Max-Planck-Institut für Kolloid- und Grenzflächenforschung

Modern photoredox transformations applied to the needs of organic synthesis

Dissertation

zur Erlangung des akademischen Grades
Doktor der Naturwissenschaften
(Doctor rerum naturalium, Dr. rer. nat.)
in der Wissenschaftsdisziplin „Organische Chemie“

eingereicht an der
Mathematisch-Naturwissenschaftlichen Fakultät
der Universität Potsdam
von

Yevheniia Markushyna

Ort und Tag der Disputation: Potsdam-Golm, 22.09.2020

Hauptbetreuer:	Prof. Dr. Dr. h.c. Markus Antonietti
Betreuer:	Prof. Dr. Bernd Schmidt Dr. Oleksandr Savatieiev
Gutachter:	Prof. Dr. Dr. h.c. Markus Antonietti Prof. Dr. Bernd Schmidt Prof. Dr. Roland Marschall

Published online on the
Publication Server of the University of Potsdam:
https://doi.org/10.25932/publishup-47766
https://nbn-resolving.org/urn:nbn:de:kobv:517-opus4-477661

Table of Contents

1. Motivation

Ever-rising demands of energy and environmental problems caused by the large-scale industries encouraged the modern society to reconsider the natural resources harvesting habits. Since the beginning of 21st century, the sustainability of human development is the biggest concern that scientists of all the areas were faced to. As science has historically developed from philosophy and as it still is one of the essential parts of it, I would like to start my PhD thesis with Aristotle, who in 4th century BC used the word "energy" for the first time. Initially, "energy" was representing a philosophical concept and had a meaning of "activity, reality, existence". In Late Latin, it was misinterpreted and started to be used with the meaning of "force", precisely "force of expression". Heading closer to our days, in 17th century, basics of a modern concept of energy were described by Gottfried Leibniz, which he called *vis viva*, meaning a "living force". In 19th century, "energy" was used instead of "*vis viva"*. However, taking a closer look on human history, Aristotle and Leibniz seem even today correct in their definitions of energy as a "living force". First fire wood and later fossil fuels as sources of energy were defining human being. However, the intensification of problems caused by wide use of natural resources has put the sustainability of this concept under question. As a result, clean and renewable energy sources, among all solar energy, have entered the scientists' horizon in many fields.[1] The power of Sun, worshipped by many ancient civilizations, has been turned to humanity once again. Inspired by the potential of solar energy, scientist have developed novel technologies powered by this, considering the estimated lifetime of Sun and Earth, everlasting source of energy. Solar energy has already been used to power solar cells,[2-4] has shown high potential in the generation of hydrogen from water,[5-7] reduction of carbon dioxide,[8-10] and degradation of organic pollutants in wastewater treatment,[11-14] as well as many more other applications.

For several decades, utilizing solar energy to power chemical transformations is one of the hottest topics also in chemistry. In general, photoinduced chemical reactions are already commonly used for quite a long time and became a part of a daily routine in organic synthesis.[15] However, ultraviolet (UV) light is usually used to afford these reactions. This requires the use of sophisticated laboratory equipment and protocols. Most of the molecules are transparent to visible light and cannot be directly excited by a photon to initiate the reaction. For such cases, photocatalysts were designed to plug the energy of visible light into a formation of chemical bonds.

The idea of utilizing light power for the synthesis of useful chemicals was proposed by Giacomo Ciamician in Science back in 1912: "*On the arid lands there will spring up industrial colonies without smoke and without smokestacks; forests of glass tubes will extend over the plants and glass buildings will rise everywhere*; *inside of these will take place the photochemical processes that hitherto have been the guarded secret of the plants*, *but that will have been mastered by human industry which will know how to make them bear even more abundant fruit than nature*, *for nature is not in a hurry and mankind is*.".[16-17] Namely, he predicted the following rapid development of new approaches utilizing solar energy instead of common harmful reagents. Since then, photochemistry is indeed constantly developing and became a big advanced field of chemistry.

Standing on the edge of material and organic chemistry, organic heterogeneous photocatalysis is gaining more and more attention of scientific community. In the last decades, numerous comprehensive organic reactions were developed, however, mainly catalyzed by homogeneous catalysts.[18] Despite all the advantages, heterogeneous materials are significantly less explored. Among heterogeneous photocatalysts, an important place is taken by carbon nitrides that are a group of polymeric semiconductors built mainly from C and N atoms.[19] Thanks to the convenient band structure, these materials are known in material chemistry as photocatalysts,[20] as a support for single metal atoms and nanoparticles,[21-23] and as electrocatalysts.[24] In recent years, they have also been successfully applied in photocatalysis of organic reactions.[25] Although the reported reactions still aim at the decomposition of organic pollutants, the number of applications in synthetic reactions is constantly growing.

In this thesis, carbon nitrides as a facile tool for accomplishing complex organic synthetic transformations will be emphasized; the application of carbon nitrides for the synthesis of small organic building blocks will be investigated and broadened; fundamental photocatalytic properties of carbon nitrides will be further investigated and their effect on the photocatalytic activity will be discussed.

2. Introduction to heterogeneous photocatalysis

2.1. Photocatalysis and its applications

Inspired by nature. Plants, microalgae and some bacteria harvest the sunlight energy to transform H_2O and CO_2 into carbohydrates by the process named photosynthesis.[26] In these photosystems, green pigments absorb a photon of light, while the obtained energy is used to excite electrons, which, in turn, power H_2O oxidation and the synthesis of NADPH. Therefore, excited electrons serve as the main drivers of photosynthesis. The similar concept is true for photocatalysis. However, as most of the compounds cannot be excited by photon directly, an external compound – "photocatalyst" – is used to produce excited electrons and to initiate the chemical transformation.

History of Photocatalysis. Mentioned in Introduction, Giacomo Ciamician, was one of the pioneers in the field to perform experiments on whether "light and light alone" would power a chemical transformation.[16-17] To power some of his reactions, he used blue and red lights. Surprisingly, he noticed that only blue light resulted in a chemical effect. This was probably the first observation of the photocatalytic reaction. Shortly later, in 1911, a bleaching of the dark blue pigment, Prussian blue, by ZnO under light illumination was published by Alexander Eibner and the keyword "photocatalysis" has entered scientific literature.[27-29] This observation initiated the interest to further experiments with ZnO as a photocatalyst, such as reduction of Ag^+ to Ag^0 in 1924.[30] Following these experiments, TiO_2 and Nb_2O_5 were also reported to drive similar reactions of reduction of silver or gold cations.[31-32] In 1938, TiO_2 was firstly tested for organic reaction. It was used as a photosensitizer for bleaching of dyes in the presence of oxygen.[33] However, due to the lack of practical applications, photocatalysis was subsided for over 25 years, up to 1970th. The "oil crisis" and environmental impacts by industrial processes motivated researchers to search for alternative energy supplies. Many research groups started to work on the UV light photoinduced effects on semiconducting solids, such as TiO_2 and ZnO. The first experiments on oxidation of organic substances were conducted. In 1964, Filimonov studied the photocatalytic oxidation of isopropanol over ZnO and TiO_2.[34] Molecules, such as O_2 and H_2O, were found to be absorbed or desorbed on the semiconductor surface under UV light irradiation. In 1972, Honda and Fujishima reported the photosensitization effect of a TiO_2 electrode for H_2O electrolysis.[35] They showed that electrolysis of H_2O with the TiO_2 electrode under UV light irradiation proceeds at lower bias voltage than normal electrolysis. In 1977,

Schrauzer and Guth used powdered TiO_2 photocatalysts with loadings of Pt or Rh metal particles for water splitting. Thus, they were first to report the photocatalytic water splitting without an additional external energy input.[36] In 1979, the first studies on CO_2 reduction, using inorganic semiconductors, were published by Fujishima.[37] These early works showed the potential of the photocatalytic approach for practical use and from 1980th an extensive work began on similar reactions, in particular, using TiO_2 as the photocatalyst.

In a broad view, reactions of converting chemicals with the help of light are commonly called as artificial photosynthesis. Sometimes, it is specifically tied to water splitting and CO_2 conversion. Indeed, these reactions have reasonably gained the most scientific attention, especially water splitting.[38] First, it is extremely important as it is the first step of natural photosynthesis. And second, it also has a great potential for practical use. In the reaction of water splitting, hydrogen is produced, which is known to be a source of clean renewable energy. The reaction of CO_2 reduction is obviously interesting due to the recent extensive global warming discussions. Not less this reaction is interesting from a chemical point of view. It involves up to 8 electrons and 8 protons in conversion to C_1 products, such as in synthesis of CH_4, and even more than 8 in synthesis of C_2 and C_3 products. These reactions along with the formation of valuable large-scale products, for example alcohols, are particularly interesting for modern chemical industry.

Since the first discoveries, photocatalytic community has been working on the understanding of fundamental principles, improving photocatalytic efficiencies, developing new methodologies, designing new photocatalysts and expanding applications of the photocatalytic approach. Photocatalysis today is a versatile tool, which has a potential of being used not only for industrial processes, but in a daily laboratory routine to run sophisticated synthetic reactions as well. Several applications of photocatalysis for performing organic reactions will be discussed in Chapter 3.

2.2. Heterogeneous photocatalysis

Main principles of photocatalysis. Photocatalysis and photocatalysts, despite countless variations, are commonly divided into two groups, homogeneous and heterogeneous, representing the physical state of the catalyst in reaction systems. The photoexcitation effect on the catalyst is shown in Figure 2.1. In case of homogeneous catalysis, photocatalyst and reactants exist in the same phase. These are typically metal complexes, such as ruthenium- and iridium-based molecular complexes or organic dyes, such as Eosin Y and Rhodamine.[39-40]

Under light irradiation, electron is exited from the highest occupied molecular orbital (HOMO) to the lowest unoccupied molecular orbital (LUMO). The photogenerated electrons and holes can further undergo redox reactions with the reactants.

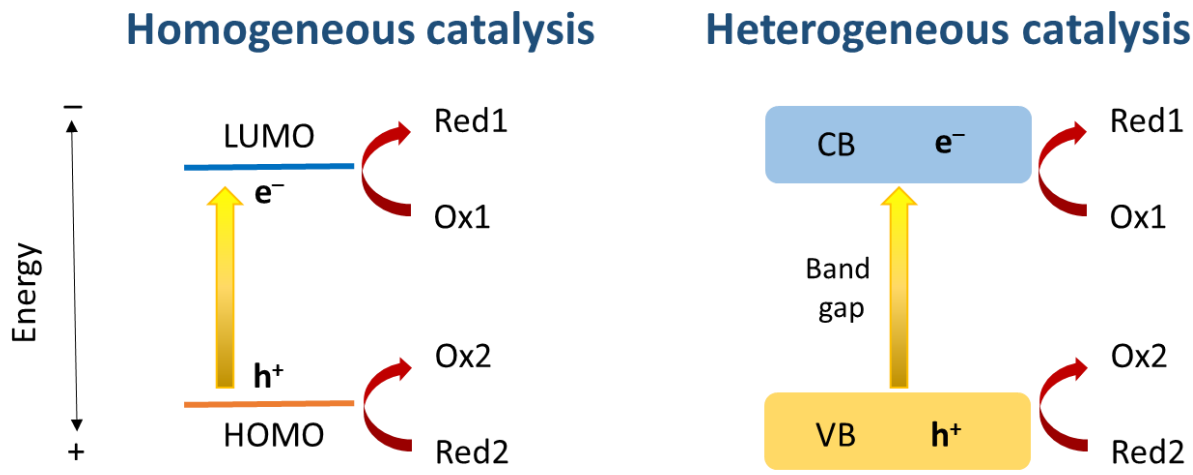

Figure 2.1. Photoexcitation of homo- and heterogeneous photocatalysts.

In heterogeneous photocatalysis, a catalyst and reactants are in the different phases. These are typically represented by metal oxides, such as TiO_2 and ZnO, and other narrow band gap semiconductors, such as carbon nitrides.[41] In solid state chemistry, equivalents of HOMO and LUMO are a valence band (VB) and a conduction band (CB) respectively. A void energy region between VB and CB is called a band gap (BG). A photon with an energy equal to or greater than the band gap excites an electron from the VB to the CB, generating an electron/hole (e^-/h) pair that undergoes redox reactions.

In general, processes happening during photocatalytic action can be described by four steps (Figure 2.2): 1) light absorption and generation of electron-hole pairs; 2) separation of the photoinduced charges; 3) transfer of charges to the surface of the catalyst; 4) utilization of charges in redox reactions.

In an ideal reaction, both the electron and hole would move to the surface and undergo a productive redox reaction with available reactants. However, movements of electrons and holes are random, and most of the photoinduced e^-/h pairs recombine, nullifying the photoexcitation act. They can recombine either in the volume or on the surface of the material. The energy released from recombination of charges can be released in the form of heat (non-radiative recombination) or light emission (radiative recombination). Ideally, each e^-/h pair should result in a reaction with reagents and recombination processes are undesirable. The recombination

rate depends on the structure, crystallinity, and particle sizes of the material and usually is in the range of ns to μs. Different methods for optimization of photocatalytic activity of carbon nitrides are reviewed in Chapter 3.1.

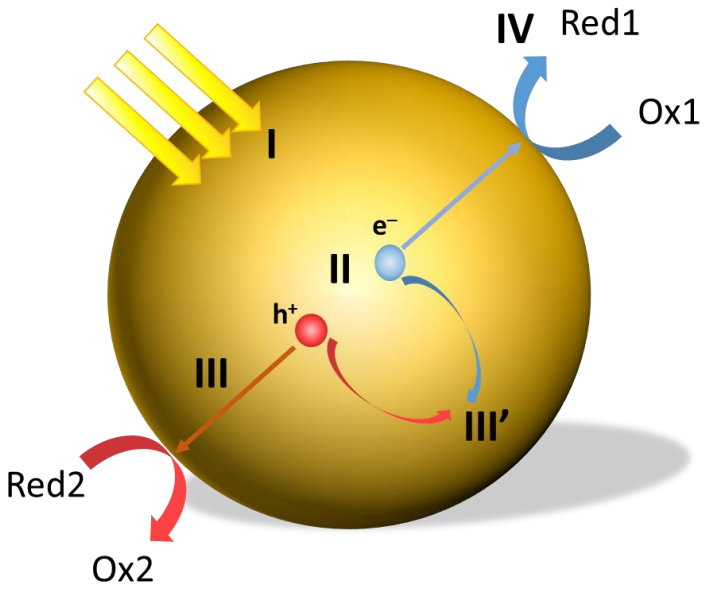

Figure 2.2. Photocatalytic process described in four steps.

A successful organic synthesis with heterogeneous photocatalyst depends on several parameters:

1. The band gap. It determines a wavelength range in which material would absorb. For excitation of an electron on the VB, the energy of the wavelength must be equal or higher than the energy of the BG.

2. Positions of the VB and CB of the semiconductor and redox potentials of the reactants. For the reaction to happen, electron acceptor must have a lower reduction potential than the CB potential of the photocatalyst. Likewise, electron donor must have a higher oxidation potential than the VB.

3. An efficient photocatalyst should effectively convert transient charge separation into redox half reactions. The recombination of photoinduced electrons and holes should be minimized. The catalyst should assist an effective separation and transfer of charges.

Heterogeneous photocatalysts are a collection of numerous solid materials of different properties. However, the most widely used among them can be grouped into metal oxides, plasmonic photocatalysts and carbon nitrides. The latter stands for the highest interest in the

present work and will be discussed in details in Chapter 3. Here, a short description of the other two groups will be given.

Metal oxides. TiO_2, Nb_2O_5 and ZnO are typical representatives of wide band gap catalysts that absorb UV light.[41] For the photoexcitation with visible light, these materials have to be modified. Adsorption of heteroatom-containing (O, S, N) substances on the metal oxide surface results in the formation of charge-transfer complexes between them, which makes a catalysis in visible range possible. Therefore, non-modified metal oxides are suitable only for reactions with heteroatom containing compounds, such as amines and alcohols.[42-44] C-H bonds of alkanes are more stable and the interaction with metal oxide is very weak. For oxidation of C-H bond a terminal oxidant, such as H_2O_2, or external heteroatom containing compound, such as SO_2, is needed.[45-46] As a result, crafting heteroatom containing compounds, for example benzyl alcohol, on the surface of metal oxides is one of the ways used for enabling catalysis under visible light.[47] Various materials with pre-adsorbed reactant are also commercially available. However, the capacity of this methodology is limited.

Plasmonic photocatalysts. The surface plasmon resonance (SPR) effect of nanostructured Au, Ag and Cu is one of the effective ways to reach a visible light photocatalysis. The absorbance spectra of the surface plasmon bands of Au spherical nanoparticles is at 530nm, Ag at 400nm, Cu at 580 nm, which enables the effective absorption of visible light.[48] The SPR effect for the photocatalytical purposes was first examined in 2008 on Au and Ag nanoparticles.[49-50] Plasmonic photocatalysts are usually supported on metal oxides, and TiO_2 is the most popular choice. The effectiveness of plasmonic metal particles can be proved by the challenging reaction of direct oxidation of sp^2 C-H bond of benzene in the synthesis of phenol.[51] Overall, despite the fact that these catalysts are effective in driving selective organic transformations, they are based on expensive noble metals. Therefore, a practical application of plasmonic photocatalysts is uncertain.

3. Photocatalysis in organic reactions: carbon nitrides versus molecular catalysts

As any other field, organic chemistry is transforming towards more sustainable and efficient processes. One of the key challenges in the field that remains open is the invention of novel methodologies to achieve highly efficient assembly of structurally complex molecules. One of the appealing approaches to pursue is to design new catalytic platforms that would enable a wide range of chemical transformations. Therefore, visible light photocatalysis is an attractive alternative to well-established protocols for the synthesis of fine chemicals. Due to the well-defined structure of homogeneous transition metal-based catalysts and organic dyes, they have been widely used to drive a wide variety of organic transformations. On the other hand, due to low cost, simple preparation procedure, and chemical stability of carbon nitride semiconductors, they have been known almost exclusively in environmental applications and water splitting. However, numerous examples of carbon nitride-based organic photocatalytic reactions have been reported within past few years.

In this chapter, synthesis methods and properties as well as different approaches for modification of carbon nitride-based materials will be discussed; the photocatalytic efficiency of carbon nitrides in organic reactions will be evaluated and compared to the widely used homogeneous catalysts in the scope of similar organic reactions, including carbon-carbon or carbon-heteroatom bond formation reactions.

This chapter is adapted from my original work: Markushyna, Y.; Smith, C. A.; Savateev, A.: Organic photocatalysis: carbon nitride semiconductors versus molecular catalysts. European Journal of Organic Chemistry (10), S. 1294 - 1309 (2020)

3.1. Synthesis and properties of carbon nitrides

A historical overview. The history of carbon nitrides (CNs) dates back to 1830s, making carbon nitride one of the oldest synthetic polymers. While attempting to achieve the formation of $(SCN)_2$ by decomposition of $Hg(SCN)_2$, Berzelius noted the formation of the ample amount of voluminous solid mass, that broke the apparatus.[52] This phenomenon boosted the development of pyrotechnic materials and was later commercialized as "Pharaoh's serpents'.[53] Years after, Liebig was also working on thiocyanates and described the formation and properties of several $C_xN_yH_z$ compounds that he named as "melamine", "melam" and "melem".[54-56] He reported the formation of the similar material to the one obtained earlier by Berzelius, to which he gave a name "melon".[54] He described, that depending on the synthesis experiment, the composition of "melon" also varies.

The history of carbon nitrides as heterogeneous photoredox catalysts started around 2006.[57] In 2009, Wang at al. reported the historical work, where they used g-CN for photocatalytic water splitting.[19] Despite the low quantum efficiency (<0.1%) reported, this work has renovated the interest in carbon nitrides as photocatalysts.

Synthesis of CNs. Modern synthesis of CN-based materials involve a thermal polymerization of various nitrogen-rich precursors. The common choices are cyanamide[19, 58] and its dimer dicyanamide,[59] melamine,[60] urea,[61] and thiourea[62] etc. The condensation processes occurring during the heating program are depicted in Figure 3.1.

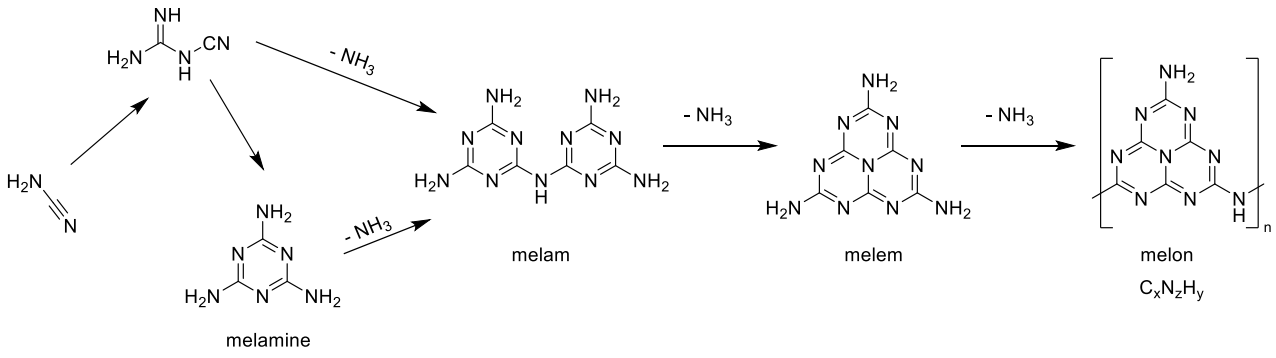

Figure 3.1. Synthesis of carbon nitride from cyanamide.

The obtained polymer can be ascribed to a general formula $C_xN_yH_z$. Following the general tendency of the reaction, the continuous elimination of ammonia should theoretically result in the formation of fully condensed graphitic g-CN based on linked heptazine units (Figure 3.2a). Theoretical studies of this structure have predicted for this carbon nitride with the C/N stoichiometric ratio 0.75 to be the most stable allotrope with the outstanding physical

properties, hardness and low compressibility comparable to that of diamond.[63-64] Although, the formation of fully condensed g-CN has not been observed up to now. Few examples of g-C_3N_4 of this stoichiometry were synthesized by alternative methods, however, they are based on the simpler (s-triazine) structure (Figure 3.2b).[65-66] This is mainly considered to be a kinetic problem.[67] Polymerization of carbon nitrides is a stepwise combination of polyaddition and polycondensation processes happening during the heating program. These transformations are hard to control, which results in different levels of condensation and therefore structural defects in the final material.

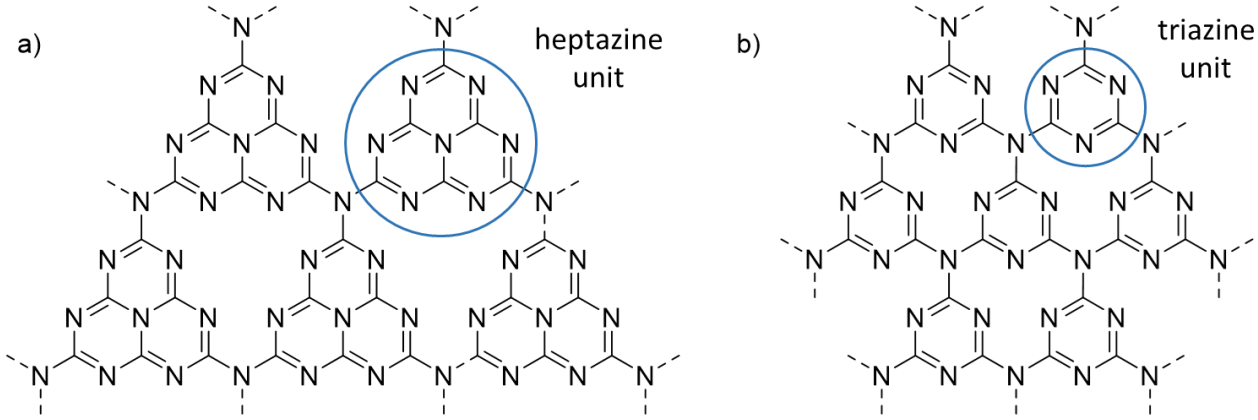

Figure 3.2. Structures of carbon nitride: a) polyheptazine (tri-s-triazine) based g-CN, b) polytriazine based g-CN.

Properties and engineering of CNs. The average C/N ratio of bulk carbon nitrides is around 0.72, and a small amount of hydrogen (2%) is also usually found. The incomplete condensation results in the presence of uncondenced amino groups, which can partially reduce the chemical inertness of the material and lead to the interactions with present reactants. Furthermore, excessive defects of incomplete condensation may also negatively affect charge migration and separation. Polymers of incomplete condensation form amorphous or semi-crystalline materials. However, a few approaches have been found to synthesize highly crystalline CNs. Schnick and co-workers isolated and identified the crystal structures of heptazine derivatives, such as melem $C_6N_7(NH_2)_3$[68] and melam $[(NH_2)_2(C_3N_3)]_2NH$[69]. This work appeared as an argument in the discussion of possible building units of CNs as well as it shows that high local crystal packing in carbon nitrides is possible. The McMillan group later reported the synthesis of a crystalline carbon nitride imide phase $C_2N_2(NH)$ with high-pressure, high-temperature (HP-HT) reaction conditions.[70-71] The synthesis of a highly crystalline carbon nitride by a simple condensation in a salt melt of LiCl/KCl has been reported by Antonietti and co-workers.[72-75] On the other hand, a trace amount of defects enhances the photocatalytic activity

of the material. Stacking defects, grain boundaries, surface terminations and structural defects seem to serve as real active sites for the reaction. In addition, introduction of "catalytically useful" defects, such as cyanamide groups, showed an improved photocatalytic activity in a hydrogen evolution reaction. 12 to 16 times higher rate and apparent quantum yield efficiency than in the reaction with unmodified catalyst were reported. [76]

Despite its non-ideal structure, g-CN showed high thermal stability up to 630 ˚C in air, while complete decomposition happens at 750 ˚C without a residue. Due to the aromatic nature of tri-s-triazine ring, the formation of π-conjugated planar layers similarly to graphite is often seen in carbon nitrides. This results in a high chemical stability and insolubility of CN-based materials in organic solvents.[77]

Directly after a condensation of organic precursors, CN materials have a surface area less than 10 m^2g^{-1} and their practical application in catalysis, where the amount of reactive sites is crucial, is limited.[62] Therefore, significant efforts were put to develop CNs with a high surface area, narrow pore size distribution, tunable pore size, uniform particle size, controllable shape and morphology. Hard and soft templating techniques allow for the formation of materials with high surface area and ordered porous structure, while at the same time retaining the chemical structure of the bulk g-CN. Mesoporous g-CN was successfully obtained from different precursors using mesoporous silica matrices as a template.[78-79] However, the "hard template" method allows for the control of surface properties of CNs only to a certain extent. Depending on the silica matrix, materials with the surface area of 86 - 439 m^2g^{-1} can be achieved.[67, 80] Despite the effectiveness and diversity of this approach, it is considered to be a time-consuming and hazardous process as the removal of the template involves the use of toxic HF or ammonium bifluorides.[81-82] A soft templating strategy was realized by Antonietti *et al.* using different surfactants or amphiphilic block polymers as structure directing agents for polymerization of dicyandiamide.[83] The application of certain templates, such as Triton X-100 (Brunauer-Emmett-Teller (BET) surface area of 76 m^2g^{-1}) and several ionic liquids (BET surface area of 81 m^2g^{-1}) resulted in good porous structures. The "soft template" method can be also merged with elemental doping. Buthylmethylimidazolium tetrafluoroborate as a "soft template" provided a CN material doped with boron and fluorine (BET surface area of 444 m^2g^{-1}).[84] In general, a "soft-templating" method is less efficient than using hard templates, but is more environmentally benign.

As a semiconductor, g-CN possesses a band gap of ca. 2.7 – 2.8 eV with the onset of light absorption around 450-460 nm.[85] The positions of CB and VB are calculated as -1.2 V and 1.5

V vs. NHE.[86] Optical and redox properties of CN-materials also depend on the synthesis strategy and can be further tuned through some band engineering techniques. These are elemental (metal or non-metal) and molecular doping.[87] An ionothermal method of synthesis or supramolecular preorganization of monomers allows for the control of polymerization process and thus, have been used for the band gap engineering. For example, by changing the molten salt from LiCl/KCl to NaCl/KCl eutectic mixtures, the band gap of a CN material changed from 1.87 to 2.2 V vs. RHE and the conduction band from –0.66 V to –0.2 V vs. RHE.[88] Synthesis of a CN in NaCl/KCl molten salt resulted in an increase of the apparent quantum yield up to 60% in the hydrogen evolution reaction.[89]

Another simple approach to control chemical and photophysical properties of CN-materials is supramolecular preorganization of monomers before calcination. This technique allows for the formation of specific morphologies and ordered structures before calcination by adjusting supramolecular interactions (hydrogen bonding, π-π interactions etc.) of the CN monomer.[90] For example, 3-amino-1,2,4-triazole oligomer was used for the synthesis of CN with the starting morphology of the precursor, while with changed optical and electronic properties.[91]

Another unique technique available for CN-based materials is molecular doping. It can be realized by copolymerization of the CN precursor with appropriate organic additives. Anchoring organic groups to CN materials can significantly change their light-harvesting properties and sufficiently narrow the band gap. Not only small functional groups, but also large functional units can be introduced into the CN framework. For example, installed hexaazatriphenylene moiety significantly narrowed the band gap of a CN.[92] Doping a CN material with carbon-rich molecules showed not only narrowing of the band gap, but also enhanced the conductivity and light-harvesting properties due to a remarkable redshift of optical absorption.[93]

Perhaps, the most widely used method for modifying electronic properties of CNs is elemental doping. Doping with non-metals, such as oxygen, fluorine, sulfur, phosphor or boron elements, is performed through substitution of C and N atoms in the CN framework. Doping with metals, Fe, Cu, Zn, Ni, instead is realized by incorporation of nanoparticles into the CN matrix. A small amount of dopant can effectively lower charge recombination rate and improve photocatalytic performance of the material. Elemental doping is an excellent tool for effective band gap engineering, as both introducing specific elements and their loadings affect the band gap position. In most cases, it results in a band gap narrowing and enhancement of the charge separation and transfer. [94-97]

Overall, chemical and thermal stability, reusability, and relatively low cost of production make carbon nitrides particularly interesting for potential industrial use. However, several issues related to relatively low catalytic efficiency, such as high charge recombination rate and poor visible light absorption, have to be solved.[98] With versatile methods for tuning chemical and photophysical properties of CNs as well as with better understanding of material composition – material properties relations, there is an obvious potential for further development and practical use of highly effective CN-based materials.

Potassium poly(heptazine imide) (K-PHI) – a promising carbon nitride for organic photocatalysis

In 2017, in Max Planck Institute of Colloids and Interfaces, a new member of carbon nitride family was synthesized - potassium poly(heptazine imide) (K-PHI) (Figure 3.3).[74] Polymerization of aminotetrazole was performed by a salt-melt method in the LiCl/KCl eutectic mixture. The obtained material showed a quite different morphology and properties compared to g-CN. The detailed characterization of K-PHI is presented in Chapter 11.4 (Figure A2).

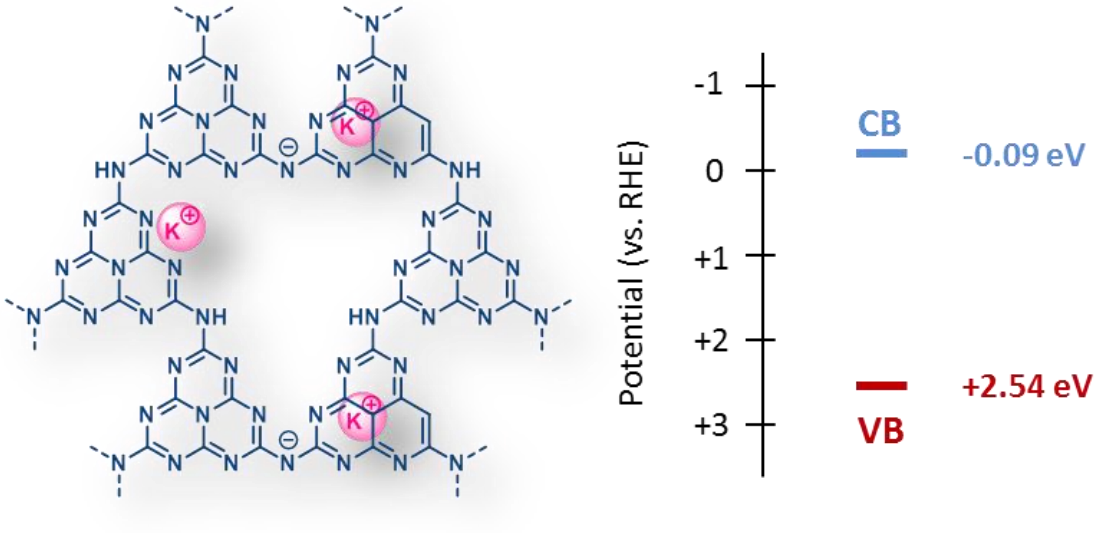

Figure 3.3. Chemical structure and band energy diagram of K-PHI.

In addition to more crystalline and ordered interlayer structure of K-PHI, it shows increased oxidative properties. The VB potential of K-PHI is 2.54 eV vs. RHE, while the one of g-CN is 1.82 eV vs. RHE.[75] Therefore, the use of K-PHI is more suitable for oxidative reactions, however reduction reactions can be catalyzed as well, as shown in Chapter 7. Despite the recent synthesis report, K-PHI has already shown an improved photocatalytic activity in many

challenging organic reactions, such as oxidation of methylarenes to disulphides,[99] synthesis of thioamides from amines and elemental sulfur[100] or cyclization of tetrahydroisoquinoline (THIQ) with chalcones.[101]

3.2. Photocatalyzed carbon-carbon bond formation reactions

In the last years increased interest in the visible light photocatalysis by chemists produced a huge variety of the photocatalytic organic reactions. Most of them are mediated by homogeneous or in other words molecular catalysts. Nevertheless, homogeneous catalysts in general possess few drawbacks, such as difficulties in separation from the product and its recovery. That is why development and application of heterogeneous catalysts deprived of these problems are highly desired. In this Chapter, performance of homogeneous molecular photocatalysts and presented earlier heterogeneous carbon nitride photocatalysts will be evaluated in the specific reactions under similar conditions. Reactions, such as carbon-carbon bond formation, carbon-carbon radical cyclization and carbon-heteroatom bond formation, will be considered.

One of the most important factors to be considered in photocatalytic reactions is redox potential of catalytic species and reactants. Potential of the valence and conduction band determine redox properties of semiconducting materials. Band potentials of carbon nitrides may significantly vary depending on the structure and method of synthesis. For example, g-C_3N_4 has more negative conduction band (CB) potential (-1.54 V vs. SCE) than that of K-PHI (-0.75 V vs. SCE), whereas valence band (VB) potential of K-PHI (1.88 V vs. SCE) is noticeably more positive than of g-C_3N_4 (1.16 V vs. SCE).

Redox potentials of the discussed catalysts are presented in Figure 3.4.

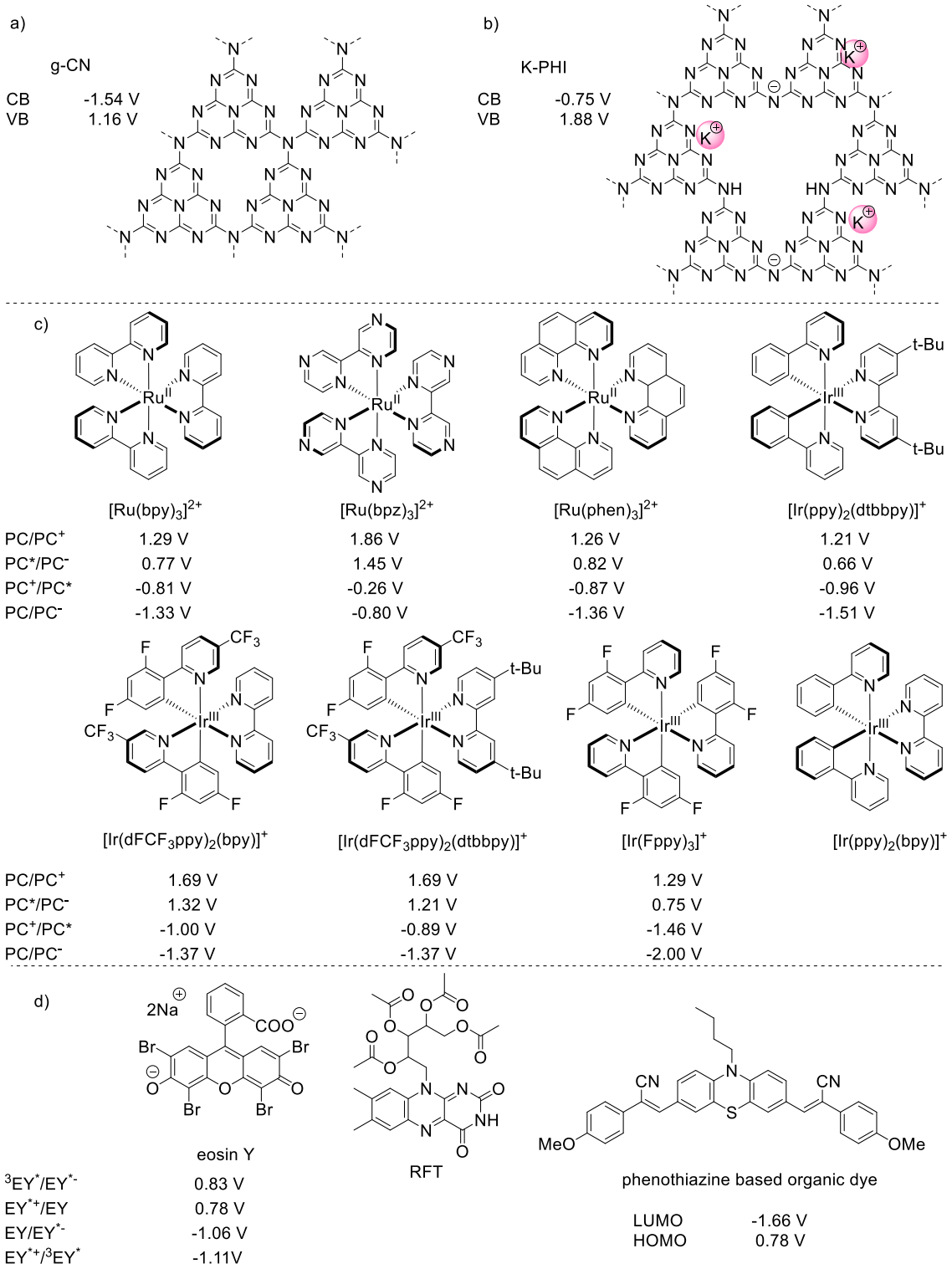

Figure 3.4. Overview of the heterogeneous carbon nitride photocatalysts and molecular photocatalysts. Catalyst structures: a) structure and aberration corrected high resolution transmission electron microscopy (AC-HRTEM) image of g-CN, b) structure and AC-HRTEM image of K-PHI, c) transition metal-based complexes, d) organic dyes. The redox potentials of eosin Y,[102] phenothiazine dye,[103] and of metal-based complexes were taken from literature.[104] The band gap potentials of carbon nitrides were taken from Savateev *et al.*[105] The potentials are given versus SCE.

Direct formation of C-C bonds is a challenging research area in organic synthesis, especially when done in an environmentally friendly manner. The tetrahydroisoquinoline (THIQ) framework is a common element in a number of natural bioactive compounds.[106] Therefore, many techniques have been developed in order to functionalize tetrahydroisoquinoline fragment,[107] including photochemical approaches.

In general, amines are known to be very good electron donors that easily undergo single electron oxidation to give an aminium radical cation, and two-electron oxidation followed by proton abstraction to give an iminium ion. Catalytically generated iminium ion intermediates can be subsequently trapped by the nucleophilic compounds to form a new bond at α-position. In 2010, Stephenson *et al.* published the photocatalyzed *aza*-Henry reaction with nitroalkanes and *N*-aryltetrahydroisoquinolines under visible light irradiation with an iridium catalyst (Scheme 3.1).[108]

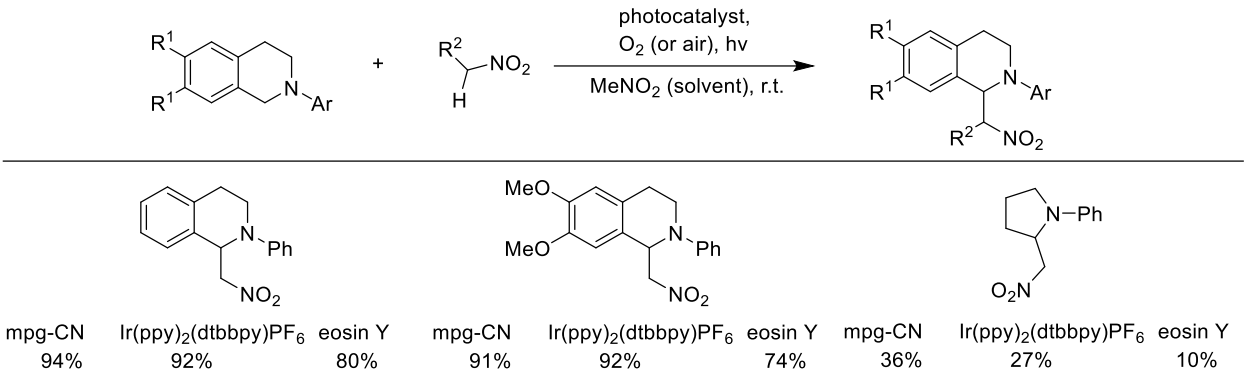

Scheme 3.1. Photocatalytic *aza*-Henry reaction with nitroalkanes and *N*-aryltetrahydroisoquinolines.

After this, König and Hari developed a transition metal free version of this reaction with eosin Y, a common organic dye (Figure 3.4).[109] Despite the high yields of the products by both methods, the drawback of these systems is the difficulty in recycling of the catalyst. Among heterogeneous catalysts, metal-free carbon nitride has been used by Blechert's group.[110] Mesoporous graphitic carbon nitride (mpg-CN) showed a comparable activity to the homogeneous systems. In all approaches, the reaction conditions were almost the same, except of course the catalyst used. In the more complicated reaction with *N*-phenylpyrrolidine, however, mpg-CN gave higher yield than both homogeneous catalysts.

The Mannich-type reaction shown in Scheme 3.2 was accomplished on tetrahydroisoquinoline substrates using proline as a co-catalyst with both mpg-CN and $Ru(bpy)_3(PF_6)_2$. The reaction proceeds *via* the formation of a nucleophilic enamine from the proline and ketone, followed by subsequent addition to the iminium ion.[110-111] This reaction catalyzed by $Ru(bpy)_3(PF_6)_2$ has

been published by Rueping and coauthors,[111] and with mpg-CN as published by Blechert *et al.* Similar product yields were achieved by catalysis with heterogeneous carbon nitride when compared to the homogeneous catalyst.[110]

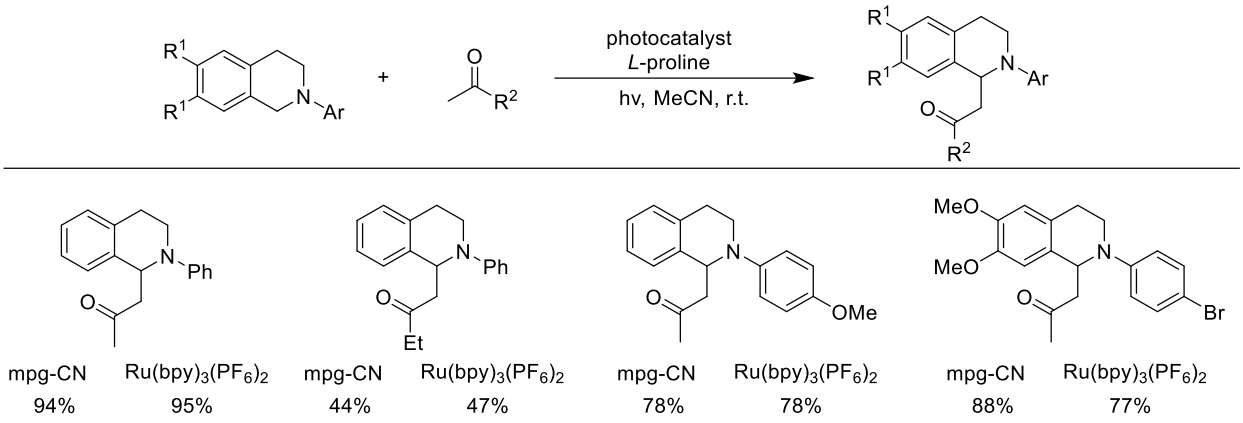

Scheme 3.2. Photocatalytic Mannich-type reaction with *N*-aryltetrahydro-isoquinolines and ketones.

In drug discovery practice, a common strategy to protect a drug candidate against *in vivo* metabolism is incorporation of electron-withdrawing groups, such as trifluoromethyl (CF_3).[112] The CF_3 moiety is typically installed by transition metal catalyzed cross-coupling reactions. However, several photochemical approaches have been recently introduced. Trifluofomethylation of arenes and heteroarenes by iridium and ruthenium photocatalysts has been reported by MacMillan *et al.* (Scheme 3.3).[113] A broad scope of products, benzene derivatives and CF_3-functionalized 5- and 6-membered heterocycles, were synthesized with moderate to excellent yields.

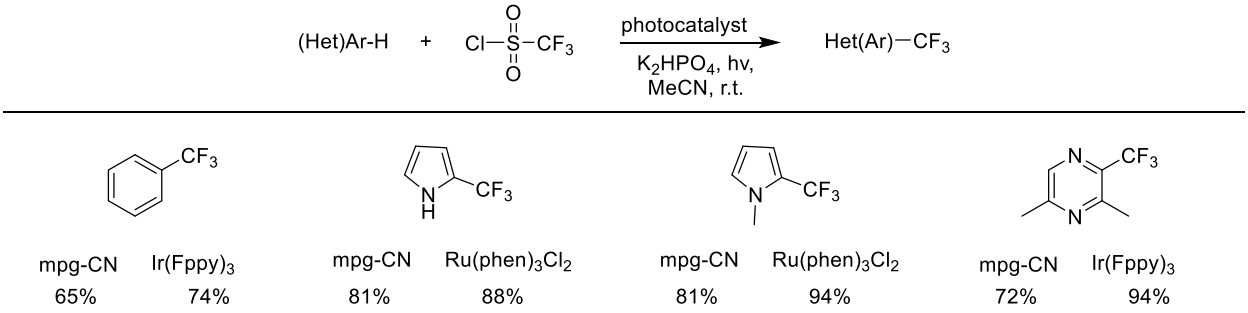

Scheme 3.3. Photocatalytic trifluoromethylation of arenes and heteroarenes.

A method with carbon nitride photocatalyst was published by Blechert *et al.*, but the yields in this case were slightly lower (Scheme 3.3).[114] Nevertheless, a large scope of heterocycles has been studied. In both cases, a CF_3 radical was generated by single-electron reduction of trifluormethanesulfonyl chloride. The value of this transformation has been shown *via* trifluoromethylation of biologically active molecules, *e.g.* caffeine.[114]

Reactions such as α-aminoalkyl radical additions, allylation, and heteroarylations, are quite well represented by homogeneous catalysis. Nevertheless, in 2018 Rueping *et al.* published several reactions involving the generation of reactive α-aminoalkyl radicals with heterogeneous g-CN.[115] Desilylative addition of α-silylamine to activated alkenes, such as 2-cyclohexenone, other cyclic unsaturated ketones (Scheme 3.4), and dicyanostyrenes (Scheme 3.5) was performed.

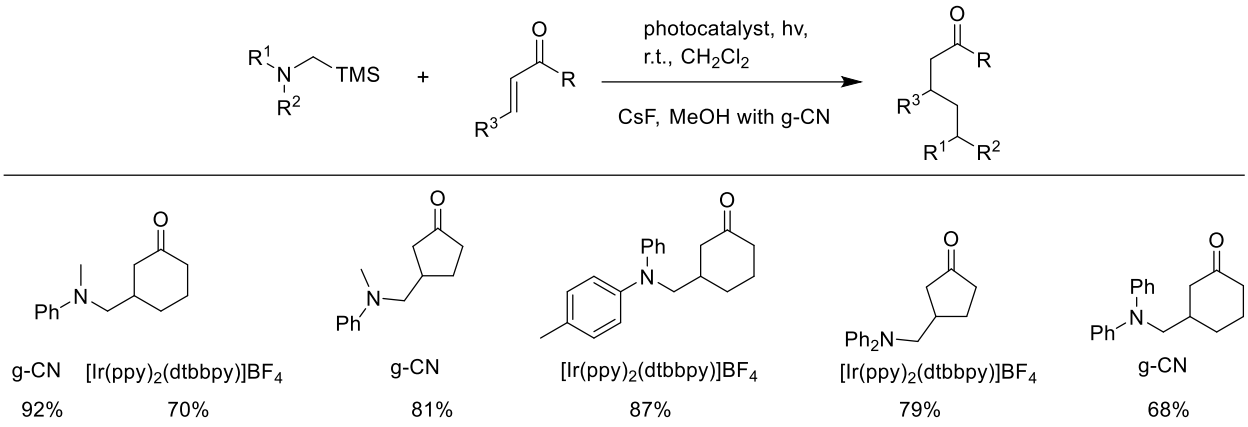

Scheme 3.4. Photocatalytic alkylamination of ketoalkenes via α-aminoalkyl radical formation.

Silyl substituted amines were chosen as substrates for the selective formation of α-aminoalkyl radicals at the desired position. This reaction catalysed by g-CN with enones required CsF as a base.[115] Variety of substituents of different electronic properties were investigated and showed no effect on the reactivity of substrate. Moreover, a study of the reaction pathway in case of catalysis by $[Ir(ppy)_2(dtbbpy)]BF_4$ was done. A primary product of the addition, silyl enol ether, was isolated.[116]

The reaction with dicyanoalkenes with the homogeneous catalyst $[Ir(ppy)_2bpy)]PF_6$ was performed with conventional amines without silyl substituent (Scheme 3.5).[117] Based on this reaction the authors showed the principal role of oxygen in the synthesis. In the presence of oxygen, selective formation of cyclic products was observed.

In the reaction catalyzed by g-CN, acrylonitrile derivatives showed excellent reactivity and higher yields in comparison to iridium-catalyzed approach.[115] To illustrate the practicability of the heterogeneous process, the catalyst was recycled for 8 times without losing its activity.

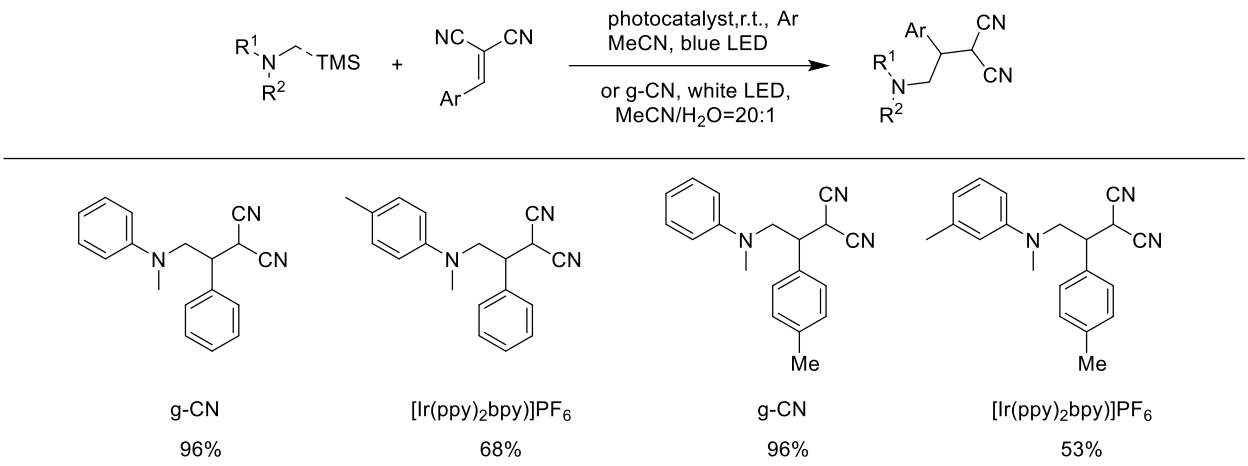

Scheme 3.5. Photocatalytic alkylamination of dicyanoalkenes.

Formation of α-aminoalkyl radicals was completed from more easily available α-amino acids (Scheme 3.6).[115, 118] Secondary amine alkyl radicals were formed through a decarboxylation process.

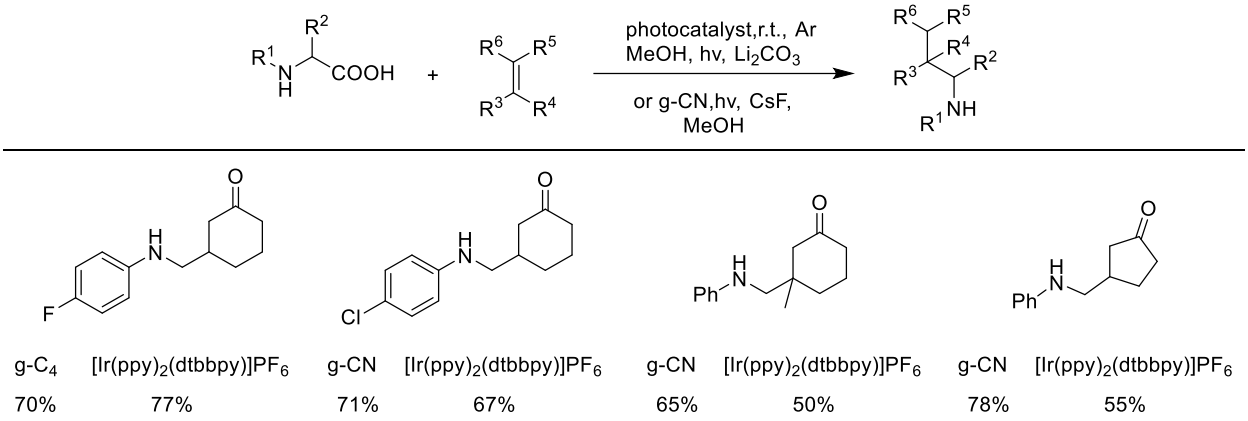

Scheme 3.6. Photocatalytic decarboxylative addition of α-amino acids to activated alkenes.

The reactivity of substrates was proven by achieving formation of a quaternary center by coupling to a sterically hindered tertiary carbon, for example to 3-methylcyclohex-2-enon. The yield was higher for carbon nitride catalyzed reactions rather than for the homogeneous catalyst $[Ir(ppy)_2(dtbbpy)]PF_6$ (65% and 50% respectively). However, only moderate yields were reported due to unselective polymerization and cycloaddition processes.

Following the additions to activated double bounds, heteroarylation was explored with g-CN as an alternative to the homogeneous catalyst $[Ir(ppy)_2(dtbbpy)]PF_6$. As a result, photocatalytic amine α-arylation was achieved by the addition of an α-amino radical to a neutral arene (Scheme 3.7).

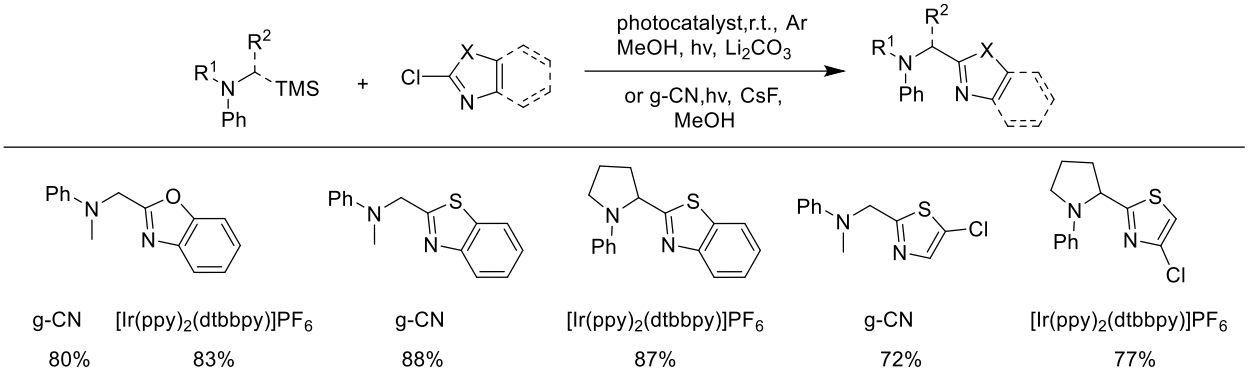

Scheme 3.7. Photocatalytic arylation through α-aminoalkyl radical addition.

Heteroarylation catalyzed by g-CN was performed in a desilylative manner.[115] Condensed five-membered heterocycles, as well as monocyclic thiasole, were tolerated under these conditions. The heterogeneous catalyzed reaction showed great performance with six-membered heterocycles as well as five- and six-membered cyclic amines.[119]

3.3. Photocatalyzed carbon-carbon radical cyclizations

The Diels-Alder reaction is a common and a powerful tool in organic synthesis for the formation of new cyclic compounds.[120] It was found that radical cations generated from electron-rich alkenes *via* photoredox catalysis react with dienes to give Diels-Alder adducts. Yoon and coauthors have published a radical cation [4+2] cycloaddition with $Ru(bpz)_3(BArF)_2$ photocatalyst (Figure 3.8).[121] They demonstrated the value of the proposed method by synthesis of natural regioisomer of heitziamide A.

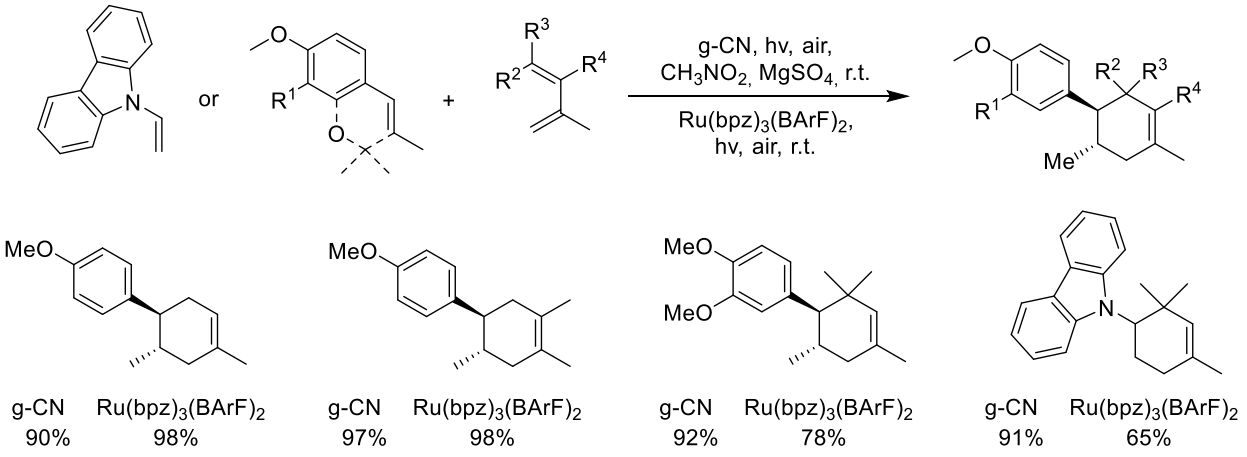

Scheme 3.8. Photocatalytic Diels-Alder cyclization.

The similar method, but with metal-free g-CN was proposed by Zhao and Antonietti, which gave comparable yields and in some cases outperformed the homogeneous catalyst.[122] In one

case, 9-vinyl-9H-carbazole, g-CN catalyst showed 91% product yield after only 1 h of irradiation compared to 65% for $Ru(bpz)_3(BArF)_2$ after 24 h of irradiation. The apparent quantum yield for g-CN in this reaction reached an outstanding value of 47%. Aerobic conditions for this reaction were required in both cases, as O_2 plays the role of electron mediator in the reaction mechanism.

Photoredox catalysts are able to reduce carbon-halogen bond by a single-electron transfer to form alkyl radicals. The photogenerated radical then reacts with the unsaturated part of the molecule to cyclize. One example of this reaction utilizing homogeneous catalysts was reported by Stephenson *et al.* (Scheme 3.9).[123] Bromomalonate was reduced to the corresponding radical and subsequently cyclized to cyclopentane *via* reaction with the double bond. The reaction is mediated by ruthenium ($Ru(bpy)_3Cl_2$) and iridium ($Ir(ppy)_2(dtbbpy)PF_6$) catalysts under visible light conditions in the presence of Et_3N as a sacrificial electron donor.

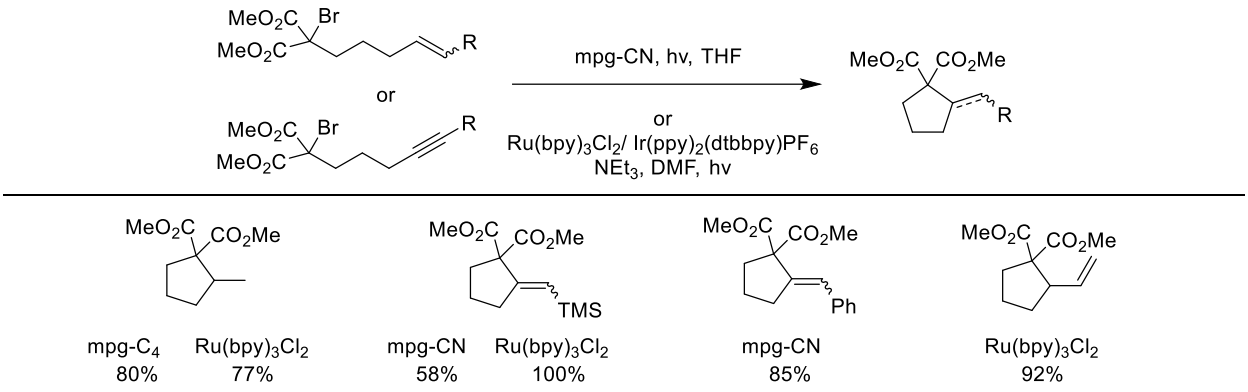

Scheme 3.9. Photocatalytic formation of cyclopentane *via* reduction of carbon-halogen bond.

Being insoluble in any organic solvent, mpg-CN was used by Blechert *et al.* in a packed bed flow photoreactor in order to increase contact with the reaction media.[124] This approach increased the selectivity and reduced the reaction time. Furthermore, THF served as both a solvent and a sacrificial electron donor.

Reductive cyclodimerization of chalcones was recently catalyzed by homogeneous $Ru(bpy)_3(PF_6)_2$ catalyst (Scheme 3.10).[125] The reaction proceeds *via* a single-electron reduction of the chalcone with its subsequent dimerization and aldol-type cyclization. The regioselectivity plays an important role in this transformation, as the only one regioisomer can be cyclized. An additional reagent for coordination of the carbonyl and enol groups, *e.g.* $Sm(OTf)_3$, was required to achieve higher selectivity toward cyclopentanol. In the heterogeneous version of this reaction, developed by Kurpil and Savateev, with the heterogeneous K-PHI photocatalyst, a coordination additive is not required, as the catalyst

itself plays a coordination role.[105] This feature of the heterogeneous photocatalysis simplifies reaction conditions and allows for high regioselectivity. In both reaction schemes, amine was used as a sacrificial electron donor.

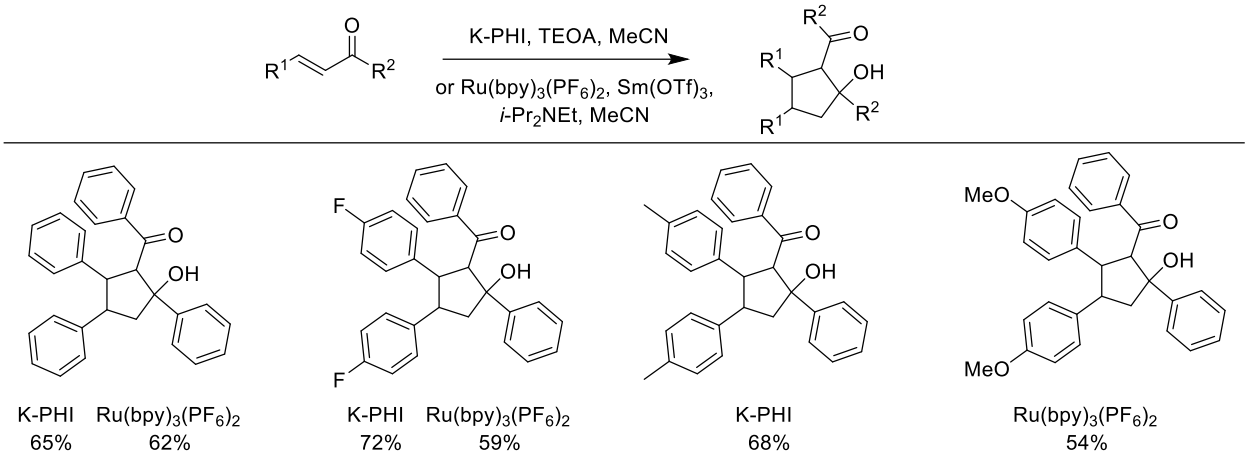

Scheme 10. Photocatalytic reductive cyclodimerization of chalcones.

Oxidation of phenols to the corresponding phenoxonium cations, followed by their coupling with alkenes is one method to build dihydrobenzofurane rings by [3+2] cycloaddition (Scheme 3.11). This reaction was catalyzed by the relatively strong oxidation photocatalyst – $Ru(bpz)_3(PF_6)_2$. When a more popular photocatalyst $Ru(bpy)_3(PF_6)_2$ was used, it was shown to be less efficient.[126] In order for the reaction to proceed efficiently, the oxidation potential of the alkene must be outside of the working range of the photocatalyst. The phenols must bear alkoxy substituents in 2- or 4- position in order to stabilize phenoxonium cation. The proposed method requires the use of $(NH_4)_2S_2O_8$ as an additional oxidant.

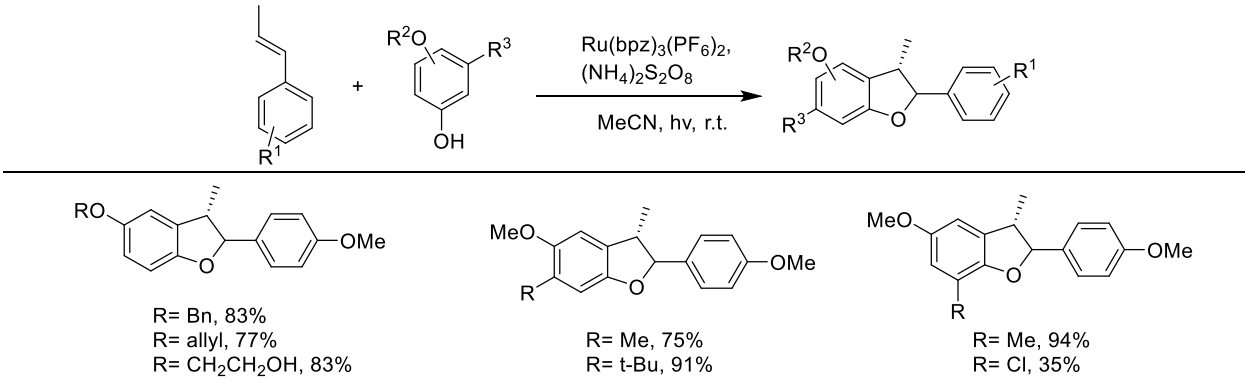

Scheme 3.11. Photocatalytic dihydrobenzofurane ring formation *via* [3+2] cycloaddition.

Another approach for building a dihydrobenzofurane fragment was shown by mpg-CN photocatalyzed oxidative dimerization of resveratrol and its analogues (Scheme 3.12).[127] Mimicking the biosynthesis of δ-viniferin, in the proposed method free oxygen was used as an

oxidizing reagent instead of $(NH_4)_2S_2O_8$, while 2,6-lutidine was used as a base. Fifteen 4-hydroxy-*trans*-stilbenes, including resveratrol, were shown to be suitable substrates. Additionally 3,4-dihydroxy-*trans*-stilbenes under the same reaction conditions gave benzodioxane-based dimers.

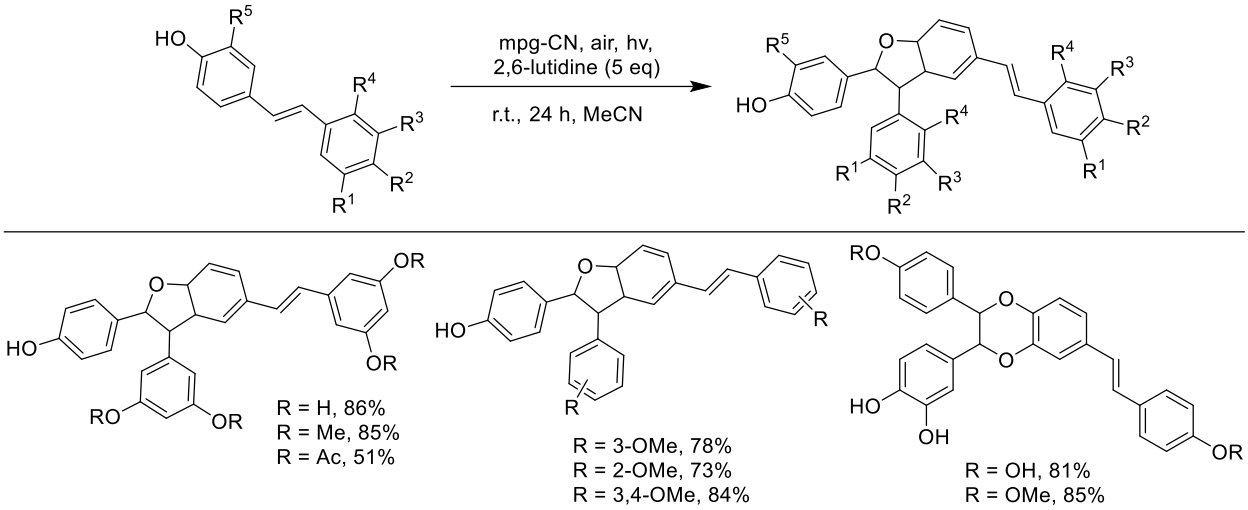

Scheme 3.12. Photocatalytic synthesis of dihydrobenzofuranes via oxidative dimerization of resveratrol and its analogues.

3.4. Photocatalyzed carbon-heteroatom bond formation reactions

The oxidation of amines is an important chemical reaction, as it is one of the key steps in synthesis of biologically active compounds in drug discovery and agrochemistry.[128-129] Photoredox catalysis has been widely presented as a suitable technique for this transformation. Both heterogeneous and homogeneous catalysts can easily oxidize amines, especially primary amines (Scheme 3.13).

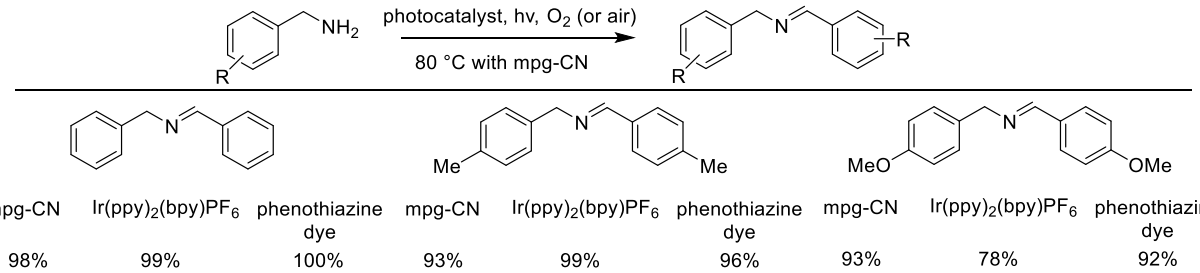

Scheme 3.13. Oxidative formation of imines by photocatalysis.

In the oxidation of amines, reactions where O_2 acts as an electron acceptor under visible light are common. This shows the advantages of the photocatalytic methods compared to the traditional purely chemical methods, when stoichiometric quantities of strong oxidants are

usually required as opposed to O_2 as an oxidant.[130-131] The transition metal-free mpg-CN was reported as a suitable photocatalyst for selective oxidation of benzylic amines to the corresponding imines.[132] Despite the high selectivity of this method, it requires a reaction temperature of 80 °C. Homogeneous version of this photocatalytic reaction mediated by $Ir(ppy)_2(bpy)PF_6$ was shown by Rueping *et al.*[133] A metal-free homogeneous catalysis under visible light with phenothiazine dye (structure is presented in the Figure 3.4) gave overall higher yields and selectivities under mild conditions.[103]

The synthetic pathways for incorporation of fluorine atoms into potential biologically active molecules has a significant interest for pharmaceutical and agrochemical areas.[134] Until recently there were no methods for direct photocatalytic carbon-fluorine bond formation. Among different carbon-heteroatom couplings, C-F bond formation has remained one of the most challenging reactions for years, because it usually requires the use of specific fluorinating reagents that are not tolerated in photocatalytic systems. Nevertheless, Selectfluor, one of the most common fluorinating reagents, was found to be suitable for this reaction in combination with the photocatalysts $Ru(bpy)_3Cl_2$ and CMB-C_3N_4 (carbon nitride prepared from cyanauric acid, melamine and barbituric acid). The first example of photocatalytic fluorination with Selectfluor was reported in 2014 with a common homogeneous catalyst $Ru(bpy)_3Cl_2$ (Scheme 3.14).[135] As substrates aryloxyacetic acid derivatives were chosen. Under the reaction conditions they release a CO_2 molecule and couple with F atom.

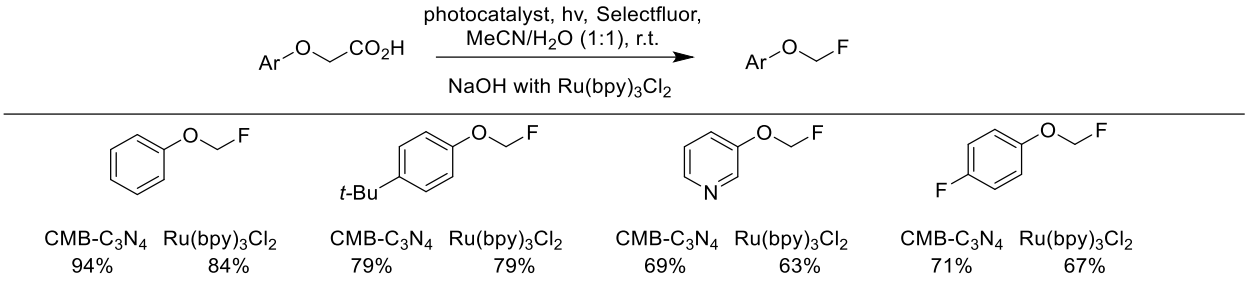

Scheme 3.14. Photocatalytic decarboxylative fluorination.

Flow reactors enhance mass and heat transfer in reactions, enable precise control over the reaction parameters, and increase the overall process efficiency and safety.[136-137] Despite these advantages, flow chemistry is barely used together with heterogeneous photocatalysis due to poor light penetration and high back pressure (packed bed reactor), or clogging and poor reproducibility (pumping a suspension).[138] In order to overcome these existing challenges, Pieber developed serial micro-batch photoreactors (SMBRs).[139] Using this technology, decarboxylative fluorination was enabled by CMB-C_3N_4 photocatalyst (Scheme 3.14). This

approach was further extended to fluorination of three different types of substrates. The practical application of this method was shown by the direct fluorination of ibuprofen. The reaction with the homogeneous catalyst $Ru(bpy)_3Cl_2$ requires the use of NaOH in excess, while the procedure with CMB-C_3N_4 was performed without any additives.

A fascinating method for the synthesis of vinyl sulfones was discovered by König and coauthors (Scheme 3.15). First, they published the method for sulfonylation of alkenes with aryl sulfinates[140] and later extended this method to alkyl sulfinates.[141] These reactions were enabled by the organic dye, eosin Y, under green light irradiation (λ_{max}=535 nm). A heterogeneous version of this reaction was performed with cyanamide- and urea-functionalized graphitic carbon nitrides (NCN-CN_x) under blue light irradiation (λ_{max}=455 nm).[142] The performance of NCN-CN_x in general is similar to homogeneous eosin Y. The reaction between styrene and benzenesulfinate under green light irradiation was achieved with g-CN modified with cyano groups.[143] For this reaction $PhNO_2$ (1 equiv.) was required as electron acceptor, and without it the yields were significantly lower.

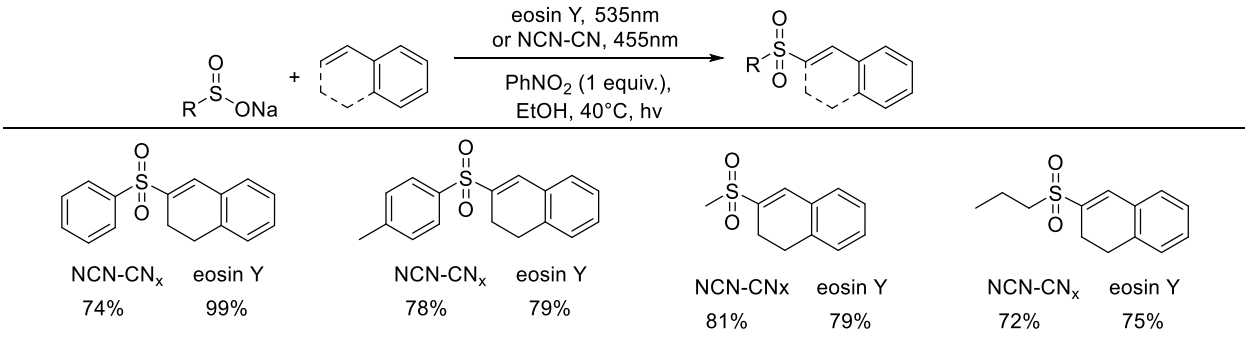

Scheme 3.15. Photocatalyzed oxidative sylfonylation of arylalkenes with sulfonates.

Halogenated products are versatile starting materials in organic synthesis, widely used for transition-metal catalyzed cross-couplings, as well as broadly presented in biologically active compounds.[144-146] Among all methods of their synthesis, oxidative halogenation of hydrocarbons is probably one of the most environmentally benign.[147] A photocatalytic version of this reaction was published by König *et al.* through mimicking the process in nature with the use of organic dye riboflavin tetraacetate (RFT) (Scheme 3.16).[148] In this method, they used *p*-methoxybenzyl alcohol as electron donor and acetic acid as a hydrogen peroxide stabilizer. Selective chlorination of aryl C-H bonds with $Ru(bpy)_3Cl_2$ photocatalyst was published as well.[149] In this approach NaCl was used as a chlorinating reagent and $Na_2S_2O_8$ as an oxidant. Selective chlorination of the aromatic C-H bond was achieved only when the α-H in benzylic position was available. The utility of the method was shown by the synthesis of several drugs

or their precursors. The heterogeneous oxidative halogenation using K-PHI photocatalyst was reported by our group and will be discussed in details in Chapter 8 as a part of my research work in Max Planck Institute.[150] The reaction was carried out under simplified conditions, using hydrochloric acid and oxygen as the only reagents.

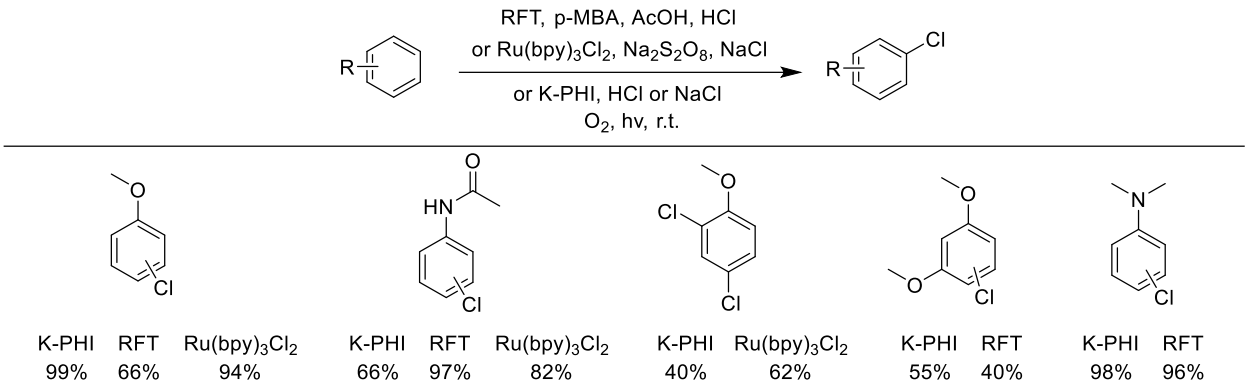

Scheme 3.16. Photocatalytic oxidative halogenation of electron-rich arenes.

All methods are in agreement with the limitation for electrophilic halogenation in aromatic ring and substitution in substrates bearing electron withdrawing groups was not achieved. Further improvement is needed to extend the scope of substrates to electron deficient aromatic systems.

Until now, only photocatalytic mono-functionalization of substrates, *i.e.* installation of one functional group or formation of one chemical bond, has been discussed. In principle, photocatalysis can be used in sequential functionalization of substrates. Ghosh, König and Antonietti implemented this idea in the sequential trifluoromethylation and bromination of trimethoxybenzene as a model compound using mpg-CN (Scheme 3.17).[151]

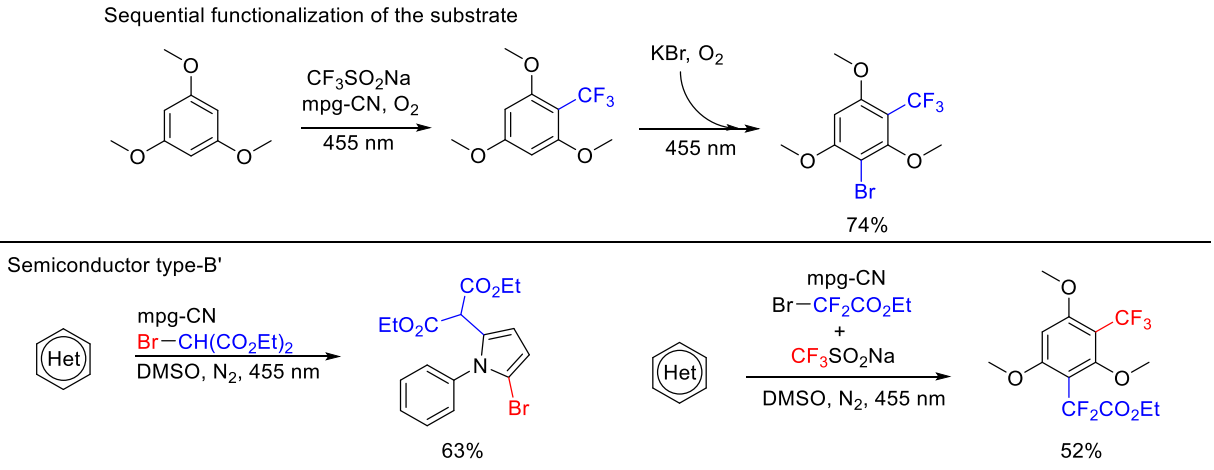

Scheme 3.17. Sequential trifluoromethylation/bromination of trimethoxybenzene (top) and semiconductor photoredox catalytic reaction mode of type B' (bottom).

Once all of the sodium trifluoromethylsulfinate was consumed, KBr was added to the reaction mixture and the photocatalytic reaction was continued to obtain polyfunctionalized benzene derivatives.

Recently, the intriguing and practical simultaneous installation of two or more functionalities at once, *i.e.* semiconductor photocatalysis of type B', was explored.[152-153] This concept was validated in the reaction of simultaneous trifluoromethylation/difluoromethylation or bromination/ alkylation of the (hetero)aromatic compounds (Scheme 3.17).[151]

All in all, the photogenerated electron-hole pair on the carbon nitride surface activates the molecules for reactions. The carbon nitride photocatalyst is insensitive to the reaction type and solvents, and it enables practically any $C(sp^2)–C(sp^3)$, $C(sp^2)–C(sp^2)$, and $C(sp^2)$–heteroatom bond forming reactions.

3.5. Dual Ni-carbon nitride photocatalysis

Transition metal-catalyzed cross-coupling reactions became a classic technique for building carbon-carbon and carbon-heteroatom bonds in a modern organic chemistry. However, these methods typically rely on rare transition metals, such as palladium, platinum, or gold. The high economic and environmental cost of such catalysis makes these systems undesirable in the long-term. Among other transition metals, nickel seems to be the most logic substitution for Pd, Pt and Au catalysts, since it is cheap, abundant and still highly active. Therefore, nickel is considered as an attractive alternative to rare metal catalysts.[154-155] Due to the higher thermodynamic stability of Ni species, the problematic β-hydride elimination in alkylmetallic complexes is suppressed, which allowed to extend the scope of electrophilic component to even sterically hindered and unactivated alkyls. Moreover, the union of nickel and photoredox catalysis has opened a new horizon in a radical and cross-coupling chemistry.[156] While photocatalytic cycle is responsible for oxidative formation of radicals, the metal catalytic cycle produces Ni(II)-alkyl complexes that subsequently trap the photocatalytically derived radical, forming Ni(III) complex. Reductive elimination from the latter leads to the formation of desired C-C (or C-Het) bond and Ni(I) complex. As the last step, photocatalyst reduces the Ni(I) complex to Ni(0), simultaneously closing two catalytic cycles.[156] In recent years, dual nickel/photoredox catalysis has been employed in cross-coupling chemistry for a variety of carbon-carbon and carbon-heteroatom coupling reactions under exceptionally mild conditions.

The combination of nickel $Ni(COD)_2$ and iridium $[Ir(dFCF_3ppy)_2bpy]PF_6$ organometallic complexes was implemented in a coupling reaction of electronically activated potassium

alkyltrifluoroborates with a variety of arylbromides. In 2014, Molander *et al*. reported a single-electron transfer-based (SET) strategy for the activation of organoboron reagents in the cross-coupling of primary benzyltrifluorobarates with substituted arylbromides (Scheme 3.18).[157]

The extremely mild conditions (visible light, ambient temperature, and absence of strong bases) resulted in the selective formation of the desired products with only unreacted arylhalide remaining. The reported approach also showed excellent functional group tolerance.

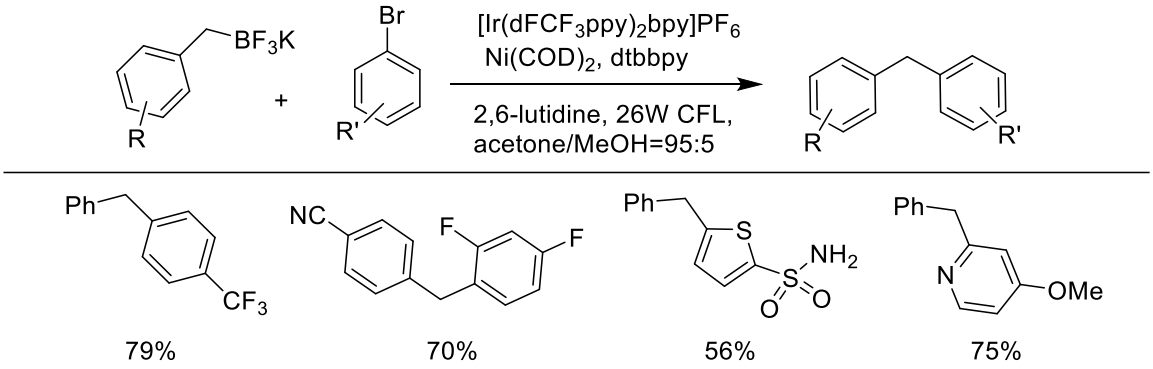

Scheme 3.18. Photocatalytic C-C coupling of primary potassium benzyltrifluoroborates with arylbromides.

In the subsequent year, Molander and co-authors reported the use of the developed SET strategy to secondary alkyltrifluorobarates (Scheme 3.19).[158] The reaction system was slightly modified to avoid formation of side products due to the higher reactivity of secondary borates. This reaction was shown to also be efficient on a gram scale.

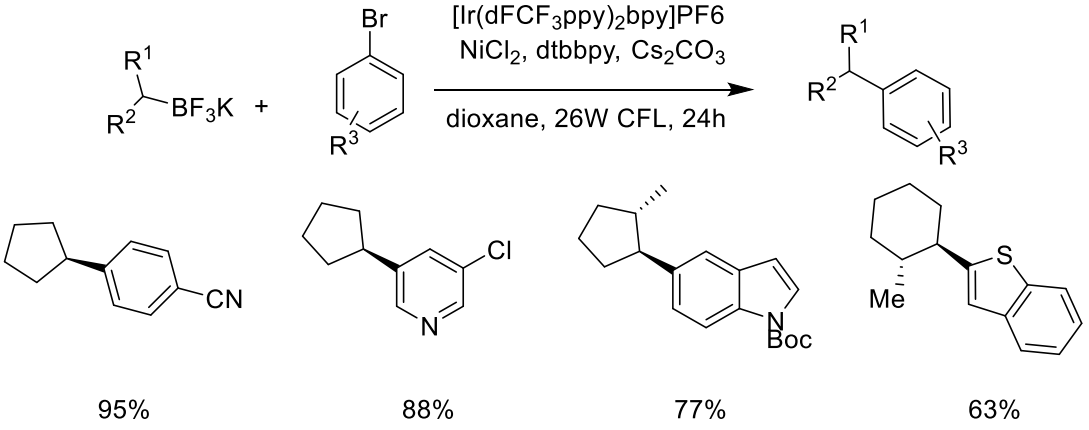

Scheme 3.19. Photocatalytic C-C coupling of secondary potassium benzyltrifluoroborates with arylbromides.

Molander and co-authors also reported a similar approach of single-electron transmetalation for the coupling of α-alkoxymethyltrifluoroborates with aryl and heteroaryl bromides to form benzyl ethers (Scheme 3.20).[159] The proposed method showed high tolerance to both heteroaryl

and alkoxymethyltrifluoroborate substrates. This approach was highly compatible with both alkenes and alkynes as demonstrated by their high yields in this reaction.

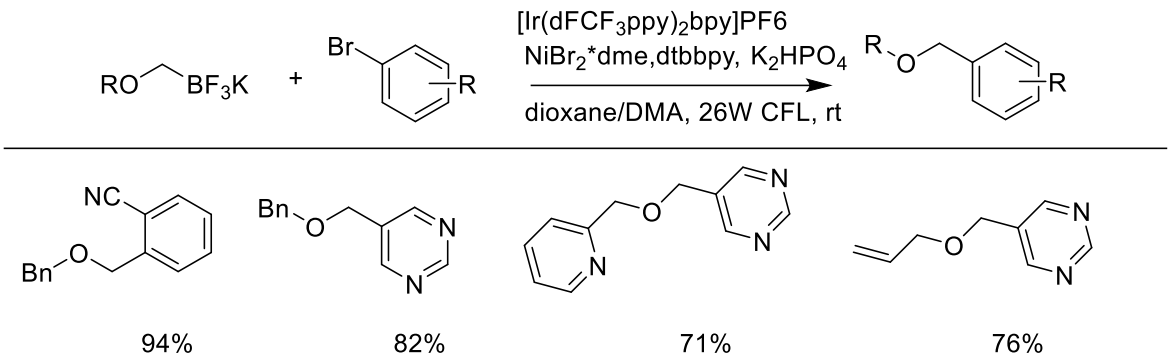

Scheme 3.20. Photocatalytic C-C coupling of primary potassium alkoxymethyltrifluoroborates with arylbromides.

Although, Pt was substituted by much cheaper Ni, the catalytic system, nevertheless, depends on using photoredox complexes of Ir that are as expensive as Pt complexes. Therefore, alternative systems should be ideally developed. Heterogeneous semiconductors are, in turn, a recyclable and cheap alternative to the expensive noble metal-based homogeneous photocatalysts. Several examples utilizing CdSe quantum dots or CdS for the dual nickel/photoredox catalysis were reported.[160-161] However, due to the high toxicity of cadmium, their use is limited and more sustainable alternatives should be found. As it was presented so far, carbon nitrides are cheap and environmentally benign alternative to the aforementioned metal complexes and are able to catalyze a broad scope of organic reactions with the same efficiency as homogeneous catalysts. Therefore, combination of CNs and Ni for dual catalysis might solve these problems. Indeed, several examples of nickel/carbon nitride dual photocatalysis were recently reported.

Synthesis of ethers *via* the coupling of alcohols with arylbromides was reported by dual catalysis of nickel with both a transition metal-based catalyst as well as with a CNs (Scheme 3.21). MacMillan *et al.* developed a system that can modulate the preferred oxidation states of nickel alkoxides in an operative catalytic cycle, which provides access to Ni species that readily participate in reductive elimination.[162] This development allowed the critical C-O bond formation step to proceed. In a similar system, CN-OA-m (a CN prepared by calcination in a molten salt of precondenced urea with oxamide) was also found to be able to stimulate reductive elimination *via* SET modification of the oxidation state of Ni complexes.[163] Both catalytic systems were effective in the selective coupling of a broad range of aliphatic alcohols and aromatic bromides.

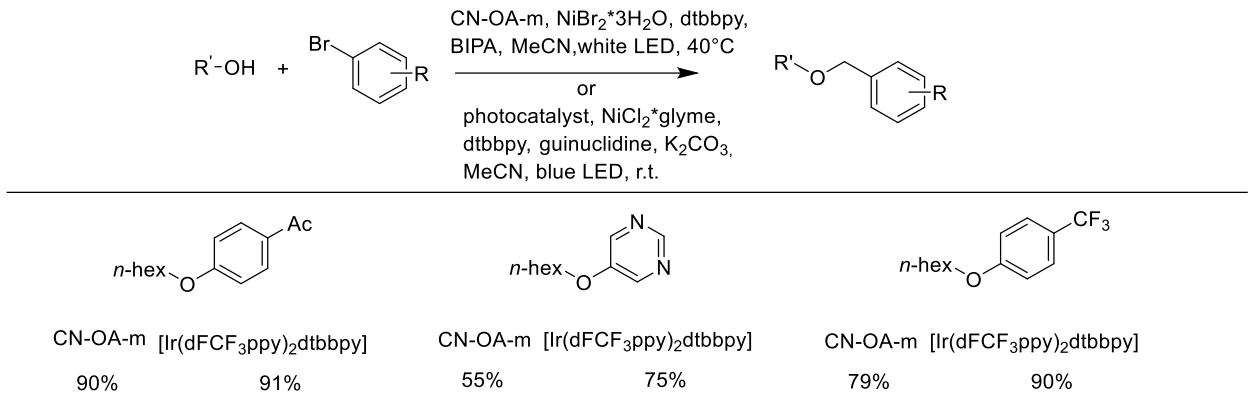

Scheme 3.21. Photocatalytic C-O coupling of alcohols and arylbromides.

Another variation of carbon-oxygen coupling by CN/Ni catalysis was shown by Pieber and co-authors (Scheme 3.22). Esterification of carboxylic acids with aryl halides was performed under mild conditions.[164] The catalyst system was shown to harvest a broad range of visible-light spectrum (up to 600nm), which was shown by *in situ* FT-IR analysis of the reaction progress. The organic semiconductor was recycled 3 times without any loss of activity. No products of the decarboxylative C-C coupling were detected, which indicates selective photosensitization rather than the described above single-electron transfer.

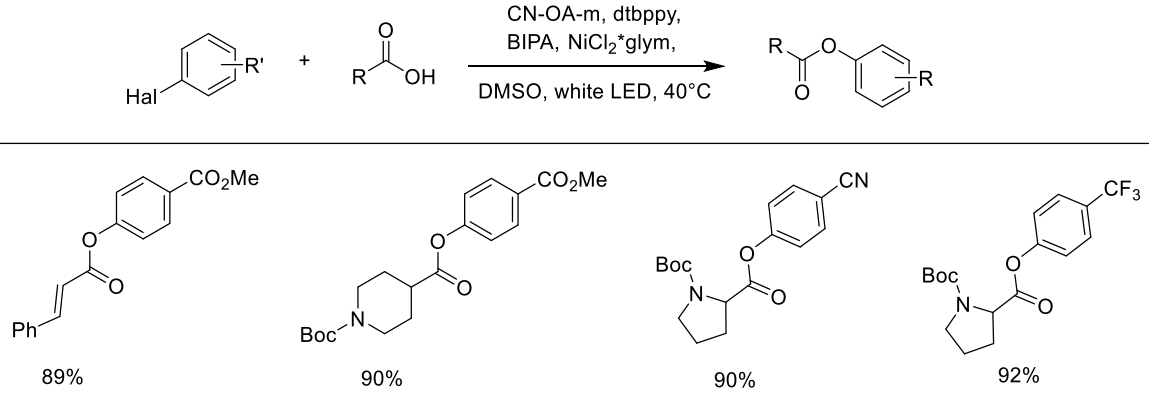

Scheme 3.22. Photocatalytic C-O coupling of carboxylic acids and arylbromides.

Recently an interesting variation of the dual catalyst system was reported by Ghosh *et al.*[165] Through the activation of C-Br bonds in electron poor aryl halides, regiospecific coupling with amines was accomplished (Scheme 3.23). The reaction conditions did not require additional ligands for nickel complexation. Generally, the reaction was performed in mild conditions at room temperature, and as a result different functional groups, such as halogen, ester, aldehyde, and cyano group, were well tolerated providing products in good to excellent yields.

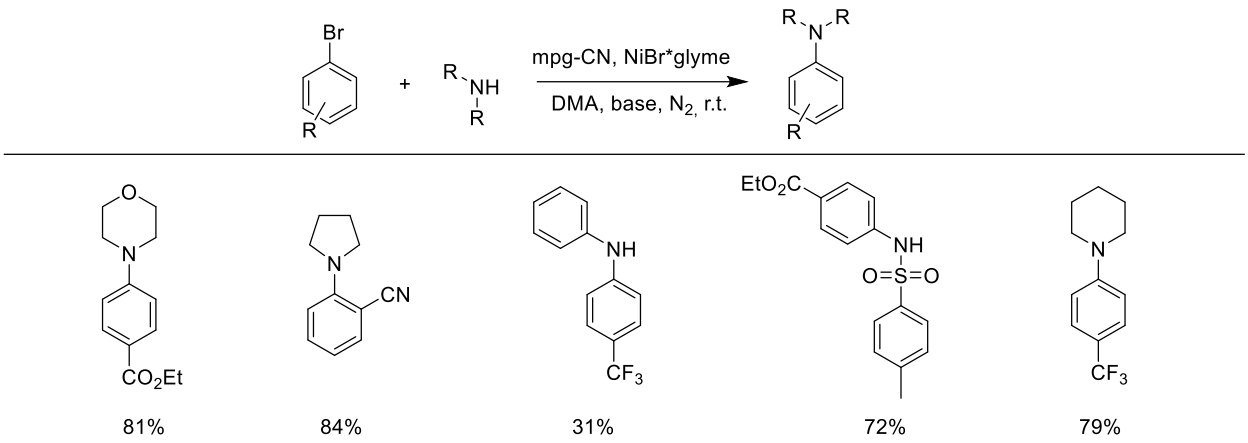

Scheme 3.23. Photocatalytic C-N coupling of amines and arylbromides.

3.6. Photocatalytic productivity of homogeneous and heterogeneous catalysts

The presented above reactions show, that overall all the catalysts show similarly good yields of the obtained products. However, the yields in general depend on the amount of the substrate used for the reaction. Therefore, certain photocatalysts can demonstrate virtually higher yields when lower substrate loadings are used. To solve this issue, a graph that correlates the product yield and the substrate amount taken for the reaction can be offered (Figure 3.5).

Three classes of the photocatalysts, *i.e.* transition metal based complexes, organic dyes and heterogeneous carbon nitride materials show a similar dispersion of yields regardless of the reaction type and substrate loading. The general tendency also shows that all photocatalysts show good performance and give good to excellent yields in the described reactions. This, in general, proves that photocatalytic approach is an efficient alternative to classic method of synthesis. The heterogeneous carbon nitride-based materials in this tendency show comparable to homogeneous catalysts productivities. With low loadings of substrates being used (up to 0.3 mmol), there is no particular difference in the performance of both molecular catalysts and CNs, with yields in the range of 60 to 100%. On the other hand, in reactions with the higher loading of substrate (0.3 – 1.2 mmol), carbon nitride materials show even better performance giving 90 – 100% yields versus 60 – 100% for metal complexes. However, the high loadings of substrate were used less frequently in CN photocatalysis, and a more thorough study should be done to establish a general trend.

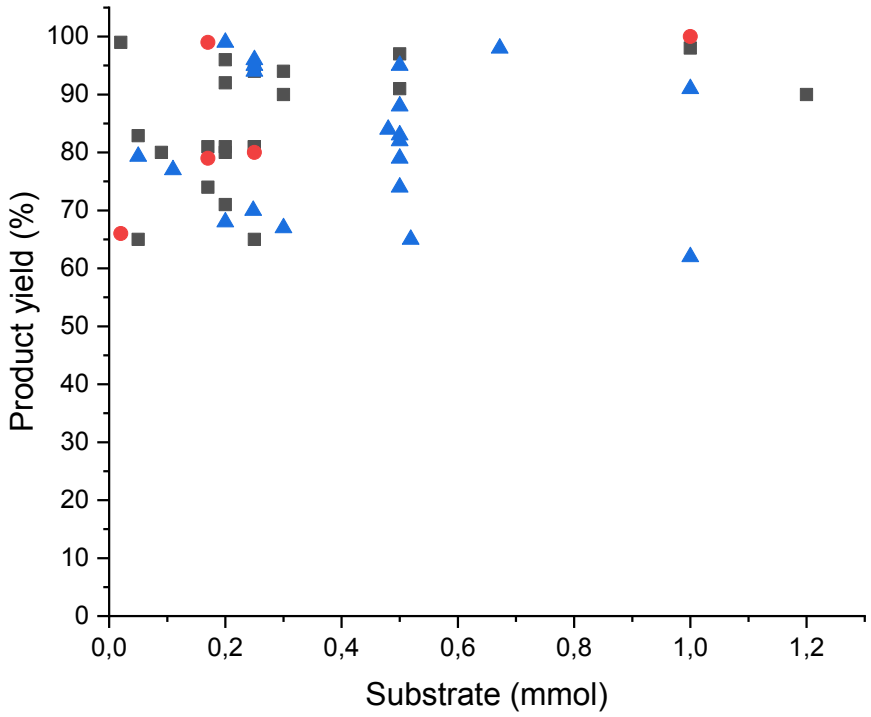

Figure 3.5. Comparison of productivities of homogeneous catalysts and carbon nitrides catalysts. Squares ■ – heterogeneous carbon nitride photocatalysts, triangles ▲ – transition metal-based photoredox complexes, circles ● – organic dyes.

3.7. Conclusion

The development of human society encouraged scientist to look for new technologies for a better use of limited natural energy resources. Years of research work made a great step towards solving these problems. Solar or wind power stations, solar powered houses and cars do not surprise anymore. However, we are still just in the beginning of revolutionary changes and the best is yet to come. Founded in the last century, photochemistry today stands for a big mature field of chemistry. Fundamental studies on water slitting, CO_2 reduction and pollutants degradation discovered fascinating properties of a special class of materials, named photocatalysts. The obvious issues using transition metal-based materials or UV light, make heterogeneous visible light catalysts and especially a group of "green" carbon nitrides very appealing for a wide use. Described in the Introduction, recent findings prove that photocatalysis is a useful tool not only for environment remediation applications, but also for complex organic reactions. As shown in Chapter 3.6, carbon nitrides efficiently catalyse different carbon-carbon or carbon-heteroatom forming reactions and show equal to transition metal-based catalysts productivity. Therefore, photocatalysis of organic reactions by CNs is a prominent tool for novel synthetic protocols. However, further studies on heterogeneous

photocatalysis from both, material and organic chemistry sides, are of a great importance on the way to fulfill the needs of modern chemistry.

Leaving a design of new photocatalytically active materials for colleagues from the material chemistry field, in this thesis, I focus on the study of photocatalytic organic reactions and mechanisms of heterogeneous approach that influence the outcome of these reactions. In next chapters, fundamental properties of carbon nitrides will be deeply investigated and reviewed from the organic chemistry standpoint; the connections between material property and photoreaction result will be established. Despite the fact that investigations at the interphase between the surface of the catalyst and homogeneous reaction media are difficult, the understanding of complex photocatalytic mechanisms of heterogeneous photocatalysis would enhance our knowledge for further successful design and application of novel photoredox active materials. With continuous progress in this field, the number of applications of heterogeneous photoredox catalysis for both lab scale synthesis and large scale solar productions will certainly develop. In addition, a tight collaboration of material and organic chemistry fields might catalyze the development of both.

In Chapter 4, the ability of carbon nitrides to store electrons will be studied and a convenient method for calculation of accumulated electrons will be proposed. The influence of this property on organic reactions will be investigated on several examples in Chapters 5-7. Through these findings, the understanding of mechanisms of photocatalytic organic reactions will be further enhanced. In Chapter 7, a combination of CN photocatalysis with a sustainable reaction media will be used for multi-electron reduction. Later on, redox properties of K-PHI will be challenged in several reactions, such as halogen anion oxidation in Chapter 8 and oxidative synthesis of sulfonyl chlorides and amides in Chapter 9. A fascinating example of chromoselective photocatalysis by K-PHI will be presented in Chapter 9 for the synthesis of three different compounds from the same starting material.

4. Green radicals of potassium poly(heptazine imide) by light and benzylamine

4.1. Overview

The tinted long-lived ionic carbon nitride radicals were recently introduced and applied in photocatalysis and energy storage. However, the reason for higher activity in the photocatalytic reactions and optimal conditions for generating such radicals still remain vague.

In this Chapter, conditions of carbon nitrides photocharging to achieve higher charge density are studied; a convenient method for quantifying electrons accumulated in the carbon nitride semiconductors is proposed; also, the number of accumulated electrons is calculated for mpg-CN and K-PHI.

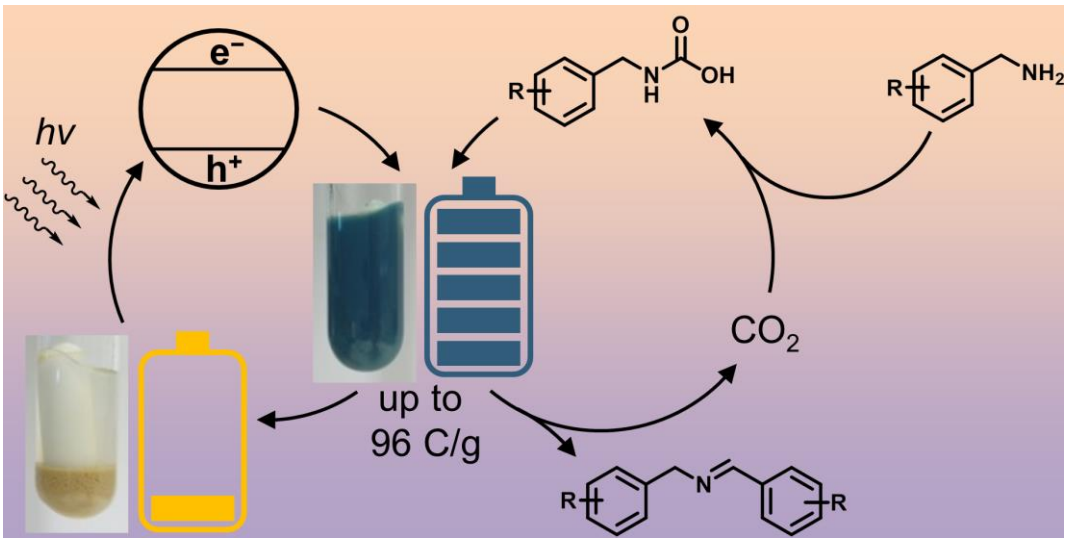

Figure 4.1. A schematic presentation of photocharging of carbon nitrides.

This chapter is adapted from my original work: Markushyna, Y.; Lamagni, P.; Teutloff, C.; Catalano, J.; Lock, N.; Zhang, G.; Antonietti, M.; Savateev, A.: Green radicals of potassium poly(heptazine imide) by light and benzylamine. Journal of Materials Chemistry A 7 (43), S. 24771 - 24775 (2019)

4.2. Results – Discussion

Recent discoveries on solar energy storage reveal that poly(heptazine imide)s are able to form long-lived radicals in the presence of electron donors under light irradiation.[166] In the present project, a detailed study of this process was performed. For convenience, a suitable acronym "IDEAS" that stands for Illumination-Driven Electrons Accumulation in Semiconductor was proposed.

The mechanism of the photocatalytic reaction grounded on IDEAS, using K-PHI as a representative photocatalyst, is sketched in Figure 4.2. On the energy scale, it can be schematically explained as follows. By absorbing a photon, K-PHI is converted to the excited state K-PHI*. Electron transfer from the HOMO of the electron donor (ED) lying above the VB of K-PHI reduces the K-PHI* and gives the negatively charged radical anion K-PHI$^{\bullet -}$. For this process, IDEAS is accompanied by a distinct color change of K-PHI and related materials from yellow to green or blue.[166-169] The energy stored in K-PHI is then released by exposing the K-PHI$^{\bullet -}$ to the electron acceptors (EA). This step leads to the recovery of K-PHI and formation of the reduced electron acceptor (EA_{red}).

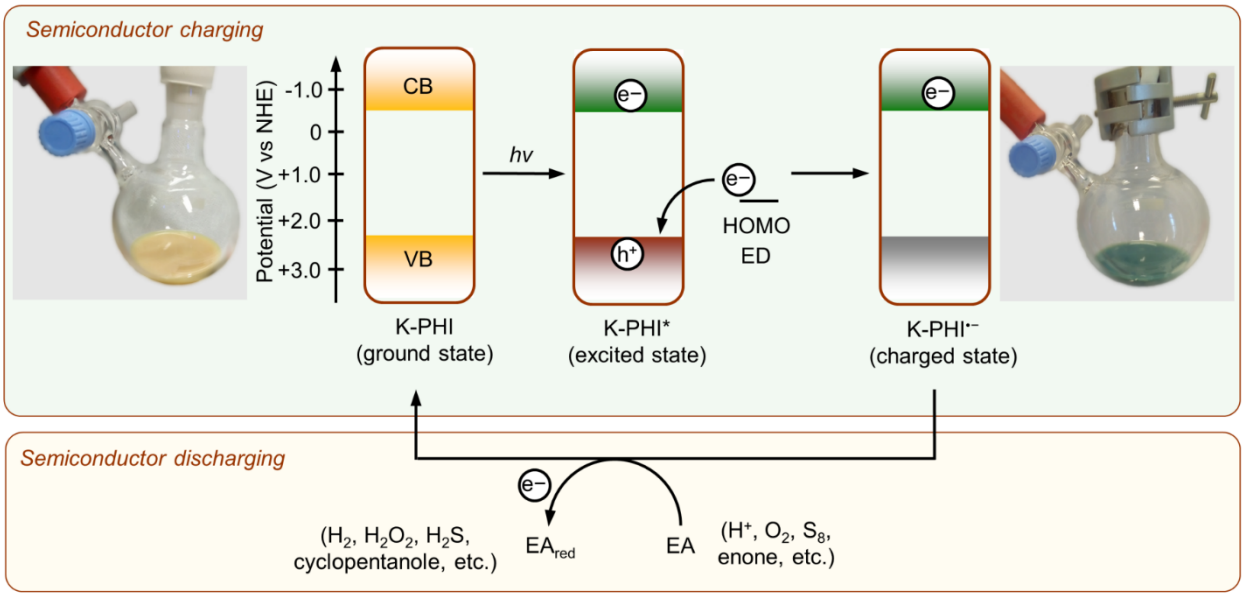

Figure 4.2. Illumination-Driven Electrons Accumulation in Semiconductor (IDEAS) for K-PHI.

For the deep investigation of IDEAS, oxidative coupling of primary amines was chosen, while the products of the amine coupling, imines, have value as precursors in synthesis of oxaziridines,[170] palladacycles,[171] or they can be photocatalytically converted to imidazoles,[172] or used in C-C reductive coupling[173] etc (Scheme 4.1).

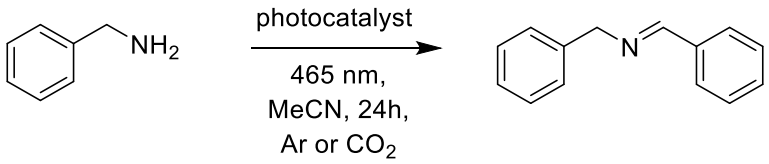

Scheme 4.1. Photocatalytic oxidative coupling of benzylamine to imine.

For quantification of accumulated electrons by IDEAS the following method was proposed. K-PHI$^{\bullet-}$ was generated *in situ* using benzylamine as an electron donor. These species of the charged catalyst have a greenish or blueish colour. After 24 h of stirring under irradiation with blue LED (λ_{max}=465 nm) a portion of methylviologen (MV^{2+}) was added to the reaction mixture in a glovebox under Ar atmosphere to avoid oxidation of K-PHI$^{\bullet-}$ by oxygen from air. MV^{2+} was reduced to the radical cation ($MV^{\bullet+}$) that has a pronounced blue colour. Figure 4.3a summarizes these observations.

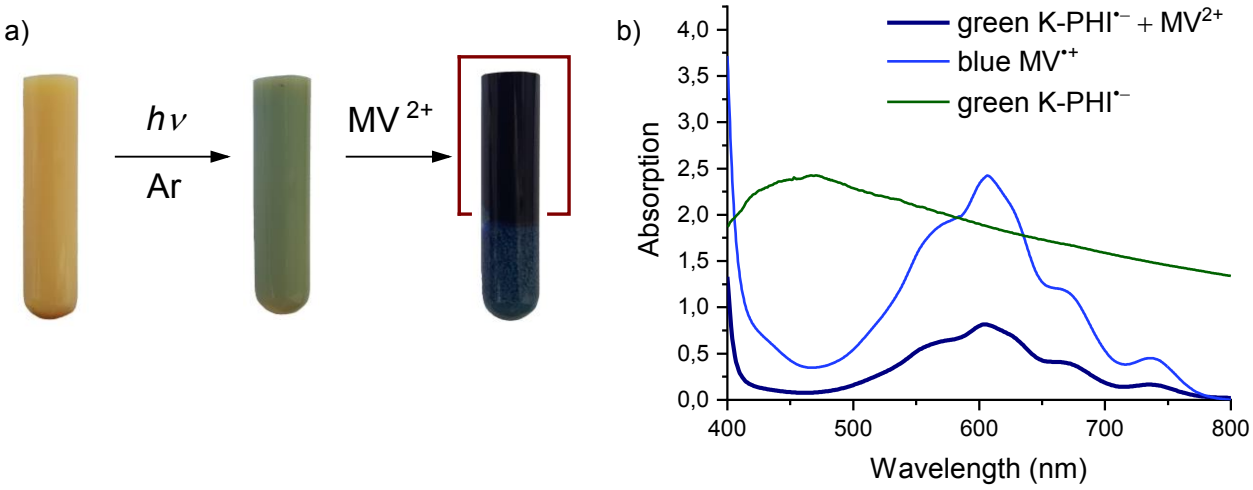

Figure 4.3. a) Visual appearance of the reaction mixture – K-PHI, benzylamine, acetonitrile, under Ar (1 bar). From left to right: reaction mixture (under Ar) before light irradiation (yellow), after light irradiation (green), after methyl viologen (MV^{2+}) addition (blue); b) Absorption spectra of green K-PHI radical anion (K-PHI$^{\cdot-}$) in MeCN; methylviologen radical cation $MV^{\cdot+}$; reaction mixture upon quenching of K-PHI$^{\cdot-}$ with methylviologen dichloride.

The amount of $MV^{\bullet+}$ produced upon K-PHI$^{\bullet-}$ quenching with MV^{2+} was determined measuring the solution absorbance (Figure 4.3b). The maximum of absorption for $MV^{\bullet+}$ was determined as 605 nm, while green K-PHI$^{\bullet-}$ does not show significant absorption at this wavelength. Negligible absorbance at 800 nm of the mixtures after MV^{2+} addition suggests that K-PHI particles completely precipitated and neither K-PHI itself nor K-PHI$^{\cdot-}$ contribute to the

absorption. Therefore, the amount of $MV^{\bullet+}$ is equal to the amount of electrons accumulated in the catalyst.

In order to find the maximum electron capacity of K-PHI, the effect of the benzylamine concentration, *i.e.* electron donor concentration, on the number of accumulated electrons was investigated. K-PHI reaches saturation at the benzylamine concentration of 60 µmol·mL^{-1}, at which the electron capacity approaches 957±82 µmol·g^{-1} (Figure 4.4a).

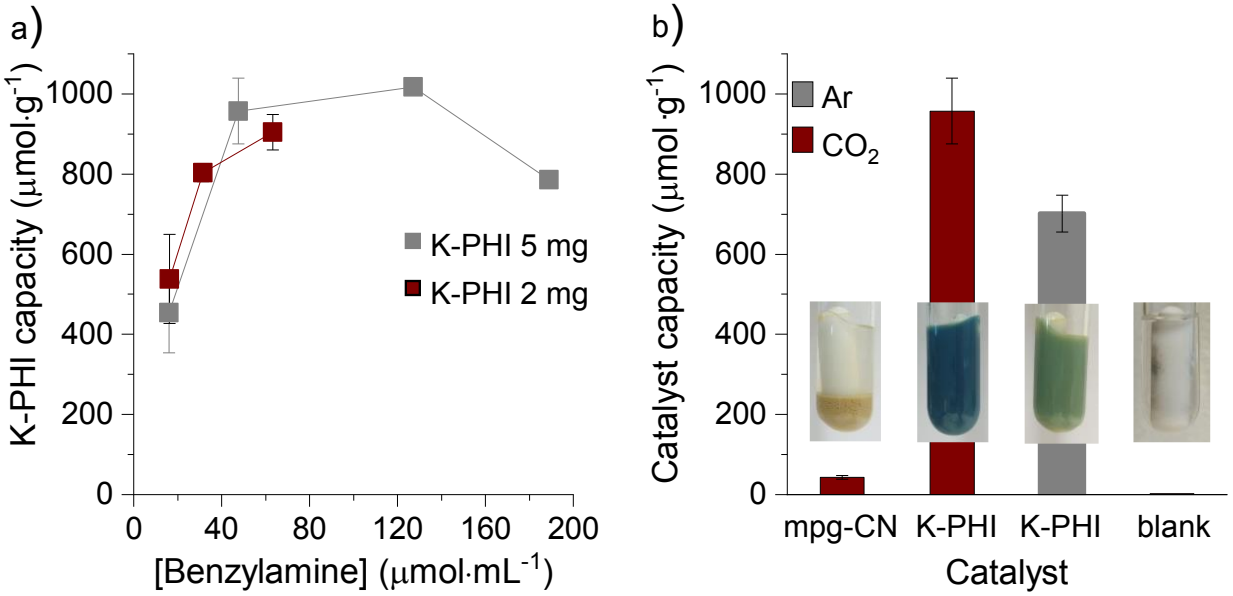

Figure 4.4. a) Capacity of K-PHI depending on the benzylamine concentration. Conditions of K-PHI$^{\bullet-}$ generation: MeCN 3 mL, CO_2 1 bar, time 24 h, T = 35 °C. Conditions of K-PHI$^{\bullet-}$ quenching: MV^{2+} 0.1 mmol; b) Electron capacity of carbon nitrides and appearance of the reaction tubes after light was switched off under Ar (1 bar) and CO_2 (1 bar). In the blank experiment no carbon nitride catalyst was added. Conditions: benzylamine 50 µmol, MeCN 1 mL, time 24 h, T = 35 °C, gas pressure 1 bar.

For comparison purposes, the ability to IDEAS of another member of CN family, mpg-CN, was investigated (Figure 4.4b). Despite mpg-CN did not show any apparent color change, IDEAS was also observed. Using the abovementioned methodology the capacity of mpg-CN was determined to be 43±5 µmol·g^{-1}. The higher surface area of mpg-CN compared to K-PHI, *i.e.* 180 m^2·g^{-1} versus 89 m^2·g^{-1}, apparently is not a decisive factor for efficient IDEAS. Instead, the microporous structure and ability of the material to stabilize negative charges observed for K-PHI are important. As the negative charge accumulated in the material by storage of negatively charged electrons must be compensated, the reason for the high electron capacity of K-PHI is, perhaps, grounded on the unique ability of the material to store H^+ species in the structure in the form of H^+ itself or NH_4^+ (Figure 4.9b). Indeed, the higher content of H atoms was detected for K-PHI after the photocatalytic reaction. A more detailed discussion is

presented at the end of the Chapter. In case of K-PHI, a deeper color was observed in the presence of CO_2 (the interaction between CO_2 and benzylamine is investigated below), which correlates with the higher electron capacity of 957±82 μmol·g^{-1} compared to 701±46 μmol·g^{-1} under Ar. Nevertheless, the achieved capacity of K-PHI under Ar using benzylamine is still 5.8 times higher compared to that using benzyl alcohol as electron donor.[167] This illustrates the much better ability of amines to quench reductively the excited state of the carbon nitride photocatalyst. In the control experiment without carbon nitride photocatalyst, MV^{2+} is not reduced by benzylamine alone.

A series of experiments with different loadings of K-PHI were performed in order to evaluate the reproducibility of the proposed method of IDEAS quantification. The number of trapped electrons versus K-PHI mass follows a linear trend, supporting the reproducibility of the method in the range of K-PHI masses up to 10 mg per experiment (Figure 4.5).

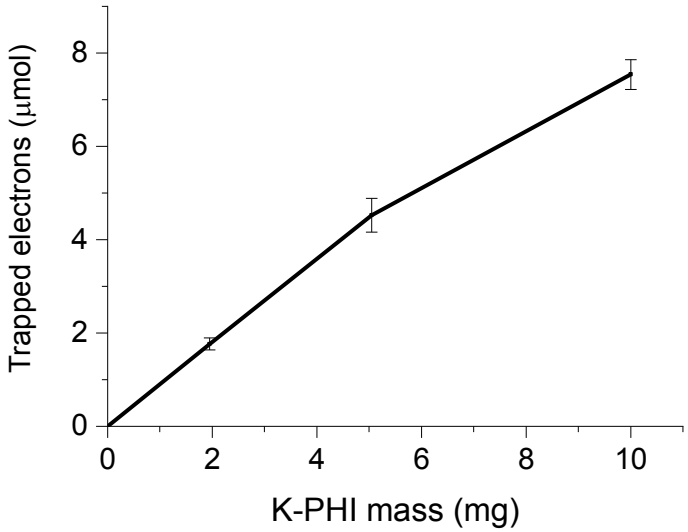

Figure 4.5. Equivalent of the number of accumulated electrons in K-PHI (y-axis) produced upon K-PHI$^{\bullet-}$ quenching with MV^{2+} versus K-PHI amount (x-axis). Conditions: initial benzylamine concentration 63 μmol·mL^{-1}, reaction temperature 35 °C, time 24 h, MeCN 3 mL, CO_2 1 bar. K-PHI$^{\bullet-}$ quenching conditions: MV^{2+} 0.1 mmol.

In order to investigate the formation of K-PHI$^{\bullet-}$, we studied a suspension of K-PHI in acetonitrile by EPR (Figure 4.6a). In the dark, a broad signal of low intensity at 3350 G (g = 2.016, after offset correction) was detected. The intensity of the signal remained almost the same when the EPR spectrum was acquired while the sample was irradiated with 461 nm (6 mW·cm^{-2}). Upon addition of benzyl amine to the sample in the dark, the broad signal at 3350 G disappeared and a narrow signal of low intensity appeared at 3370 G (g = 2.0048). Under light irradiation the intensity of the signal increased drastically supporting that K-PHI* was quenched by benzylamine and K-PHI$^{\bullet-}$ radical formed.

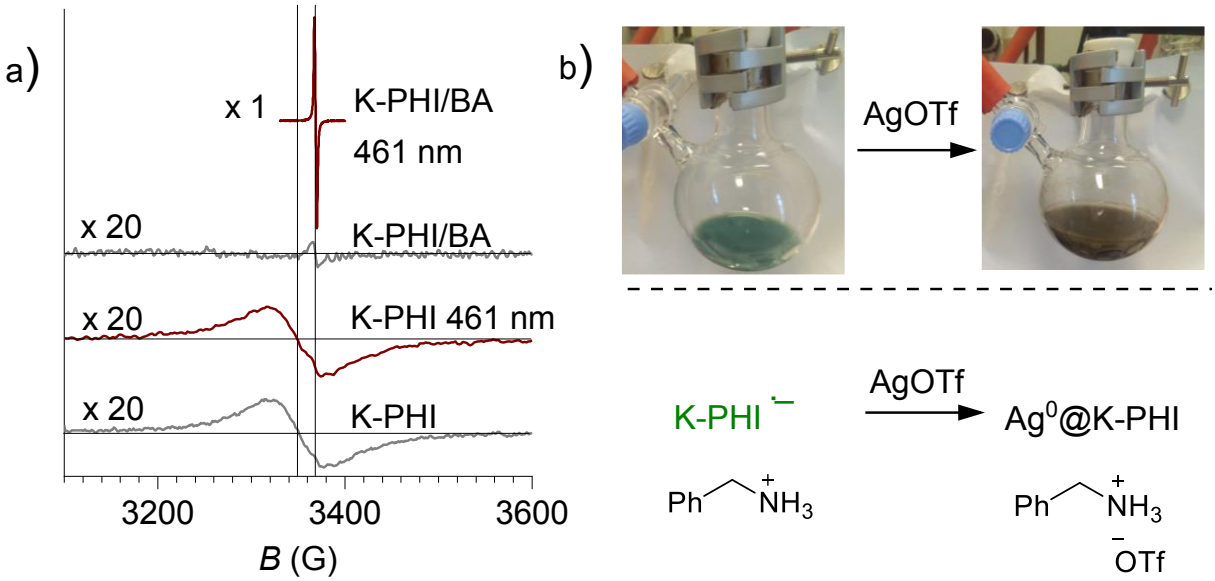

Figure 4.6. a) EPR spectra. EPR spectra of K-PHI suspension in MeCN in dark (grey line) and under 461 nm light (brown curve) irradiation (BA – benzylamine); b) Quenching of K-PHI$^{\bullet-}$ with AgOTf. Reaction was performed under CO_2. Appearance of the reaction mixture and schematic representation of the quenching reaction.

Finally, K-PHI$^{\bullet-}$ can be quenched not only with MV^{2+}, but also with AgOTf, necessarily under oxygen-free conditions. In this case, Ag^{+} is instantly reduced to Ag^{0} (Figure 4.6b). Formation of Ag^{0} was confirmed by the presence of (111) and (200) diffraction peaks in the powder X-Ray diffraction pattern of the resulting solid (Figure 4.7a).

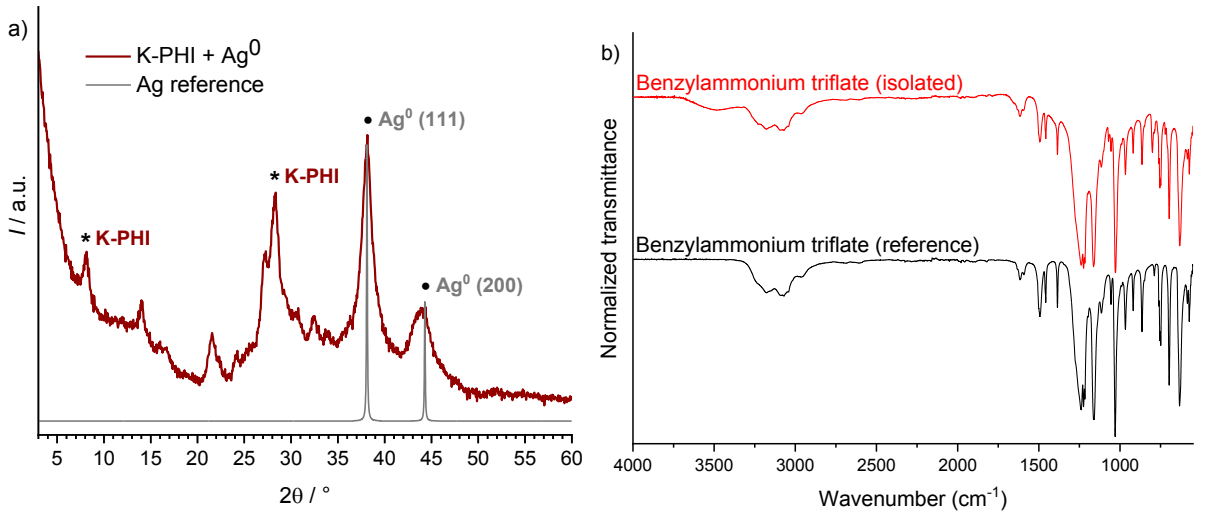

Figure 4.7. a) PXRD pattern of Ag@KPHI generated upon K-PHI$^{\bullet-}$ quenching with AgOTf. Reference X-Ray diffraction pattern of Ag^{0} taken from the literature;[174] b) FT-IR spectra of benzylammonium triflate isolated upon K-PHI$^{\bullet-}$ quenching with AgOTf (red, top) and prepared by neutralization of benzylamine with HOTf (black, bottom).

Upon the reaction mixture workup, benzylammonium triflate was isolated (Figure 4.7b). It suggests that the negative charge of K-PHI$^{\bullet-}$ is compensated partially by benzylammonium cations. Taking into account successful quenching of K-PHI$^{\bullet-}$ with AgOTf and MV^{2+} and their standard redox potentials, $E(Ag/Ag^{+})^{0}$ = +0.80 V and $E(MV^{2+}/MV^{\bullet-})^{0}$ = –0.5 V vs. SHE, energetically the SOMO of the K-PHI$^{\bullet-}$ lies at the potential more positive than –0.5 V vs. SHE. The electron capacity of K-PHI approaches 957±82 μmol·g^{-1} under CO_2 atmosphere. Given that the molecular weight of a K-PHI monomer unit is 223 g·mol^{-1} (Figure 4.8),[175] it can be concluded that every 4th heptazine unit bears an uncoupled electron.

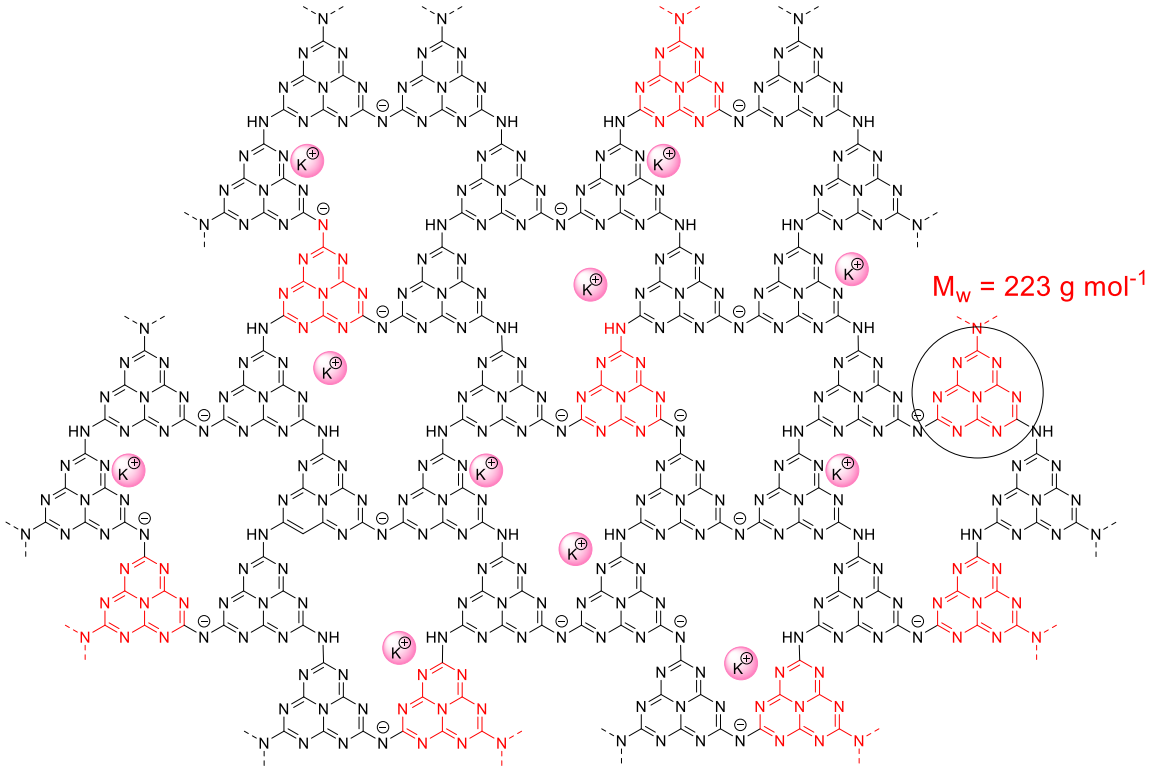

Figure 4.8. Ideal structure of K-PHI. Every 4th heptazine unit that might bear an electron is marked with red.

Taking into account that K-PHI is represented by particles with the average diameter of 100 nm, the volume-to-surface ratio of heptazine units is 26. In other words, in order to achieve such high density of trapped electrons, they must be stored not only on the surface of the material, but be distributed in the bulk of the K-PHI particles. These results underline similarity between the cathode of the electric battery and the K-PHI nano particle.

In order to elucidate a path of benzylamine oxidation, several experiments in CD_3CN using ^{15}N-labeled benzylamine were performed. A solution of amine was purged with CO_2 for several minutes and the ^{15}N, ^{1}H and ^{13}C NMR spectra were recorded. According to the results, benzylamine-^{15}N was quantitatively converted into benzylcarbamic acid (Figure 4.9a). Therefore, benzylcarbamic acid is a more plausible electron donor than benzylamine itself, if

the reaction is performed in the presence of CO_2. Also the full reaction was performed using benzylamine-^{15}N. In the ^{15}N NMR spectrum of the reaction mixture after irradiation for 24 h, we have registered a signal of the ^{15}N-imine at 329.3 ppm and a broad peak at -1.4 ppm that corresponds to either $^{15}NH_3$ or $^{15}NH_4^+$ (Figure 4.9b). The formation of $^{15}NH_4^+$ species by binding of H^+ to released ammonia might be favorable in order to compensate the negative charge of accumulated electrons in the material.

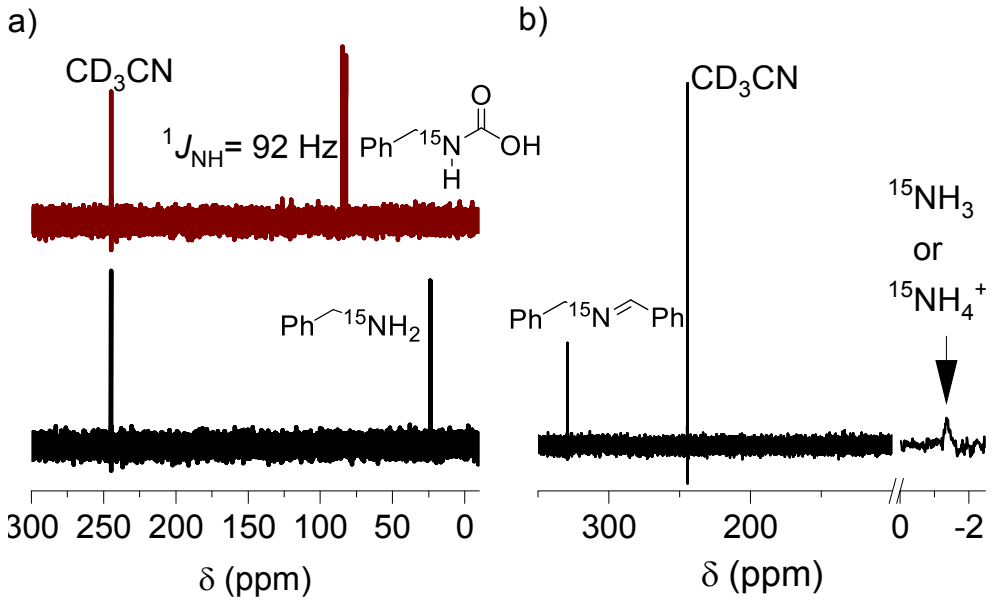

Figure 4.9. a) ^{15}N NMR spectrum of a benzylamine-^{15}N solution in CD_3CN:DMSO-d_6 (4:1) before (bottom) and after (top) saturation with CO_2; b) ^{15}N NMR spectrum of the reaction mixture in CD_3CN after the photocatalytic experiment. The up-field area was magnified and expanded for clarity.

The stoichiometry of benzylamine coupling to imine requires evolution of 1 equivalent of H_2. However, the amount of H_2 detected by GC-TCD (1.48 nmol, Figure A5) was substantially lower than expected from the reaction of benzylamines coupling (25 µmol). This is another piece of evidence for the hypothesis that hydrogen is presumably stored in K-PHI. Elemental analysis of the spent K-PHI showed increased content of hydrogen, 2.60±0.01 wt.% versus 2.23±0.03 wt.%, compared to the fresh catalyst. The increased hydrogen content translates into 18.5 µmol of H^+ (or 9.25 µmol of H_2) that is close to the typical experiment of benzylamines coupling, *i.e.* 25 µmol (reagents loading as in Figure 4.4b). These results suggest that not only electrons, but also protons from the reaction of benzylamines coupling are stored in K-PHI and compensate negative charge.

4.3. Conclusion

In this Chapter, conditions of the carbon nitride radical anion generation by IDEAS were elaborated, while the number of accumulated electrons was measured by quenching the carbon nitride radical anion with a common redox indicator – methylviologen dichloride. The method is generally applicable for the characterization of semiconducting materials regarding their ability to accumulate electrons. Carbon nitride materials can be charged up to at least 957±82 $\mu mol \cdot g^{-1}$ using benzylamine as convenient electron donor in the atmosphere of CO_2. Every 4^{th} heptazine unit in K-PHI thus holds an uncoupled electron, which means electrons are stored not only on the surface of the material but also in the volume. The mechanistic studies and the post-catalytic investigation of K-PHI catalyst revealed that apart of electrons material shows the ability to store protons, which indeed is essential for compensation of the large negative charge to avoid the 'Coulomb collapse'. Therefore, the specific morphology of K-PHI in comparison to mpg-CN allows for a storage of electrons as well as protons in the framework. However, the structure of K-PHI-H species is not clear and further studies should be undertaken. Optimization of the poly(heptazine imide) structure toward higher capacity in IDEAS is one of the strategies to enhance further the photocatalytic performance of the material. Further studies on CO_2 fixation and the use of CO_2 in organic synthesis may be conducted. Also the understanding of photocharging process may enhance the development of dark photocatalysis and multi-electron processes by carbon nitride semiconductors.

5. Advantages in using cheap CO_2 to favour photocatalytic oxidation of benzylamines

5.1. Overview

In the previous chapter, the positive effect of CO_2 on the electron accumulation process in carbon nitrides was established. However, a deeper investigation of the CO_2 role in the benzylamine coupling to imines is needed. Considering the environmental issues related to global warming, the utilization of CO_2 as an inexpensive reaction medium during the photocatalytic reactions stands for the high interest.

In this chapter, the role of CO_2 in the photocatalytic oxidative coupling of primary amines to the corresponding imines is investigated; the influence of water content on the imine formation efficiency is established; CO_2 as an alternative inexpensive reaction medium to commonly used Ar is revised.

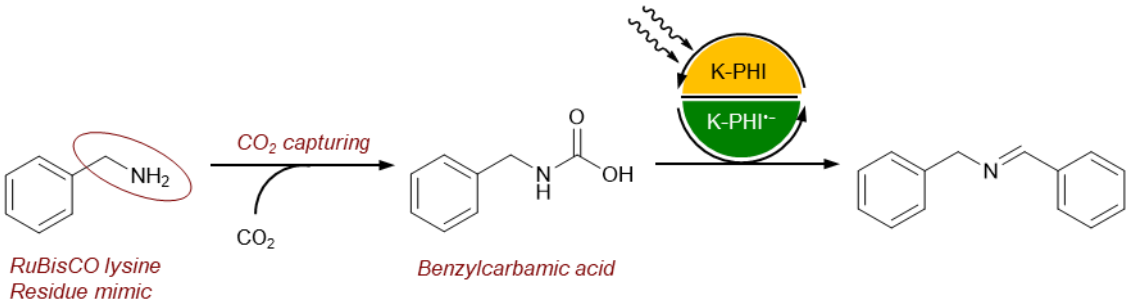

Figure 5.1. Coupling of benzylamine to imine with K-PHI.

This chapter is adapted from my original work: Markushyna, Y.; Lamagni, P.; Catalano, J.; Lock, N.; Zhang, G.; Antonietti, M.; Savateev, A.: Advantages in using inexpensive CO_2 to favor photocatalytic oxidation of benzylamines. ACS Catalysis 10 (13), S. 7336 - 7342 (2020). Copyright 2020 American Chemical Society

5.2. Results – Discussion

In the previous chapter, the benefits of using benzyl amines as electron donors were disscused. It was also found, that the model reaction of coupling of benzyl amines to imines proceeds faster under CO_2 atmosphere than under Ar. Thus, CO_2 benefits the IDEAS of K-PHI. However, the coupling of benzylamines to imines is also interesting itself. Imines are valuable precursors in synthesis of oxaziridines,[170] palladacycles,[171] or they can be photocatalytically converted to imidazoles,[172] or used in C-C reductive coupling,[173] etc. Imines are also used in the synthesis of various heterocycles (*e.g.* piperidin-2-ones, having physiologic action)[176] and in titrimetric determination of organolithium compounds.[177]

Surveying some of the reaction conditions applied to the photocatalytic coupling of amines (Scheme 5.1), Su *et al.* used a mpg-CN photocatalyst in combination with O_2 as a terminal oxidant to couple benzylamines.[132] In a similar reaction, Raza and co-workers used WS_2 nanosheets as photocatalyst.[178] Similar reaction schemes are also included in the works of Yang *et al.* and of Kumar *et al.*, who used Au/TiO_2 and CuO_2/CQDs, respectively.[179-180] Furukawa *et al.* employed a Nb_2O_5 photocatalyst and O_2 as electron acceptor.[181] Liu *et al.* applied Pt nanoparticles in combination with metal-organic framework (MOF) PCN-777.[182] In this chapter, the conversion of benzylamines to the corresponding imines with a CN material, K-PHI, is investigated.

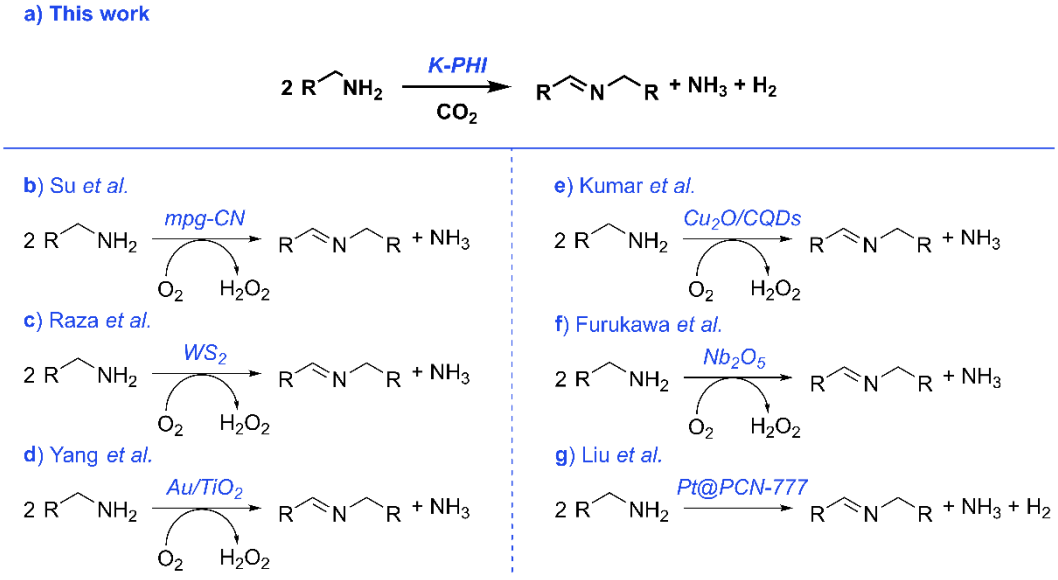

Scheme 5.1. Simplified comparison of the mechanisms for oxidative benzylamine coupling in this work (a) and in other works reported in literature.

In order to verify the possibility of using primary amines for capturing CO_2 and to verify their photocatalytic coupling using K-PHI, a series of preliminary tests in acetonitrile under various conditions was performed (Table 5.1). Benzylamine was chosen as a representative substrate.

Table 5.1. Screening of the reaction conditions.[a]

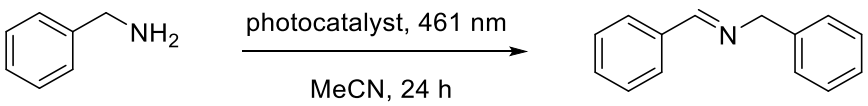

Entry	Photocatalyst	Time (h)	Environment	H_2O addition (μmol)	Yield[b]
1	K-PHI	24	CO_2	-	88%
2	mpg-CN	24	CO_2	-	38%
3	K-PHI	24	Ar	-	34%
4	K-PHI	24	Ar	10	42%
5	K-PHI	24	Ar	50	50%
6	K-PHI	24	Ar	200	73%
7[c]	K-PHI	24	CO_2 (dry)	-	74%
8[d]	K-PHI	24	CO_2	-	1%
9	-	24	CO_2	-	4%
10	-	24	Ar	-	7%
11	K-PHI	4	CO_2	-	65%
12	mpg-CN	4	CO_2	-	22%
13[e]	K-PHI	24	CO_2	-	74%
14[e]	mpg-CN	24	CO_2	-	52%
15[e]	K-PHI	24	Ar	-	13%
16[f]	K-PHI	24	^{13}C-CO_2	-	65%

[a] Reaction conditions: benzylamine 0.05 mmol; photocatalyst 5 mg; MeCN 3 mL; pressure 1 bar; T_{bath} = 35 °C; light intensity 51.70(3) mW cm^{-2} (blue LED, λ_{max} 461 nm); relative standard deviation of the method is 5%; [b] ^1H NMR yields; [c] Conditions as in entry 1, but CO_2 was passed through a column filled with P_2O_5 before entering the reaction tube, in order to remove moisture. [d] conditions as in entry 1, except that the reaction was performed in the dark; [e] conditions as in entries 1-3, but using 1 mL CD_3CN instead of 3 mL MeCN; [f] conditions as in entry 1, but using ^{13}C-labelled CO_2.

The yield of the corresponding imine, N-benzylidene benzylamine, was 88% when the reaction mixture was degassed and subsequently purged with CO_2 followed by irradiation with blue

light (λ_{max}=461 nm) (entry 1). When a different carbon nitride was used, *i.e.* mpg-CN, the conversion decreased to 38% (entry 2). On the other hand, substitution of CO_2 with Ar resulted in imine yield of 34% (entry 3). No conversion was expected, as no electron acceptor was added to the reaction mixture. However, the small degree of conversion can be explained by trace amounts of moisture (Table A1).[183] The experiments performed in wet acetonitrile with variable amount of explicitly added water (entries 4-6) suggested that indeed H_2O enhances the yield of the imine. To further prove the catalytic role of H_2O, CO_2 was passed through a column filled with P_2O_5 desiccant before being bubbled in MeCN. The imine yield decreased from 88% to 74%, revealing that H_2O indeed co-participates in the photocatalytic oxidative coupling of benzylamines (entry 7). Without light, almost no imine was produced (entry 8). Without catalyst, benzylamine is stable under light irradiation both in the presence of CO_2 and under Ar (entries 9-10). Furthermore, in the presence of K-PHI already after 4 h of irradiation, the yield of the imine was 65%, while in the presence of mpg-CN only 22% (entries 11, 12). Higher yield of the imine in case of K-PHI is explained by faster benzylamine oxidation *via* IDEAS, *i.e.* by better capacity of the photocatalyst of storing unpaired electrons and readily donating them to an electron acceptor, described in the previous chapter. Using a more concentrated reaction mixture in CD_3CN gave the imine with slightly lower yield, but it also allowed for quasi *in situ* characterisation of the reaction mixture by ^{1}H NMR (entry 13). Under similar conditions, mpg-CN produced the imine in 52% yield (entry 14). When the reaction was performed under Ar, the yield of imine was 13% (entry 15). Finally, experiments were conducted using ^{13}C-labelled CO_2 to prove that CO_2, despite having a key role in mediating these photocatalytic reactions, is not photocatalytically reduced by K-PHI (entry 16).

A modified setup was used for experiments with ^{13}C-CO_2 (Figure 5.2). Labelled ^{13}C-CO_2 was produced by thermal decomposition of ^{13}C-labelled $NaHCO_3$ and used to saturate the photoreactor as shown at Figure 5.3. (A detailed procedure is described in section A11.6) Chamber A was filled with ^{13}C-$NaHCO_3$ and connected to the flow of Ar. Then, while flushing Ar, Chamber A was heated to 230 °C. This led to the decomposition of ^{13}C-$NaHCO_3$ into H_2O vapour and $^{13}CO_2$ which were carried towards the second Chamber. Chamber B was used to trap the formed water. The CO_2/Ar gas mixture was bubbled through the solution of benzylamine and subsequently through the $Ba(OH)_2$ solution to monitor CO_2 formation through precipitation of ^{13}C-$BaCO_3$. After 30 min, the tube with reaction mixture was closed and irradiated as usually for 24h.

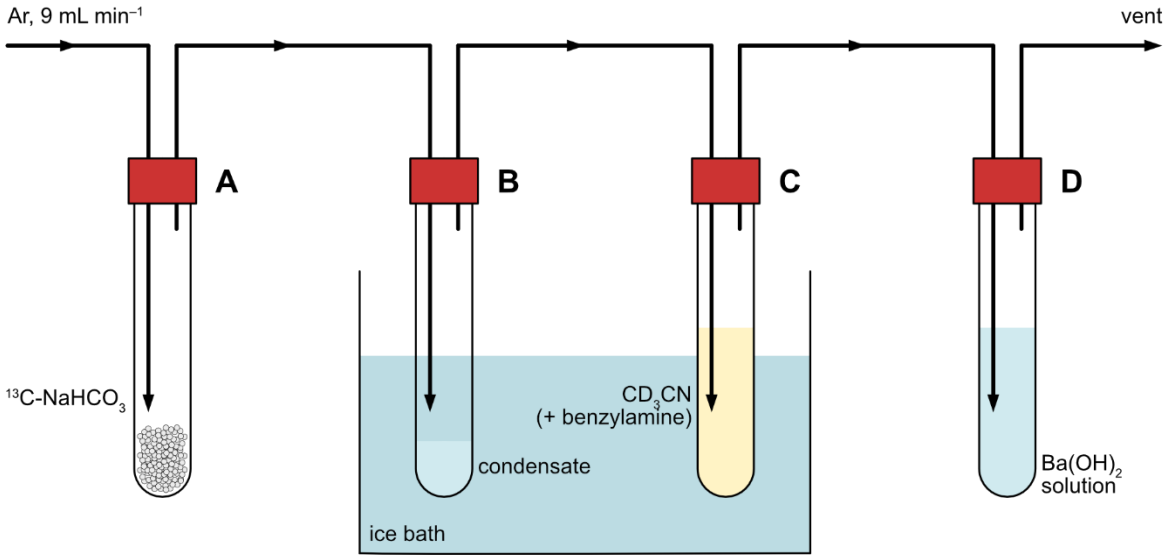

Figure 5.2. Setup used for thermal decomposition of ^{13}C-$NaHCO_3$ and generation of ^{13}C-CO_2 to be used in photocatalytic oxidative coupling of benzylamines.

These experiments showed no conversion of CO_2 to any reduction products, further confirming what was observed with other characterization techniques such as HPLC and GC-TCD. Except for the CD_3CN solvent peaks, only the signals belonging to unreacted benzylamine and to the imine product are observed in ^{1}H and ^{13}C NMR spectra. (Figures A10, A11)

The scope of substrates for imine synthesis by the proposed method was further extended to other benzylamines. The corresponding imines were obtained with 72-96% yields (Scheme 5.2). Electron donating *m*-CH_3 and *o*-CH_3 groups gave the products in higher yields, while *p*-CH_3 and *p*-OCH_3 in lower yield. Similarly, electron withdrawing *o*-F group decreased the yield, while *p*-F slightly increased the yield. Analysis of the data on Scheme 5.2 reveals that no distinct correlation between the nature of substituents and the yield of the imine exist. Apparently, this is a result of quite similar oxidation potentials of substituted benzylamines, *i.e.* 1.203-1.242 V vs. Ag/AgCl (sat. KCl)[184] and a much more positive oxidation potential of K-PHI, 2.54 eV vs. RHE.[75] (*R*)- and (*S*)-1-phenylethan-1-amines gave the imines in slightly lower yields apparently due to steric effect of the methyl groups next to the reactive N-centre. Furan-based amines gave the product in much lower yield presumably due to a side reaction of furan ring oxidation.

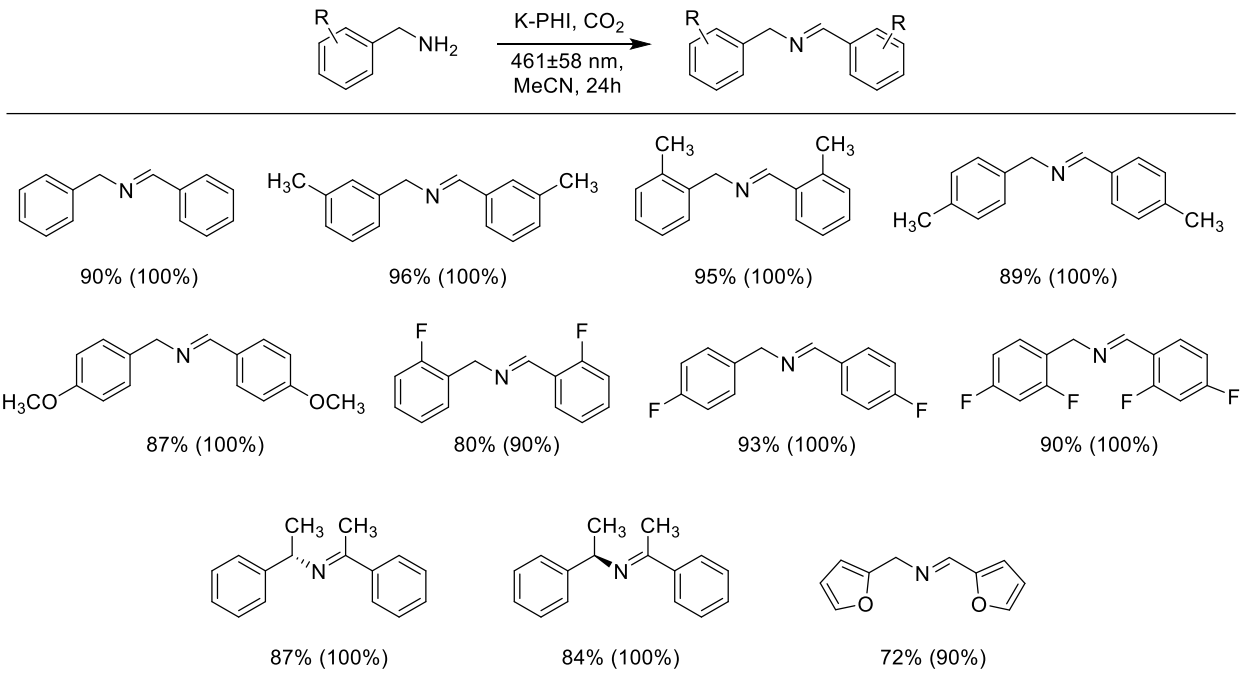

Scheme 5.2. The scope of substituted benzylamines investigated in this work. ^{1}H NMR yields are given in percent. Conversion of benzylamines is given in parentheses. Reaction conditions: amine substrate 0.05 mmol; K-PHI 5 mg; MeCN 3 mL; CO_2 1 bar; T_{bath} = 35 °C; light intensity 51.70(3) mW cm^{-2} (blue LED, λ_{max}=461 nm).

The mechanism of the benzylamine condensation was investigated using ^{15}N-labeled benzylamine. The quantitative conversion of the ^{15}N-benzylamine to ^{15}N-benzylcarbamic acid in excess of CO_2 was already confirmed in the previous chapter (^{15}N NMR of the carbamic acid is presented on the Figure 4.7a). This proves that benzylcarbamic acid participates in the photocatalytic reaction rather than benzylamine itself when CO_2 is chosen as reaction environment. Figure 5.3a shows the yield of imine depending on the load of K-PHI. The imine yield increased when a larger amount of K-PHI was employed. This fact correlates well with the ability of K-PHI to store electrons. This gives another piece of evidence that IDEAS plays a role in the benzylamine oxidation, as a higher load of K-PHI can host a larger number of electrons from the benzylamine electron donor. On the other hand, the yield of the imine under Ar was almost the same when 5 mg and 40 mg of K-PHI were used, suggesting that even though more catalytic sites were provided, the reaction proceeds slower in the absence of CO_2. This observation strengthens the hypothesis that the benzylcarbamic intermediate indeed boosts the photocatalytic reaction thanks to its better electron donor properties compared to benzylamine. As previously mentioned, the conversion in Ar, around 7-34%, is explained by the presence of trace amounts of water, which could participate as electron acceptor and also due to IDEAS (Table 5.1, entries 4-6). The yield of the imine was higher when the reaction was performed at lower temperature both using K-PHI and mpg-CN (Figure 5.3b). It might be

explained by destabilisation of the intermediates on the path of imine formation and lower solubility of CO_2 at elevated temperature.

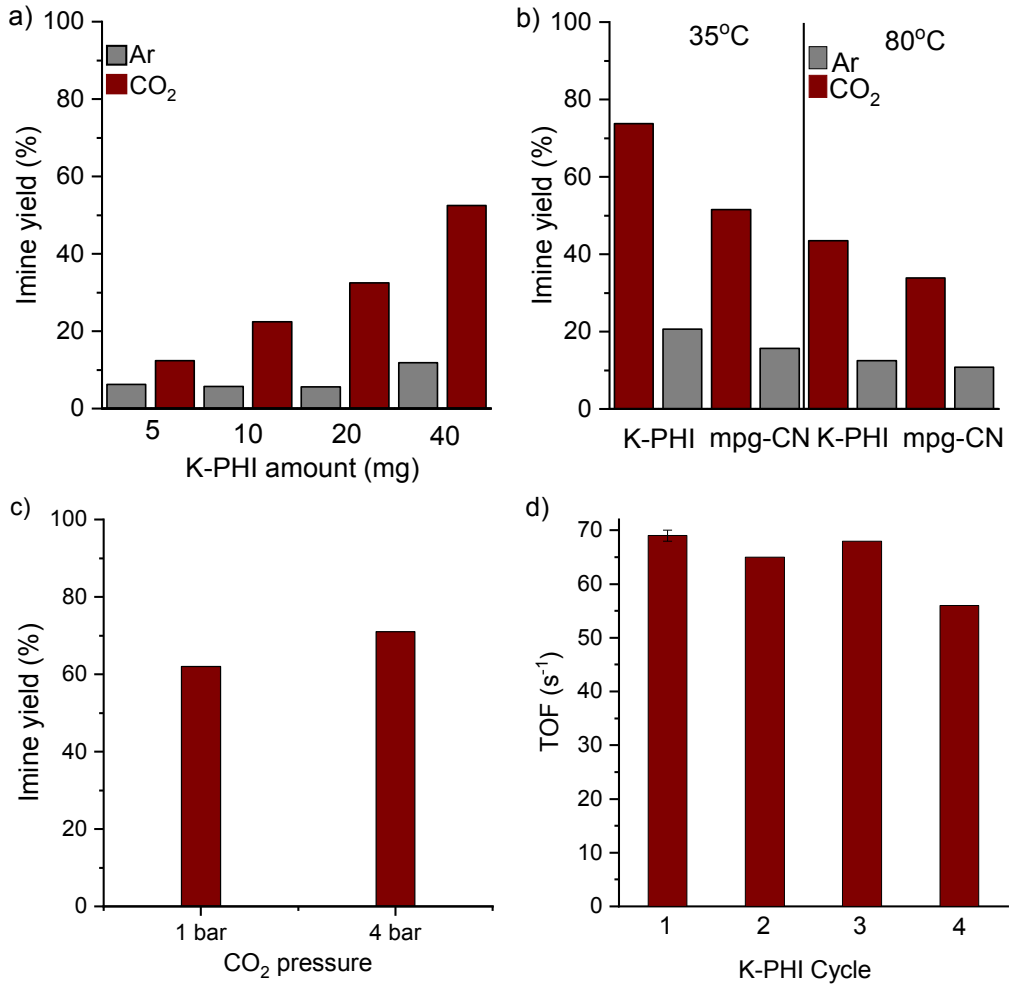

Figure 5.3. a) The effect of the catalyst loading on the imine yield (non-optimized conditions). Conditions: benzylamine 0.2 mmol, T = 35 °C, MeCN 3 mL, 72 h, 461 nm; b) Temperature- and catalyst dependent yield of the imine. Conditions: photocatalyst 5 mg, benzylamine 0.05 mmol, CD_3CN 1 mL, 24 h, 461 nm; c) the effect of CO_2 pressure on the imine yield. Conditions: K-PHI 40 mg, benzylamine: 0.05 mmol, CD_3CN 3 mL, 24 h, 461 nm; d) Turnover frequency (TOF) of K-PHI particles in conversion of benzylamine after several uses. The photocatalyst was washed with water and MeCN between each cycle.

The CO_2 pressure had almost no effect on the yield of the imine (Figure 5.3c), fact that suggests that the molecule is regenerated during each photocatalytic cycle when the benzylcarbamic acid reacts to form the final imine product. From the K-PHI particle size distribution and the conversion of benzylamine, the turnover frequency (TOF) of a single nano photoreactor with the average size 94 nm (Figure A1) was calculated to be 69±1 s^{-1} (Figure 5.3d). After four cycles using the same photocatalyst, the TOF remained at the level of 56 s^{-1}.

Summarizing the obtained results, the following photocatalytic mechanism of benzylamine condensation was proposed (Scheme 5.3). Mechanism of the reaction mediated by CO_2 is schetched in Scheme 5.3a. CO_2 binds to benzylamine to form benzylcarbamic acid. When K-PHI is brought in its excited state K-PHI* upon illumination, this carbamic acid promptly donates 1 electron to K-PHI*, turning into its radical cation **1** and forming the long-lived tinted radical anion K-PHI$^{\bullet-}$ (detected by EPR). The compound **1** is suspected to release CO_2 and 2 protons, maybe undergoing a first release of formic acid and its subsequent fast photolysis. CO_2 is then reintroduced in the catalytic cycle, whereas protons are absorbed by K-PHI itself (it was disscussed in Chapter 4). Product analysis and experiments with ^{13}C-labelled CO_2 also allowed us to confirm that CO_2 is regenerated during the photocatalytic cycle rather than being converted to other compounds (Figure A10, A11). The new intermediate **2** is presumably generated, which reacts with a second benzylcarbamic acid molecule to produce the desired imine product, with concomitant release of CO_2 and NH_3 (detected *via* NMR in both $^{15}NH_3$ and $^{15}NH_4^+$ forms, Figures 4.7b and A6).

When moisture is present, H_2O can act as electron acceptor instead of the benzylcarbamic acid coupling intermediates, as already suggested in literature.[132, 185-187] In this case, benzylamine is the electron donor, and not its carbamic acid, and forms the corresponding radical cation (Scheme 5.3b). Usually, oxygen is needed to start the photocatalytic reaction: it receives 1 electron from the excited photocatalyst to generate the reactive radical anion $O_2^{\bullet-}$. In the present case, the working conditions are oxygen-free using CO_2 or Ar as reaction atmosphere. As claimed by Yu *et al.*, the photocatalyst may generate O_2 by performing water splitting under anaerobic conditions.[187] This may indeed be the case, as poly(heptazine imide) carbon nitrides are efficient photocatalysts for this reaction.[188] $O_2^{\bullet-}$ and the benzylamine radical cation react to provide H_2O_2 and phenylmethanimine. The latter molecule reacts with a second benzylamine molecule to give the desired imine and ammonia. The former H_2O_2 leads to the same products in a 2-step mechanism, by producing another phenylmethanimine molecule as intermediate and subsequently the imine. In the proposed system, in photocatalysis under CO_2-saturated conditions water is also peresent. Therefore, both mechanisms are expected to be simultaneously followed, with one being favoured over the other depending on the relative concentration of CO_2 and H_2O in MeCN. In a typical reaction, in 3 mL MeCN there are approximately 837 μmol CO_2 (solubility ~ 0.279 M)[189] and 19.5 μmol H_2O, therefore photocatalysis is expected to proceed mainly through formation of the benzylcarbamic acid intermediate.

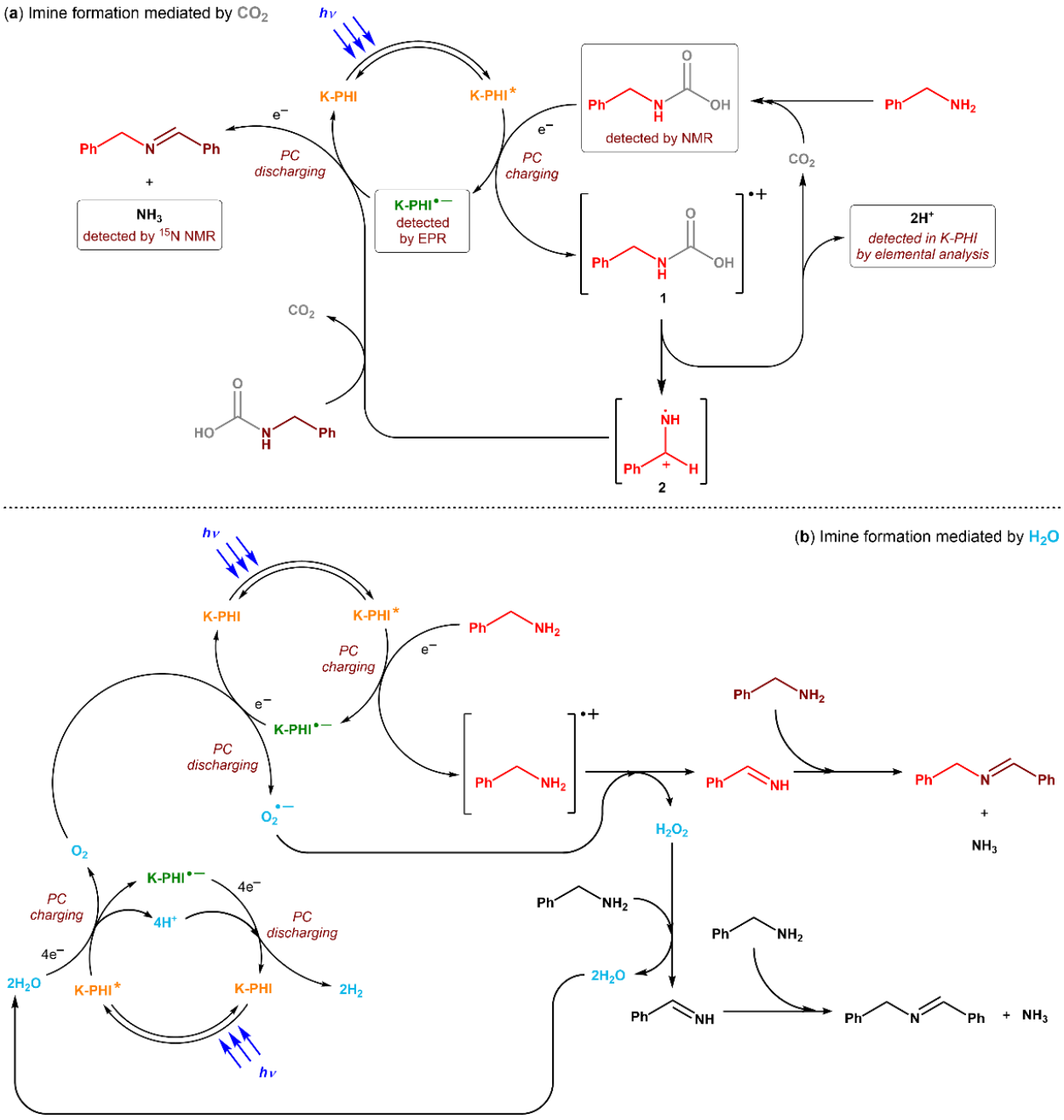

Scheme 5.3. Proposed mechanisms for photocatalytic oxidative coupling of benzylamines to N-benzylidene benzylamine in presence of a) CO_2 or b) H_2O.

In summary, according to the proposed mechanism, the consecutive push-pull of electrons mediated by K-PHI allows for the successful coupling of two benzylamine molecules, stepping through benzylcarbamic acid intermediates. K-PHI works similarly to a battery by charging (*i.e.* reduction of K-PHI* to K-PHI$^{\bullet-}$) and discharging (*i.e.* oxidation of K-PHI$^{\bullet-}$ back to K-PHI). Showing a better ability to even out the input and output flow of electrons *via* IDEAS, this material outperforms the standard choice carbon nitride photocatalyst mpg-CN.

5.3. Conclusion

The feature of carbon nitride materials to store electrons has a clear influence on their performance in the oxidative coupling of benzylamines in the presence of CO_2. Thus, higher conversion of benzylamine correlates with higher electron capacity of the employed photocatalyst. Having the comprehensive data on charge storage ability of carbon nitrides and their performance in coupling of benzylamines, we conclude that IDEAS is responsible for faster kinetics. Benzylamine captures CO_2 and stores it in the form of benzylcarbamic acid, while IDEAS accelerates the photocatalytic reaction by rapid oxidation of the benzylcarbamic acid. IDEAS mediated by benzylamine and combined with CO_2 as amine activating agent was applied for preparation of a series of synthetically useful imines with 72-96% yield. CO_2 was demonstrated to favour and accelerate the photocatalytic oxidative coupling of benzylamines by producing a more efficient electron donor: benzylcarbamic acid. Moreover, the moisture present in the solvent or in the gas steam was confirmed to promote the imine formation, as well, by acting as electron acceptor in the photocatalytic cycle. The charged photocatalyst acts as an "electron pump", readily injecting unpaired electrons into an available electron acceptor (*e.g.* CO_2 or H_2O). Therefore, matching a photocatalyst with large electron capacity with an efficient electron donor may be envisioned as a method to boost the photocatalytic reaction.In the light of these two experimental observations, we conclude that wet streams of CO_2, such as flue gas streams from cement industry, are a convenient and inexpensive alternative as reaction atmosphere to highly expensive and pure inert gases used in laboratory research such as Ar.

6. Tetramerization of benzylic amines to diazetidines-1,3 employing intrinsic charge storage property of semiconductors under visible light irradiation

6.1. Overview

The role of photogenerated holes in semiconductor materials is almost exclusively associated with the oxidation of substrates, i.e. electron transfer. Only little is known about holes acting as Lewis acid sites. Working on the projects described above, formation of interesting compounds, diazetidines-1,3, under Ar armosphere was noticed.

Therefore, in this chapter, the application of the standard reaction of benzylamines oxidation will be broadened to formation of hardly-accessible diazetidines-1,3. The intrinsic property of K-PHI to accumulate electrons is further investigated and the role of photogenerated holes in the mentioned reaction will be studied.

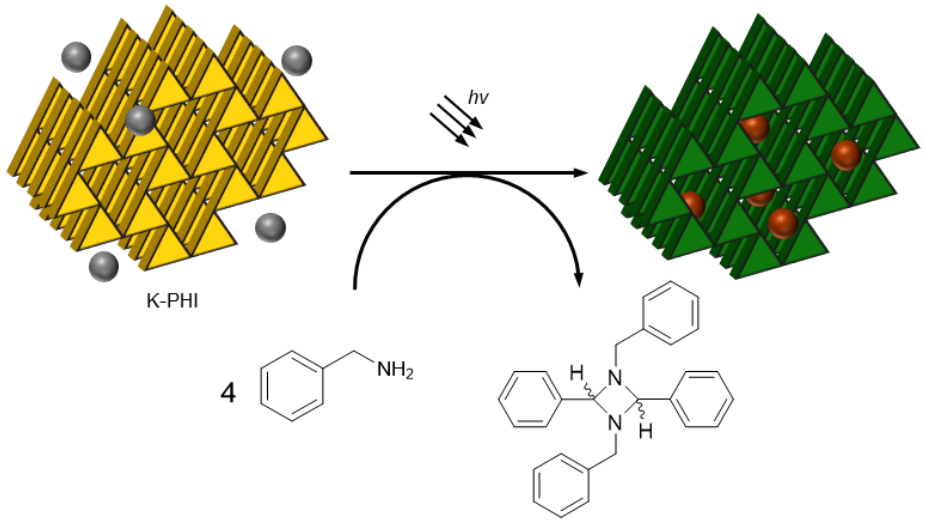

Figure 6.1. Overview of the Chapter 6.

6.2. Results – Discussion

Diazetidines-1,3 are rather scarcely presented in the literature.[190,191,192,193] This class of compounds is prepared mainly by photolysis of imines under UV irradiation.[194,195,196,197,198] The reaction is capricious and very sensitive to the substituents, even those located aside from the reactive center.[199] The situation is further complicated by instability of diazetidines-1,3 – some of them spontaneously decompose in solution.[200,195] These factors make them really evasive class of strained heterocycles.

Oxidative coupling of benzylic amines to imines in the presence of electron acceptors, such as O_2, is one of the most studied photocatalytic reactions reported to date and the mechanism has been thoroughly investigated. In particular, Wang et al. concluded that the photogenerated holes are not only involved in the redox process, but it also facilitates elimination of ammonia from the intermediary *gem*-diamine (Figure 6.2), *i.e.* hole works as Lewis acid.[201] We concede that quenching of the photogenerated holes in the reaction of benzylamines coupling, will suppress elimination of ammonia from the *gem*-diamine and therefore alter the outcome of the photocatalytic reaction. In this approach, the formation of diazetidine-1,3 as the product instead of exclusively imine formation when the reaction is performed in the presence of electron acceptors was observed.

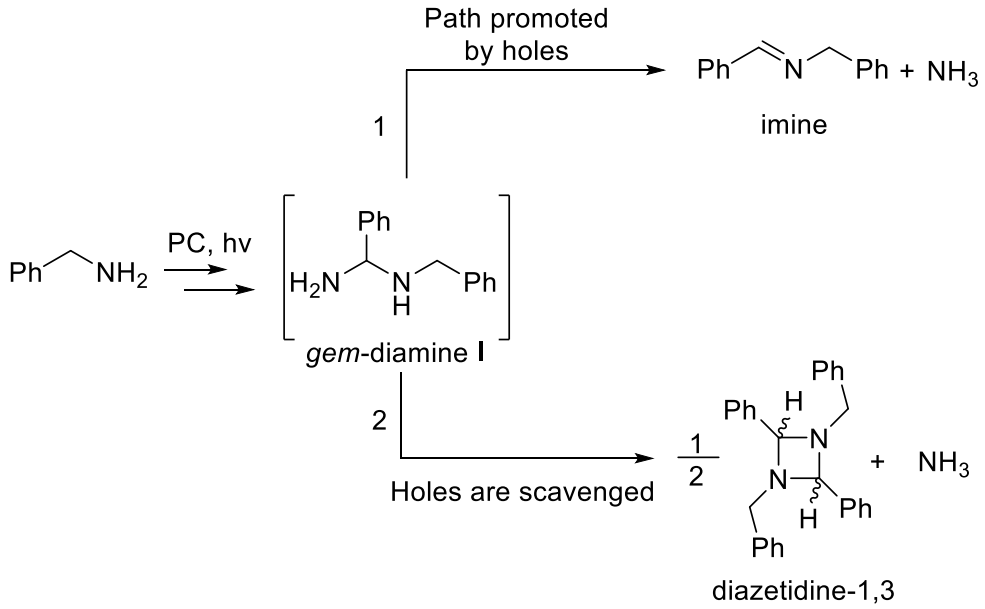

Figure 6.2. Two paths of benzylamine photocatalytic oxidative coupling: 1) convenient path in the presence of electron acceptor; 2) developed in this project path of diazetidine-1,3 synthesis.

In the very first experiment, performed dispersing K-PHI in thoroughly degassed solution of benzylamine in MeCN under blue light irradiation (465 nm) 78% conversion of benzylamine

along with the formation of the imine (50%) was observed. Careful examination of ^{1}H NMR spectrum indeed revealed formation of diazetidines-1,3 in 19% yield (Figure 6.3). Due to significantly different boiling point, diazetidines-1,3 were separated from the imine and unreacted benzylamine by distillation in vacuum.

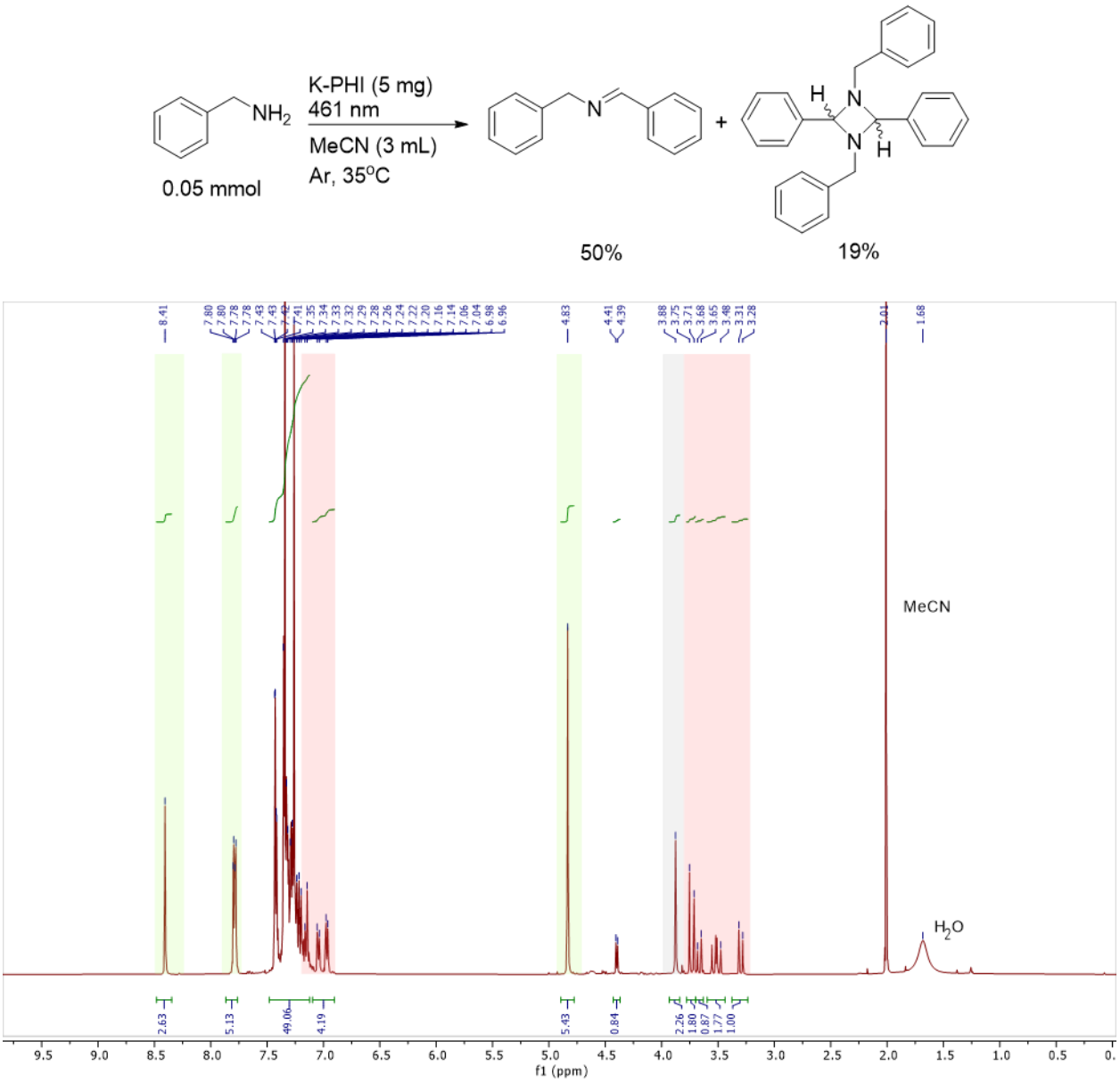

Figure 6.3. Oxidation of benzylamine under Ar atmosphere: reaction scheme and ^{1}H NMR spectra of the reaction mixture after irradiation. Reaction conditions: benzylamine 0.05 mmol; K-PHI 5 mg; MeCN 3 mL; Ar 1 bar; irradiation with blue LED (λ_{max}=465 nm).

Analysis of the 1,3-dibenzyl-2,4-diphenyl-1,3-diazetidine structure reveals that this heterocycle can have several diastereomers. In *cis*-isomer the phenyl rings are located on the one side from the plane of the four-membered ring, while in *trans*-isomer – on the opposite sides (Figure 6.4a). As expected the *cis*- and *trans*-diastereomers also have different chemical

shifts in ^{1}H NMR spectrum. Diastereotopic benzylic protons appear as doublets. Similarly, in ^{15}N NMR spectrum of the crude reaction mixture obtained using ^{15}N-labeled benzylamine two signals, 49.8 ppm and 47.6 ppm, corresponding to the diazetidine-1,3 diastereomers were detected (Figure 6.4b).

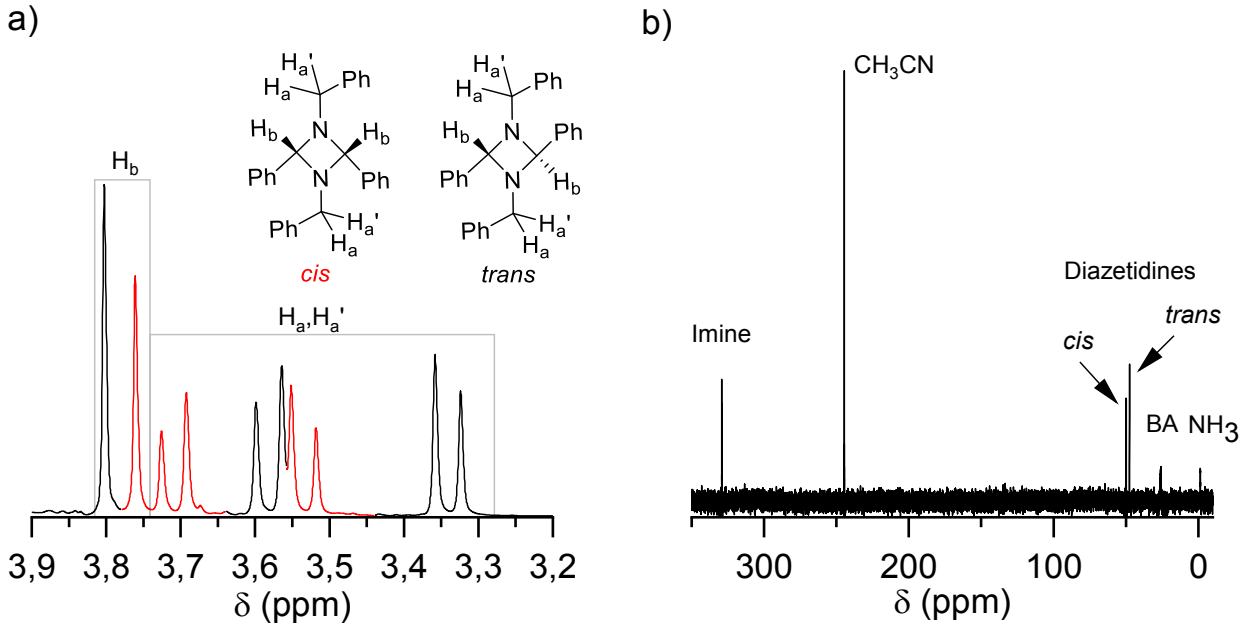

Figure 6.4. 1,3-dibenzyl-2,4-diphenyl-1,3-diazetidine *cis-/trans-* isomers in NMR spectra: a) ^{1}H NMR spectrum of the diazetidines-1,3 mixture (in $CDCl_3$). Slightly lower intensity of the *cis*-isomer is due to lower solubility of this compound compared to the *trans*-isomer; b) ^{15}N NMR spectrum (in CH_3CN) of the reaction mixture using ^{15}N-benzylamine as the reagent.

As a sequence of different symmetry, *cis*- and *trans*-isomers have different physical forms – one is a solid at room temperature, while another is a liquid. Using this feature, diazetidines isomers were separated by fractional crystallization from acetonitrile. Chromatography was not suitable as the diazetidines-1,3 readily decompose on silicagel. C_1 and C_2 carbon atoms in ^{13}C NMR spectra of pure $^{15}N_2$-labeled diazetidines-1,3 appear as doublet of doublets, suggesting that carbon is clutched between two ^{15}N atoms (Figure 6.5a). Therefore, NMR spectra confirmed that diazetidines-1,3 and not diazetidines-1,2 were synthesized. High resolution mass-spectra (HR-MS) of two diastereomers as well as $^{15}N_2$-labeled counterparts are similar and agree with the calculated mass of these compounds (Figures A13-A16). FT-IR spectra of both isomers are almost identical except that one isomer shows pronounced peak at 1260 cm^{-1} (Figure 6.5b). According to the results of the normal mode analysis performed at ωB97X-D//6-31G(d) level of theory (Table A3), this band is mainly attributed to the asymmetric stretching vibration in the C_2N_2 ring in the molecule of *cis*-isomer (Figure A17). Correlating the

experimental FT-IR and ^{1}H NMR spectra with the results of modeling, we conclude that *cis*-isomer is a solid at room temperature, while *trans*-isomer is a liquid.

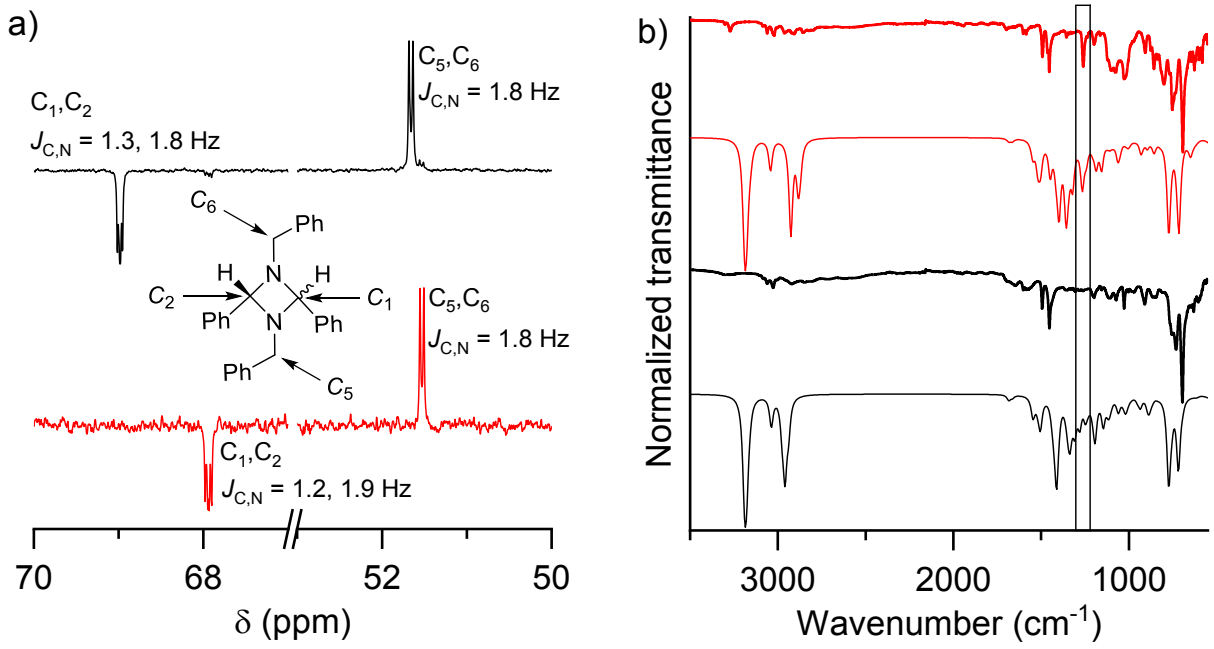

Figure 6.5. a) ^{13}C APT NMR spectrum of *cis*-diazetidine-1,3 and *trans*-diazetidine-1,3 in CD_3CN. b) Experimental (FT-IR in neat) and simulated (gas phase) IR spectra of *cis*- and *trans*-diazetidine-1,3.

A scope of substrates was extended to 20 amines (Scheme 6.1). Among them only benzylamines bearing electron withdrawing substituents, i.e. one or several fluorine atoms and CF_3-group, gave the diazetidines-1,3 also as a mixture of *cis*- and *trans*-isomers (1:1). Amines holding electron donating groups gave exclusively imines. These results suggest that electron withdrawing groups stabilize the intermediate in the reaction path of diazetidines-1,3 synthesis. The effect of fluorine atoms might also constitute in hydrogen bonding with the hydroxylated surface of K-PHI that additionally stabilizes the intermediate on the surface of K-PHI.

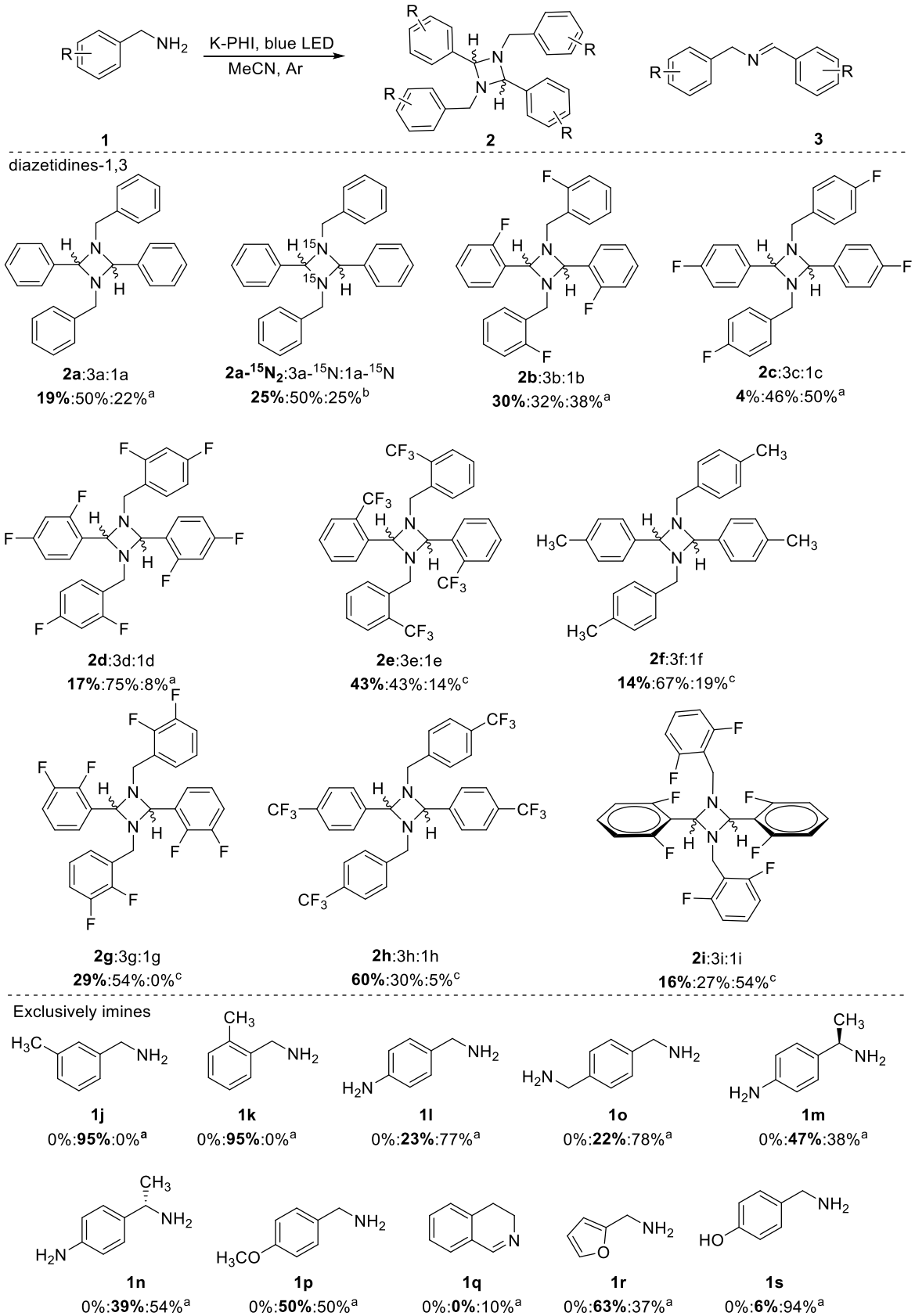

Scheme 6.1. Reactivity of substituted benzylamines. Ratio between the diazetidines-1,3 (*cis*- and *trans*-isomers), imine and unreacted amine was calculated from the ^{1}H NMR spectra; [a] 24 h; [b] 72 h; [c] 48 h.

The *gem*-diamine **I** (Figure 6.2) has been postulated as the intermediate in benzylamines oxidation, but it has not been observed or isolated apparently due to its high reactivity. However, when geminal amino groups are incorporated into the cycle, the *gem*-diamine may be isolated and it was, in fact, suggested as the intermediate in synthesis of diazetidines-1,3.[202]

In order to further confirm the mechanism of diazetidines-1,3 formation, the following experiments were performed. Irradiation of the mixture of benzylamine, K-PHI in MeCN in the presence of different electron acceptors, such as O_2,[201] S_8[100] and $CHCl_3$[203] gave exclusively imine, suggesting that holes, when are not quenched, promote the path of imine formation. The experiment without solvent resulted in 23% benzylamine conversion, while yield of diazetidines was 15%, suggesting that under the standard conditions residual water in MeCN (400 ppm) works as an electron acceptor.

On the other hand, addition of different electron donors such as Et_3N, benzylalcohol and triethylamine to N-benzylidene benzylamine did not give the diazetidine-1,3 either, suggesting that diazetidines are not the products of imine dimerization. Additional experiments employing 2,3-diphenylaziridine, stanic halide complex of phenylmethaneimine $SnCl_2 \cdot (PhCH{=}NH \cdot HCl)_2$ did not give the diazetidines, rulling out these compounds as the intermediates.

Screening of different common photocatalysts in the reaction of benzylamine coupling under Ar revealed that in all these cases the major product is imine. However, semiconductors, such as different types of carbon nitrides, CdS under blue light and TiO_2 under UV irradiation (λ_{max}=365 nm), gave diazetidines-1,3 in 1-19% yield (Figure 6.5a), while molecular catalysts did not give diazetidine-1,3.

Using the developed earlier procedure, a number of electrons accumulated in the tested semiconductors was determined by titration with methylviologen (Figure 6.6b). Thus, Na-PHI showed comparable capacity (2.74 μmol) to that of K-PHI (2.12 μmol). Other semiconductors, mpg-CN, TiO_2, CdS, and WO_3, showed lower but still detectable capacity in IDEAS, 0.08-0.40 μmol. Reaction mixture containing molecular catalysts, such as $Ir(ppy)_3$, did not show solution staining upon addition of MV^{2+}. Therefore, only semiconductors from the tested catalysts mediate tetramerization of benzylamine.

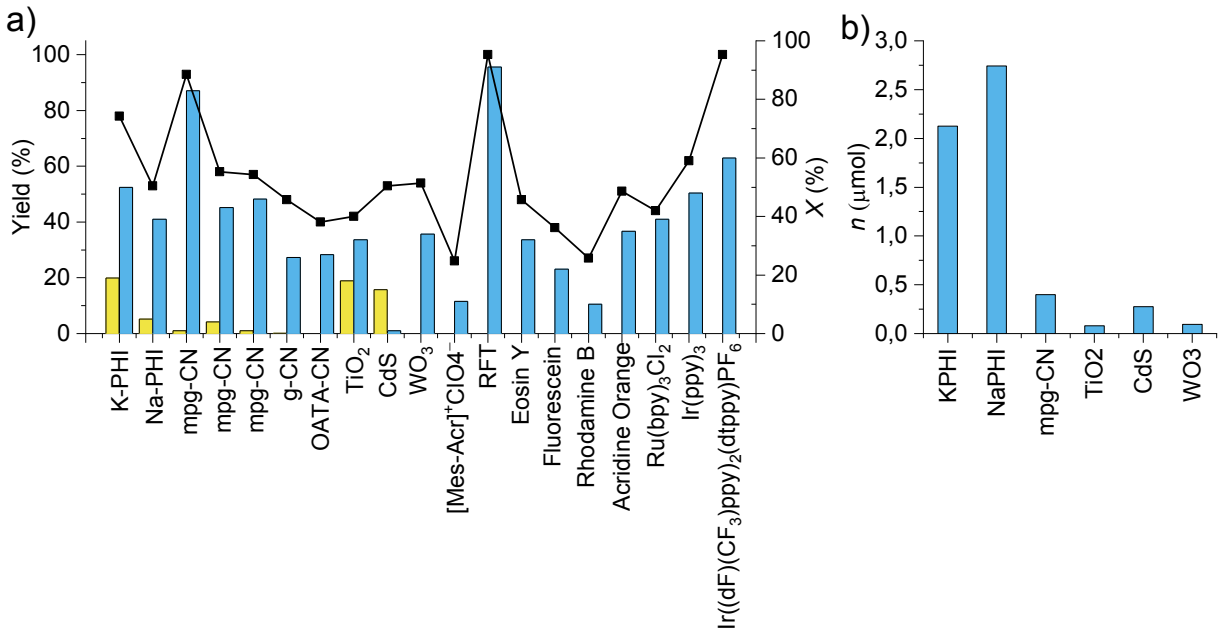

Figure 6.6. Mechanistic studies. a) Catalysts screening. Conditions: benzylamine 0.05 mmol; catalyst 5 mg; MeCN 3 mL; Ar 1 bar; time 24 h; light intensity 51.7±0.03 mW·cm^{-2} (blue LED). b) IDEAS of chosen semiconductors.

Given the experimental data, the following mechanism of benzylamines coupling was proposed (Figure 6.7). The mechanism includes utilizing intrinsic electron storage property of the semiconductor, exemplified on K-PHI as the most studied semiconducting material in this regard. Excitation of K-PHI with blue light leads to the formation of the hole and electron. Quenching of the photogenerated holes by electrons from benzylamine accompanied by H^+ transfer leads to the formation of phenylmethaneimine (PhCH=NH) and K-PHI-H_2. The structure of the latter is not completely clear. However, based on the recent reports we conclude that this material is radical by nature, while H^+ are weakly bound and compensate negative charge. It is supported by distinct signal in EPR spectrum and increased hydrogen content as evidenced by elemental analysis.[204] In addition, Lau et al. showed that addition of Pt nanoparticles to the material of similar structure leads to the evolution of H_2.[205] Release of H_2 under such mild conditions in our opinion would not be possible, if hydrogen was covalently bound to the carbon nitride framework. Nucleophilic addition of benzylamine to the phenylmethanimine gives *gem*-diamine **I**. This intermediate can undergo two reaction paths. In the presence of electron acceptors, 'naked' holes promote evolution of NH_3 and formation of the imine. However, when the holes are scavenged, two *gem*-diamine **I** molecules exist long enough to undergo dimerization and form one diazetidine-1,3 molecule and two NH_3 molecules.

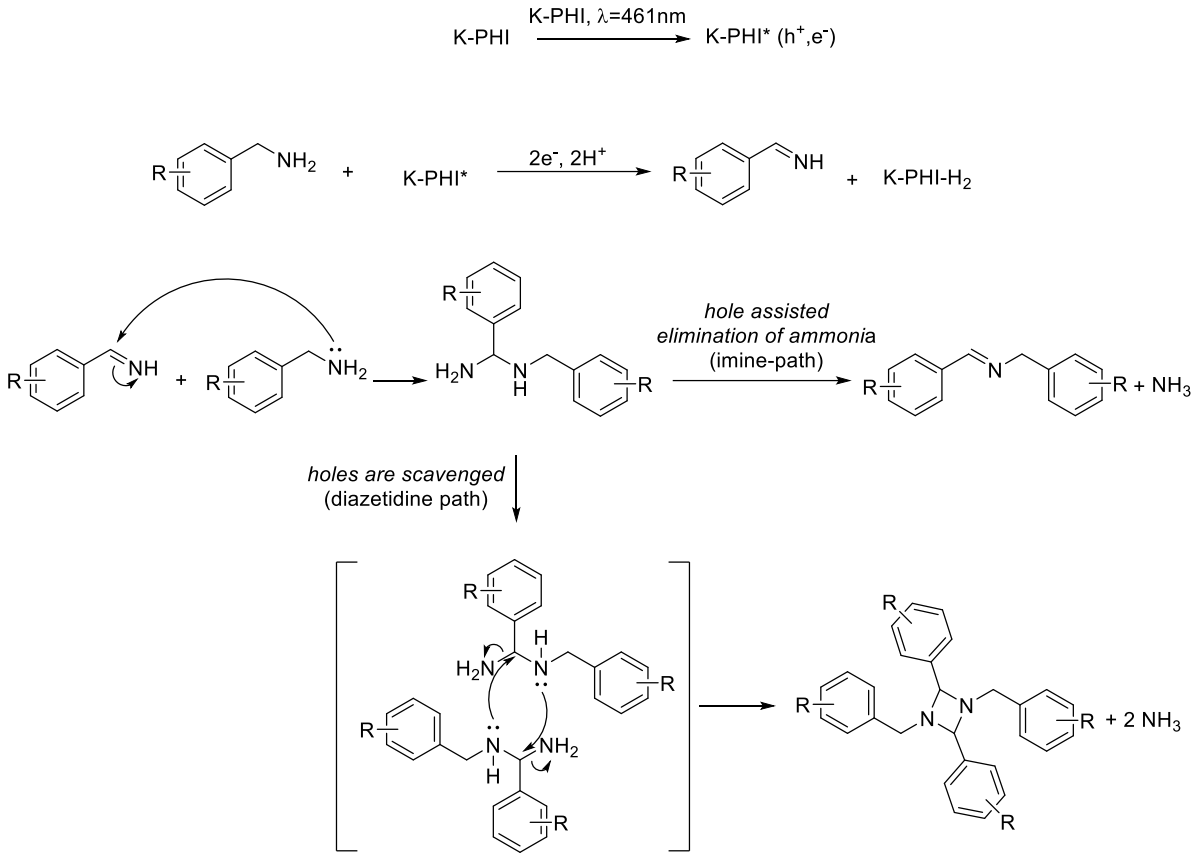

Figure 6.7. A proposed mechanism of diazetidine-1,3 formation.

diazetidines-1,3 properties

Due to the limited availability, the properties of diazetidine-1,3 are poorly studied. Therefore, the next step of this project was to investigate basic physico-chemical properties of *cis*-diazetidine-1,3 and *trans*-diazetidine-1,3. First, the cyclic voltammetry experiments were conducted to investigate redox properties of diazetidines-1,3. Similarly to amines, they showed onset of oxidation current at +0.55 V vs. $Ag/AgNO_3$ (Figure 6.8a). Next, a thermal behavior of both was investigated. The crystalline *cis*-isomer melts at +135 ºC (Figure 6.8b). Liquid isomer does not crystallize down to —150 °C. The structure of the diazetidine-1,3 was preserved after 3 cycles of fast and short-duration heating followed by cooling.

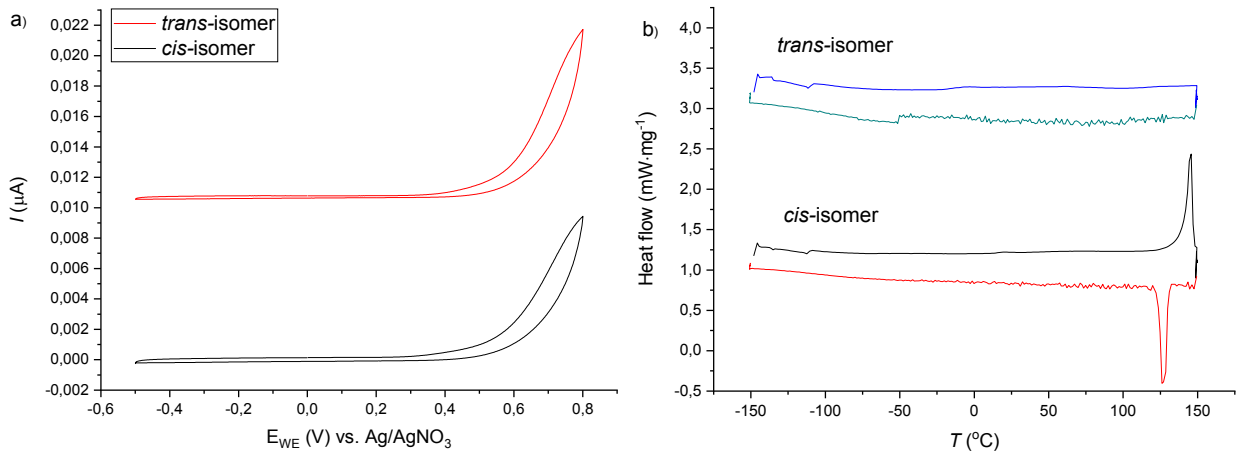

Figure 6.8. a) Cyclic voltammetry and b) differential scanning calorimetry (DSC) of *cis-/trans*-diazetidine-1,3.

Considering unusual structure of diazetidines, their thermal stability was also investigated. Surprisingly, both isomers were stable up to 200 °C upon relatively fast heating (5 °C min^{-1}), but lose 80% of weight at ca. 300 °C (Figure 6.9).

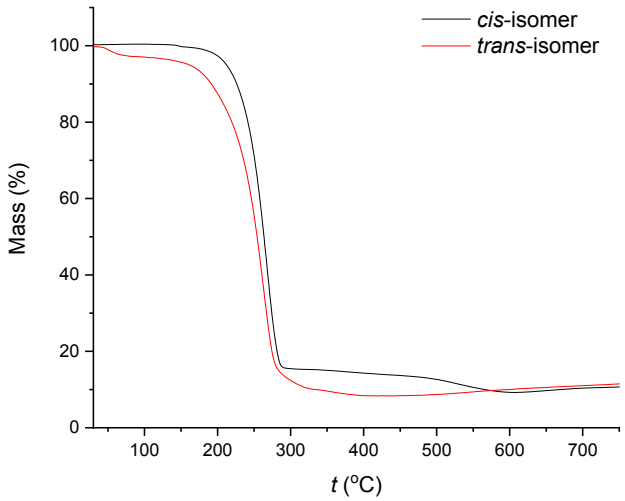

Figure 6.9. Thermal gravimetric analysis (TGA) of *cis-/trans*-diazetidine-1,3.

Decomposition pathways of both isomers are similar as supported by a similar set of charged species registered by TGA-MS (Figures A18-A21, Table A4). Analysis of TGA-MS data reveals that diazetidines decomposition apparently proceeds *via* ring-opening followed by formation of 1) two benzonitirle molecules and two toluene molecules or 2) two phenylmethanimine molecules and presumably one diphenylacetylene molecule (Scheme 6.2;

detailed path of diazetidine decomposition with suggested structures of charged intermediates is sketched in Figure A22).

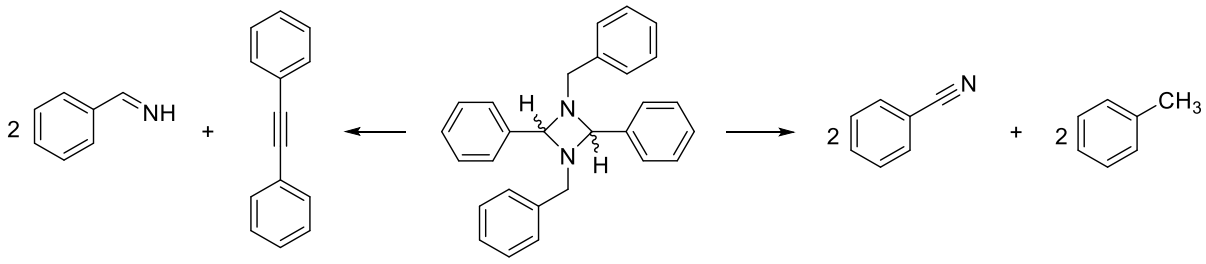

Scheme 6.2. Paths of diazetidines thermal decomposition.

6.3. Conclusion

In this chapter, K-PHI and a series of other semiconductors were shown to enable tetramerization of benzylic amines to diazetidines-1,3. Additionally, the properties of hardly-accessible diazetidines-1,3 have been studied. This reaction has been made possible employing the intrinsic property of semiconductor materials to accumulate electrons without adding apparent electron acceptors. The discussed reaction shows that photogenerated holes are involved not only in redox process, but also act as Lewis acid sites. Given that photocatalysis strongly relies on using sacrificial electron acceptors, performing the known reaction without apparent electron acceptors can, in principle, alter the well-explored paths and give molecules with unexpected properties, such as diazetidines-1,3 prepared herein.

7. One-pot photocalalytic reductive formylation of nitroarenes via multielectron transfer by carbon nitride in functional eutectic medium

7.1. Overview

In the past years, organic semiconductor photocatalysis has made remarkable advances in developing efficient chemical routes for building complex molecular structures. Until now, most efforts were focused on optimizing the semiconducting photocatalyst, while solvents were largely ignored. Deep eutectic solvents (DES) are prepared from abundant, sustainable resources, which makes them an affordable alternative to ionic liquids.

In this Chapter, a combination of photocatalysis with K-PHI and sustainable media, DESs, is used to enable a multi-electron reduction of nitro compounds. A series of DESs with adjustable physico-chemical properties are designed for the use as both reaction medium and electron donor; by means of two compositions of DES, two pathways for the NO_2 group reduction are proposed – the formylative reduction to N-arylformamides or the reduction to bare anilines.

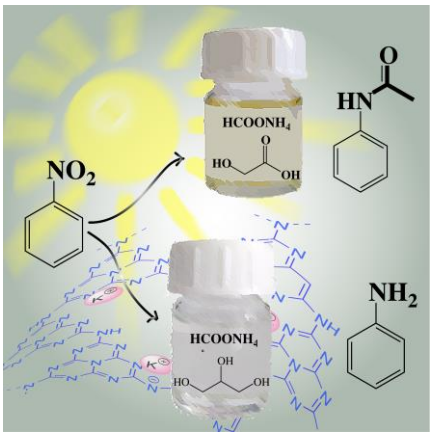

Figure 7.1. Two variations of reduction of nitro group presented in this Chapter.

This chapter is adapted from my original work: Markushyna, Y.; Völkel, A.; Savateev, A.; Antonietti, M.; Filonenko, S.: One-pot photocalalytic reductive formylation of nitroarenes via multielectron transfer by carbon nitride in functional eutectic medium. Journal of Catalysis 380, S. 186 - 194 (2019)

7.2. Results – Discussion

The eutectic media for this reaction were designed in the way to efficiently conduct photocatalytic reaction, namely to form colorless transparent liquid as a main requisition for using visible light, and at the same time to provide reagents necessary for reduction and subsequent formylation of the substrates. The choice of components was restricted to low molecular weight compounds, in order to overcome high viscosity intrinsic of the designed DES, which hinders their practical use. The components are easily reachable from renewable sources and have a much lower price compared to ionic liquids.

The use of ammonium formate for catalytic reductive formylation of nitroaromatic compounds is already known.[206-208] It is an attractive source of carbon for attaching CO, CHO, or methyl groups and can be used similarly to formic acid as a sustainable and affordable reducing agent, easily available as a major product of biomass processing.[209-210] Therefore, ammonium formate as an already low melting hydrogen bond acceptor (HBA) was used and complemented with the two different hydrogen bond donors (HBDs) - neutral and acidic. The smallest α-hydroxy acid and glycerol were used expecting to achieve lower viscosity of the mixture and to enlarge freezing point depletion. In order to evaluate the role of the DES components in the reduction and formylation reactions, several different eutectic mixtures were prepared, including a number of blinds (Table 7.1), namely, combining choline chloride with glycolic or formic acid HBD.

Table 7.1. Composition of the eutectic media and molar ratio of the components.*

Eutectic media	**HBA**	**HBD**	**Molar ratio**
DES1	Ammonium formate	glycolic acid	1:1
DES2	Ammonium acetate	glycolic acid	1:1
DES3	Ammonium formate	glycerol	1:1
DES4	Choline chloride	glycolic acid	1:1
DES5	Choline chloride	formic acid	1:2
DES6	Choline chloride	urea	1:2

*Eutectic mixtures were prepared by mixing corresponding components at 40°C until a transparent liquid formed

Ammonium acetate was combined with glycolic acid in order to test the possibility of one-pot reductive acetylation in the eutectic medium. Choline chloride:formic acid DES5 eutectic

mixture was prepared to reveal the activity of HCOOH in the photocatalytic reductive formylation with K-PHI. Conventional choline chloride:urea DES6 was used as a medium for a blank experiment.

Applicability of the medium to host the reaction largely depends on its physical properties allowing its practical use for industrial processes. The main physicochemical properties of the proposed DES were measured and are presented in Table 7.2.

Table 7.2. Physicochemical properties of eutectic media.

Eutectic media	Density, g cm^{-3} (25 °C)	Viscosity, mPas (25 °C)	Glass transition temperature, °C
DES1	1.32	317.0	-60.3
DES2	1.25	1486.7	-54.1
DES3	1.24	476.2	*
DES4	1.20	-	9.6
DES5	1.16	27.3	*
DES6	1.25[211]	750[212]	12[213]

* No glass transition detected.

As ammonium formate was used as an electron donor before and K-PHI, thanks to IDEAS, can accumulate up to hundred micromoles of electrons, the combination of such reaction media and photocatalytic approach is very promising. Therefore, the formed reaction media were tested for the reduction of nitro group. As DES1, formed from ammonium formate and glycolic acid, can act as both reducing agent and reaction media, no other electron donor was used. As a result, a quantitative conversion of nitrotoluene was observed (Table 7.3, entry 1). Furthermore, the only detected product of reduction was *N*-(p-tolyl)formamide – derivative of aniline. The photocatalytic reaction with K-PHI obviously leads to full reduction of nitro group to amino group and further formylation. This proves the high potential of the designed system for reduction reactions. Investigation of the reaction conditions through blank reactions proved that the presence of photocatalyst and light is necessary to conduct the reaction, as no conversion was observed. (Table 7.3, entries 2-4). The study of the effect of temperature on *N*-(p-tolyl)formamide yield was done as well (Table 7.3, entries 5-8). The higher temperature resulted in a higher conversion but led to a lower selectivity, which is rather typical for a photochemical reaction. Therefore, the ambient temperature 30 °C was chosen as an optimal temperature for this reaction.

Table 7.3. Reaction conditions optimization of *p*-nitrotoluene reduction.[a]

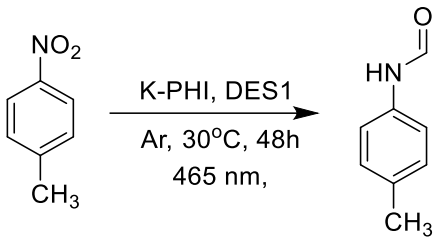

Entry	Photocatalyst	Light	Temperature, °C	Time, h	Conversion,[b]%	Yield,[c]%
1[d]	K-PHI (5 mg)	465 nm	30	48 h	100	85
2	-	465 nm	30	48 h	0	0
3	K-PHI (5 mg)	-	30	48 h	0	0
4	-	-	80	24 h	0	0
5	K-PHI (5 mg)	465 nm	30	24 h	61	55
6	K-PHI (5 mg)	465 nm	45	24 h	58	52
7	K-PHI (5 mg)	465 nm	60	24 h	88	78
8	K-PHI (5 mg)	465 nm	80	24 h	85	73
9[e]	K-PHI (5 mg)	465 nm	30	48 h	100	87
10[f]	K-PHI (5 mg)	465 nm	30	48 h	100	85
11	mpg-CN (5 mg)	465 nm	30	48 h	9	8
12	H-PHI (5 mg)	465 nm	30	48 h	38	35
13	g-CN (5 mg)	465 nm	30	48 h	1	traces

[a] nitrotoluene 0.1 mmol; K-PHI 5 mg; DES1 (ammonium formate : glycolic acid) 0.2 mL; T = 25 °C; Ar, LED module 465 nm; [b] determined by ^{1}H HMR; [c] total yield of *cis-/trans-* isomers determined by ^{1}H HMR; [d] first run; [e] second run; [f] third run.

Heterogeneous K-PHI can be easily recycled from the reaction mixture and used again. After three cycles of using the same catalyst no change in the catalyst's activity was observed (Table 7.3, entries 1, 9-10). In order to compare performance of K-PHI, the reaction with other types of CN catalysts was carried out. The results showed that reaction with mpg-CN results in only 9% conversion (Table 7.3, entry 11), while H-PHI gives higher conversion of 38% (Table 7.3,

entry 12), however not reaching the conversion of 100% obtained with K-PHI at the same conditions. With g-CN catalyst only traces of the product were detected (Table 7.3, entry 13). It should be mentioned that acid treatment of carbon nitride, as in case of H-PHI, typically increases surface zeta-potential.[214] Taking into account this fact and results from the Table 7.3, considerably higher performance of K-PHI compared to mpg-CN and H-PHI, these can be attributed to two factors: 1) electron buffering in the K-PHI and 2) negatively charged poly(heptazine imide) framework (while K^+ compensate the negative charge). Negatively charged surface of K-PHI is apparently beneficial for improved interaction with the reagent molecule.

This simple approach was further extended to a scope of nitroarenes presented in Scheme 7.1.

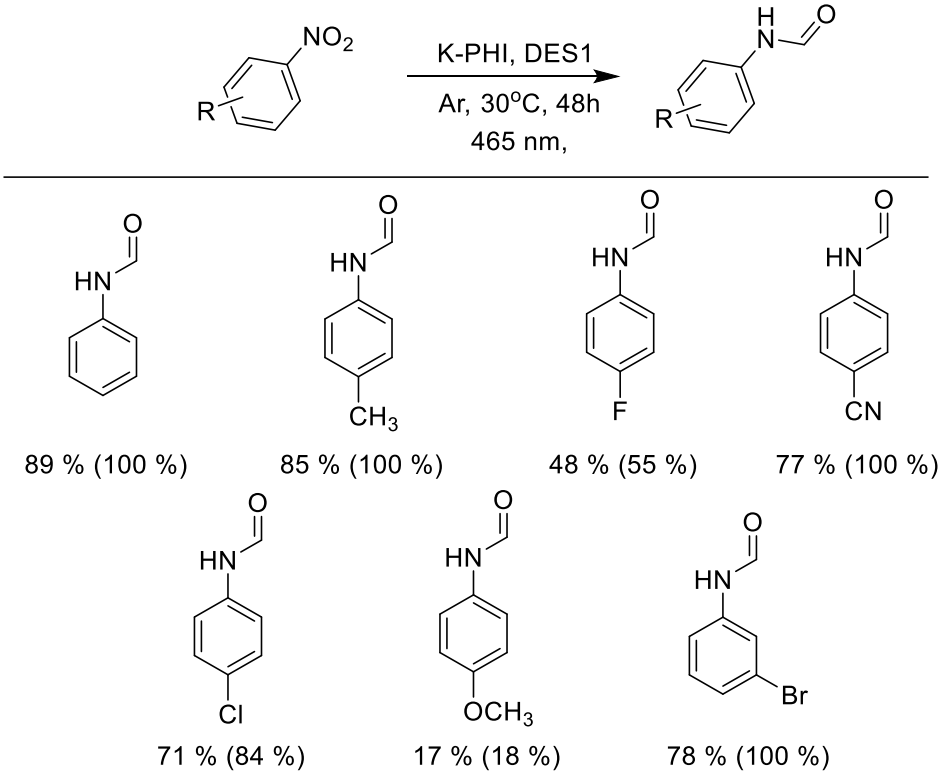

Scheme 7.1. Reduction of nitroarenes to N-arylformamides catalyzed by K-PHI. Conditions: substrate 0.1 mmol; K-PHI 5 mg; DES1 (ammonium formate: glycolic acid) 0.2 mL; T = 30 ˚C; Ar, LED module 465 nm. Yield and conversion (given in parentheses) determined by ^{1}H HMR. The yields are given for *cis-/trans-* isomers.

The proposed method can indeed be used for the reduction of both electronically rich and electronically poor compounds. Generally, when polar organic solvents are used, substrates with electron withdrawing groups have lower yields compared to those with electron donating substitutes.[215] Similar tendency is observed in the reactive eutectic media, which is probably

due to its polar nature. Overall, it is possible to say that weak electron donating groups, such as halogens and alkyl substituents, do not have a strong influence on the conversion and yield. However, in case of a substrate with a strong electron donating group (4-methoxynitrobenzene), considerably lower yield of the product was observed, while in conventional organic solvents it doesn't have a considerable effect. This peculiar property probably resulted from specific interactions between the 4-methoxynitrobenzene and components of DES. Despite the various yields, selectivity towards formylated aniline was preserved in all substrates.

To take the advantages of the reductive formylation, this reaction medium was used to run *in situ* cyclization of the intermediary formamides. As a result, we proposed a method for synthesis of benzimidazole as shown in Scheme 7.2. In this reaction, three steps are accomplished in one pot: 1) reduction of nitro group, 2) formylation of NH_2 group and 3) heterocyclization. The product was obtained in 85% yield.

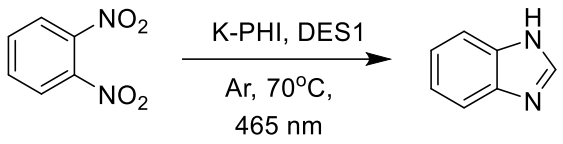

Scheme 7.2. Photocatalytic synthesis of benzimidazole via reductive formylation of 1,2-dinitrobenzene.

To get closer to the mechanism of the reaction, the influence of DES components on the reaction was investigated. Combinations of ammonium formate and glycolic acid with other compounds were studied (Table 7.4). Only DES5 (choline chlorid and formic acid) gave N-phenylformamide, however with extremely low 3% yield. Interesting result was found using ammonium formate and glycerol medium – no N-phenylformamide was detected, but instead aniline was formed in 86% yield. DES screening data suggest that formate (either anion or formic acid) is crucial for the reduction of the nitro group, while to formylate the amino group effectively formic acid is required to be generated in the eutectic media, as most formylating agents are reactive formyl derivatives generated *in situ*.

Table 7.4. Study of the different DES compositions in nitrobenzene reductive formylation.

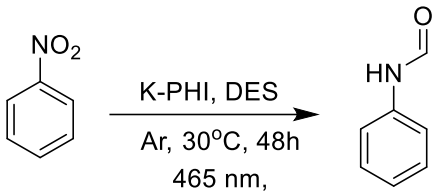

Entry	DES	Yield,%
1	DES1	100
2	DES2	0
3	DES3	0[a]
4	DES4	0
5	DES5	3
6	DES6	0

[a] The main product is aniline in 86% yield.

The direct selective aniline synthesis is interesting as well. A series of aromatic nitrocompounds was reduced to aminoderivatives using the ammonium formate: glycerol DES3 (Scheme 7.3).

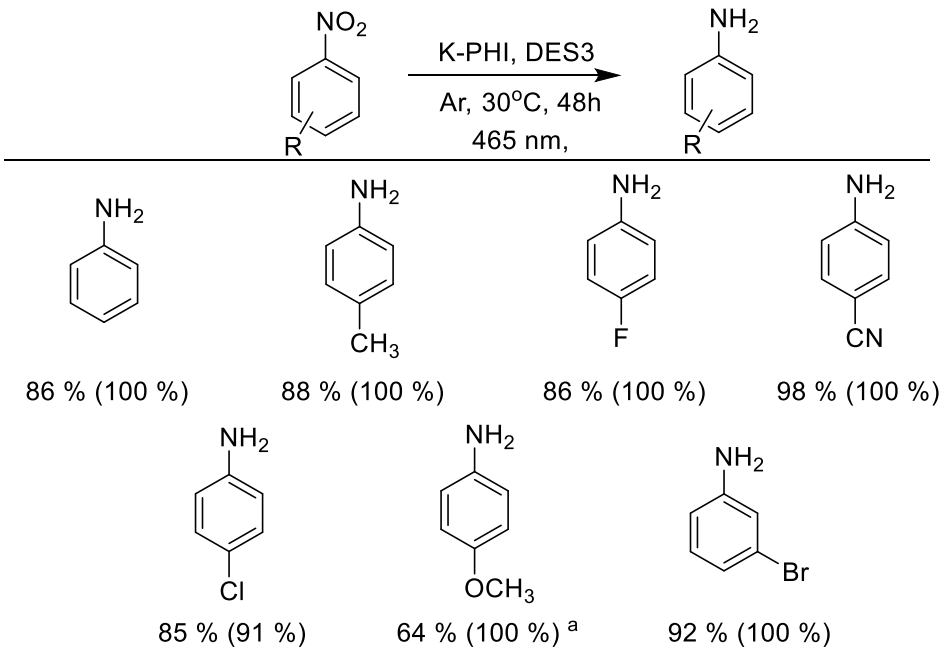

Scheme 7.3. Reduction of nitroarenes to anilines catalyzed by K-PHI. Conditions: substrate 0.1 mmol; K-PHI 5 mg; DES3 (ammonium formate: glycerol) 0.2 mL; T = 30 ˚C; Ar, LED module 465 nm. Yield and conversion (given in parentheses) determined by ^{1}H HMR. [a] The other product is N-(4-methoxyphenyl)formamide.

Similarly to formylative amination, the lower conversion of the substrate with a strong electron donating group (*p*-methoxynitrobenzene) was observed. Indeed, in all cases higher yields of the primary amines were obtained. Thus, the direction of the reduction of aromatic nitro compounds either to N-arylformamidines or anilines was selectively controlled by choice of the reactive medium.

The mechanism of the nitroarenes photocatalytic formylative reduction is sketched in Scheme 7.4.

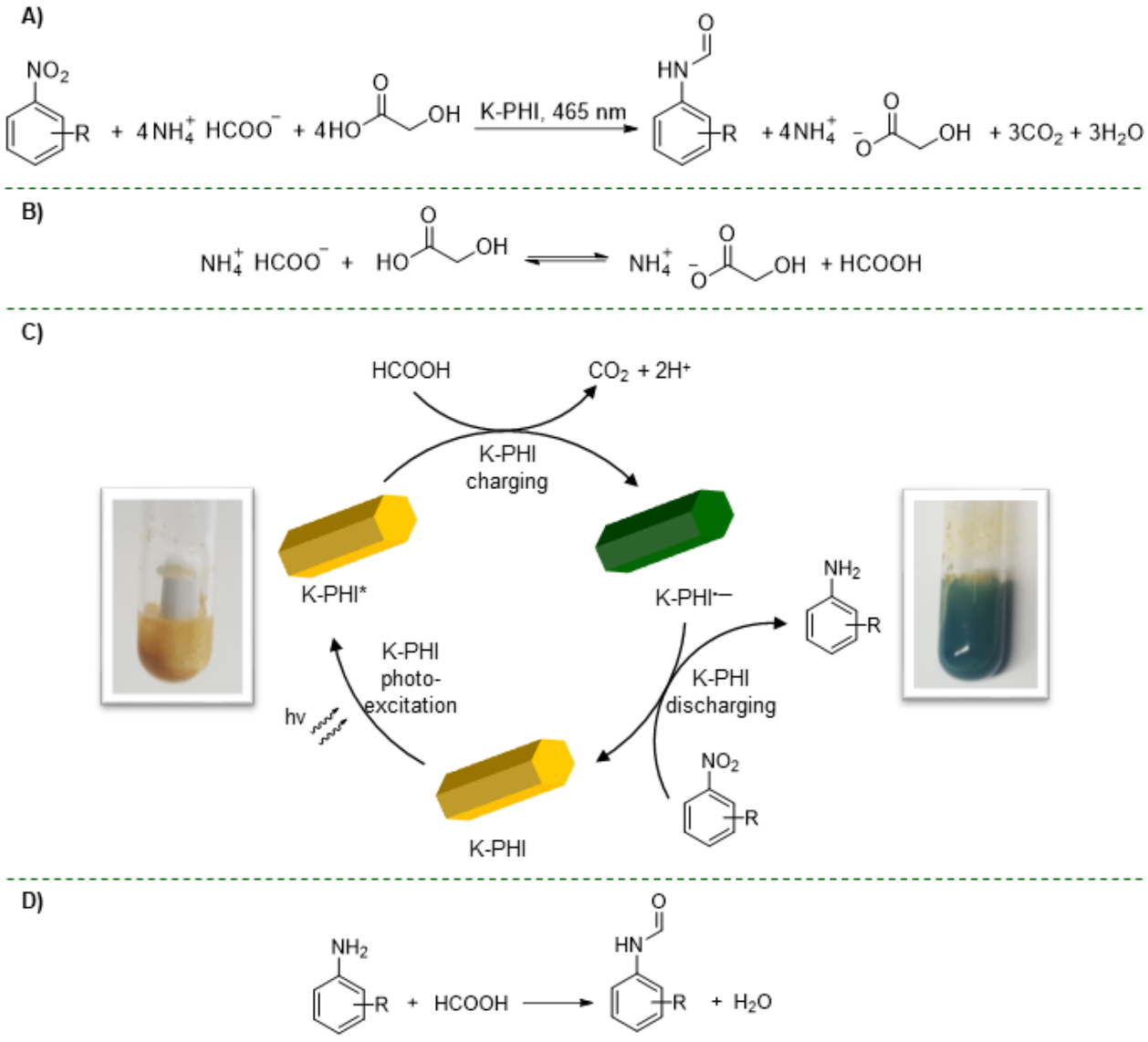

Scheme 7.4. The proposed mechanism of the photocatalytic reductive formylation of nitroarenes. A) Overall reaction equation; B) *In situ* formation of formic acid; C) Multi-electron photocatalytic reduction of the nitroarene by K-PHI; D) Formylation of the arylamine.

The overall equation describing the process is shown in Scheme 7.4a. In the first step, formic acid is formed reversibly *in situ* from ammonium formate and glycolic acid (Scheme 7.4b). The equilibrium is constantly shifted to the right as formic acid is gradually consumed. In the second step, K-PHI is converted to the excited state K-PHI* by absorbing a photon. Due to relatively low oxidation potential of formic acid (+0.4 V vs. RHE),[216] electron transfer from formic acid to the K-PHI* leads to the blue radical anion, K-PHI$^{\bullet-}$ appearance. Charging of K-PHI is accompanied by decomposition of formic acid that is converted into CO_2 and $2H^+$. Evolution of CO_2 was proved by precipitation of $BaCO_3$ upon bubbling reactor headspace gas through $Ba(OH)_2$ solution (Figure A23). During the step of K-PHI$^{\bullet-}$ discharging, protons from the formic acid decomposition and electrons stored in the semiconductor are transferred to the nitro-compound. The photocatalyst is recovered and aniline is expelled. In the last step, free formic acid reacts with aniline and gives the corresponding formamide.

As mentioned before, in the proposed reaction system, substrates with electron withdrawing groups, such as nitrile group, lead to a higher conversion/yield of the reduced product. During the photocatalytic process, charging of K-PHI as a result of reduction by formed HCOOH to the radical-anion K-PHI$^{\bullet-}$ occurs faster than the opposite discharging. This leads to accumulation of negatively charged K-PHI$^{\bullet-}$ species in the reaction mixture. Therefore, the interactions, such as adsorption on the catalyst's surface and discharging of the catalyst, between negatively charged K-PHI$^{\bullet-}$ and lower density substrate occur easier and faster than with the electron rich substrates.

Only products of the full reduction of nitro group have been detected in the studied reaction. The main product is formylated amine, while the other detected product is aniline. This also shows that reduction and formylation are separated processes and occur sequentially. We have not detected other intermediate reduction products, e.g. diazo-compounds. Given that K-PHI can store up to 1000 mmol of electrons per one gram of the material by IDEAS (Chapter 4), it can be concluded that indeed a rather concerted multi-electron reduction takes place.

7.3. Conclusion

In this project, a step forward was done to shift the organic reaction of reduction of nitroarenes to the demands of green chemistry. Two new eutectic media were designed using affordable and sustainable components that are able to efficiently host the photocatalytic reaction and simultaneously provide the reagents for it. Seven N-arylformamides in 17–89% yield and seven substituted anilines in 64-98% yield were prepared within the developed sustainable approach.

The high charge storage ability of K-PHI proved to be benefitial for organic synthesis once again, this time to accomplish a multi-electron reduction of nitro group. Analyzing obtained data, the following requirements to the DES chemical structure in the reaction of nitro group formylative reduction can be outlined: 1) DES should be liquid at the reaction temperature (in this case, 30–80 ˚C); 2) DES should contain formate anion – an effective reductant and formylating agent; 3) DES should contain acidic HBD, e.g. glycolic acid, to provide access to formic acid required for the formylation step.

8. Halogenation of aromatic hydrocarbons by halide anion oxidation with K-PHI photocatalyst

8.1. Overview

In the previous chapters, most attention was paid to the fascinating ability of semiconductors to store charges, especially high electron capacity of K-PHI, and its influence on the reaction outcome. However, another crucial characteristic of semiconductors, the redox potentials of CB and VB, were not highlighted yet.

In this Chapter, the highly positive VB potential of K-PHI is used to photooxidize halide anions (Cl^-, Br^-) in aqueous media to promote oxidative halogenation of electron rich aromatic compounds. The detailed study of the mechanism will be provided.

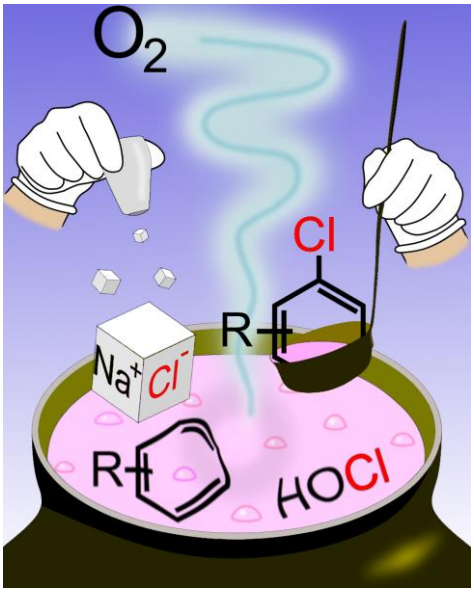

Figure 8.1. An overview of the Chapter 8.

This chapter is adapted from my original work: Markushyna, Y.; Teutloff, C.; Kurpil, B.; Cruz, D.; Lauermann, I.; Zhao, Y.; Antonietti, M.; Savateev, A.: Halogenation of aromatic hydrocarbons by halide anion oxidation with poly(heptazine imide) photocatalyst. Applied Catalysis B: Environmental 248, S. 211 - 217 (2019)

8.2. Results – Discussion

Reaction conditions of photocatalytic chlorination of anisole

Chlorinated and brominated hydrocarbons are a pivot of the chemical industry – they are important reagents and solvents. From the available methods, oxidative halogenation is probably the least harmful method to synthesize halogenated hydrocarbons.[217] According to this approach a halide-anion (Cl^- or Br^-) is oxidized *in situ* by H_2O_2 or $S_2O_8^{2-}$ to generate an electrophilic "Hal^+" species, which in turn enable electrophilic halogenation of the aromatic substrate.

Carbon nitrides have been already applied in H_2O_2 production upon O_2 reduction,[218] but the possibility to couple this reaction on the photooxidation side with oxidative halogenation of the aromatic compounds was not taken into account. This approach is beneficial compared to non-photocatalytic version (H_2O_2/HCl mixture), because H_2O_2 is generated *in situ* in micro quantities right before consumption (and does nor have to be added) and is potentially surface-bound, and still in its activated form. Therefore substrate over-chlorination or over-oxidation is minimized.[219]

Hering and König have shown that a multicomponent system including riboflavin tetraacetate (RFT) as a homogeneous photocatalyst, HCl, O_2, 4-methylbenzylalcohol and acetic acid, can be used to run oxidative chlorination of aromatic compounds under irradiation with λ=455 nm.[219] These conditions were used as a starting point in this project, except that RFT was replaced by the heterogeneous K-PHI photocatalyst. Indeed, a quantitative conversion of anisole along with excellent selectivity when benzylalcohol was used as electron/proton donor was observed (Table 8.1, entry 1). The effect of temperature on the *p*-chloroanisole yield was also studied. In the presence of benzyl alcohol and acetic acid, higher yield was obtained at higher temperature (Table 8.1, entries 4-5). On the other hand, using ^{i}PrOH as electron donor without acetic acid the dependence was opposite – lower yield of chloroanisoles was observed at higher temperature (Table 8.1, entries 6-8). These results can be explained as follows. Benzyl alcohol gives more stable radical upon oxidation than ^{i}PrOH. Furthermore, under the König's conditions acetic acid is converted into peracetic acid, the oxidazing agent, that is more stable at elevated temperature compared to H_2O_2 produced under the simplified conditions. Having these results, further experiments were performed at 30 °C, the optimal temperature for this process. The other common alcohols, *e.g.* EtOH and MeOH, were also tested under these conditions. In these cases, conversion of anisole was lower (Table 8.1, entries 9-12), which can

be explained by lower stability of the intermediary radical cation formed during the alcohol oxidation. However, the choice of ^{i}PrOH can be justified as an environmentally friendly reagent as the product of its oxidation is acetone.

Table 8.1. Optimization of reaction conditions of anisole chlorination with electron donor.[a]

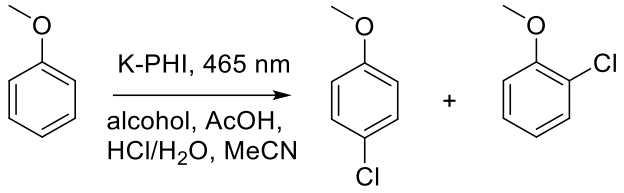

Entry	Electron donor	Temperature, °C	Time, h	Conversion,[b]%	Yield,[c]%
1	BnOH	30	13	100	97 (1:0.31)
2	BnOH	30	3	47	46 (1:0.39)
3	BnOH	45	3	49	38 (1:0.08)
4	BnOH	60	3	63	61 (1:0.4)
5	BnOH	80	3	66	65 (1:0.37)
6	^{i}PrOH	30	3	47	46 (1:0.39)
7	^{i}PrOH	60	3	52	33 (1:0.56)
8	^{i}PrOH	80	3	0	0
9[d]	BnOH	30	13	100	98 (1:0.31)
10[d]	^{i}PrOH	30	13	93	91 (1:0.41)
11[d]	EtOH	30	13	66	61 (1:0.35)
12[d]	MeOH	30	13	80	73 (1:0.38)

[a] conditions: anisole 0.02 mmol; HCl (36 wt.%) 0.1 mL; K-PHI 4mg; acetic acid 0.2 mmol; alcohol 0.12 mmol; MeCN 0.5 mL; light source 465 nm; [b] determined by ^{1}H NMR using N,N-dimethylaniline as an internal standard; [c] total yield of *o*- and *p*-chloroanisole. The ratio between *o*- and *p*-chloroanisole is given in parentheses. The ratio between isomers was determined by ^{1}H NMR using *N,N*-dimethylaniline as an internal standard; [d] K-PHI 1 mg.

Because of highly positive VB potential of K-PHI, +2.54 V vs. RHE, Cl^- theoretically can be oxidized to "Cl^+" *via* a two electron process (E^0 = +1.36 V) by the photocatalyst itself, without using auxiliary reagents – acetic acid and alcohol. In this desired case, we really take the "naked" catalyst and use both photogenerated electron and hole for the reaction. Under these simplified conditions, 65% conversion of anisole along with the high selectivity after only 12 h was observed (Table 8.2, entry 1). When the amount of K-PHI was increased to 4 mg and the time of irradiation to 24 h, quantitative conversion of anisole was obtained (entry 2).

Table 8.2. Reaction conditions optimization of anisole chlorination.[a]

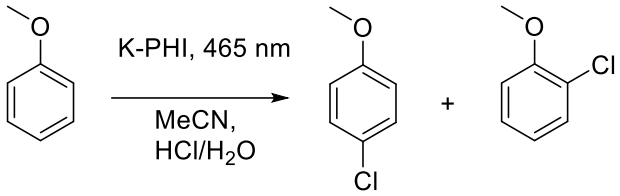

Entry	Photocatalyst	T, °C	Time, h	Conversion,[b]%	Yield,[c]%
1	K-PHI (1 mg)	30	12	65	64 (1:0.32)
2[d]	K-PHI (4 mg)	30	24	100	99 (1:0.31)
3[e]	K-PHI (4 mg)	30	24	78	75 (1:0.31)
4f	K-PHI (4 mg)	30	24	61	53 (1:0.33)
5[g]	K-PHI (4 mg)	30	24	39	35 (1:0.35)
6[h]	K-PHI (4 mg)	30	24	100	99 (1:0.34)
7[i]	K-PHI (1 mg)	30	13	28	26 (1:0.41)

[a] anisole 0.02 mmol; HCl (36 wt.%) 0.1 mL; MeCN 0.5 mL; electron scavenger – O_2; LED module (λ_{max}=465 nm). [b] determined by ^{1}H HMR using *N,N*-dimethylaniline as an internal standard; [c] total yield of *o*- and *p*-chloroanisole. The ratio between *p*- and *o*-chloroanisole was determined from ^{1}H NMR spectra and is given in parentheses. [d] first run; [e] second run; [f] third run; [g] fourth run; [h] K-PHI was recovered and washed with KOH; [i] triethylammonium chloride (TEACl) 0.2 mmol was used as a source of Cl^-; H_2SO_4 (0.2 mmol).

After few cycles of using the same catalyst, an essential drop of activity of K-PHI was observed. (entries 3-5). The result can be explained by highly acidic reaction conditions that led to the substitution of potassium by hydrogen. Furthermore, the hypothesis was supported by Energy Dispersive X-Ray Analysis (EDX). Potassium content in fresh K-PHI was 10.44

wt.%, while after the photocatalytic reaction it decreased to 0.11 wt.%. Nevertheless, potassium can be easily and quickly returned into K-PHI structure by treatment of the spent catalyst with KOH. As suggested by EDX analysis, potassium content in the regenerated sample was 10.07 wt.%, while X-Ray diffraction pattern and FT-IR spectrum of the regenerated sample and the starting material were identical. The regenerated K-PHI gave the same activity as the fresh material (entry 6). The experimental data unambiguously indicate the correlation between potassium content in the photocatalyst and its activity in the oxidative chlorination of anisole and may be explained as follows. Potassium cations in the structure of K-PHI compensate negative charge localized at nitrogen atoms. Making comparison with the structures of *N*-chlorocompounds, e.g. *N*-chlorosuccineimide, chloranmine-T etc., negatively charged N-atoms are essential for chlorine coordination by K-PHI. At the same time, coordination of Cl atoms by covalent carbon nitrides, *i.e.* g-CN or H-PHI, is also possible, but obviously less efficient. Therefore, covalent carbon nitrides are significantly less active in the chlorination reaction (Table 8.3).

Table 8.3. Photocatalyst screening for chlorination of anisole.[a]

Entry	Photocatalyst	Conversion,[b]%	Yield,[c]%
1	K-PHI	100	99 (1:0.31)
2	Na-PHI	39	35 (1:0.32)
4	H-PHI	46	43 (1:0.33)
5	g-CN	44	42 (1:0.29)
6	$Ru(bpy)_3Cl_2$	100	97 (1:0.22)[h]
7	$Ir(ppy)_3$	0	0
8	RFT	0	0

[a] anisole 0.02 mmol; HCl (36 wt.%) 0.1 mL; photocatalyst 4 mg, MeCN 0.5 mL; T = 30 °C; electron scavenger – O_2; LED module 465 nm; [b] determined by ^{1}H HMR using *N,N*-dimethylaniline as an internal standard; [c] total yield of *o*- and *p*-chloroanisole. The ratio between *p*- and *o*-chloroanisole was determined from ^{1}H NMR spectra and is given in parentheses.

Under water-free conditions and using triethylammonium chloride (TEACl) as a Cl^- source, anisole gave products of chlorination (Table 8.2, entry 7) too. Nevertheless, an acidic medium and a solvent stabilized Cl^+ are essential to close the reaction path as explained in Figure 8.4.

For comparison purposes, different forms of carbon nitrides were studied. The obtained data are presented in Table 8.3. Thus, Na-PHI[175] gave chloroanisoles in 35% yield. H-PHI[220] produced chloroanisoles with 43% yield. Similarly, g-CN gave chloroanisoles with 42% yield. Among the investigated homogenous catalysts, only $Ru(bpy)_3$ worked in this reaction, but recovery of this photocatalyst is still challenging. RFT, without acetic acid and alcohol, did not furnish any chloroanisoles.

In order to evaluate the effect of H_2O_2 concentration on the reaction of anisole chlorination, the experiments using a mixture of H_2O_2 and HCl were conducted. In this case, conversion of anisole was 100%, while selectivity of *p*-chloroanisole was only 6%. The main products were dichloroanisole (41%) and trichloroanisole (51%). These results underline the advantage of the photocatalytic approach versus non-photocatalytic.

The structure of the photocatalyst before and after the photocatalytic reaction was investigated by EDX and X-Ray Photoelectron spectroscopy (XPS) (Figure 8.2).

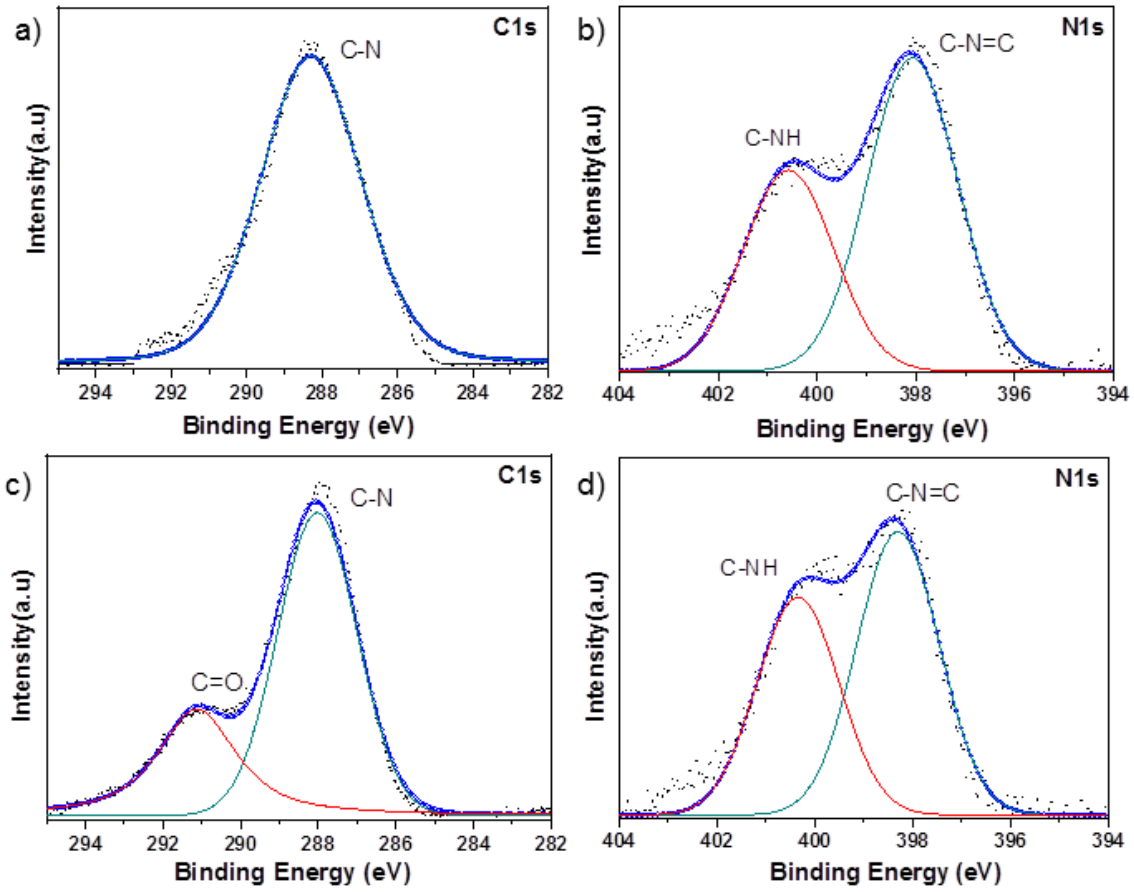

Figure 8.2. X-Ray Photoelectron spectroscopy (XPS): a) C 1s spectrum of fresh K-PHI, b) N 1 s spectrum of fresh K-PHI, c) C 1s spectrum of K-PHI after the photochlorination reaction, d) N 1s spectrum of K-PHI after the photochlorination reaction.

The results suggest that under the reaction conditions the surface of K-PHI underwent some chemical changes. Thus, XPS analysis reveals that the surface of the photocatalyst has partially hydrolyzed as suggested by the appearance of the peak at 291.2 eV in the C 1s spectrum, which is related to the surface C=O bonds. Similarly, in N 1s spectrum a fraction of NH_x groups observed as a peak at 400.4 eV increased. Possibly, these changes are a result of partial hydrolysis of K-PHI, in particular C-N=C bonds. Furthermore, EDX analysis revealed that Cl content in the catalyst increased from 0.7 wt.% to 2.31 wt.% after the reaction.

Presence of Cl in K-PHI after the reaction was also confirmed by XPS analysis (Figure 8.3). Typically, chlorine bound to carbon atom appears above 200 eV, while peaks at 197.2 eV and 198.7 eV in Cl 2p spectrum are apparently derived from inorganic chlorine, *e.g.* Cl^-.[221] All in all, the structure of K-PHI was subjected to partial hydrolysis during the photocatalytic chlorination. Nevertheless, these changes are not critical for the photocatalytic activity as can be concluded from the recycling and regeneration experiments.

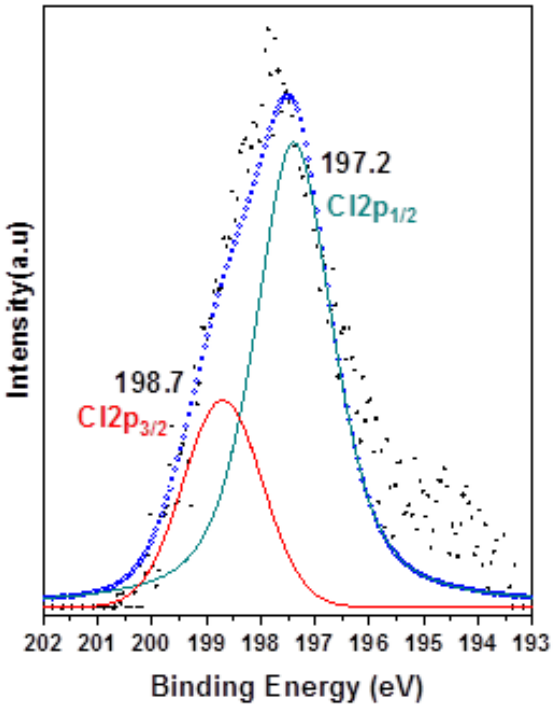

Figure 8.3. X-Ray Photoelectron spectroscopy (XPS) of Cl bonds in K-PHI after photochlorination reaction.

Oxidative halogenation of aromatic hydrocarbons catalysed by K-PHI

This very practical approach, using aqueous HCl and O_2 as the only reagents, was further extended to chlorinate electron rich aromatic compounds. A series of chlorinated benzenes was synthesized under the similar conditions (Scheme 8.1). The reaction went smoothly with the

substrates bearing strong EDG (electron donating group). With such substrates conversion and yield were almost quantitative. In case of moderate EDG (acetanilide), the yield and conversion were moderate. The reaction with weak EDG did not proceed or led to chlorination of the side chain.

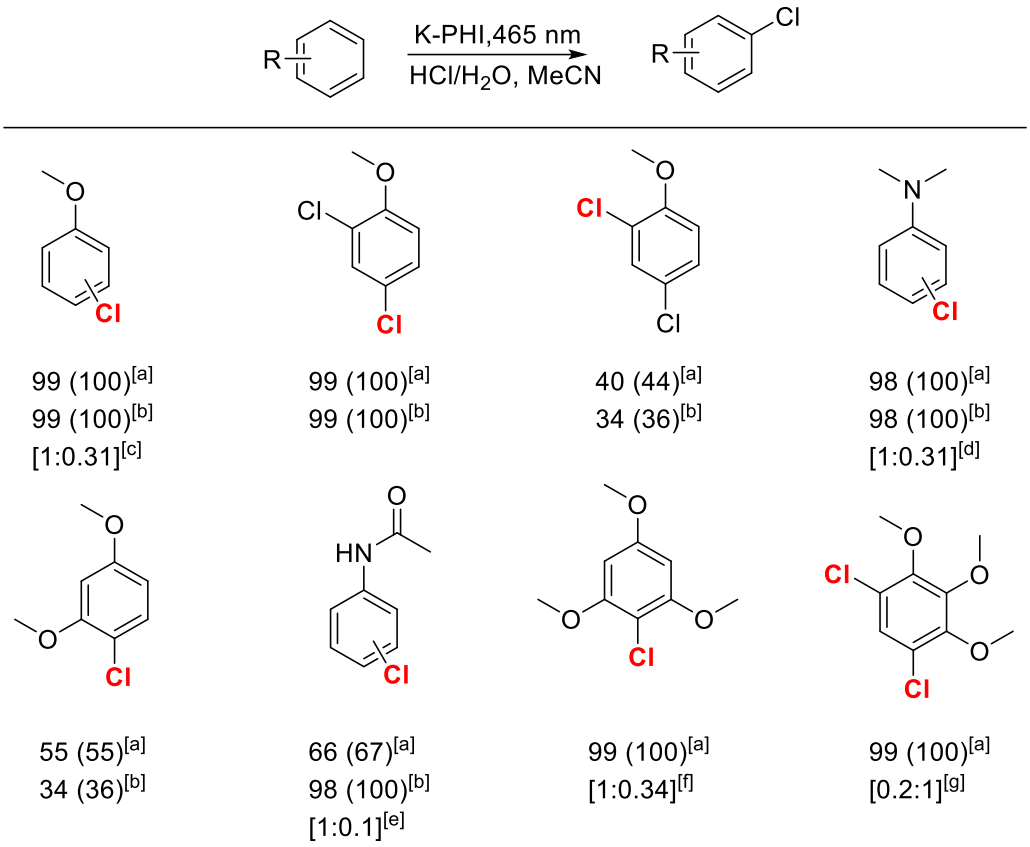

Scheme 8.1. Chlorination of aromatic substrates catalyzed by K-PHI. [a] Substrate 0.02 mmol; HCl (36 wt.%) 0.1 mL; MeCN 0.5 mL; K-PHI 4 mg; electron scavenger – O_2; LED module 465 nm; temperature 30 °C; 24 h. Conversion (given in parentheses) and yield were determined by ^{1}H NMR using *N*,*N*-dimethylaniline or anisole (in case of *N*,*N*-dimethylaniline) as an internal standard. [b] The values obtained when chlorination was performed according to the method A using alcohol as electron donor. [c] The ratio between *p*- and *o*-chloroanisole. [d] The ratio between *p*- and *o*-chloro-N,N-dimethylaniline. [e] The ratio between *N*-(4-chlorophenyl)acetamide and *N*-(2-chlorophenyl)acetamide; [f] the ratio between mono- and dichloro-1,3,5-trimethoxybenzene; [g] The ratio between di- and trichloro-1,2,3-trimethoxybenzene.

The proposed approach of halide anion oxidation was also applied in oxidative bromination reaction under the photocatalytic conditions using aqueous HBr as Br^- source and H^+ donor. The results are summarized in Scheme 8.2. Bromination as well as chlorination worked well with the substrates bearing strong EDG substituents, such as -OMe, -NMe_2, and led to the quantitative conversion and yield. In case of cresols, weak EDG substituents, the reaction occurred not only in the aromatic ring but gave also substantial amount of side-chain

brominated products. Different behavior of cresols compared to the other substrates is explained by the ability of these molecules to give relatively stable benzyl radicals. Therefore, the side chain bromination readily proceeds *via* radical substitution along with electrophilic substitution at the aromatic ring. According to the mechanism described below, radical bromination can be promoted by the formed hydrogen peroxide, which is well-known to act as initiator in radical reactions.

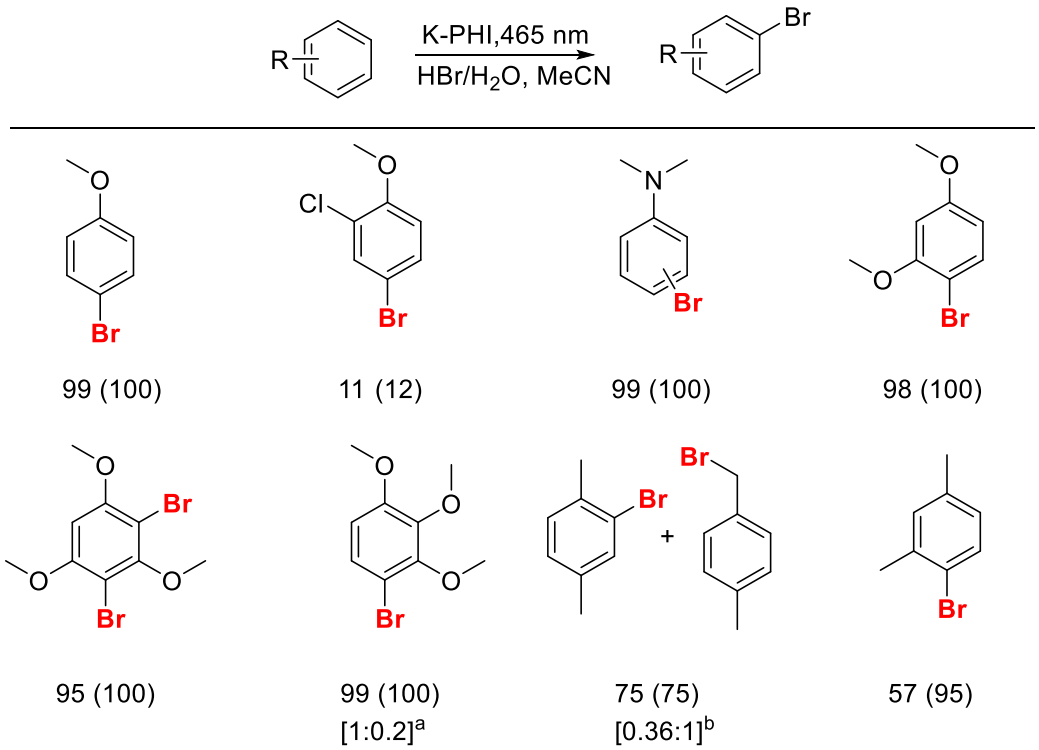

Scheme 8.2. Bromination of aromatic substrates catalyzed by K-PHI. Reaction conditions: substrate 0.02 mmol; HBr (48 wt.%) 0.1 mL; MeCN 0.5 mL; K-PHI 4 mg; electron scavenger – O_2; LED module 465 nm; temperature 30 °C; 24 h. Conversion (given in parentheses) and yield were determined by ^{1}H NMR using *N*,*N*-dimethylaniline or anisole (in case of *N*,*N*-dimethylaniline) as an internal standard. [a] The ratio between mono- and dibromo-1,2,3-trimethoxybenzene is given in brackets. [b] The ratio between aryl- and alkyl- substituted *p*-cresol is given in brackets.

Given that 97% of all water on Earth is sea water with sodium chloride as a major solute, we have used for curiosity this abundant resource (a 35 g·L^{-1} solution of NaCl in water) to run photocatalytic oxidative chlorination of anisole. Chloroanisoles were indeed formed: 62% conversion of anisole and 51% yield using NaCl solution as a source of chlorine were achieved. In accord with the results above, in this case halogenation worked well with the substrates bearing strong EDG too (Scheme 8.3). It should be mentioned that the yields here were not

optimized, *e.g.* by pH variation, as the main purpose was to illustrate the principal possibilities of the use of NaCl.

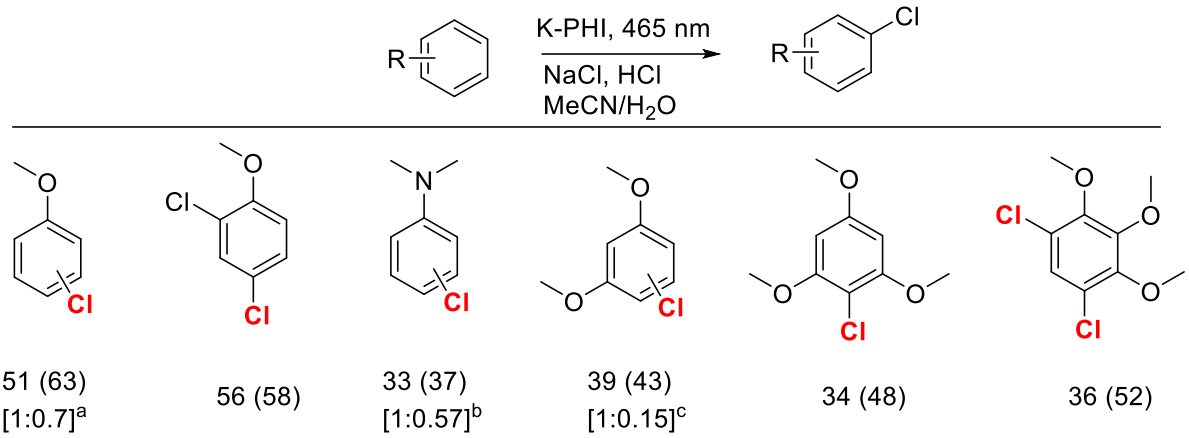

Scheme 8.3. Chlorination of aromatic substrates catalyzed by K-PHI with NaCl. Reaction conditions: substrate 0.06 mmol; HCl (36 wt.%) 20 µL; MeCN 5 mL; K-PHI 5 mg; electron scavenger – O_2; LED module 465 nm; T = 30 °C; 24 h. Conversion (given in parentheses) and yield were determined by ^{1}H NMR using *N*,*N*-dimethylaniline or anisole (in case of *N*,*N*-dimethylaniline) as an internal standard. [a] The ratio between *p*- and *o*-chloroanisole. [b] The ratio between *p*- and *o*-chloro-*N*,*N*-dimethylaniline. [c] The ratio between 4-chloro and 2-chlorodimethoxybenzene.

Mechanism of the oxidative photohalogenation reaction with K-PHI

The mechanism of the oxidative halogenation photocatalyzed by K-PHI is sketched in Figure 8.4. Upon excitation with visible light a bound hole-electron pair is formed. At the conduction band site, O_2 being an electron scavenger is reduced to H_2O_2. As evidenced by the EPR spectrum in the Figure 8.4a, the intensity of the signal related to the uncoupled electron in the catalyst in the presence of the hole scavenger (benzyl amine) under irradiation is much intense and sharper compared to the EPR spectrum in dark.[222] This is explained by the formation of the radical anion of K-PHI in the presence of electron donor. When all components of the chlorination reaction were mixed together, under the irradiation and in the dark there was no significant difference between the EPR spectra, proving that in this case O_2 from the air acts as an electron scavenger, while Cl^- acts as an electron donor. The formation of H_2O_2 was confirmed by its colored complex with Ti(IV), which gave the additional absorption at 400 nm (Figure 8.4b). The ultimate product of O_2 reduction, hydrogen peroxide, reacts readily with the large excess of water and hydrochloric acid giving a rise to the active electrophilic species "HOCl" as the chlorinating agent. This "HOCl" subsequently reacts with anisole in an electrophilic aromatic substitution reaction. At the VB of K-PHI, oxidation of Cl^- to Cl^+ *via* a two-electron process takes place by the photogenerated holes.

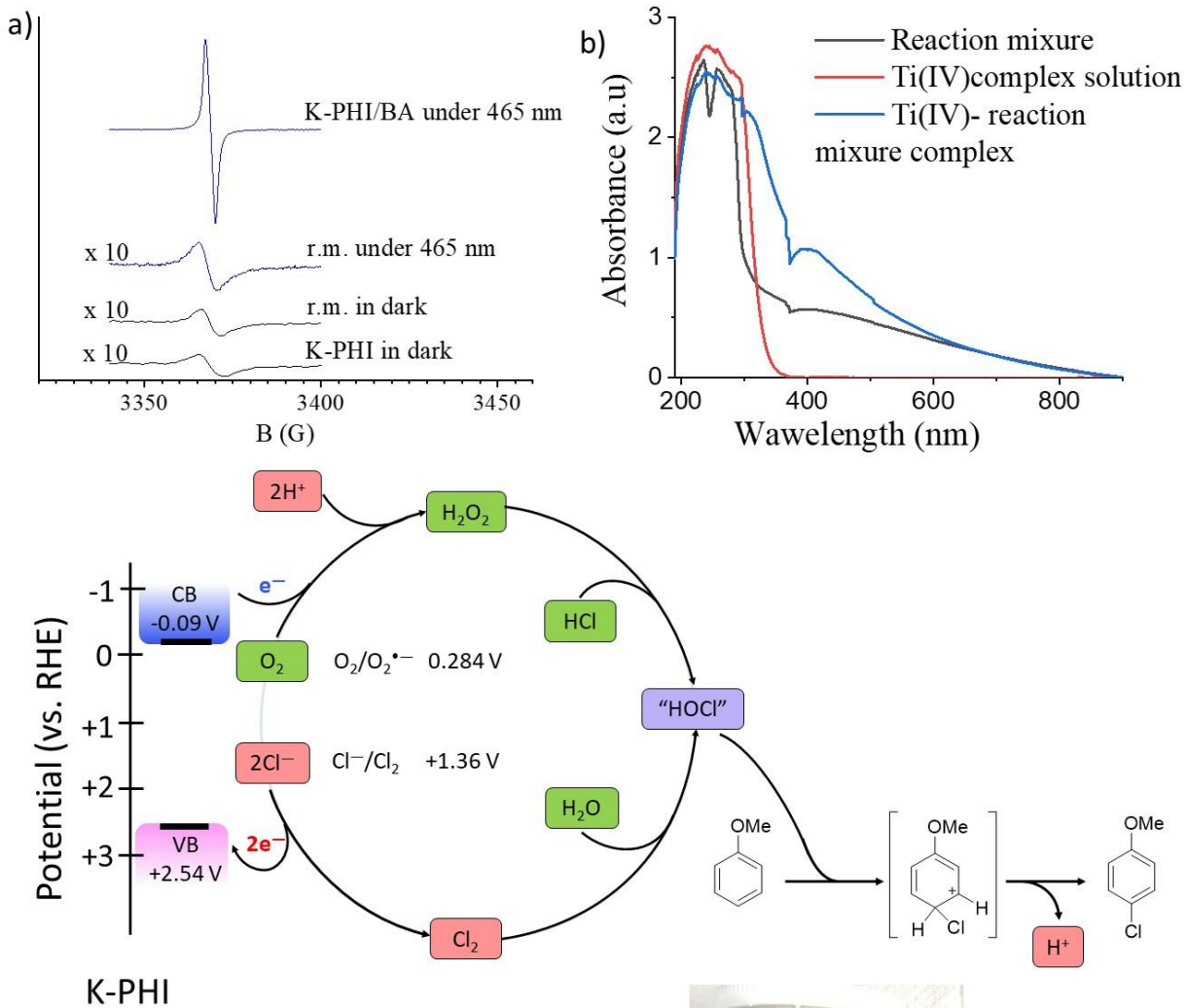

c)

Reagent	Quenches	Yield, %
TEOA	holes	99
O_2	electrons	99
Catalase	H_2O_2	99

d)

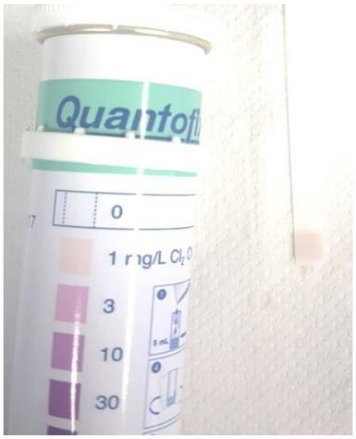

Figure 8.4. A proposed mechanism of electrophilic halogenation *via* Hal^- photooxidation and O_2 reduction, both resulting in the reactive "HOCl" species. Anisole is given as an example. a) EPR spectra of the reaction mixture (anisole 0.02 mmol, HCl , MeCN) in dark and under irradiation (465 nm) magnified 10 times; EPR spectrum of K-PHI in the presence of hole scavenger (benzylamine) under light irradiation (465 nm) b) UV-vis spectra of the reaction mixture and its complex with Ti(IV) d) active chlorine detection using Quantofix Chlorine test strip. c) results of the reactions with different quenchers.

The chloride anion was previously reported as a hole scavenger for both TiO_2 and carbon nitride as the photocatalysts.[223-224]. Quenching of the potentially surface bound Cl^+ by water under liberation of H^+ leads to the active electrophilic "HOCl" species. The presence of active chlorine was detected by Quantofix Chlorine test strips (Figure 8.4d). The relative stability of Cl^+ species in acidic media can be explained as follows. The formation of active species occurs not in the solution, but on the surface and in the pores of the material, which might result in the stabilization of such species by negatively charged surface of K-PHI. Furthermore, the negatively charged nitrogen atoms in PHI structure might bind Cl^+ to form N-Cl bonds as in common organic reagents, similarly to N-Chlorosuccinimide. The exact structure of the active species hiding Cl^+ remains under debate, and herein, for the convenience of mechanism explanation, it is denoted as "HOCl". To prove that formation of "HOCl" occurs *via* two different pathways, the reaction in the presence of few quenchers was carried out (Figure 8.4c). As a result, triethanolamine (TEOA, hole scavenger) and catalase (H_2O_2 scavenger) did not affect the product yield, which means that formation of HOCl proceeds by two different pathways independently: 1) from H_2O_2 and HCl and 2) quenching Cl_2 with H_2O.

In agreement with the proposed mechanism is its high selectivity – only mono chlorinated products were obtained. This implies that the process is electrophilic rather than radical. Moreover, conversion and selectivity observed with both the original König's method and without hole scavenger (benzyl alcohol) are the same, which proves that the reaction proceeds *via* formation of the same electrophilic agent. Interesting, when dry 1,4-dioxane saturated with HCl was used as the solvent and the Cl^- source, 1,4-dioxane polychlorination along with chloroanisoles were detected (Figure 8.5).

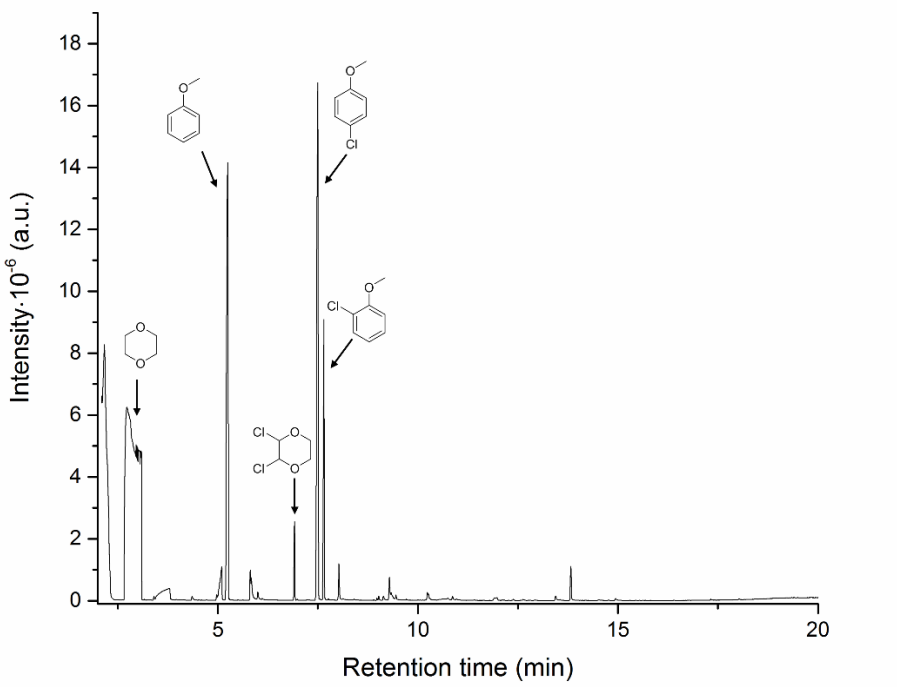

Figure 8.5. Chromatogram of anisole oxidative chlorination performed in 1,4-dioxane saturated with HCl.

This experiment suggests that the presence of water is important to quench Cl^+ *in situ* to give the electrophilic "HOCl" species rather than reacting with Cl^- to give Cl_2. The first enters the electrophilic substitution reaction rather than the radical chlorination reaction typical for Cl_2 under light irradiation.

8.3. Conclusion

In this Chapter, the oxidation potential of K-PHI was shown to be positive enough to oxidize halogen anions to form electrophilic "HOHal" species under visible light. According to the mechanism of this reaction, "HOHal" species can be generated along both paths of photoredox chemistry: 1) quenching of Hal^+, the product of Hal^- two electron oxidation, by water and 2) reaction between H_2O_2, the product of O_2 reduction, with HCl. The generated electrophilic "HOCl" species were employed in oxidative halogenation of electron rich aromatic compounds. A solution of NaCl in water, seawater mimic, was also demonstrated to serve as a suitable chlorinating agent. In addition, it was shown that the proposed approach is also applicable for bromination of aromatic compounds. Potentially, this reaction can also be expanded to run polyhalogenation of aromatic compounds, if water is replaced by a more oxidation stable, but ion solvating medium, e.g. ionic liquids.

9. Chromoselective catalytic synthesis of sulfonylchlorides and sulfamides

9.1. Overwiev

The main component of photocatalysis is obviously light. Would it not be beneficial to alter the reaction selectivity by simply changing the light source? The recent trend in photocatalysis, chromoselective synthesis, offers this unique opportunity. However, the applications are limited to few examples only.

Sulfur is one of the earliest known elements, and its healing power was known to Greeks since antiquity. Since sulfanilamide Prontosil (Daniel Bovet was awarded the Nobel Prize in 1957) became the basis of antibiotics,[225] the sulfonamide group is an ever-present motif in biologically active compounds.[226] Analysis of the common synthesis methods reveals that sulfonyl amide group formation is usually the endpoint of the synthetic route, while other sulfonyl derivatives, such as sulfonyl chlorides, serve as a main point for derivatization.

In this Chapter, the CN semiconductor K-PHI is used for the synthesis of three different products from thioacetates and thiols simply varying energy of incident photons maintaining other conditions identical. Two methods for the synthesis of sulfonyl chlorides of electronically rich and poor structures are proposed. In addition, the application of the method will be extended for the direct one-step synthesis of sulfonyl amides.

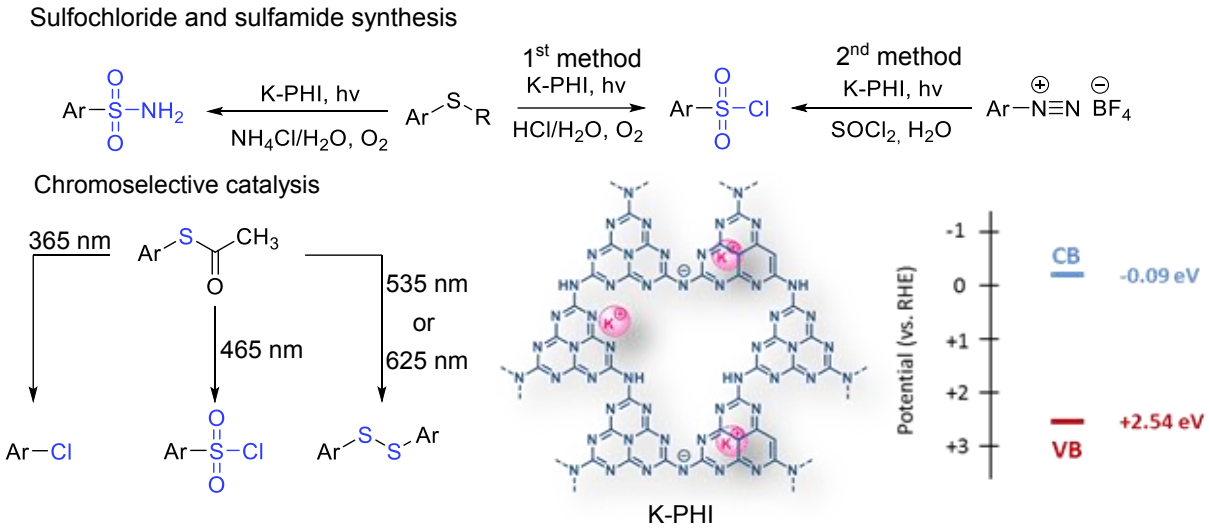

Figure 9.1. The overview of the results presented in the Chapter 9.

9.2. Results - Discussion

The intense efforts have been focused on developing of procedures for sulfonyl amides synthesis and numerous methods have been reported so far.[227] A traditional and most common strategy for the synthesis of complex sulfonyl amides is the addition – elimination process. Sulfonyl chlorides are the most common substrates in this type of reaction. They react with the alkyl or aryl amine to form the corresponding sulfonamide (Scheme 9.1).[228]

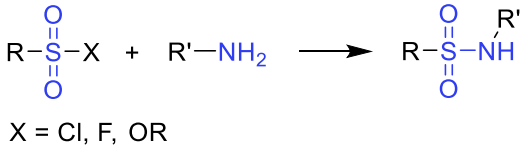

Scheme 9.1. Classical route to sulfonamides.

As a result, the difficulties in sulfonyl amides synthesis come not from the sulfonamide formation step itself, but rather from the synthesis of sulfonyl chlorides. Apart from the application in sulfonyl amide synthesis, sulfonyl chlorides are also used in common laboratory practice for synthesis of several other important functional groups including sulfonyl fluorides, sulfonate esters, sulfones, and sulfinic acids. In photocatalysis, upon one-electron reduction, sulfonyl chlorides give alkyl- and aryl radicals and are used in organic reactions.[229]

It is more than important in organic synthesis not only to conduct the reaction, but rather to provide good selectivity for it. The selectivity is one of the key points in catalysis, when several reaction paths exist. Among different external stimuli that could be possibly used to change selectivity of the reaction, photocatalysis possesses a unique one – energy of incident photons. Several works dedicated to chromoselective catalysis represent an exclusive possibility to tune the reaction outcome by simply changing the light color.[230-232]

One of the most common and classic methods for the synthesis of sulfonyl chlorides is oxidative chlorination of thiocompounds. In this project, as substituted thioacetates are common substrates for oxidative sulfonylchlorination, S-phenylthioacetate was chosen as a model compound. Under blue light irradiation, using HCl in water/acetonitrile mixture and O_2 as electron acceptor, K-PHI afforded phenylsulfonyl chloride in 93% yield (Table 9.1, entry 1). Analysis of the reaction conditions showed that all the components and light are necessary to accomplish the reaction (Table 9.1, entries 2-6).

Table 9.1. Optimization of reaction conditions for phenylsulfonyl chloride synthesis.[a]

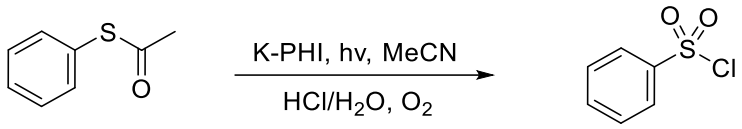

Entry	K-PHI	HCl	Light	Atmosphere	Temperature, ˚C	Yield,%
1	4 mg	HCl/H_2O	465 nm	O_2	25	93
2	-	HCl/H_2O	465 nm	O_2	25	0
3	4 mg	-	465 nm	O_2	25	0
4	4 mg	HCl/H_2O	-	O_2	25	0
5	4 mg	HCl/H_2O	465 nm	Ar	25	0
6[b]	4 mg	HCl/dioxane	465 nm	O_2	25	0
7	4 mg	HCl/H_2O	465 nm	O_2	25	0
8	4 mg	HCl/H_2O	465 nm	O_2	45	0
9	4 mg	HCl/H_2O	465 nm	O_2	60	0

[a] S-Phenylthioacetate 0.035 mmol, K-PHI 4 mg; HCl (36 wt.% in water) 50 μL, H_2O 0.2 mL, MeCN 0.5 mL, T = 25 °C, electron scavenger – O_2, LED module 465 nm, [b] HCl in 1,4-dioxane (4 mol·L^{-1}) 0.2 mL.

The study of the temperature effect revealed that under elevated temperatures no formation of sulfonyl chloride was observed. This might be due to the lower stability of intermediates at high temperatures. Therefore, all further experiments were carried out at ambient temperature.

With regards to a heterogeneous nature of K-PHI, the semiconductor was recycled after the reaction. In the second run using the recovered material, the yield of phenylsulfonyl chloride dropped to 10% (Table 9.2, entry 2). In Chapter 8, it was explained that loss of potassium and partial hydrolysis takes place under the acidic conditions. Considering zeolite-like nature of K-PHI, potassium cations were installed back into the poly(heptazine imide) by treatment with KOH solution, which led to the recovery of the K-PHI activity (Table 9.2, entry 3). For comparison purposes, other types of carbon nitrides and several common homogeneous photoredox complexes were studied in this reaction. Surprisingly, other CN materials and molecular photoredox complexes led to the recovery of starting phenylthioacetate (Table 9.2, entries 4-10). Using the same setup the reaction was performed on 1.4 mmol scale (Table 9.2, entry 11). Furthermore, the utility of the method was proven by the reaction at direct sunlight, which led to the full conversion of the substrate in only 5 hours (Table 9.2, entry 11).

Table 9.2. Semiconductors and molecular photoredox complexes screening. [a]

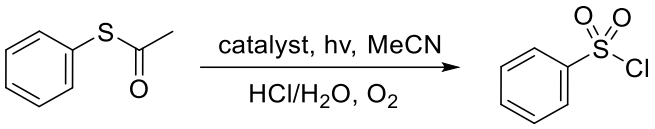

Entry	Material	Light	Time	Conversion,%	Yield,%
1	K-PHI	465 nm	20 h	100	93
2[b]	K-PHI	465 nm	20 h	15	10
3[c]	K-PHI	465 nm	20 h	100	91
4	mpg-CN	465 nm	20 h	0	0
5	g-CN	465 nm	20 h	0	0
6	H-PHI	465 nm	20 h	0	0
7	Na-PHI	465 nm	20 h	0	0
8	RFT	465 nm	20 h	0	0
9	$Ru(bpy)_3Cl_2$	465 nm	20 h	0	0
10	$Ir(ppy)_3$	465 nm	20 h	0	0
11[d]	K-PHI	465 nm	20 h	100	90
12[e]	KPHI	sunlight	4 h	100	95

[a] S-Phenylthioacetate 0.035 mmol, photocatalyst 4 mg, HCl (36 wt.% in water) 50 μL, H_2O 0.2 mL, MeCN 0.5 mL, T = 25 °C, electron scavenger – O_2, LED module 465 nm; [b] recycled catalyst; [c] catalyst recovered with KOH, [d] S-phenylthioacetate 1.4 mmol, K-PHI 4 mg; [e] S-phenylthioacetate 0.035 mmol, K-PHI 4 mg, HCl (36 wt.%) 0.1 mL, H_2O 0.1 mL, MeCN 0.5 mL, T = 25 °C, electron scavenger – O_2, sunlight 70 $mW \cdot cm^{-2}$.

Taking into account reports on chromoselective catalysis by carbon nitrides and molecular catalysts[230,231,232] and multiple reaction paths available for S-phenylthioacetate[233,234,235,236] under the redox conditions, the impact of light source wavelength on selectivity of S-arylthioacetates reactivity was explored. For this experiment, three substrates with different electronic properties were chosen: electron rich 4-methoxyphenylthioacetate, electron deficient 2-trifluorophenylthioacetate and bare phenylthioacetate. The result of the reactions of these substrates under selected wavelengths is shown in Scheme 9.2.

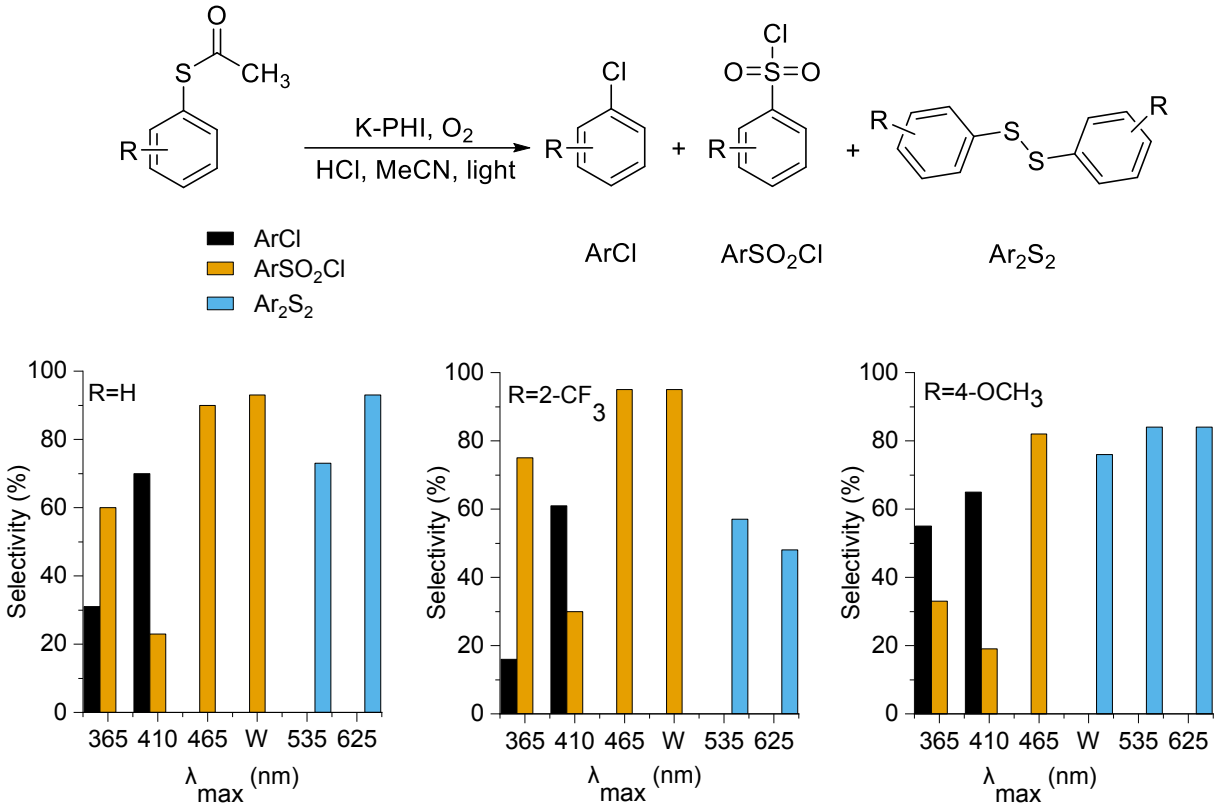

Scheme 9.2. Chromoselective thioacetate oxidation with K-PHI. Conditions: S-Arylthioacetate 0.035 mmol; K-PHI 4 mg; HCl (36 wt.%) 0.1 mL; H_2O 0.1 mL; MeCN 0.5 mL; T = 25 °C; electron scavenger – O_2; irradiation with LED of specific wavelength. λ_{max} denotes maximum emission wavelength of the LED declared by the manufacturer or determined from emission spectra (Figure A30). W stands for LED emitting white light. Conversion is given for reactions where formation of one substrate was observed.

Regardless of the electronic structure of substrate, under UV light irradiation the major product was arylchloride. Phenylthioacetate and 2-trifluorophenylthioacetate under white (λ=410-800 nm) and blue light (λ_{max}=465 nm) irradiation gave selectively sulfonyl chlorides, while for electron rich 4-methoxyphenylthioacetate only blue light was suitable to obtain the corresponding sulfonyl chloride with 61% yield. Moreover, under white light 4-methoxyphenylthioacetate has been converted to the corresponding disulfide. For all substrates, green (λ_{max}=535 nm) and red (λ_{max}=625 nm) photons resulted in formation of diaryldisulfides. The light source screening tests suggest that UV light is preferable for the synthesis of arylchlorides. When synthesis of arylsulfonyl chlorides from arylthioacetates is the target reaction, blue light works the best for all substrates, while white light – for electrondeficient ones. Irradiation with red light is preferable for synthesis of diaryldisulfides from arylthioacetates.

The proposed method was further used for the synthesis of various aromatic sulfonyl chlorides using appropriate light source (Scheme 9.3).

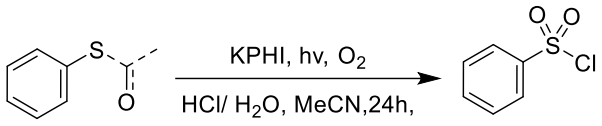

Substrate	Product	Substrate	Product	Substrate	Product
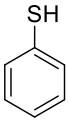	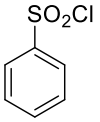 90 (100)[a]	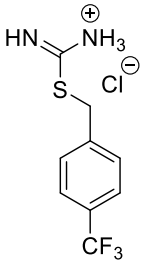	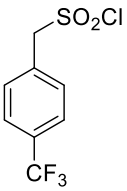 95 (100)[b]	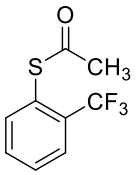	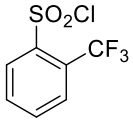 98 (100)[b]
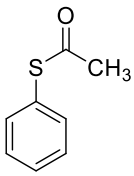	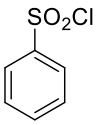 93 (100)[b]	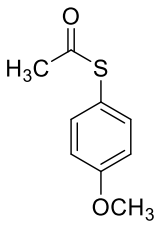	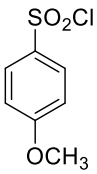 82 (89)[a]	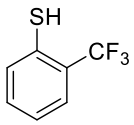	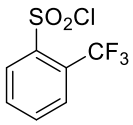 78 (100)[a]
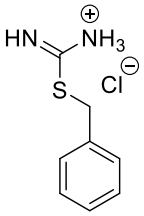	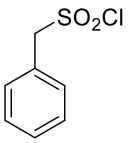 65 (100)[a]	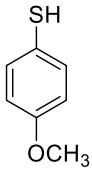	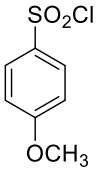 61 (69)[a]	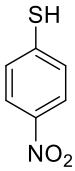	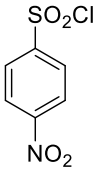 71 (91)[c]

Scheme 9.3. Scope of substrates used in oxidative synthesis of sulfonyl chlorides. Conditions: Substrate 0.035 mmol; K-PHI 4 mg; HCl (36 wt.%) 0.1 mL; H_2O 0.1 mL; MeCN 0.5 mL; T = 25 °C; electron scavenger – O_2; irradiation with LED module. [a] irradiation with LED module 465 nm (46,2 mW cm^{-2}); [b] irradiation with white LED (139,3 mW cm^{-2}); c irradiation with LED module 465 nm (22,6 mW cm^{-2}); yield and conversion (given in parentheses) are given in% and were determined by ^1H NMR.

The proposed method allows for using different thioderivatives as starting substrates, such as bare thioles, thioacetates, and isothiouronium salts. Nature of the thioprecursor does not affect the reaction pathway and the product can be obtained in good yields. For example, phenyl sulfonyl chloride was synthesized from phenylthiol with 85% yield and from phenylthioacetate with 93% yield under the same conditions. Analysis of the obtained results showed that substrates bearing electron withdrawing groups (EWG), such as 4-trifluoromethylphenylthioacetate, gave only arylchlorides. As this can be a result of harsh reaction medium, milder reaction conditions were applied, and therefore less intense source of

light, the white LED, was used. Indeed, sulfonyl chlorides were obtained with good yields. Unsubstituted phenylsulfonyl chloride can be obtained under both sources of light with the same good yields.

Despite synthesis of sulfonyl chlorides is the most challenging on the pathway towards sulfonyl amides, it would be certainly beneficial to develop a method for the direct synthesis of the latter in one step. Slightly modifying the described above procedure, this was achieved. Using NH_4Cl, several sulfonyl amides were synthesized, however blue light was required for all (Scheme 9.4).

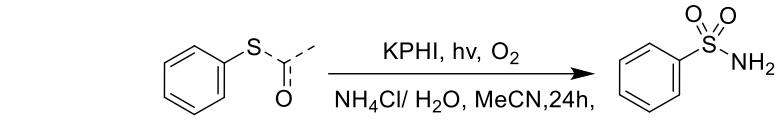

Substrate	Product	Substrate	Product
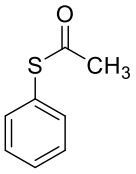	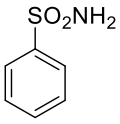	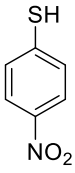	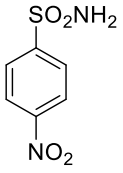
	81 (100)		67 (89)
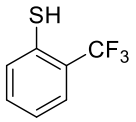		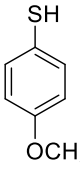	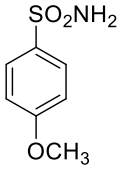
	25 (100)		25 (80)

Scheme 9.4. Scope of substrates used in oxidative synthesis of sulfonyl amides. Conditions: Substrate 0.035 mmol; K-PHI 4 mg; NH_4Cl 10 mg; H_2O 0.2 mL; MeCN 0.5 mL; T = 25 °C; electron scavenger – O_2; irradiation with LED module 465 nm (46,2 mW cm^{-2}); yield and conversion (given in parentheses) are given in% and were determined by ^1H NMR.

To extend the scope of sulfonyl chlorides bearing Br-, Cl-, CN- and MeO_2C- groups, a strategy proposed originally for homogeneous Ru-based catalyst was applied.[237] After replacing Ru-complex by K-PHI and minor adjustments, a series of functionalized sulfonylchlorides were obtained from diazonium salts (Scheme 9.5).

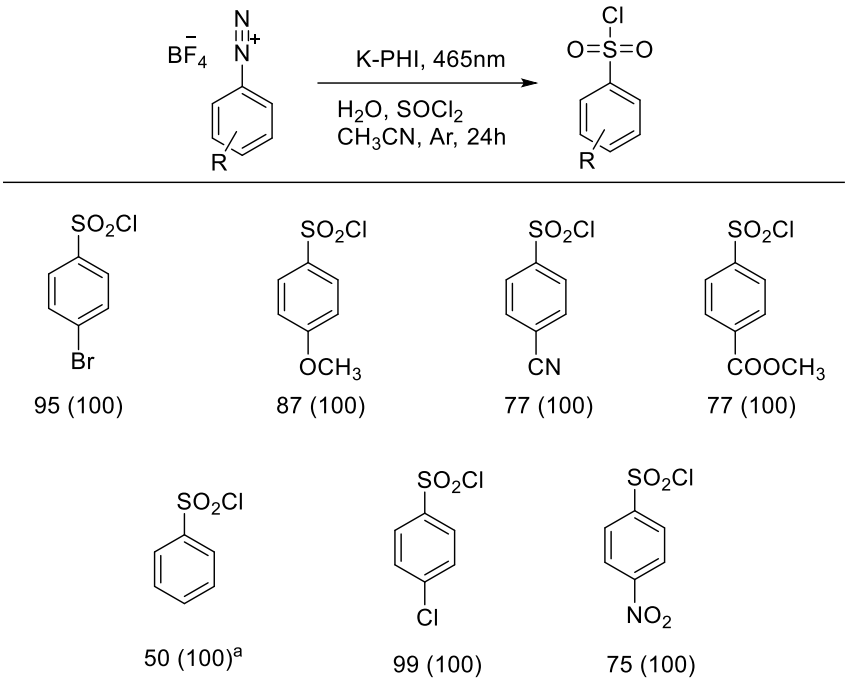

Scheme 9.5. Scope of substrates used in a Meerwein-type synthesis of sulfonyl chlorides. Conditions: substrate 0.025 mmol; K-PHI 4 mg; $SOCl_2$ (19 µL, 0.16 mmol); H_2O (5 µL, 0.28 mmol); MeCN 1 mL; T = 25 °C; atmosphere – Ar; [a] CH_2Cl_2 (1 mL) instead of acetonitrile; yield and conversion (given in parentheses) are given in% and were determined by ^1H NMR

Mechanism discussion

In order to propose the mechanism for the chromoselective transformations of thioacetates, several experiments were conducted. First, non-photocatalytic transformation of thioacetates and sulfonyl chlorides should be excluded. Irradiation of S-phenylthioacetate with 365 nm, 465 nm and 523 nm without K-PHI resulted in zero conversion of the substrate suggesting that chlorobenzene, phenylsulfonylchloride, and disulfide are products of the photocatalytic process. Irradiation of phenylsulfonylchloride with 365 nm, 465 nm, and 525 nm with and without K-PHI also gave zero conversion of the substrate, suggesting that chlorobenzene and diphenyldisulfide did not derive from phenylsulfonylchloride, but the path of formation is governed by the photon wavelength (Table A9, A10).

A general concept of the proposed mechanism of sulfonyl chlorides synthesis from thioderivatives is sketched in Figure 9.2. However, a deeper investigation is needed and further mechanistic studies will be conducted. Absorption of a photon leads to the formation of the singlet excited state of K-PHI that undergoes singlet-triplet intersystem crossing and followed by energy transfer produces singlet oxygen ($^1O_2$). Earlier it was shown that intraband states in K-PHI are responsible for the sequential energy transfer and $^1O_2$ sensitization. In the context

of the discussed sulfonylchloride synthesis, Na-PHI did not give any desired product – indeed there are no intraband states that could be involved in $^1O_2$ sensitization and otherwise would be observed as bands in the visible region of the absorption spectrum (Figure A31).

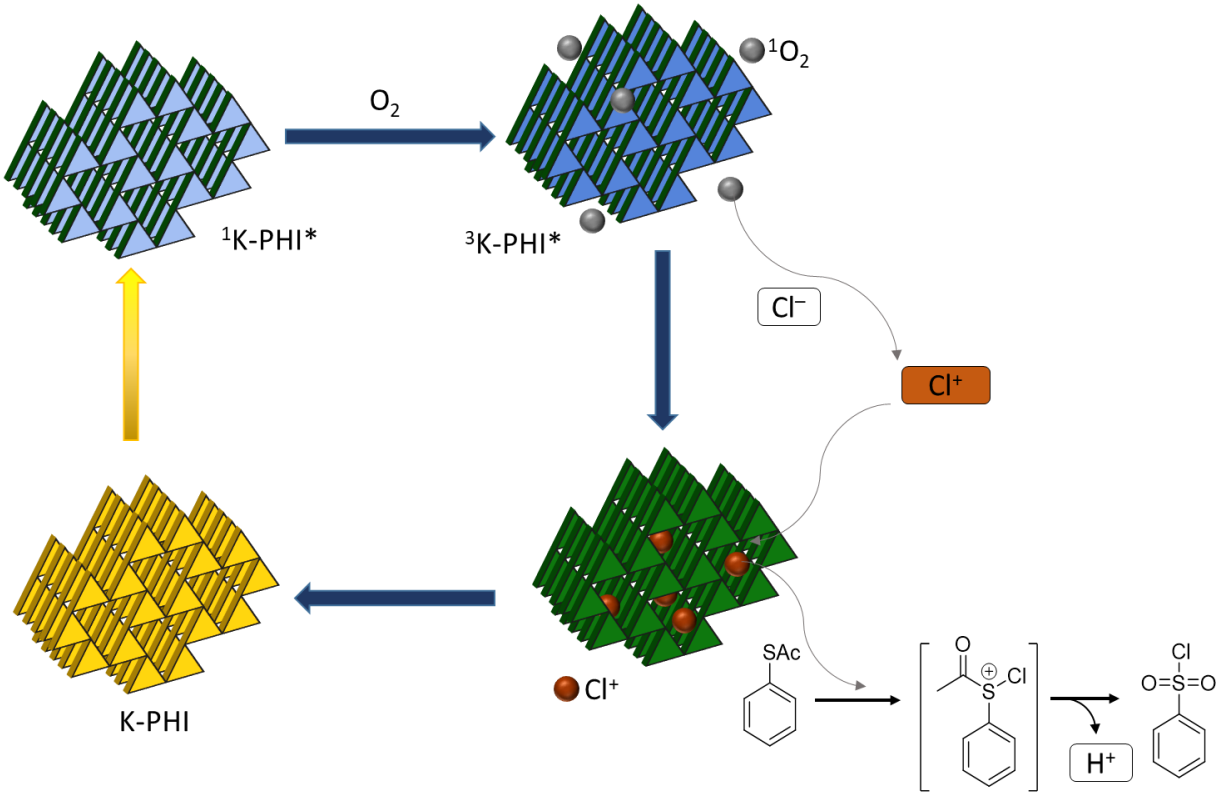

Figure 9.2. Schematic representation of the mechanism of sulfonyl chloride synthesis catalyzed by K-PHI

On the other hand, RFT, $Ir(ppy)_3$, and $Ru(bpy)_3Cl_2$ studied in Table 9.1 are known to produce $^1O_2$. Nevertheless, these compounds did not give any sulfochloride either. Therefore, it can be concluded that the property of the material to generate $^1O_2$ is compulsory, but not sufficient for sulfochloride synthesis. The reason for K-PHI being the only active material in the discussed reaction (Table 9.1) is negatively charged polymeric anion that apparently serves as a temporary storage for Cl– anion oxidation product – Cl^+ or other chlorine species in higher oxidation states. The local structure of the adduct between poly(heptazine imide) anion and active chlorine might be similar of that of *N*-chlorosuccinimide (NCS) – a common source of active chlorine in organic synthesis. Indeed, chemical synthesis of sulfonylchlorides from phenylthioacetate and NCS has been reported.[233]

9.3. Conclusions

In this Chapter, the photocatalytic approach was explored for the synthesis of highly useful organic compounds – sulfonyl amides and their most common precursors – sulfonyl chlorides.

Indeed, two synthetic methods for the synthesis of aromatic sulfonyl chlorides were developed. Oxidative halogenation was found to be an appropriate technique for the electron deficient substrates, whereas sulfochlorination of arene diazonium salts can be used for both electron rich and electron poor substarates. In addition, the possibility of using the method for direct synthesis of sulfonyl amides was shown. A unique component of the photocatalytic approach, light irradiation, allowed for the choromoselective synthesis of different products of thioacetates oxidation. Indeed, three products can be achieved at the same reaction conditions using different lights. The high performance and the practical potential of the proposed method was also shown by reaction at the direct sunlight with a yield of 95% in 5 hours. The further development of chromoselective transformations might serve as a unique platform for the synthesis of different compounds under standardized conditions, only varying the wavelengths of excitation photons. Regarding the chromoselective synthesis with K-PHI presented in this project, further mechanistic studies must be conducted in order to investigate a potential of chromoselective approach for another reactions.

10. Conclusion and Outlook

This thesis is focused on investigation of inherent photocatalytic properties of carbon nitrides that play a significant role in organic photoredox reactions and broadening the applications of heterogeneous catalysis in synthetic organic chemistry. A deep understanding of the reaction outcome – photocatalyst properties connection has been a core of my PhD project.

In the first presented project, the unique semiconductor property to store electrons upon excitation was investigated. The process was given a name - Illumination-Driven Electrons Accumulation in Semiconductor (IDEAS) and was examined for carbon nitrides, mpg-CN and K-PHI. A convenient method for calculation of IDEAS using the reaction of benzylamine oxidation and a common redox indicator, methylviologen, was proposed. Mechanistic studies for the photoinduced electron storage in CNs were conducted. They reveal that not only electrons but also protons are stored in semiconductor to compensate negative charge. The number of trapped electrons for K-PHI was calculated as high as 957±82 $\mu mol \cdot g^{-1}$ under CO_2 atmosphere and 701±46 $\mu mol \cdot g^{-1}$ under Ar, while for mpg-CN it is only 43±5 $\mu mol \cdot g^{-1}$. These results reveal that other structural properties are more important for the process rather than just a high surface area.

The role of CO_2 in the reaction of benzylamine coupling was investigated in Chapter 5. The results suggest that upon CO_2 quenching, benzylamine forms a more efficient electron donor – benzylcarbamic acid. This result combined with IDEAS accelerates the reaction compared to the reaction under Ar atmosphere. Using the proposed method a scope of imines was synthesised with 72-96% yield. In addition, the present moisture in the solvent and gas stream was shown to favour imine formation. Therefore, wet streams of CO_2 might serve as an inexpensive alternative to Ar.

Comparing reaction mixture compositions obtained in the reaction under CO_2 and Ar atmospheres, a formation of additional product, diazetidine-1,3, was detected using Ar, while only imines were achieved under CO_2. In Chapter 6, the tetramerization of benzylic amines to diazetidines-1,3 was studied. While diazetidines-1,3 are quite exotic structures and are not easily achievable, using the proposed method 10 compounds were synthesized, however, limited to the substrates with electron deficient substituents. Revising common photocatalysts, only semiconducting materials were found to be able to catalyze the tetramerization, while common homogeneous materials led to the formation of imines exclusively. The IDEAS was investigated for these semiconductors (CdS, TiO_2) and calculated to be several times lower

than for carbon nitrides K-PHI and Na-PHI. Considering the fact that only limited information available about these compounds, the physical properties of the diazetidines were studied.

Accumulated electrons in carbon nitride K-PHI can be further injected in the present electron acceptor, working as an "electron pump". However, charging and discharging of K-PHI have different kinetics. Due to the high affinity of K-PHI to electrons, electron donor oxidation happens faster than the subsequent discharging of K-PHI$^{\bullet-}$. In the presence of suitable electron donors, this leads to the excessive accumulation of electrons in the material. Multiple electrons can be further injected in the electron acceptor at ones to accomplish a multi-electron reduction reaction. In Chapter 7, the multi-electron reduction of nitroarenes was combined with the novel sustainable media – deep eutectic solvents (DES). In the developed system, DES served as both reaction media and electron donor. Seven N-arylformamides in 17–89% yield and seven substituted anilines in 64-98% yield were synthesized within this approach.

Overall, in Chapters 4-7, the intrinsic feature of carbon nitrides to accumulate electrons was studied from different angles. First, understanding of the IDEAS allowed for the formation of unique compounds – diazetidines-1,3 that are otherwise unavailable using electron acceptors; second, allowed for the highly efficient multi-electron reduction, thanks to the boosted kinetics of electron accumulation.

In the next chapters, the other important property of photocatalyst – redox potentials of VB and CB – was under scrupulous revision. In Chapter 8, K-PHI was shown to be able for the direct oxidation of halide anions to accomplish electrophilic halogenation of aromatic ring. The mechanistic studies revealed that the reaction can occur through two independent pathways, either through Hal^{-} oxidation or through H_2O_2–formation by O_2 reduction. The proposed method was used for chlorination, as well as for bromination of eight substrates bearing electron donating substituents. In addition, NaCl solution, a seawater mimic, was successfully used for chlorination.

In the last project, a unique component of photocatalytic approach – light – was used as a tool for changing the selectivity of reaction. The chromoselective synthesis of three different compounds from S-thiacetates and thiols is presented in Chapter 9. First of all, an oxidative chlorination was used for the synthesis of sulfonyl chlorides bearing electron withdrawing substituents with 61 – 98 % yields. The method was extended to the direct synthesis of sulfonyl amides under blue light irradiation. To accomplish synthesis of sulfonyl chlorides with electron donating substituents, another method was proposed, namely sulfoclorination of arene

diazonium salts. Using the same reaction conditions as for oxidative chlorination only varying the irradiation wavelength, two other compounds can be synthesized form the same starting material. Under irradiation with 365 nm and 410 nm LED, the selectivity of the reaction was shifted towards formation of aryl chlorides. Irradiation with 465 nm and white (410-800 nm) LED leads to the formation of sulfonyl chlorides, while with 535 nm and 625 nm LED – to the disulfides. Furthermore, the high performance and potential for practical use of the method was shown through the reaction under direct sunlight with a pronounced yield of 95% in 5 hours.

All in all, this thesis presents the possibilities of carbon nitrides materials beyond broadly investigated environmental applications, such as water splitting, CO_2 conversion and wastewater treatment. In this thesis, carbon nitrides are revised from the point of rather common laboratory use than large-scale applications, however not excluding the last. Indeed, CNs were shown to be able to catalyze several challenging reactions from the synthetic organic chemistry, such as synthesis of imines, diazetidines-1,3, halogenated arenes, aromatic sulfonyl chlorides and amides. The photocatalytic approach allows for using, first of all, mild conditions, which is one of the most important requirements for the selective synthesis. Selective synthesis, in turn, is one of the key problems in organic chemistry, where commonly more than one path for transformation exists. Indeed, selective transformations were achieved in all presented projects. Photocatalysts in general and carbon nitrides in special are very diverse materials with different physico-chemical properties and, what is more important, with broad possibilities for modification. The application of materials out of established protocols allows for studying the material from various prospections, sometimes revealing new properties and potential use where not expected. Therefore, the interdisciplinary approach for the investigation of heterogeneous catalysis, better understanding of material property – photocatalytic effect connections, will undoubtedly lead to the design of novel efficient materials with desired properties that will allow for selective environmentally benign methods in chemistry, including organic synthesis.

11. Appendix

11.1 List of abbreviations

AC-HRTEM	Aberration corrected high resolution transmission electron microscopy
BA	Benzyl amine
BET	Brunauer-Emmett-Teller
BG	Band gap
CB	Conduction band
CN	Carbon nitride
DES	Deep eutectic solvent
DHPIQ	Dihydropyrroloisoquinolines
DMA	Dimethylacetamide
DMSO	Dimethyl sulfoxide
DSC	Differential scanning calorimetry
EA	Electron acceptor
ED	Electron donor
EDG	Electron donating group
EDX	Energy Dispersive X-Ray
EPR	Electron paramagnetic resonance
e^-/h	Electron-hole
EWG	Electron withdrawing group
EY	Eosin Y
FT-IR	Fourier-transform infrared spectroscopy
GC-MS	Gas chromatography-mass spectrometry
GC-TCD	Gas chromatograhpy with thermal conductivity detector
g-CN	Graphitic carbon nitride
Hal	Halogen
HOMO	Highest occupied molecular orbital
HR-MS	High resolution mass-spectra
HBA	Hydrogen bond acceptor
HBD	Hydrogen bond donor
H-PHI	poly(heptazine imide)
IDEAS	Illumination-Driven Electrons Accumulation in Semiconductor
K-PHI	Potassium poly(heptazine imide)
LED	Light-emitting diode
LUMO	Lowest unoccupied molecular orbital
Me	Methyl
MeOH	Methanol
MeCN	Acetonitrile
MV	Methylviologen
MOF	Metal-organic framework
mpg-CN	Mesoporous graphitic carbon nitride

NHE	Normal hydrogen electrod
NCS	N-chlorosuccinimide
NMR	Nuclear magnetic resonance
Na-PHI	Sodium poly(heptazine imide)
PC	Photocatalyst
RHE	Reversible hydrogen electrode
PXRD	Powder X-Ray diffraction
RFT	Riboflavin tetraacetate
SCE	Saturated calomel electrode
SET	Single-electron transfer
SHE	Standard hydrogen electrode
SMBR	Serial micro-batch photoreator
SPR	Surface plasmon resonance
TEOA	Triethanolamine
THF	Tetrahydrofuran
THIQ	Tetrahydroisoquinoline
TGA-MS	Thermogravimetric analysis –mass spectrometry
TEM	Transmission electron microscopy
TOF	Turnover frequency
TON	Turnover number
UV	Ultraviolet
VB	Valence band
XPS	X-Ray Photoelectron spectroscopy

11.2. Materials

(*R*)-(+)-α-methylbenzylamine (98%, Sigma Aldrich), (^{15}N)benzylamine (98 atom% ^{15}N, Sigma Aldrich), (*1S,2R*)-(+)-2-Amino-1,2-diphenylethanol (99%, Sigma Aldrich), (Ir[dF(CF_3)ppy]$_2$(dtbpy))PF_6 (Sigma Aldrich), (*S*)-(−)-α-methylbenzylamine (99%, Sigma Aldrich), 1,2,3,4-tetrahydroquinoline (≥95%, TCI), 1,2-Dinitrobenzene (99%, Sigma Aldrich), 1,3-dimethoxybenzene (≥98%, Sigma Aldrich), 1-Bromo-3-nitrobenzene (97%, Sigma Aldrich), 1-Chloro-4-nitrobenzene (99%, Sigma Aldrich), 1-Fluoro-4-nitrobenzene (99%, Sigma Aldrich), 2-(Aminomethyl)furan (99%, Sigma Aldrich), 2,3-difluorobenzylamine (97%, Alfa Aesar), 2,4-difluorobenzylamine (98%, TCI), 2,6-difluorobenzylamine (97%, Alfa Aesar), 2-fluorobenzylamine (98%, TCI), 2-methylbenzylamine (98%, Alfa Aesar), 2-trifluoromethylbenzylamine (98%, Alfa Aesar), 2-trifluoromethylthiophenole (≥95%, Maybridge), 3-methylbenzylamine (98%, Acros Organics), 4-Aminobenzylamine (98%, ACROS Organics), 4-fluorobenzylamine (98%, TCI), 4-Hydroxybenzylamine (Sigma Aldrich), 4-methoxybenzylamine (98%, Acros Organics), 4-methoxythiophenole (98%, Acros Organics), 4-methylbenzylamine (98%, Acros Organics), 4-Nitroanisole (99%, ACROS Organics), 4-nitrobenzene thiol (≥95%, TCI), 4-Nitrobenzonitrile (97%, Sigma Aldrich), 4-nitrotoluene (99%, Sigma Aldrich), 4-Trifluoromethyl)benzylamine (98%, Alfa Aesar), 4-trifluoromethylbenzylchloride (98%, Alfa Aesar), Acetonitrile (≥99.8%, Sigma Aldrich), acetonitrile-d3 (99.8 atom% D, Sigma Aldrich), acetyl chloride (≥98%, Sigma Aldrich), Acridine orange (90%, Sigma Aldrich), ammonium acetate (98%, Sigma Aldrich), ammonium formate (98%, AnalaR NORMAPUR), anisole (≥99%, Sigma Aldrich), argon 5.0 (99.999%, water content 3 vol. ppm), Benzonitrile (98%, Fluka), benzyl alcohol (≥99%, Sigma Aldrich), benzyl chloride (99%, Sigma Aldrich), benzylamine (99%, Sigma Aldrich), Cadmium sulfide (98%, Sigma Aldrich), carbon dioxide (99.5%, water content 67 vol. ppm), chloroform-d (99.8 atom% D, Sigma Aldrich), choline chloride (98%, Acros Organics), dichloromethane (≥99.9%, Sigma Aldrich), Diisopropyl azodicarboxylate (94%, Acros Organics), Eosin Y (99%, Sigma Aldrich), ethanol (99.8%, Sigma Aldrich), Fluorescein (Ph.Eur., Sigma Aldrich), Fukuzumi dye (Sigma Aldrich), glycerol (99%, Fluca BioChemika), glycolic acid (98%, Alfa Aesar), HCl (37 wt.%, Carl-Roth), HCl in 1,4-dioxane (4 mol·L-1, TCI), Hydrogen chloride in diethyl ether (2N solution, Acros Organics), methyl viologen dichloride hydrate (98%, Sigma Aldrich), N,N-dimethylaniline (99%, Sigma Aldrich), N-chlorosuccinimide (≥98%, TCI), nitrobenzene (99%, Sigma Aldrich), N-phenylacetanide (99%, Across Organic), o-chloroanisole (98%, Sigma Aldrich), p-chloroanisole (99.5%, Dr.

Ehrenstorfer GmbH), p-Xylylenediamine (99%, Sigma Aldrich), Rhodamin B (≥95%, Sigma Aldrich), Riboflavin (pharma grade, AppliChem), sodium sulphate (≥99%, Sigma Aldrich), S-phenylthioacetate (≥98%, Alfa Aesar), thionyl chloride (≥99%, Sigma Aldrich), thiophenol (97%, Sigma Aldrich), Tin(II) chloride (98%, Alfa Aesar), Titanium dioxide (99,98%, Sigma Aldrich), Triethylamine (99,5%, Sigma Aldrich), Triphenylphosphine (99%, Acros Organics), Tris(2,2′-bipyridyl)dichlororuthenium(II) hexahydrate (99,95%, Sigma Aldrich), Tris[2-phenylpyridinato-C2,N]iridium(III) (99%, Sigma Aldrich), Tungsten(VI) oxide (99,8%, Sigma Aldrich), urea (98%, Sigma Aldrich).

Light source was a LED module composed of 10 × 10 LED units. The screw-capped tubes (total volume 5 mL) were used to perform photocatalytic experiments. Emission spectrum of the blue LED: λ = 461(58) nm and transmittance of the tube is shown on the Figure A1.

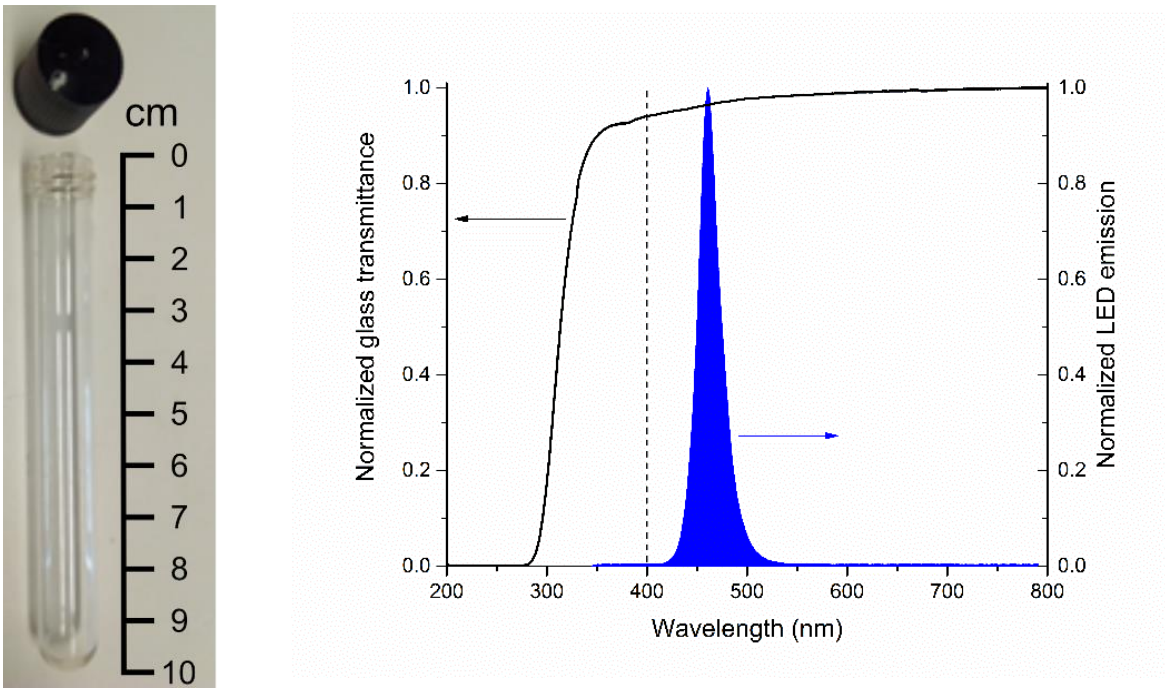

Figure A1. Photoreactor tube used in the photocatalytic experiments (left). Emission spectrum of the LED module (filled) and transmission of the glass tube used for photocatalytic tests (black line) (right).

11.3 Characterization methods

Nuclear magnetic resonance spectroscopy (NMR). Spectra were recorded at ambient temperature on Agilent 400 MHz (at 400 MHz for Protons, 101 MHz for Carbon-13 and 41 MHz for Nitrogen-15). Chemical shifts are reported in ppm versus solvent residual peak: $CDCl_3$ - 7.26 ppm in ^1H NMR, 77.16 ppm in ^{13}C NMR; CD_3CN – 1.94 ppm in ^1H NMR, 1.32, 118.26 ppm in ^{13}C NMR, 44.76 ppm in ^{15}N NMR; D_2O – 4.79 ppm in ^1H NMR; DMSO – 2.50

ppm in ^{1}H NMR, 39.52 in ^{13}C NMR). NMR spectroscopy is a non-destructive technique to analyse the composition of the mixtures, to determine purity of the sample and chemical structure of the analysed compound. The principle of the method relies on a nuclear spin of elemental isotopes. The most common isotopes are ^{1}H, ^{13}C, ^{19}F, ^{15}N, ^{31}P that have a nuclear spin of ½.

Gas chromatography-mass spectrometry (GC-MS). GC-MS of samples were measured using an Agilent 6890 Network GC System coupled with Agilent 5975 Inert Mass Selective detector (electron ionization) and a capillary column (HP-5MS, 30 m, 0.25 mm, 0.25 micron). GC-MS is an analytical technique used to identify and quantify different substances in the test sample. The method is used for analysis of volatile compounds only as the sample is first volatized in gas chromatograph. After the column, components are ionized and accelerated. As a result, ions are separated based on the mass-to-charge (m/z) ratios. Sensitivity of the method is very high as it allows to identify even trace amounts of substance and therefore, is a highly useful technique for investigation of purity of the sample.

High-resolution mass spectral (HR-MS) data were obtained using Waters XEVO G2-XS QTOF with Aquity H-Class (HPLC). The application of the method is the same as of GC/LC-MS, but it requires the use of specialized instrumentation, such as high resolution column and high resolution mass spectrometer. The method is used to improve identification of targeted compound, determining its exact molar mass upon isotope dilution.

Fourier transform infrared (FT-IR) spectra were recorded on Thermo Scientific Nicolet iD5 spectrometer equipped with an attenuated total reflection unit with diamond applying a resolution of 4 cm^{-1}. FT-IR is a vibrational spectroscopic technique that allows for qualitative analysis of samples as it is used to identify functional groups in compounds. The principle of the method relies on the asymmetric molecular stretching, vibration, and rotation of chemical bonds under IR irradiation.

Powder X-Ray diffraction (PXRD) patterns were measured on a Bruker D8 Advance diffractometer equipped with a scintillation counter detector with CuKα radiation ($\lambda = 0.15418$ nm) applying 2θ step size of 0.05° and counting time of 3 s per step. All reference patterns are taken from the database ICDD PDF-4+ (2012 and 2013 edition). XRD provides information about the structure of the crystalline materials. Diffraction peaks in XRD pattern are directly related to the atomic distances in the crystal structure. The position of the diffraction peaks is

determined by the distance between the parallel planes of atoms. Bragg's law describes the diffraction of the wavelength:

$$n\lambda = 2dsin(\theta),$$

where θ is a diffraction angle of the X-ray beam, d is a distance between planes, and n is the order of diffraction.

Nitrogen adsorption/desorption measurements were performed after degassing the samples at 150 °C for 20 hours using a Quantachrome Quadrasorb SI-MP porosimeter at 77.4 K. The specific surface area was calculated by applying the Brunauer-Emmett-Teller (BET) model to adsorption isotherms for $0.05 < p/p0 < 0.3$ using the QuadraWin 5.11 software package. Method involves the adsorption of the gaseous nitrogen by the material at different pressures. The volume of adsorbed gas is recorded and the information is processed based on mathematical models. The method provides information about the surface area of the sample and its pores size distribution.

High resolution transmission electron microscopy (HR-TEM). The measurements were acquired using a double-corrected Jeol ARM200F, equipped with a cold field emission gun and a Gatan GIF Quantum. The used acceleration voltage was 200 kV and the emission was set to 10 μA in order to reduce beam damage. In the TEM microscope, an electron beam of wavelengths in the order of picometers is generated and transmitted through the sample. These small wavelengths allow to study the sample on a nanoscale range and to visualize the sample's morphology, for example, on a fluorescent screen.

Scanning electron microscopy (SEM) images were obtained on a LEO 1550-Gemini microscope. Shimadzu UV 2600 was used to reveal the optical absorbance spectra of powders. *Energy disperse X-ray (EDX)* analysis and morphology observation by scanning electron microscope (SEM) were performed on JSM-7500F (JEOL) equipped with an Oxford Instruments X-MAX80 mm2 detector. Similarly to TEM, method employs an electron beam. However, electrons scattered back from the sample are recordered, while in TEM, electrons that pass through are detected. Obtained images give information about the samples structure.

Electron paramagnetic resonance (EPR) spectra at X-band (9 GHz) and room temperature were recorded on a lab-built spectrometer comprised of an ER041 MR microwave bridge with 4122 SHQE probe head, AEG electromagnet controlled by ER081S/BH15 power supply/controller (Bruker Biospin, Karlsruhe, Germany), a SR810 lock-in amplifier (Stanford Research Systems, USA), and a 53181A frequency counter (Agilent Technologies, USA).

N@C60 was used as g-standard for magnetic field calibration.[238] The concept of EPR is similar to NMR, but electron spins instead of nuclear are excited. The technic is useful for qualitative and quantitative analysis of metal complexes and organic radicals. EPR is a useful technique for investigation of reaction mechanisms that include formation of radicals. EPR is also used to investigate electronic properties of intermediates, which is essential for understanding their reactivity.

X-ray photoelectron spectroscopy (XPS) measurements were carried out in an ultrahigh vacuum (UHV) spectrometer equipped with a VSW Class WA hemispherical electron analyzer. A dual anode Al Kα X-ray source (1486.6 eV) was used as incident radiation. Survey and high resolution spectra were recorded in constant pass energy mode (44 and 22 eV, respectively). During the UPS (He I excitation energy hν=21.23 eV) measurements a bias of 15.32 V was applied to the sample, in order to avoid interference of the spectrometer threshold in the UP spectra. The values of the valence band maximum (VBM) are determined by fitting a straight line into the leading edge.

The XPS measurements in Chapter 7 were performed at the CISSY setup. Mg-Kα-irradiation with an energy of 1253.6 eV was used for excitation. Photoelectrons were analyzed with a VG CLAM 4 hemispherical analyzer. The energy calibration was performed using the Au4f7/2 line, which was set to a binding energy of 84 eV.

XPS provides qualitative and quantitative information about the surface composition of the sample, as a typical analysis depth is less than 5 nm. In XPS, electrons from the inner shell of the atom (core electrons) are investigated. The method gives information about elemental composition, density of electronic states, chemical and electronic state of the elements in the studied material.

Ultraviolet-visible (UV-Vis) spectroscopy was performed on a Shimadzu UV 2600spectrometer equipped with an integrating sphere. Method provides information about optical and electronic properties of material through the light absorption ability. Band gaps of semiconductors can be calculated *via* Tauc plots.

UV-vis absorption spectra of $MV^{\bullet+}$ in MeCN were recorded using T-70 spectrometer.

Light intensity of the LED module was measured by PM400 Optical Power and Energy Meter equipped with the integrating sphere S142C and purchased from Thorlabs.

Elemental analysis was accomplished as combustion analysis using a Vario Micro device. Method allows to identify the elemental ratios of C, N, H, and S atoms in a sample. The sample

is combusted in oxygen atmosphere and gaseous products formed upon decomposition are analysed.

Photoluminescent (PL) emission spectra were recorded on Jasco FP-8300 fluorescence spectrometer equipped with integrating sphere. Method gives information about optical and electronic properties of the studied compound. Under excitation with the beam of light (for example, 360 nm) electrons in the material are excited to the higher energy level and then relax to the ground energy level emitting light, usually visible light. The method is useful to determine excitonic properties and recombination rates in semiconductors.

Thermogravimetric analysis – mass specrroscopy (TGA-MS) was recorded using a thermo microbalance TG 209 F1 Libra (Netzsch, Selb, Germany) coupled with a Thermostar Mass spectrometer (Pfeiffer Vacuum; Asslar/Germany) with a ionization energy of 75 eV. The method is used to measure the change in mass of a sample upon heating with a defined rate and at the same time gives qualitative information on the evolved products.

Gas chromatograms with thermal conductivity detector (GC-TCD) were collected using Agilent Technologies 7890B gas chromatography system equipped with a thermal conductivity detector (TCD). Method allowed for analysis of the gas produced during the photocatalytic experiment. The separation of the gaseous species was performed with an Agilent select permanent gases/CO_2 capillary column set. The latter was consisting of two parallel columns that combine CP Molsive 5 Å for permanent gas analysis, and CP PoraBOnD Q for CO_2 analysis. The detector and oven temperatures used were 200 and 45 °C, respectively. Ar was used as a carrier phase with a flow rate of 14 mL min^{-1}. The injection was performed with a 250-µL gas-tight syringe from SGE Analytical Science. A calibration gas consisting of 20% CO_2, 5% CO, 5% CH_4, 2% H_2, and 1% C_2H_6 mixed in Ar, injected in known volumes, was used to obtain the calibration curve that allowed the quantification of the gas products.

High-performance liquid chromatography (HPLC) of samples from Chapter 5 was performed using an Agilent 1100 Series HPLC System, fitted with a refractive index detector (RID). Samples were prepared by filtration of the liquid phase with 200 nm Nylon filters to remove solid K-PHI particles and by subsequent dilution of 0.1 mL of the MeCN phase with 0.4 mL of mQ-H_2O. For methanol detection, a Rezex ROA-Organic Acid H^+ (8%) column from Phenomenex, heated to 70 °C, was used. The eluent was 5 mM sulphuric acid, with isocratic elution at 0.4 mL/min. The run time was 40 min per sample.

Electrochemical measurements were performed in three electrode cell equipped with the Ar inlet and magnetic stir bar using Biologic potentiostat to control the potential of the working electrode (WE) and EC-Lab v. 10.40 software for data logging. Glassy carbon (diameter 3 mm) was used as a WE, Ag wire in $AgNO_3$ (0.01M) with tetrabutylammonium perchlorate (0.1M) in MeCN as a reference electrode (RE), Pt wire as a counter electrode. Measurements were performed at room temperature (20-25 °C). A solution of tetrabutylammonium perchlorate (0.1M) in MeCN was used as electrolyte. Electrochemical cell was filled with the electrolyte (10 mL). Solution was stirred while dry argon was passed through the solution for ca. 10 min at the rate ca. 5 mL·min^{-1}. Cycling voltammetry (CV) curves were acquired after every 2-3 min in order to confirm absence of the redox peak related to the $O_2/O_2^{\bullet-}$ redox couple centred at ca. −1.19 V vs. RE. CV measurements were performed without stirring, while flow of argon was by-passed above the solution. When no apparent redox peaks at ca. −1.19 V vs. RE were observed, analyte (20 μmol) was added to the electrolyte. The mixture was briefly stirred in order to dissolve the compound. The electrochemical cell was placed into the grounded Faraday's cage. CV curves were acquired scanning continuously the region from 0 V to +2 V, from +2 V to −2 V and back from −2 V to 0 V. Typically 3 scans were acquired. The scanning rate was 50 mV·s^{-1}. After the CV measurement was finished, ferrocene (3.72 mg, 20 μmol) was added to the electrolyte. The solution was stirred for ca. 2 min in order to completely dissolve ferrocene. CV measurements were repeated scanning the region from +0.5 V to −0.5 V at the scanning rate 50 mV·s^{-1}. The potential of the WE was then recalculated using the equation:

$$U_{corr} = U_{WE} - E_{Fc/Fc^+} = U_{WE} - E_{Fc/Fc^+}$$

where U_{WE} – potential of the WE versus RE, V; E_{Fc/Fc^+} – the redox potential of the Fc/Fc^+ couple versus the RE. Determined as an average between reduction and oxidation peaks of the Fc/Fc^+, V.

11.4. Synthesis of photocatalysts

<u>mpg-CN preparation</u>

mpg-CN was prepared according to the procedure described in literature.[151] Cyanamide (3.0 g) and Ludox HS-40 (7.5 g) were mixed in a 10 mL glass vial. The mixture was stirred at room temperature for 30 min until cyanamide has completely dissolved. The resultant solution was stirred at +60°C for 16 h until water has completely evaporated. The magnetic stirrer bar was

removed and white solid was transferred to the porcelain crucible and heated under N_2 flow in the oven. The temperature was increased from room temperature to 550 °C within 4 h and maintained at 550°C for 4 h. The crucible was spontaneously cooled to room temperature. The solid from the crucible was briefly grinded in the mortar and transferred to the polypropylene bottle. A solution of $(NH_4)HF_2$ (0.24 g·mL^{-1}, 50 mL) was added and suspension was stirred at room temperature for 24 h. The solid was filtered, thoroughly washed with water, once with ethanol and dried in vacuum (55°C, 20 mbar) overnight.

g-CN preparation

g- CN was prepared according to the following procedure. Dicyandiamide (15 g) was heated to 600 °C with a ramp 2.4 °C under N_2 flow. After cooling to room temperature, solid was finely ground in mortar.

H-PHI preparation

H-PHI was prepared according to the following procedure. A suspension of K-PHI (408 mg) in HCl (18 mL, 0.1 M) was stirred at room temperature for 24 h. The suspension was subjected to centrifugation (13000 rpm, 10 min). Supernatant layer was decanted and deionized water (2 mL) was added to the solid. The solid was dispersed by vortex mixer and centrifuged (13000 rpm, 10 min) again. Supernatant layer was decanted and washing procedure was repeated in total 7 times until suspension pH 7. The solid was dried in vacuum overnight.

K-PHI preparation

K-PHI was synthesized according to a previously described procedure.[239] A mixture of lithium chloride (3.71 g), potassium chloride (4.54 g) and 5-aminotetrazole (1.65 g) was ground in ball mill for 5 min at the shaking rate 25 s^{-1}. Reaction mixtures were transferred into porcelain crucibles and covered with lids. Crucibles were placed in the oven and heated under constant nitrogen flow (15 L·min^{-1}) and atmospheric pressure at a following temperature regime: heating from room temperature to 550 °C for 4 hours, annealing at 550 °C for 4 hours. After completion of the heating program, the crucibles were allowed to cool slowly to room temperature under nitrogen flow. The crude products were removed from the crucibles, washed with deionized water (100 mL) for 3 hours in order to remove salts, then filtered, extensively washed with deionized water and dried in a vacuum oven (20 mbar) at 50 °C for 15 h.

K-PHI was characterized by different techniques and the summary is given in Figures A2, A3.[240] The number and position of diffraction peaks in the PXRD pattern are identical to the ones reported earlier.[241,242] The valence band maximum in K-PHI determined by ultraviolet

photoelectron spectroscopy (UPS) is located at ~2.5 V (Figure A2e). K-PHI has a main onset of absorption at 460 nm related to π-π* transitions and a band of lower intensity with the edge at 650 nm (n-π* transitions) (Figure A2f). Using the π-π* band as responsible for the photocatalytic activity optical band gap of 2.72 eV was determined. K-PHI shows maximum of fluorescence at ~500 nm upon sample excitation with 350 nm (Figure A2g). K-PHI does not possess distinct porosity as evidenced by the N_2 sorption isotherm (Figure A2h). The specific surface area is 89 $m^2 \cdot g^{-1}$. FT-IR shows peaks typical for K-PHI and carbon nitrides in general: 800 cm^{-1} (heptazine out-of-plane bending), 916 cm^{-1}, 985 cm^{-1} (symmetric vibrations of the metal–NC_2 moiety), 1116 cm^{-1}-1390 cm^{-1} (C-O stretch), 1574 cm^{-1} (secondary amine N-H bend), 1653 cm^{-1} (primary amine N-H bend), 2184 cm^{-1} (nitrile stretch), 2500-3600 cm^{-1} (N-H stretch) (Figure A2i).[243] In water K-PHI falls into particles from ca. 50 to 200 nm in diameter with the average size 94 nm (Figure A2j). The ordered structure of the catalyst is readily observed in the high resolution transmission electron microscopy (HR-TEM) image of K-PHI (Figure A2l). Relaxation of the excited state via radiative path occurs within 0.66 ns (Figure A3).

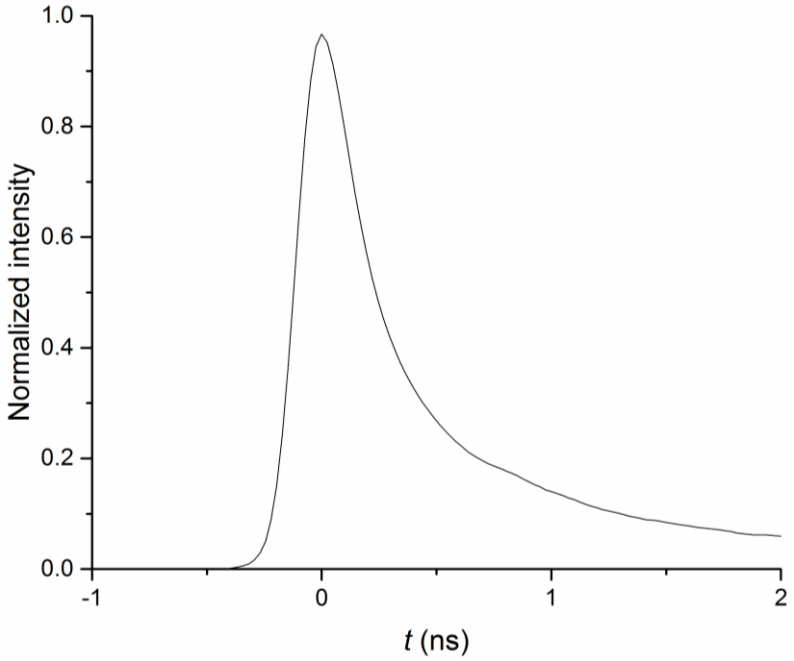

Figure A3. Time-resolved fluorescence spectrum of K-PHI particles suspension in degassed MeCN excited with 405 nm.

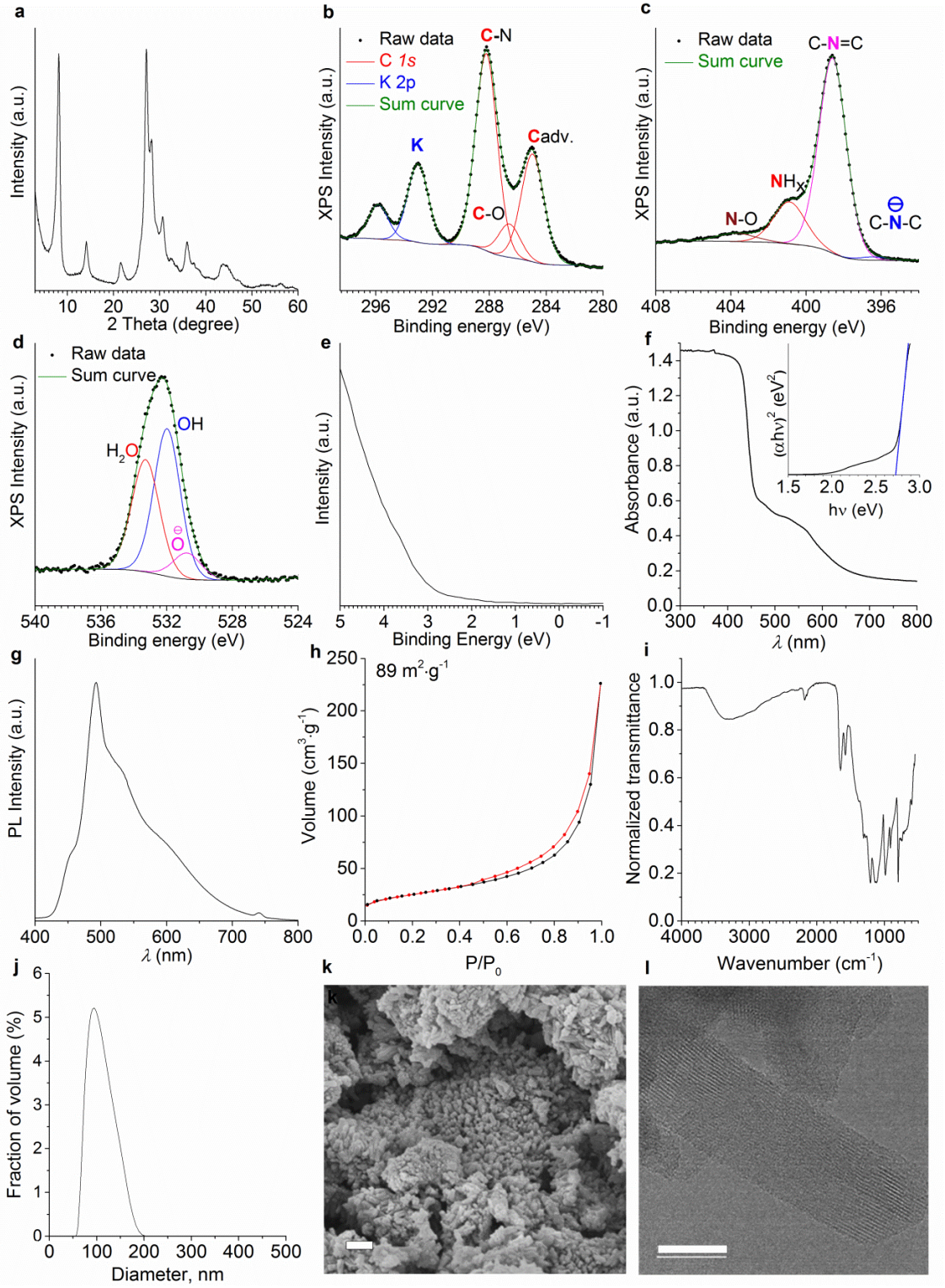

Figure A2. K-PHI characterization. a) PXRD pattern of K-PHI; b) XPS C 1s and K 2p spectra of K-PHI; c) XPS N 1s spectrum of K-PHI; d) XPS O 1s spectrum of K-PHI; e) UPS spectrum of K-PHI; f) UV-vis absorption spectrum of K-PHI with Tauc plot as inset assuming that K-PHI is a direct semiconductor; g) PL spectrum of K-PHI obtained upon excitation with 350 nm; h) N_2 sorption isotherm measured at 77 K. BET surface area; i) FT-IR spectrum of K-PHI; j) Dynamic light scattering (DLS) analysis of K-PHI suspension in water; k) representative SEM image of K-PHI photocatalyst. Scale bar 200 nm; l) AC-HRTEM image of K-PHI photocatalyst. Scale bar 20 nm.

Pt@K-PHI preparation

To the suspension of KPHI (300 mg) in ethanol (70 mL) NaBH4 (12 mg) was added. After 5 min, 8% solution of chloroplatinic acid in water (78 μL) diluted with water (50 mL) was added dropwise. The mixture was stirred for 30 min and additional portion of NaBH4 (12 mg) was added. After stirring for 30 min, catalysts was separated by centrifugation, washed 3 times with water (10 mL) and dried.

Na-PHI preparation

Na-PHI was prepared according to the literature procedure. [244] Melamine (1 g) was grinded with NaCl (10 g). Reaction mixture was transferred into a porcelain crucible and covered with lid. Crucible was placed in the oven and heated under constant nitrogen flow (15 $L \cdot min^{-1}$) to 600 °C with a heating rate of 2.3 °C/min, held at 600 °C for 4 hours, then allowed to cool down. The crude product was removed from the crucible, washed with deionized water (100 mL), isolated by filtration, then thoroughly washed with deionized water on the filter (100 mL) and dried in a vacuum oven at 50 °C for 15 h.

RFT synthesis

RFT was prepared according to the following procedure. Riboflavin (0.5 g) was suspended in a mixture of acetic acid (20 mL) and acetic anhydride (20 mL). To the mixture $HClO_4$ (70%, 0.1 mL) was added dropwise and the resulting mixture was stirred at 40 °C for 1h. After cooling, water (40 mL) was added and mixture was extracted with CH_2Cl_2 (4 times, 50 mL). Organic layer was washed with water (twice, 40 mL) and NaHCO3 (solution 40 mL), dried with Na_2SO_4 and concentrated.

11.5. Supplementary information to the Chapter 4

A procedure of K-PHI radical anion quenching with methyl viologen

A thick-walled glass tube equipped with a Teflon valve and side arm was charged with benzylamine (0.2 mmol), K-PHI (typically 5 mg, or other mass if specified), MeCN (3 mL, *V* in the equation below) and a stir bar. The mixture was degassed using freeze-pump-thaw method (3 times, liquid nitrogen, residual pressure $7 \cdot 10^{-5}$ bar) and refilled with CO_2 (1 bar). The mixture was stirred at 35 °C under blue LED irradiation (λ_{max} = 461 nm, $0.0517 \pm 3 \cdot 10^{-5}$ $mW \cdot cm^{-2}$) for 24 h. The tube with the reaction mixtures was transferred into the glove box (residual O_2 concentration <0.1 ppm, residual H_2O concentration <0.1 ppm) and 0.1 mmol of methyl viologen dichloride was added to each mixture. The tube end was covered with the PTFE-separator and firmly closed with a cap. The sealed tube was removed from the glove box

and the mixture was vigorously stirred for 3 h. The color of the reaction mixture changed from greenish to deep blue. The catalyst was allowed to precipitate at the bottom of the tube. The tubes were again transferred into the glove box and solutions for UV-vis analysis were prepared: V_2 volume of the reaction mixture was taken from each tube and diluted with MeCN to the total volume V_1. These solutions in a closed screw capped QS quartz cuvette were used for UV-vis measurements. For calculations of trapped electrons average numbers of three measurements were used.

Number of electrons (μmol) trapped in K-PHI was calculated according to the equation:

$$N = \frac{A \cdot V_1}{\varepsilon \cdot L \cdot V_2} \cdot V \cdot 1000$$

A – absorbance of $MV^{\cdot+}$ solution at 605 nm; V_1 – volume of the diluted solution, which was used for the analysis, mL; V_2 – volume of the reaction mixture with $MV^{\cdot+}$ taken for analysis, mL; ε – extinction coefficient of $MV^{\cdot+}$, $M^{-1}cm^{-1}$; L – optical path of the QS quartz cuvette, cm; V – total volume of the reaction mixture, mL.

Preparation of N-benzylidene benzylamine

A screw-capped tube (5 mL) was charged with benzylamine (0.05 mmol), K-PHI (5 mg), MeCN (3 mL) and magnetic stir bar. The mixture was degassed using freeze-pump-thaw method (3 times, liquid nitrogen, residual pressure $7 \cdot 10^{-5}$ bar) and refilled with CO_2. The mixture was stirred at 35 °C under blue LED irradiation (λ_{max} = 461 nm, $0.0517 \pm 3 \cdot 10^{-5}$ $mW \cdot cm^{-2}$) for 24 h. After that time, the catalyst was separated by centrifugation. The acetonitrile solution was concentrated in vacuum and analyzed by ^1H NMR. NMR spectrum was identical to the reported earlier.[245]

^1H NMR (400 MHz, $CDCl_3$) δ 8.40 (s, 1H), 7.78 (dd, J = 6.7, 2.6 Hz, 2H), 7.45 – 7.31 (m, 8H), 4.82 (s, 2H).

A procedure of K-PHI radical anion quenching with AgOTf

A screw-capped tube (5 mL) was charged with benzylamine (0.2 mmol), K-PHI (5 mg), MeCN (3 mL) and magnetic stir bar. The mixture was degassed using freeze-pump-thaw method (3 times, liquid nitrogen, residual pressure $7 \cdot 10^{-5}$ bar) and refilled with CO_2. Four tubes were prepared using the same amount of the reagents. The mixture was stirred at 35 °C under blue LED irradiation (λ_{max} = 461 nm, $0.0517 \pm 3 \cdot 10^{-5}$ $mW \cdot cm^{-2}$) for 72 h. The tubes were transferred into the glove box (residual O_2 concentration <0.1 ppm, residual H_2O concentration <0.1 ppm).

Reaction mixtures of dark green color from four tubes were combined in a 50 mL Schlenk flask. Schlenk flask was covered with a rubber septum and removed from the glove box. A freshly prepared solution of silver(I) triflate in deoxygenated water (17.6 mL, 0.0681 mol·L^{-1}) was injected through the septum into the Schlenk flask. Suspension immediately changed color from green to black. The solid was separated by centrifugation (13000 rpm, 5 min), washed with water, acetonitrile and ethanol. The solutions were combined and concentrated in vacuum (50 °C, 20 mbar). The resulting residue was washed with benzene, dried in vacuum (50°C, 20 mbar) and was identified as benzylammonium triflate.

Preparation of (^{15}N)benzylcarbamic acid

An NMR tube was charged with (^{15}N)benzylamine (5 µL), CD_3CN (0.4 mL) and DMSO-d_6 (0.1 mL). CO_2 was bubbled through the solution for 1 minute and NMR spectra were recordered.

^{1}H NMR (400 MHz, CD_3CN) δ 7.26 (ddt, J = 21.2, 13.9, 7.2 Hz, 5H), 6.69 (dt, J = 92.1, 6.2 Hz, 1H), 4.18 (d, J = 5.9 Hz, 2H). ^{13}C NMR (101 MHz, CD_3CN) δ 158.59 (d, J = 24.8 Hz), 141.19, 129.04, 127.74, 127.45, 125.40, 44.69 (d, J = 11.6 Hz). ^{15}N NMR (41 MHz, CD_3CN) δ 83.49 (d, J = 92.3 Hz).

Preparation of benzylcarbamic acid

CO_2 was passed through a solution of benzylamine (80 µL) in MeCN (5 mL). White precipitate was filtered of and washed briefly with MeCN. Yield: 41%.

Degradation of benzylcarbamic acid

A screw-capped tube (5 mL) was charged with benzylcarbamic acid (0.05 mmol), K-PHI (5 mg), MeCN (3 mL) and magnetic stir bar. The mixture was degassed using freeze-pump-thaw method (3 times, liquid nitrogen, residual pressure $7\cdot10^{-5}$ bar) and refilled with CO_2. The mixture was stirred at 35 °C under blue LED irradiation (λ_{max} = 461 nm, $0.0517\pm3\cdot10^{-5}$ mW·cm^{-2}) for 24 h. Catalyst was separated by centrifugation. An aliquot (0.3 mL) of the MeCN solution was transferred into the NMR tube, CD_3CN (0.3 mL) and CH_2Cl_4 (0.5 µL) as an internal standard were added to the NMR tube.

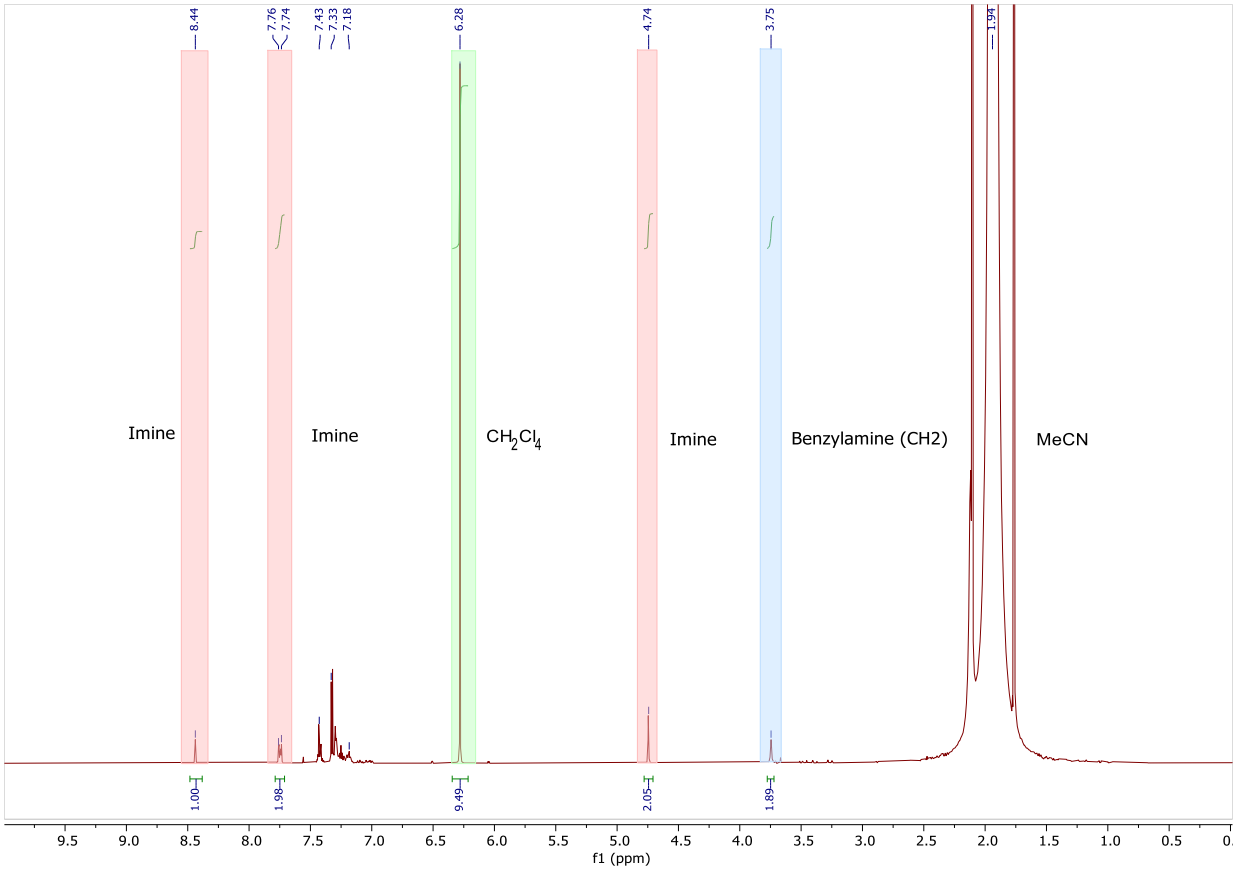

Figure A4. ^{1}H NMR spectrum of the reaction mixture obtained using benzylcarbamic acid as an electron donor in IDEAS experiment. Characteristic proton peaks of imine, benzylamine and internal standard are labeled.

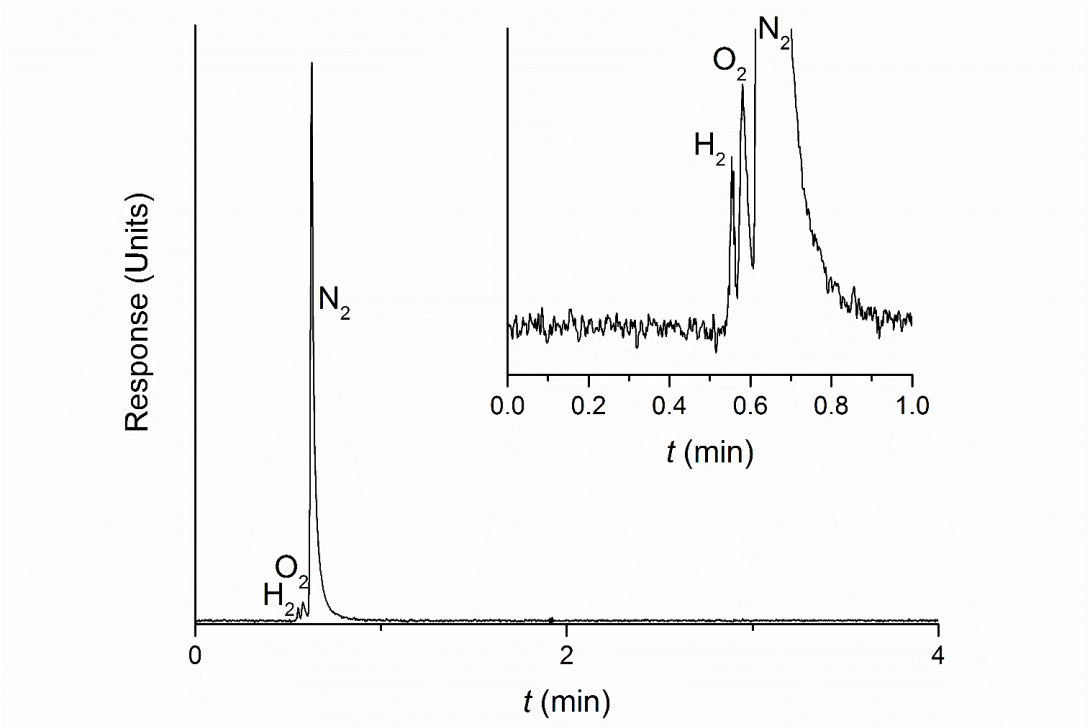

Figure A5. GC-TCD of the reaction mixture headspace. The peaks of N_2 and O_2 are due to imperfect connection between the syringe barrel and a plunge during transfer the reaction mixture head space from the reactor to gas chromatograph. The amount of H_2 quantified in this experiment was 1.48 nmol.

11.6. Supplementary information to the Chapter 5

Typical procedure for preparation of imines from benzylamines

A screw-capped tube (5 mL) was charged with benzylamine (0.05 mmol), K-PHI (5 mg), MeCN (3 mL) and magnetic stir bar. The mixture was degassed using freeze-pump-thaw method (3 times, liquid nitrogen, residual pressure $7 \cdot 10^{-5}$ bar) and refilled with CO_2. The mixture was stirred at 35 °C under blue LED irradiation (λ_{max} = 461 nm, $0.0517 \pm 3 \cdot 10^{-5}$ mW·cm^{-2}) for 24 h. After that time the catalyst was separated by centrifugation. The acetonitrile solution was concentrated in vacuum (50 °C, 100 mbar) and analyzed by ^{1}H NMR.

Extraction of ammonium formate from K-PHI with D_2O/HCl.

A screw-capped tube (5 mL) was charged with ^{15}N-labeled benzylamine (0.2 mmol), K-PHI (5 mg), MeCN (3 mL) and a magnetic stir bar. The mixture was degassed using freeze-pump-thaw method (3 times, liquid nitrogen, residual pressure 7×10^{-5} bar) and refilled with CO_2. The mixture was stirred at 35 °C (oil bath temperature) under blue LED irradiation (λ_{max} = 461 nm, 51.70(3) mW cm^{-2}) for 72 h. The catalyst was separated by centrifugation (3 min, 13000 rpm): the liquid phase was decanted and the catalyst was washed with acetonitrile (3 times, 2 mL each) using the centrifuge (3 min, 13000 rpm) to separate the catalyst. Acetonitrile solutions were combined, concentrated in vacuum, and analysed by ^{1}H NMR. The centrifuged solid was further washed with water (2 mL), using the centrifuge (3 min, 13000 rpm) to separate the catalyst. This was transferred into a 5-mL vial and D_2O (0.4 mL) and HCl (20 µL, 37 wt.%) were added. The suspension was stirred at room temperature for 60 h. The catalyst was separated by centrifugation (5 min, 13000 rpm) and washed with D_2O (0.2 mL). The aqueous solutions were combined directly in a NMR tube and analysed by ^{1}H NMR.

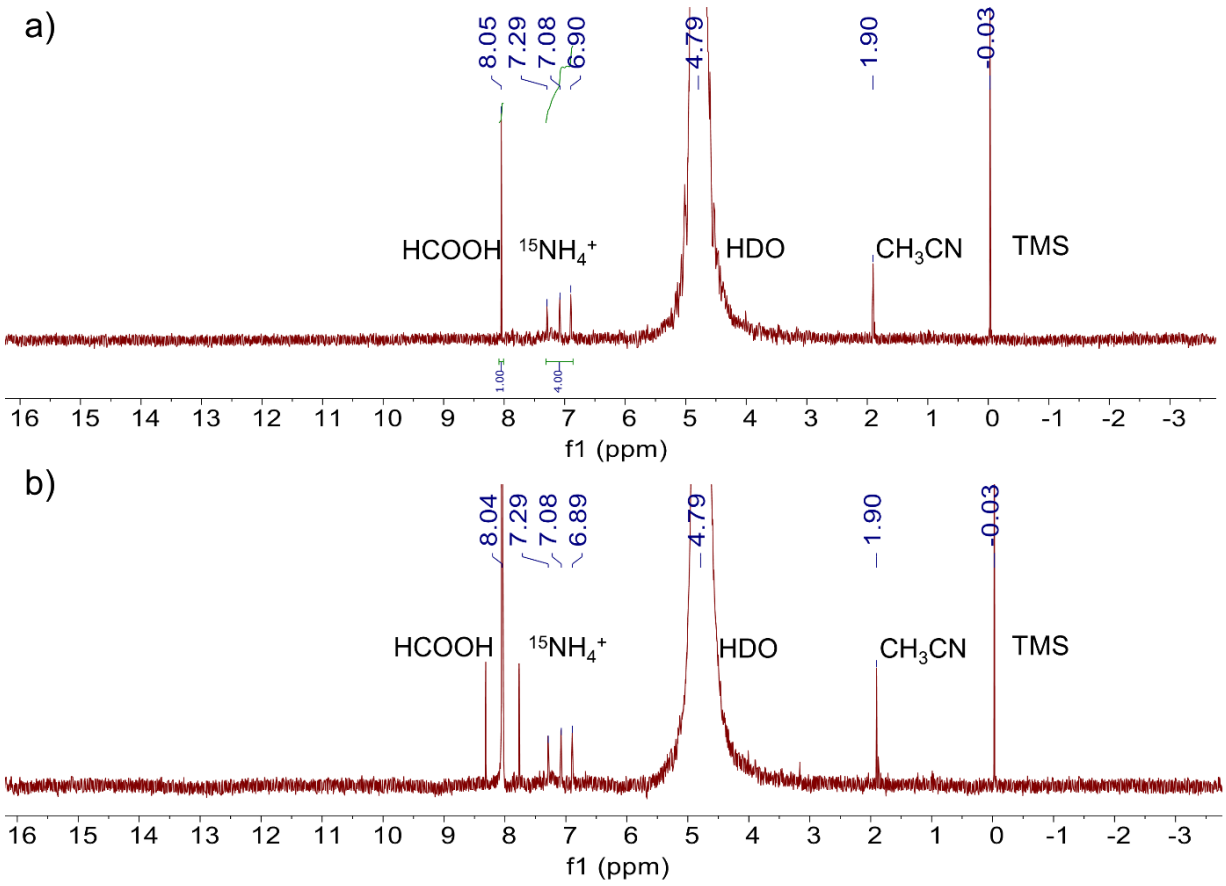

Figure A6. a) ^{1}H NMR spectrum of the solution obtained after extraction of K-PHI with D_2O/HCl; b) ^{1}H NMR spectrum of the solution after addition of formic acid (0.5 µL) to the same NMR tube. The intensity of the singlet at 8.05 ppm was enhanced and no additional peak around ~8 ppm appeared. Therefore, the singlet at 8.05 ppm is related to the formyl proton in the molecule of formic acid.

Table A1. Water content for various solvent/gas combinations in a 6 mL photoreactor tube. [a]

Combination	Component	H_2O content[a]	$V_{component}$ / mL	Amount of H_2O / µmol (ppm)
1	CH_3CN	0.005%	3	8.3
	Ar	0.0003%	3	0.2
			Total:	8.5 (147)
2	CH_3CN	0.005%	3	8.3
	CO_2	0.0067%	3	11.2
			Total:	19.5 (338)
3	CD_3CN	0.02%	1	11.1
	Ar	0.0003%	5	0.8
			Total:	11.9 (613)
4	CD_3CN	0.02%	1	11.1
	CO_2	0.0067%	5	18.6
			Total:	29.7 (1528)

[a] As declared by the supplier.

Turnover frequency (TOF) calculation

TOF was calculated using the following equation:

$$\mathrm{TOF} = \frac{\mathrm{TON}}{t} = \frac{N_{BA}}{t \cdot m \cdot N_{KPHI}} = \frac{N_{BA}}{t \cdot m \cdot \frac{1}{d \cdot 10^{-21} \cdot \sum_{i=1}^{n} w_i \cdot v_i}}$$

$$= \frac{N_{BA}}{t \cdot m \cdot \frac{1}{\frac{1}{6} \cdot \pi \cdot d \cdot 10^{-21} \cdot \sum_{i=1}^{n} w_i \cdot (l_i)^3}}$$

where TON – turn over number, number of benzylamine molecules converted by a single K-PHI particle; t – reaction time, in s; m – mass of K-PHI taken for the photocatalytic experiment, in g; N_{KPHI} – specific number of K-PHI particles per gram of the material (10^{15} g^{-1}, estimated from dynamic light scattering in a previous work[204]), in g^{-1}; d – density of K-PHI (2.00(13) g cm^{-3}), in g cm^{-3}; N_{BA} – number of benzylamine molecules converted by K-PHI during the photocatalytic experiment, mol^{-1}; w_i – fraction of volume of the K-PHI particles of size l_i (from dynamic light scattering[204]); l_i – particle size, in nm.

Stability of K-PHI over recycling experiments

K-PHI was recovered after photocatalysis by means of centrifugation. The separated solid was collected and washed twice with 2 mL of MeCN and subsequently with two more washes using 2 mL of H_2O. The material was dried and then used again for another 24 h cycle of photocatalysis. This procedure was repeated in order to utilise the same photocatalyst for a total of four cycles. Even though the imine yield did not follow a clear trend among experiments, a still decent conversion of benzylamine to N-benzylidene benzylamine was obtained after the 4th cycle of photocatalysis (Table A2). FT-IR analysis (Figure A7a) of the photocatalyst before and after the first photocatalytic experiment showed that the kind of functional groups in K-PHI did not change upon reaction: no peaks disappeared, and no new signals appeared. Nevertheless, changes in relative intensities may suggest small modifications of the C=N bonds in the structure of the catalyst (*e.g.* different intensity ratio at ~1570-1650 cm^{-1}). PXRD characterisation (Figure A7b) also confirms that, despite the preservation of the overall crystalline structure of K-PHI, some changes did take place upon reaction. In fact, the diffraction peak around 27° shifted to 28°, which is clear indication of a reduced interlayer distance.

Table A2. Imine yield during recycling experiments.[a]

Entry	Photocatalyst	Time (h)	Environment	Yield
S1	K-PHI, 1st run	24	CO_2	88%
S2	K-PHI, 2nd run	24	CO_2	63%
S3	K-PHI, 3rd run	24	CO_2	80%
S4	K-PHI, 4th run	24	CO_2	67%

[a] Reaction conditions: benzylamine 0.05 mmol; photocatalyst 5 mg; MeCN 3 mL; pressure 1 bar; T_{bath} = 35 °C; light intensity 52 mW cm^{-2} (blue LED, λ_{max} = 461 nm); relative standard deviation of the method is 5%.

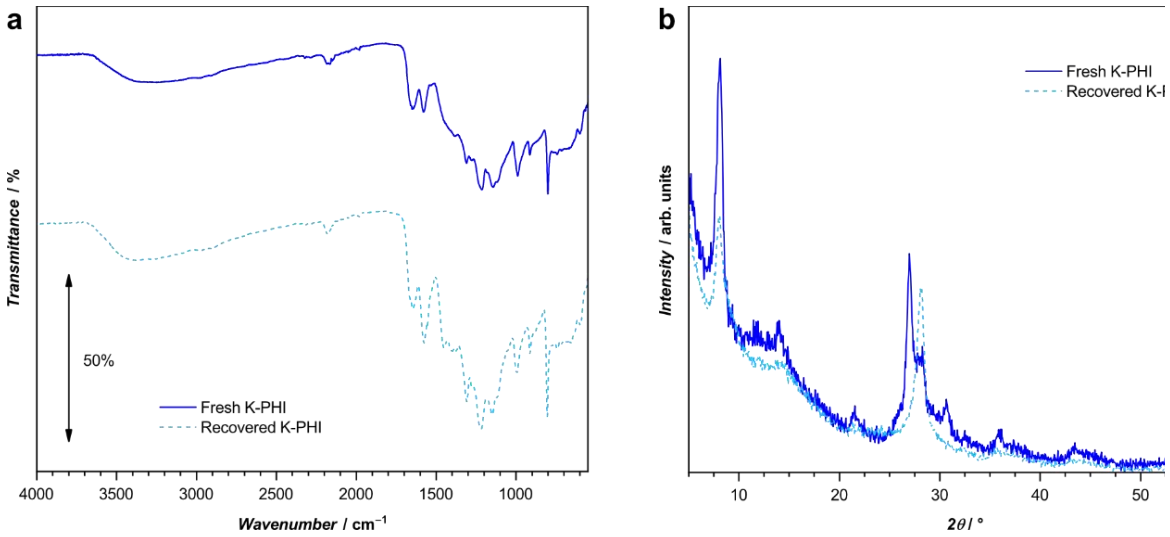

Figure A7. Characterisation of K-PHI before (blue, solid line) and after (light blue, dashed line) 24 h of photocatalysis, by means of a) FT-IR and b) PXRD techniques.

Detection of CO_2 reduction products

In order to confirm the regeneration of CO_2 over the photocatalytic cycle proposed in Scheme 5.3, various analysis were performed with the aim of detecting eventual reduction products. The observation of such compounds would suggest that CO_2 is at least partially consumed during the photocatalytic oxidative coupling of benzylamines. Comparing the band positions of K-PHI and the standard reduction potentials of CO_2 (Figure A8), it is possible to observe that only some reduction products are potentially accessible *via* direct photoreduction of CO_2. Among these, MeOH and CH_4 are thermodynamically accessible but they also have larger kinetic energy barriers. Other products such as CO and HCOOH have too negative standard reduction potentials and cannot be directly reduced by K-PHI. In contrast, mpg-CN shows its conduction band at more negative energy potentials and it could potentially reduce CO_2.

Indeed, this has been demonstrated in scientific literature.[246-249] However, no products of CO_2 reduction were observed in our case.

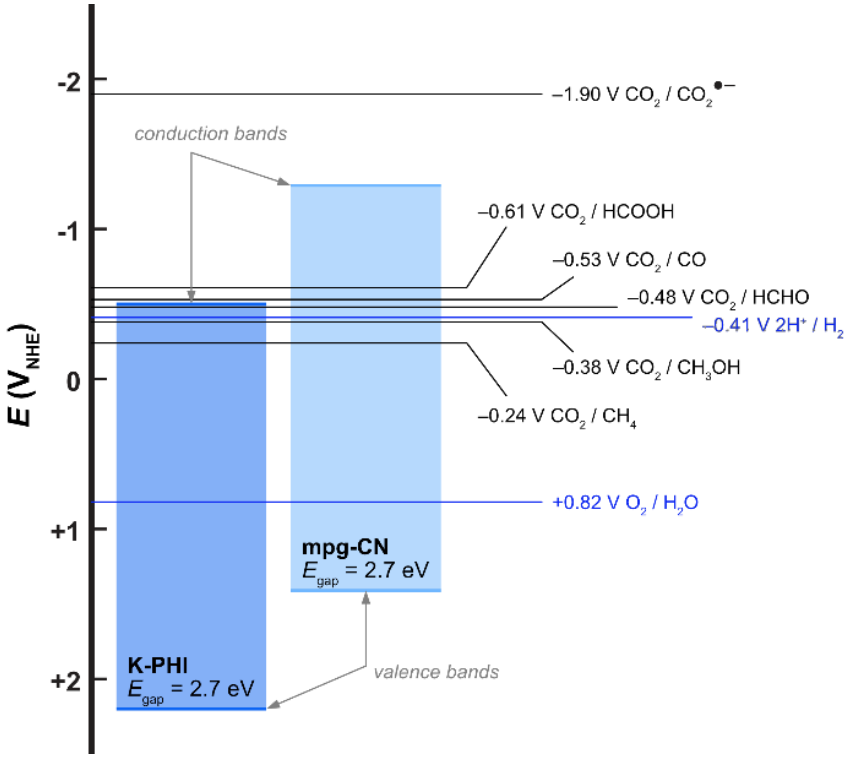

Figure A8. Band positions for K-PHI and for mpg-CN displayed together with CO_2 standard reduction potentials on the same potential energy scale.

Methanol – HPLC was used to investigate the formation of this product in the liquid phase. Only a peak relative to the reaction medium, MeCN, was observed. Therefore, the formation of MeOH was excluded.

Carbon monoxide or methane – GC-TCD was used to analyse the pre-run and post-run headspace of photoreactor to verify the potential conversion of CO_2 to gas products such as CO and CH_4. CO_2 reduction product were not detected, and only traces of H_2 were observed by means of GC-TCD.

Formic acid – two strategies were used to verify the conversion of CO_2 to formate/formic acid. On one hand, after the photocatalytic experiment with ^{15}N-labeled benzylamine, ammonium formate was extracted from K-PHI structure using a mixture of D_2O/HCl. In the ^{1}H NMR spectrum of the solution we detected the formyl proton at 8.05 ppm, while a triplet at 7.08 ppm is presumably due to $^{15}NH_4^+$ (Figure 5.3). The amount of ammonium formate obtained from the photocatalyst after the first extraction was 0.14 µmol, which is substantially lower than the amount of imine produced photocatalytically in the same reactor, namely 50 µmol. The

suspected that the relatively low yield of formic acid with respect to the imine could be due to the easiness of formic acid decomposition under the photocatalytic conditions.[250-252] In a control experiment, a continuous stream of N_2 was purged in a tube loaded with a known amount of HCOOH, benzylamine and K-PHI. Under blue light irradiation, evolution of CO_2 was detected by passing the gaseous products through an aqueous $Ba(OH)_2$ solution, as a $BaCO_3$ precipitated was observed according to the reaction $Ba(OH)_2 + CO_2 \rightarrow BaCO_3 + H_2O$ (Figure A12).

These experiments suggest that under the applied reaction conditions formic acid could in principle be formed to some extent and subsequently decompose back into CO_2 with simultaneous evolution of H_2. As discussed before, only traces of H_2 were detected by means of gas chromatography and a significant amount of H atoms were trapped into the photocatalyst. However, since no reduction product was directly observed neither in the gaseous (*e.g.* CO or CH_4) or in the liquid phase (*e.g.* MeOH, HCOOH), we are not able to confirm that CO_2 is significantly being reduced during photocatalysis.

Experiments with ^{13}C-labelled CO_2.

A modified setup was used for this kind of experiments (Figure A9). Labelled ^{13}C-CO_2 was produced by thermal decomposition of ^{13}C-labelled $NaHCO_3$ and used to saturate the photoreactor according to the following procedure. A total of 4 chambers were connected in series to perform the experiments. A Schlenk flask (referred to as Chamber A) was filled with 0.245 g ^{13}C-$NaHCO_3$ and connected to a second Chamber B *via* a syringe-tube-syringe bridge. A line with Ar was connected to Chamber A and the flow rate was set to 9 mL min^{-1}. Chamber B was connected with a similar syringe-tube-syringe bridge to Chamber C. Chamber C (the standard 6 mL glass vial used for photoreactions in this work) was loaded with 3 mL CD_3CN, 5 mg K-PHI and 0.05 mmol benzylamine. Deuterated acetonitrile was used to measure NMR spectra after the reaction without evaporating the solvent, because CO_2 reduction products might be volatile. Chamber B and C were placed in an ice bath to trap H_2O (from bicarbonate thermal decomposition) and to lower CD_3CN temperature (during the following heating of chamber A). Chamber C was connected to Chamber D with another syringe-tube-syringe bridge. This last Chamber D was loaded with a water solution containing 50 mg $Ba(OH)_2$ to monitor CO_2 formation through precipitation of ^{13}C-$BaCO_3$ and was exposed to atmosphere.

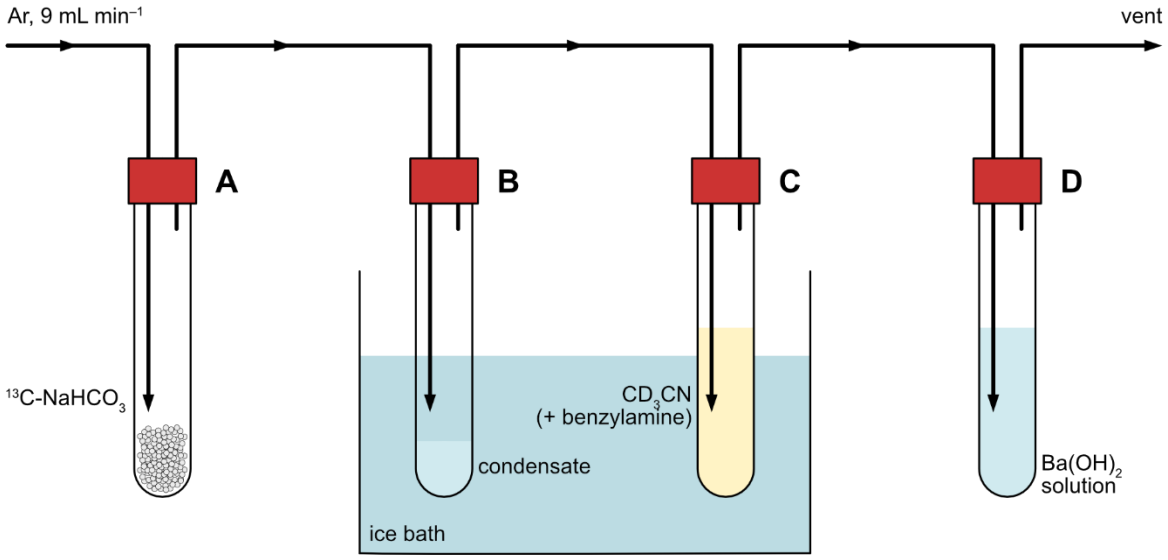

Figure A9. Setup used for thermal decomposition of ^{13}C-NaHCO$_3$ and generation of ^{13}C-CO2 to be used in photocatalytic oxidative coupling of benzylamines.

First, the system was flushed with Ar for 20 min to remove air from the chambers. Then, while flushing Ar, Chamber A was heated to 230 °C. This led to the decomposition of ^{13}C-NaHCO$_3$ into H_2O vapour and $^{13}CO_2$ which were carried towards the second Chamber. The CO_2/Ar gas mixture was bubbled through the CD_3CN and subsequently through the $Ba(OH)_2$ solution for 30 min. After this time, no more precipitation of ^{13}C-$BaCO_3$ was observed and the thermal decomposition of ^{13}C-NaHCO$_3$ was considered finished. At this point, the tube with reaction mixture was closed and irradiated as usually for 24 h. After this time, 0.5 mL aliquots of the reacted solution were sampled and ^{1}H and ^{13}C NMR spectra were recorded (Figures A10 and A11).

Control experiments with standard CO_2 were performed in a similar manner by replacing labelled ^{13}C-NaHCO$_3$ with common $NaHCO_3$. The change of setup affected the imine yield, probably due to a not complete saturation in CO_2 of the deuterated solvent and the differences in moisture contamination. Nevertheless, the tests with CO_2 and ^{13}C-CO_2 showed consistent imine formation: 69% and 65%, respectively.

These experiments showed no conversion of CO_2 to any reduction products, further confirming what observed with other characterization techniques such as HPLC and GC-TCD. Except for the CD_3CN solvent peaks, only the signals belonging to unreacted benzylamine and to the imine product are observed in ^{1}H and ^{13}C NMR spectra. In Figure A11, only the peak belonging to ^{13}C-CO_2 (~125 ppm) is present, and no reduction products are formed.

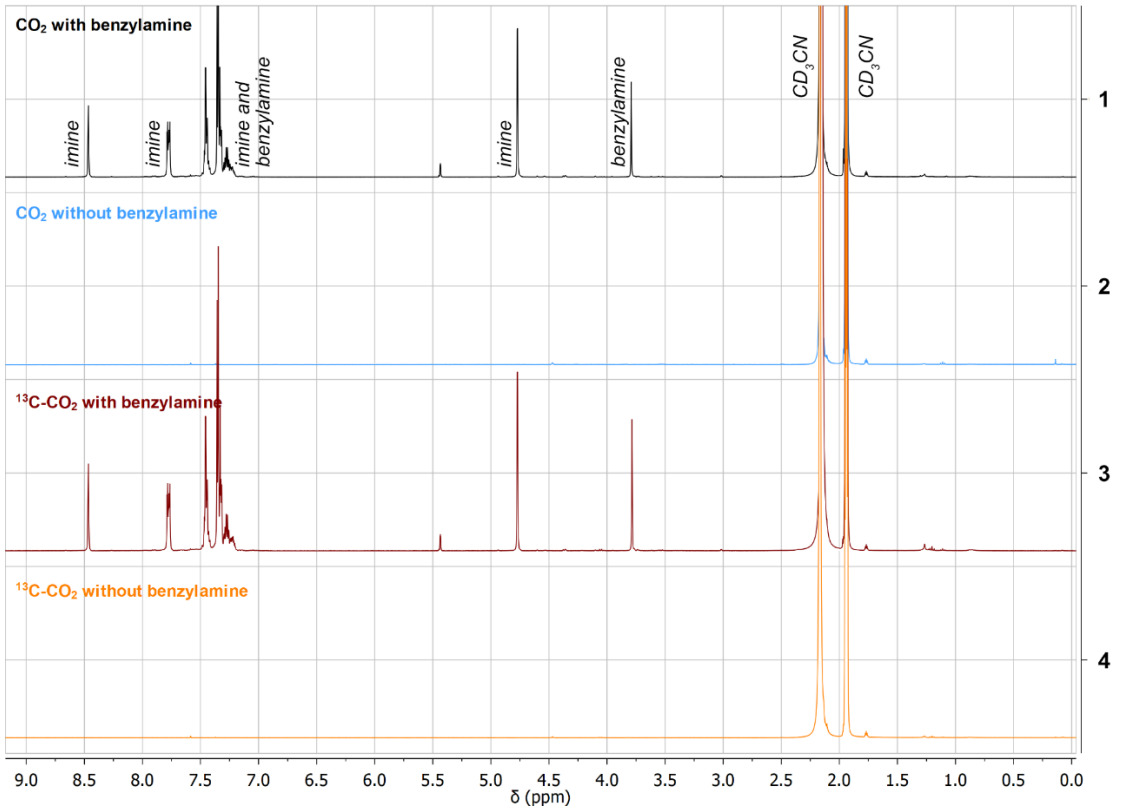

Figure A10. ^{1}H NMR spectra relative to the experiments for CO_2 reduction products detection using 1) standard and 3) labelled ^{13}C-CO_2 in the presence of benzylamine. The respective blank experiments in absence of the benzylamine substrate are shown in 2) and 4).

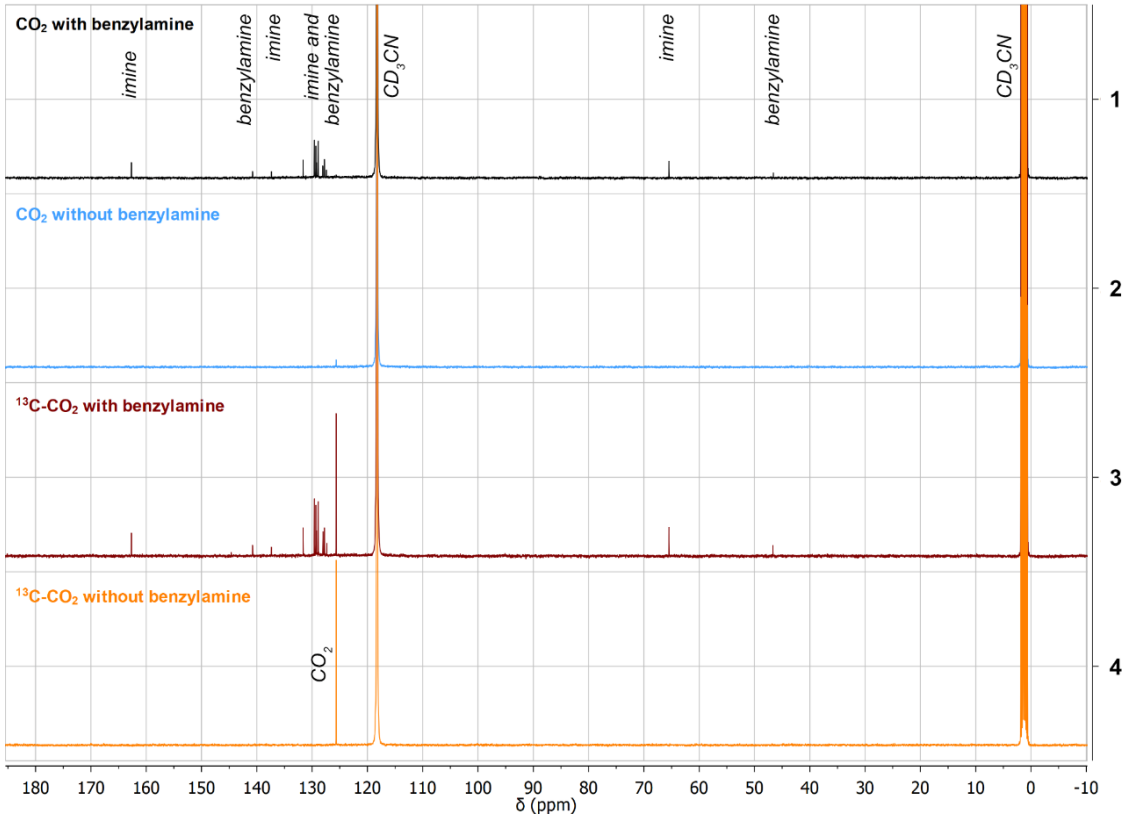

Figure A11. ^{13}C NMR spectra relative to the experiments for CO_2 reduction products detection using 1) standard and 3) labelled ^{13}C-CO_2 in the presence of benzylamine. The respective blank experiments in absence of the benzylamine substrate are shown in 2) and 4).

A procedure of photocatalytic decomposition of formic acid and CO_2 trapping with $Ba(OH)_2$.

A tube with condenser and gas inlet (5 mL) was charged with benzylamine (0.05 mmol), K-PHI (5 mg), formic acid (4.1 µL, 50 umol), MeCN (5 mL), and a magnetic stir bar. The mixture was degassed using freeze-pump-thaw method (3 times, liquid nitrogen, residual pressure 7×10^{-5} bar) and refilled with nitrogen. Then the nitrogen flow was set as 1 bubble per second. The gas above the reaction mixture was bubbled through a solution of 18.9 mg $Ba(OH)_2$ in 2 mL of water. The mixture was stirred under blue LED irradiation (λ_{max} = 461 nm, 51.70(3) mW cm^{-2}) at room temperature for 24 h. White precipitate of $BaCO_3$ was collected by centrifugation, washed 3 times with water, dried, and analyzed with PXRD.

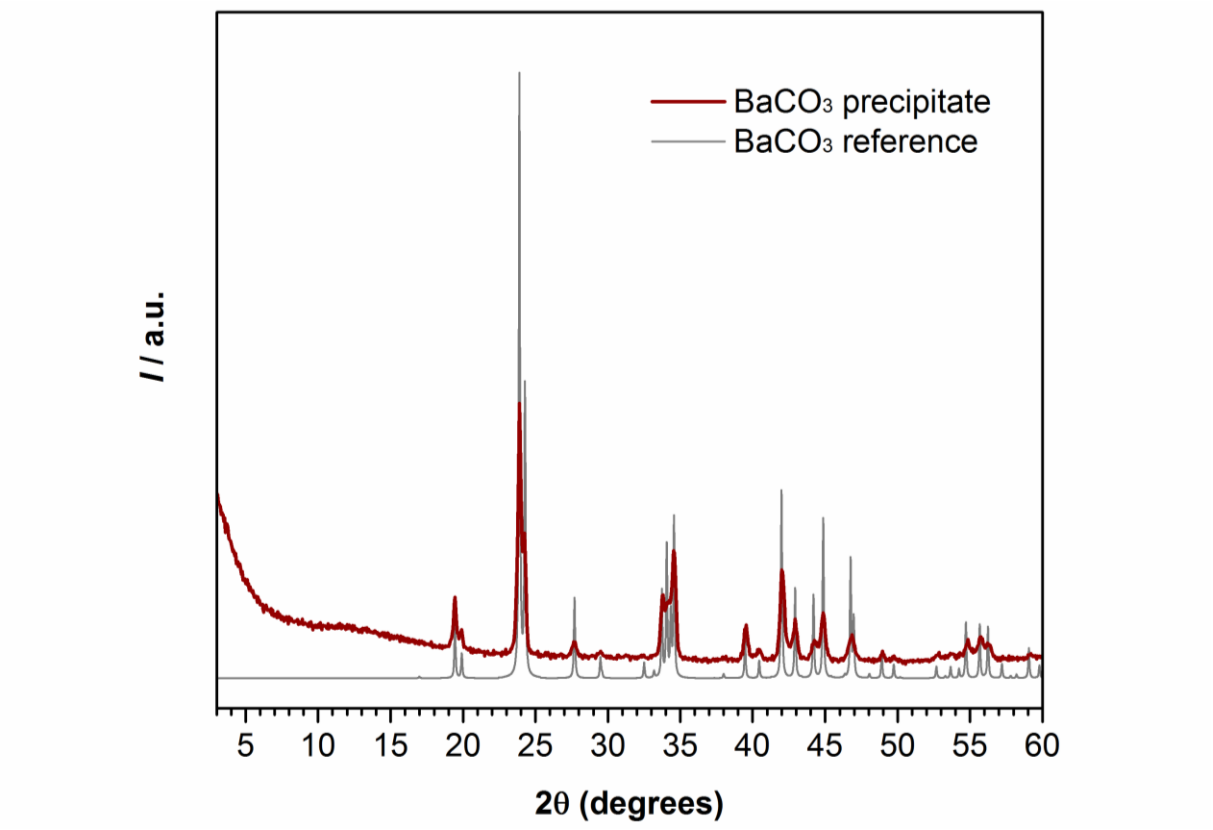

Figure A12. PXRD pattern of the precipitate after the photolysis test of formic acid (blue) compared with the diffraction pattern of $BaCO_3$ as found in literature reference.[253]

11.7. Supplementary information to the Chapter 6

2(R),3(R)-diphenylaziridine synthesis.

A solution of PPh_3 (0.32 g, 1.22 mmol) and NEt_3 (0.39 mL, 2.81 mmol) in THF (5 mL) was cooled in an ice bath. The solution of DIAD (0.21 g, 1.03 mmol) in THF (5 mL) was added dropwise at 10 °C. The reaction was stirred at 10 °C for 30 min until precipitate formed. Then,

the solution of (*1S,2R*)-(+)-2-amino-1,2-diphenylethanol (0.2 g, 0.94mmol) in THF (5 mL) was added dropwise at 10 °C and the mixture was left with stirring at room temperature overnight. The reaction mixture was concentrated and diluted with Et_2O (20 mL), washed with water (5 mL), dried over Na_2SO_4 and concentrated. The residue was purified by column chromatography to afford the product in 80% yield.

^{1}H NMR (400 MHz, $CDCl_3$) δ 7.43 – 7.26 (m, 1H), 3.10 (s, 1H), 1.58 (s, 1H). ^{13}C NMR (101 MHz, $CDCl_3$) δ 139.63, 128.67, 127.37, 125.51, 43.81.

Preparation of the aldimine stannic chloride complex $(PhCH{=}NH{\cdot}HCl)_2{\cdot}SnCl_2$

The complex was prepared according to the literature procedure.[254]

Under Ar atmosphere, 2M HCl in Et_2O (5 mL) was added to the $SnCl_2$ (2.8 g, 14.56 mmol). After stirring for 10 min, another portion of 2M HCl in Et_2O (10 mL) was added. After stirring for another 20 min, the last portion of 2M HCl in Et_2O (10 mL) was added resulting in forming of two liquid layers. Then, benzonitrile (0.5 g, 4.85 mmol) was added dropwise and the reaction mixture was stirred overnight. The formed precipitate was filtered, washed with Et2O (10 mL) and dried. The product was obtained as a white solid with 90% yield.

Synthesis of diazetidines-1,3

A screw-capped tube (5 mL) was charged with benzylamine (0.05 mmol), K-PHI (5 mg), MeCN (3 mL) and magnetic stir bar. The mixture was degassed using freeze-pump-thaw method (3 times, liquid nitrogen, residual pressure $7{\cdot}10^{-5}$ bar) and refilled with Ar. The mixture was stirred at 35 °C under blue LED irradiation (λ_{max} = 461 nm, $0.0517{\pm}3{\cdot}10^{-5}$ mW·cm^{-2}) for 24 h (or 48 h, 72 h where specified). After that time, the catalyst was separated by centrifugation. The acetonitrile solution was concentrated in vacuum (50 °C, 100 mbar) and analyzed by ^{1}H NMR.

For 1,3-dibenzyl-2,4-diphenyl-1,3-diazetidine-1,3

The concentrated reaction mixture was subjected to further purification. The crude mixture was placed in a Schlenk flask equipped with a septum and cold finger. The Schlenk flask was evacuated (liquid nitrogen, residual pressure $7{\cdot}10^{-5}$ bar), the cold finger was filed with liquid nitrogen and the Schlenk flask was immersed into a water bath (60 °C). The Schleck flask was maintained under these conditions for 20 min, liquid nitrogen was removed from the cold finger, and the flask was removed from the bath and refilled with Ar. A liquid/solid that condensed on the cold finger was quantitatively collected and transferred as a solution in $CDCl_3$

into NMR tube (‘fraction B’, contains imine and unreacted benzylamine). The residue from the Schlenk flask was dissolved in $CDCl_3$ and quantitatively transferred into NMR tube (‘fraction C’, a mixture of diazetidine-1,3 diastereomers). MMR spectra for both fractions were recordered.

A solution from the NMR tube containing diazetidine-1,3 diastereomers was quantitatively transferred into 2 mL vial, solvent was evaporated passing a flow of nitrogen above the liquid. The residue was dissolved in a small amount of MeCN (~200 uL) upon heating to 50 ^oC. The solution was allowed to cool slowly to room temperature and then placed for 20 min in the freezer (-20 ^oC). The liquid was carefully collected into a separate vial (‘fraction D’, *trans*-isomer, liquid). The solid after recrystallization – ‘fraction E’, *cis*-isomer, solid. If fraction E is not pure, recrystallization is repeated. The obtained isomers were characterized by NMR and HR-MS.

(*2S,4S*)-1,3-dibenzyl-2,4-diphenyl-1,3-diazetidine-1,3

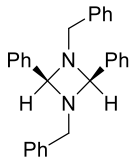

^1H NMR (400 MHz, $CDCl_3$) δ 7.29 – 7.08 (m, 19H), 7.02 (d, J = 5.6 Hz, 1H), 6.94 (d, J = 6.3 Hz, 4H), 3.76 (s, 2H), 3.51 (d, J = 13.7 Hz, 2H), 3.28 (d, J = 13.7 Hz, 2H). ^{13}C NMR (101 MHz, $CDCl_3$) δ 139.9 (d), 128.7, 128.6, 128.4, 128.1, 127.9, 127.0, 67.0, 50.9. HR-MS found 390,2417; 391,2153; 392,2187 (calculated 390,2096; 391,2130; 392,2163)

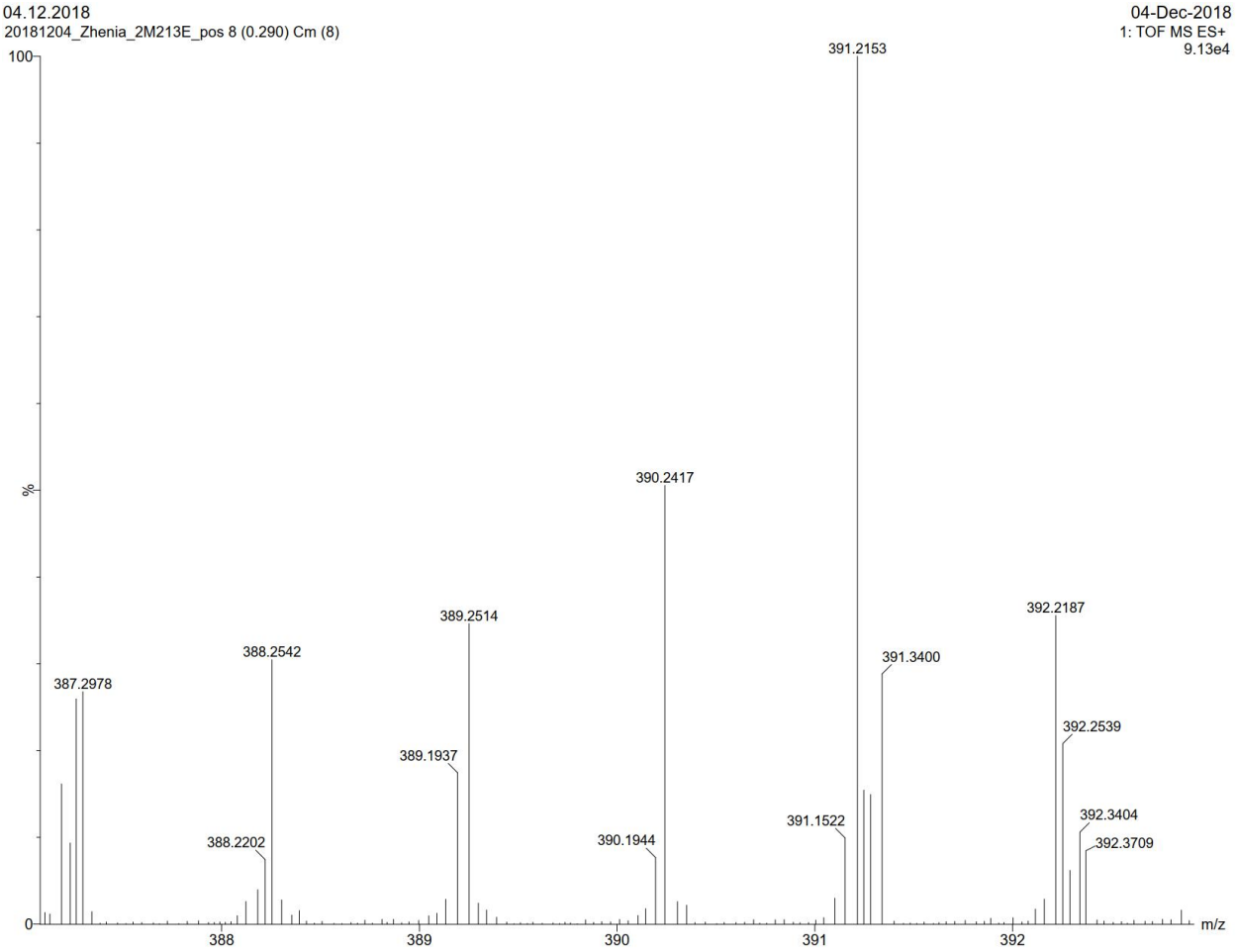

Figure A13. HR-MS spectrum of (*2S,4S*)-1,3-dibenzyl-2,4-diphenyl-1,3-diazetidine-1,3.

(*2R,4R*)-1,3-dibenzyl-2,4-diphenyl-1,3-diazetidine-1,3

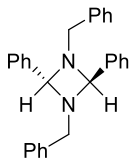

^{1}H NMR (400 MHz, $CDCl_3$) δ 7.33 – 7.26 (m, 8H), 7.25 – 7.21 (m, 3H), 7.21 – 7.11 (m, 7H), 7.08 (d, *J* = 7.8 Hz, 4H), 3.83 (s, 2H), 3.75 (d, *J* = 13.2 Hz, 2H), 3.56 (d, *J* = 13.3 Hz, 2H). ^{13}C NMR (101 MHz, $CDCl_3$) δ 139.2 (d, *J* = 19.1 Hz), 128.6, 128.4, 128.3, 128.1, 127.5, 127.3, 67.7, 51.0. HR-MS found 390,2020; 391,2148; 392,2179 (calculated 390,2096; 391,2130; 392,2163)

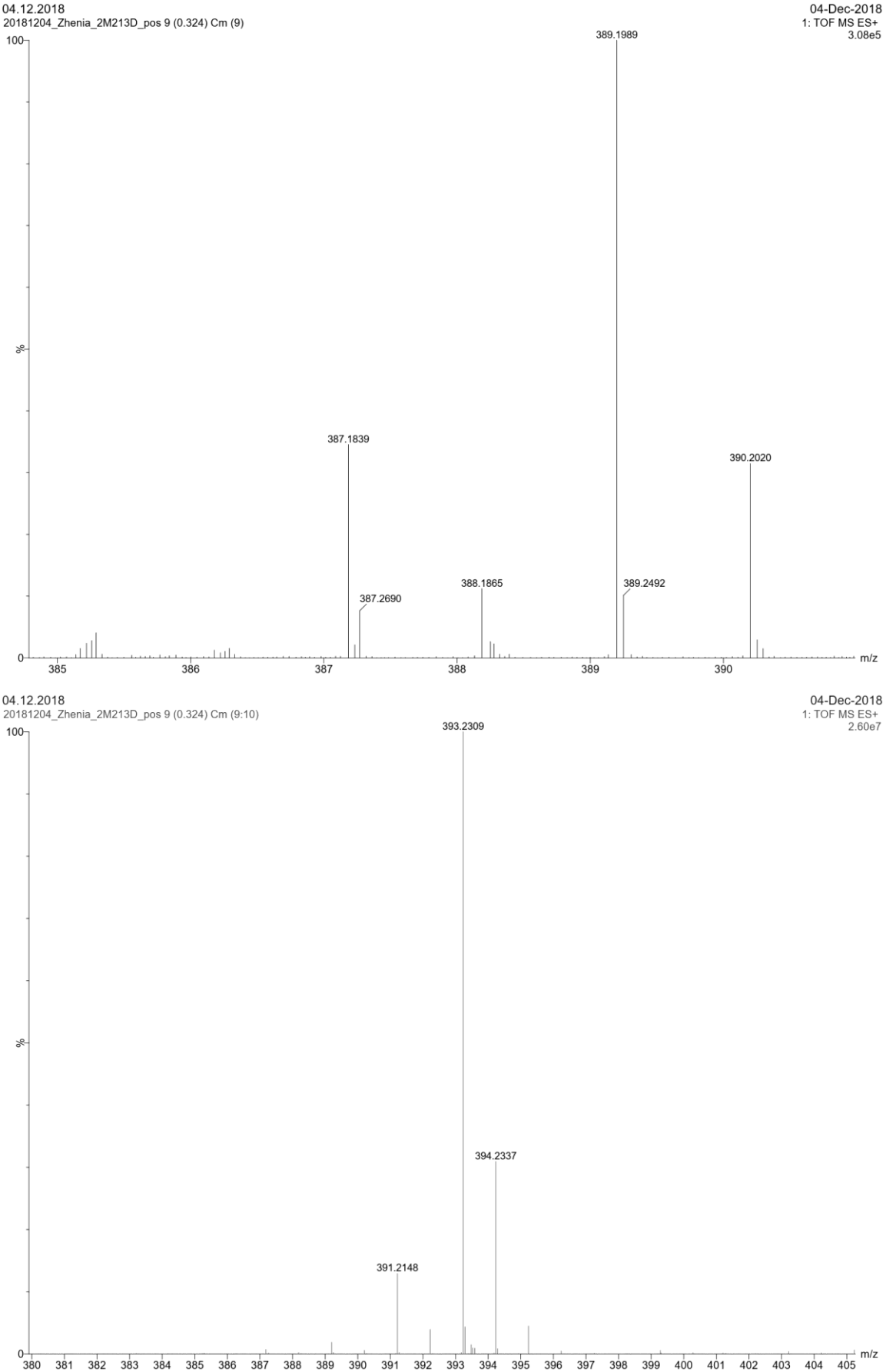

Figure A14. HR-MS spectrum of (*2R,4R*)-1,3-dibenzyl-2,4-diphenyl-1,3-diazetidine-1,3.

(*2S,4S*)-1,3-dibenzyl-2,4-diphenyl-1,3-diazetidine-1,3-$^{15}N_2$

^{15}N-benzylamine was used for the synthesys. Reaction time 72 h.

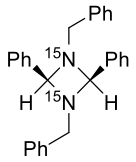

^{1}H NMR (400 MHz, CD_3CN) δ 7.35 – 7.14 (m, 16H), 7.03 (d, *J* = 6.7 Hz, 4H), 3.77 (s, 2H), 3.50 (d, *J* = 13.5 Hz, 2H), 3.29 (d, *J* = 13.6 Hz, 2H). ^{13}C NMR (101 MHz, CD_3CN) δ 142.3 (d, *J* = 1.9 Hz), 141.7, 129.4, 129.0, 128.9, 128.8, 128.1, 127.5, 68.0 (dd, *J* = 4.5, 3.0 Hz), 51.5 (d, *J* = 4.5 Hz). ^{15}N NMR (41 MHz, CD_3CN) δ 49.8. HR-MS found 393,2072; 394,2247 (calculated 392,2037; 393,2070; 394,2104)

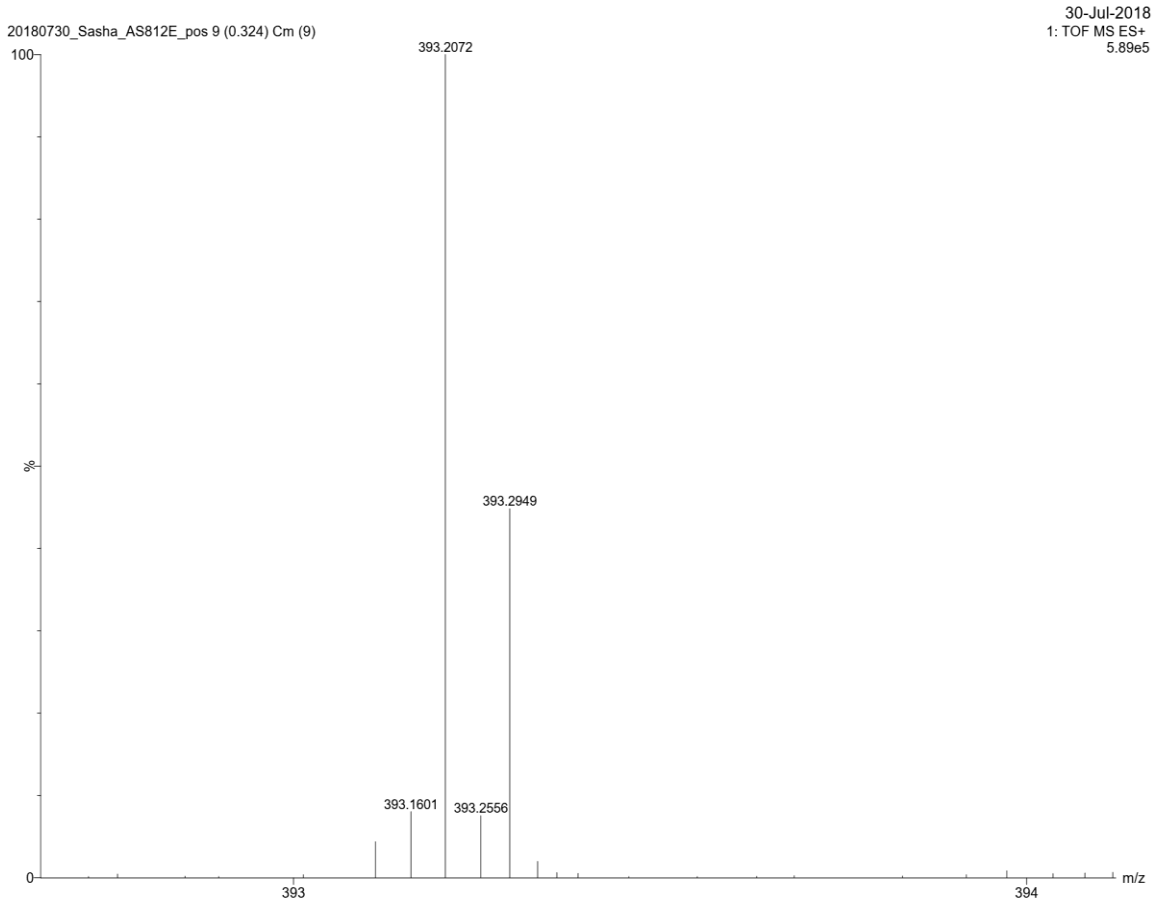

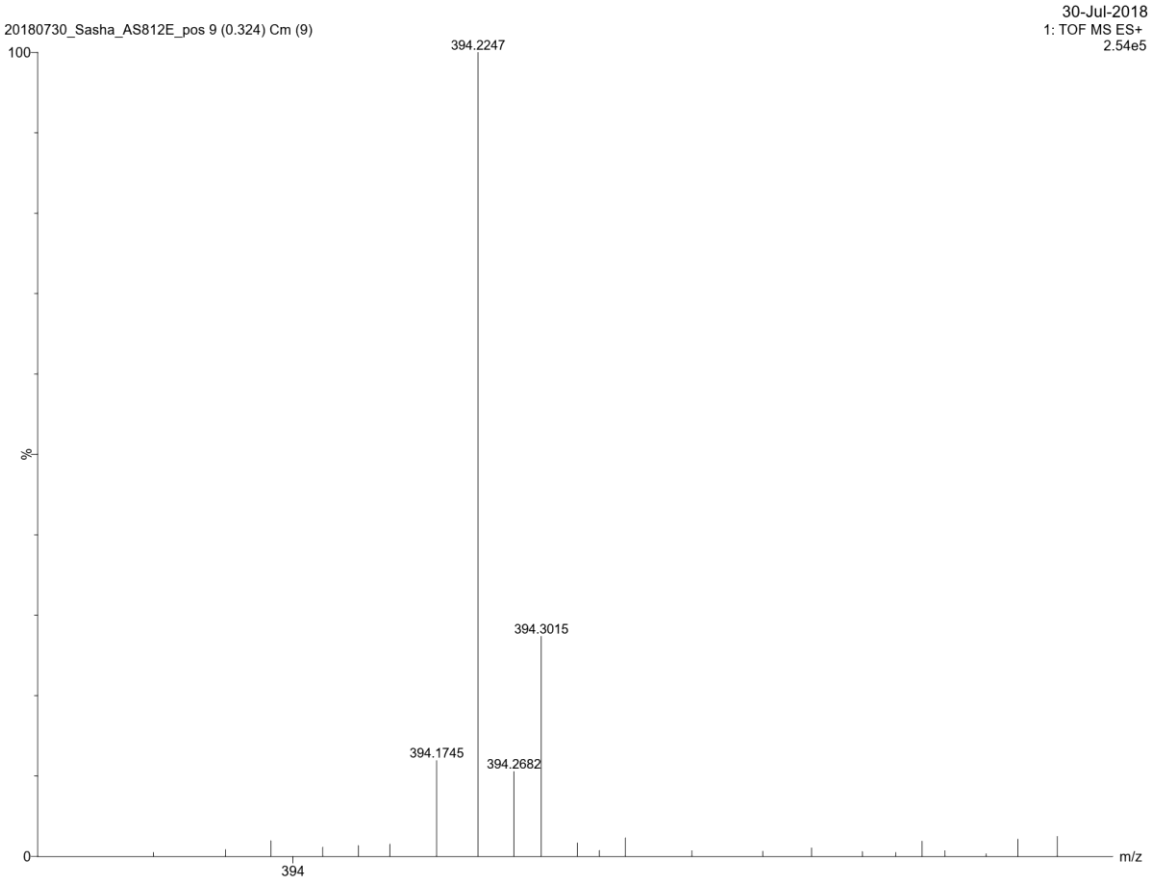

Figure A15. HR-MS spectrum of (*2S,4S*)-1,3-dibenzyl-2,4-diphenyl-1,3-diazetidine-1,3-$^{15}N_2$.

(*2R,4R*)-1,3-dibenzyl-2,4-diphenyl-1,3-diazetidine-1,3-$^{15}N_2$

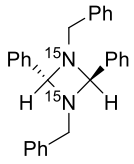

^{1}H NMR (400 MHz, CD_3CN) δ 7.26 (dq, *J* = 16.0, 8.8, 8.1 Hz, 13H), 7.16 – 7.05 (m, 11H), 3.70 (s, 2H), 3.56 (d, *J* = 13.4 Hz, 2H), 3.42 (d, *J* = 13.3 Hz, 2H). ^{13}C NMR (101 MHz, CD_3CN) δ 142.7, 141.9, 129.2, 129.1, 128.9, 128.7, 127.6, 127.5, 69.1 – 68.8 (m), 51.7 (d, *J* = 4.7 Hz). ^{15}N NMR (41 MHz, CD_3CN) δ 49.7. HR-MS found 392, 2044; 394,2197 (calculated 392,2037; 393,2070; 394,2104)

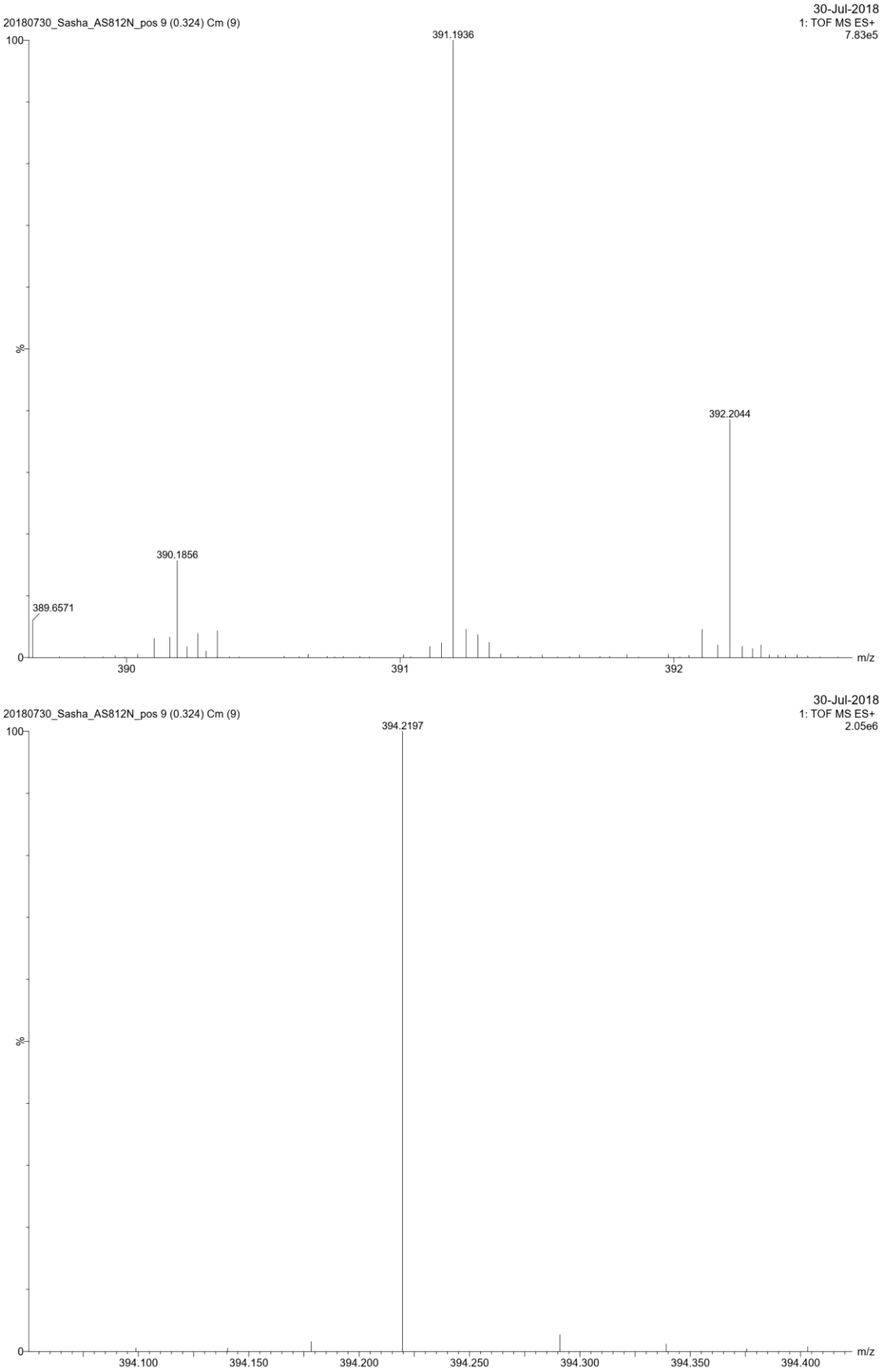

Figure A16. HR-MS spectrum of (*2R,4R*)-1,3-dibenzyl-2,4-diphenyl-1,3-diazetidine-1,3-$^{15}N_2$.

Theoretical modeling of cis- and trans-diazetidine-1,3 FT-IR spectra.

The calculations were performed at ωB97X-D//6-31G(d) level of theory.

The IR spectra of isomers are similar except for intense band at 1260 cm^{-1}, which is present in the spectrum of E and absent in the spectrum of D. According to the results of the normal mode analysis performed at ωB97X-D//6-31G(d) level of theory (Table A3), this band is mainly attributed to the asymmetric stretching vibration in the C_2N_2 ring in the molecule of *cis*-isomer:

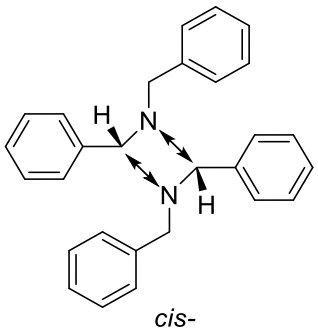

cis-

Figure A17. Schematic representation of asymmetric stretching vibration in the C_2N_2 ring in the molecule of *cis*-isomer.

Table A3. Frequencies of the main bands in the IR spectra of diazetidines (cm^{-1}) and their assignment

D = trans	E = cis	Assignment
3084, 3060, 3027	3084, 3061, 3021	$\nu(CH)_{Ph}$
2922, 2849	2962, 2908, 2858	$\nu(CH_2)$
1494	1493	$\nu(CC)_{Ph}$
1453	1454	$\nu(CC)_{Ph} + \delta(CH)$
–	1355	$\nu_s(C_2N_2) + \delta(CH)$
–	1260	$\nu_{as}(C_2N_2)$
1199	1199	$\nu(H_2C–N) + \delta(CH)$
–	1163	$\delta(NCN) + \delta(CH)$
1155	–	$\nu(CN) + \delta(CH)$
1073, 1027	1074, 1026	$\delta(CCC)_{Ph}$
910	906	$\gamma(CH)_{Ph}$
862	857	$\delta(CNC)$
732, 695	753, 693	$\gamma(CH)_{Ph}$

Abbreviations: ν, stretching; δ, in-plain bending; γ, out-of-plain bending; as, asymmetric; s, symmetric; Ph, phenyl.

Attempts to trigger imine dimerization using different electron donors

A screw-capped tube (5 mL) was charged with N-benzylidenebenzylamine (0.025 mmol), electron donor (0.1 mmol, 4 eqv.) K-PHI (5 mg), MeCN (3 mL) and magnetic stir bar. The mixture was degassed using freeze-pump-thaw method (3 times, liquid nitrogen, residual pressure $7 \cdot 10^{-5}$ bar) and refilled with Ar. The mixture was stirred at 30 °C under blue LED irradiation (λ_{max} = 461 nm, $0.0517 \pm 3 \cdot 10^{-5}$ mW·cm^{-2}) for 48 h. After that time, the catalyst was separated by centrifugation. The reaction mixture was concentrated in vacuum (50 °C, 100 mbar) and analyzed by ^{1}H NMR.

Electron donor used for the reaction: trimethylamine, benzyl alcohol, triethanolamine. No diazetidine formation was detected.

Experiments to check if Diphenylazeridine is intermediate of diazetidine synthesis

A screw-capped tube (5 mL) was charged with *2(R),3(S)*-diphenylaziridine (0.025 mmol), K-PHI (5 mg), MeCN (3 mL) and magnetic stir bar. The mixture was degassed using freeze-pump-thaw method (3 times, liquid nitrogen, residual pressure $7 \cdot 10^{-5}$ bar) and refilled with Ar. The mixture was stirred at 30 °C under blue LED irradiation (λ_{max} = 461 nm, $0.0517 \pm 3 \cdot 10^{-5}$ mW·cm^{-2}) for 48 h. After that time, the catalyst was separated by centrifugation. The reaction mixture was concentrated in vacuum (50 °C, 100 mbar) and analyzed by ^{1}H NMR. Imine was formed with 20% yield. Diazetidine was not detected.

Experiments to check if Benzaldimine is intermediate of diazetidine synthesis

Experiment with benzaldimine stannic chloride complex $(PhCH{=}NH{\cdot}HCl)_2SnCl_2$

A screw-capped tube (5 mL) was charged with $(PhCH{=}NH{\cdot}HCl)_2SnCl_2$ (0.075 mmol), K-PHI (5 mg), MeCN (3 mL) and magnetic stir bar. The mixture was degassed using freeze-pump-thaw method (3 times, liquid nitrogen, residual pressure $7 \cdot 10^{-5}$ bar) and refilled with Ar. The mixture was stirred at 30 °C under blue LED irradiation (λ_{max} = 461 nm, $0.0517 \pm 3 \cdot 10^{-5}$ mW·cm^{-2}) for 48 h. After that time, the catalyst was separated by centrifugation. The reaction mixture was concentrated in vacuum (50 °C, 100 mbar) and analyzed by ^{1}H NMR. Diazetidine was not detected.

Experiment with $(PhCH{=}NH{\cdot}HCl)_2SnCl_2$ and triethylamine

A screw-capped tube (5 mL) was charged with $(PhCH{=}NH{\cdot}HCl)_2SnCl_2$ (0.075 mmol), triethylamine (0.22 mmol) K-PHI (5 mg), MeCN (3 mL) and magnetic stir bar. The mixture was degassed using freeze-pump-thaw method (3 times, liquid nitrogen, residual pressure $7 \cdot 10^{-5}$ bar) and refilled with Ar. The mixture was stirred at 30 °C under blue LED irradiation (λ_{max}

= 461 nm, 0.0517±3·10^{-5} mW·cm^{-2}) for 48 h. After that time, the catalyst was separated by centrifugation. The reaction mixture was concentrated in vacuum (50 °C, 100 mbar) and analyzed by ^{1}H NMR. Diazetidine was not detected.

Experiment with (PhCH=NH·HCl)$_2$SnCl$_2$ and benzylamine

A screw-capped tube (5 mL) was charged with (PhCH=NH·HCl)$_2$SnCl$_2$ (0.1 mmol), benzylamine (0.8 mmol), CD_3CN (1 mL) and magnetic stir bar. The mixture was degassed using freeze-pump-thaw method (3 times, liquid nitrogen, residual pressure 7·10^{-5} bar) and refilled with Ar. The mixture was stirred at 30 °C for 48 h. After that time, the catalyst was separated by centrifugation and reaction mixture was analyzed by ^{1}H NMR. Imine was formed with 12% yield. Diazetidine was not detected.

Oxidation of benzylamine with Pt@K-PHI

A screw-capped tube (5 mL) was charged with benzylamine (0.05 mmol), Pt@K-PHI (5 mg), MeCN (3 mL) and magnetic stir bar. The mixture was degassed using freeze-pump-thaw method (3 times, liquid nitrogen, residual pressure 7·10^{-5} bar) and refilled with Ar. The mixture was stirred at 30 °C under blue LED irradiation (λ_{max} = 461 nm, 0.0517±3·10^{-5} mW·cm^{-2}) for 24 h. After that time, the catalyst was separated by centrifugation. The reaction mixture was concentrated in vacuum (50 °C, 100 mbar) and analyzed by ^{1}H NMR. Imine was formed with 94% yield. Diazetidine was not detected.

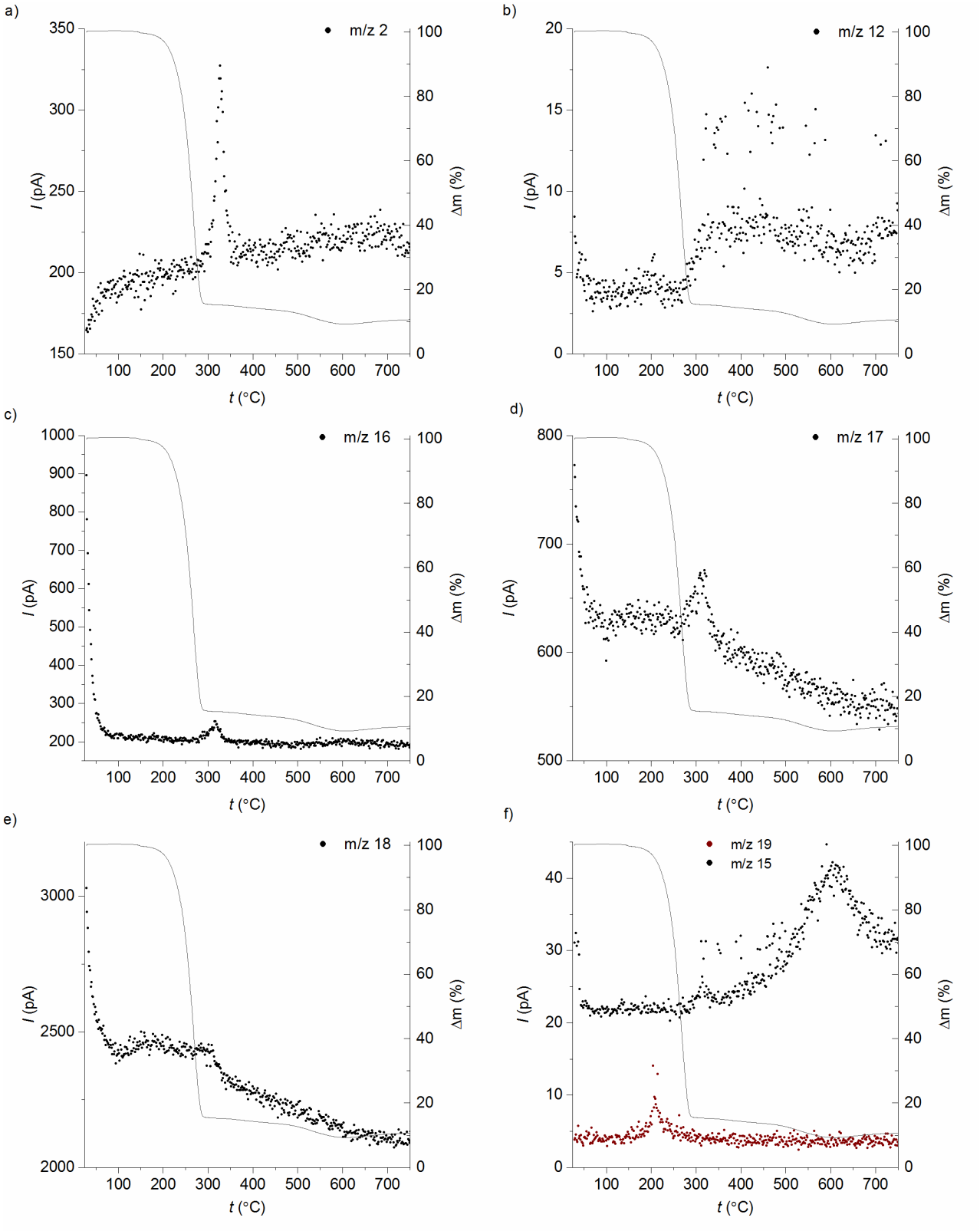

Figure A18. TGA-MS data of *cis*-diazetidine. Channels with m/z 2 (a), 12 (b), 16 (c), 17 (d), 18 (e) and 15, 19 (f) are shown.

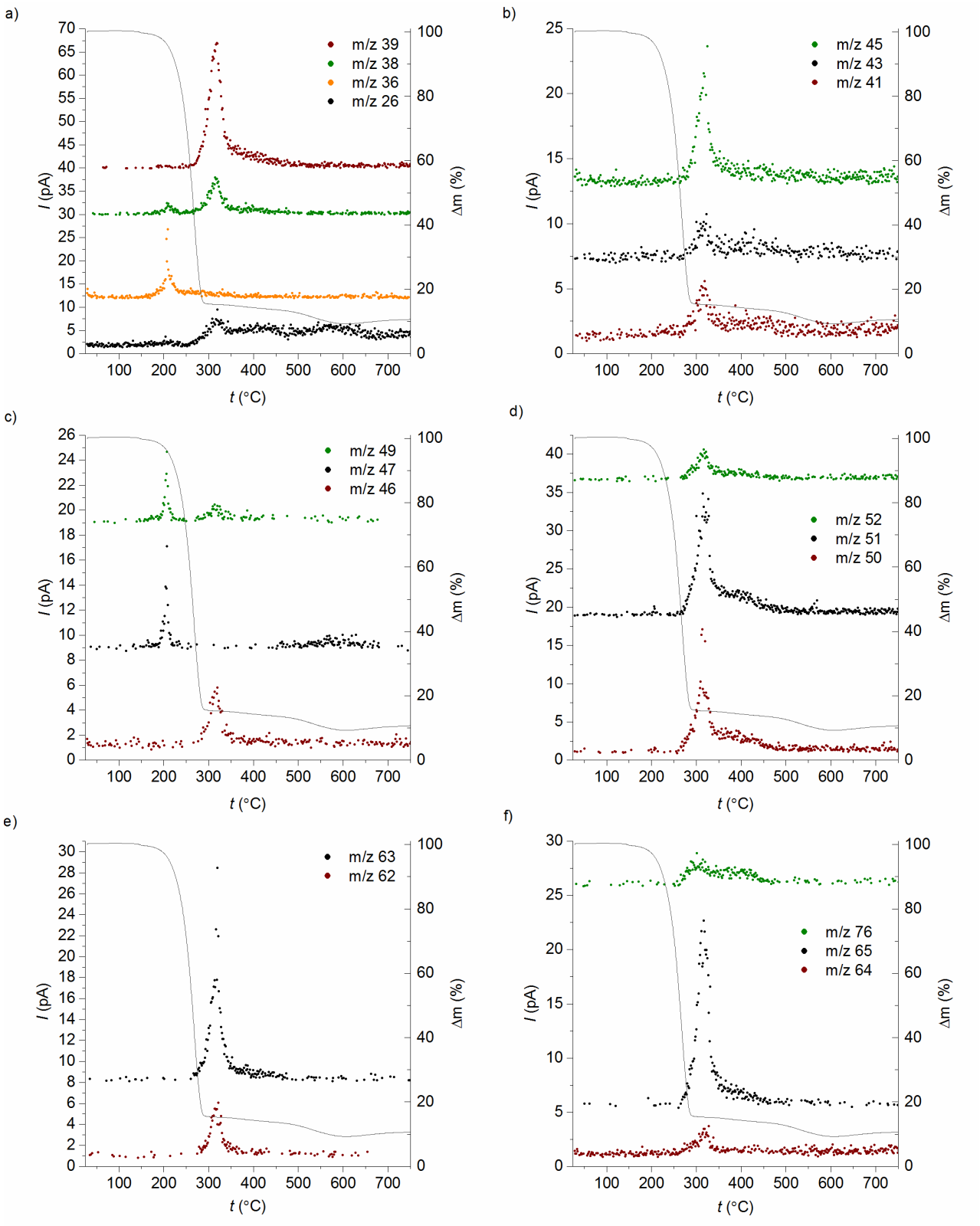

Figure A19. TGA-MS data of *cis*-diazetidine. Channels with m/z 26, 36, 38, 39 (a), 41, 43, 45 (b), 46, 47, 49 (c), 50, 51, 52 (d), 62, 63 (e) and 64, 65, 76 (f) are shown.

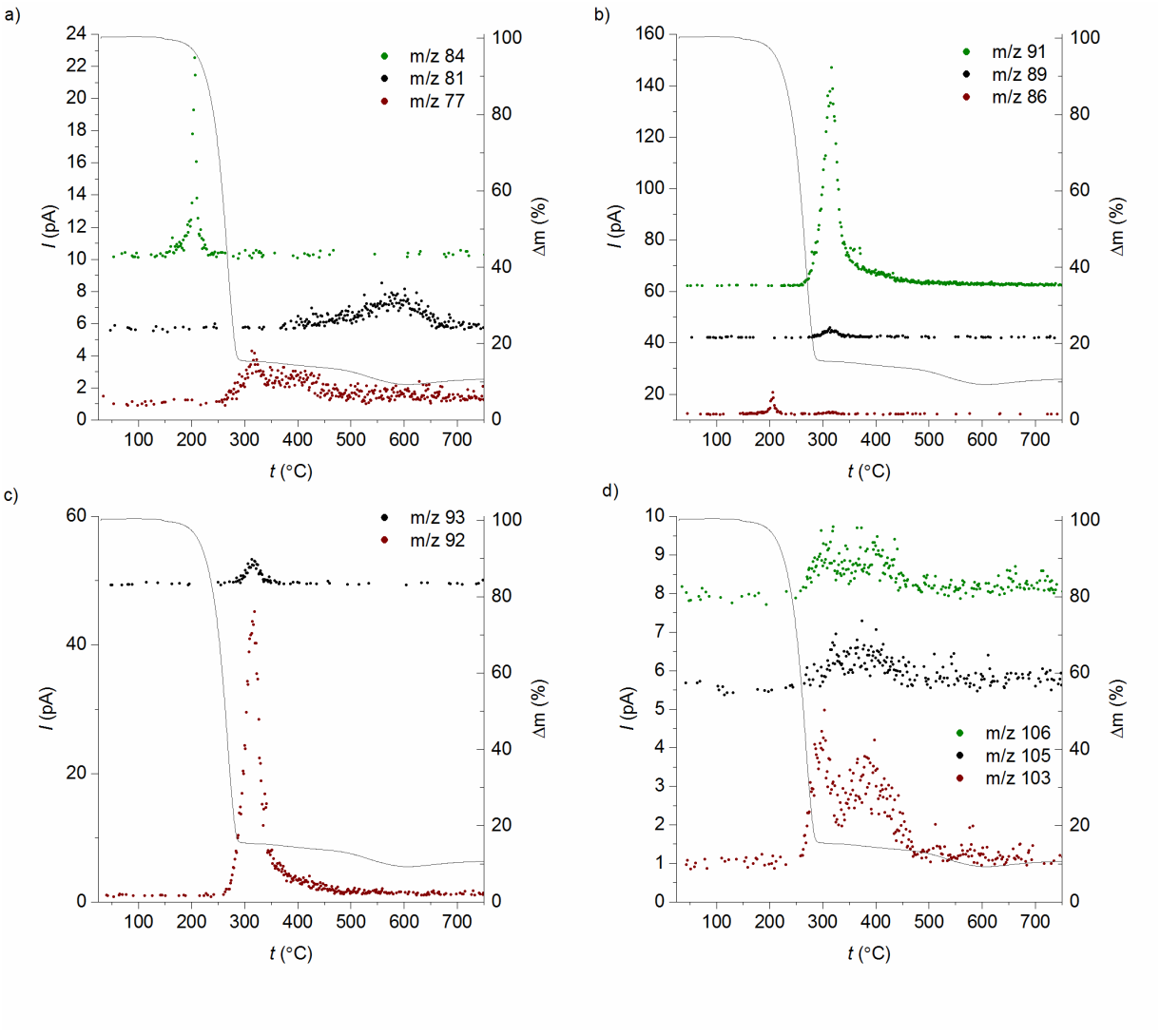

Figure A20. TGA-MS data of *cis*-diazetidine. Channels with m/z 77, 81, 84 (a), 86, 89, 91 (b), 92, 93 (c), 103, 105, 106 (d) are shown.

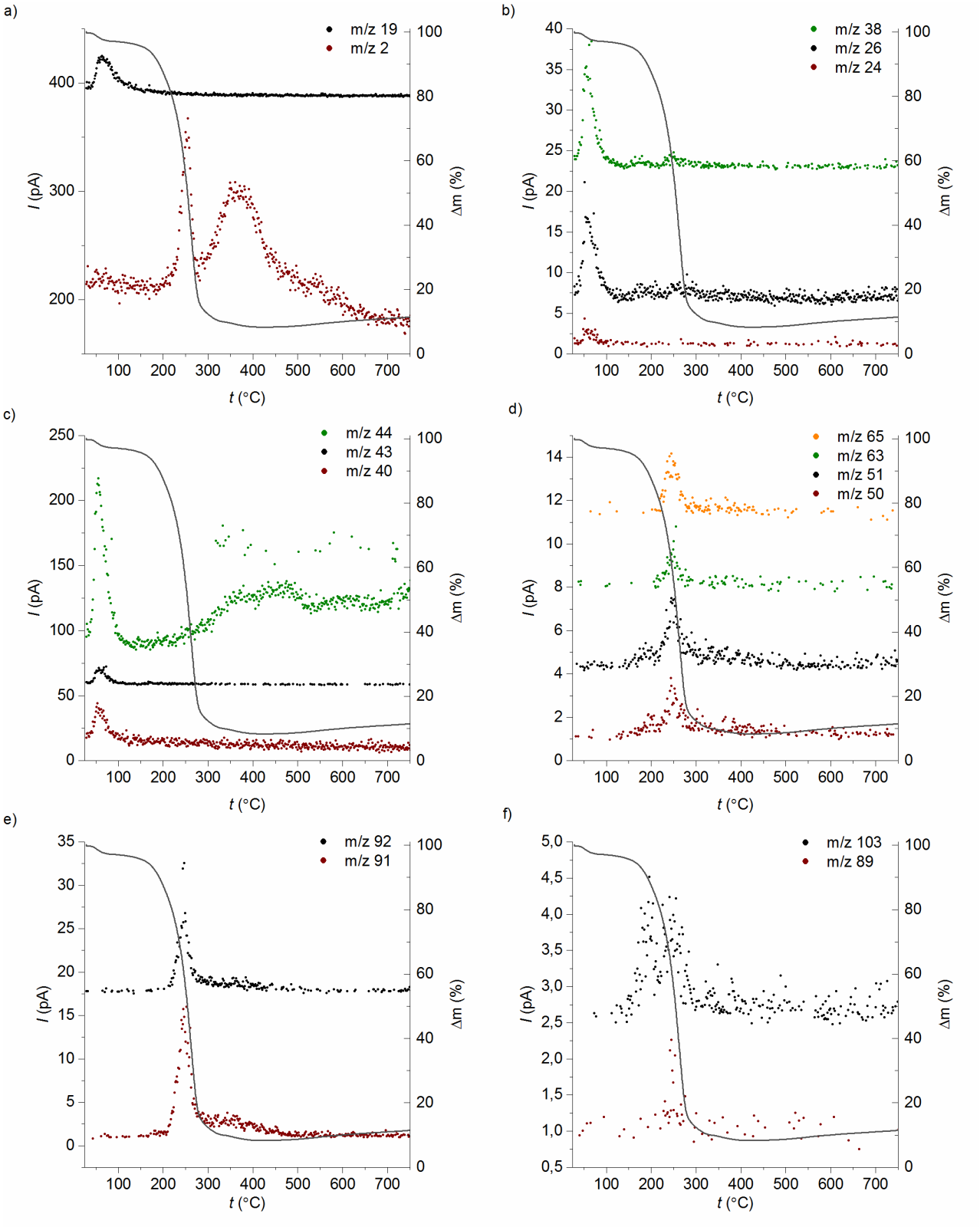

Figure A21. TGA-MS data of *trans*-diazetidine. Channels with m/z 2, 19 (a), 24, 26, 38 (b), 38, 40, 43, 44 (c), 50, 51, 63, 65 (d), 91, 92 (e) and 89, 103 (f) are shown.

Table A4. Current peak intensity for different m/z channels.

Cis-diazetidine		Trans-diazetidine	
m/z	Current peak maximum I (pA)	m/z	I (pA)
2	130	2	40
12	4	19	150
15	20	24	2
16	50	26	10
17	50	38	15
18	125	40	4
19	5	43	2
26	5	44	13
36	5	50	3
38	7	51	3
39	28	63	3
41	4	65	2
43	3	89	1
45	12	91	15
46	4	92	15
47	5	103	2
49	6		
50	10		
51	18		
52	4		
62	6		
63	20		
64	3		
65	18		
76	2		
77	3		
81	2		
84	14		
86	1		
89	0,5		
91	9		
92	50		
93	5		
103	4		
105	1		
106	2		

[a] Channels with current peak ≥0.5 pA are shown.

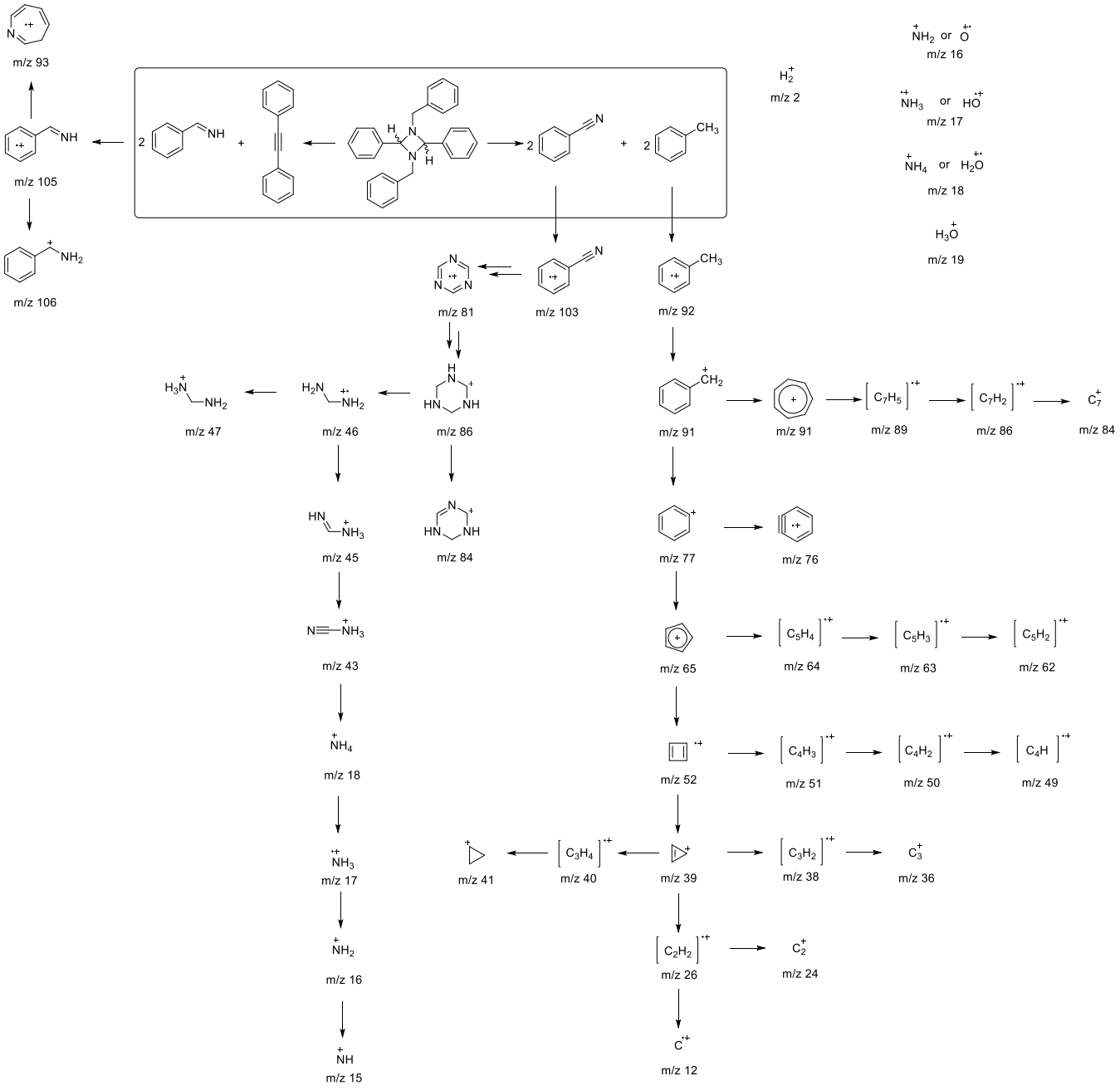

Figure A22. Paths of diazetidines thermal decomposition. Structures of charged species registered by TGA-MS are based on the assumption that molecules undergo one-electron ionization.

11.8. Supplementary information to the Chapter 7

The eutectic media used in this paper were prepared by mixing corresponding components, preliminarily dried under vacuum at room temperature overnight, with subsequent constant mixing at 40 °C until the transparent liquids were formed. The components used for eutectic media preparation and their molar ratio are described in Table 7.2.

Photocatalytic synthesis of N-arylformamides

A glass vial was charged with the nitroarene (0.04 mmol), K-PHI (5 mg) and the corresponding DES (0.2 mL). The mixture was degassed (residual pressure $9 \cdot 10^{-5}$ bar) and refilled with Ar (1 bar). The reaction mixture was stirred at 25 °C under light irradiation (λ_{max} = 465 nm, 51.7±0.03 $mW \cdot cm^{-2}$) for 48 h. After that, 0.5 mL of water were added, and the organic product was for analytics extracted with 2 mL of ethyl acetate. The layers were separated and organic layer was concentrated in vacuum. Resulted residue was analyzed by ^{1}H NMR and GC-MS analysis.

Photocatalytic synthesis of benzimidazole

The Glass vial was charged with the o-dinitrobenzene (0.04 mmol), K-PHI (5 mg) and DES3 (0.2 mL). The mixture was degassed (residual pressure 9·10-5 bar) and refilled with Ar (1 bar). The reaction mixture was stirred at 70 °C under irradiation (λ_{max} = 465 nm, 51.7±0.03 $mW \cdot cm^{-2}$) for 5 days. After that, 2 mL of water was added, the catalyst was removed and the solution was analyzed by GC-MS.

Photocatalytic synthesis of N-arylformamides with CO2 trapping

Into a tube with gas inlet (5 mL) was placed p-nitrotoluene (0.16 mmol), K-PHI (5 mg), DES1 (0.8 mL) and magnetic stir bar. The mixture was degassed (residual pressure 9·10-5 bar) and refilled with nitrogen. The mixture was stirred under blue LED irradiation (λ_{max} = 465 nm) and room temperature with nitrogen flow of 1 bubble per second for 24 h. The evolved gases were bubbled through the solution of $Ba(OH)_2$ (23 mg, 0.14 mmol) in water (2 mL). Precipitate which formed from $Ba(OH)_2$ was collected by centrifugation, washed 3 times with water, dried, and analyzed with PXRD confirming the formation of $BaCO_3$.

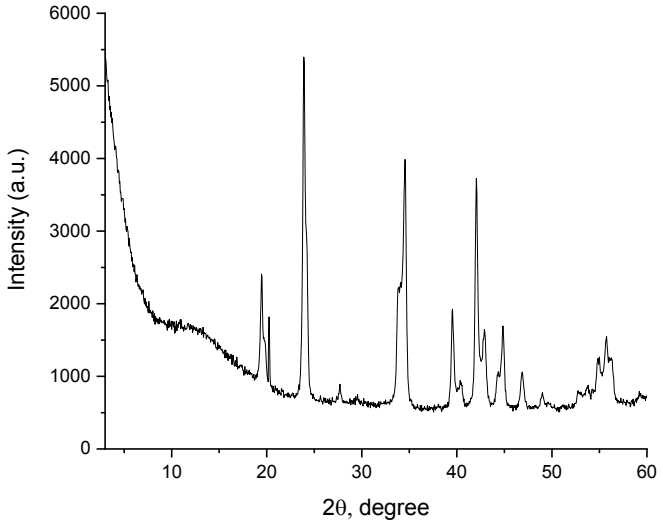

Figure A23. PXRD pattern of $BaCO_3$.

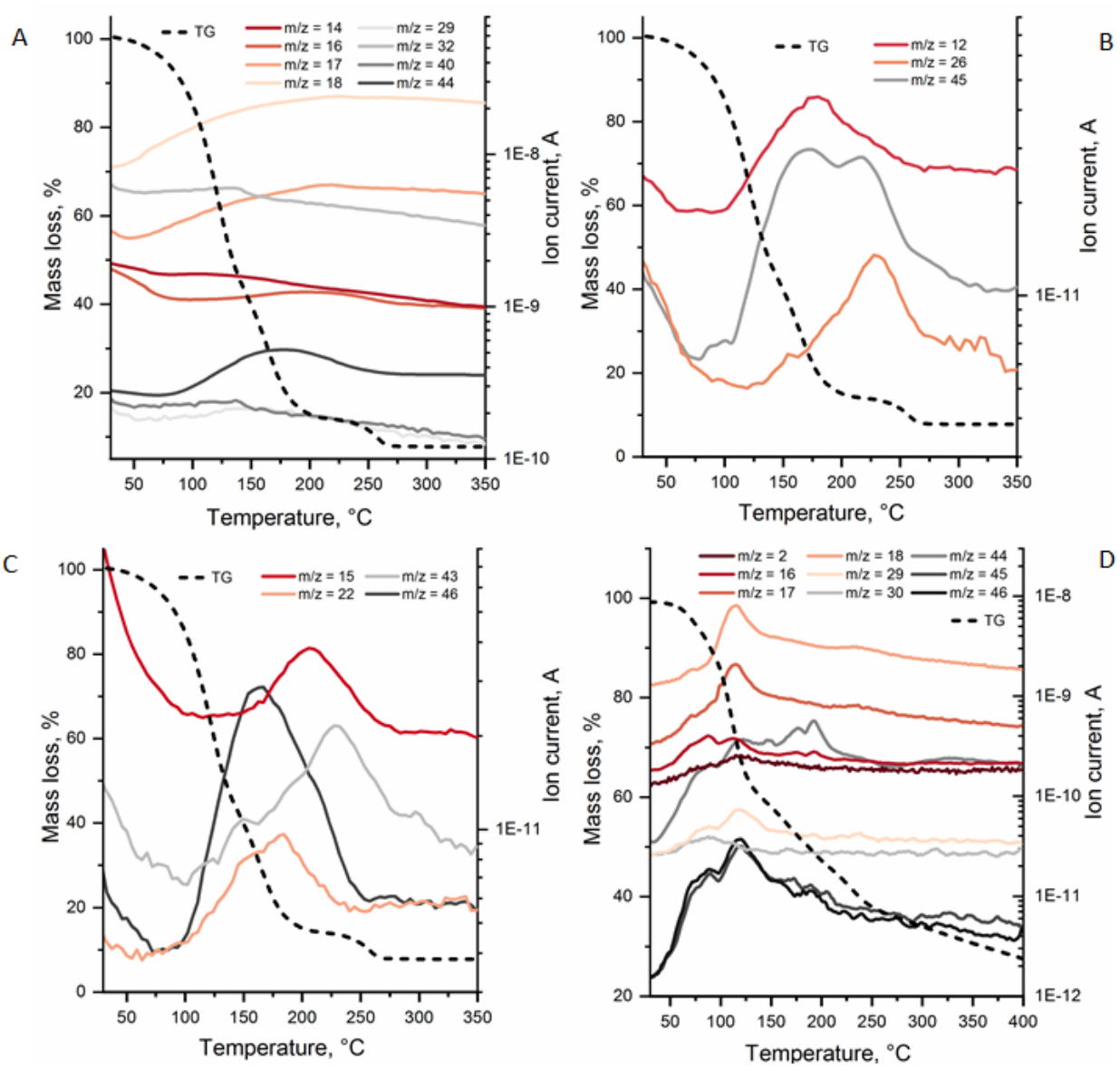

Figure A24. TGA-MS analysis of the DES1 (A-C) and DES3 (D) reactive media using a heating rate of 2.5 °C /min under helium.

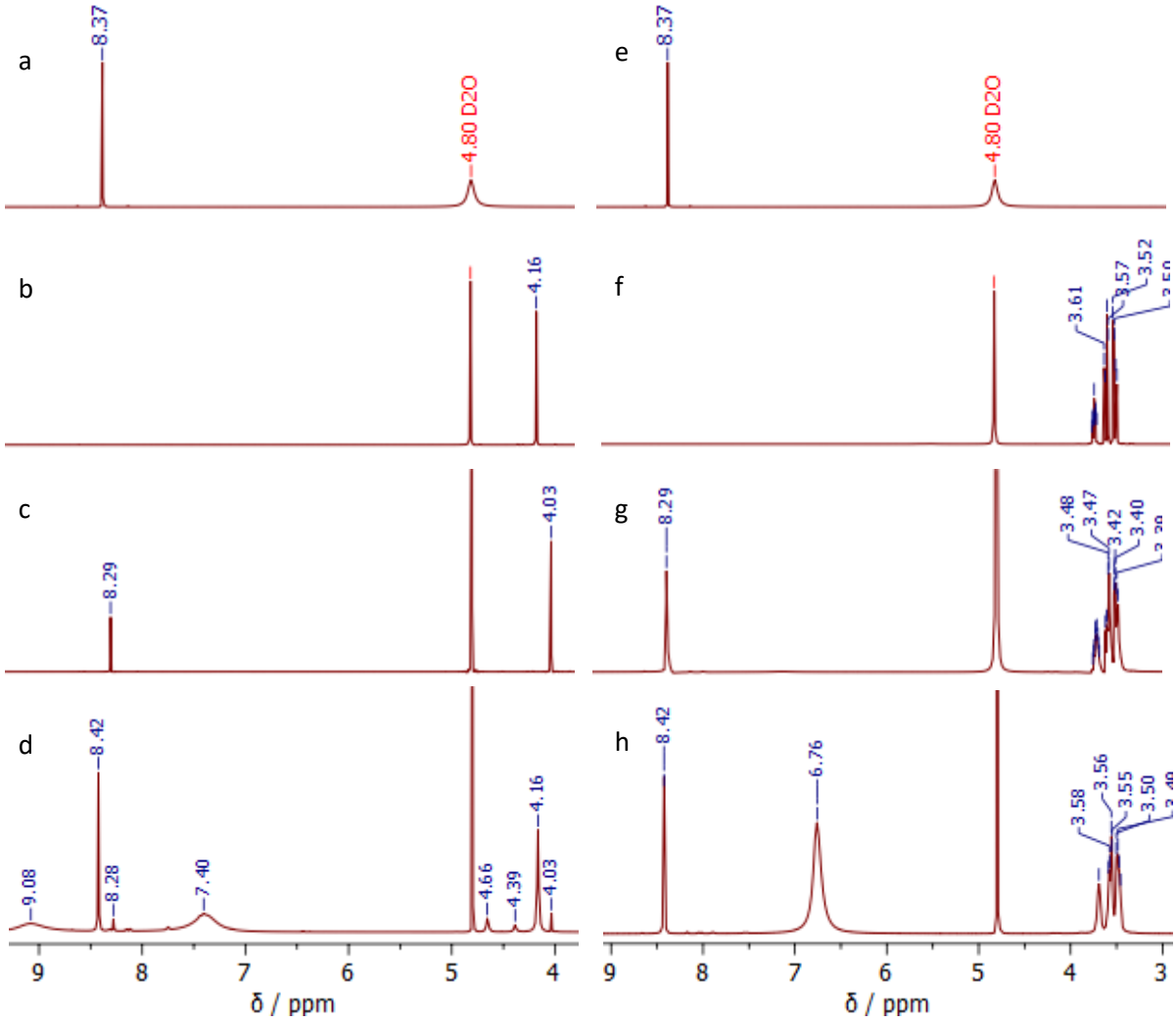

Figure A25. NMR spectra of neat ammonium formate (a,e), glycolic acid (b), and glycerol (f), water solution of ammonium formate and glycolic acid (c), water solution of glycerol and ammonium formate (g), and eutectic media ammonium formate / glycolic acid (d) and ammonium formate / glycerol (h)

11.9. Supplementary information to the Chapter 8

Method A (König method) for the photocatalytic chlorination

In a vial, a substrate (0.02 mmol), together with HOAc (0.2 mmol, 10 eq.) and benzylalcohol (0.12 mmol, 6 eq.) were dissolved in acetonitrile (0.5 mL) and HCl (0.1mL, 36 wt.% HCl). Then K-PHI (1 mg) was added and the reaction mixture was irradiated under stirring at 30 °C for 12 h under O_2 atmosphere. After the irradiation $CDCl_3$ (0.7 mL) and water (0.1 mL) were added to the reaction mixture. The layers were separated and organic layer was analyzed by ^1H NMR using the internal standard (*N*,*N*-dimethylaniline (0.01 mmol) or anisole (0.01 mmol) in case of *N*,*N*-dimethylaniline chlorination).

Method B (pure aqueous conditions, using electron and hole) for the photocatalytic chlorination

In a vial, a substrate (0.02 mmol) was dissolved in acetonitrile (0.5 mL). HCl (0.1 mL, 36 wt.%, 1.2 mmol) and K-PHI (4 mg) were added. The reaction mixture was stirred under light irradiation at 30 °C for 24 h under O_2 atmosphere. After the irradiation $CDCl_3$ (0.7 mL) and water (0.1 mL) were added to the reaction mixture. The layers were separated and organic layer was analyzed by ^1H NMR using the internal standard (*N*,*N*-dimethylaniline (0.01 mmol) or anisole (0.01 mmol) in case of N,N-dimethylaniline chlorination). In the catalytic cyclic experiments K-PHI was washed with acetonitrile (2 times, 2 mL each), water (2 times, 2 mL each), dried in vacuum overnight and used again.

General procedure for the photocatalytic bromination

A vial was charged with a substrate (0.02 mmol), K-PHI (4 mg), HBr (0.1 mL, 47 wt.%, 0.9 mmol) and acetonitrile (0.5 mL). A suspension was irradiated at vigorous stirring at 30 °C for 24 h under O_2 atmosphere. After the irradiation $CDCl_3$ (0.7 mL) and water (0.1 mL) were added to the reaction mixture. The layers were separated and organic layer was analyzed by ^1H NMR or GC-MS using the internal standard (*N*,*N*-dimethylaniline (0.01 mmol) or anisole (0.01 mmol) in case of *N*,*N*-dimethylaniline chlorination).

Procedure of K-PHI regeneration

K-PHI after the reaction was separated by centrifugation, washed with acetonitrile (2 times, 2 mL each) and with water (2 times, 2 mL each). KOH solution (9 mL, 0.1 M) was added to the catalyst and suspension was stirred for 20 h. The catalyst was separated by centrifugation, washed with water (3 times, 3 mL each), once with methanol and dried in vacuum overnight.

Method of the photocatalytic chlorination with NaCl

In a vial a substrate (0.06 mmol) was dissolved in acetonitrile (5 mL). HCl (20 µL, 36 wt.%), NaCl (48.8 mg), water (1.4 mL) and K-PHI (5 mg) were added. The reaction mixture gave two liquid phases – organic and aqueous. The reaction mixture was vigorously stirred under light irradiation at 30 °C for 24 h under O_2 atmosphere. After the irradiation organic phase was separated and acetonitrile was distilled off, but some water left. $CDCl_3$ (0.5 mL) was added to the residual water, layers were separated and organic layer was analyzed by ^1H NMR using the internal standard (dimethylaniline (0.01 mmol)).

Oxidative chlorination of anisole using a mixture of HCl and H_2O_2

A mixture of anisole (0.02 mmol), HCl (0.1 mL, 36 wt.%, 1.2 mmol), H_2O_2 (80 µL, 30 wt.%, 0.08 mmol) in acetonitrile (0.5 mL) was stirred at 30 °C for 24 h in dark. $CDCl_3$ (0.7 mL) was added to the reaction mixture, organic phase was separated, dried over anhydrous Na_2SO_4 and analyzed by ^{1}H NMR using *N*,*N*-dimethylaniline (0.01 mmol) as internal standard.

Table A5. Variation of components in anisole chlorination reaction.[a]

Entry	K-PHI	BnOH	HOAc	Light	Electron scavenger	Yield,[b]%
1	+	+	+	+	**+ (O_2)**	**98 (1:0.31)**
2	+	+	-	+	+ (O_2)	0
3	-	+	+	+	+ (O_2)	0
4	+	+	+	+	— (N_2)	0
5	+	+	+	-	+ (O_2)	0

[a] reaction conditions: K-PHI 4 mg; anisole 0.02 mmol; HCl (36 wt.%) 0.1 mL; acetic acid 0.2 mmol; benzyl alcohol 0.12 mmol; acetonitrile 0.5 mL; light source 461 nm. [b] determined by ^{1}H NMR using N,N-dimethylaniline as an internal standard. The ratio between *o*- and *p*-chloroanisole is given in parentheses.

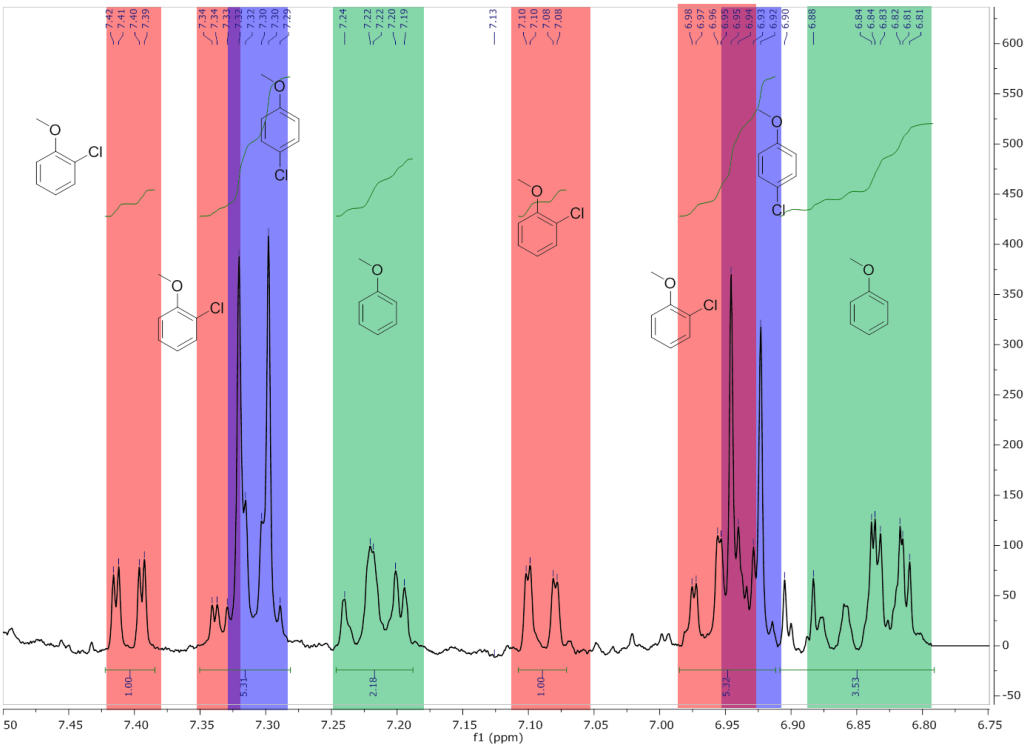

Figure A26. An exemplary ^{1}H NMR spectrum of anisole chlorination reaction mixture. Signals of hydrogen atoms in anisole are highlighted with green color, *p*-chloroanisole – blue color and *o*-chloroanisole – red color.

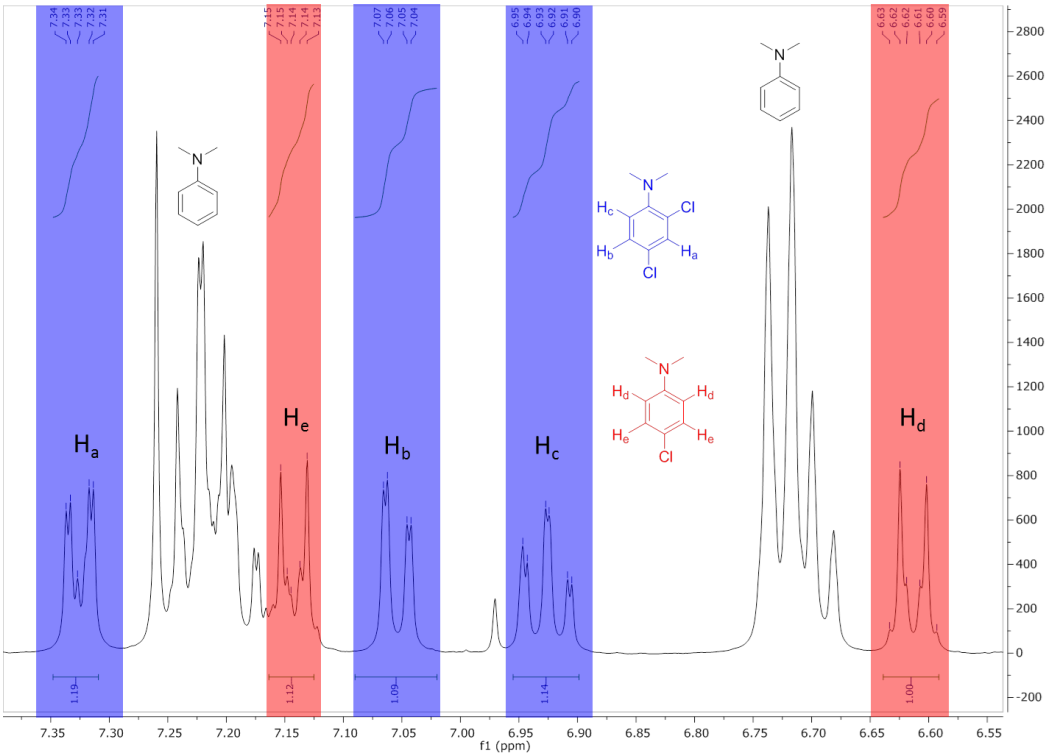

Figure A27. An exemplary ^{1}H NMR spectrum of N,N-dimethylaniline chlorination reaction mixture. Signals of hydrogen atoms in 4-chloro-N,N-dimethylaniline are highlighted with red color, 2,4-dimethyl-N,N-dimethylaniline – with blue color.

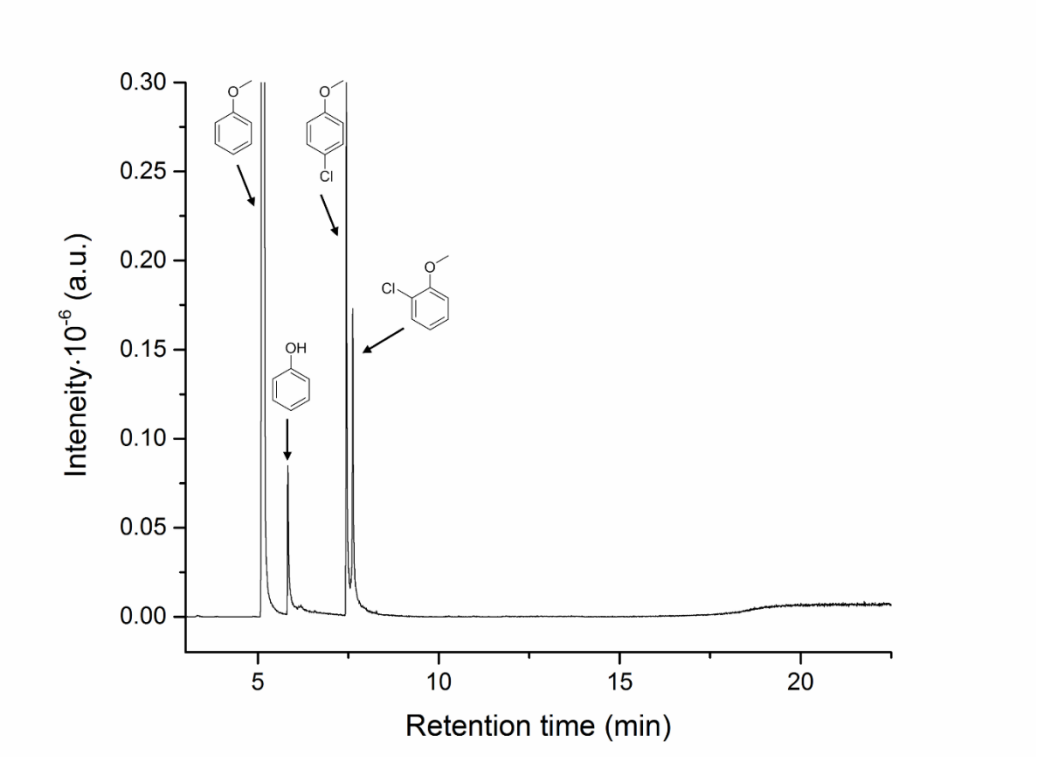

Figure A28. Chromatogram of anisole oxidative chlorination performed in NaCl water solution.

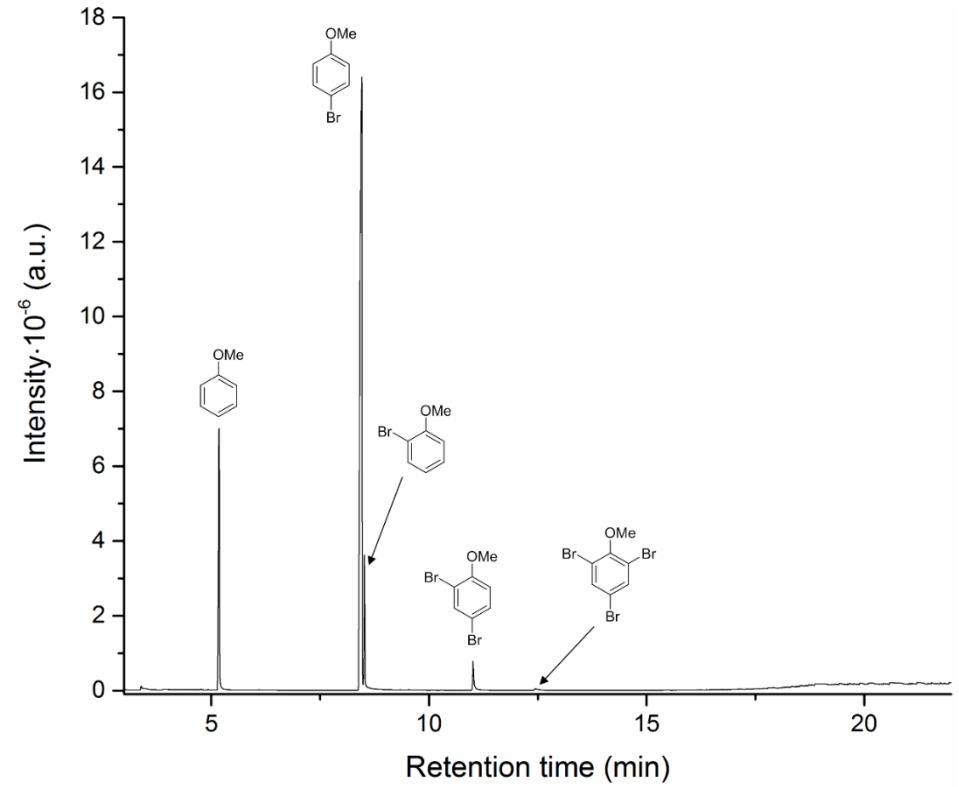

Figure A29. Chromatogram of anisole oxidative bromination (reaction mixture).

11.10. Supplementary information to the Chapter 9

Light sources

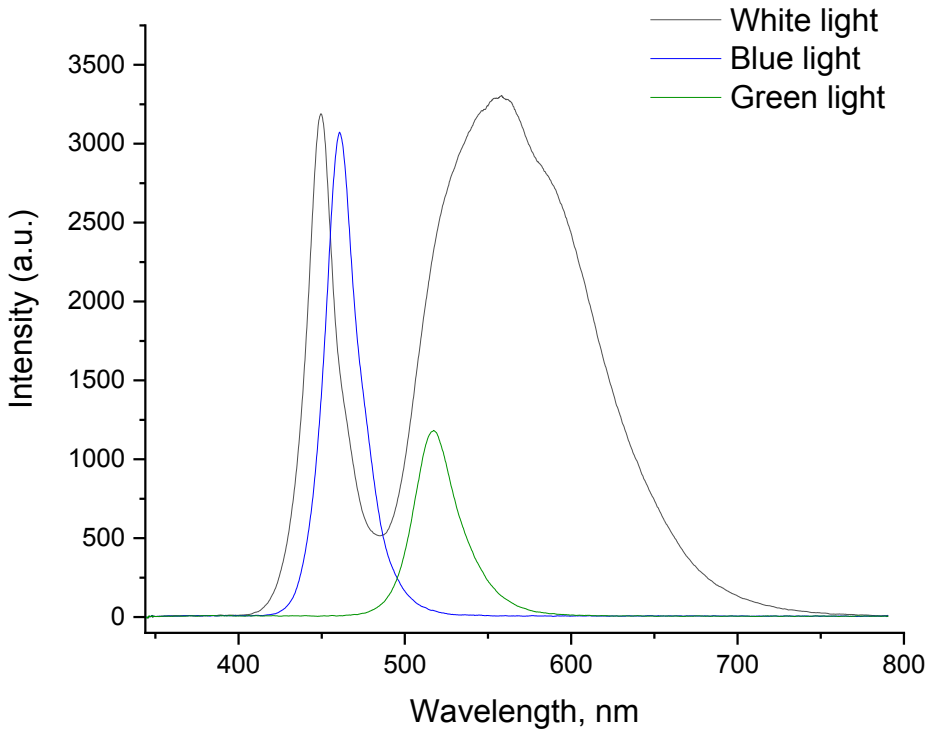

Figure A30. Emission spectra of white, blue and greed LEDs.

Table A6. Optical power of LEDs*

	Light	Wavelength, nm	Power, mW cm^{-2}
1	UV	365	17.1
2	Violet	410	64.7
3	Blue	465	46.2
4	Blue 50%	465	22.6
5	White	410-800	139.3
6	Green	520-525	20.5
7	Red	620-625	29.9

* Optical power was measured at the distance of 10 cm.

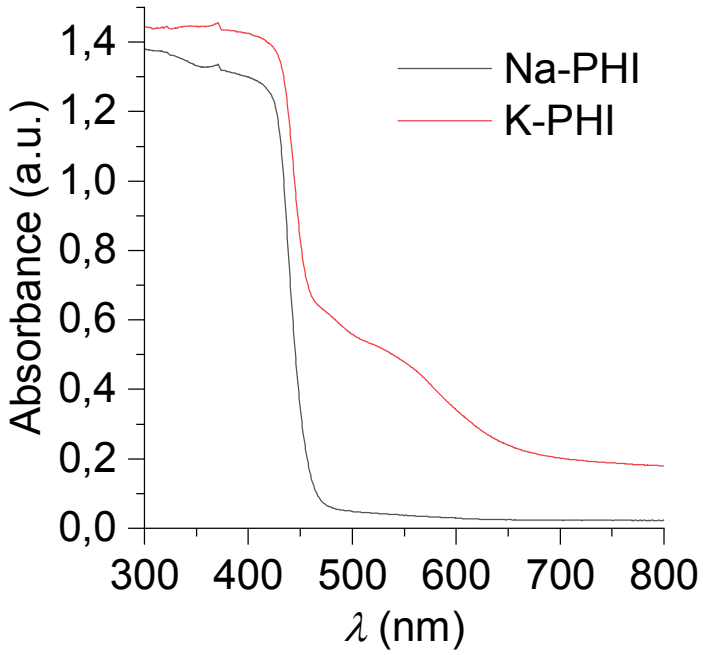

Figure A31. UV-vis absorption spectra of Na-PHI (grey) and K-PHI (red).

Synthesis of arenediazonium tetrafluoroborates

The diazonium salts have been prepared according to the reported procedure.[255] Typically, a solution of $NaNO_2$ (0.69 g, 10 mmol) was added dropwise to a cooled on the ice bath solution of arylamine (10 mmol) in HBF_4 (3.54 mL, 27 mmol) upon stirring. The reaction mixture was stirred on the ice bath for additional 2 h. Precipitate was separated by filtration, dissolved in acetone (150 mL) and maintained at -20 °C overnight. Transparent crystals precipitated.

Diethylether (200 mL) was added and suspension was maintained at -20 °C for 1 h, solid was separated by filtration, washed with cold diethylether (2 times 5 mL) and dried on filter.

4-bromobenzenediazonium tetrafluoroborate

Yield: 86%. ^{1}H NMR (400 MHz, DMSO) δ 8.57 (d, *J* = 9.0 Hz, 2H), 8.26 (d, *J* = 9.0 Hz, 2H). ^{13}C NMR (101 MHz, DMSO) δ 136.59, 134.57, 134.03, 115.76.

4-methoxybenzenediazonium tetrafluoroborate

Yield 78%. ^{1}H NMR (400 MHz, DMSO) δ 8.61 (d, *J* = 9.4 Hz, 2H), 7.48 (d, *J* = 9.4 Hz, 2H), 4.04 (s, 3H). ^{13}C NMR (101 MHz, DMSO) δ 168.78, 136.17, 117.30, 103.43, 57.51.

4-cyanobenzenediazonium tetrafluoroborate

Yield: 88%. ^{1}H NMR (400 MHz, DMSO) δ 8.84 (d, *J* = 8.9 Hz, 2H), 8.46 (d, *J* = 8.9 Hz, 2H). ^{13}C NMR (101 MHz, DMSO) δ 134.87, 133.08, 121.78, 121.13, 116.45.

4-(methoxycarbonyl)benzenediazonium tetrafluoroborate

Yield: 65%. ^{1}H NMR (400 MHz, DMSO) δ 8.79 (d, *J* = 8.8 Hz, 2H), 8.44 (d, *J* = 8.8 Hz, 2H), 3.95 (s, 3H). ^{13}C NMR (101 MHz, DMSO) δ 163.89, 137.44, 133.21, 130.69, 120.36, 54.34.

Benzenediazonium tetrafluoroborate

Yield 71%. ^{1}H NMR (400 MHz, DMSO) δ 8.66 (d, *J* = 7.6 Hz, 2H), 8.26 (t, *J* = 7.6 Hz, 1H), 7.98 (d, 2H). ^{13}C NMR (101 MHz, DMSO) δ 140.87, 132.71, 131.28, 116.11.

4-chlorobenzenediazonium tetrafluoroborate

Yield: 85%. ^{1}H NMR (400 MHz, DMSO) δ 8.69 (d, *J* = 9.0 Hz, 2H), 8.11 (d, *J* = 9.0 Hz, 2H). ^{13}C NMR (101 MHz, DMSO) δ 146.51, 134.44, 131.64, 114.82.

4-nitrobenzenediazonium tetrafluoroborate

Yield: 97%. ^{1}H NMR (400 MHz, DMSO) δ 8.92 (d, *J* = 9.3 Hz, 2H), 8.72 (d, *J* = 9.3 Hz, 2H). ^{13}C NMR (101 MHz, DMSO) δ 153.21, 134.52, 126.07, 121.95.

Synthesis of S-benzylisothiourea hydrochloride and S-(4-trifluoromethylbenzyl)isothiourea hydrochloride

In a round bottom flask with a reflux condenser benzylchloride (8 mmol), thiourea (8 mmol) and ethanol (5 mL) were placed. The mixture was refluxed for 2 h and cooled to room temperature. The resulting solution was concentrated under reduced pressure. The formed precipitate was washed with EtOAc (5 mL), filtered, dried and analyzed by ^{1}H and ^{13}C NMR.

S-benzylisothiourea hydrochloride

Yield: 93%. ^{1}H NMR (400 MHz, DMSO) δ 9.19 (s, 4H), 7.46 – 7.28 (m, 5H), 4.49 (s, 2H). ^{13}C NMR (101 MHz, DMSO) δ 169.01, 135.09, 129.03, 128.87, 128.06, 34.15.

S-(4-trifluoromethylbenzyl)isothiourea hydrochloride

Yield: 86%. ^{1}H NMR (400 MHz, DMSO) δ 9.17 (s, 4H), 7.77 (d, J = 8.2 Hz, 2H), 7.65 (d, J = 8.1 Hz, 2H), 4.58 (s, 2H). ^{13}C NMR (101 MHz, DMSO) δ 168.62, 140.57, 129.79, 128.57, 125.73, 125.69, 122.81, 33.32.

Synthesis of 4-methoxybenzene thioacetate and 2-trifluoromethylbenzene thioacetate

In a round bottom flask aryl thiol (0.7 mmol) and trimethylamine (1.4 mmol, 2 eqv.) were dissolved in dichloromethane (15 mL). Solution was cooled with ace bath to 0 °C and acetyl chloride (1.05 mmol, 1.5 eqv.) in dichloromethane (5 mL) was added dropwise (exothermic reaction). Reaction was kept with stirring overnight at room temperature. Then solution was washed with water (3 times 5mL), dried over $NaSO_4$, concentrated and analyzed by ^{1}H NMR.

4-methoxybenzene thioacetate

^{1}H NMR (400 MHz, $CDCl_3$) δ 7.32 (d, J = 8.9 Hz, 2H), 6.94 (d, J = 8.9 Hz, 2H), 3.83 (s, 2H), 2.40 (s, 3H). ^{13}C NMR (101 MHz, $CDCl_3$) δ 195.40, 160.74, 136.18, 118.72, 114.96, 55.44, 30.06.

2-trifluoromethylbenzene thioacetate.

^{1}H NMR (400 MHz, $CDCl_3$) δ 7.79 (d, J = 7.8 Hz, 1H), 7.66 – 7.50 (m, 3H), 2.46 (s, 3H). ^{13}C NMR (101 MHz, $CDCl_3$) δ 192.68, 139.04, 132.40, 130.05, 127.24, 127.19, 121.94, 30.39.

Sulfonyl chlorides synthesis

Method 1 from thiols and their derivatives

In a glass vial a substrate (0.04 mmol) was dissolved in acetonitrile (0.5 mL). HCl (0.1 mL, 36 wt.%, 1.2 mmol), water (0.1 mL) and K-PHI (4 mg) were added. The reaction mixture was stirred under light irradiation at room temperature for 24 h under O_2 atmosphere. After the irradiation $CHCl_3$ (3 mL) and water (0.3 mL) were added to the reaction mixture. The layers were separated, organic layer was dried over $NaSO_4$ and concentrated under reduced pressure. Residue was analyzed by ^{1}H NMR. The NMR spectral data match to the reported earlier.[256-257]

Benzenesulfonyl chloride

^{1}H NMR (400 MHz, $CDCl_3$) δ 8.04 (d, 2H), 7.74 (t, 1H), 7.62 (t, 2H).

2-trifluoromethylbenzenesulfonyl chloride

^{1}H NMR (400 MHz, $CDCl_3$) δ 8.35 (d, *J* = 8.7 Hz, 1H), 7.97 (d, *J* = 7.4 Hz, 1H), 7.92 – 7.79 (m, 2H).

4-nitrobenzenesulfonyl chloride

^{1}H NMR (400 MHz, $CDCl_3$) δ 8.46 (d, *J* = 9.1 Hz, 2H), 8.24 (d, *J* = 9.6 Hz, 2H).

4-methoxybenzenesulfonyl chloride

^{1}H NMR (400 MHz, $CDCl_3$) δ 7.98 (d, *J* = 9.0 Hz, 2H), 7.05 (d, *J* = 9.0 Hz, 2H), 3.93 (s, 3H).

Benzylsulfonyl chloride

^{1}H NMR (400 MHz, $CDCl_3$) δ 7.55 – 7.42 (m, 5H), 4.87 (s, 2H).

4-trifluoromethylbenzylsulfonyl chloride

^{1}H NMR (400 MHz, $CDCl_3$) δ 7.72 (d, *J* = 8.2 Hz, 2H), 7.62 (d, *J* = 8.2 Hz, 2H), 4.92 (s, 2H).

Method 2 from arenediazonium tetrafluoroborates

A glass vial was charged with arenediazonium salt (0.025 mmol), and K-PHI (4 mg), acetonitrile (1 mL) (or chloroform for phenyldiazonium tetrafluoroborate) and the solution was purged with N_2 for 5 min. Then, water (5 μL, 0.28 mmol) and $SOCl_2$ (19 μL, 0.16 mmol) were added. The reaction mixture was stirred under blue LED irradiation (465 nm, 46 $mW \cdot cm^{-2}$) at room temperature for 24 h. After the irradiation solution was concentrated under reduced pressure and analyzed by ^{1}H NMR. The NMR spectral data match to the reported earlier.[258]

4-bromobenzenesulfonyl chloride

^{1}H NMR (400 MHz, $CDCl_3$) δ 7.91 (d, *J* = 8.8 Hz, 2H), 7.77 (d, *J* = 8.8 Hz, 2H).

4-cyanobenzenesulfonyl chloride

^{1}H NMR (400 MHz, DMSO) δ 7.81 (d, *J* = 8.4 Hz, 2H), 7.74 (d, *J* = 8.4 Hz, 2H).

4-(methoxycarbonyl)benzene sulfonyl chloride

^{1}H NMR (400 MHz, DMSO) δ 7.92 (d, *J* = 8.3 Hz, 2H), 7.71 (d, *J* = 8.3 Hz, 2H), 3.84 (s, 3H).

4-chlorobenzenesulfonyl chloride

^{1}H NMR (400 MHz, DMSO) δ 7.63 – 7.55 (m, 2H), 7.37 (d, *J* = 8.5 Hz, 2H).

4-nitrobenzenesulfonyl chloride

^{1}H NMR (400 MHz, DMSO) δ 8.21 (d, *J* = 8.8 Hz, 2H), 7.83 (d, *J* = 8.8 Hz, 4H).

4-methoxybenzenesulfonyl chloride

^{1}H NMR (400 MHz, DMSO) δ 7.52 (d, *J* = 8.7 Hz, 2H), 6.86 (d, *J* = 8.7 Hz, 2H).

Sulfonyl amides synthesis

In a glass vial a substrate (0.04 mmol) was dissolved in acetonitrile (0.5 mL). NH_4Cl (10mg, 0.19 mmol), water (0.2 mL) and K-PHI (4 mg) were added. The reaction mixture was stirred under blue LED (465 nm, 46 mW·cm^{-2}) irradiation at room temperature for 24 h under O_2 atmosphere. After the irradiation $CHCl_3$ (3 mL) and water (0.3 mL) were added to the reaction mixture. The layers were separated, organic layer was dried over $NaSO_4$ and concentrated under reduced pressure. Residue was analyzed by ^{1}H NMR. The NMR spectral data match to the reported earlier.[259-260]

Benzenesulfonyl amide

^{1}H NMR (400 MHz, $CDCl_3$) δ 7.93 (d, *J* = 7.2 Hz, 1H), 7.62 – 7.51 (m, 3H).

4-nitrobenzenesulfonyl amide

^{1}H NMR (400 MHz, $CDCl_3$) δ 8.34 (d, *J* = 8.9 Hz, 2H), 8.10 (d, *J* = 8.9 Hz, 2H).

4-methoxybenzenesulfonyl amide

^{1}H NMR (400 MHz, $CDCl_3$) δ 7.86 (d, *J* = 9.0 Hz, 2H), 6.98 (d, *J* = 8.9 Hz, 2H), 3.83 (s, 3H).

Synthesis of benzenesulfonyl chloride

N-chlorosuccinimide (4.85 g, 4 eqv.) was dissolved in a mixture of hydrochloric acid (2 mL, 2M) and acetonitrile (10 mL). The solution was cooled to 5 °C and thiophenol (1 g, 9 mmol) in acetonitrile (5 mL) was added dropwise. The reaction mixture was stirred at 5 °C for 10 min and was let warm up to room temperature for 30 min. Water (5 mL) was added to the reaction mixture and it was extracted with ether (3 times, 10 mL). Organic solution was dried over $NaSO_4$ and concentrated. Precipitate was filtered off, washed with cold ether (2 mL). Filtrate was purified by column chromatography. Yield 86%.

^{1}H NMR (400 MHz, $CDCl_3$) δ 8.06 (d, *J* = 8.1 Hz, 2H), 7.76 (t, *J* = 7.5 Hz, 1H), 7.64 (t, *J* = 7.9 Hz, 2H). ^{13}C NMR (101 MHz, $CDCl_3$) δ 135.39, 129.85, 127.15.

Synthesis of phenylsulfonyl chloride under sunlight

In a glass vial S-phenylthioacetate (0.04 mmol) was dissolved in acetonitrile (0.5 mL). HCl (0.1 mL, 36 wt.%, 1.2 mmol), water (0.1 mL) and K-PHI (5 mg) were added. The reaction mixture was stirred under direct sunlight irradiation (69 $mW \cdot cm^{-2}$ at reactor surface, 10am 04 June 2019 at 52°24'53.2"N 12°58'11.4"E) at ambient temperature for 5 h under O_2 atmosphere. After the irradiation $CHCl_3$ (3 mL) and water (0.3 mL) were added to the reaction mixture. The layers were separated, organic layer was dried over $NaSO_4$ and concentrated under reduced pressure. Residue was analyzed by ^1H NMR.

Procedure of K-PHI regeneration

K-PHI after the reaction was separated by centrifugation, washed with acetonitrile (2 times, 2 mL each) and with water (2 times, 2 mL each). KOH solution (9 mL, 0.1 M) was added to the catalyst and suspension was stirred for 20 h. The catalyst was separated by centrifugation, washed with water (3 times, 3 mL each), once with methanol and dried in vacuum overnight.

Supplementary Note 1

For the case with phenyldiazonium tetrafluoroborate reaction was carried out in dichloromethane, as it reacts with acetonitrile to form phenylacetamide ^1H NMR spectra of which is presented below.

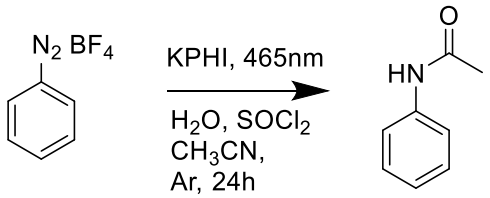

Table A7. Optimization of S-phenylthioacetate oxidation reaction conditions.[a]

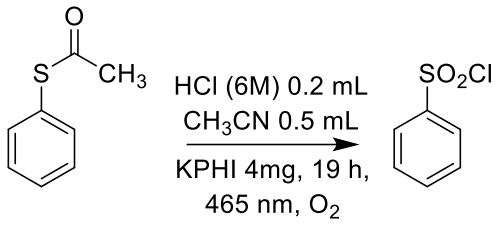

Entry	Substrate	KPHI	HCl, 6M	MeCN	Atmosphere	Light, nm	Yield,%
1	5 mg	4 mg	0.2 mL	0.5 mL	O_2	465	93
2	5 mg	-	0.2 mL	0.5 mL	O_2	465	0
3	5 mg	4 mg	-	0.5 mL	O_2	465	0
4	5 mg	4 mg	0.2 mL	0.5 mL	Ar	465	0
5	5 mg	4 mg	0.2 mL	0.5 mL	O_2	dark	0
6	5 mg	4 mg	HCl/dioxane	0.5 mL	O_2	465	0

[a] S-Phenylthioacetate 0.035 mmol; photocatalyst 4 mg; HCl (36 wt.%) 50 μL; H_2O 0.2 mL; MeCN 0.5 mL; T = 25 °C; electron scavenger – O_2; LED module 465 nm.

Table A8. S-phenylthioacetate oxidation varying temperature. [a]

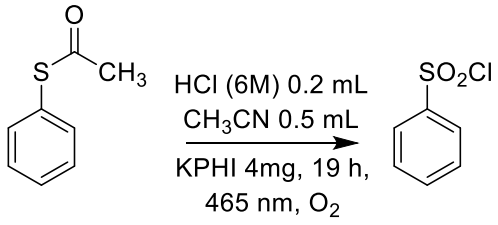

Entry	substrate	KPHI	HCl 6M	MeCN	Atmosphere	Temperature, °C	Yield,%
1	5 mg	4 mg	0.2 mL	0.5 mL	O_2	30	90
2	5 mg	4 mg	0.2 mL	0.5 mL	O_2	45	0
3	5 mg	4 mg	0.2 mL	0.5 mL	O_2	60	0

[a] S-Phenylthioacetate 0.035 mmol; photocatalyst 4 mg; HCl (36 wt.%) 50 μL; H_2O 0.2 mL; MeCN 0.5 mL; electron scavenger – O_2; LED module 465 nm.

Table A9. Sulfonyl chlorides photolysis.[a]

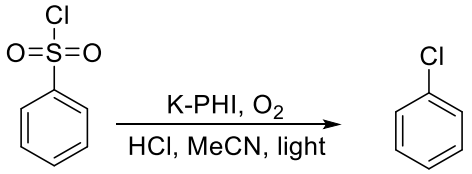

Entry	λ_{max}, nm	K-PHI, mg	Conversion,%	Yield,%
1	365	5 mg	0	0
2	465	5 mg	0	0
3	523	5 mg	0	0
4	365	-	0	0
5	465	-	0	0
6	525	-	0	0

[a] Phenylsulfonyl chloride 0.035 mmol; photocatalyst 5 mg; HCl (36 wt.%) 0.1 mL; H_2O 0.1 mL; MeCN 0.5 mL; electron scavenger – O_2; LED module irradiation.

Table A10. S-phenylthioacetate photolysis. [a]

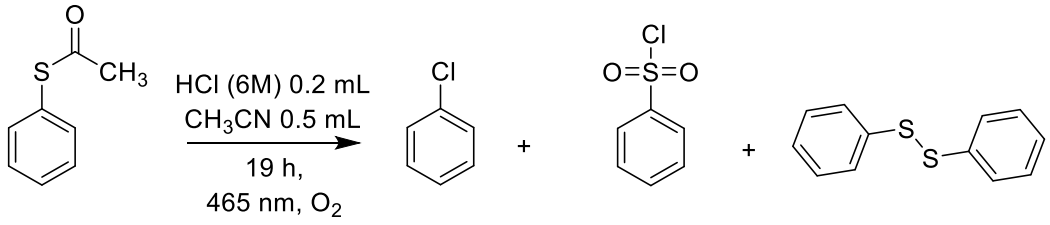

Entry	λ_{max}, nm	Conversion,%	Yield,%
1 ZM 806-2	365	0	0
2 ZM 803-6	465	0	0
3 ZM 806-1	523	0	0

[a] S-Phenylthioacetate 0.035 mmol; HCl (36 wt.%) 0.1 mL; H_2O 0.1 mL; MeCN 0.5 mL; electron scavenger – O_2; LED module irradiation.

NMR spectra

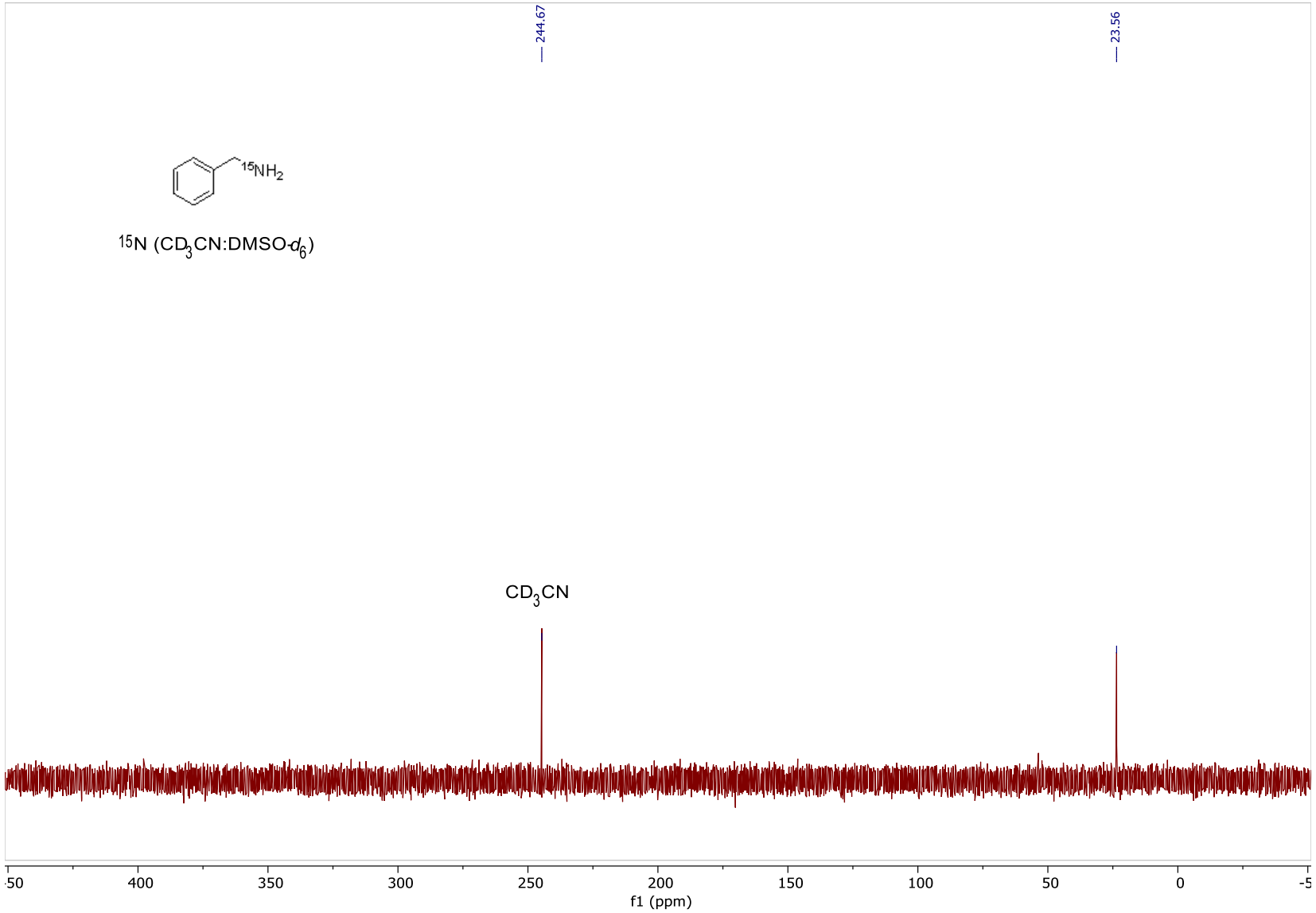
244.67
23.56
$^{15}NH_2$
^{15}N (CD_3CN:DMSO-d_6)
CD_3CN
400
350
300
250
200
150
100
50
0
f1 (ppm)

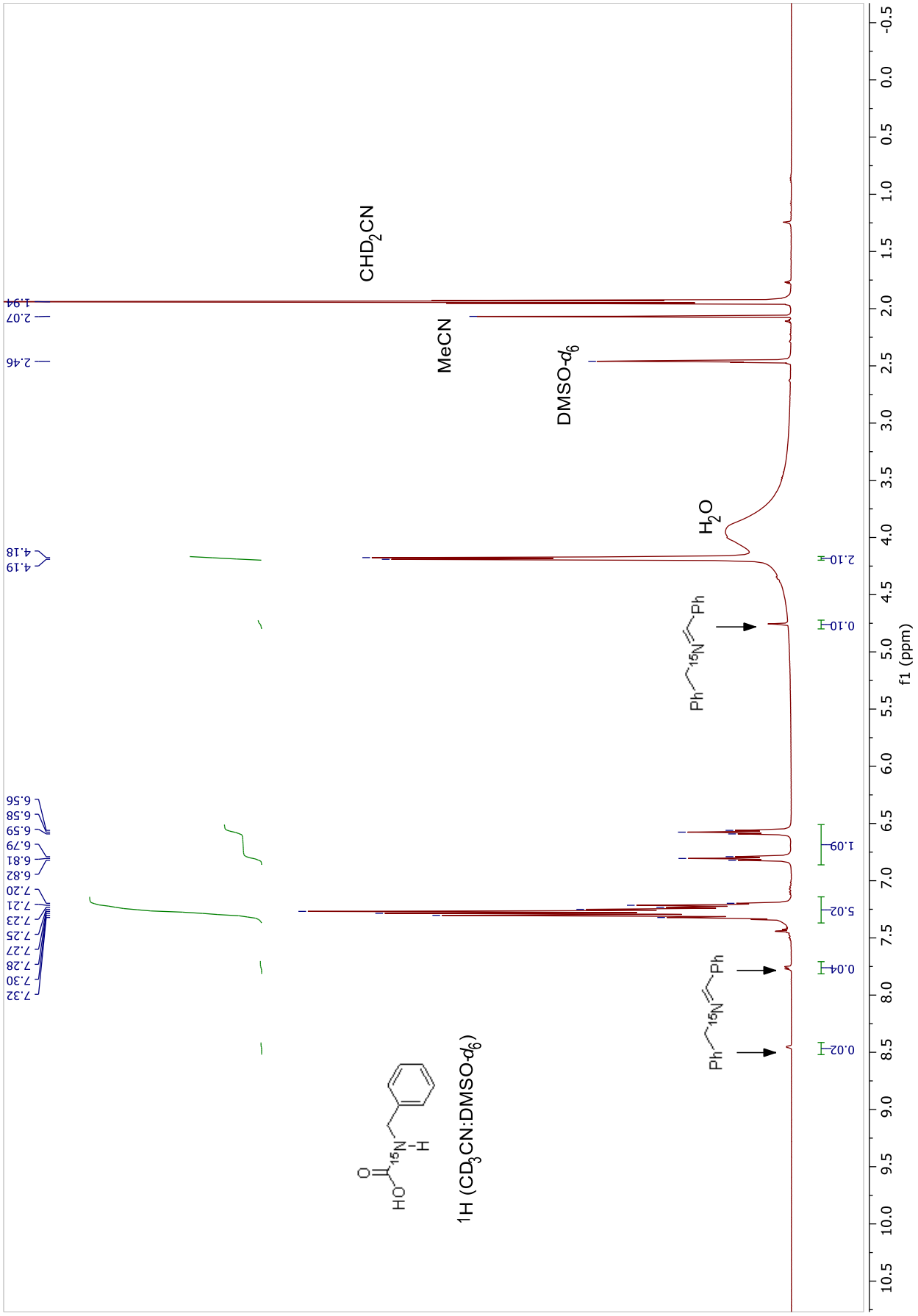
^{1}H (CD_3CN:DMSO-d_6)
CHD_2CN
MeCN
DMSO-d_6
H_2O
f1 (ppm)

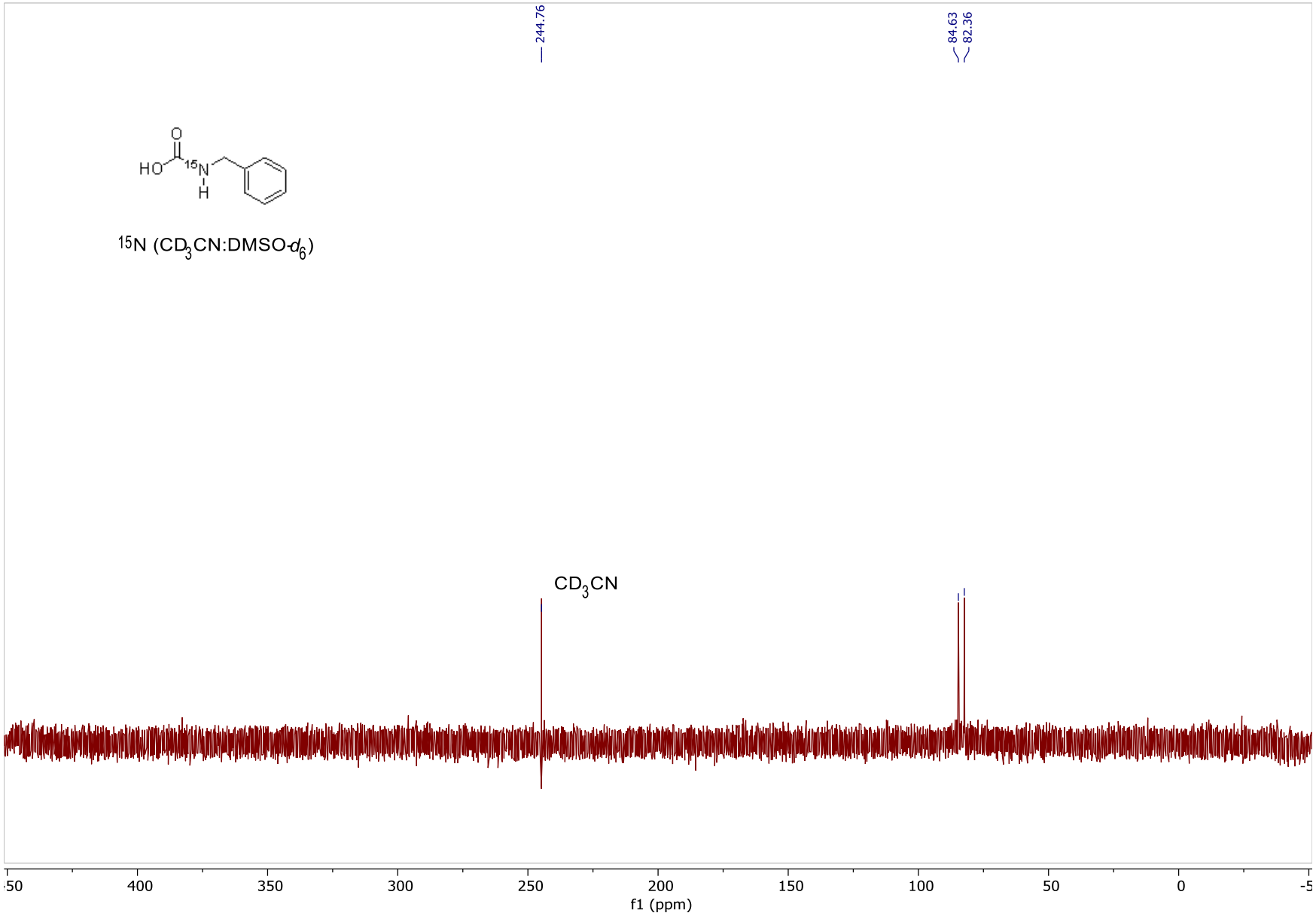
244.76
84.63
82.36
HO
O
15N
H
15N (CD3CN:DMSO-d6)
CD3CN
f1 (ppm)

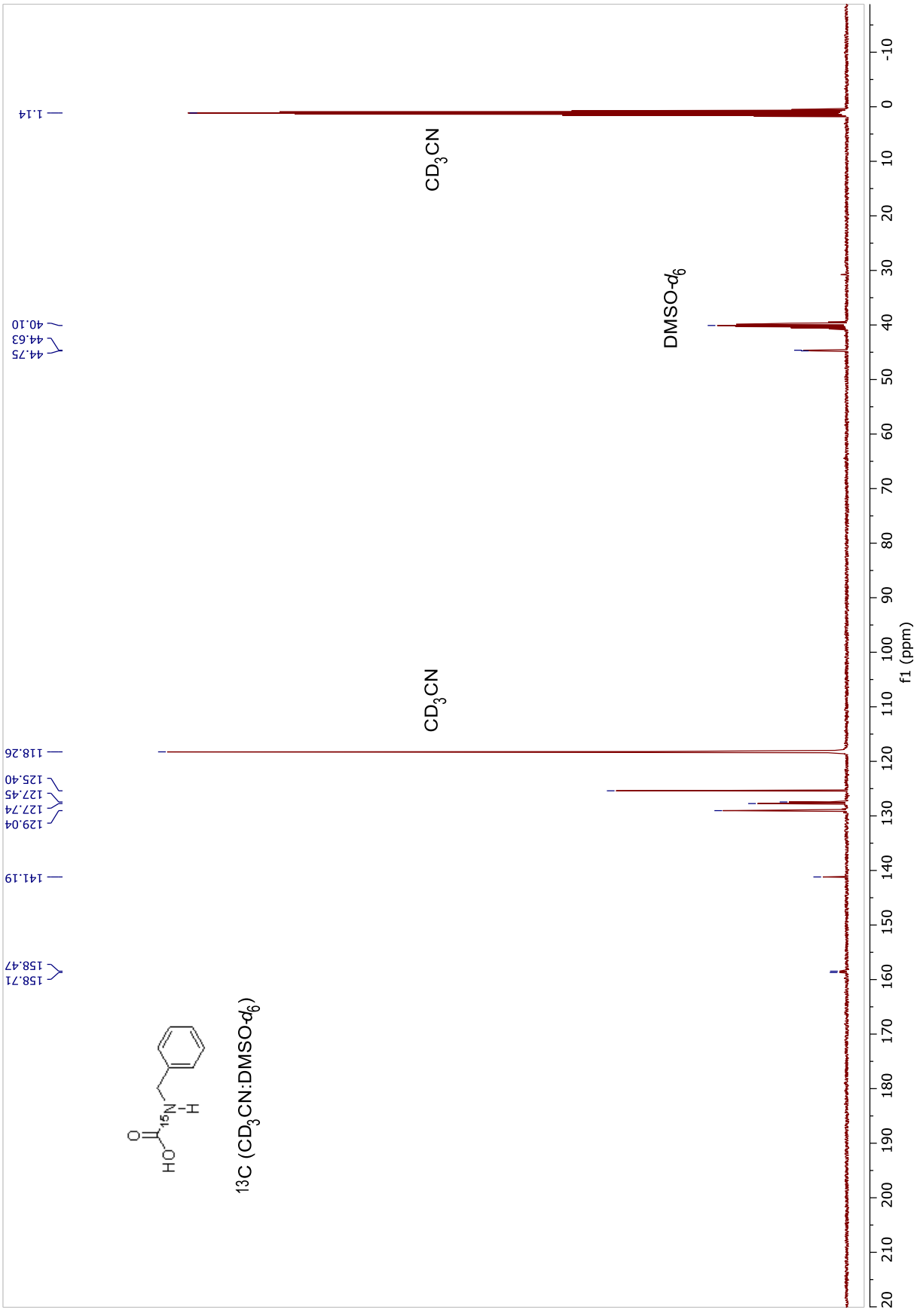
158.71
158.47
141.19
129.04
127.74
127.45
125.40
118.26
44.75
44.63
40.10
1.14
CD3CN
CD3CN
DMSO-d6
f1 (ppm)
13C (CD3CN:DMSO-d6)

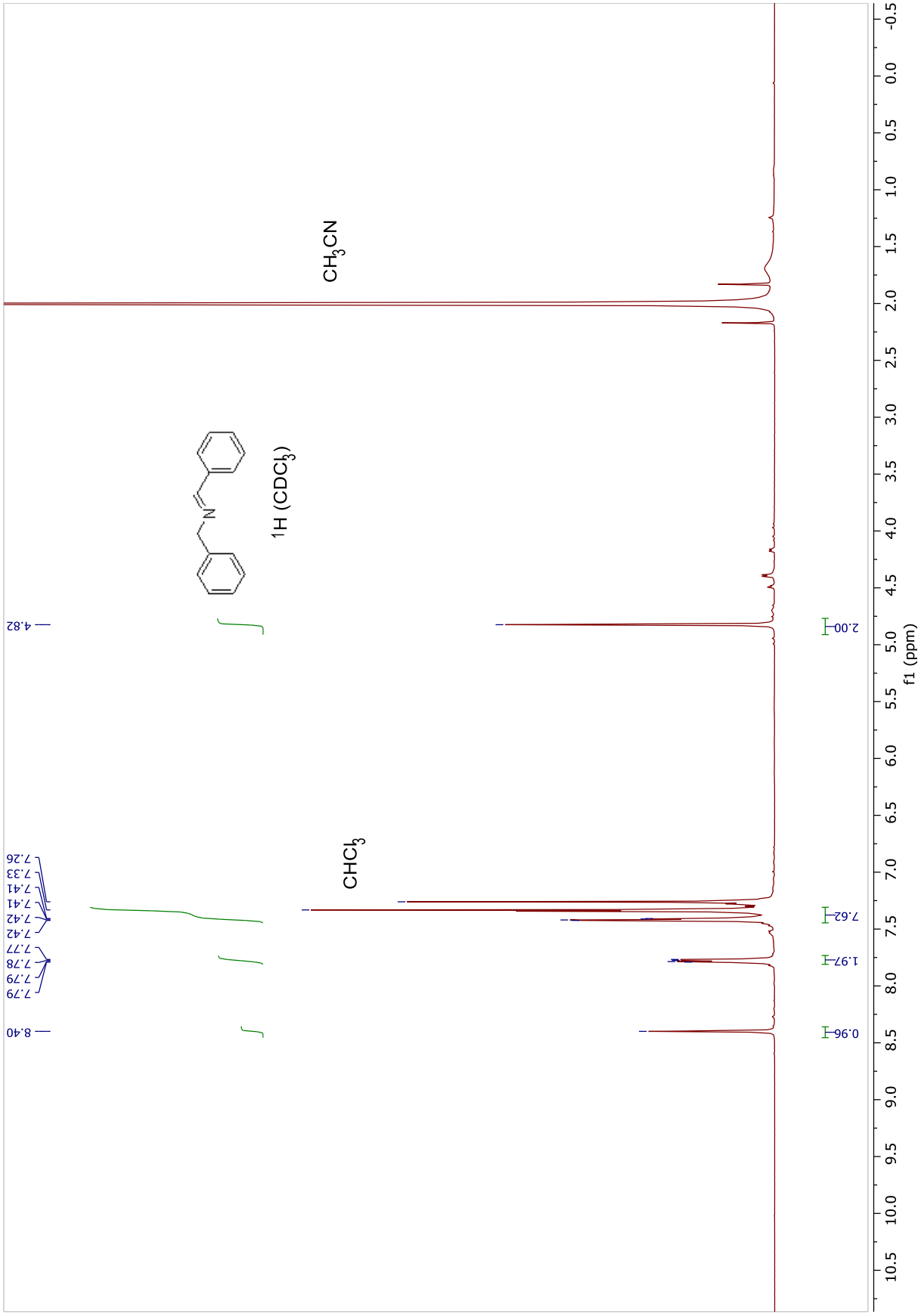
8.40
7.79
7.79
7.78
7.77
7.42
7.42
7.41
7.41
7.33
7.26
4.82
CHCl3
1H (CDCl3)
CH3CN
2.00
7.62
1.97
0.96
f1 (ppm)

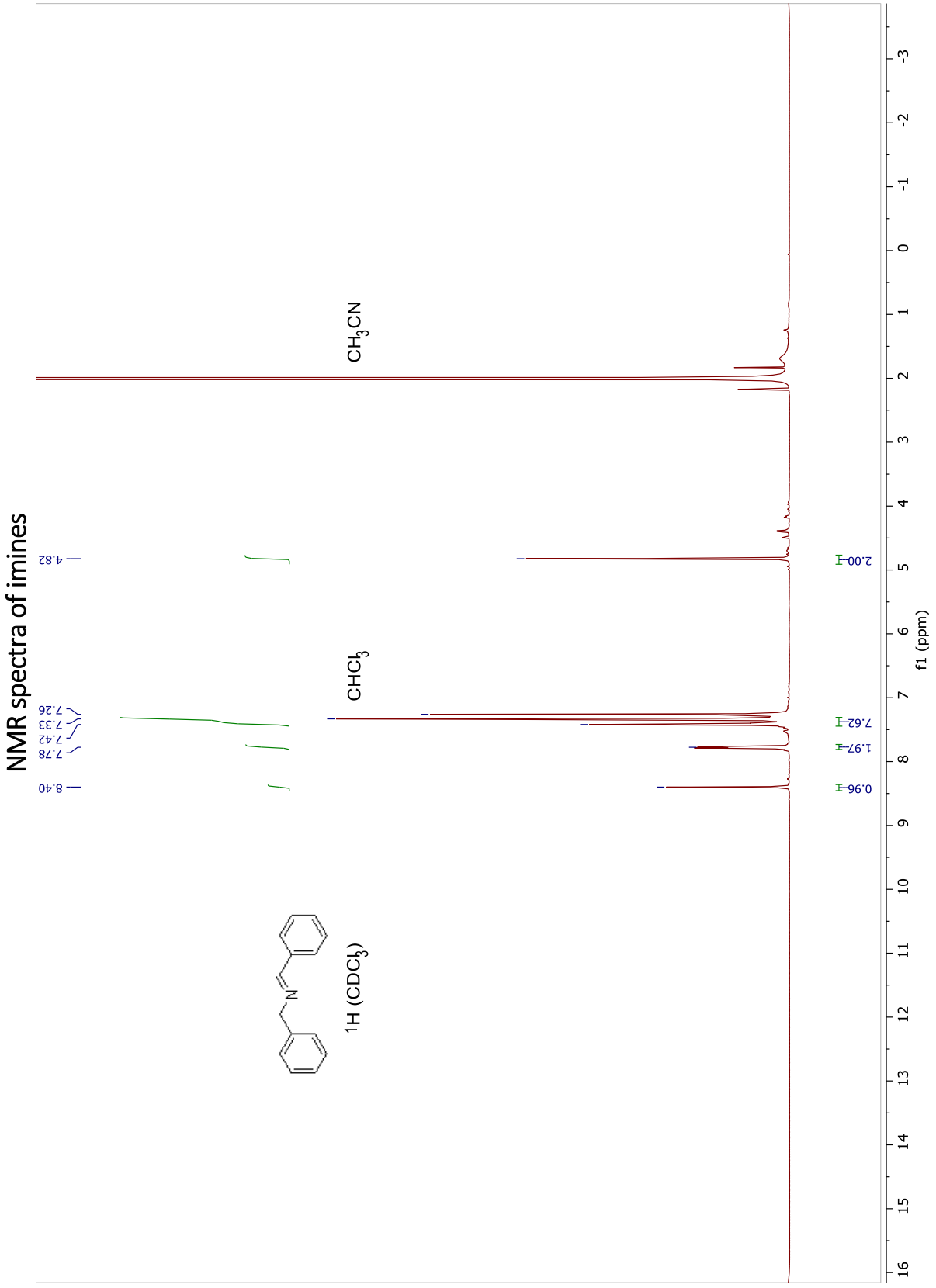
NMR spectra of imines
^{1}H (CDCl$_3$)
CHCl$_3$
CH$_3$CN
8.40
7.78
7.42
7.33
7.26
4.82
0.96
1.97
7.62
2.00
f1 (ppm)

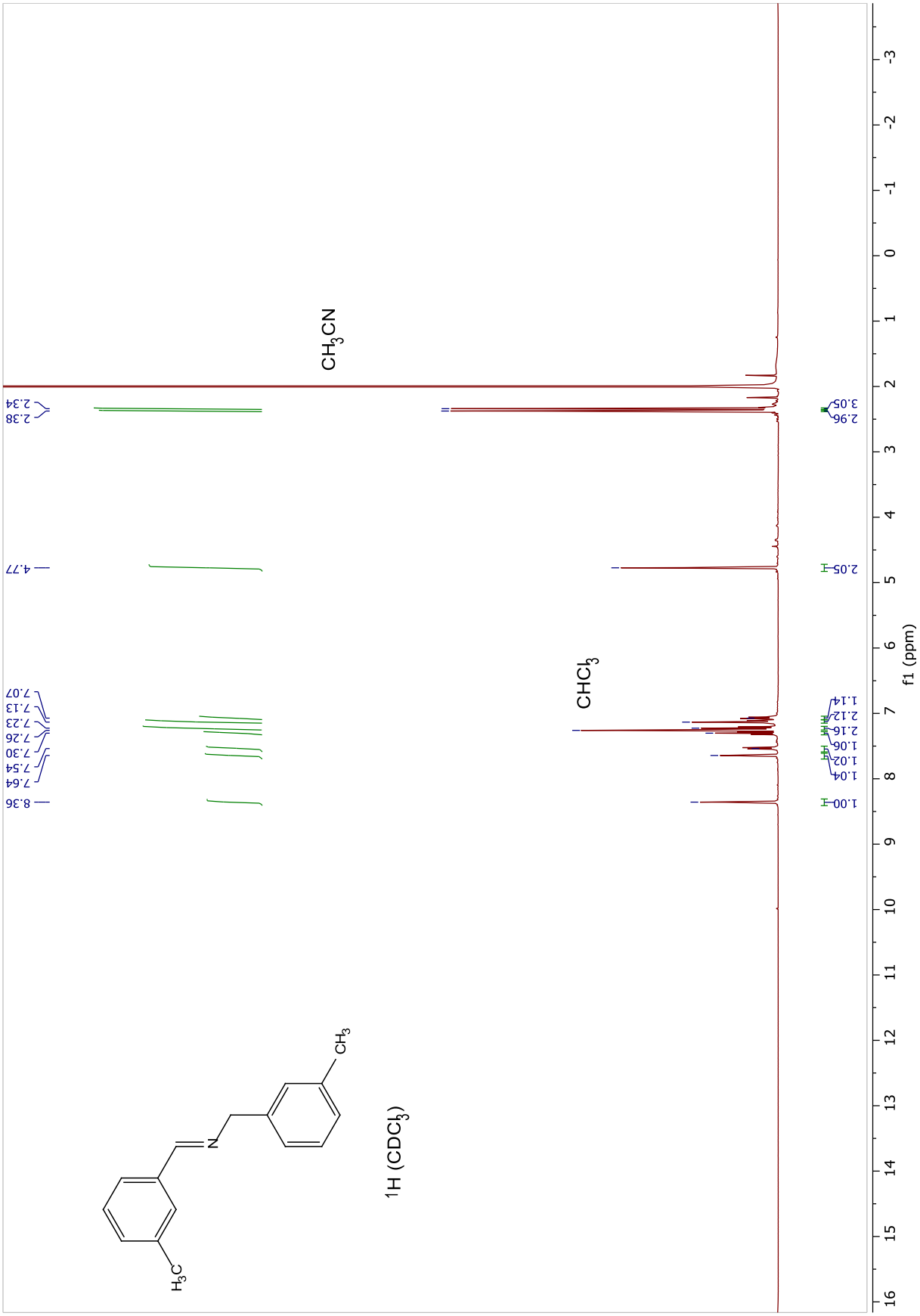
^{1}H ($CDCl_3$)
CH_3CN
$CHCl_3$
f1 (ppm)

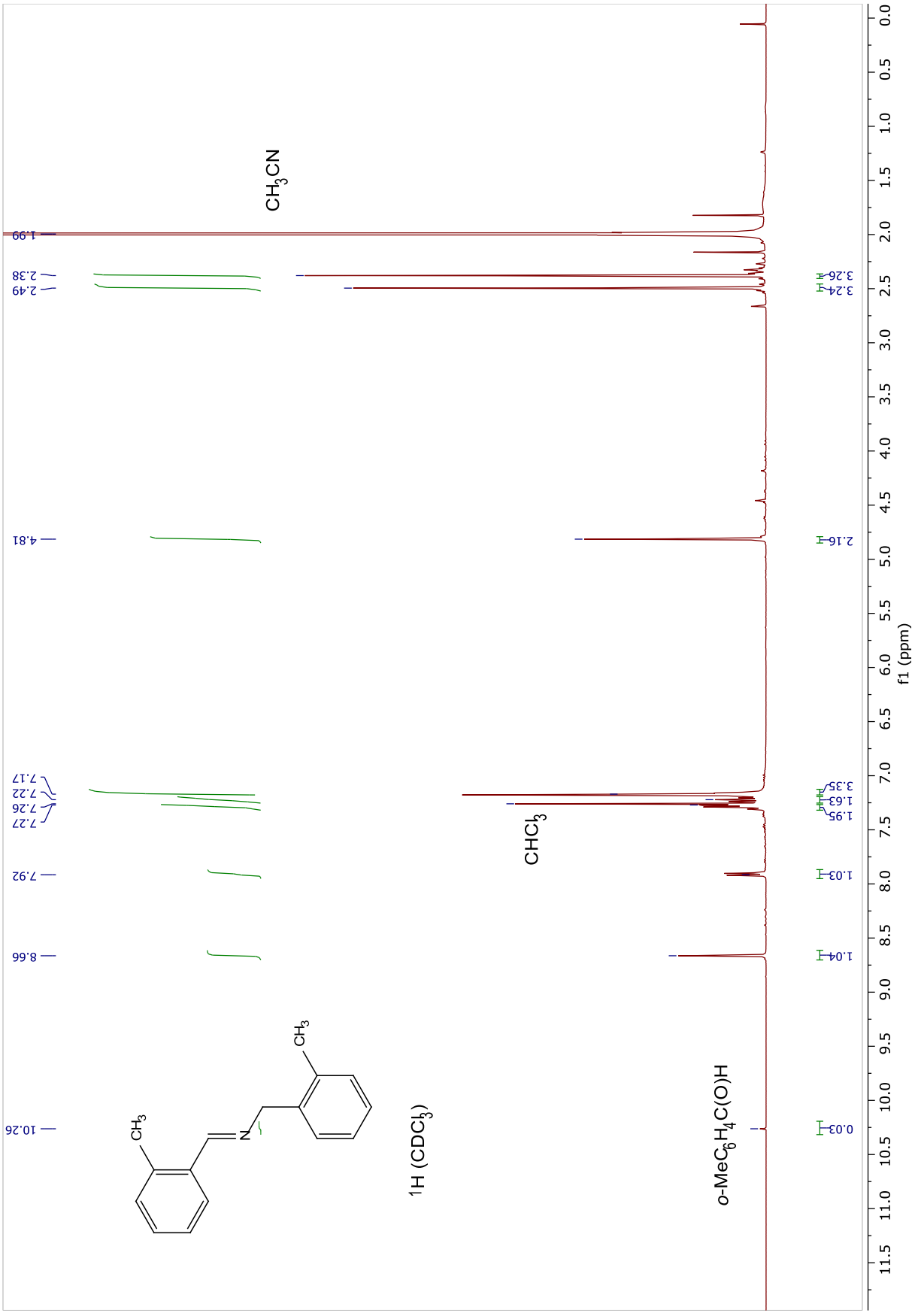
10.26
8.66
7.92
7.27
7.26
7.22
7.17
4.81
2.49
2.38
1.99
3.26
3.24
2.16
1.95
1.63
3.35
1.03
1.04
0.03
CH3CN
CHCl3
1H (CDCl3)
o-MeC6H4C(O)H
f1 (ppm)

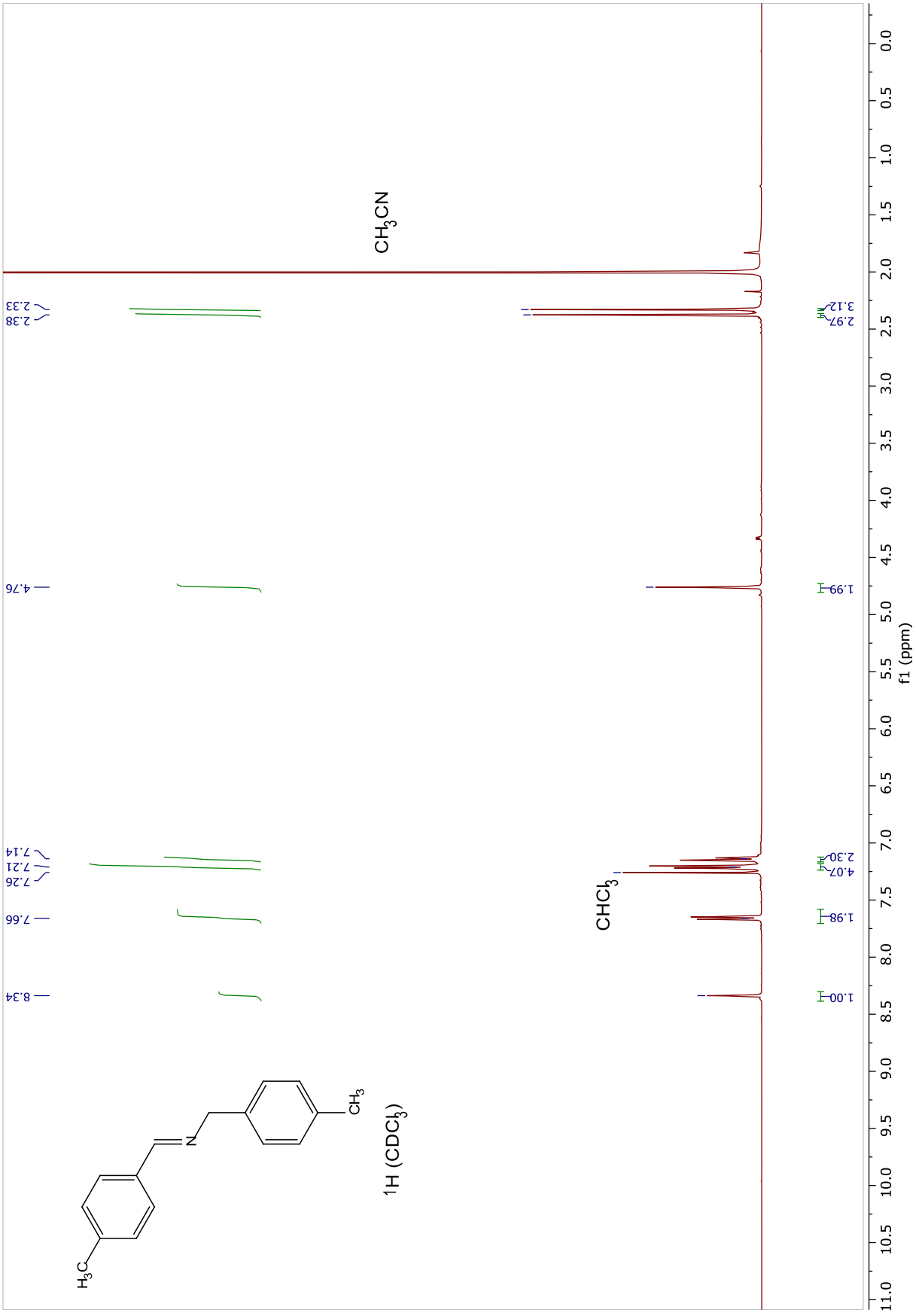
^{1}H (CDCl$_3$)
CH_3CN
$CHCl_3$
f1 (ppm)

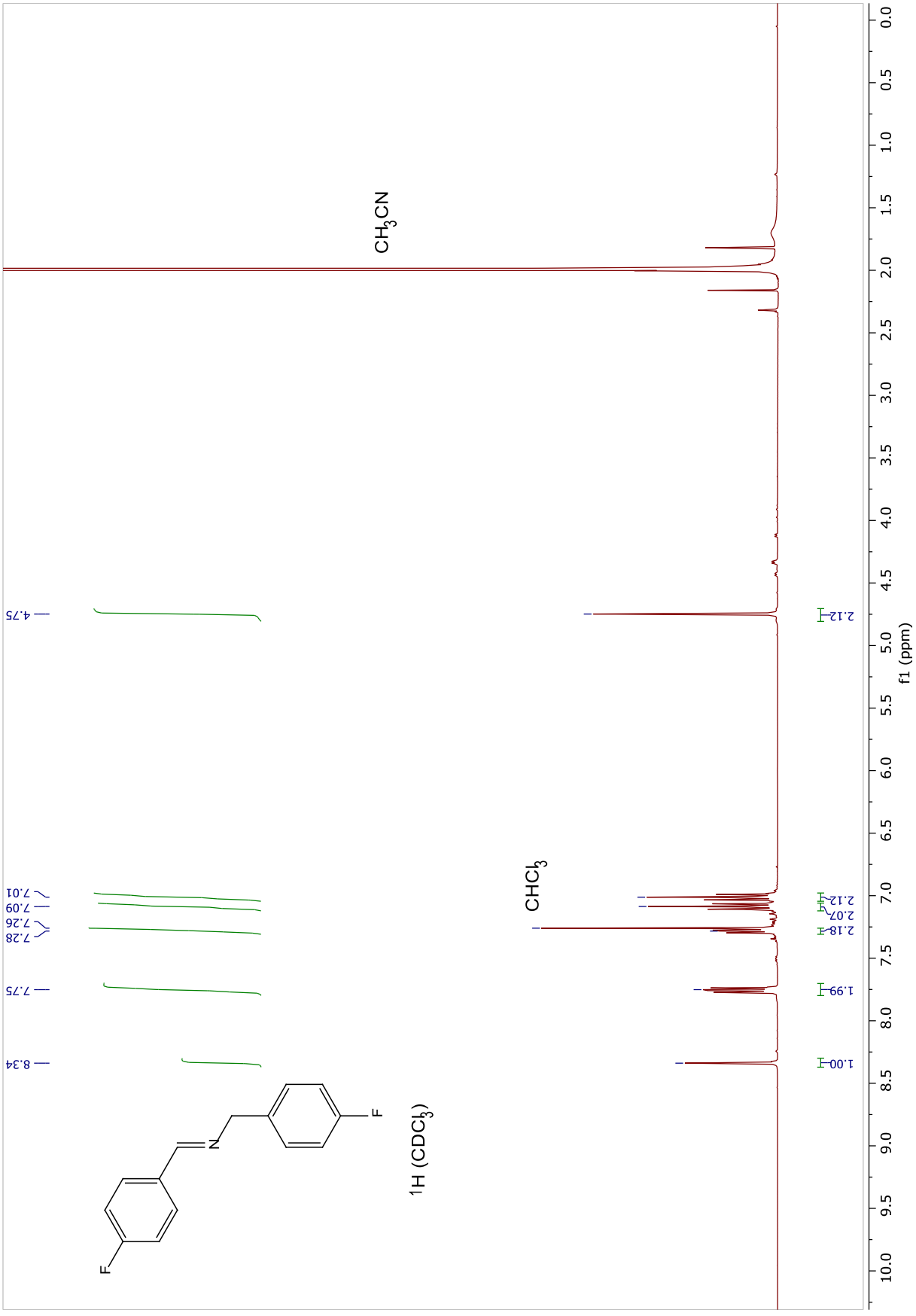
^{1}H (CDCl$_3$)
F
N
F
8.34
7.75
7.28
7.26
7.09
7.01
4.75
CHCl$_3$
CH$_3$CN
1.00
1.99
2.18
2.07
2.12
2.12
f1 (ppm)

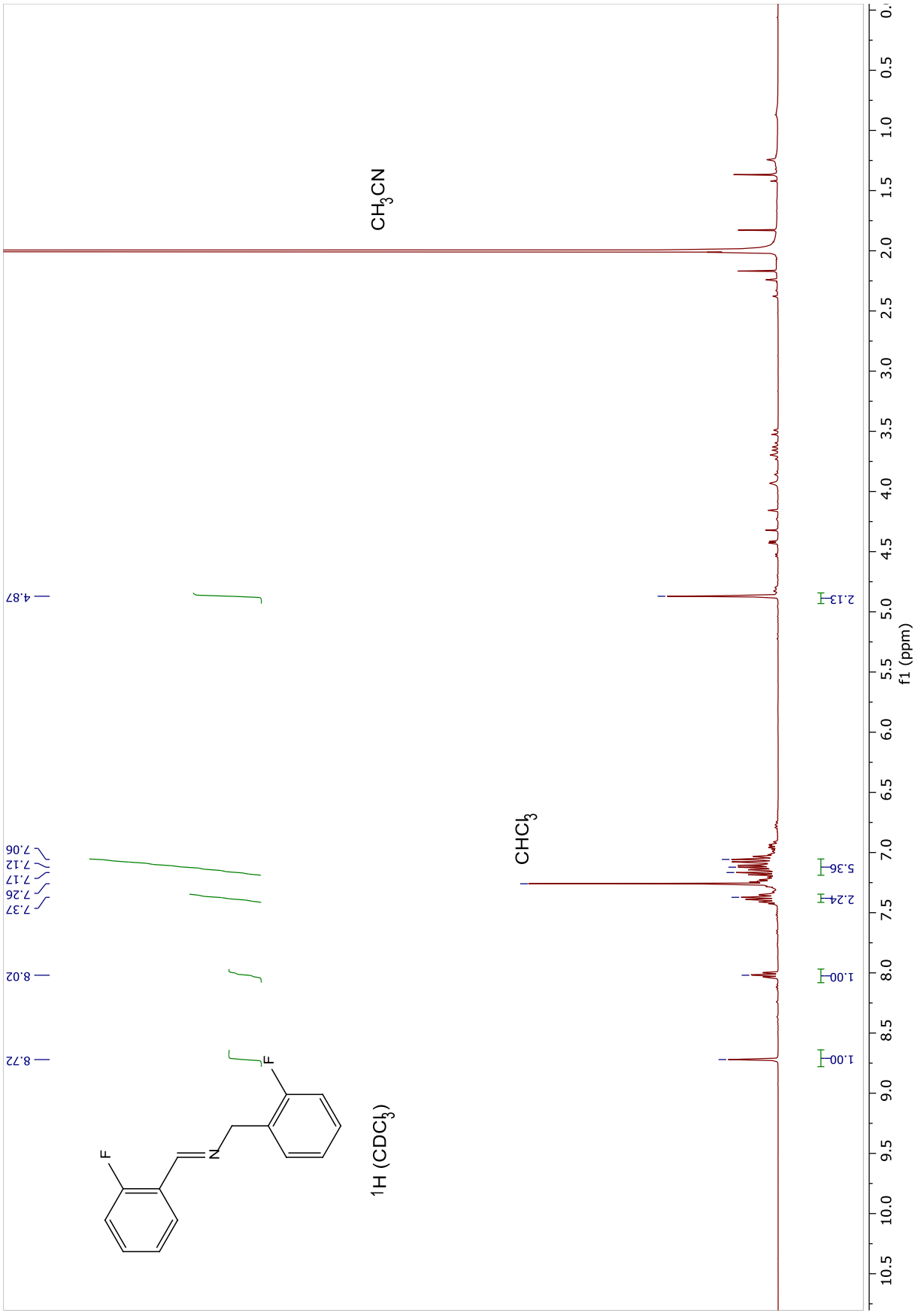
F
N
F
^{1}H (CDCl$_3$)
8.72
8.02
7.37
7.26
7.17
7.12
7.06
4.87
CHCl$_3$
CH$_3$CN
1.00
1.00
2.24
5.36
2.13
f1 (ppm)

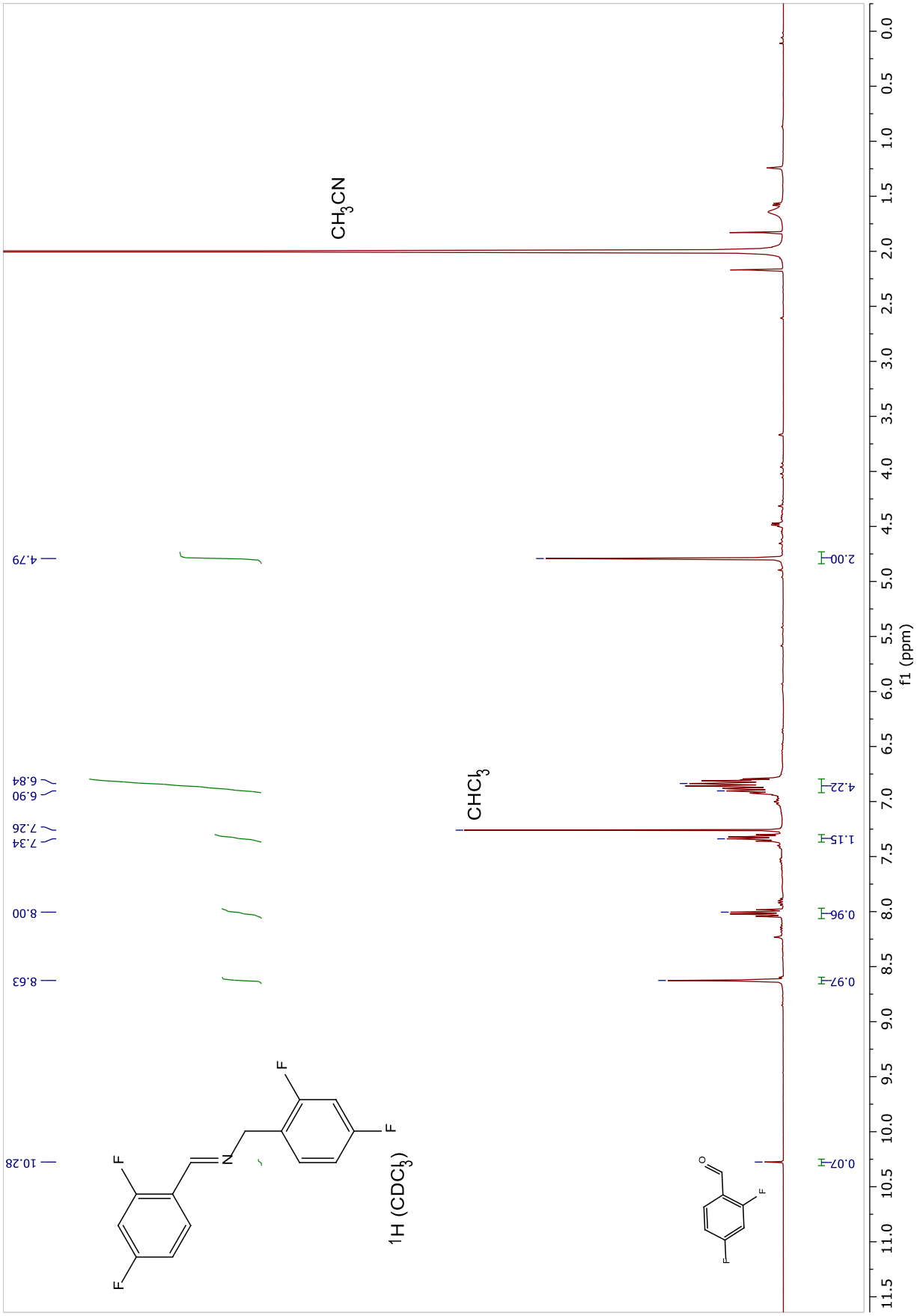
10.28
8.63
8.00
7.34
7.26
6.90
6.84
4.79
0.07
0.97
0.96
1.15
4.22
2.00
CHCl3
CH3CN
1H (CDCl3)
F
F
F
F
N
O
F
f1 (ppm)

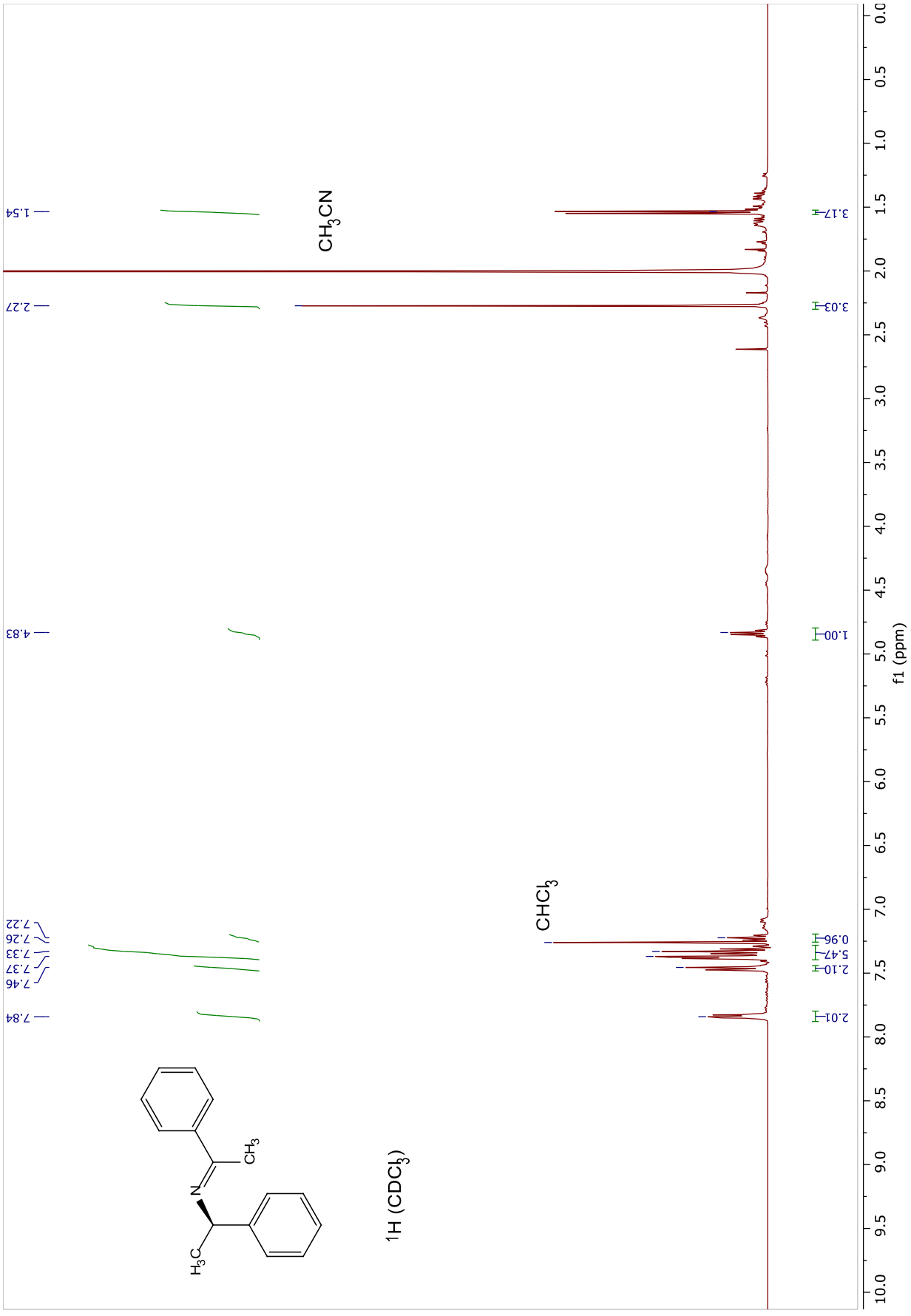
^{1}H ($CDCl_3$)
CH_3CN
$CHCl_3$
f1 (ppm)

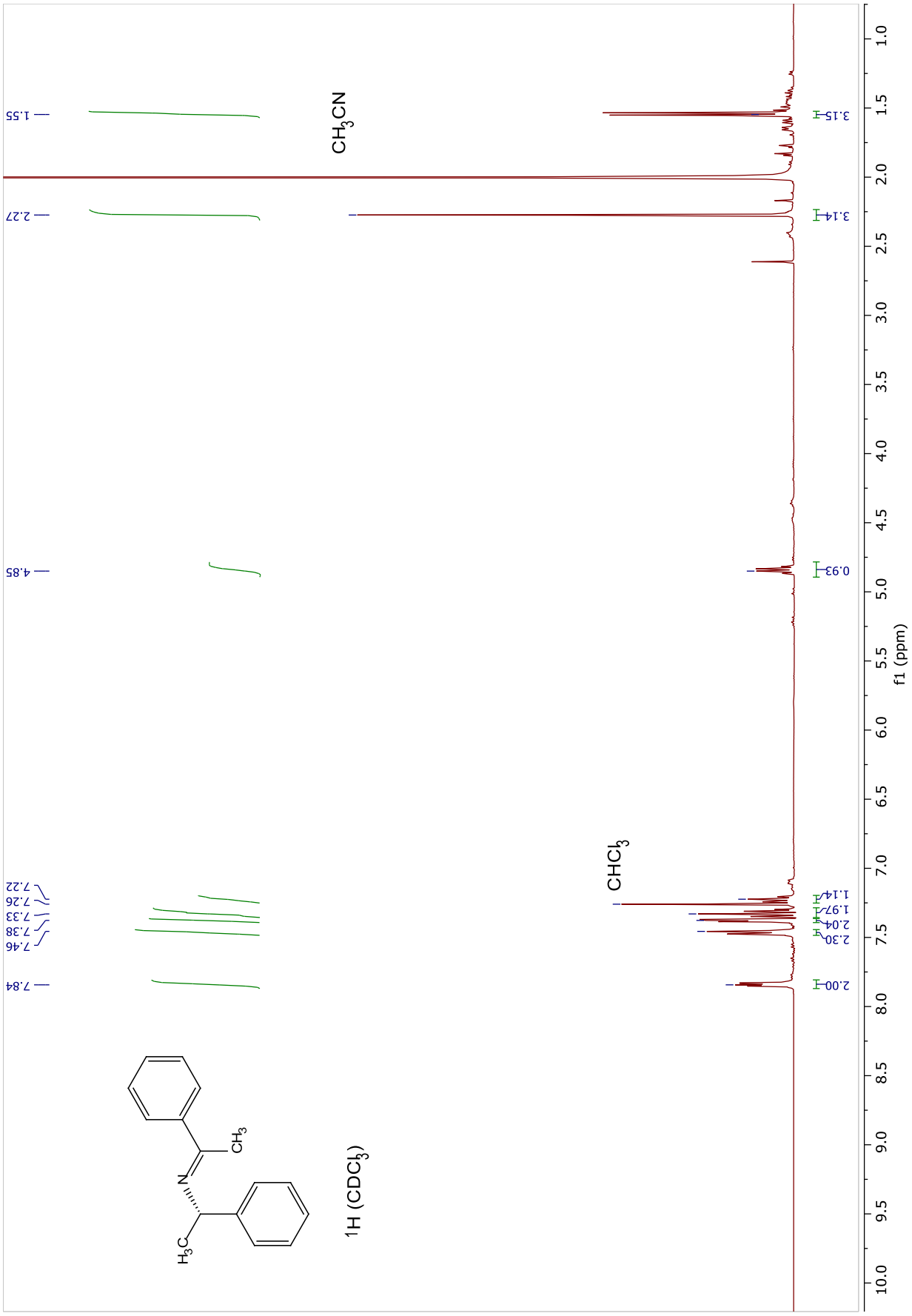
^{1}H (CDCl$_3$)
CHCl$_3$
CH$_3$CN
f1 (ppm)

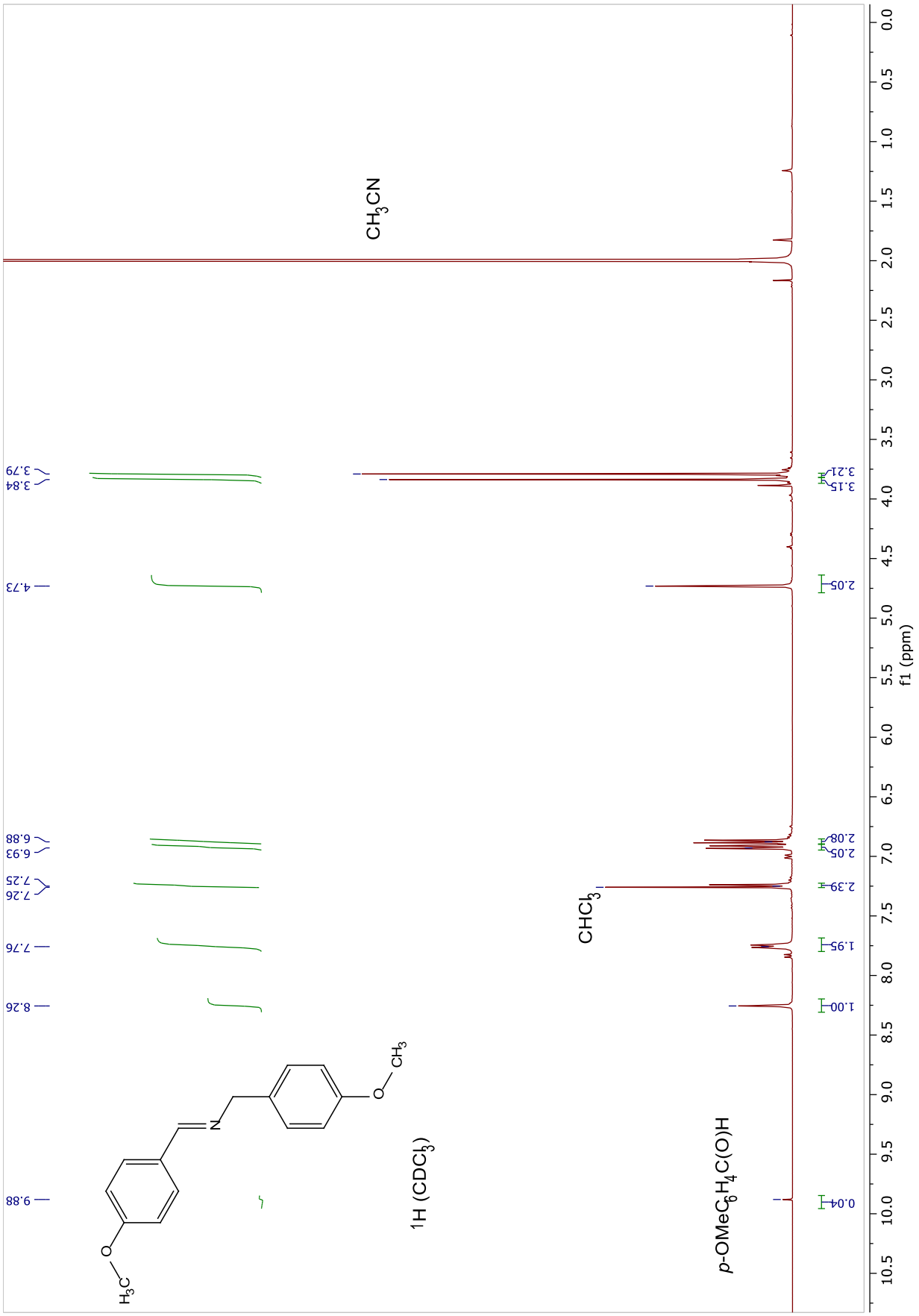
9.88
8.26
7.76
7.26
7.25
6.93
6.88
4.73
3.84
3.79
3.21
3.15
2.05
2.08
2.05
2.39
1.95
1.00
0.04
CH3CN
CHCl3
1H (CDCl3)
p-OMeC6H4C(O)H
f1 (ppm)

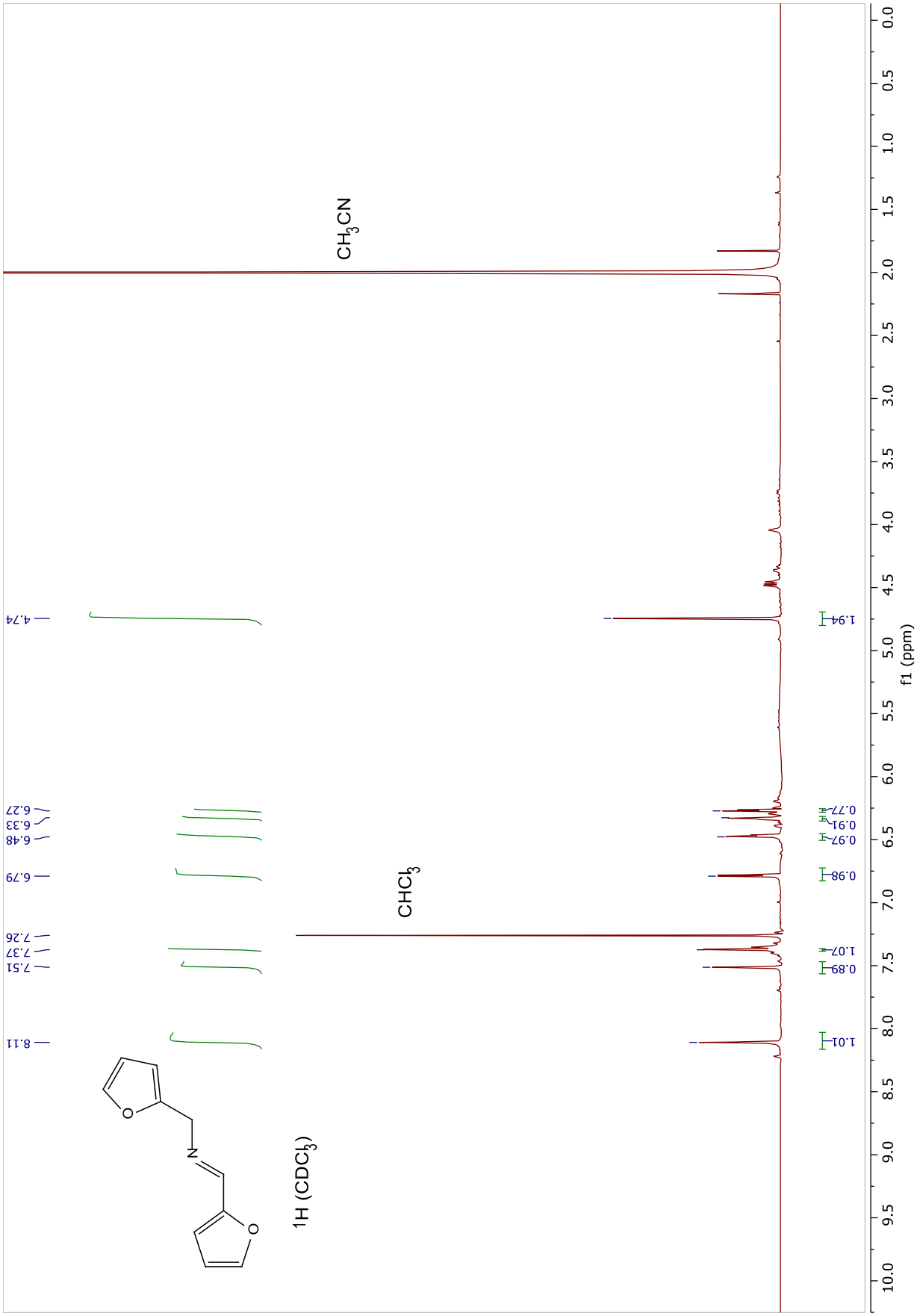
^{1}H (CDCl$_3$)
CHCl$_3$
CH$_3$CN
8.11
7.51
7.37
7.26
6.79
6.48
6.33
6.27
4.74
1.01
0.89
1.07
0.98
0.97
0.91
0.77
1.94
f1 (ppm)

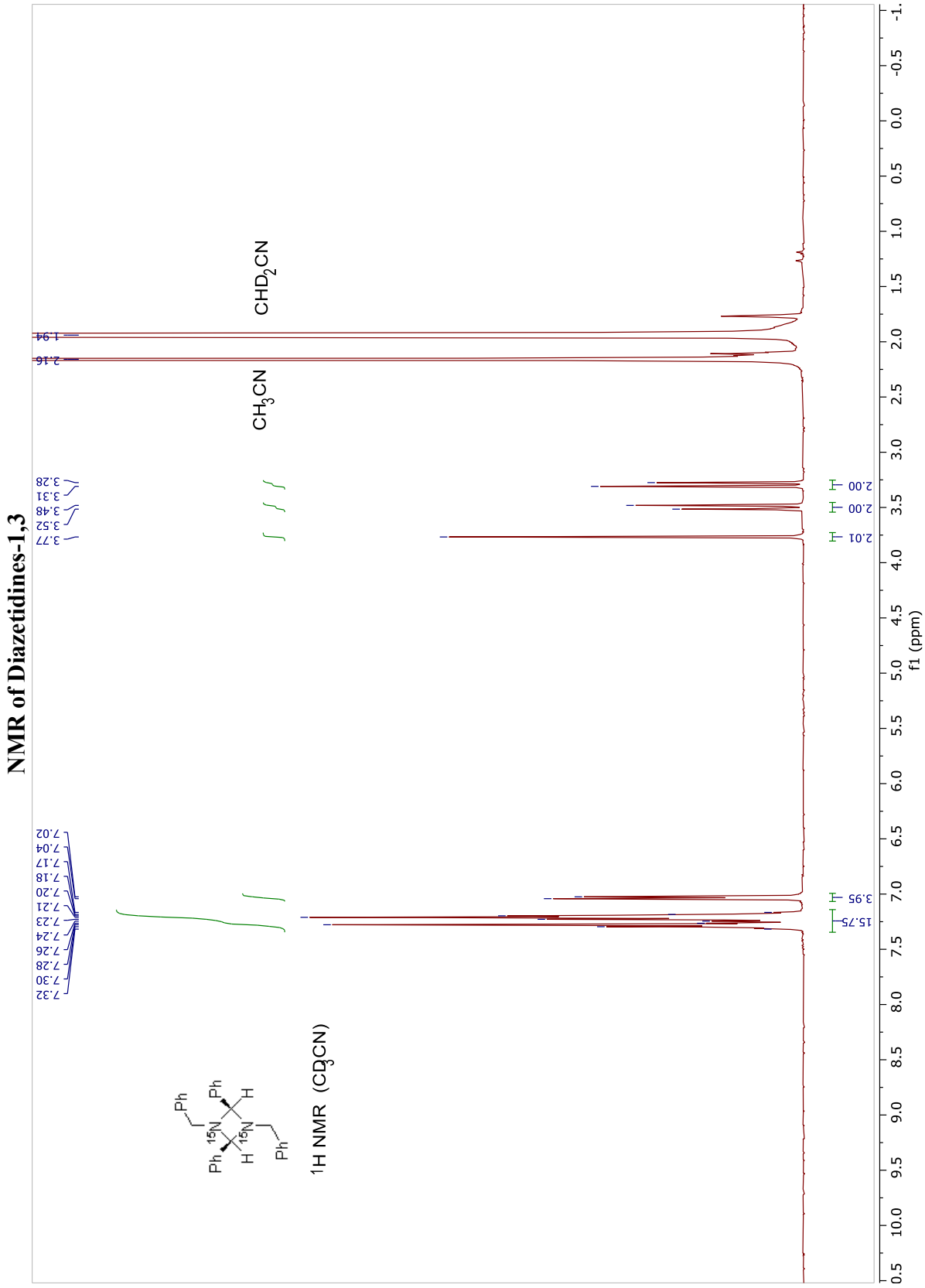
NMR of Diazetidines-1,3
1H NMR (CD3CN)
CHD2CN
CH3CN
f1 (ppm)

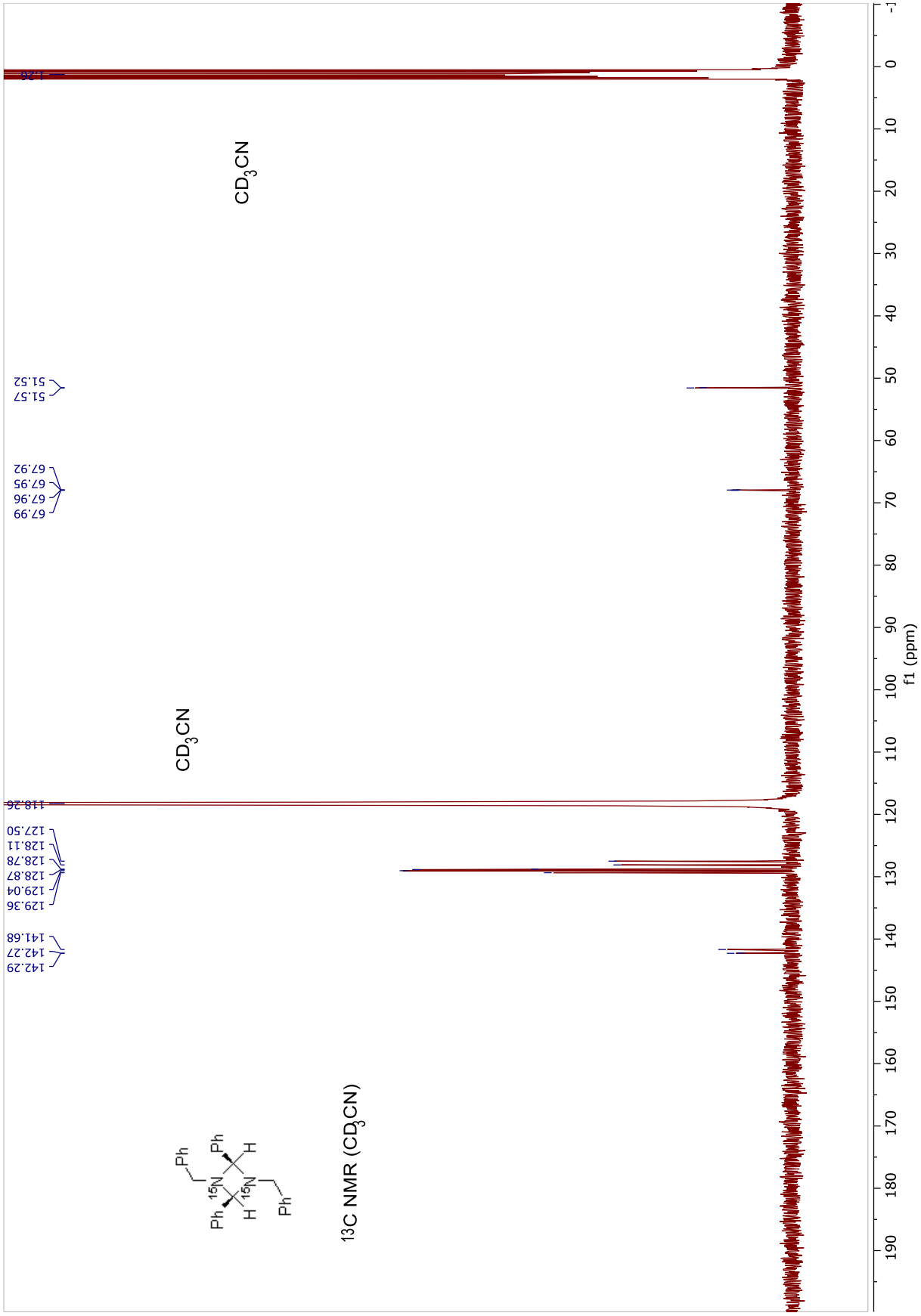
1.28
51.57
51.52
67.99
67.96
67.95
67.92
118.26
127.50
128.11
128.78
128.87
129.04
129.36
141.68
142.27
142.29
CD3CN
CD3CN
13C NMR (CD3CN)
Ph
Ph
H
15N
15N
H
Ph
Ph
f1 (ppm)

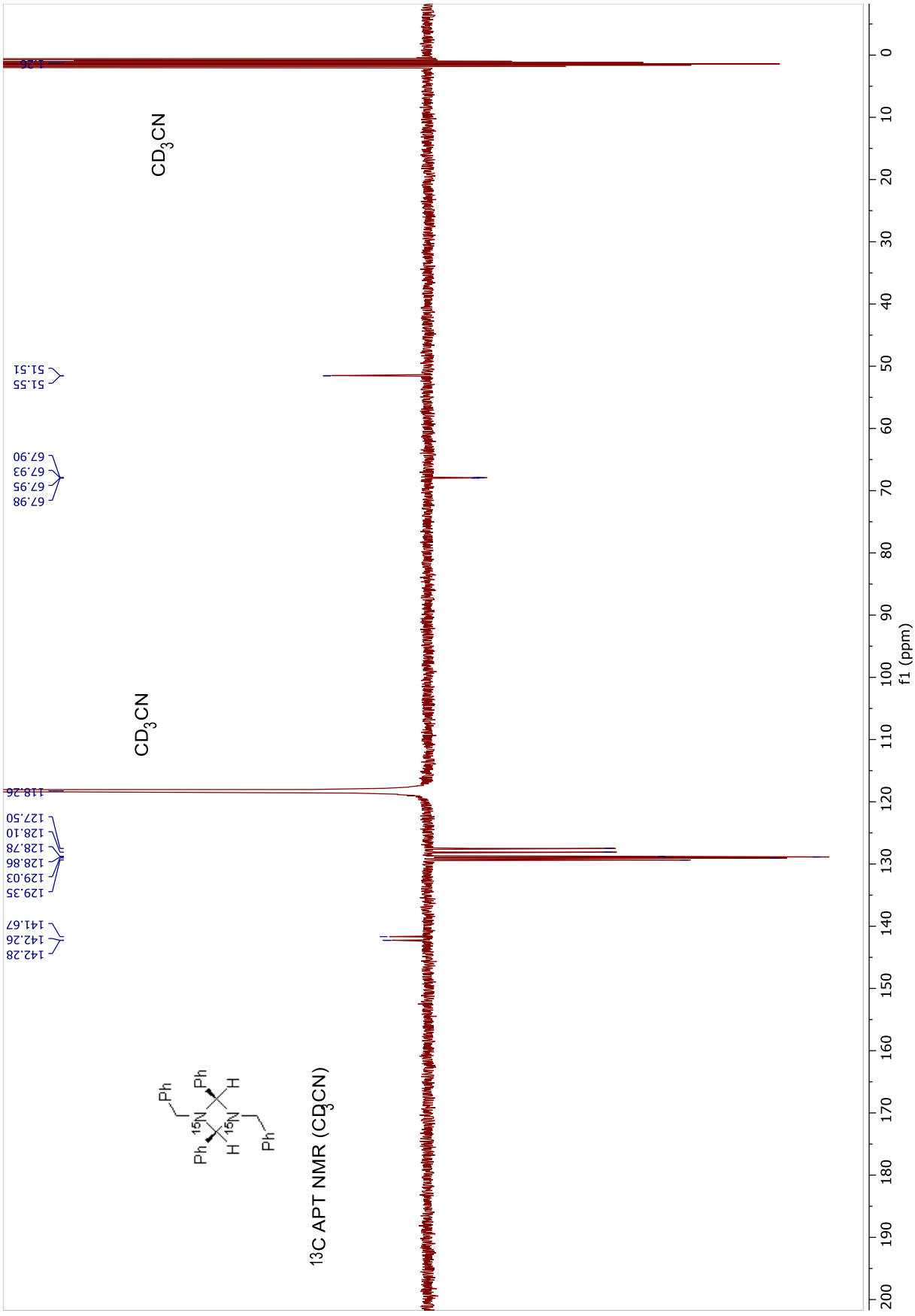
142.28
142.26
141.67
129.35
129.03
128.86
128.78
128.10
127.50
118.26
67.98
67.95
67.93
67.90
51.55
51.51
CD3CN
CD3CN
13C APT NMR (CD3CN)
Ph
Ph
15N
15N
H
H
Ph
Ph
f1 (ppm)

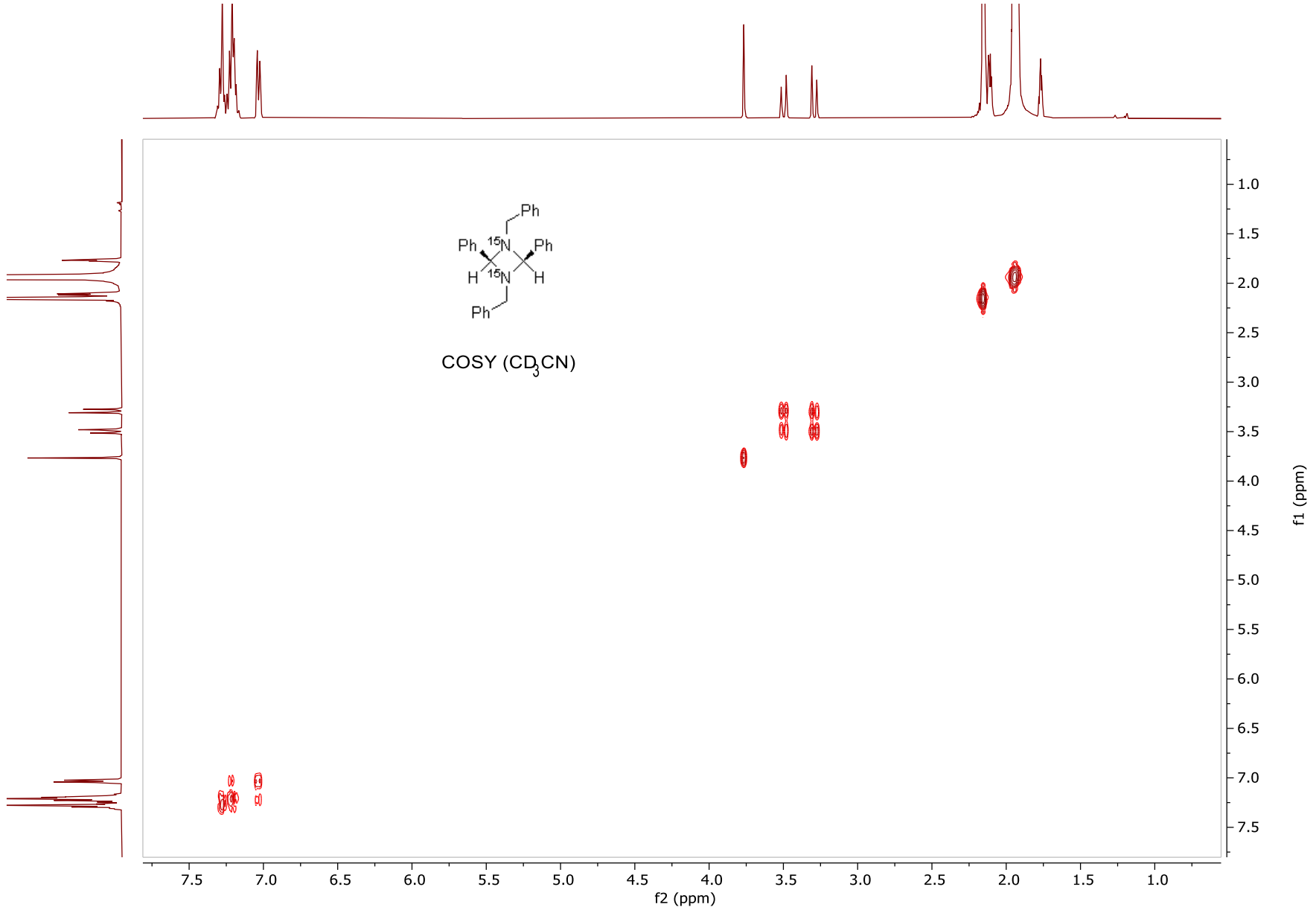
Ph
Ph
15N
Ph
H
15N
H
Ph
COSY (CD3CN)
7.5
7.0
6.5
6.0
5.5
5.0
4.5
4.0
3.5
3.0
2.5
2.0
1.5
1.0
f2 (ppm)
f1 (ppm)

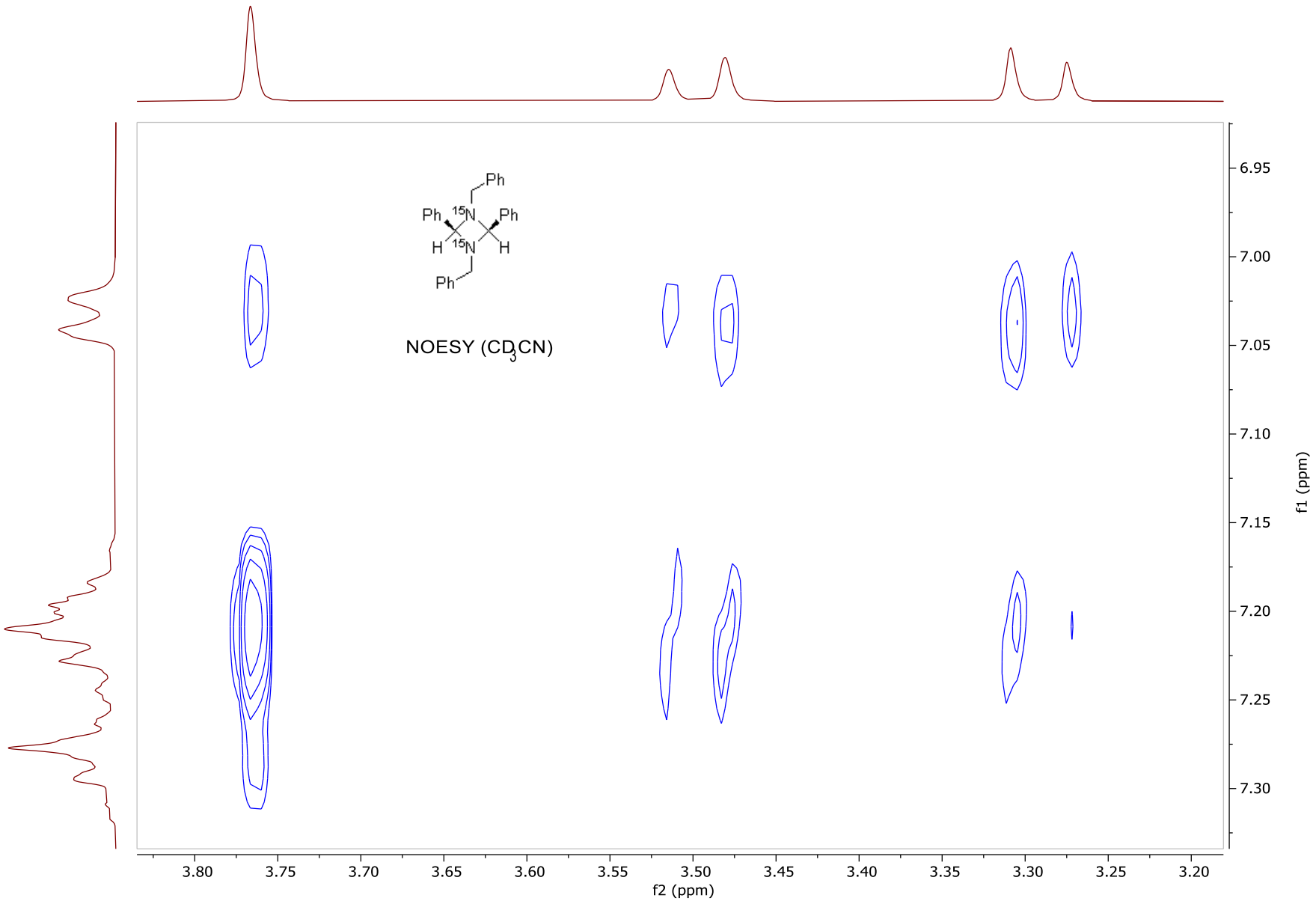
Ph
Ph
15N
Ph
H
15N
H
Ph
NOESY (CD3CN)
6.95
7.00
7.05
7.10
7.15
7.20
7.25
7.30
f1 (ppm)
3.80
3.75
3.70
3.65
3.60
3.55
3.50
3.45
3.40
3.35
3.30
3.25
3.20
f2 (ppm)

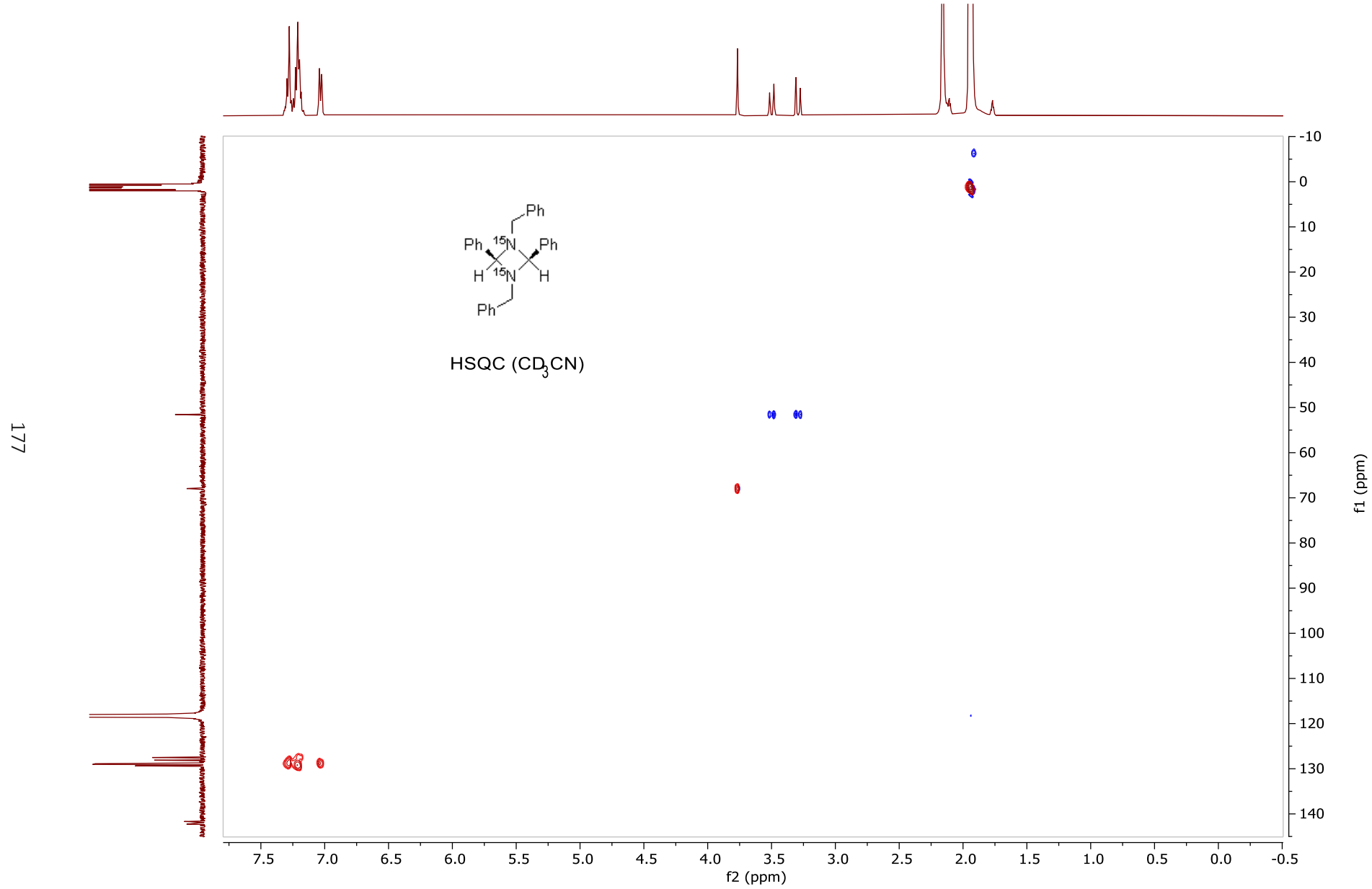
Ph
Ph
15N
Ph
H
15N
H
Ph
HSQC (CD3CN)
f2 (ppm)
f1 (ppm)
7.5
7.0
6.5
6.0
5.5
5.0
4.5
4.0
3.5
3.0
2.5
2.0
1.5
1.0
0.5
0.0
-0.5
-10
0
10
20
30
40
50
60
70
80
90
100
110
120
130
140

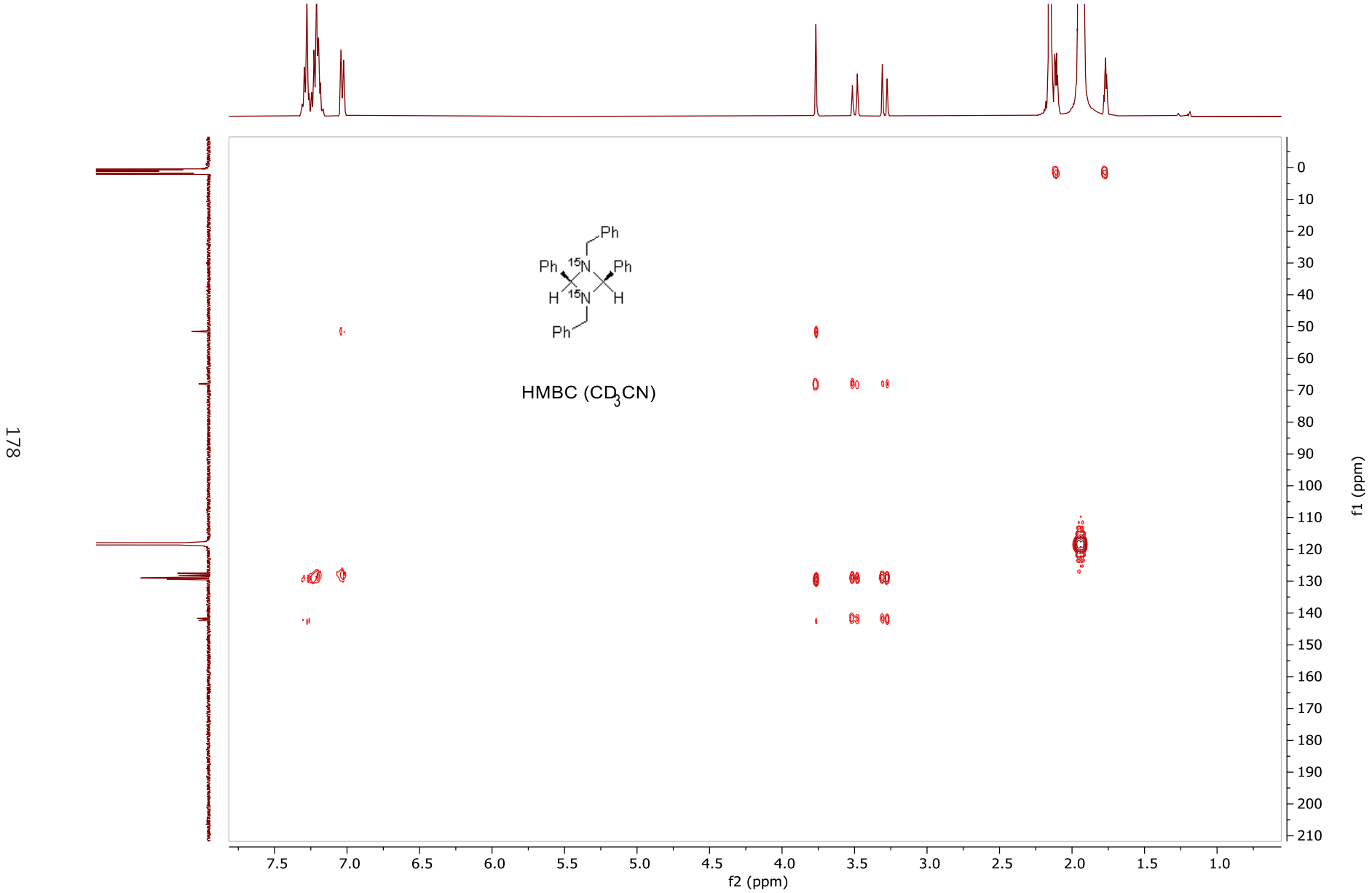
Ph
Ph
15N
Ph
H
15N
H
Ph
HMBC (CD3CN)
0
10
20
30
40
50
60
70
80
90
100
110
120
130
140
150
160
170
180
190
200
210
f1 (ppm)
7.5
7.0
6.5
6.0
5.5
5.0
4.5
4.0
3.5
3.0
2.5
2.0
1.5
1.0
f2 (ppm)

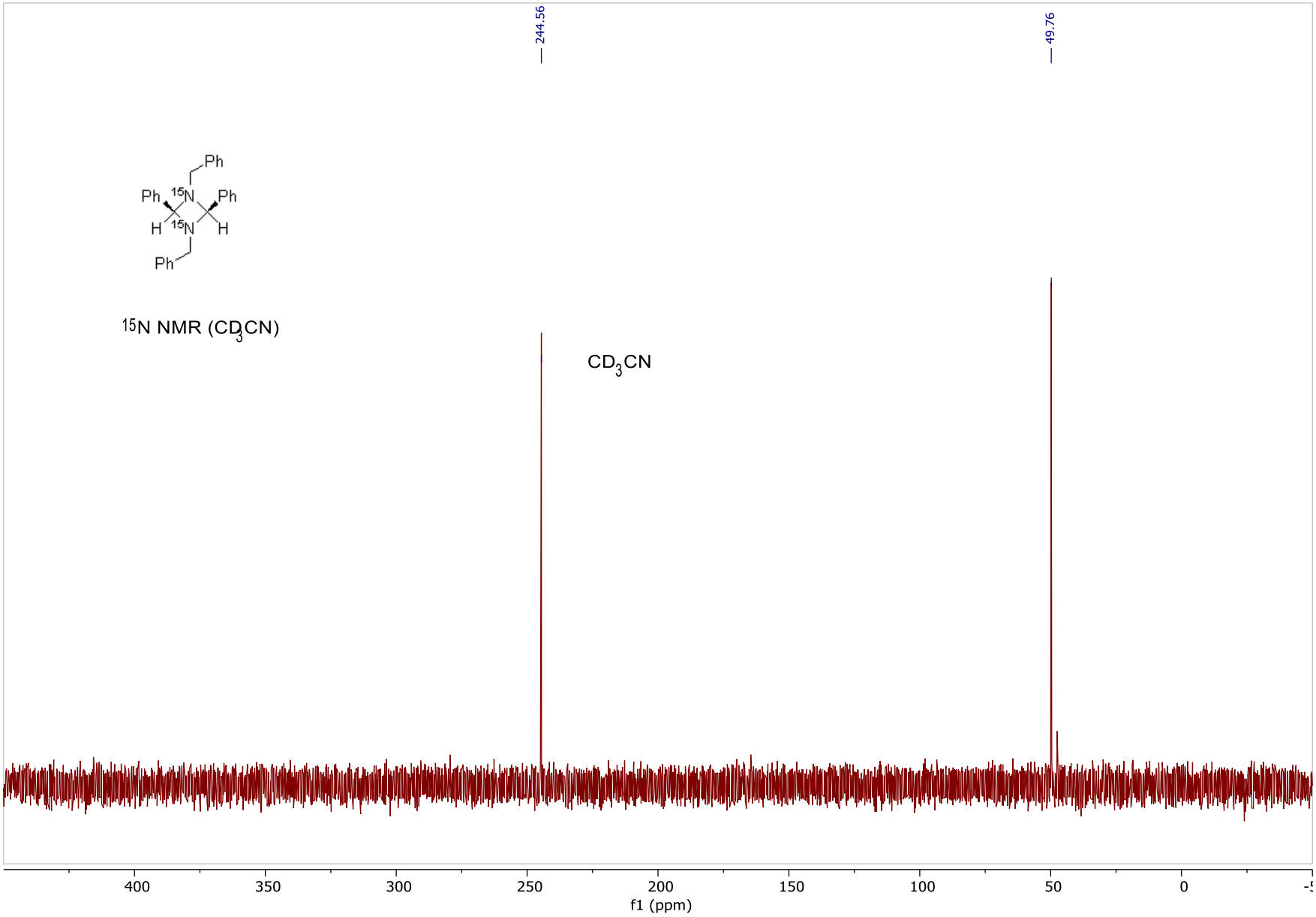
244.56
49.76
Ph
Ph
15N
Ph
H
15N
H
Ph
15N NMR (CD3CN)
CD3CN
400
350
300
250
200
150
100
50
0
f1 (ppm)

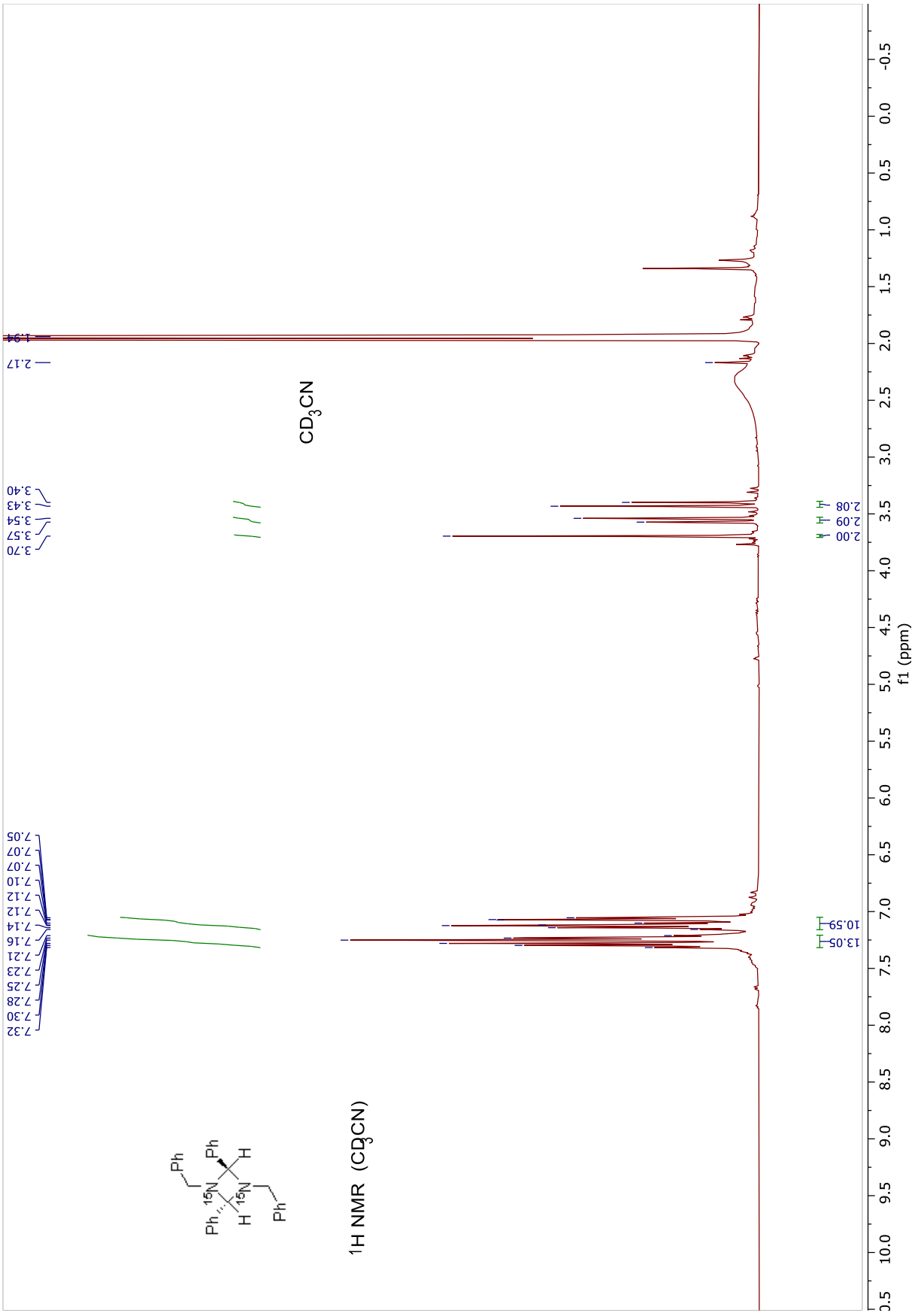
^{1}H NMR (CD$_3$CN)
CD$_3$CN
Ph
Ph
H
Ph
^{15}N
^{15}N
Ph
H
7.32
7.30
7.28
7.25
7.23
7.21
7.16
7.14
7.12
7.12
7.10
7.07
7.07
7.05
3.70
3.57
3.54
3.43
3.40
2.17
1.94
2.00
2.09
2.08
10.59
13.05
f1 (ppm)

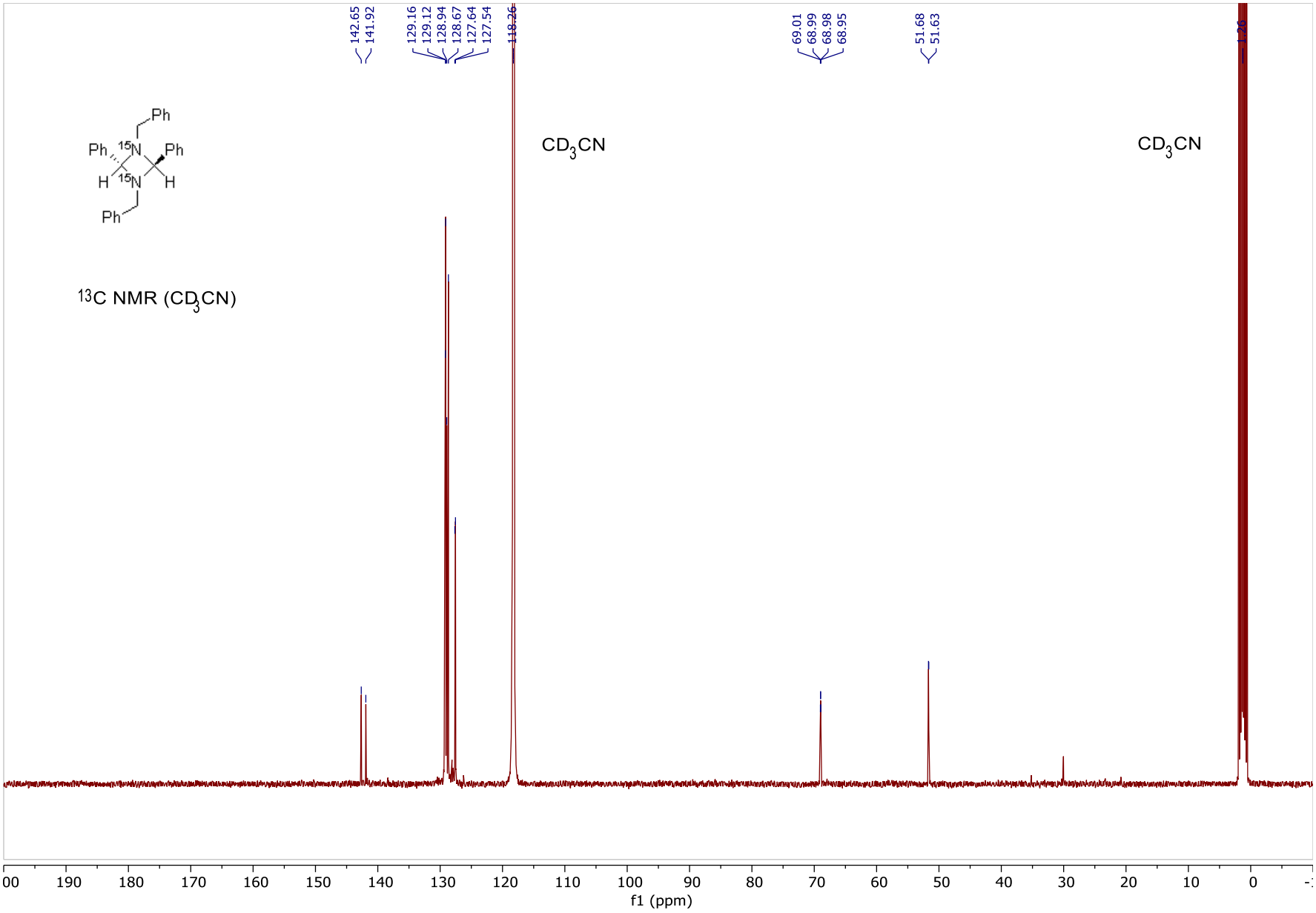
142.65
141.92
129.16
129.12
128.94
128.67
127.64
127.54
118.26
69.01
68.99
68.98
68.95
51.68
51.63
1.26
Ph
Ph
15N
Ph
H
15N
H
Ph
13C NMR (CD3CN)
CD3CN
CD3CN
f1 (ppm)

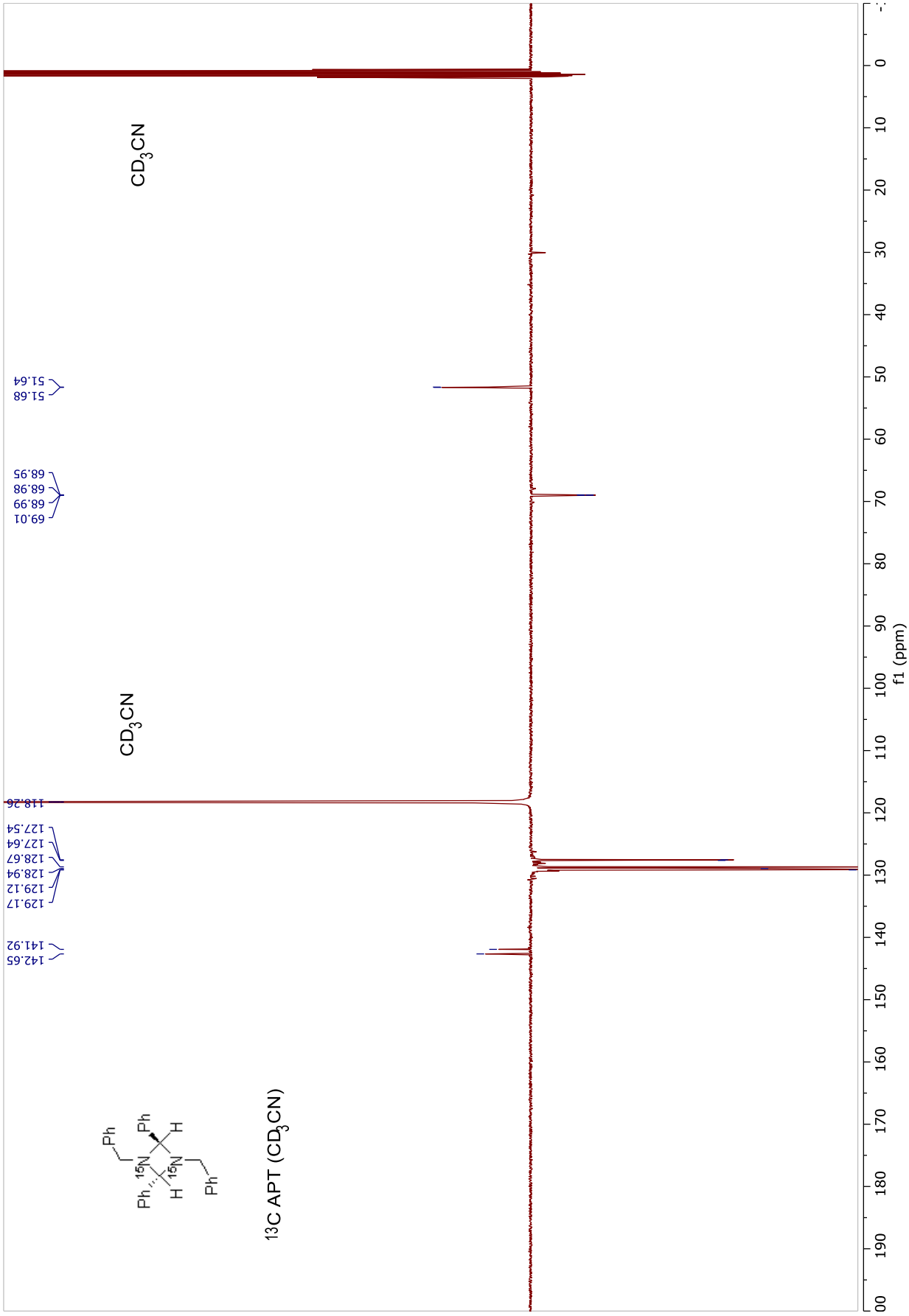
142.65
141.92
129.17
129.12
128.94
128.67
127.64
127.54
118.26
69.01
68.99
68.98
68.95
51.68
51.64
CD3CN
CD3CN
13C APT (CD3CN)
Ph
Ph
H
15N
15N
H
Ph
Ph
f1 (ppm)

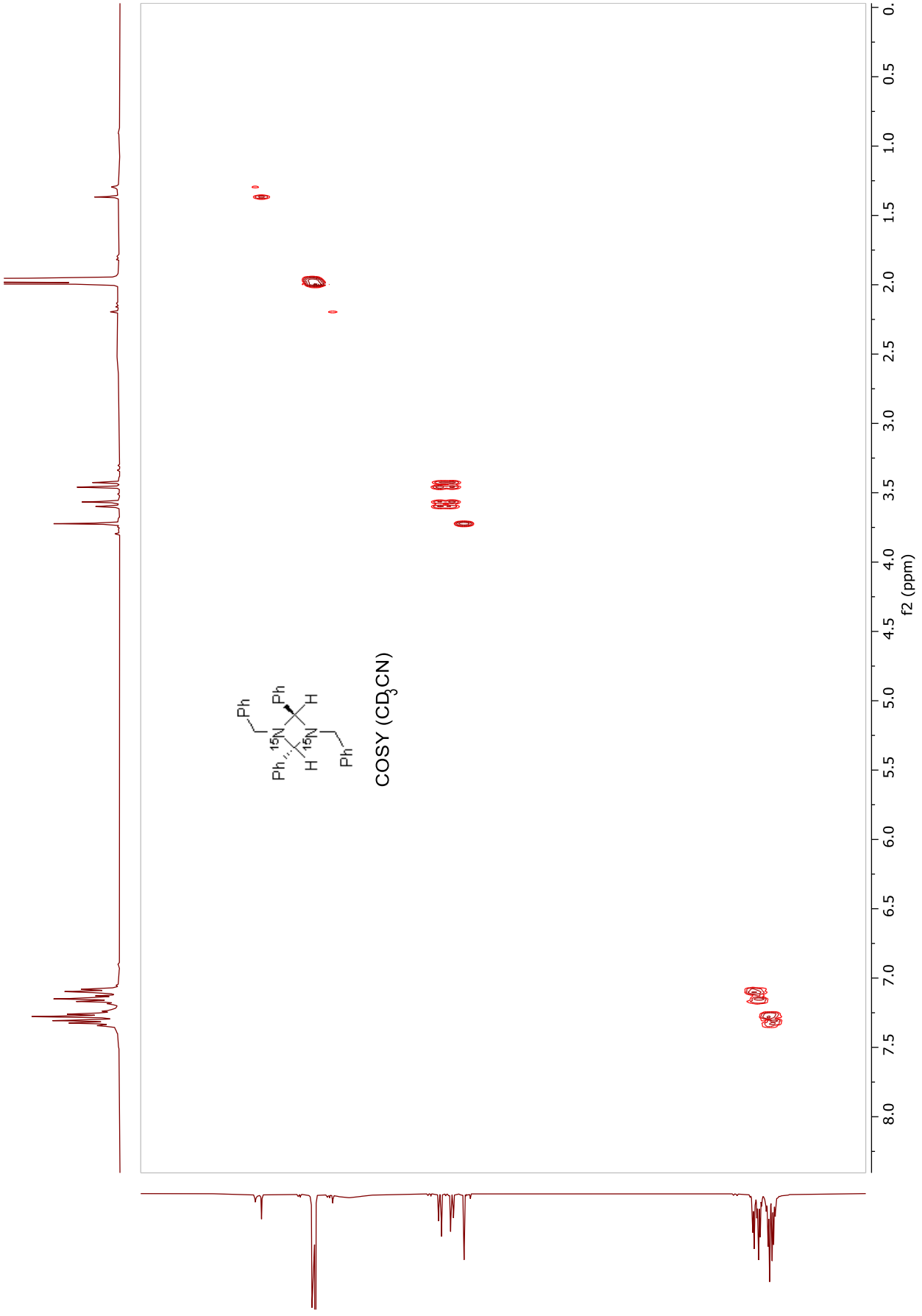
COSY (CD_3CN)
Ph
Ph
H
^{15}N
^{15}N
Ph
H
Ph
0.
0.5
1.0
1.5
2.0
2.5
3.0
3.5
4.0
4.5
5.0
5.5
6.0
6.5
7.0
7.5
8.0
f2 (ppm)

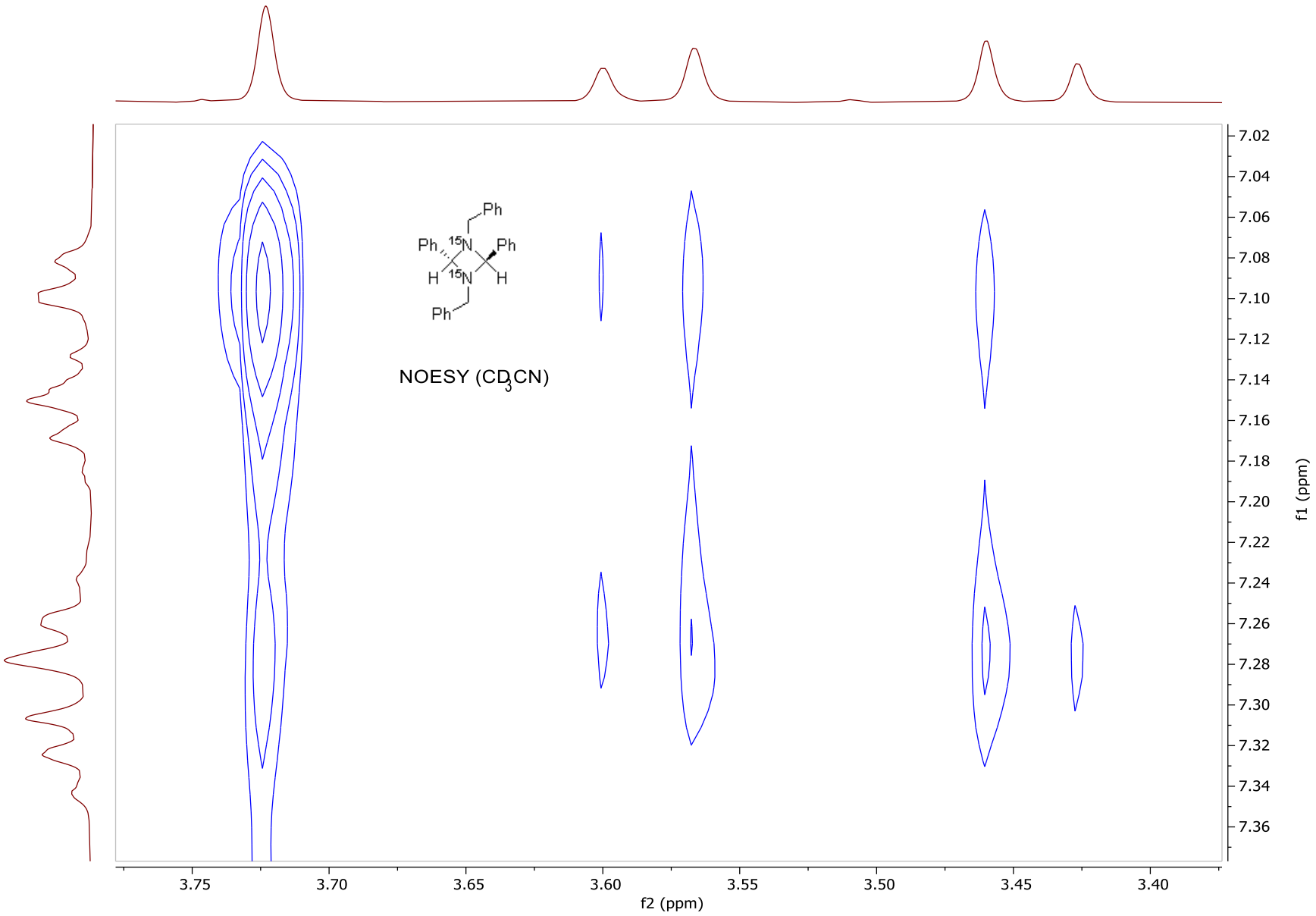
Ph
Ph
15N
Ph
H
15N
H
Ph
NOESY (CD3CN)
7.02
7.04
7.06
7.08
7.10
7.12
7.14
7.16
7.18
7.20
7.22
7.24
7.26
7.28
7.30
7.32
7.34
7.36
f1 (ppm)
3.75
3.70
3.65
3.60
3.55
3.50
3.45
3.40
f2 (ppm)

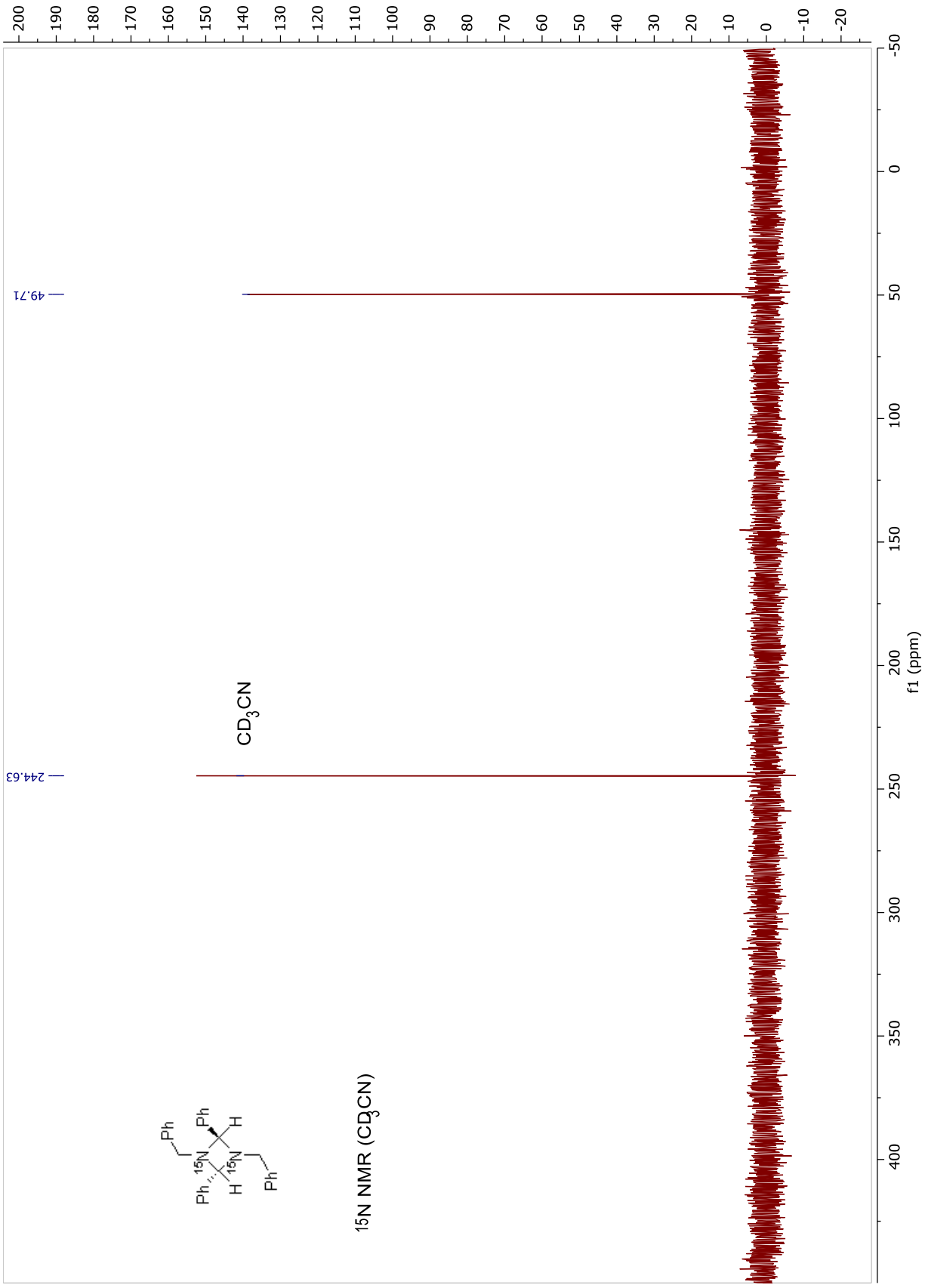
200
190
180
170
160
150
140
130
120
110
100
90
80
70
60
50
40
30
20
10
0
-10
-20
-50
0
50
100
150
200
250
300
350
400
f1 (ppm)
49.71
244.63
CD3CN
15N NMR (CD3CN)
Ph
Ph
15N
H
Ph
15N
H
Ph

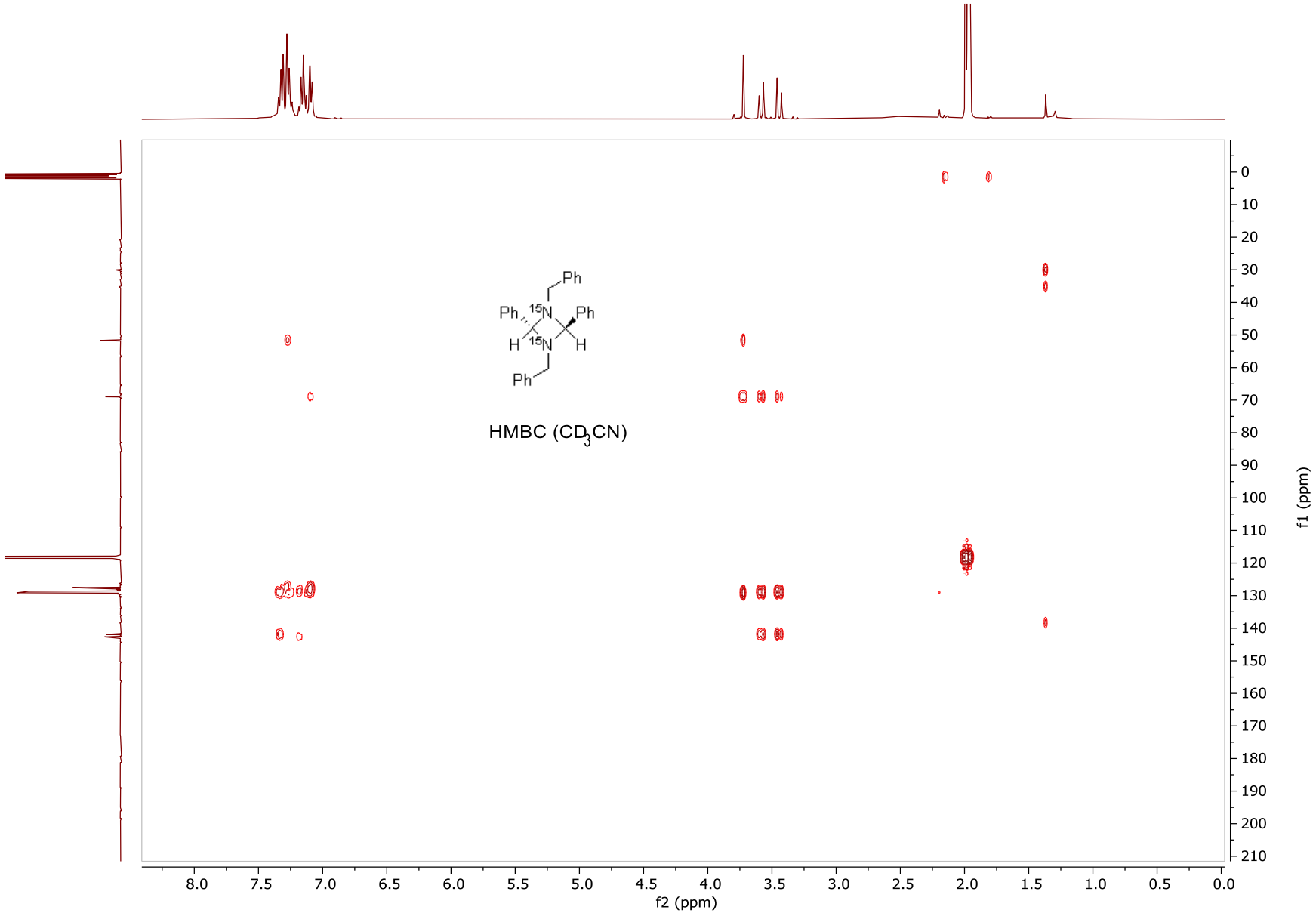
Ph
Ph
15N
Ph
H
15N
H
Ph
HMBC (CD3CN)
f2 (ppm)
f1 (ppm)
8.0
7.5
7.0
6.5
6.0
5.5
5.0
4.5
4.0
3.5
3.0
2.5
2.0
1.5
1.0
0.5
0.0
0
10
20
30
40
50
60
70
80
90
100
110
120
130
140
150
160
170
180
190
200
210

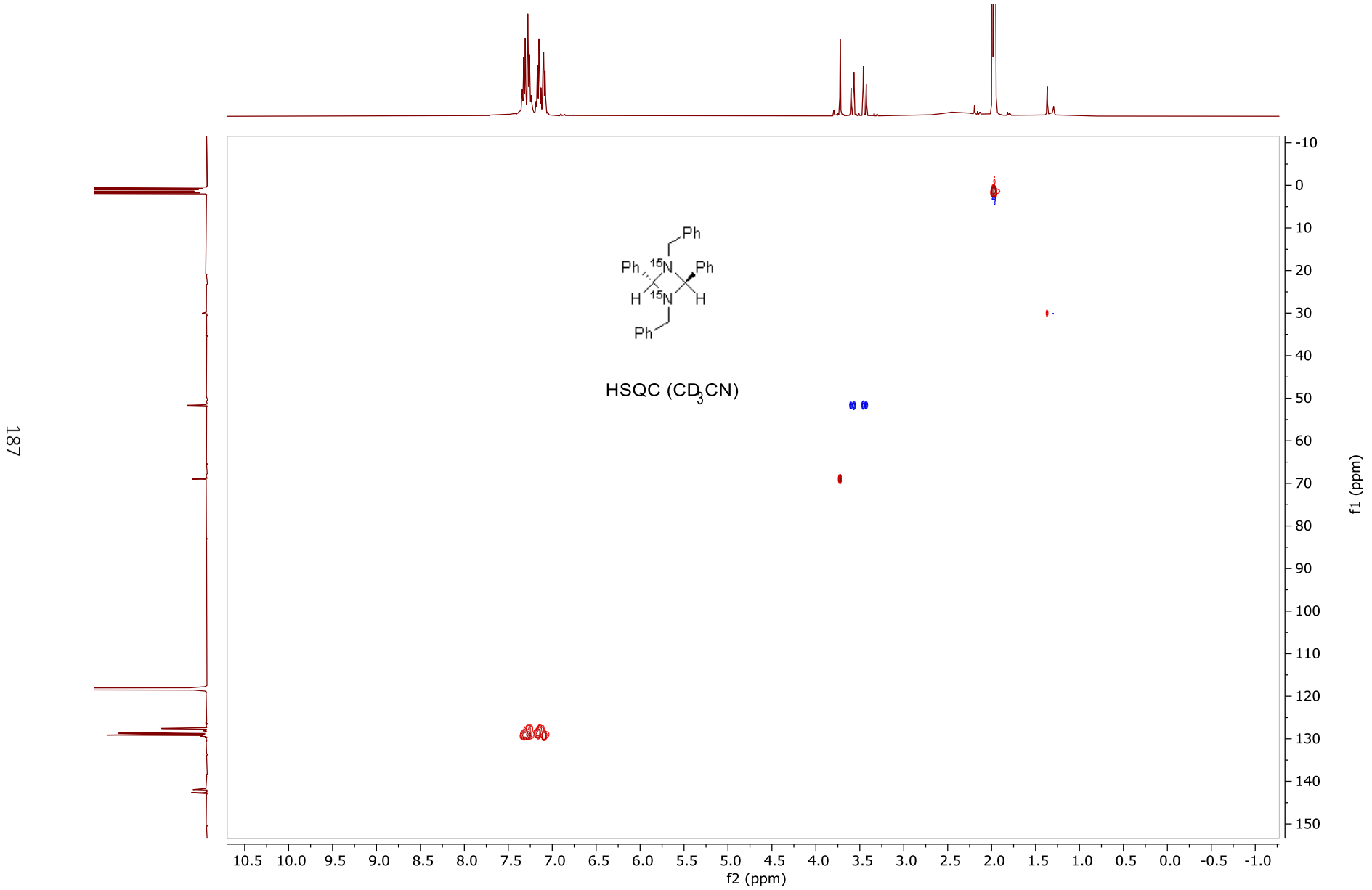
Ph
Ph
15N
Ph
H
15N
H
Ph
HSQC (CD3CN)
-10
0
10
20
30
40
50
60
70
80
90
100
110
120
130
140
150
f1 (ppm)
10.5
10.0
9.5
9.0
8.5
8.0
7.5
7.0
6.5
6.0
5.5
5.0
4.5
4.0
3.5
3.0
2.5
2.0
1.5
1.0
0.5
0.0
-0.5
-1.0
f2 (ppm)

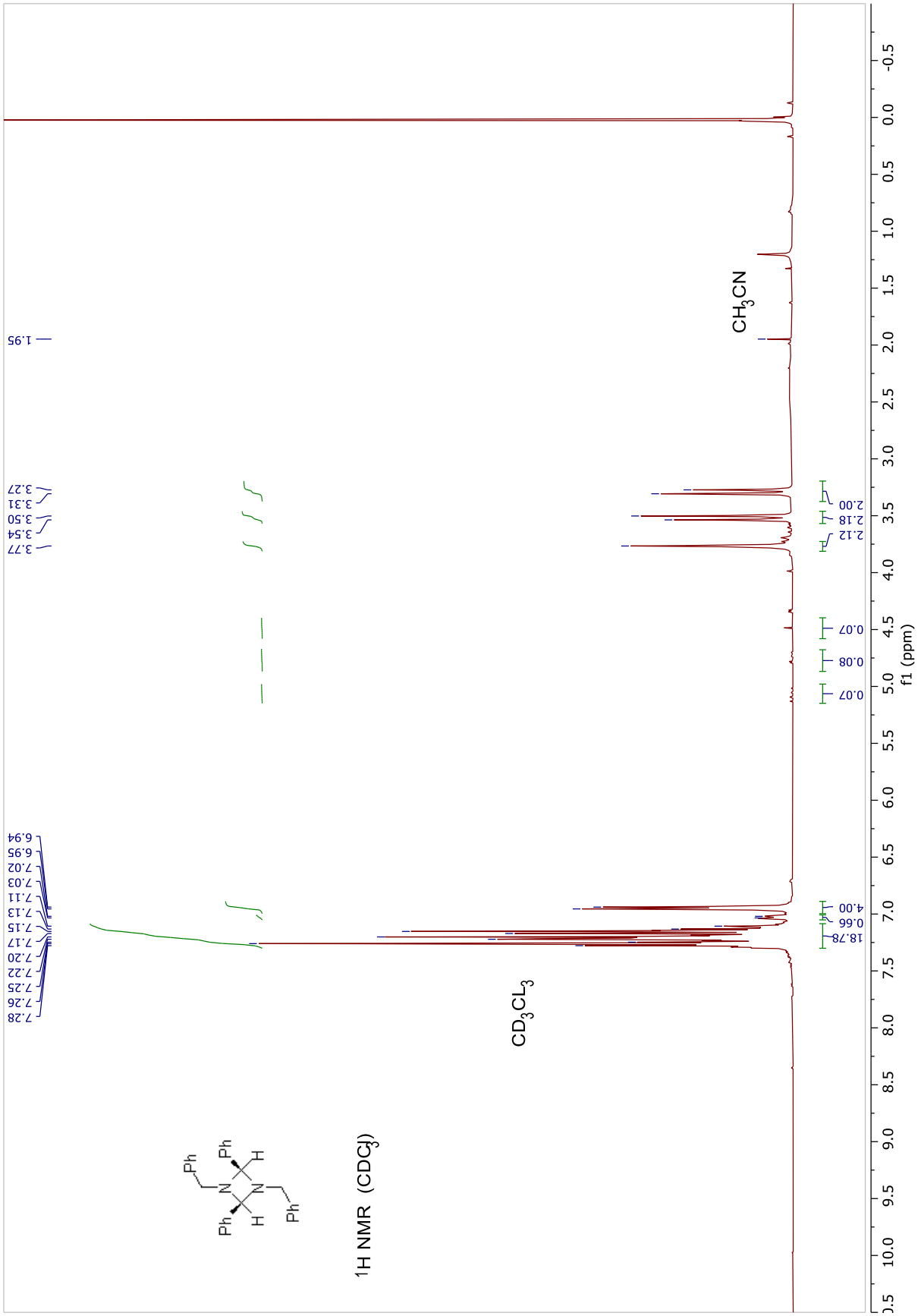
1H NMR (CDCl3)
CD3CL3
CH3CN
Ph
Ph
H
N
N
H
Ph
Ph
7.28
7.26
7.25
7.22
7.20
7.17
7.15
7.13
7.11
7.03
7.02
6.95
6.94
3.77
3.54
3.50
3.31
3.27
1.95
18.78
0.66
4.00
0.07
0.08
0.07
2.12
2.18
2.00
f1 (ppm)

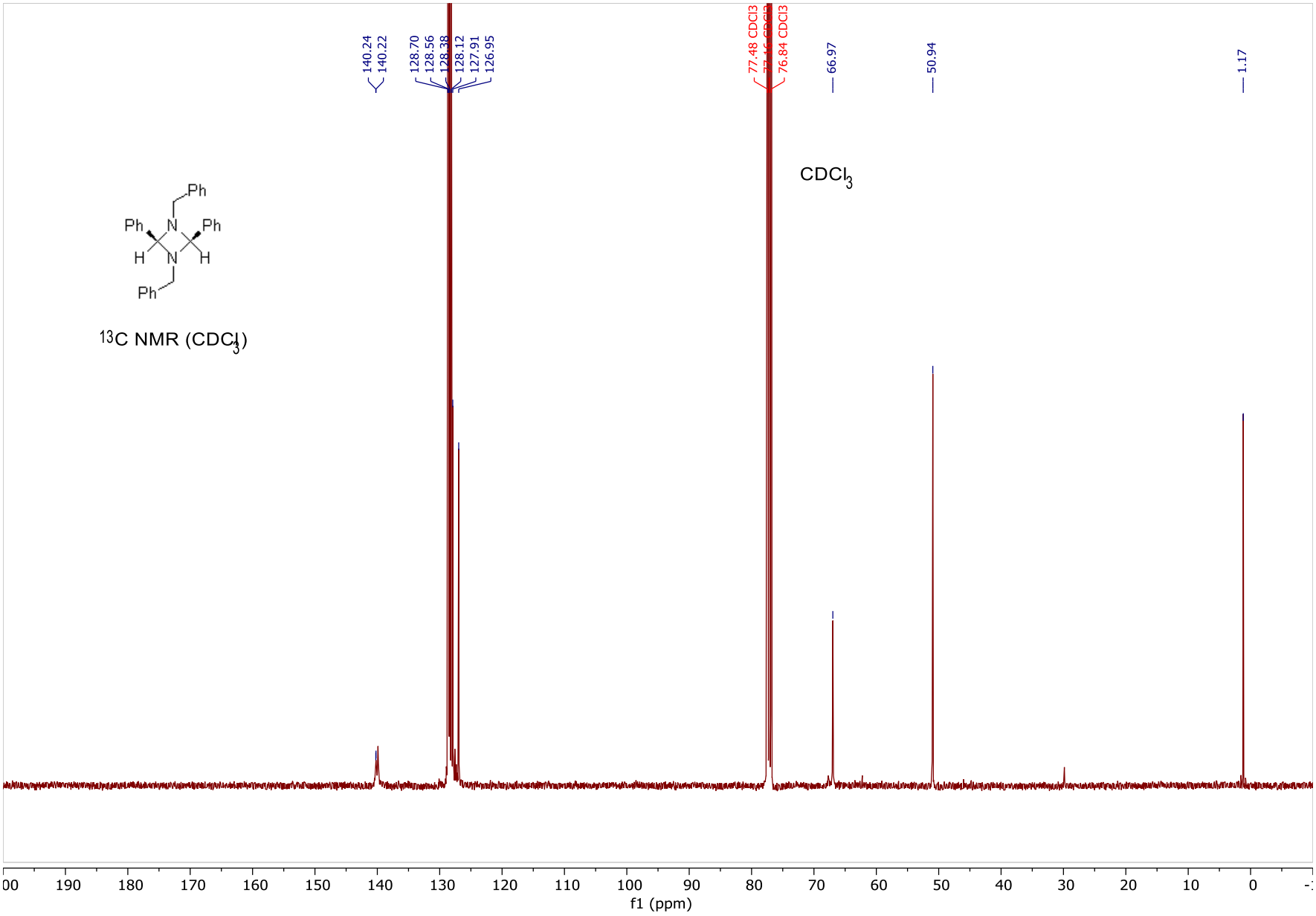
140.24
140.22
128.70
128.56
128.38
128.12
127.91
126.95
77.48 CDCl3
77.16 CDCl3
76.84 CDCl3
66.97
50.94
1.17
CDCl3
Ph
Ph
N
Ph
H
N
H
Ph
13C NMR (CDCl3)
f1 (ppm)

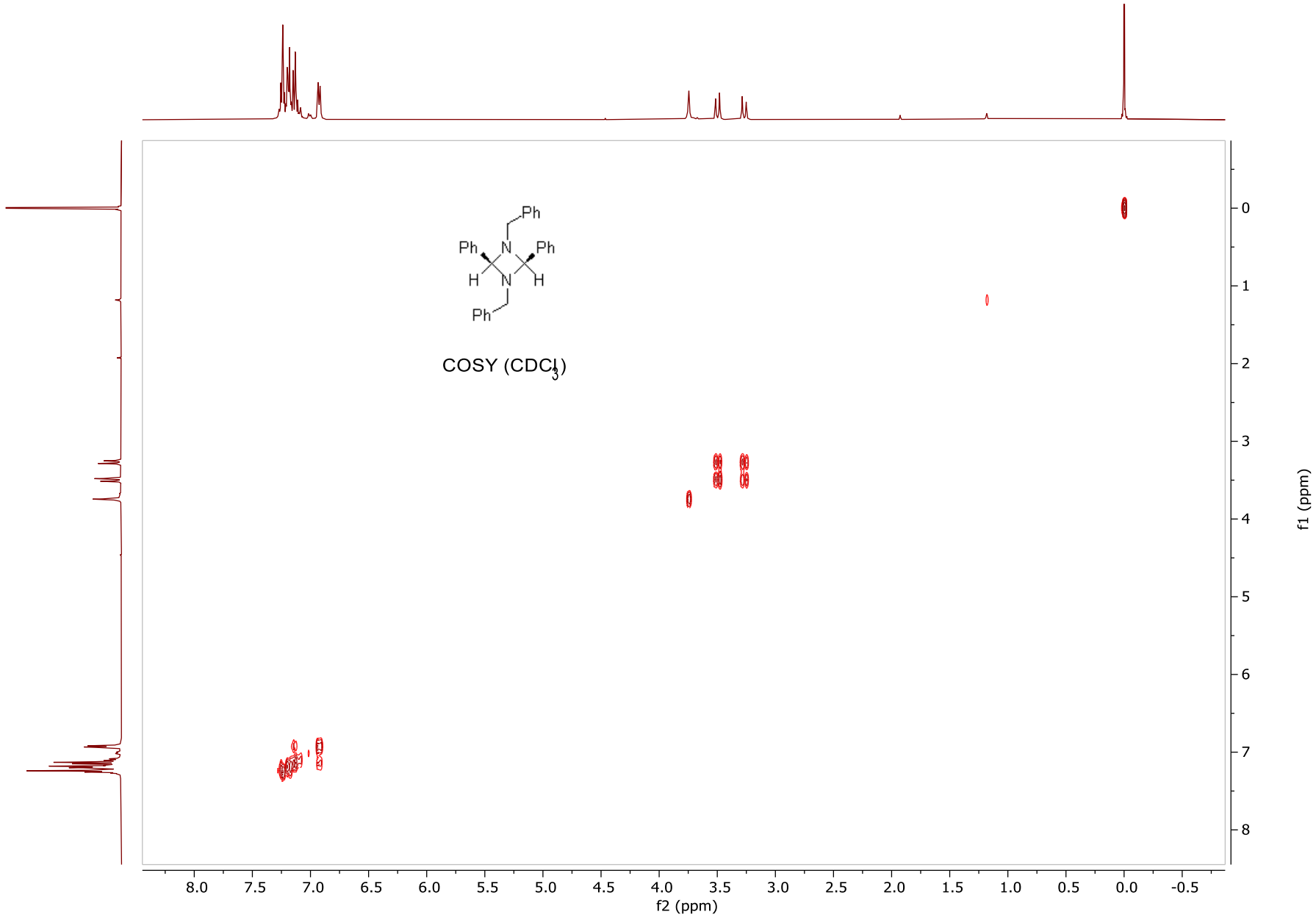
Ph
Ph
N
Ph
H
N
H
Ph
COSY (CDCl3)
f2 (ppm)
f1 (ppm)
8.0
7.5
7.0
6.5
6.0
5.5
5.0
4.5
4.0
3.5
3.0
2.5
2.0
1.5
1.0
0.5
0.0
-0.5
0
1
2
3
4
5
6
7
8

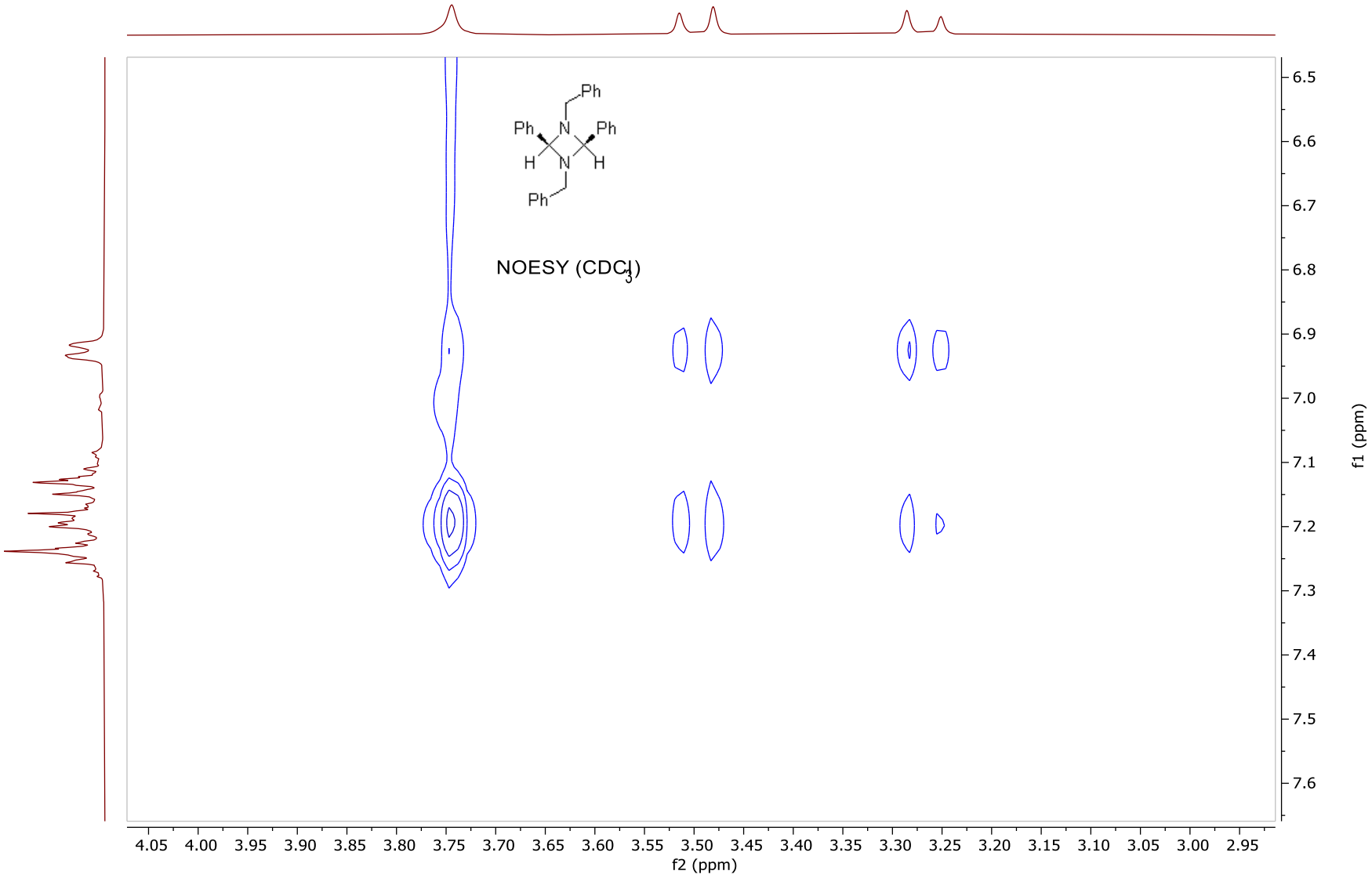
Ph
Ph
N
Ph
H
N
H
Ph
NOESY (CDCl3)
6.5
6.6
6.7
6.8
6.9
7.0
7.1
7.2
7.3
7.4
7.5
7.6
f1 (ppm)
4.05
4.00
3.95
3.90
3.85
3.80
3.75
3.70
3.65
3.60
3.55
3.50
3.45
3.40
3.35
3.30
3.25
3.20
3.15
3.10
3.05
3.00
2.95
f2 (ppm)

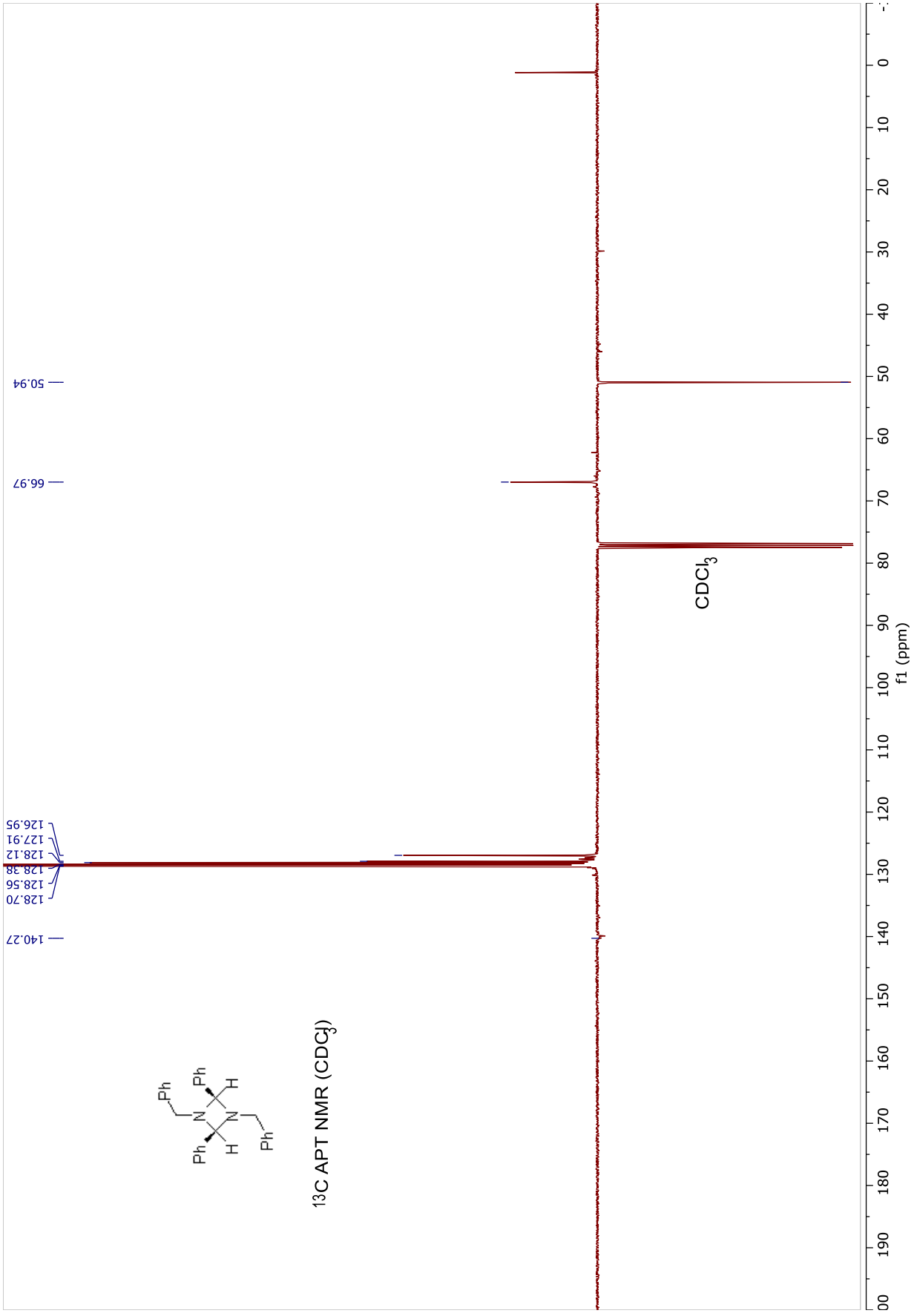
^{13}C APT NMR ($CDCl_3$)
Ph
Ph
H
N
N
H
Ph
Ph
140.27
128.70
128.56
128.38
128.12
127.91
126.95
66.97
50.94
$CDCl_3$
f1 (ppm)

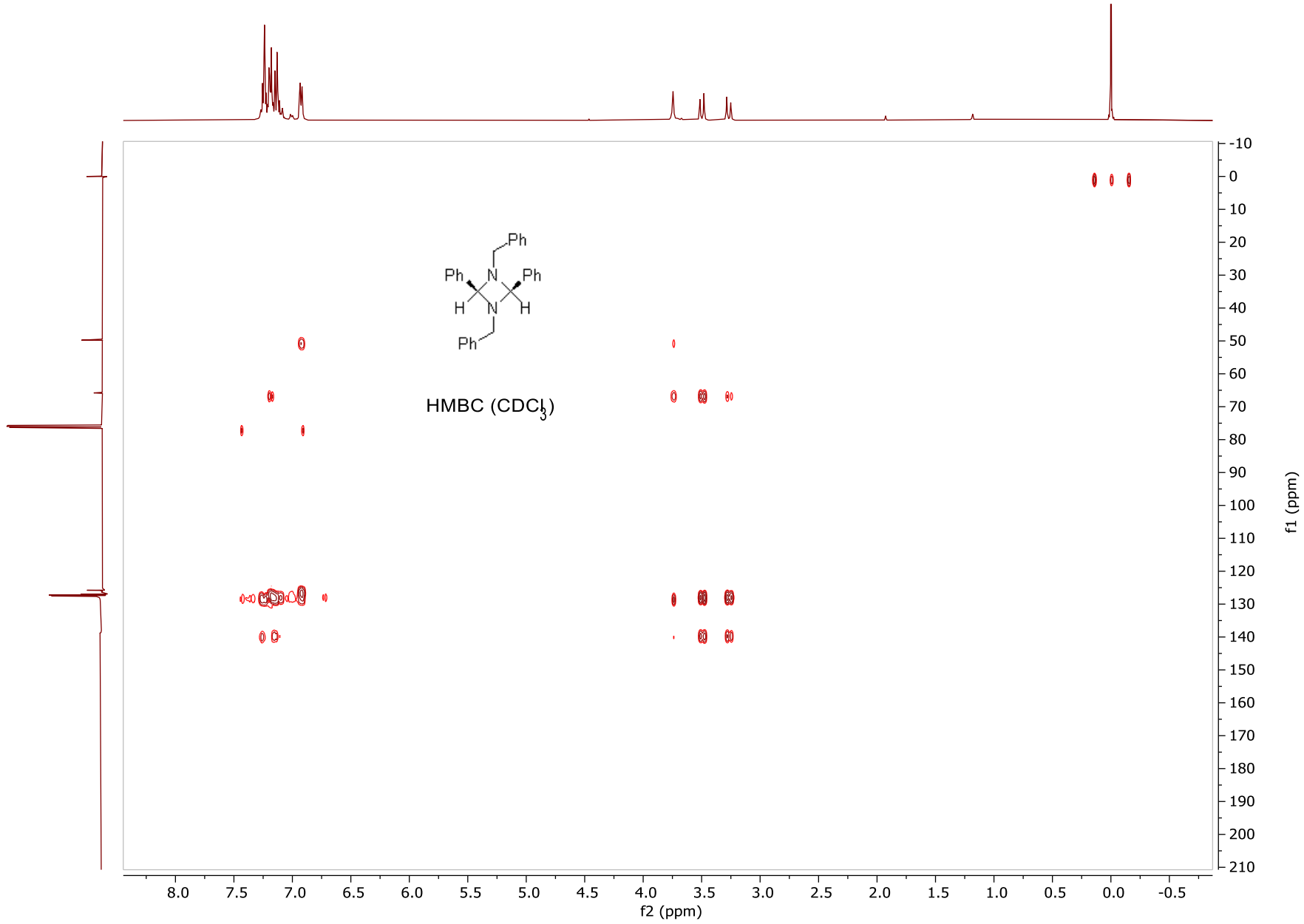
Ph
Ph
N
Ph
H
N
H
Ph
HMBC (CDCl3)
-10
0
10
20
30
40
50
60
70
80
90
100
110
120
130
140
150
160
170
180
190
200
210
f1 (ppm)
8.0
7.5
7.0
6.5
6.0
5.5
5.0
4.5
4.0
3.5
3.0
2.5
2.0
1.5
1.0
0.5
0.0
-0.5
f2 (ppm)

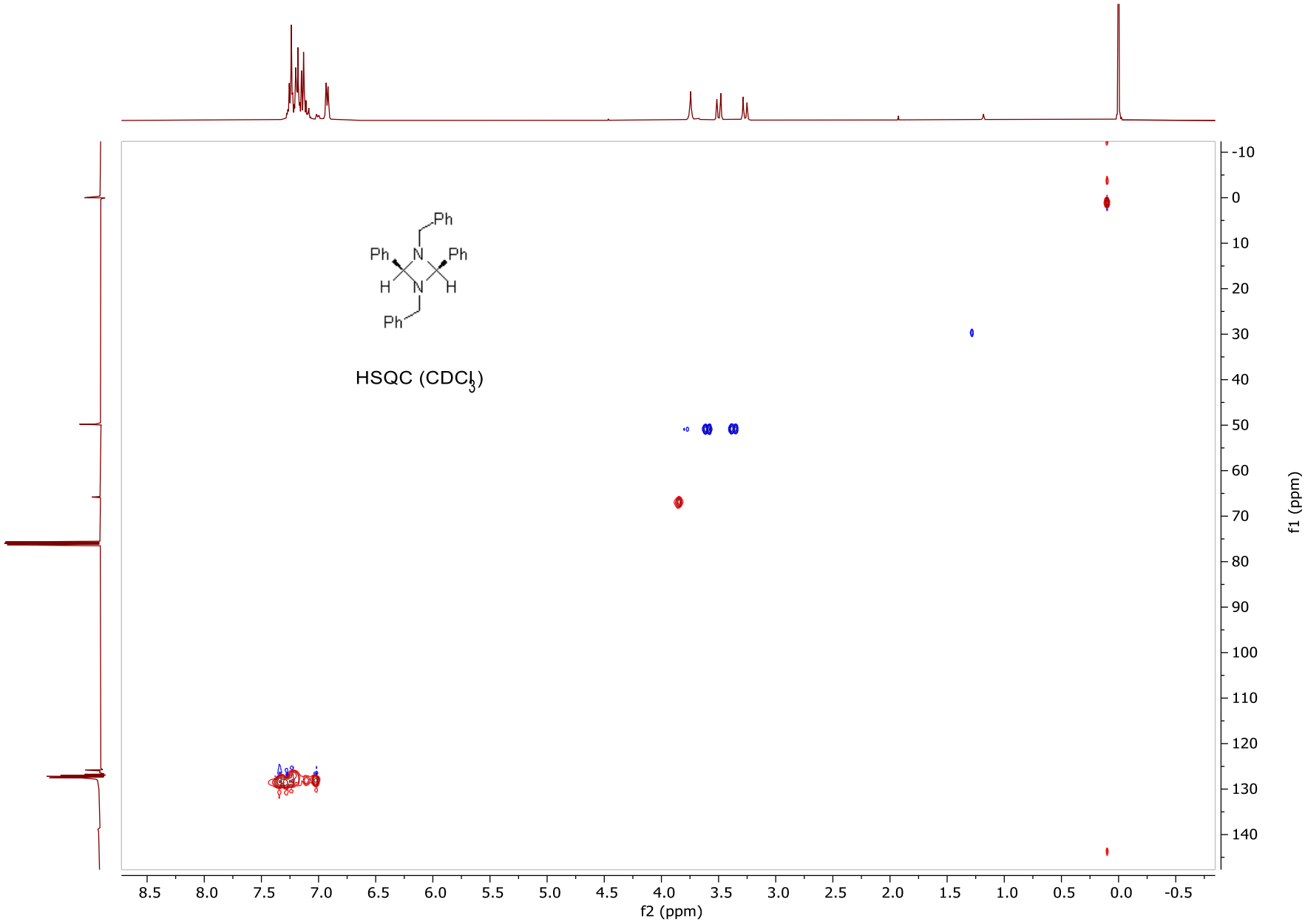
Ph
Ph
N
Ph
H
N
H
Ph
HSQC (CDCl3)
f2 (ppm)
f1 (ppm)

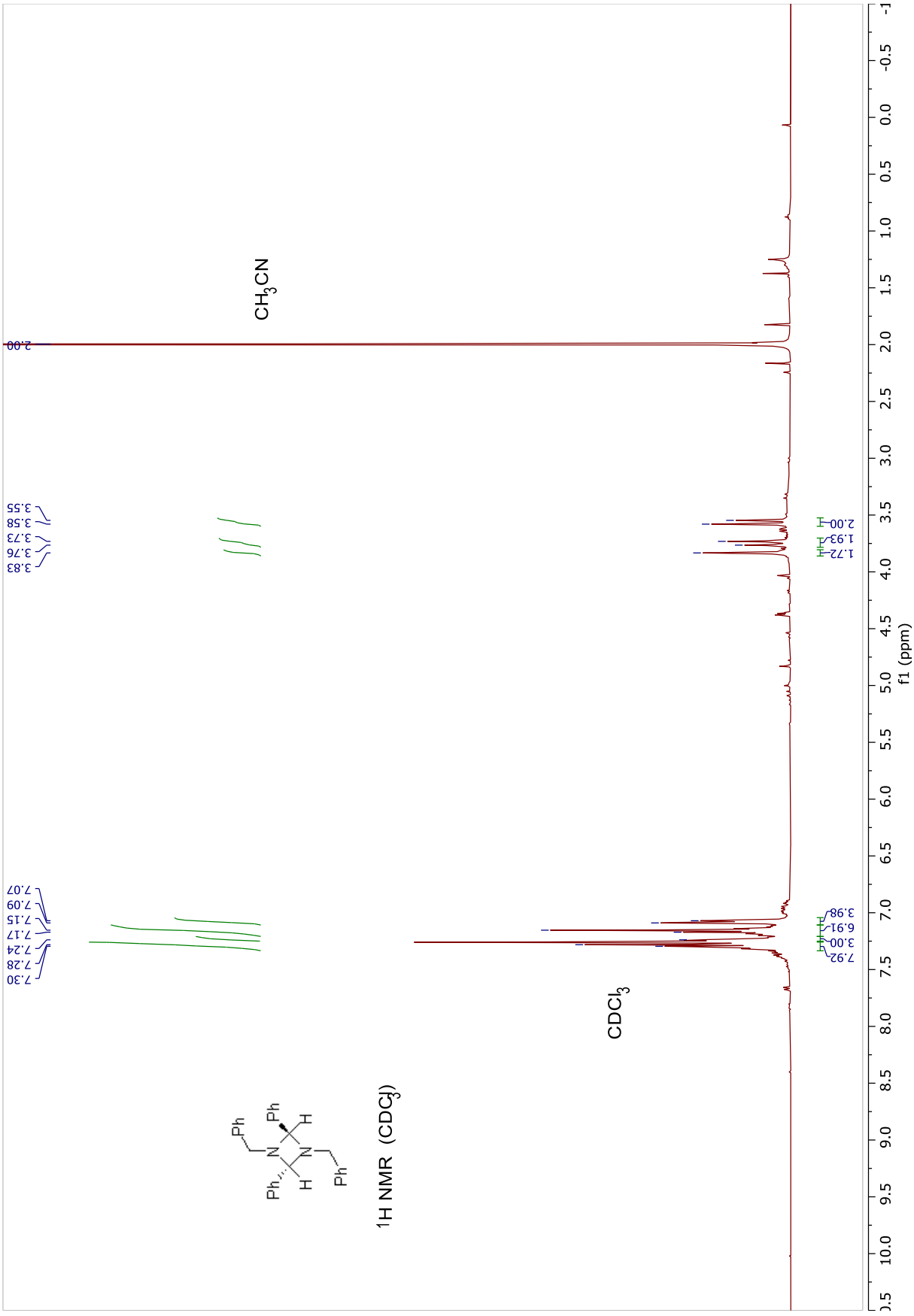
^{1}H NMR (CDCl$_3$)
CDCl$_3$
CH$_3$CN
f1 (ppm)

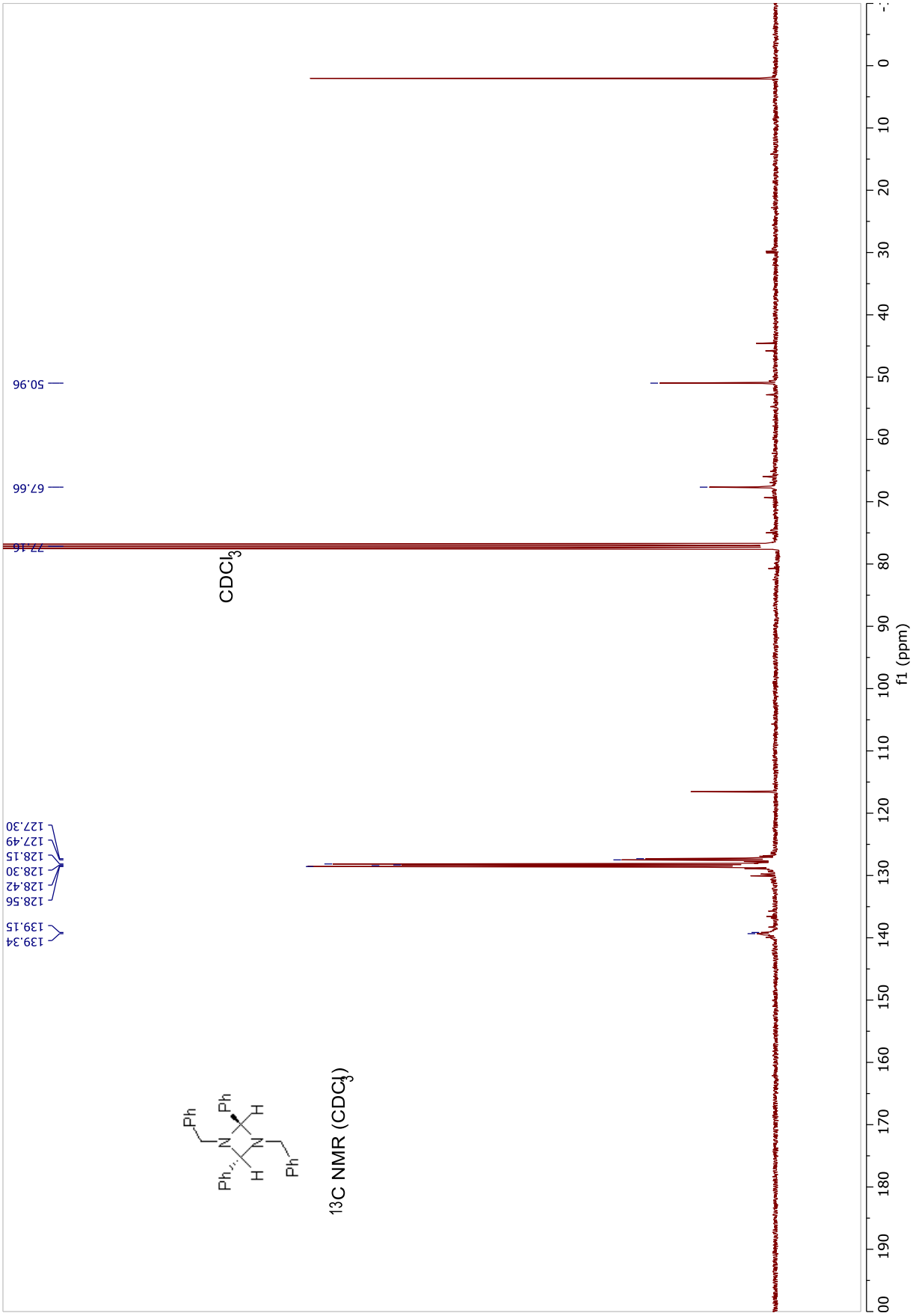
^{13}C NMR ($CDCl_3$)
$CDCl_3$
50.96
67.66
77.16
127.30
127.49
128.15
128.30
128.42
128.56
139.15
139.34
f1 (ppm)

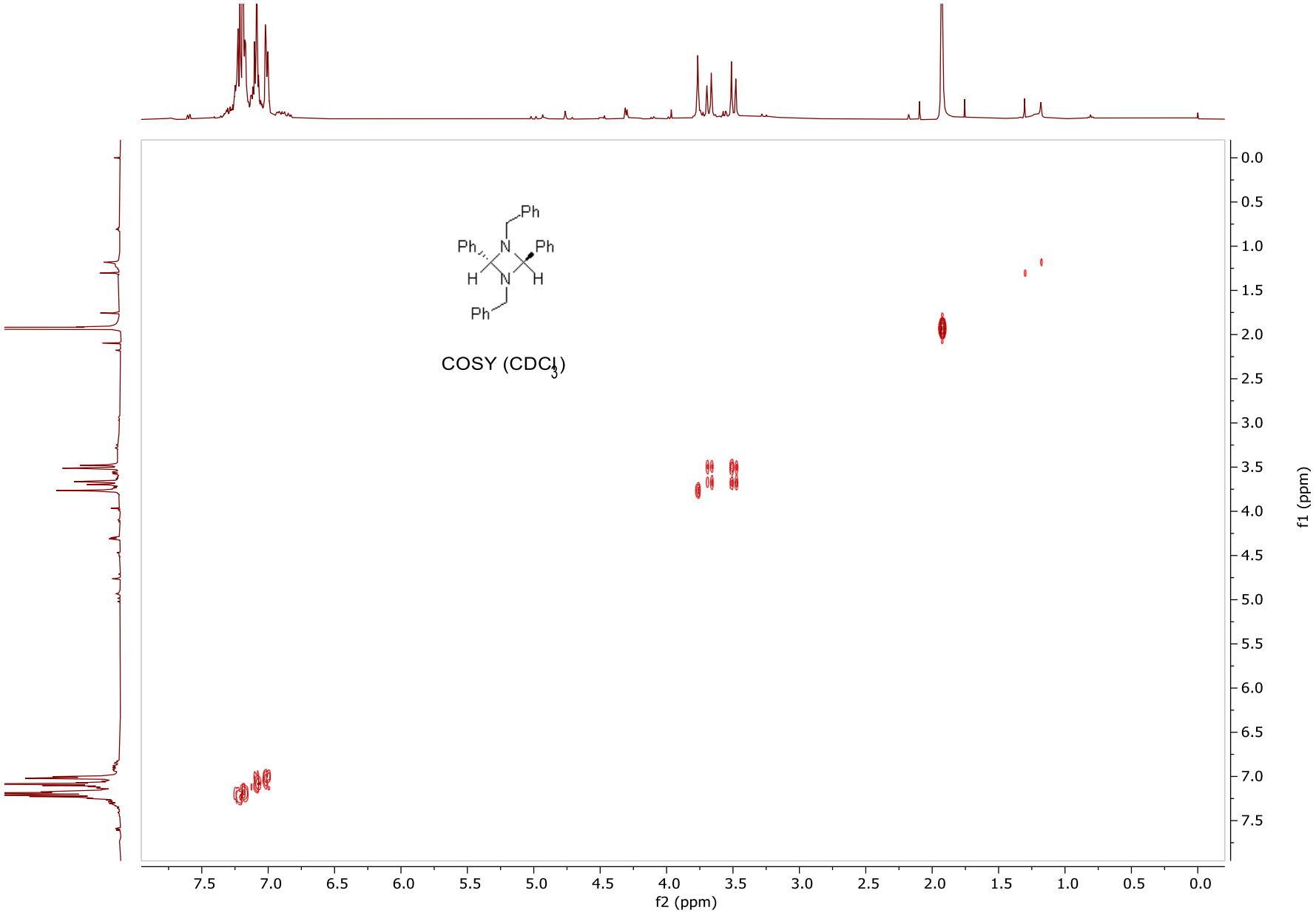
Ph
Ph
N
Ph
H
N
H
Ph
COSY (CDCl3)
f2 (ppm)
f1 (ppm)
7.5
7.0
6.5
6.0
5.5
5.0
4.5
4.0
3.5
3.0
2.5
2.0
1.5
1.0
0.5
0.0

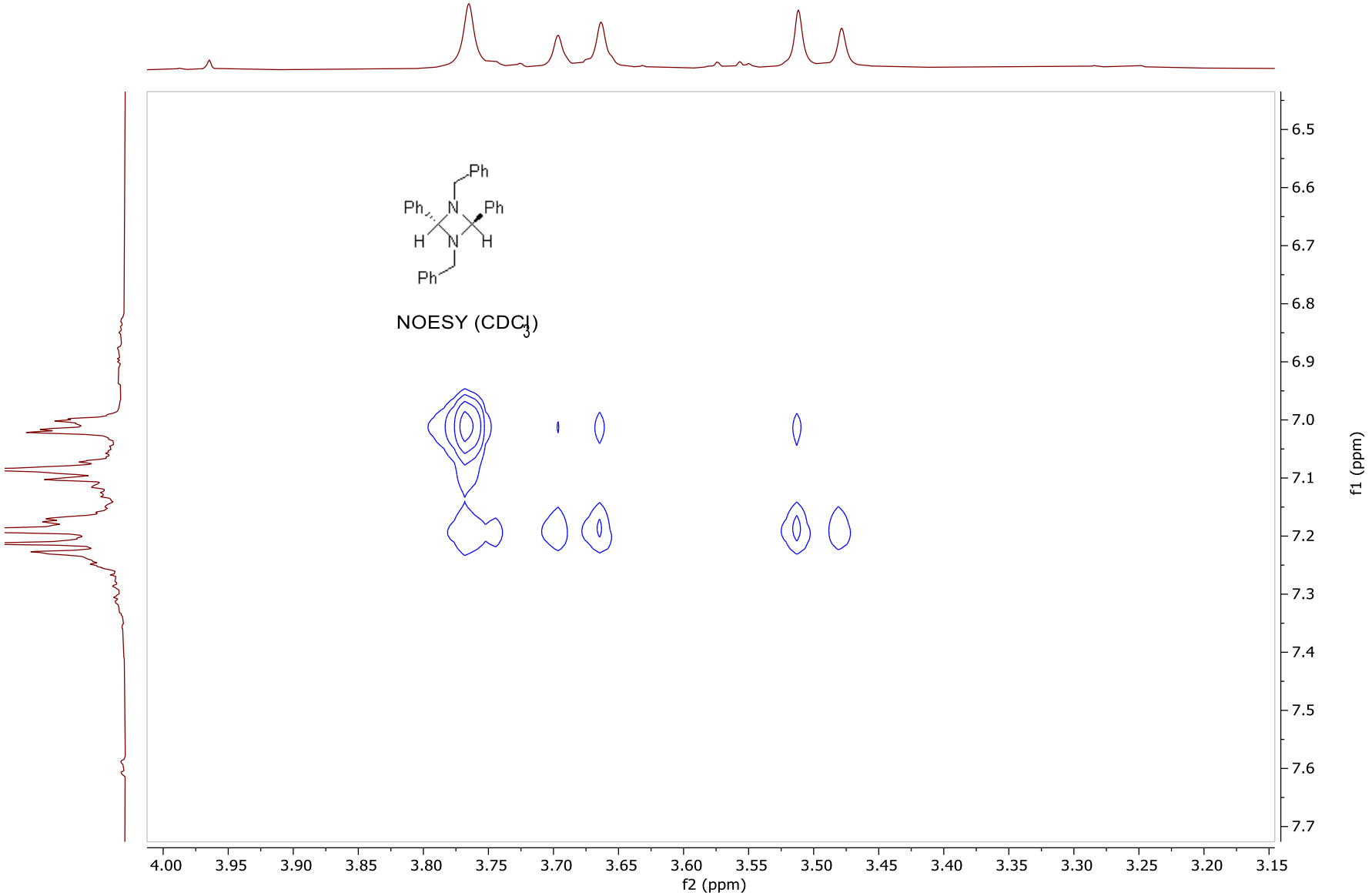
Ph
Ph
N
Ph
H
N
H
Ph
NOESY (CDCl3)
6.5
6.6
6.7
6.8
6.9
7.0
7.1
7.2
7.3
7.4
7.5
7.6
7.7
f1 (ppm)
4.00
3.95
3.90
3.85
3.80
3.75
3.70
3.65
3.60
3.55
3.50
3.45
3.40
3.35
3.30
3.25
3.20
3.15
f2 (ppm)

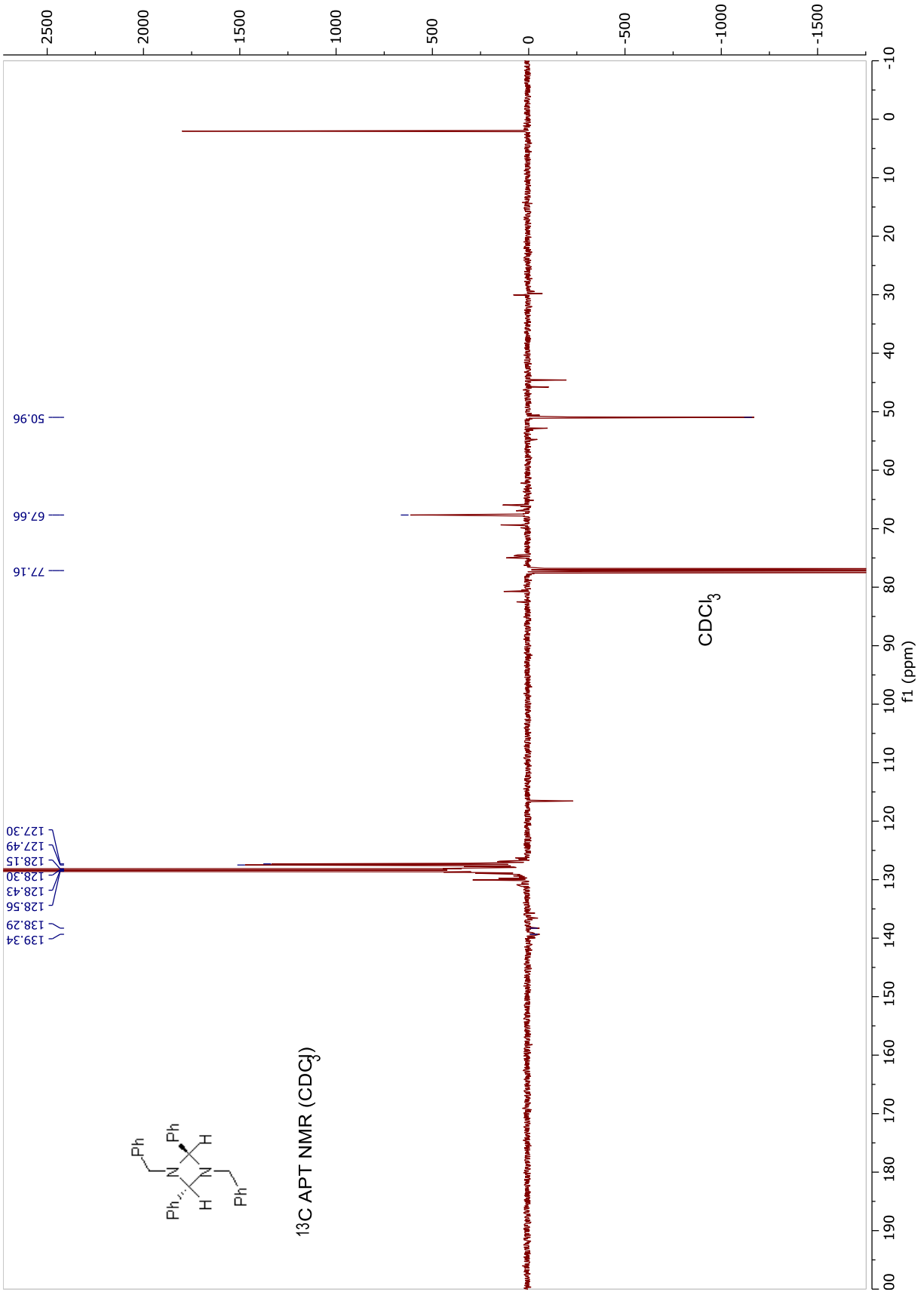
13C APT NMR (CDCl3)
CDCl3
f1 (ppm)
139.34
138.29
128.56
128.43
128.30
128.15
127.49
127.30
77.16
67.66
50.96
Ph
Ph
N
H
Ph
Ph
N
H
Ph

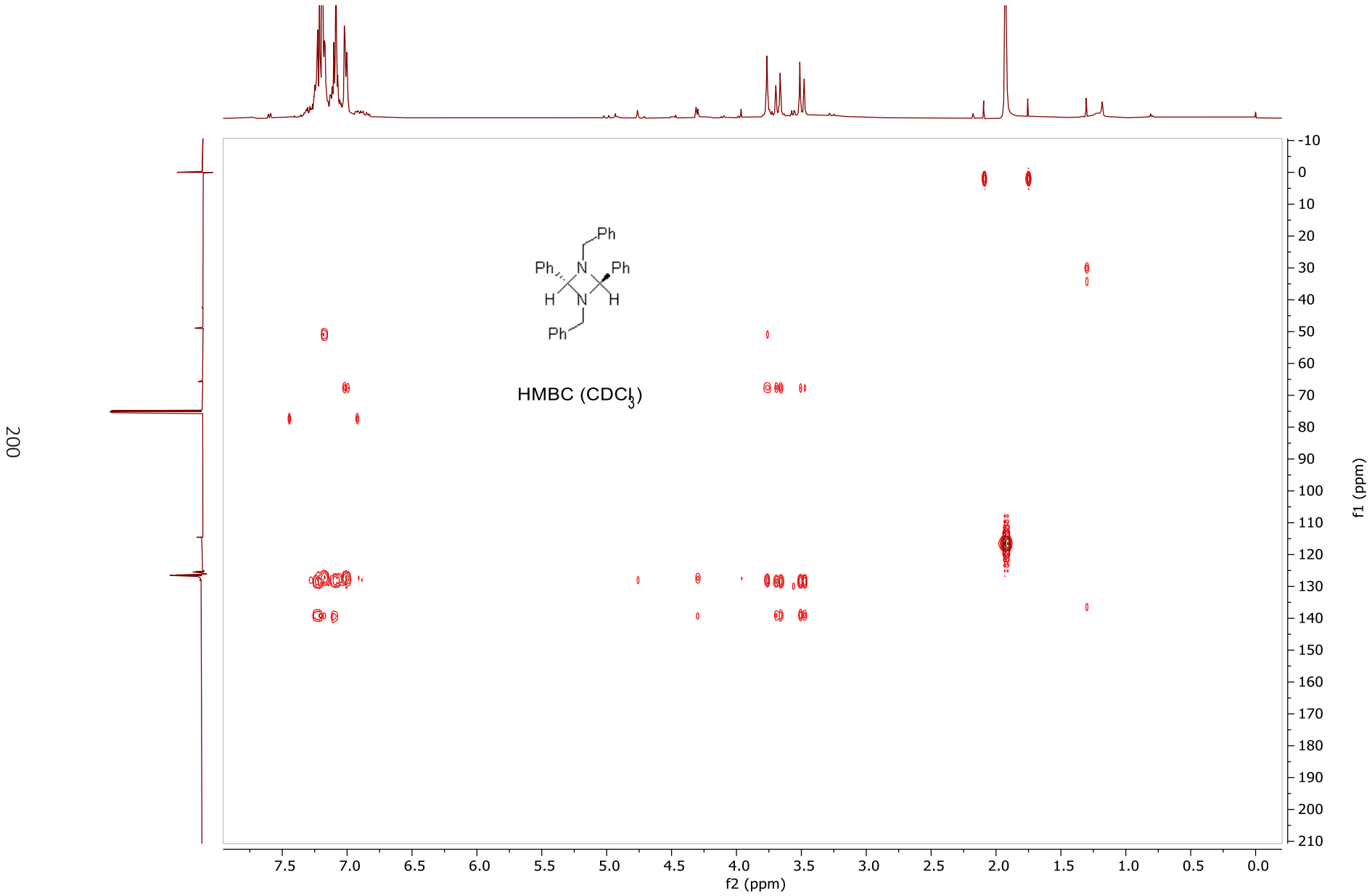
Ph
Ph
N
Ph
H
N
H
Ph
HMBC (CDCl3)
200
-10
0
10
20
30
40
50
60
70
80
90
100
110
120
130
140
150
160
170
180
190
200
210
f1 (ppm)
7.5
7.0
6.5
6.0
5.5
5.0
4.5
4.0
3.5
3.0
2.5
2.0
1.5
1.0
0.5
0.0
f2 (ppm)

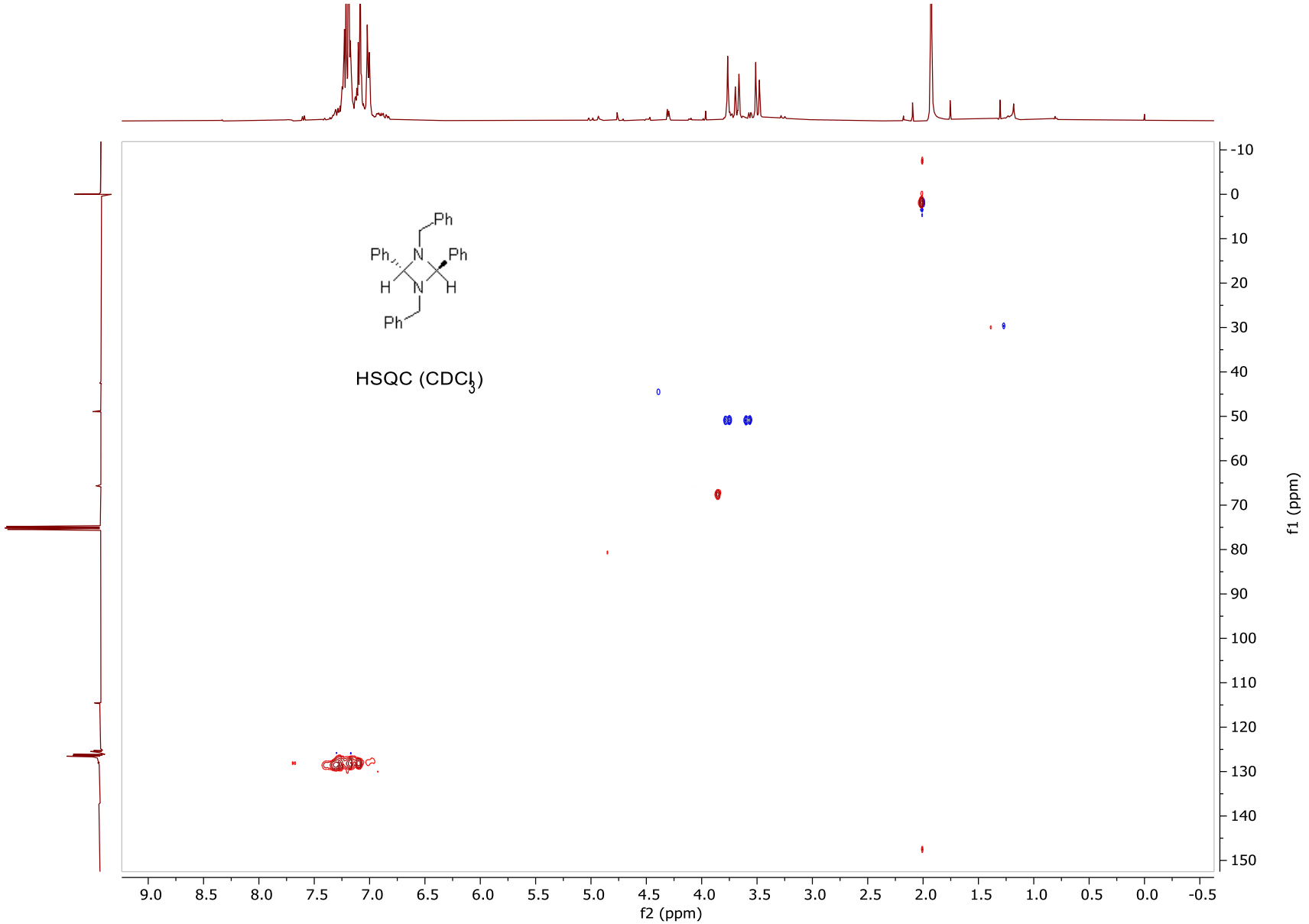
Ph
Ph
N
Ph
H
N
H
Ph
HSQC (CDCl3)
f2 (ppm)
f1 (ppm)
9.0
8.5
8.0
7.5
7.0
6.5
6.0
5.5
5.0
4.5
4.0
3.5
3.0
2.5
2.0
1.5
1.0
0.5
0.0
-0.5
-10
0
10
20
30
40
50
60
70
80
90
100
110
120
130
140
150

Reaction mixtures NMR

Red rectangles mark peaks of the diazetidines-1,3 protons; green rectangles mark peaks of the imine protons; grey rectangles mark peaks of the amine protons.

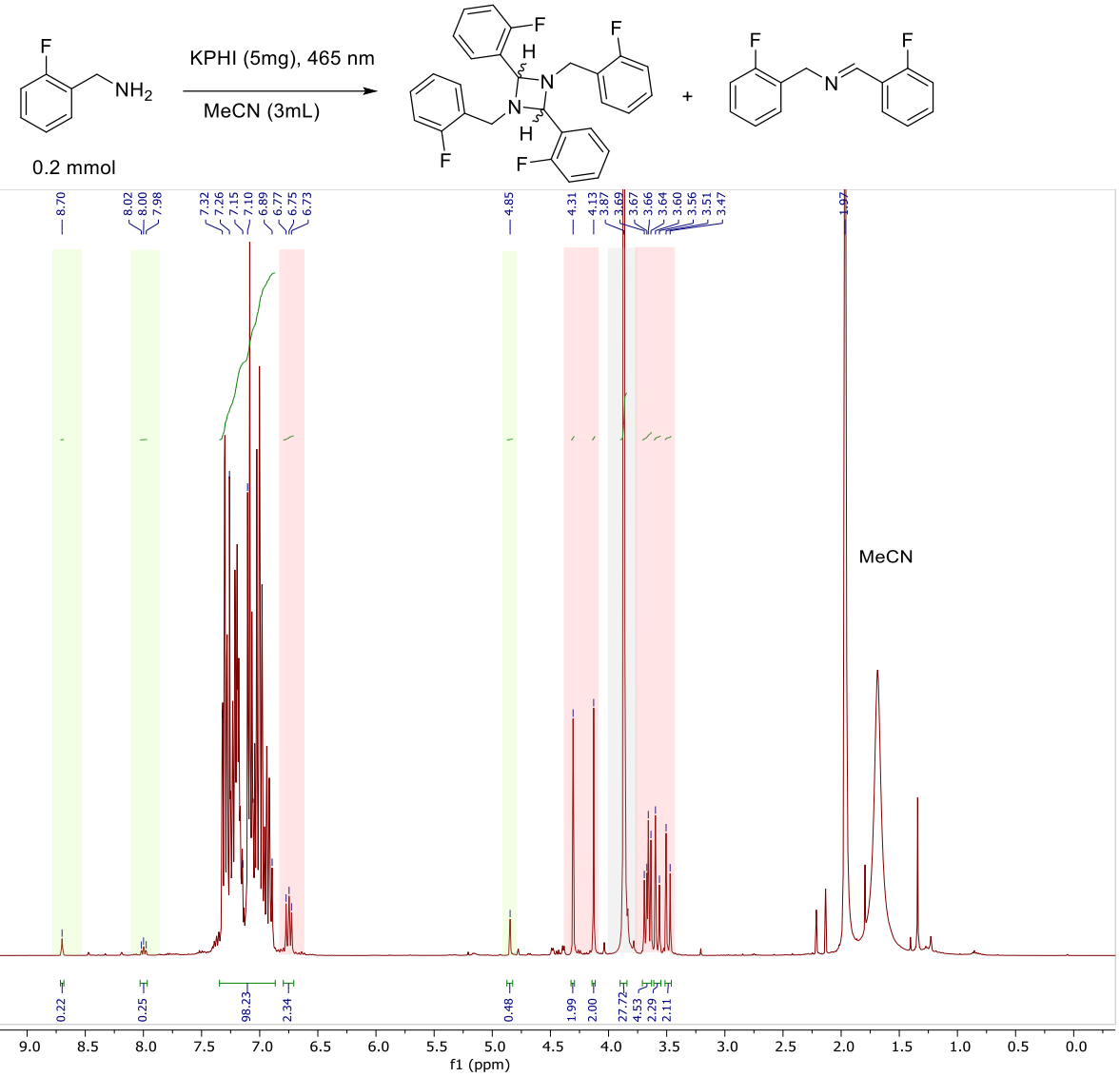

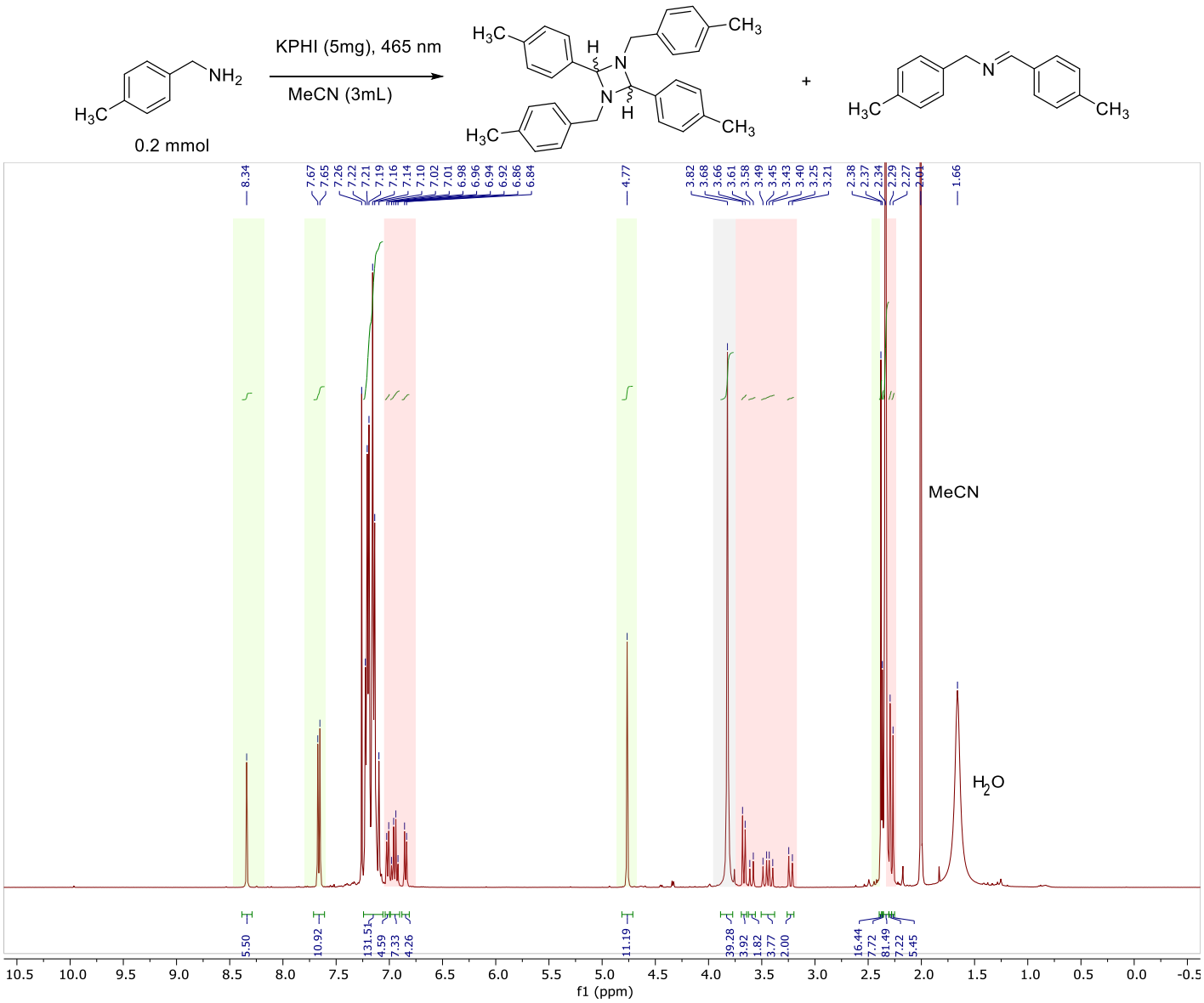
KPHI (5mg), 465 nm
MeCN (3mL)
0.2 mmol
MeCN
H2O
f1 (ppm)

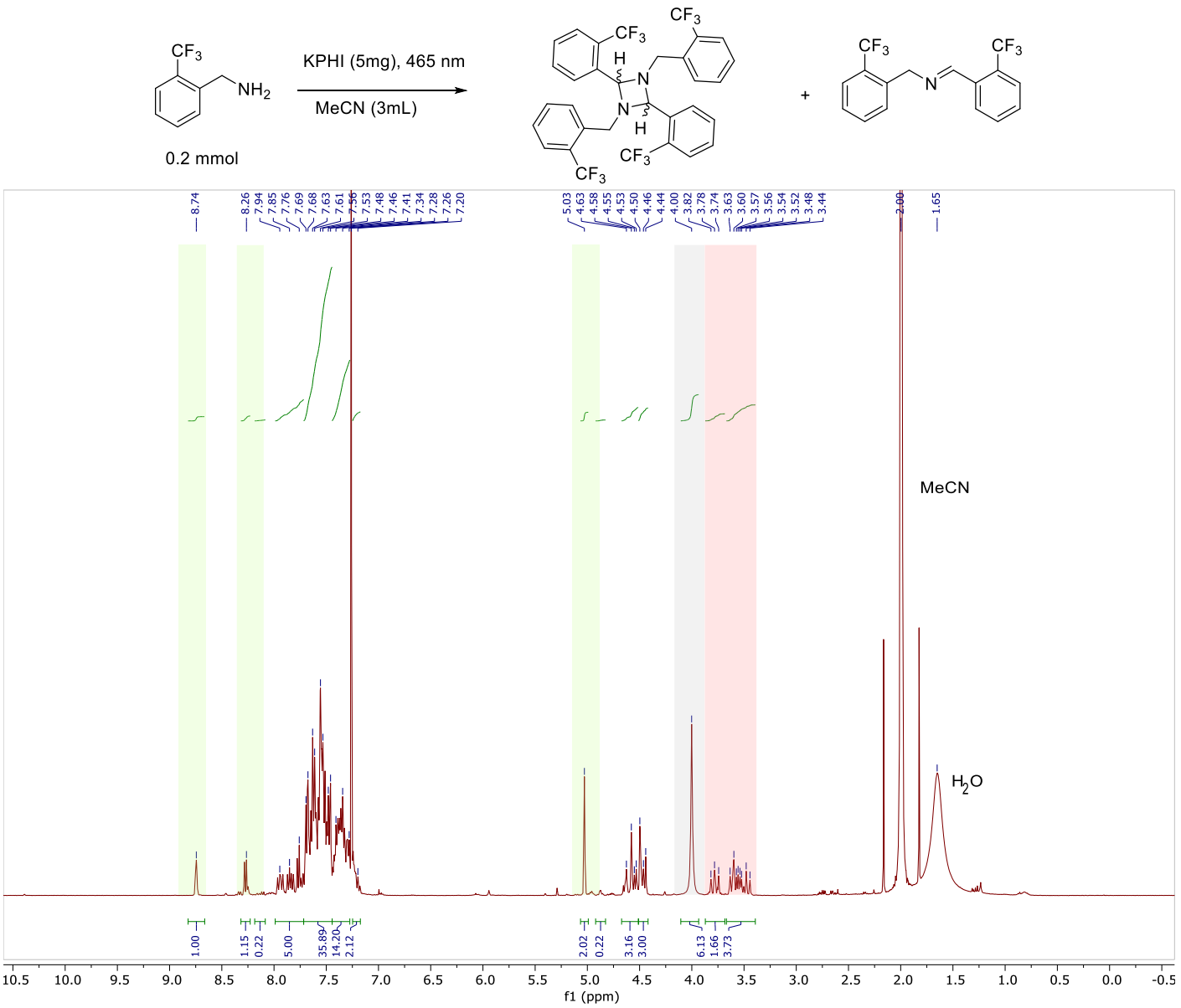
CF3
NH2
0.2 mmol
KPHI (5mg), 465 nm
MeCN (3mL)
CF3
CF3
H
N
N
H
CF3
CF3
+
CF3
N
CF3
MeCN
H2O
f1 (ppm)

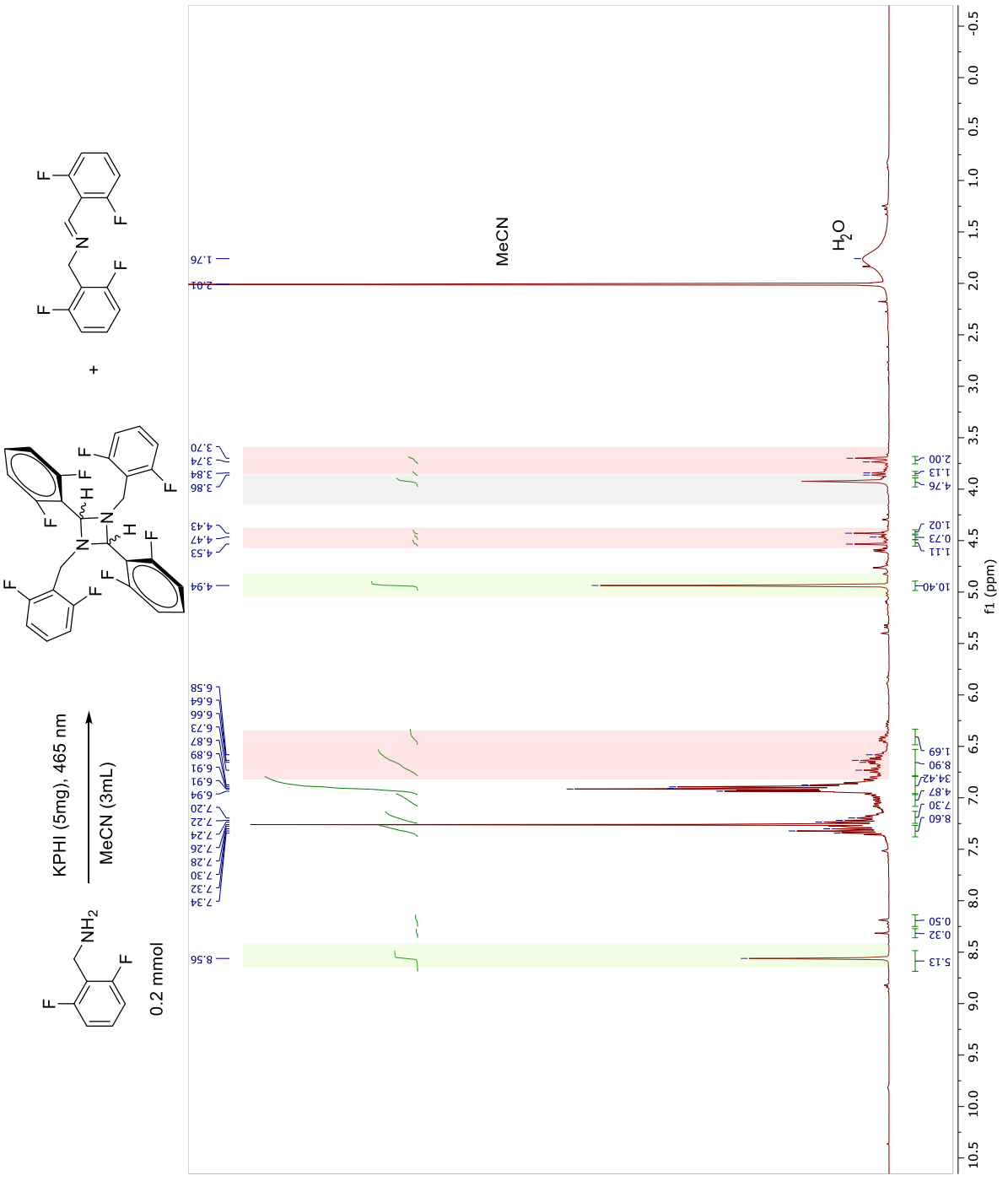
KPHI (5mg), 465 nm
MeCN (3mL)
0.2 mmol
+
MeCN
H2O
f1 (ppm)

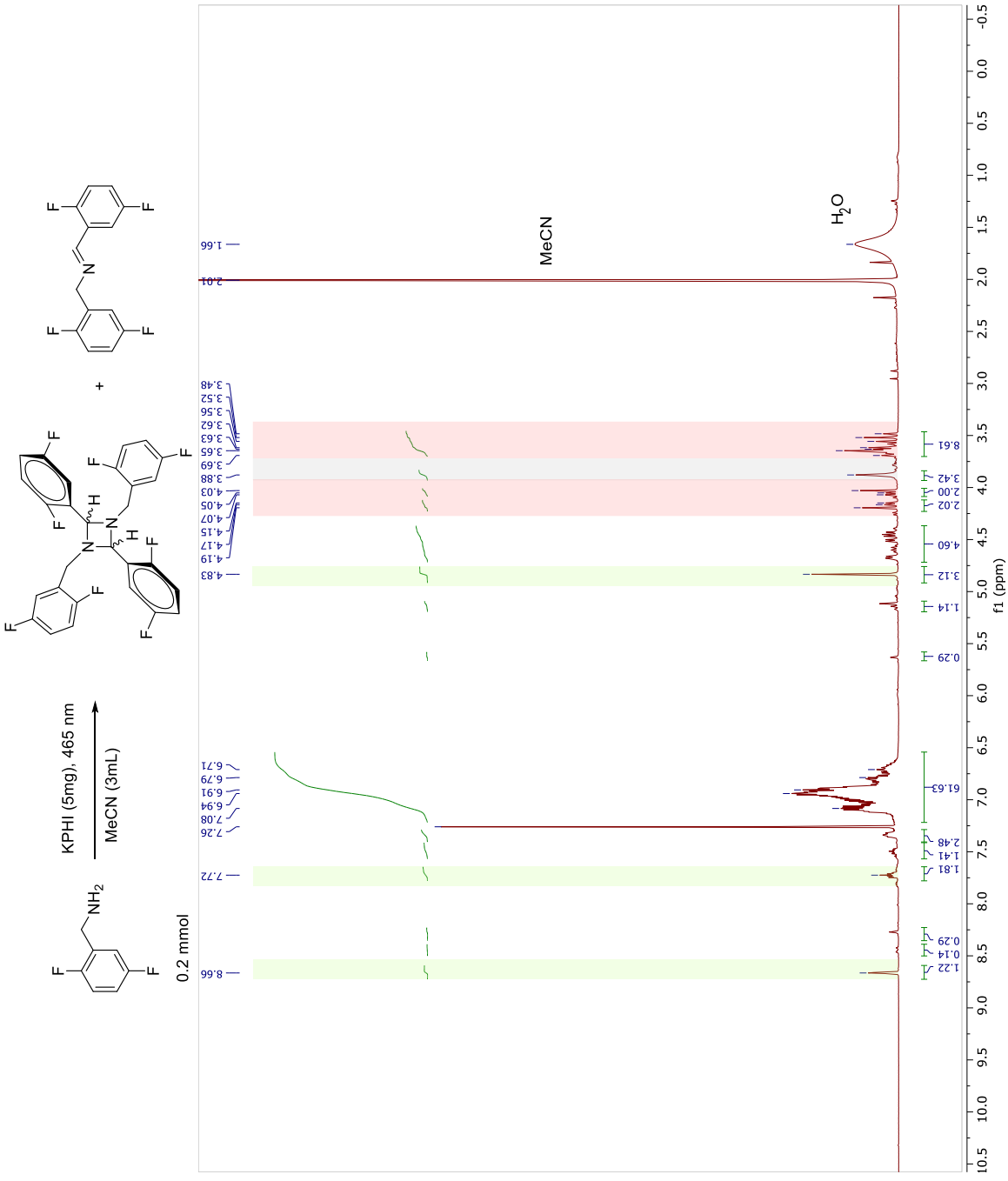
KPHI (5mg), 465 nm
MeCN (3mL)
0.2 mmol
MeCN
H2O
f1 (ppm)

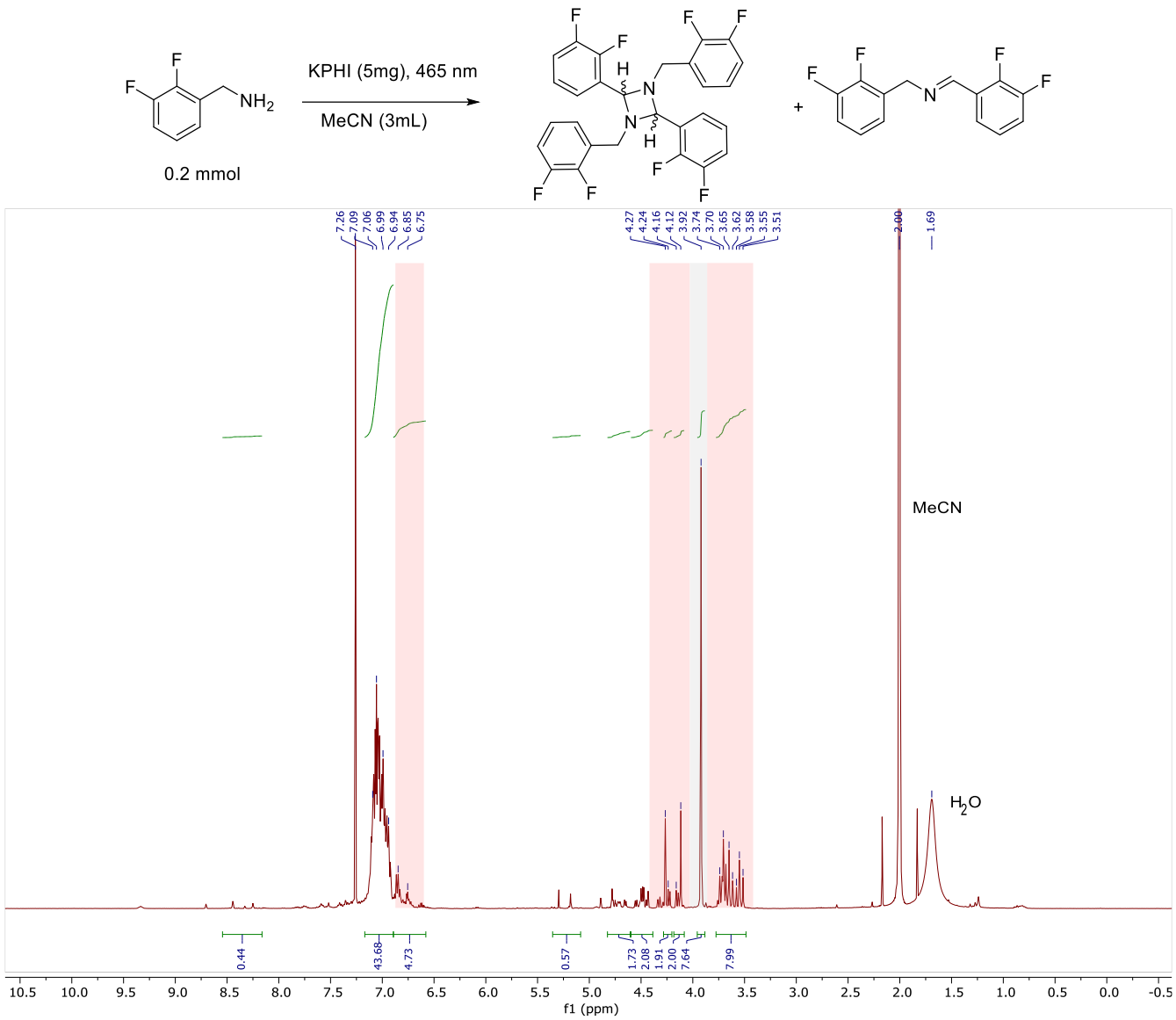
KPHI (5mg), 465 nm
MeCN (3mL)
0.2 mmol
MeCN
H2O
f1 (ppm)

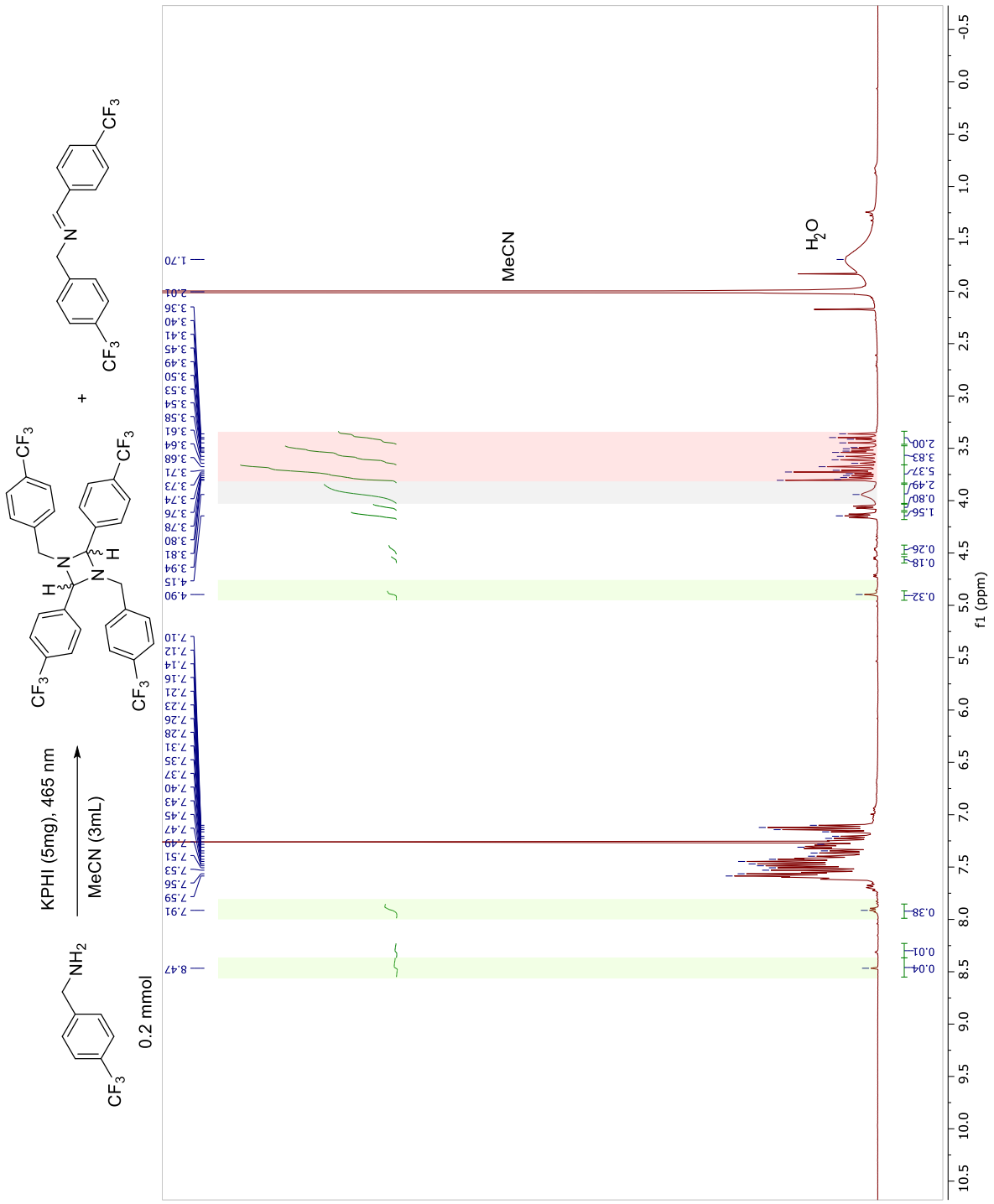
KPHI (5mg), 465 nm
MeCN (3mL)
0.2 mmol
MeCN
H2O
f1 (ppm)

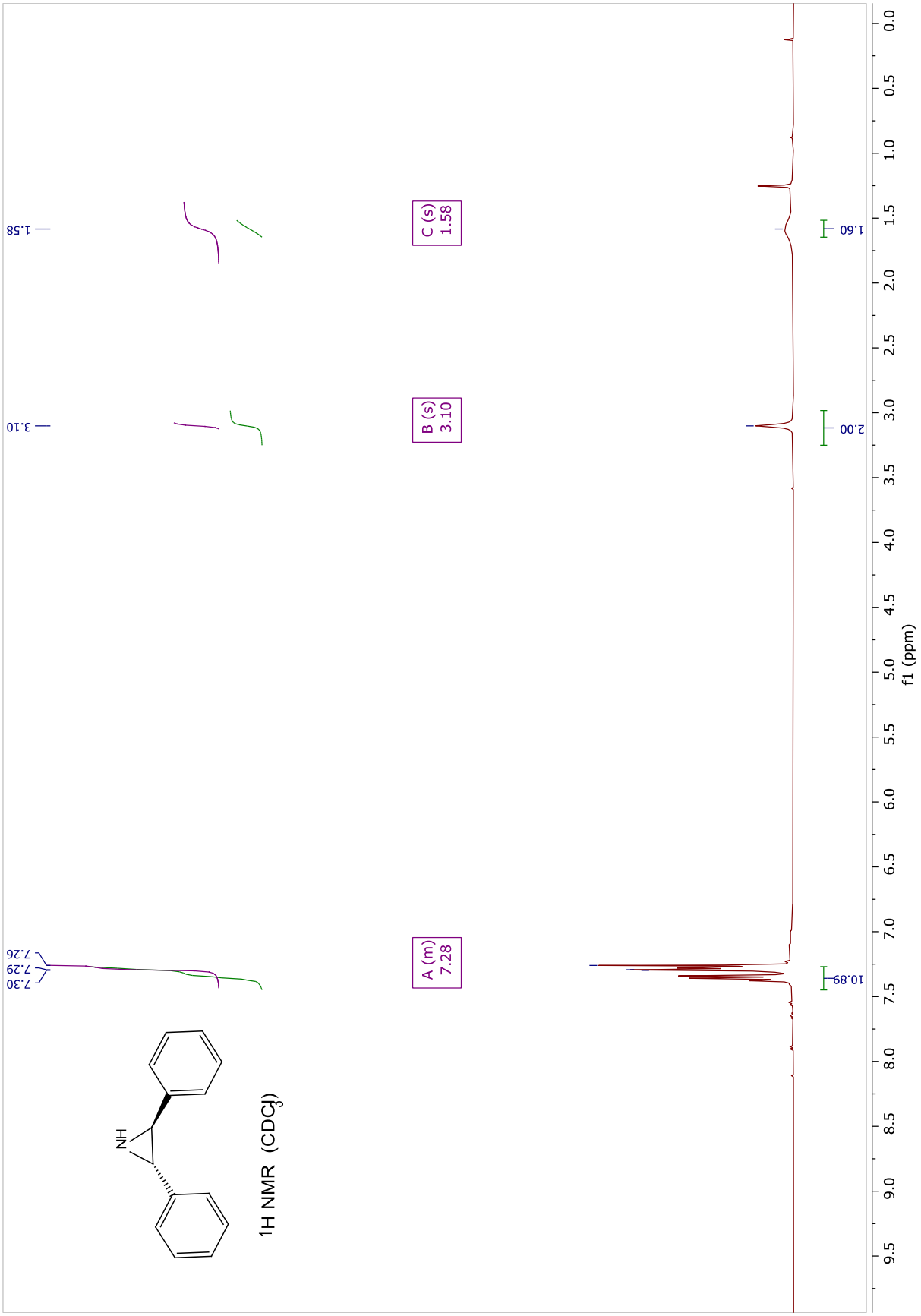
^{1}H NMR (CDCl$_3$)
NH
7.30
7.29
7.26
3.10
1.58
A (m)
7.28
B (s)
3.10
C (s)
1.58
10.89
2.00
1.60
f1 (ppm)

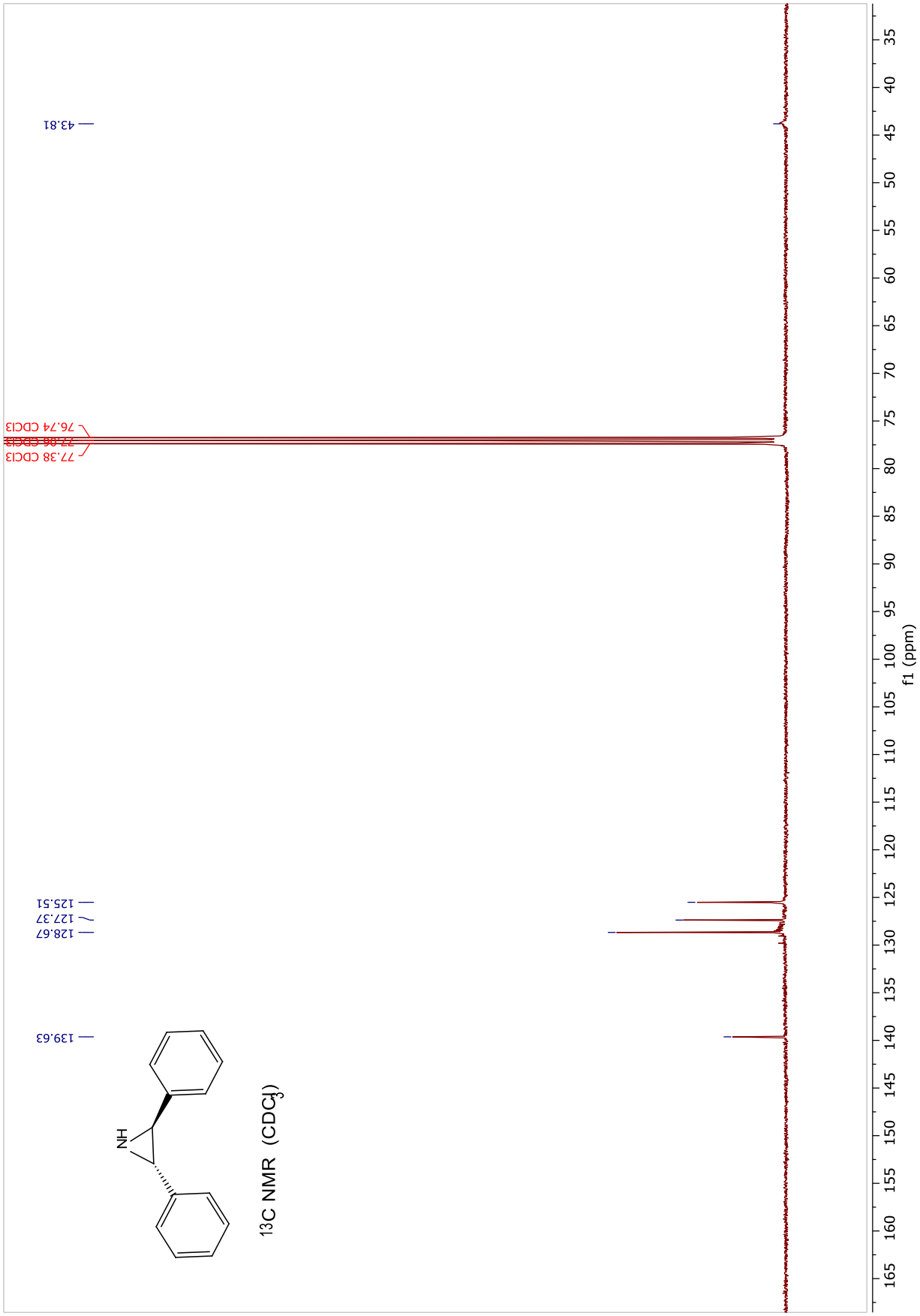
139.63
128.67
127.37
125.51
77.38 CDCl3
27.08 CDCl3
76.74 CDCl3
43.81
HN
13C NMR (CDCl3)
f1 (ppm)

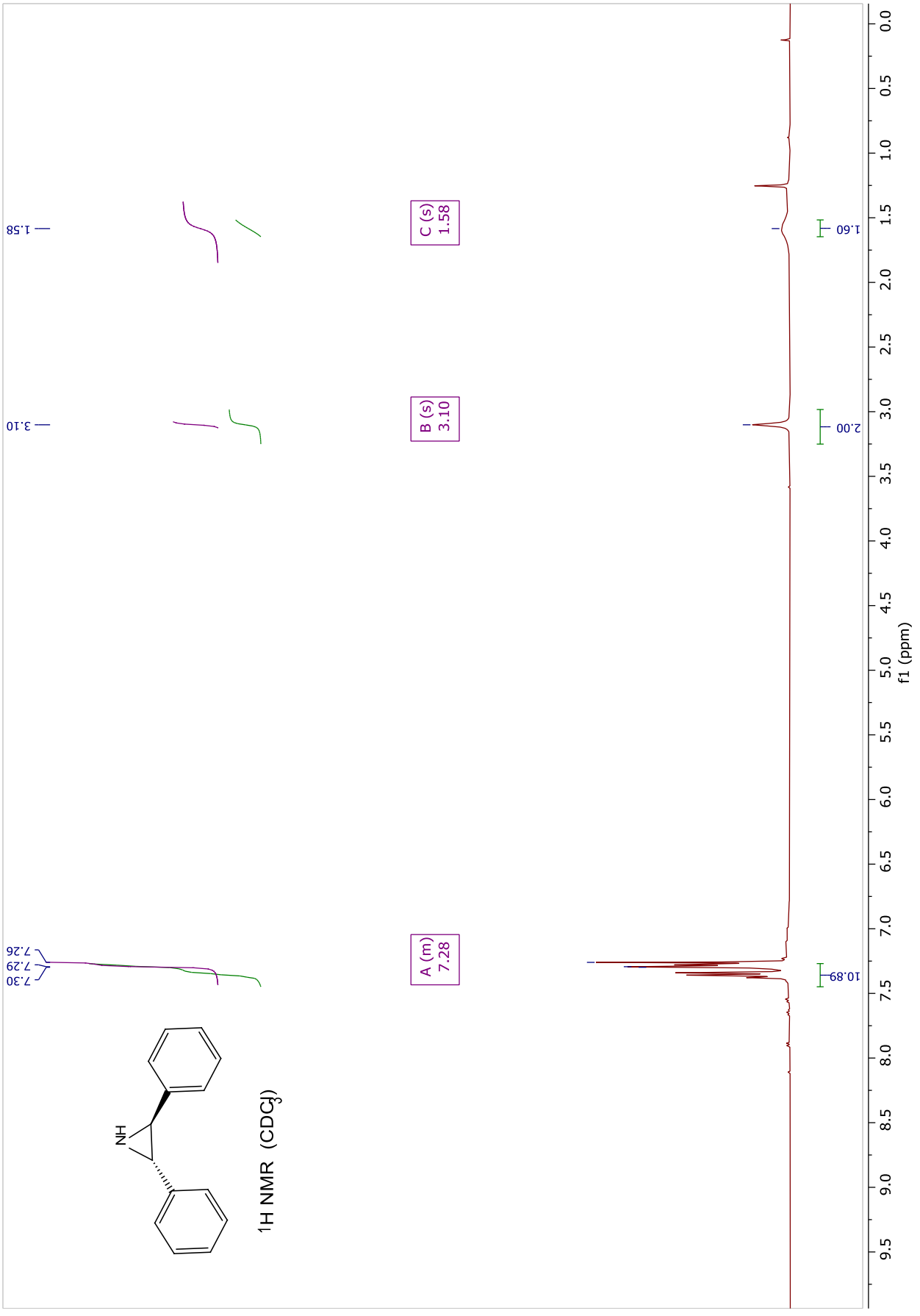
^{1}H NMR (CDCl$_3$)
NH
7.30
7.29
7.26
A (m)
7.28
B (s)
3.10
C (s)
1.58
10.89
2.00
1.60
3.10
1.58
f1 (ppm)

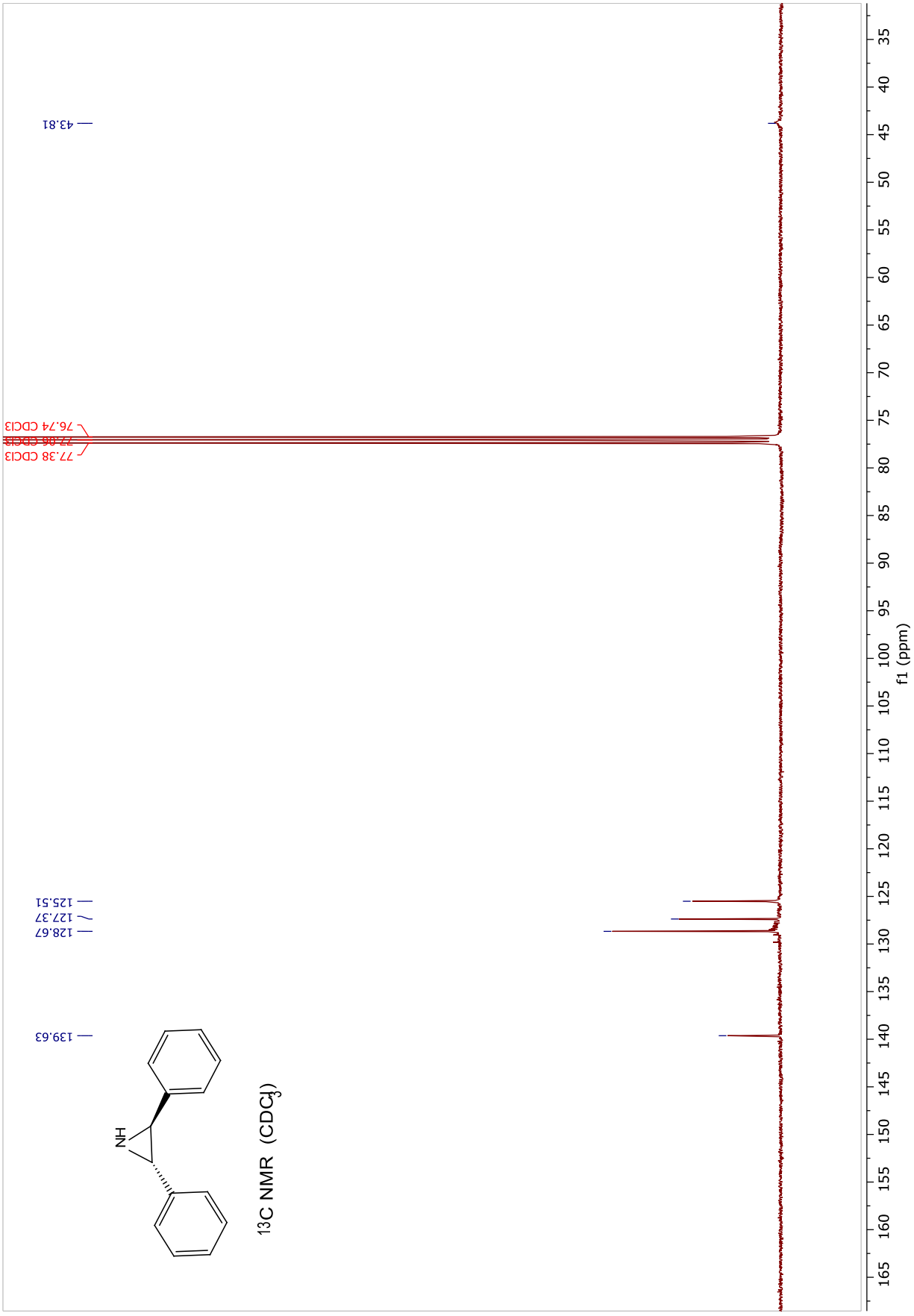
139.63
128.67
127.37
125.51
77.38 CDCl3
77.06 CDCl3
76.74 CDCl3
43.81
NH
13C NMR (CDCl3)
f1 (ppm)

NMR spectra of sylfonyl chlorides

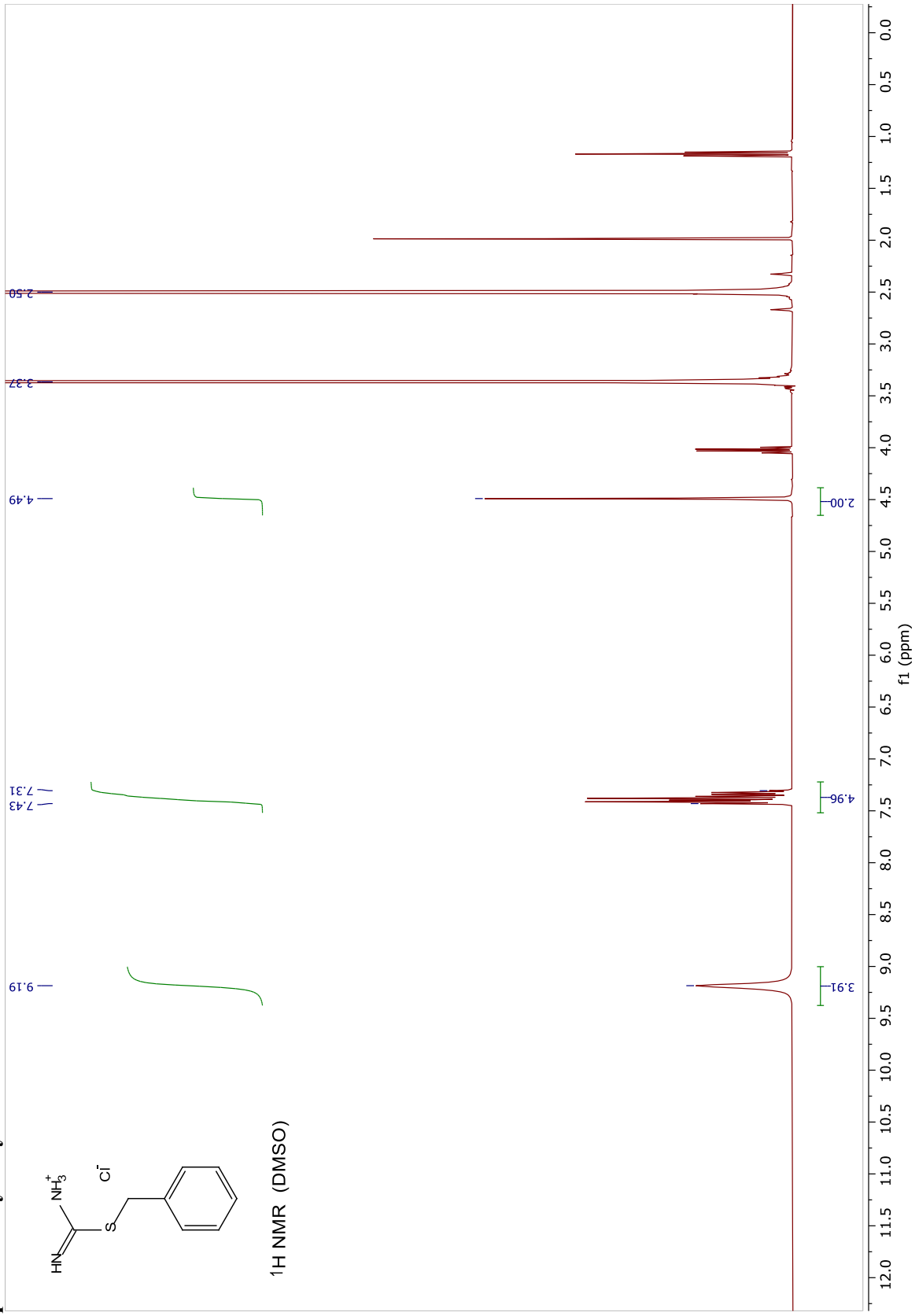

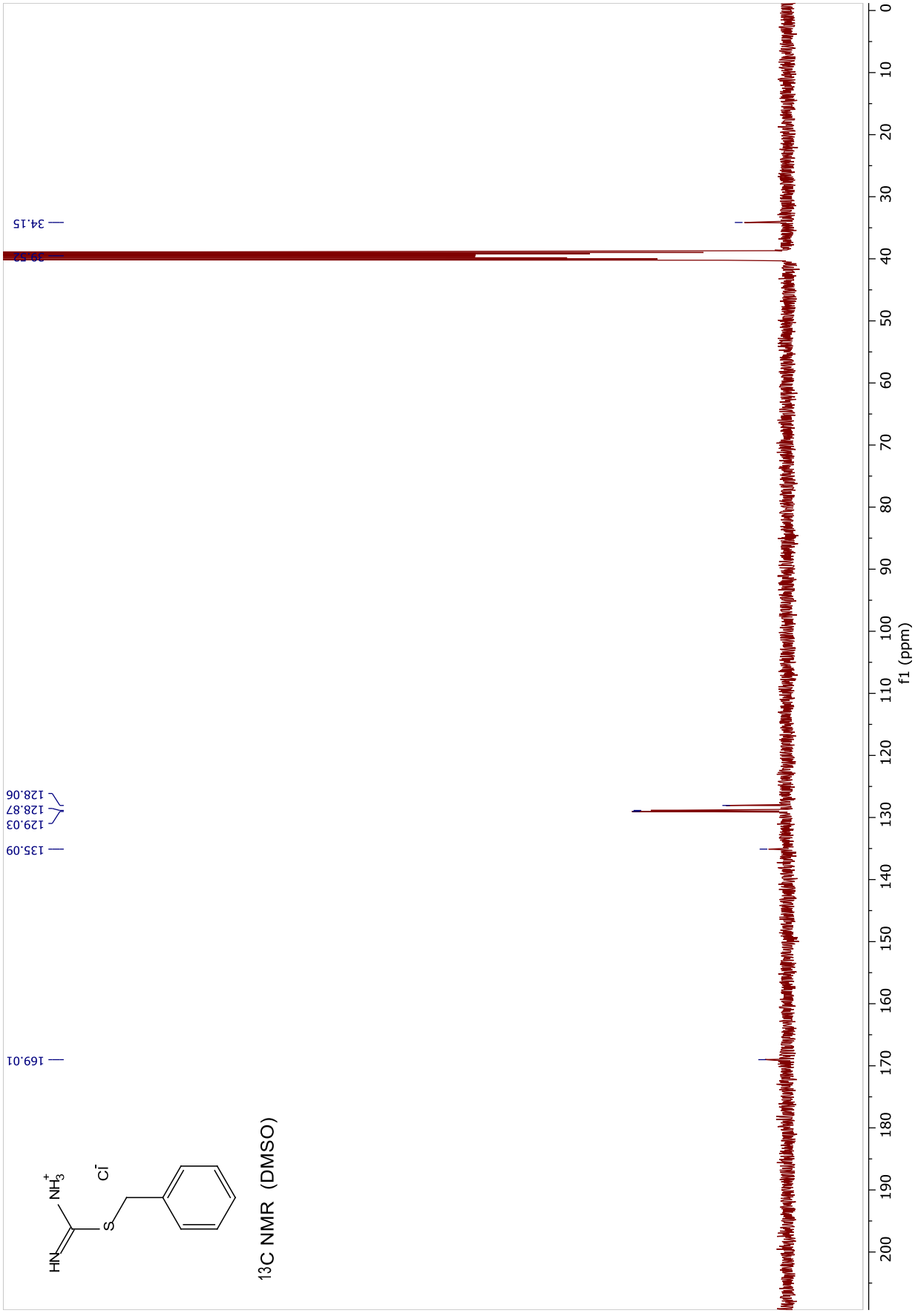
34.15
39.52
128.06
128.87
129.03
135.09
169.01
^{13}C NMR (DMSO)
HN
S
Cl$^-$
NH$_3^+$
0
10
20
30
40
50
60
70
80
90
100
110
120
130
140
150
160
170
180
190
200
f1 (ppm)

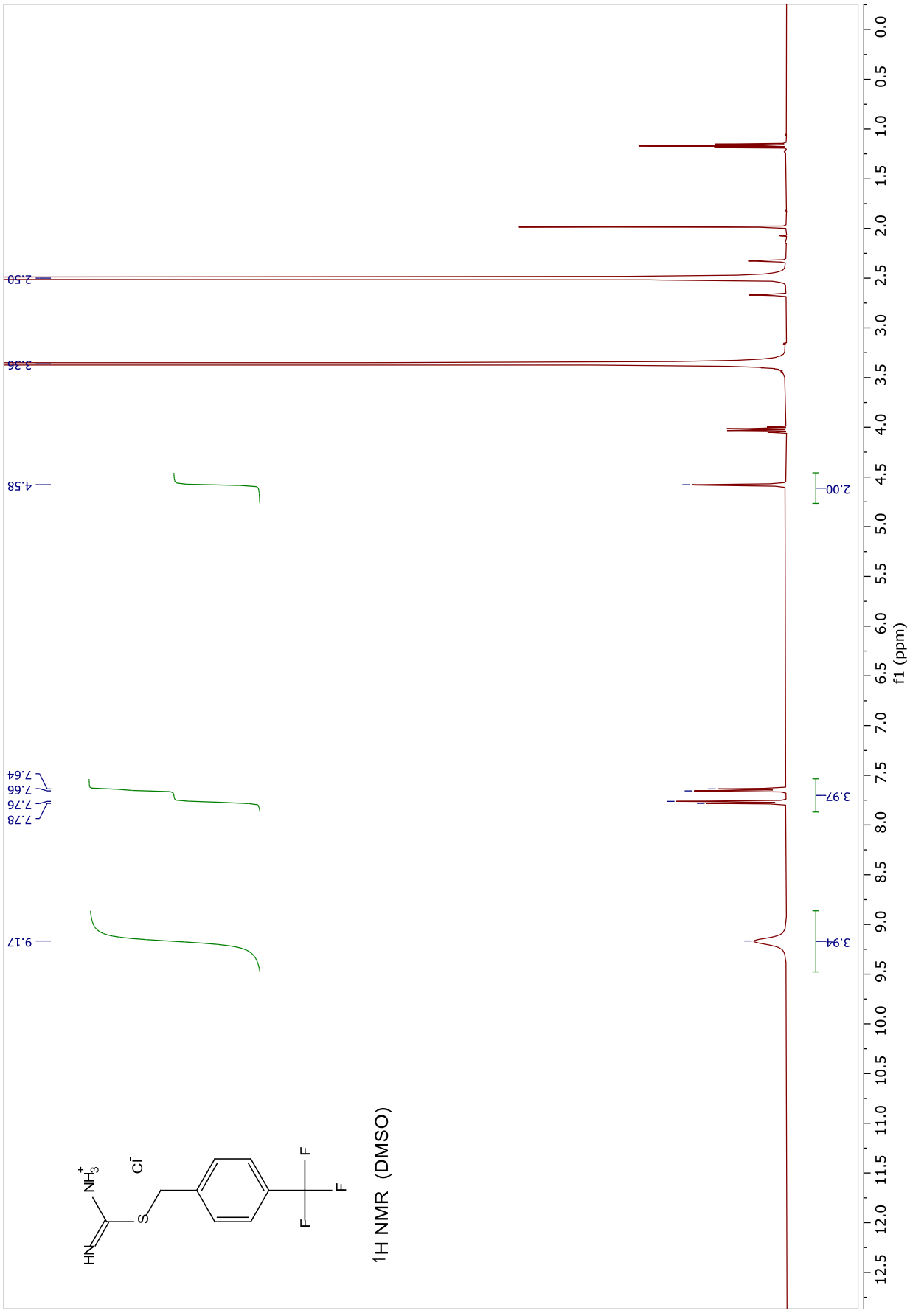
^{1}H NMR (DMSO)
HN
NH$_3^+$
S
Cl$^-$
F
F
F
9.17
7.78
7.76
7.66
7.64
4.58
3.36
2.50
3.94
3.97
2.00
f1 (ppm)

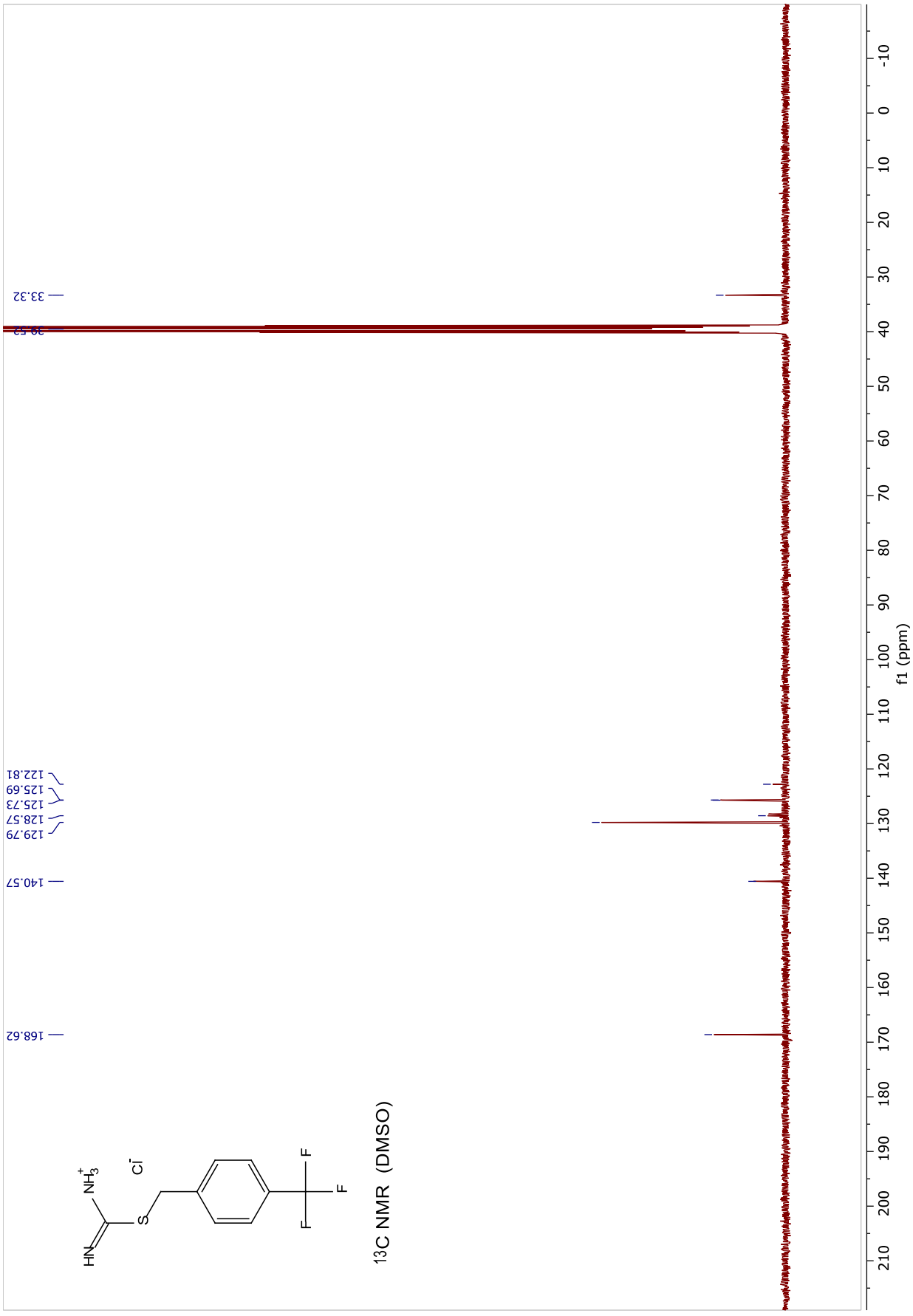
^{13}C NMR (DMSO)
HN
NH$_3^+$
S
Cl$^-$
F
F
F
168.62
140.57
129.79
128.57
125.73
125.69
122.81
39.52
33.32
f1 (ppm)

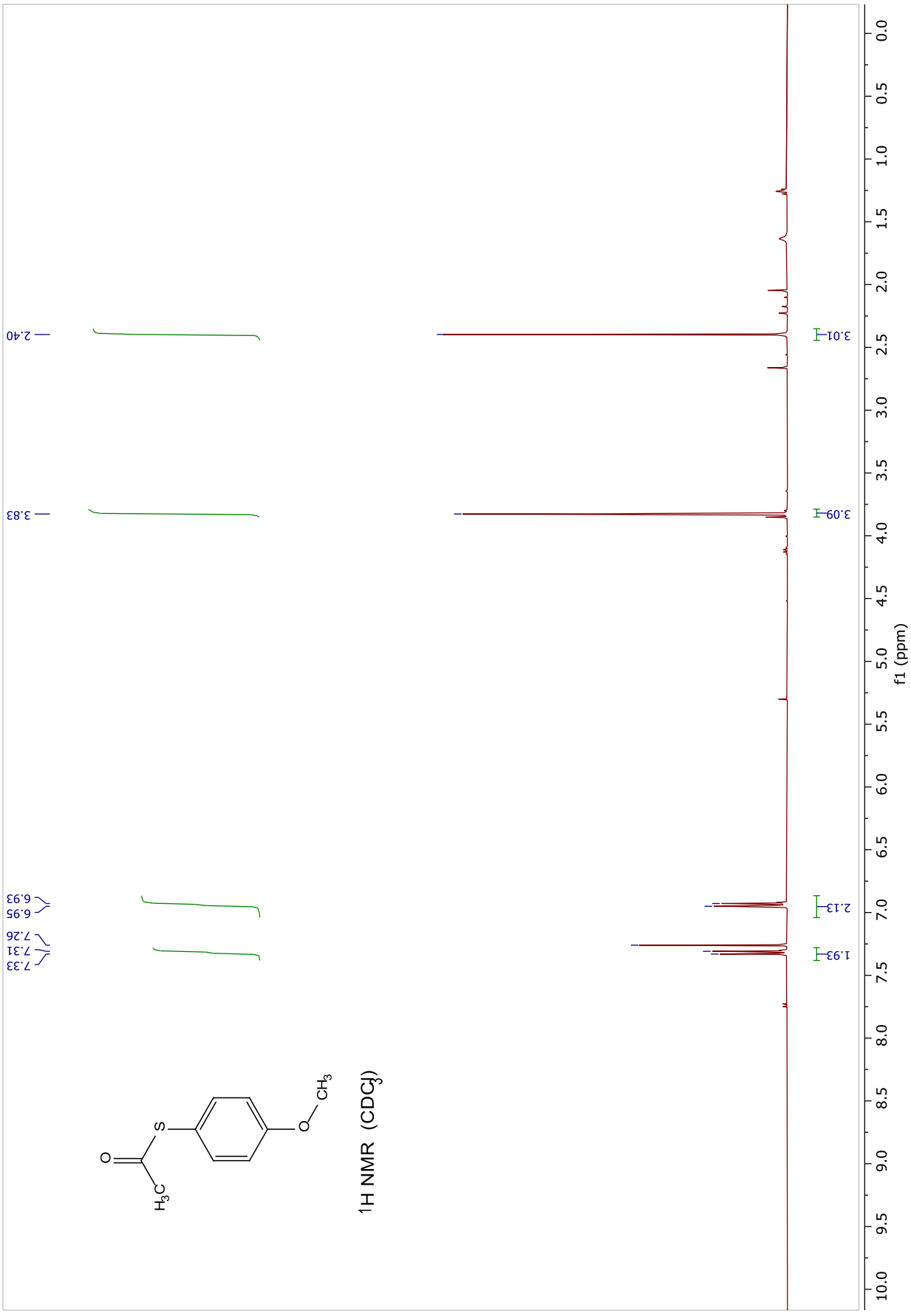
2.40
3.83
6.93
6.95
7.26
7.31
7.33
3.01
3.09
2.13
1.93
f1 (ppm)
^{1}H NMR (CDCl$_3$)
O
S
O
CH$_3$
H$_3$C

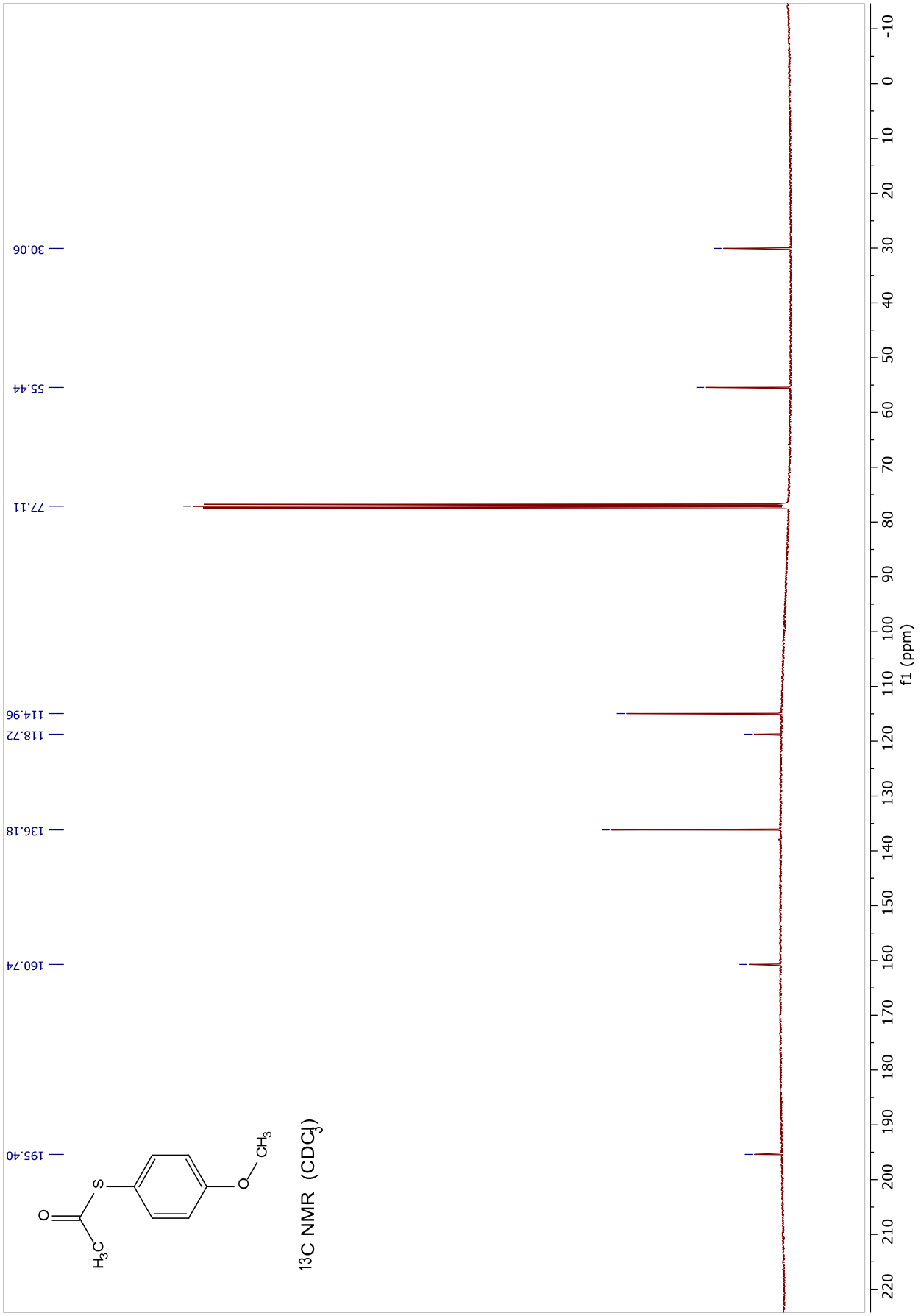
195.40
160.74
136.18
118.72
114.96
77.11
55.44
30.06
^{13}C NMR (CDCl$_3$)
f1 (ppm)

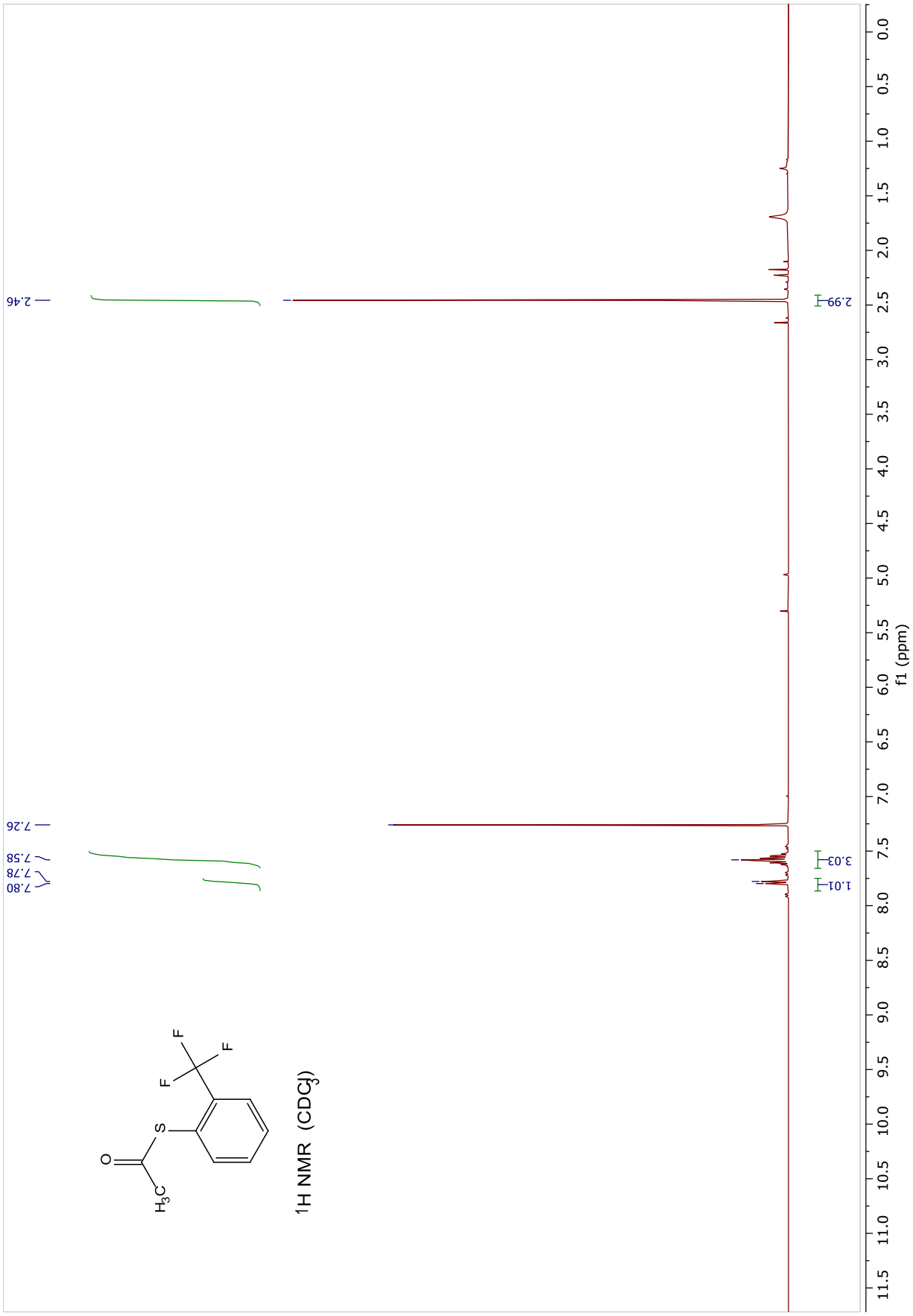
2.46
7.26
7.58
7.78
7.80
2.99
3.03
1.01
f1 (ppm)
^{1}H NMR (CDCl$_3$)
O
S
F
F
F
H$_3$C

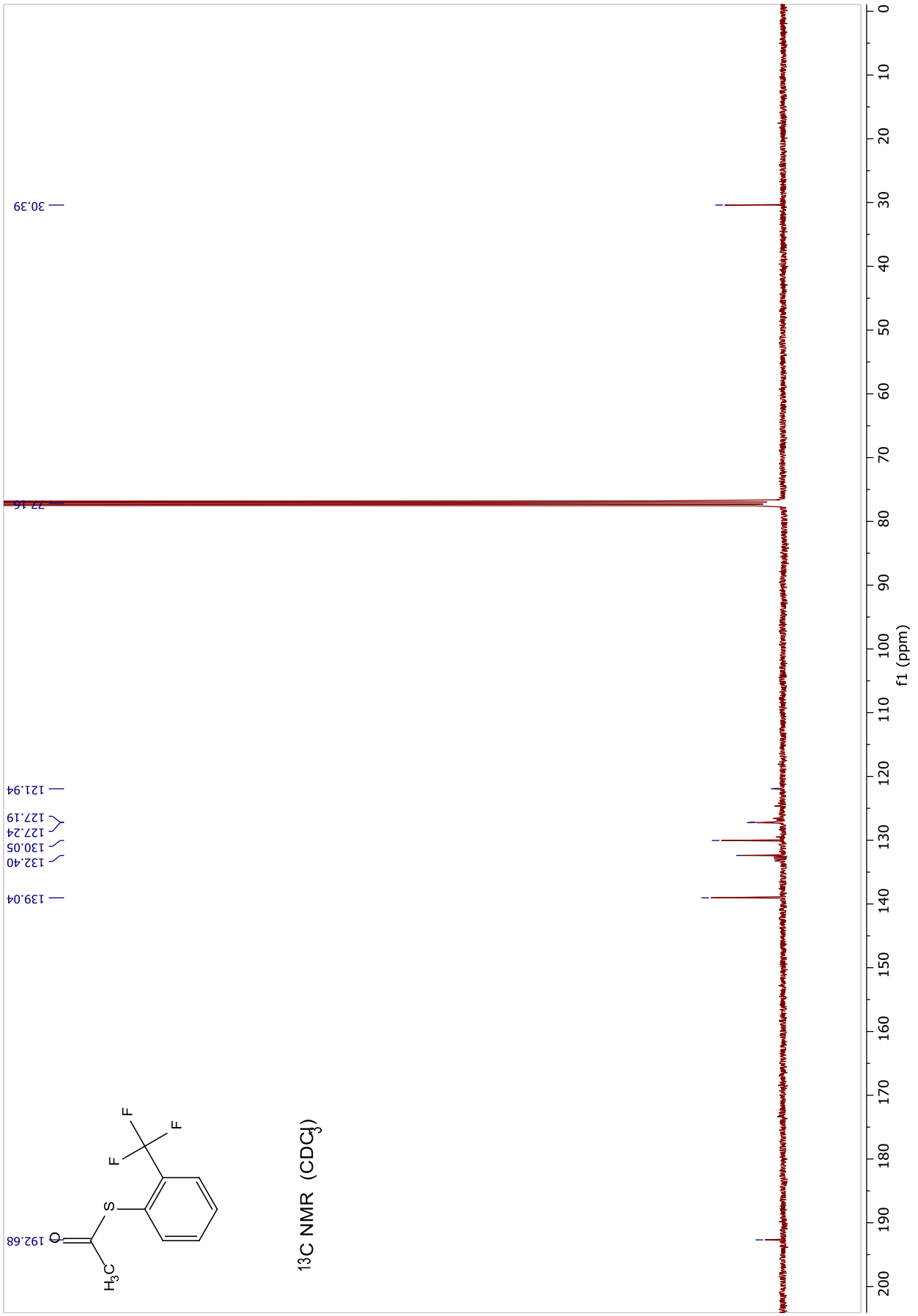
192.68
139.04
132.40
130.05
127.24
127.19
121.94
77.16
30.39
^{13}C NMR (CDCl$_3$)
f1 (ppm)

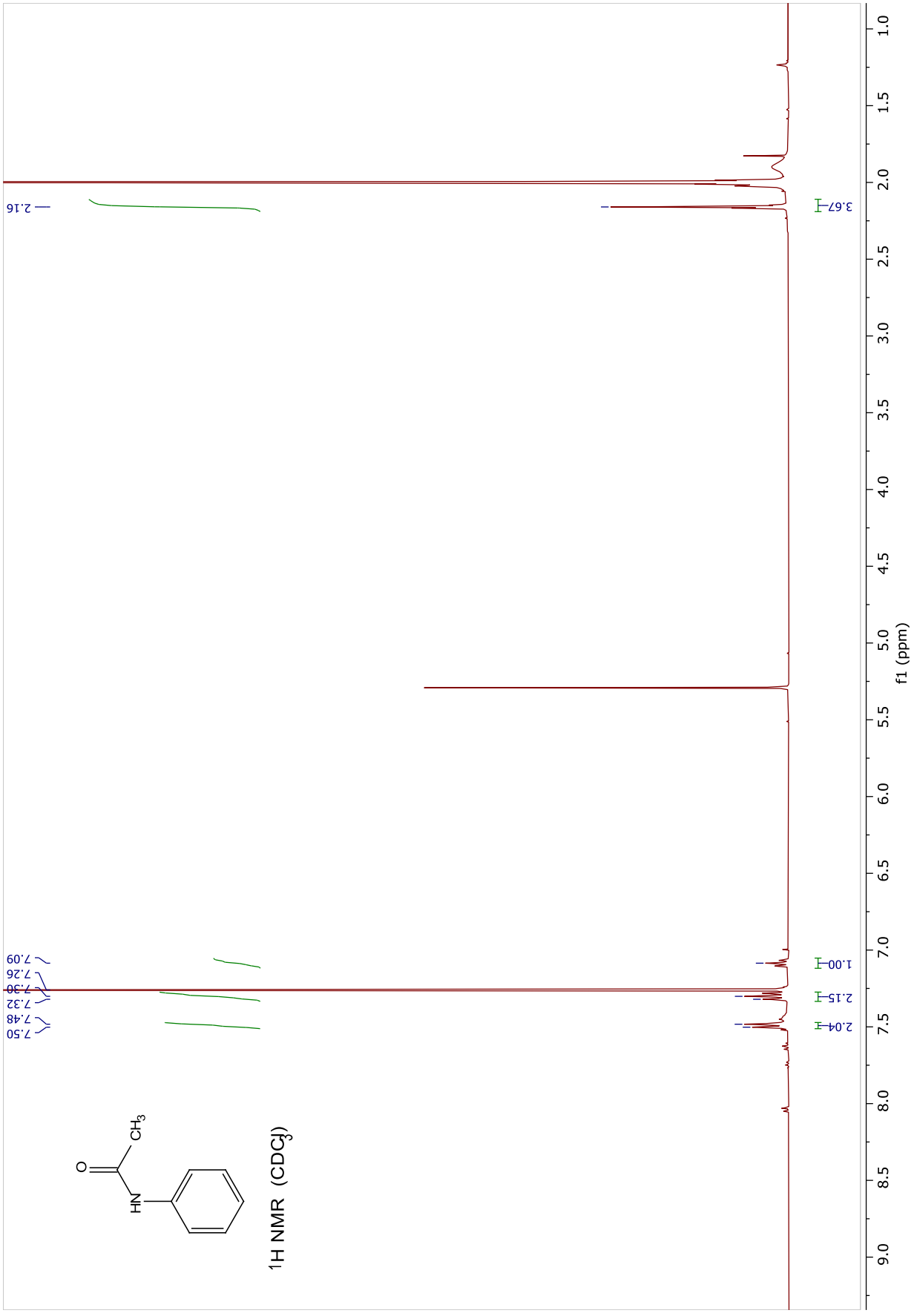
2.16
3.67
7.09
7.26
7.30
7.32
7.48
7.50
1.00
2.15
2.04
1.0
1.5
2.0
2.5
3.0
3.5
4.0
4.5
5.0
5.5
6.0
6.5
7.0
7.5
8.0
8.5
9.0
f1 (ppm)
O
HN
CH3
1H NMR (CDCl3)

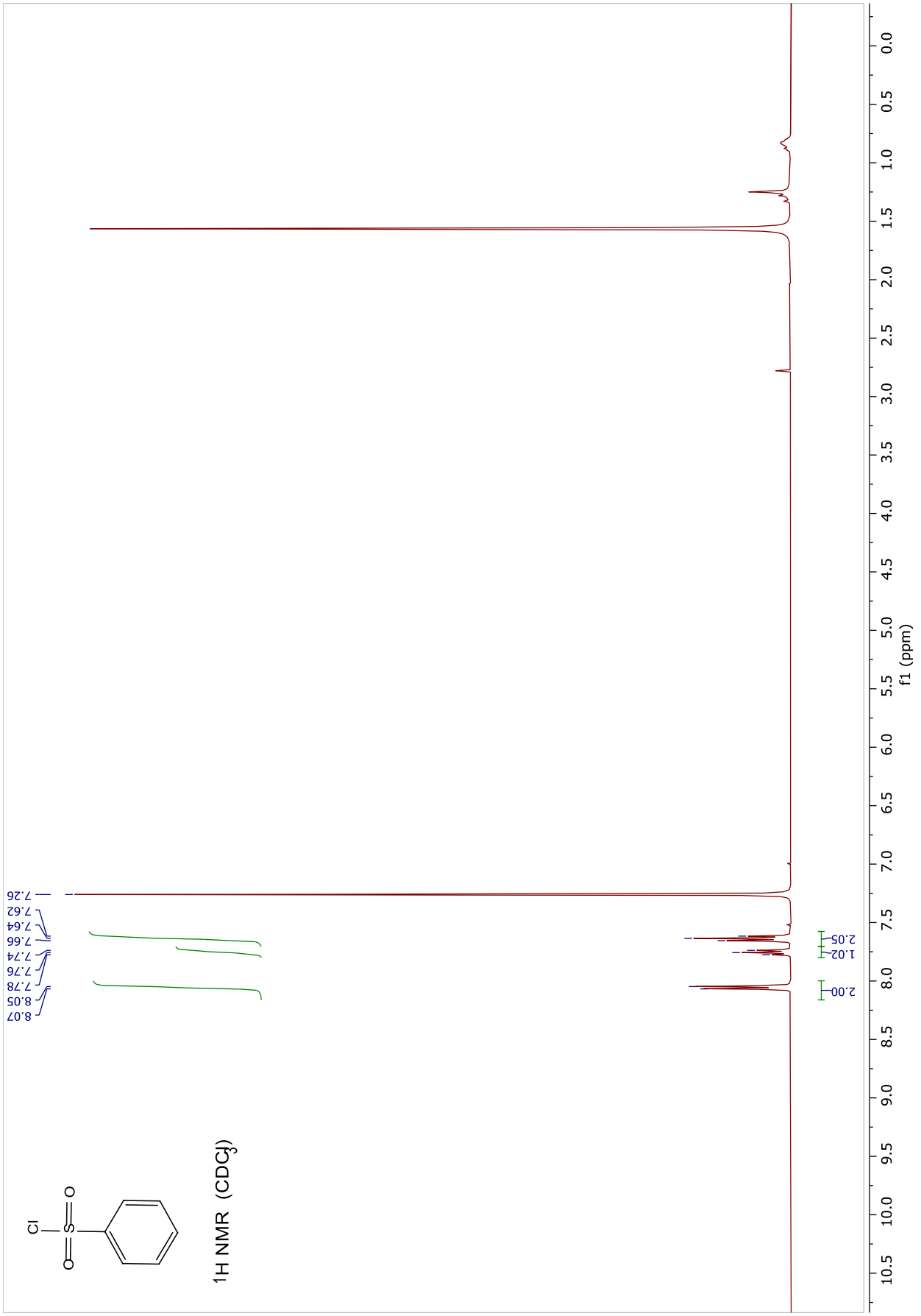
^{1}H NMR (CDCl$_3$)
Cl
S
O
O
8.07
8.05
7.78
7.76
7.74
7.66
7.64
7.62
7.26
2.00
1.02
2.05
f1 (ppm)

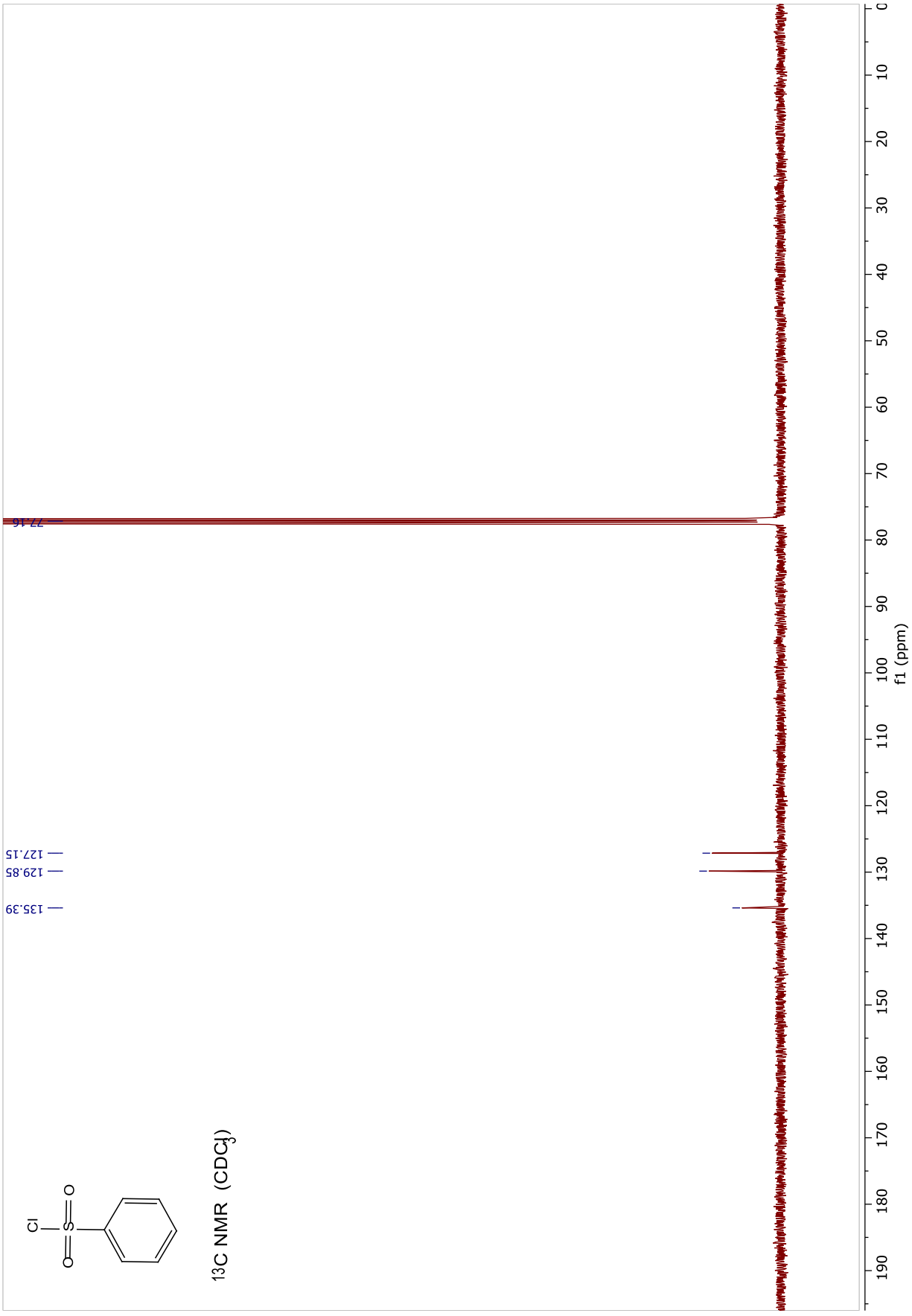
^{13}C NMR (CDCl$_3$)
77.16
127.15
129.85
135.39
f1 (ppm)

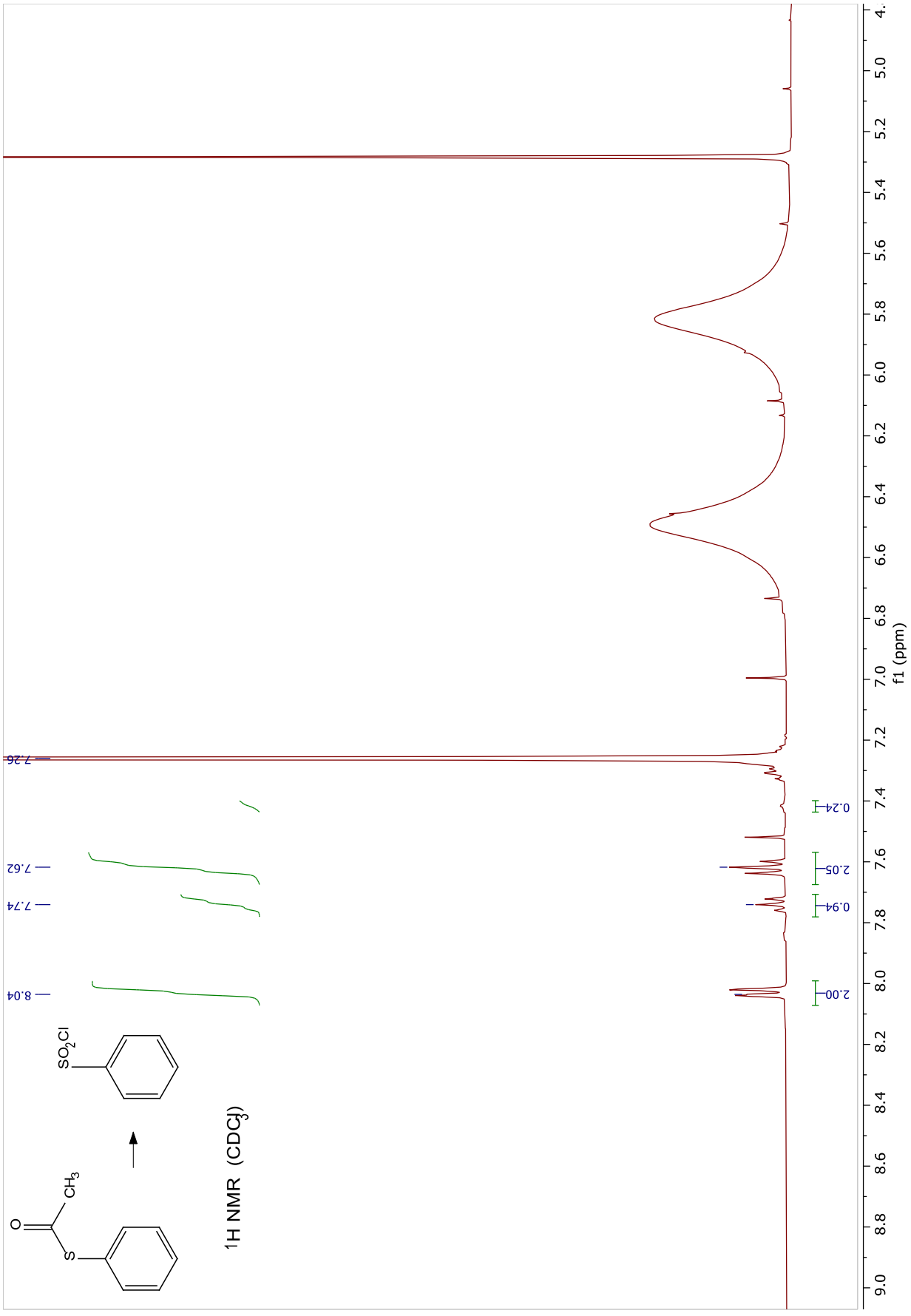
^{1}H NMR (CDCl$_3$)
O
S
CH$_3$
SO$_2$Cl
8.04
7.74
7.62
7.26
2.00
0.94
2.05
0.24
f1 (ppm)

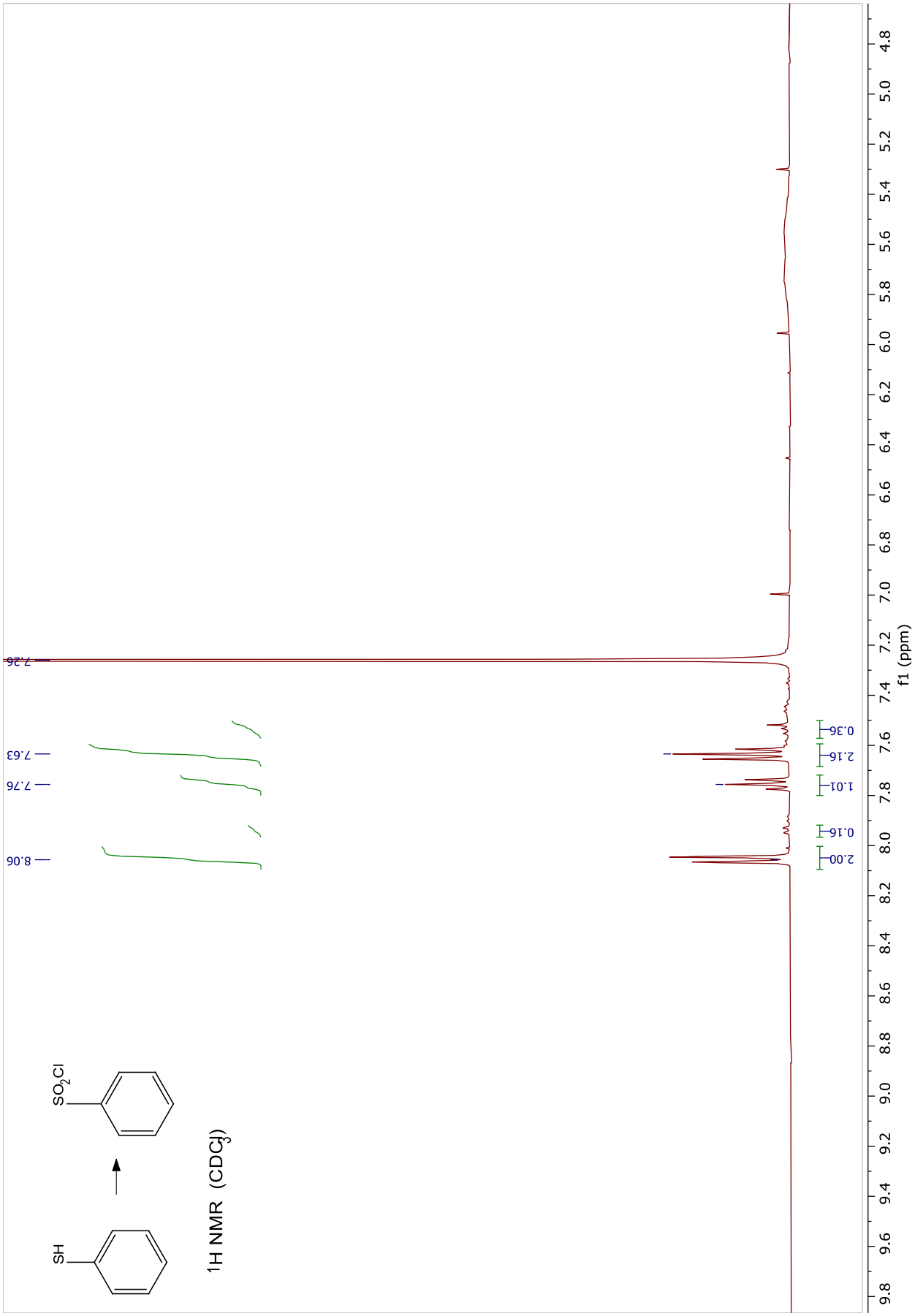
SH
SO2Cl
1H NMR (CDCl3)
7.26
7.63
7.76
8.06
0.36
2.16
1.01
0.16
2.00
f1 (ppm)

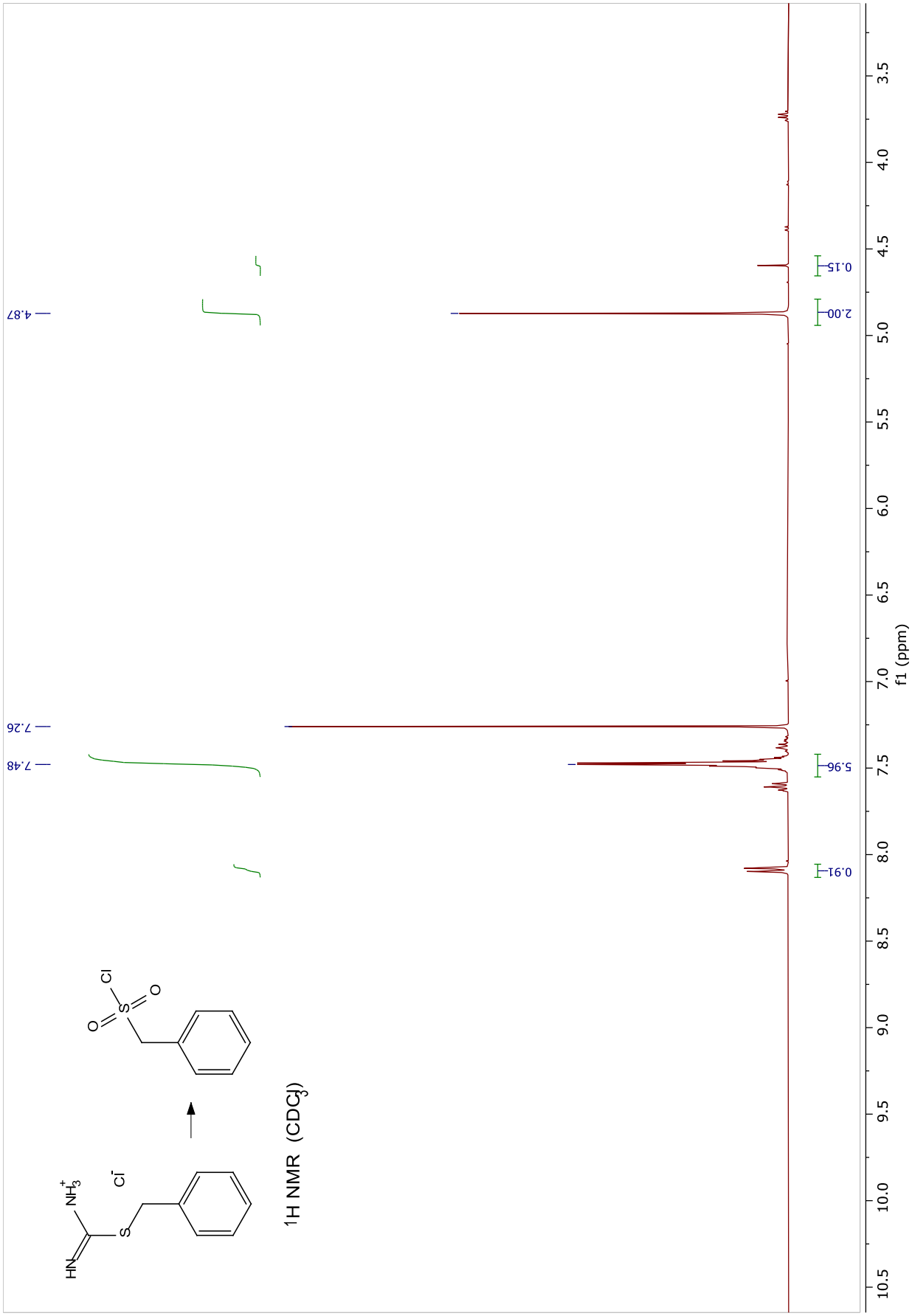
4.87
7.26
7.48
0.15
2.00
5.96
0.91
10.5
10.0
9.5
9.0
8.5
8.0
7.5
7.0
6.5
6.0
5.5
5.0
4.5
4.0
3.5
f1 (ppm)
^{1}H NMR (CDCl$_3$)

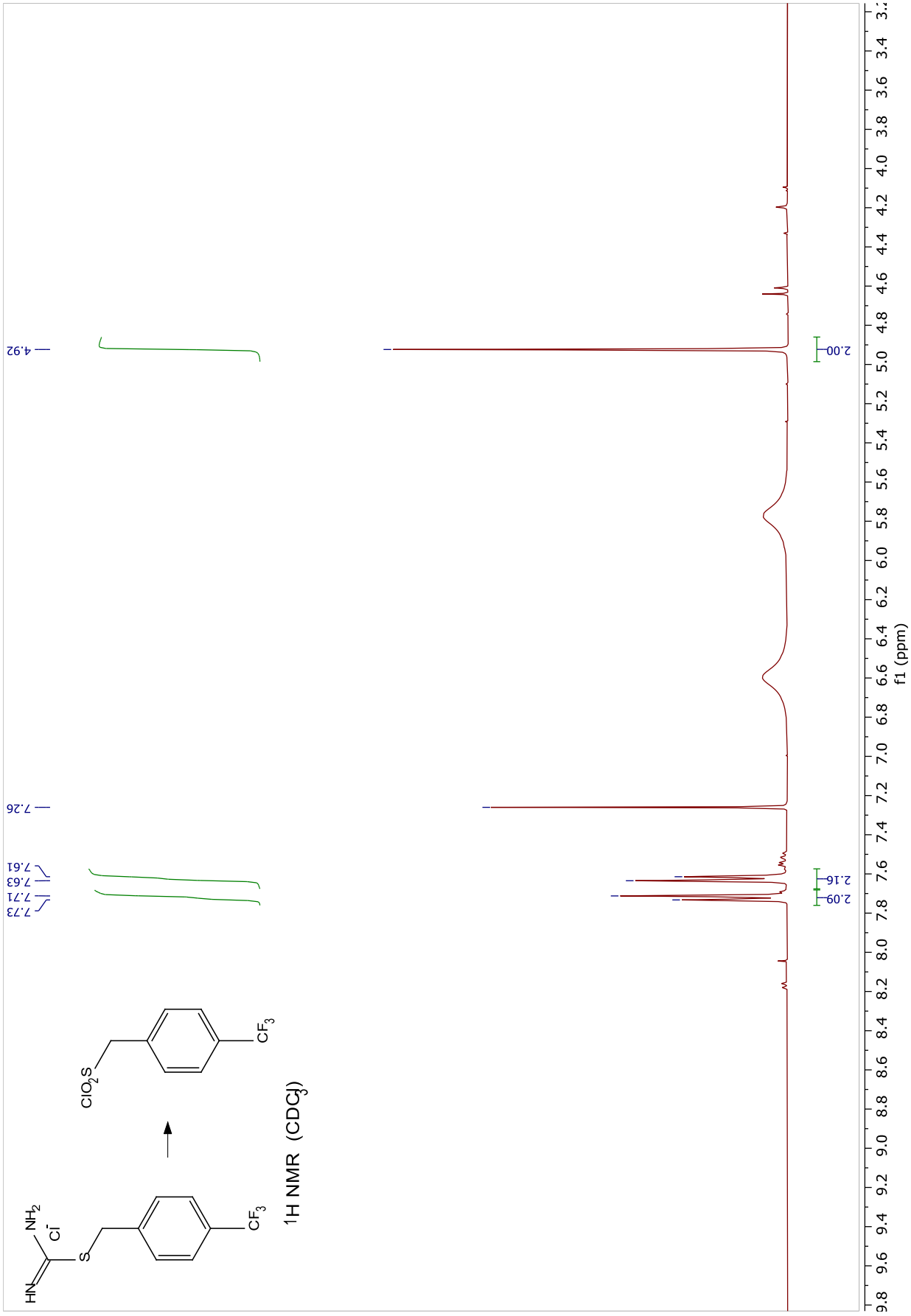
4.92
7.73
7.71
7.63
7.61
7.26
2.00
2.16
2.09
f1 (ppm)
^{1}H NMR (CDCl$_3$)
NH$_2$
Cl$^-$
HN
S
CF$_3$
ClO$_2$S
CF$_3$

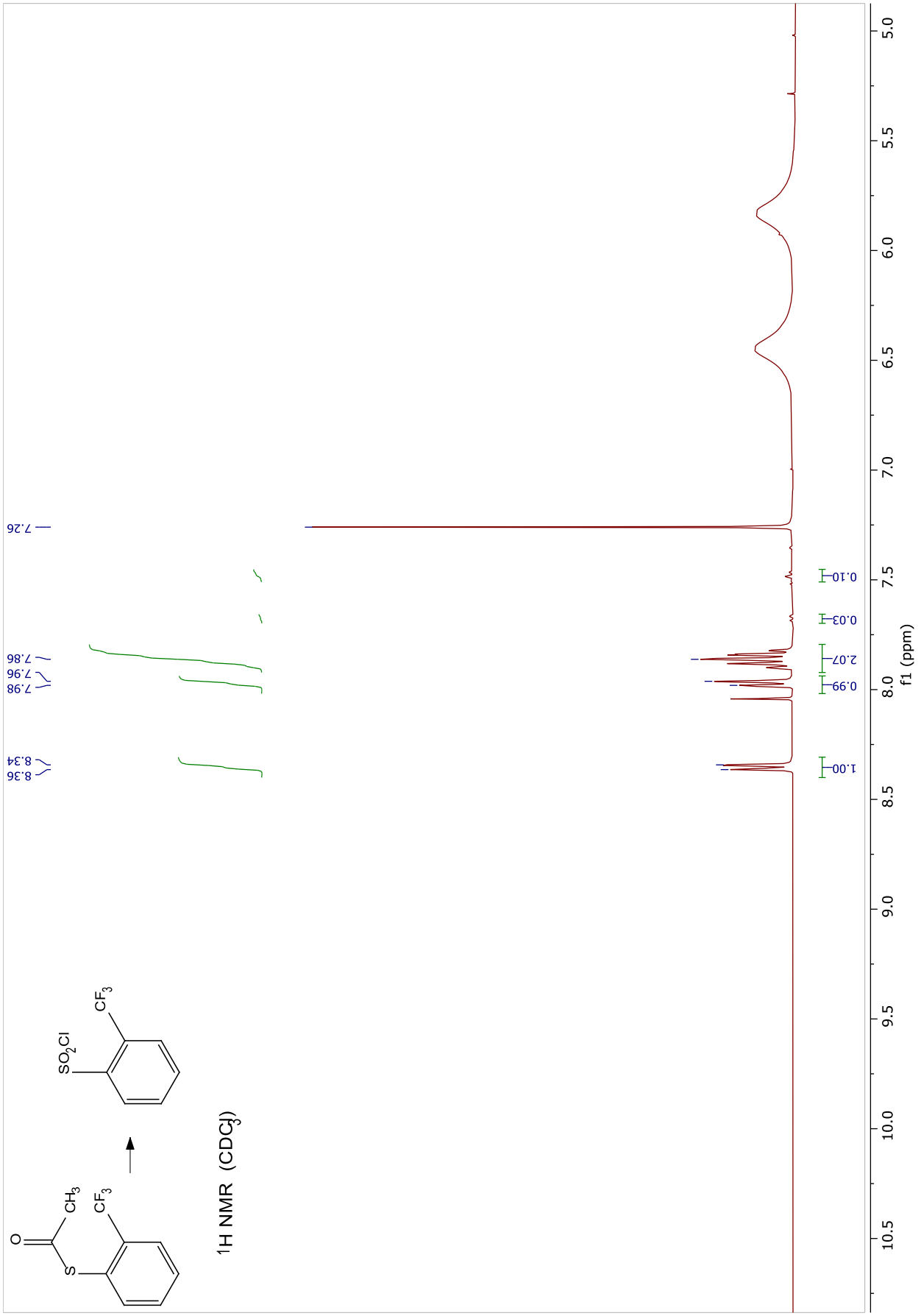
O
CH3
S
CF3
SO2Cl
CF3
1H NMR (CDCl3)
8.36
8.34
7.98
7.96
7.86
7.26
1.00
0.99
2.07
0.03
0.10
f1 (ppm)

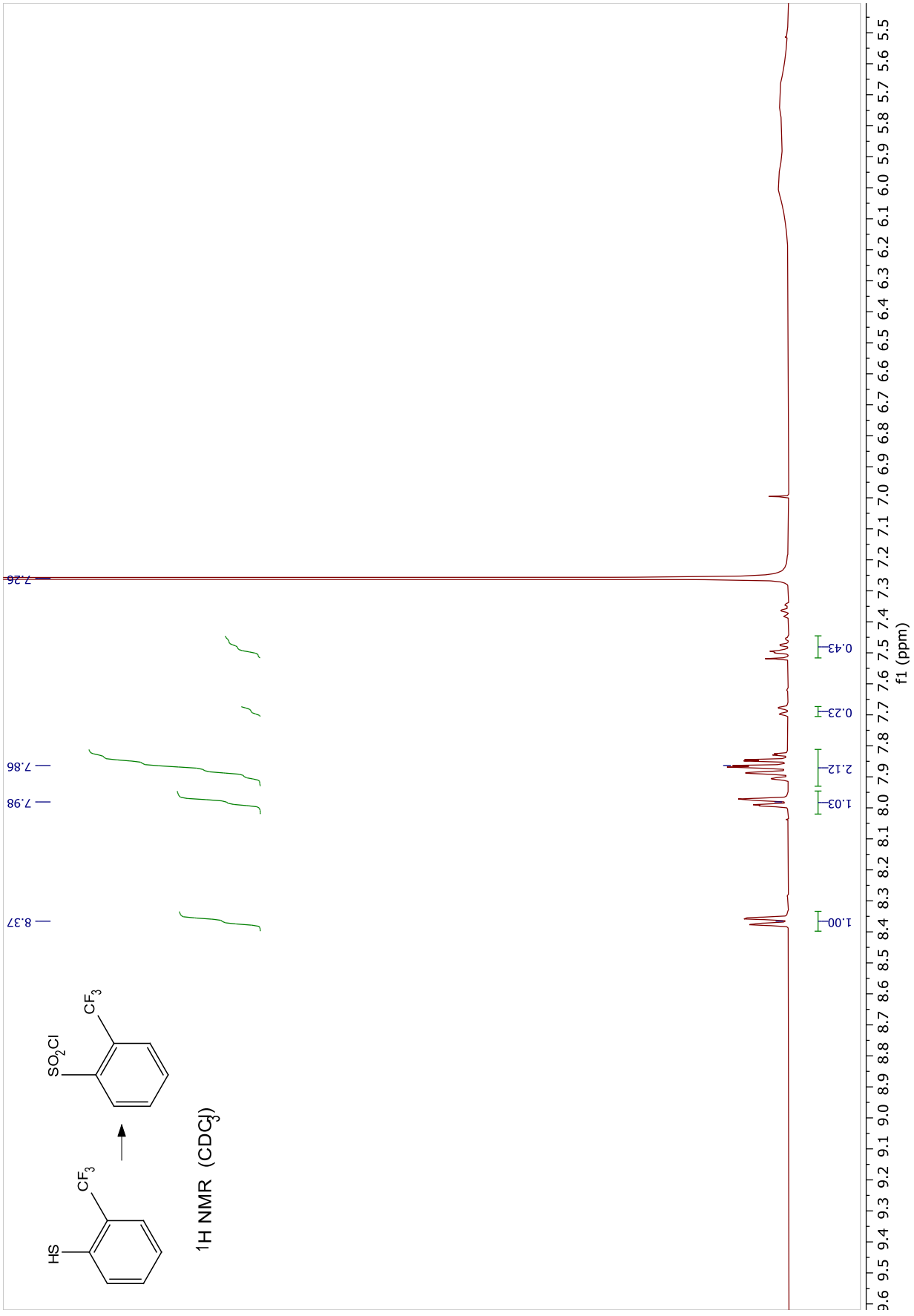
HS
CF3
SO2Cl
CF3
1H NMR (CDCl3)
8.37
7.98
7.86
7.26
1.00
1.03
2.12
0.23
0.43
f1 (ppm)

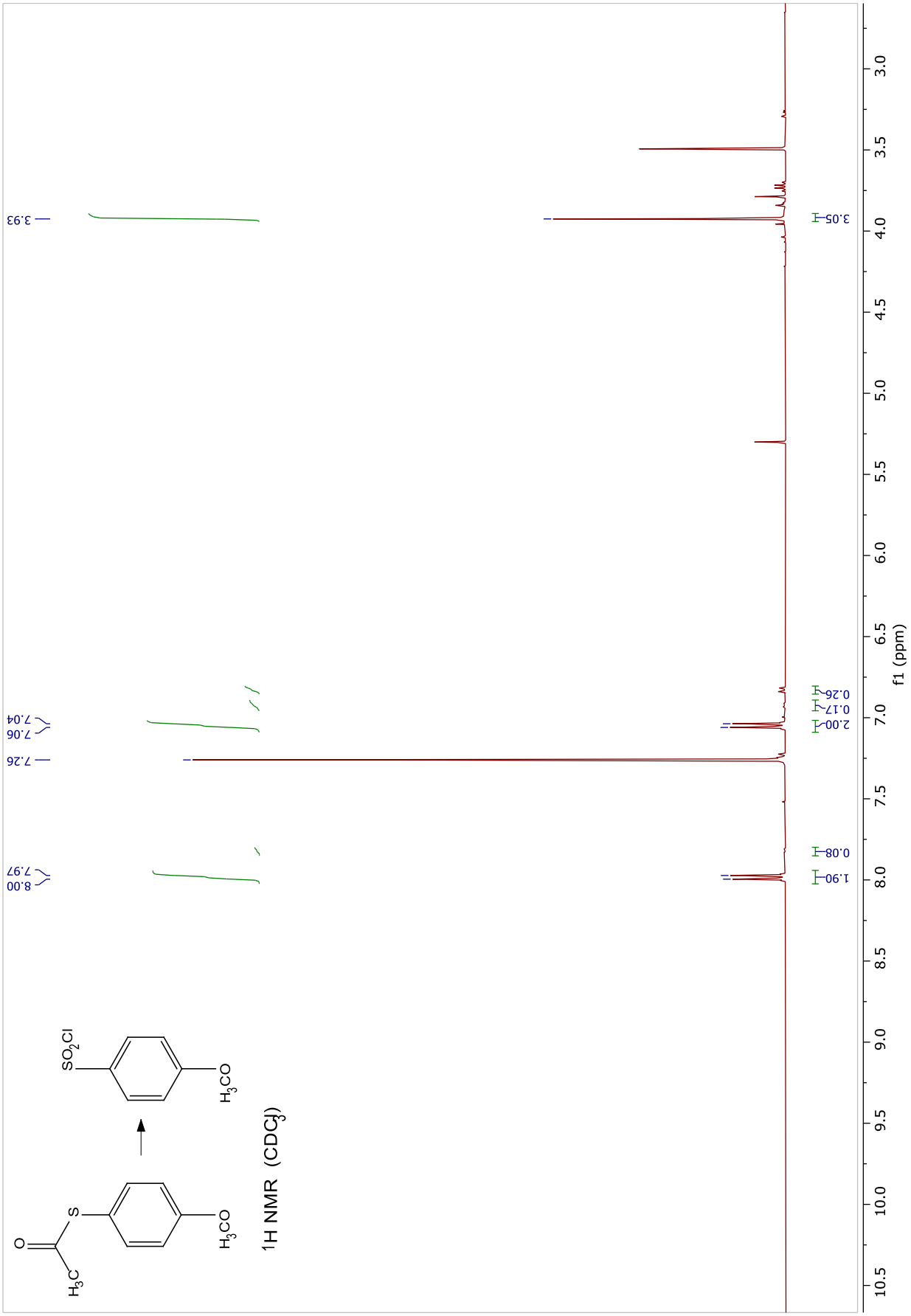
^{1}H NMR (CDCl$_3$)
H_3C
O
S
H_3CO
SO_2Cl
H_3CO
8.00
7.97
7.26
7.06
7.04
3.93
3.05
2.00
1.90
0.26
0.17
0.08
f1 (ppm)

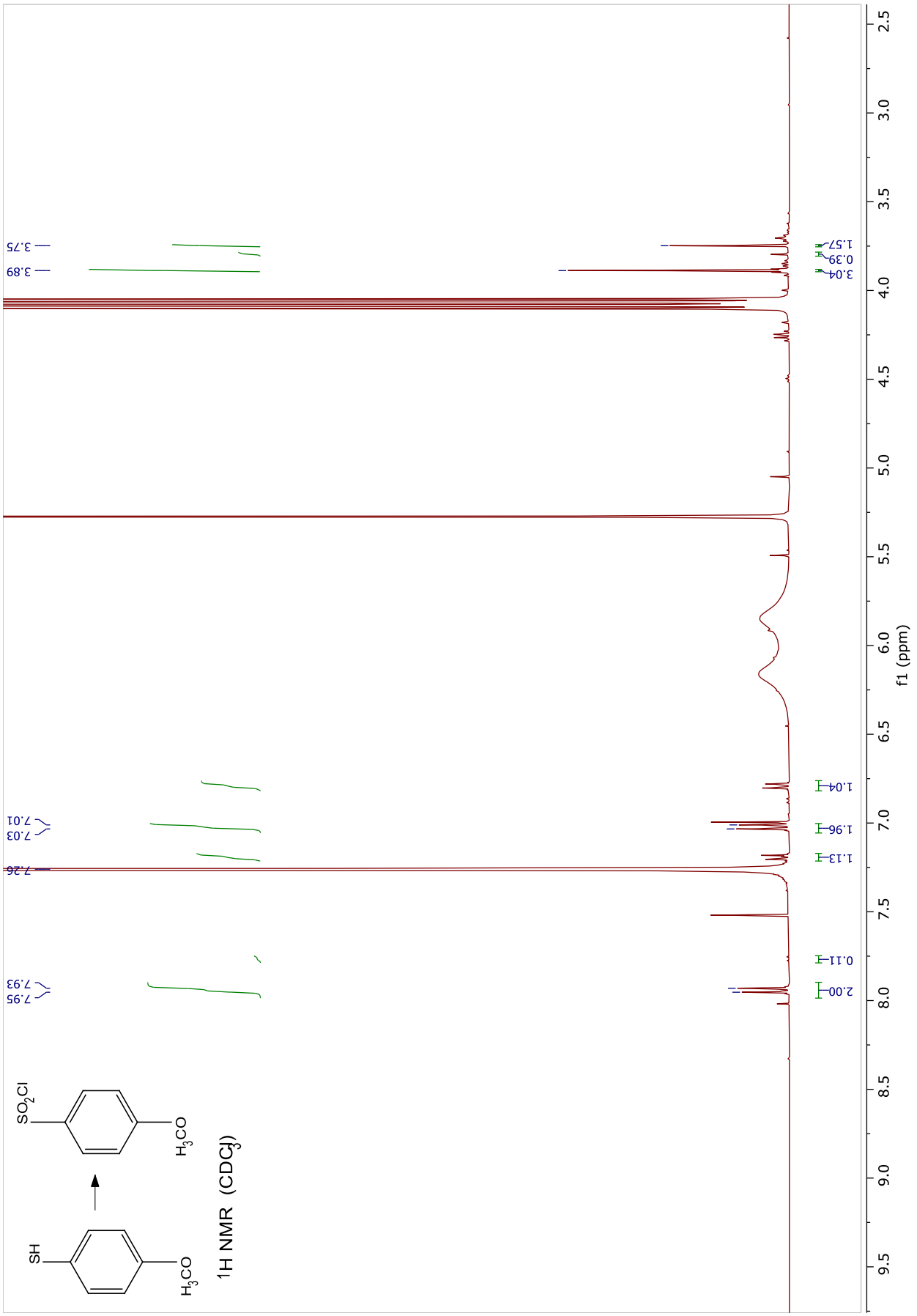
SH
H3CO
SO2Cl
H3CO
1H NMR (CDCl3)
7.95
7.93
7.26
7.03
7.01
3.89
3.75
1.57
0.39
3.04
2.00
0.11
1.13
1.96
1.04
f1 (ppm)

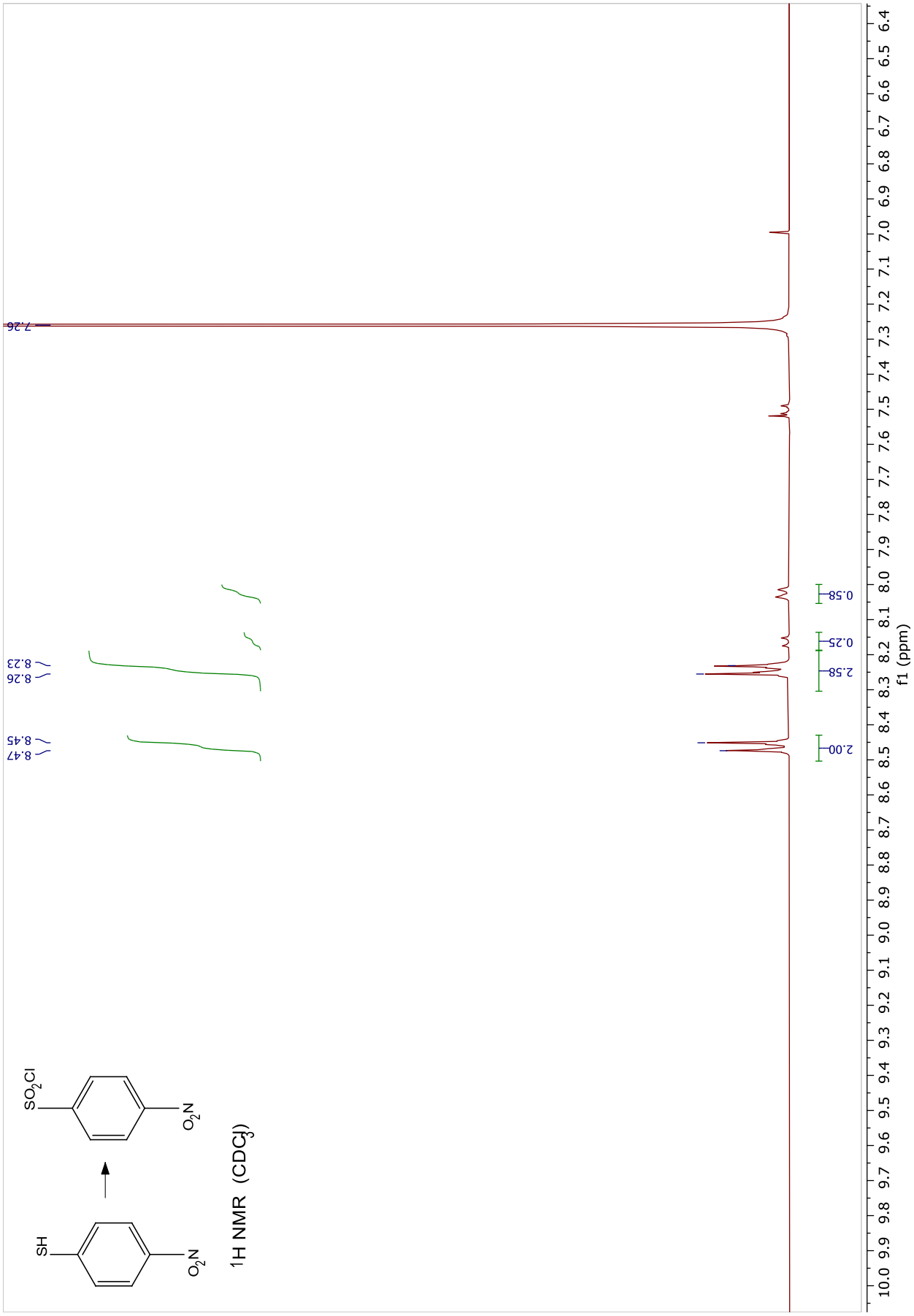
SH
O2N
SO2Cl
O2N
1H NMR (CDCl3)
7.26
8.47
8.45
8.26
8.23
2.00
2.58
0.25
0.58
f1 (ppm)

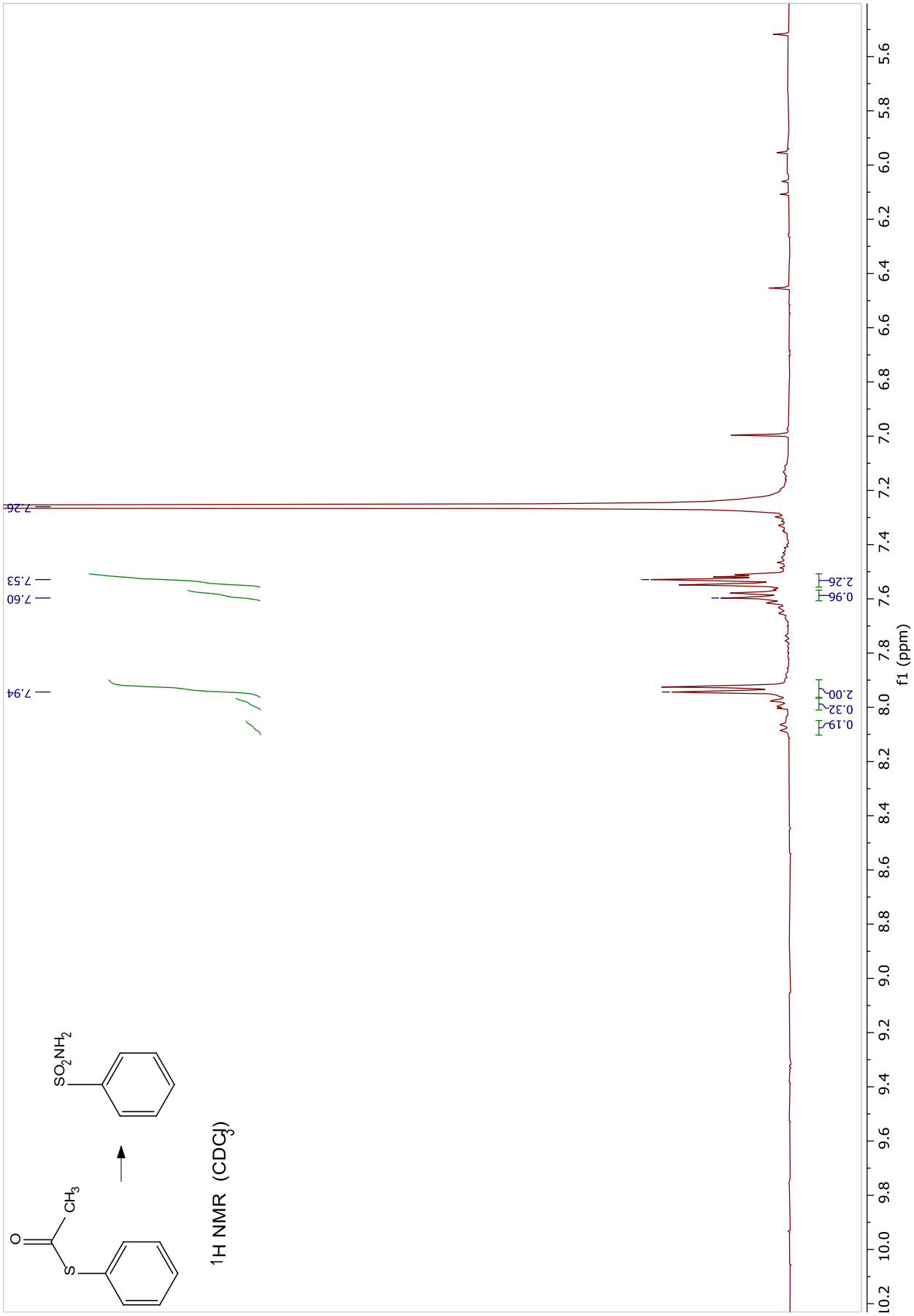
^{1}H NMR (CDCl$_3$)
7.26
7.53
7.60
7.94
2.26
0.96
2.00
0.32
0.19
f1 (ppm)

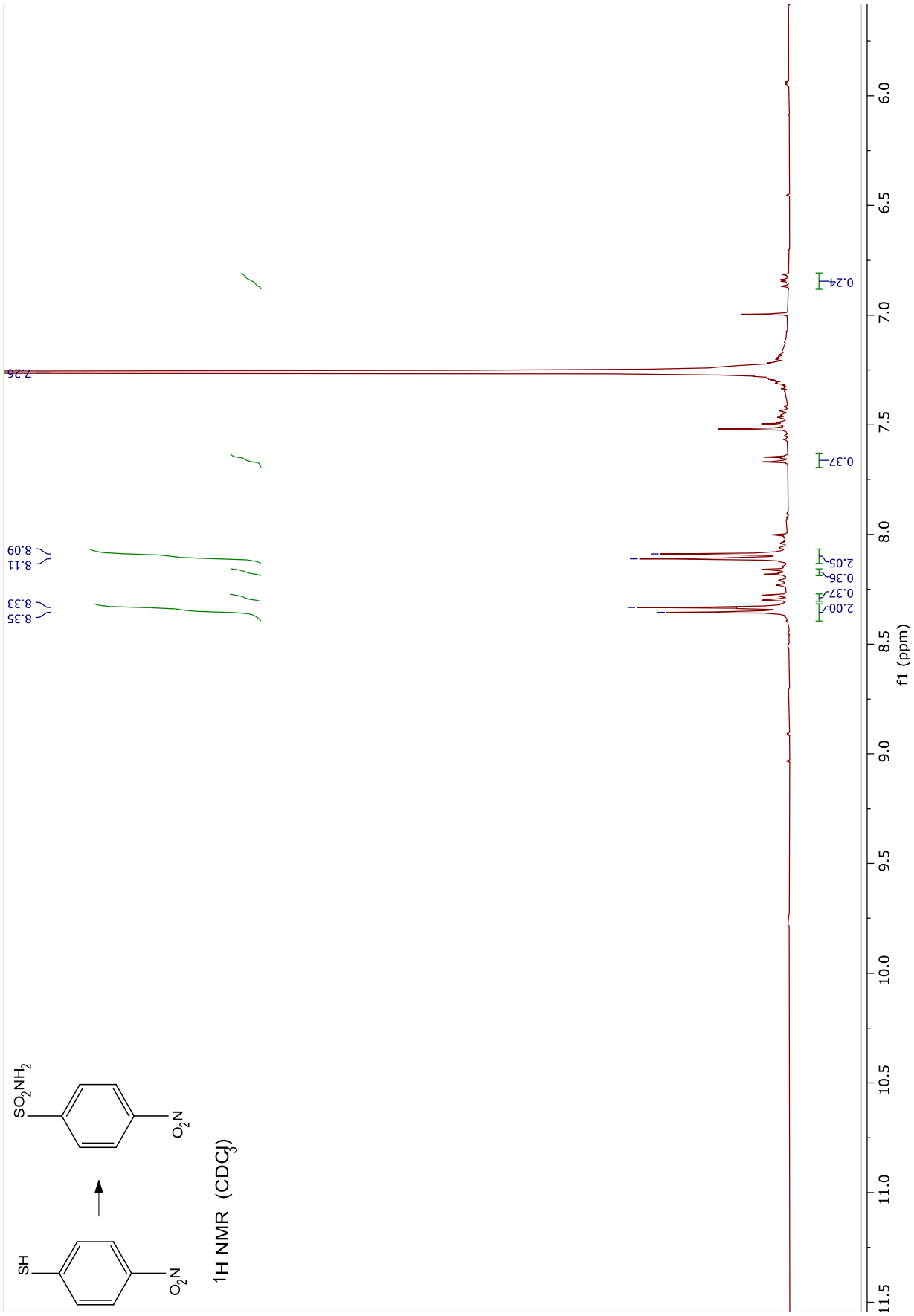
SH
O2N
SO2NH2
O2N
1H NMR (CDCl3)
8.35
8.33
8.11
8.09
7.26
0.24
0.37
2.05
0.36
0.37
2.00
6.0
6.5
7.0
7.5
8.0
8.5
9.0
9.5
10.0
10.5
11.0
11.5
f1 (ppm)

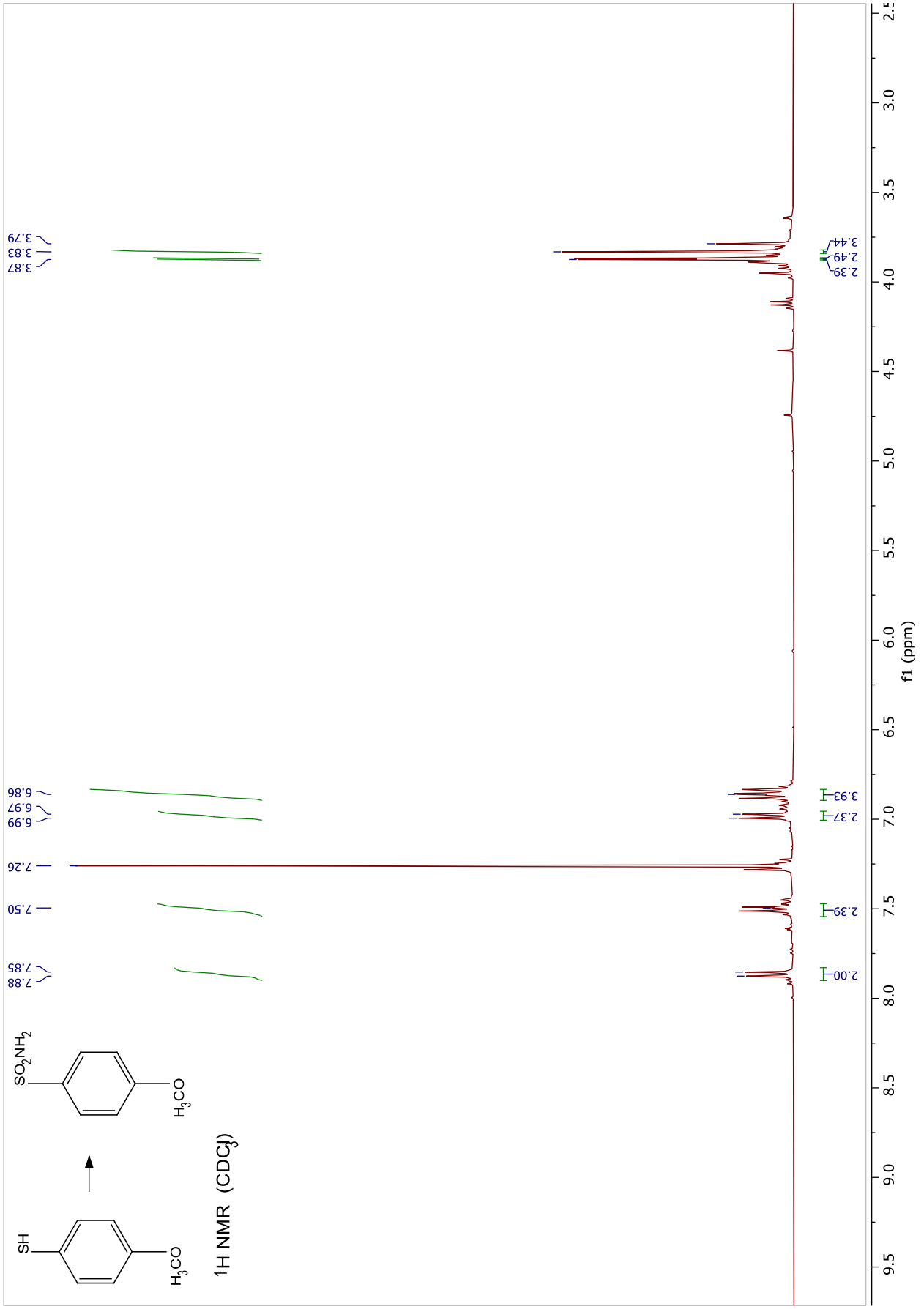
^{1}H NMR (CDCl$_3$)
SH
H_3CO
SO_2NH_2
H_3CO
7.88
7.85
7.50
7.26
6.99
6.97
6.86
3.87
3.83
3.79
2.00
2.39
2.37
3.93
3.44
2.49
2.39
f1 (ppm)

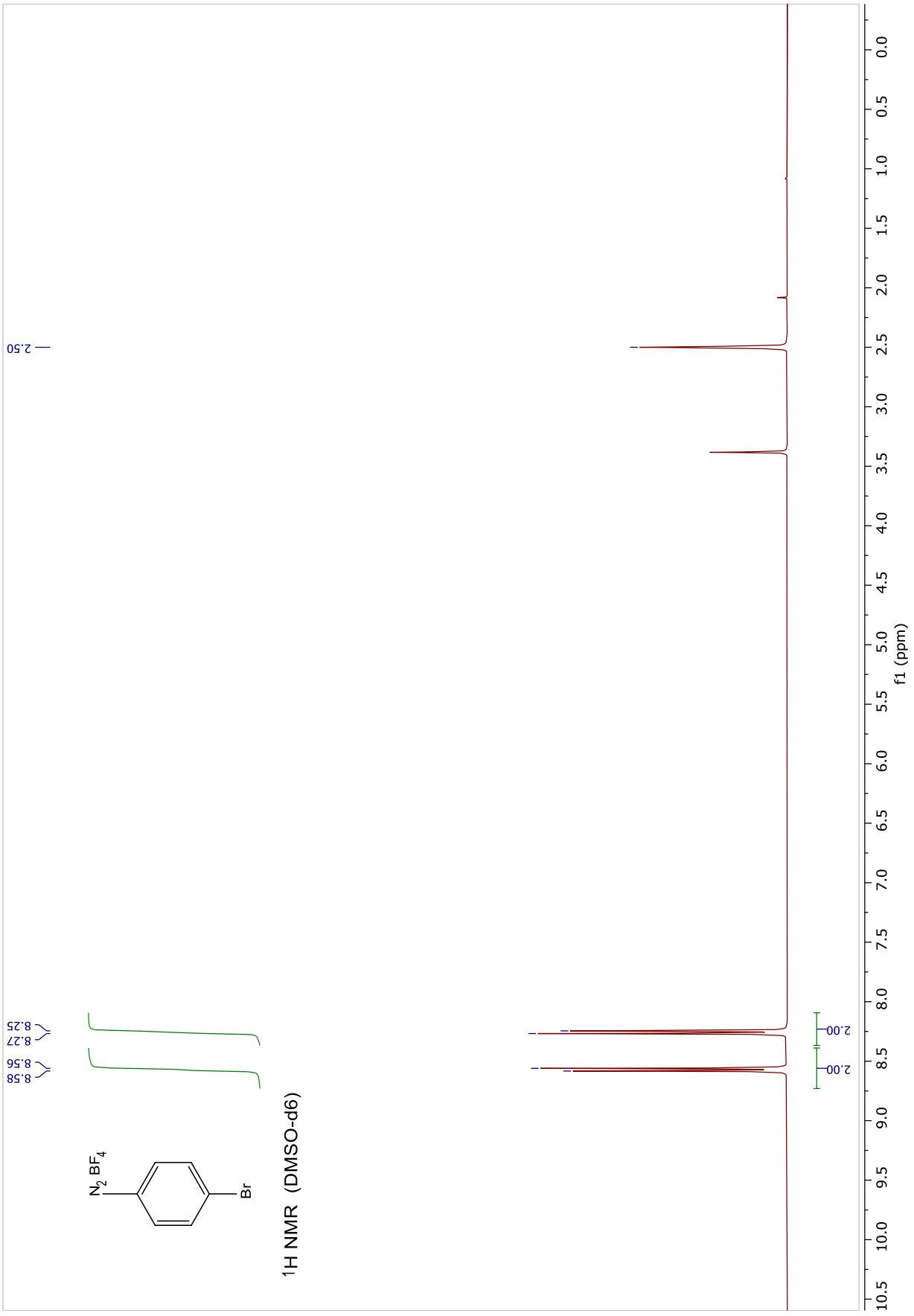
2.50
8.58
8.56
8.27
8.25
2.00
2.00
^{1}H NMR (DMSO-d6)
N_2 BF_4
Br
f1 (ppm)

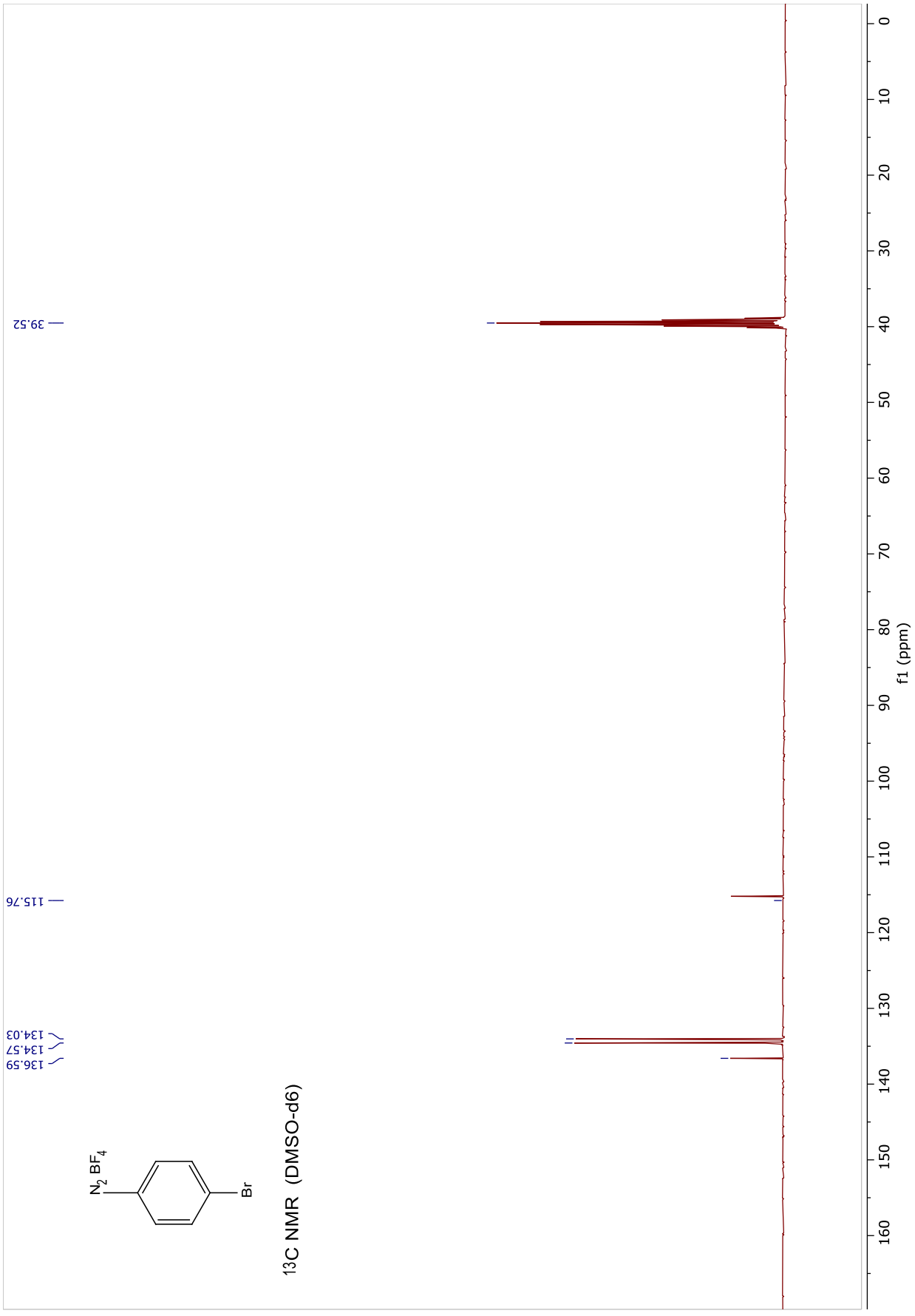
39.52
115.76
136.59
134.57
134.03
^{13}C NMR (DMSO-d6)
N_2 BF_4
Br
f1 (ppm)

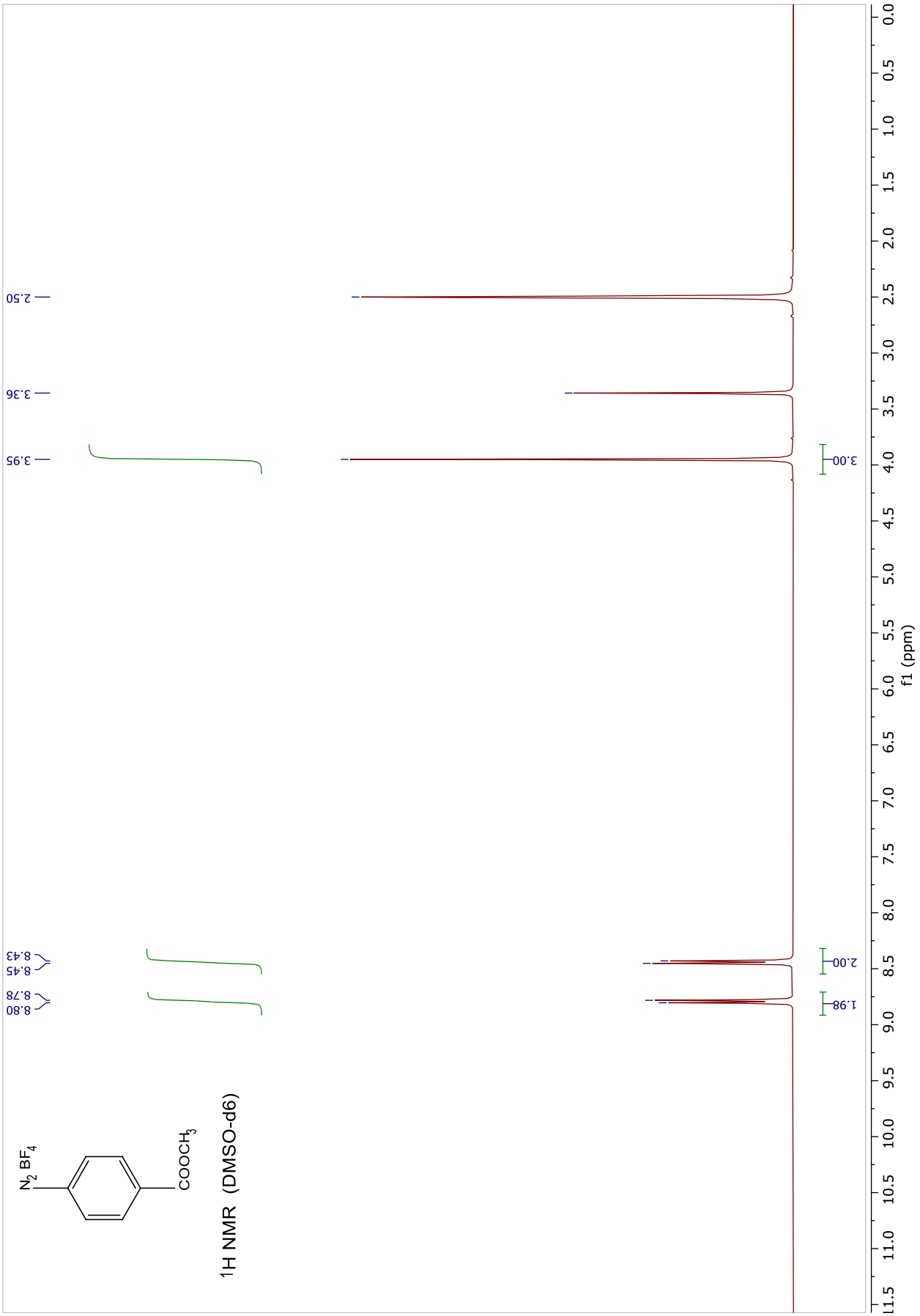
^{1}H NMR (DMSO-d6)
N_2BF_4
$COOCH_3$
8.80
8.78
8.45
8.43
3.95
3.36
2.50
1.98
2.00
3.00
f1 (ppm)

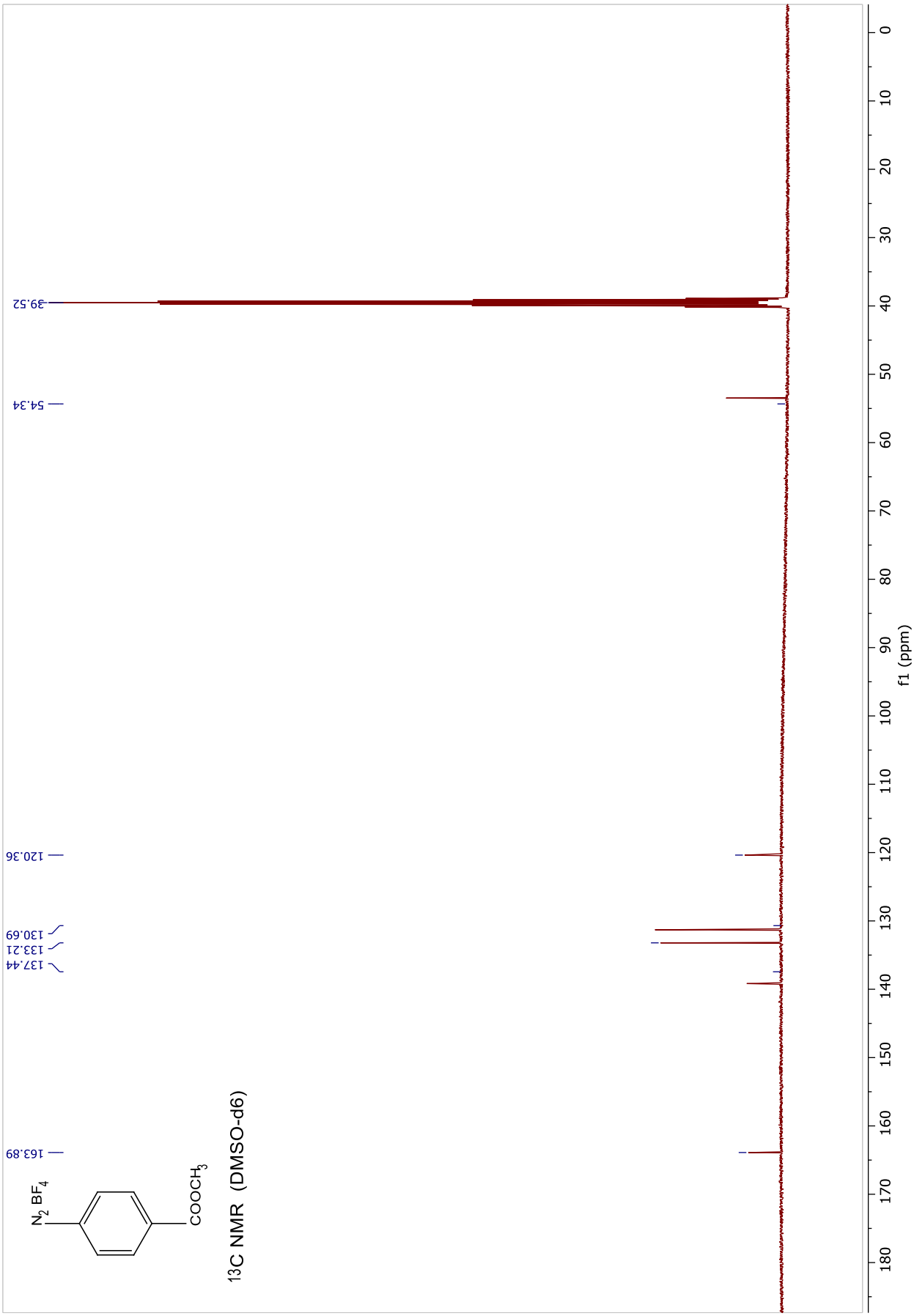
39.52
54.34
120.36
130.69
133.21
137.44
163.89
^{13}C NMR (DMSO-d6)
N_2 BF_4
$COOCH_3$
f1 (ppm)

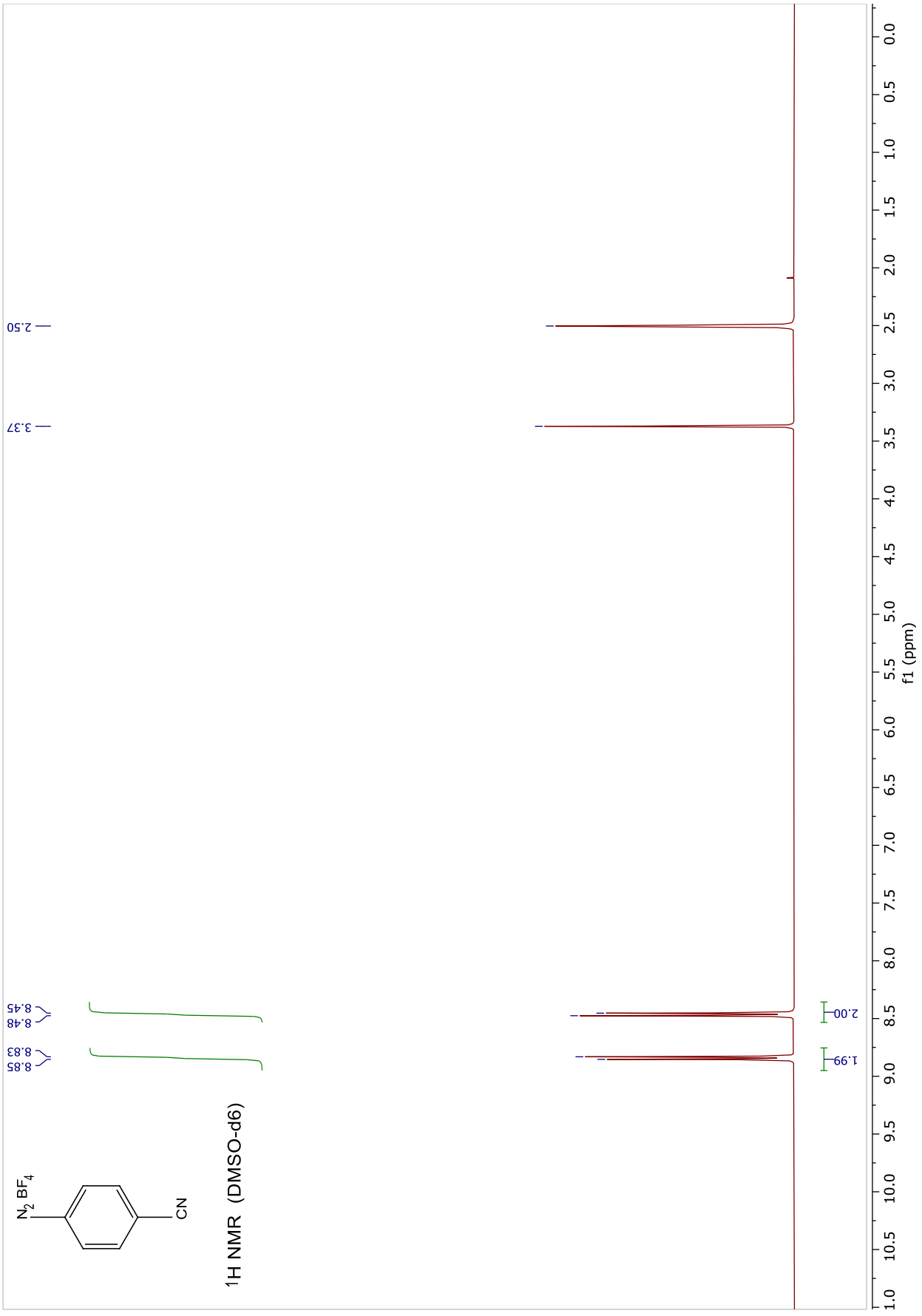
2.50
3.37
8.45
8.48
8.83
8.85
2.00
1.99
^{1}H NMR (DMSO-d6)
N_2 BF_4
CN
f1 (ppm)

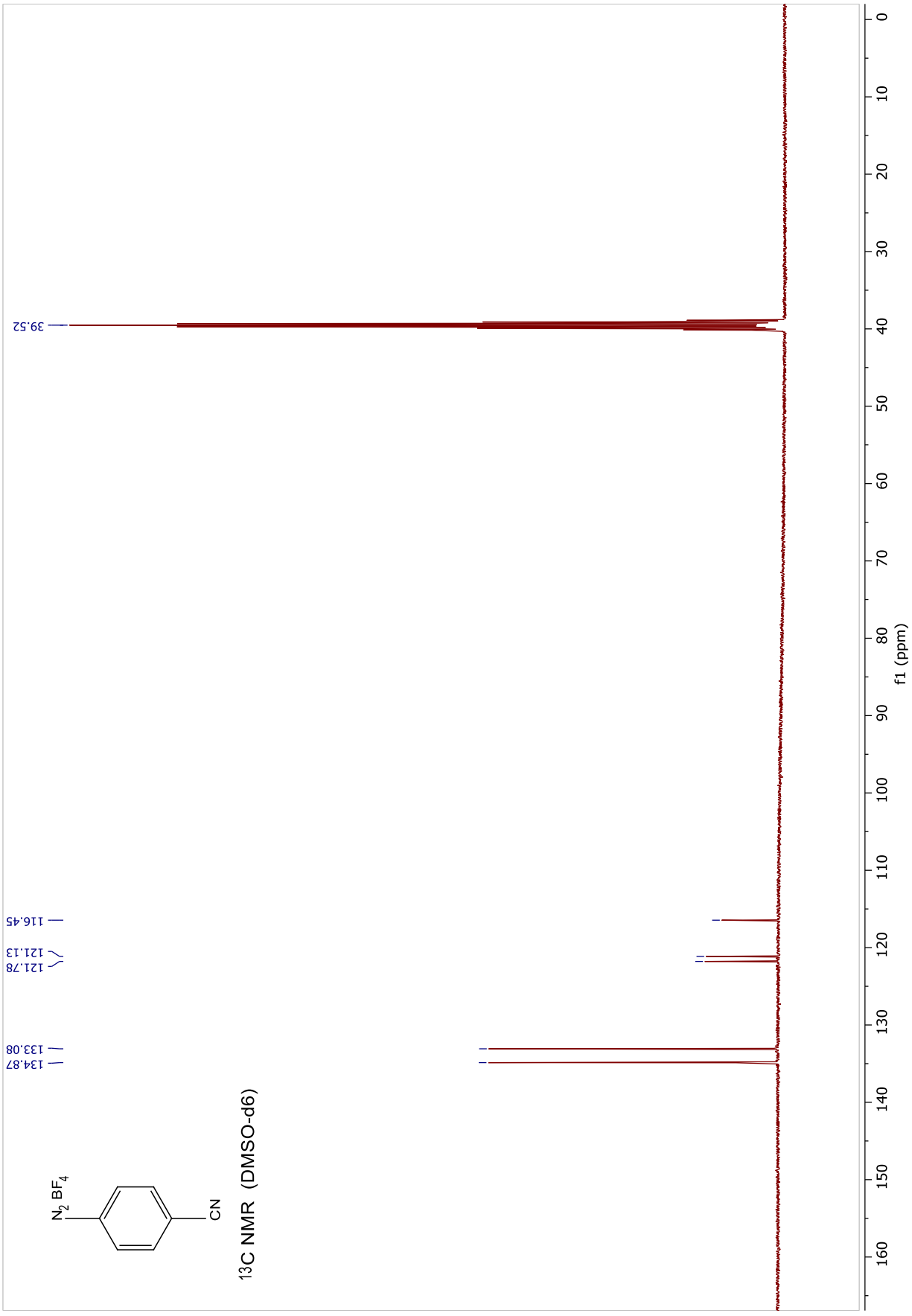
39.52
116.45
121.13
121.78
133.08
134.87
^{13}C NMR (DMSO-d6)
N_2 BF_4
CN
f1 (ppm)

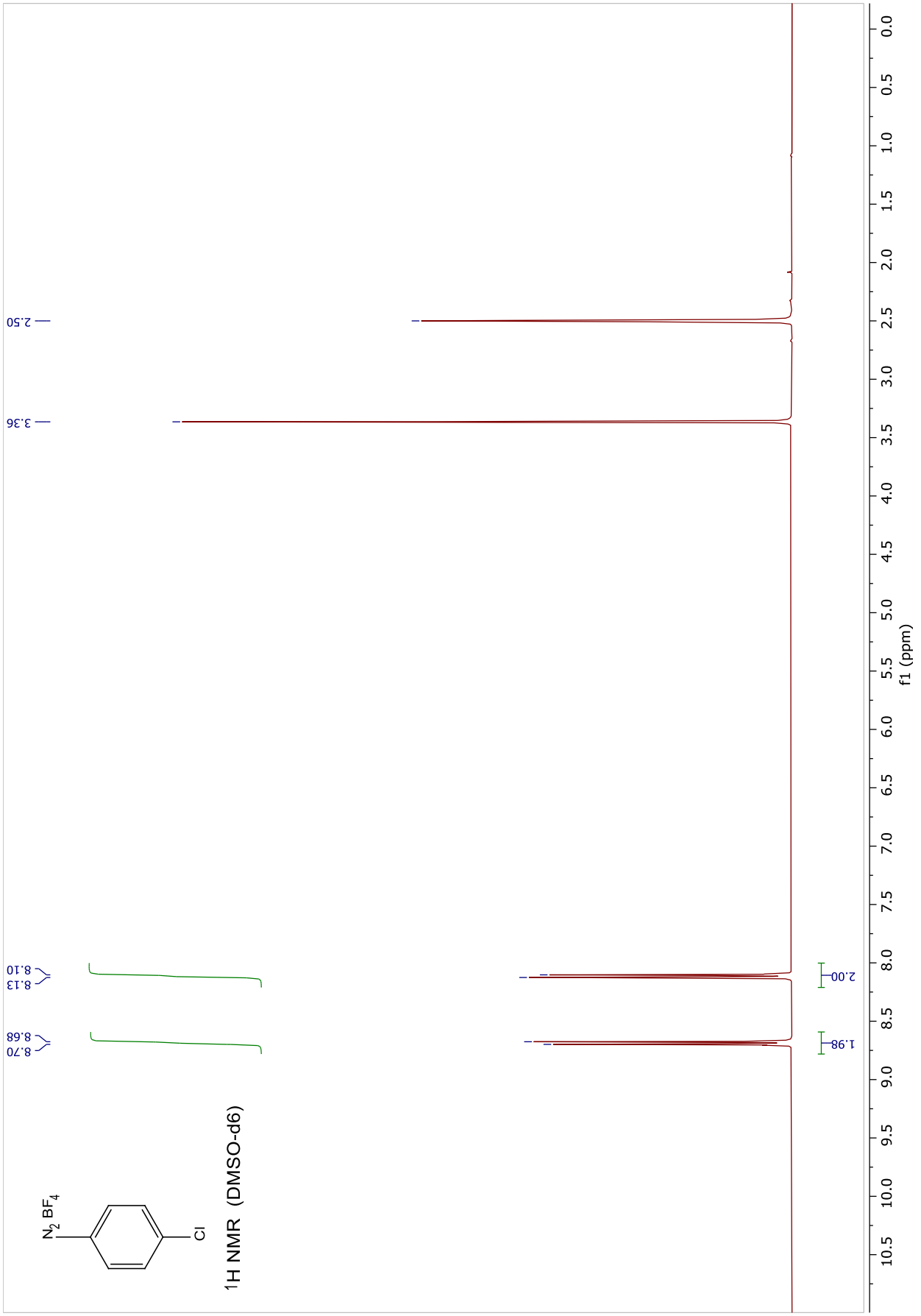
2.50
3.36
8.10
8.13
8.68
8.70
2.00
1.98
f1 (ppm)
^{1}H NMR (DMSO-d6)
N_2 BF_4
Cl

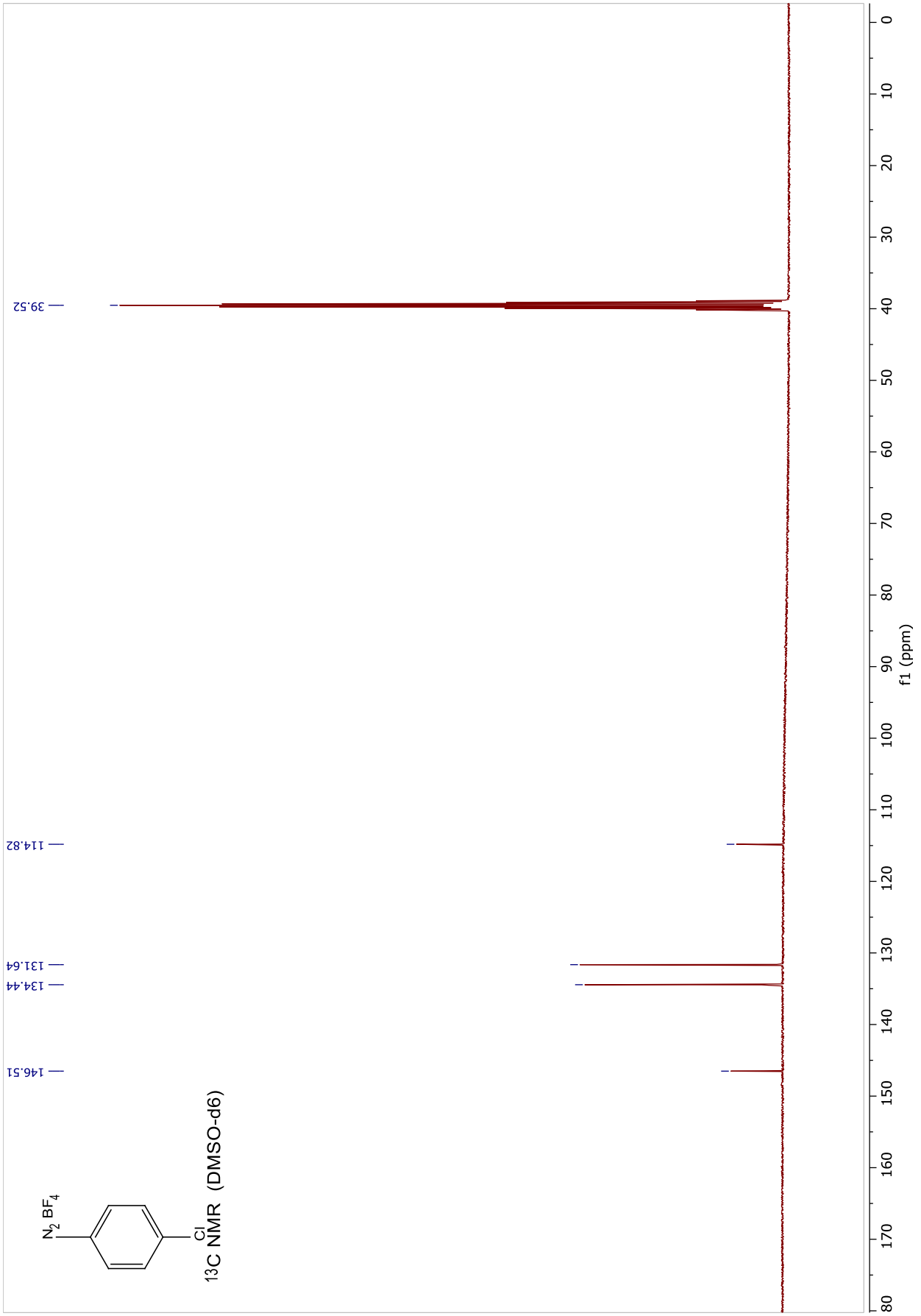
^{13}C NMR (DMSO-d6)
N_2 BF_4
Cl
146.51
134.44
131.64
114.82
39.52
f1 (ppm)

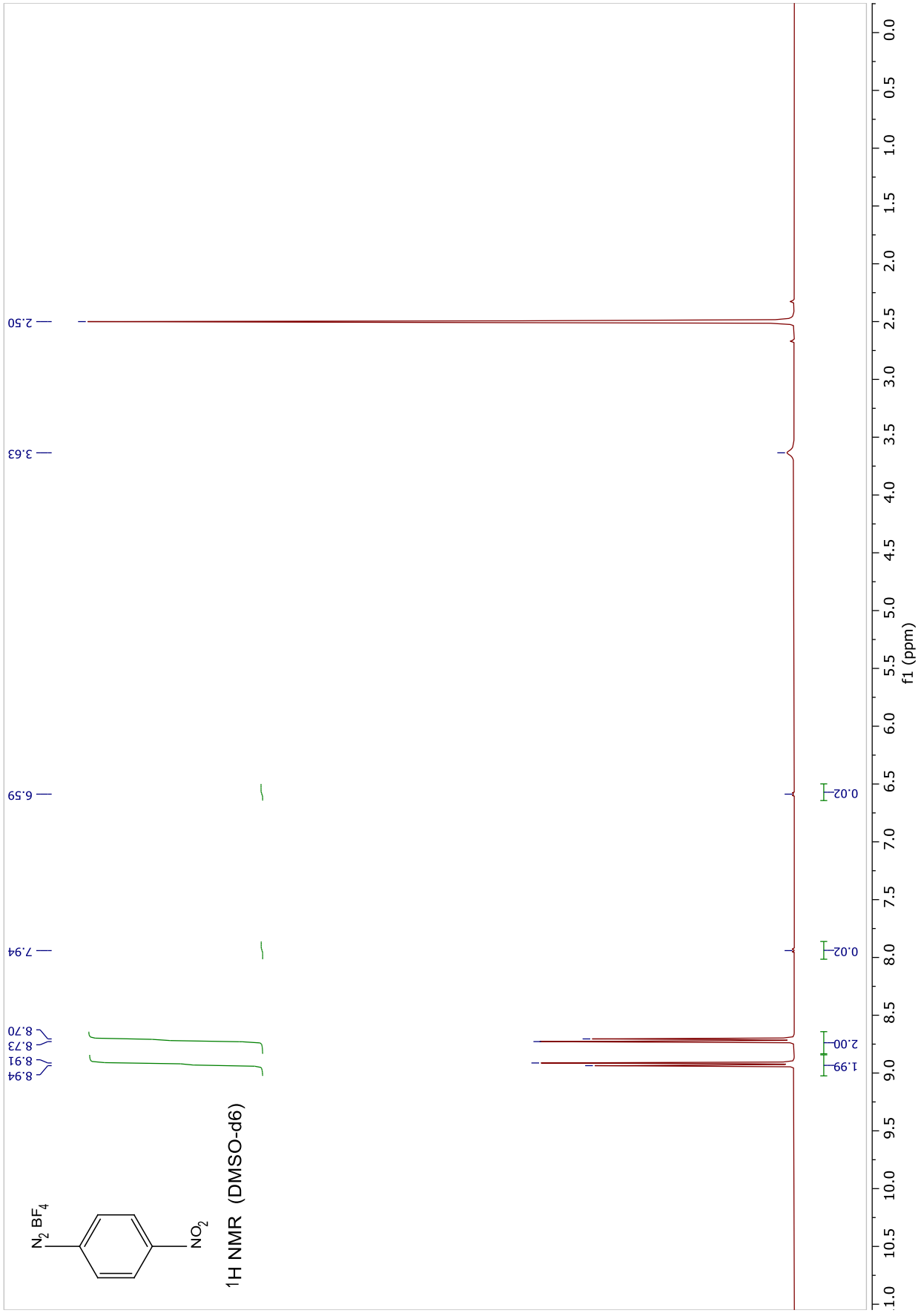
^{1}H NMR (DMSO-d6)
N_2 BF_4
NO_2
8.94
8.91
8.73
8.70
7.94
6.59
3.63
2.50
1.99
2.00
0.02
0.02
0.02
f1 (ppm)

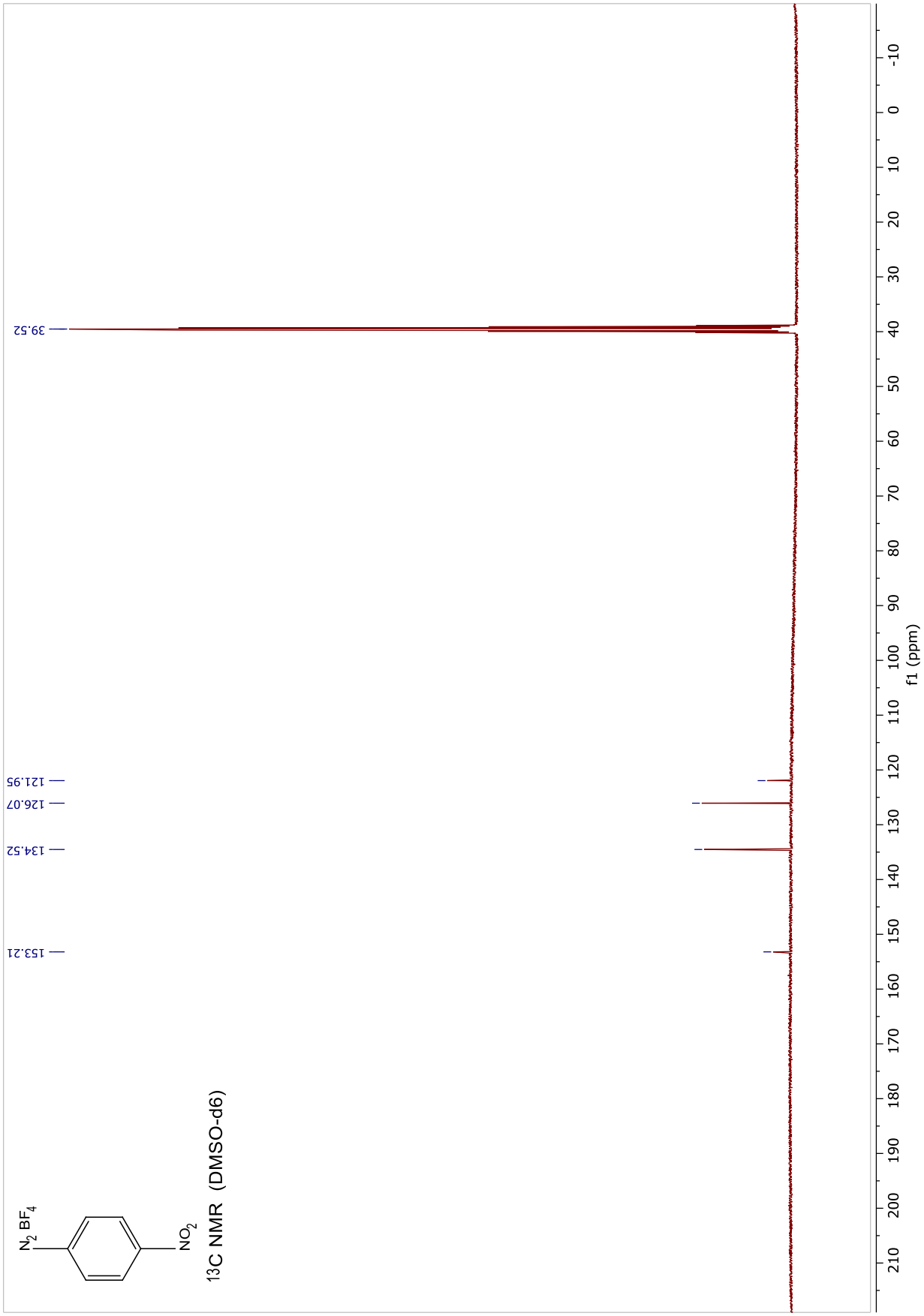
^{13}C NMR (DMSO-d6)
N_2BF_4
NO_2
153.21
134.52
126.07
121.95
39.52
f1 (ppm)

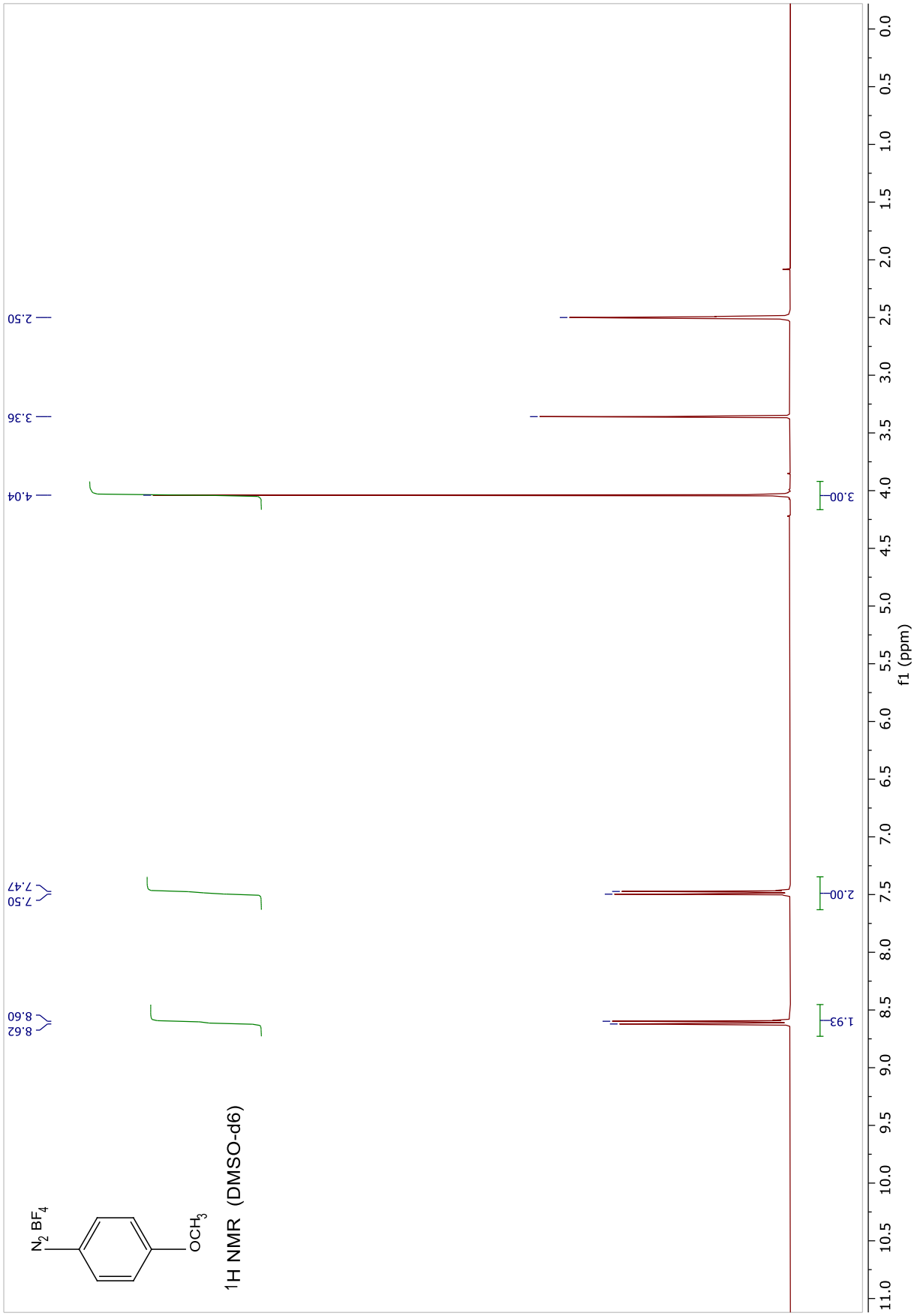
^{1}H NMR (DMSO-d6)
N_2 BF_4
OCH_3
8.62
8.60
7.50
7.47
4.04
3.36
2.50
1.93
2.00
3.00
f1 (ppm)

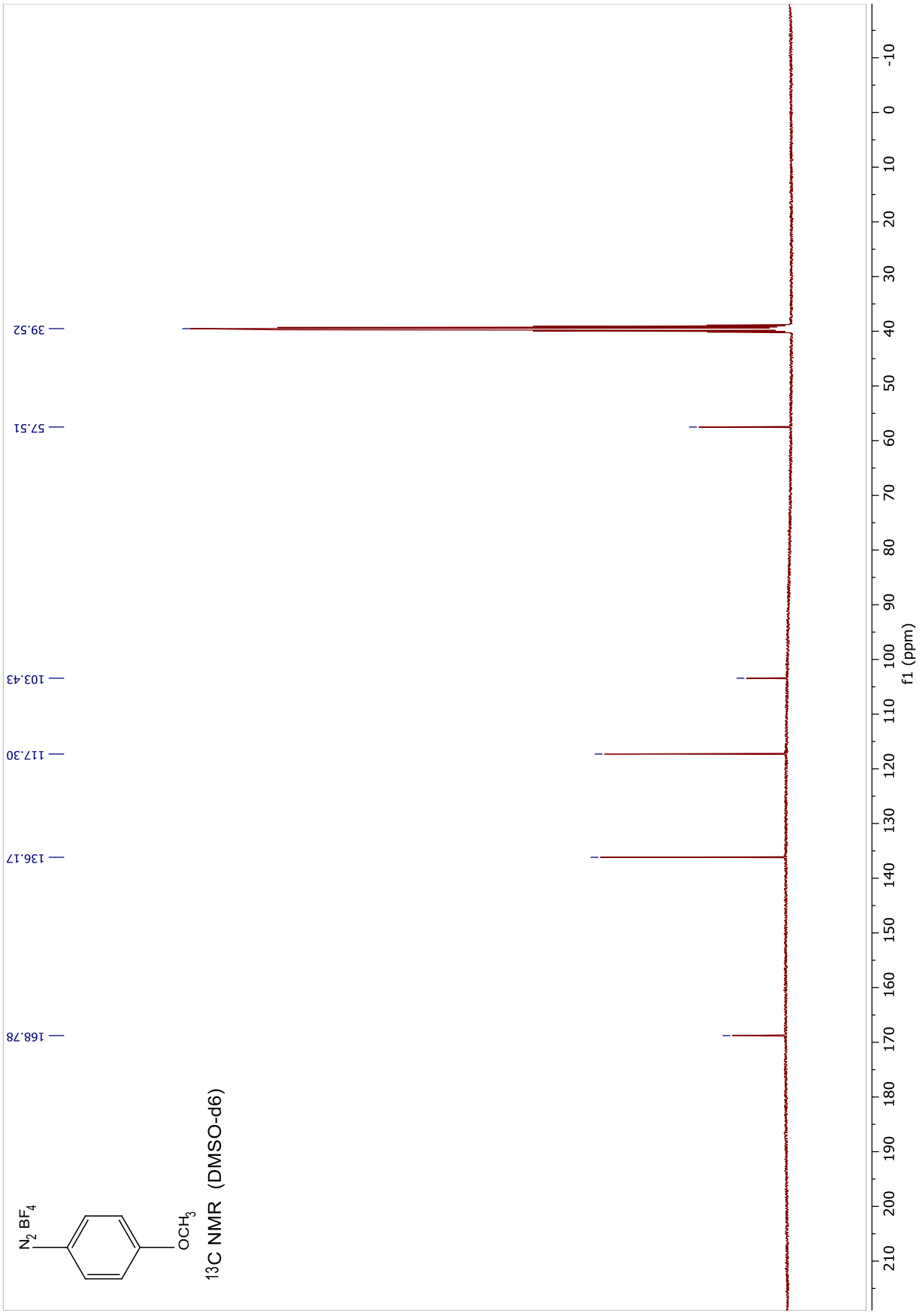
^{13}C NMR (DMSO-d6)
N_2 BF_4
OCH_3
168.78
136.17
117.30
103.43
57.51
39.52
f1 (ppm)

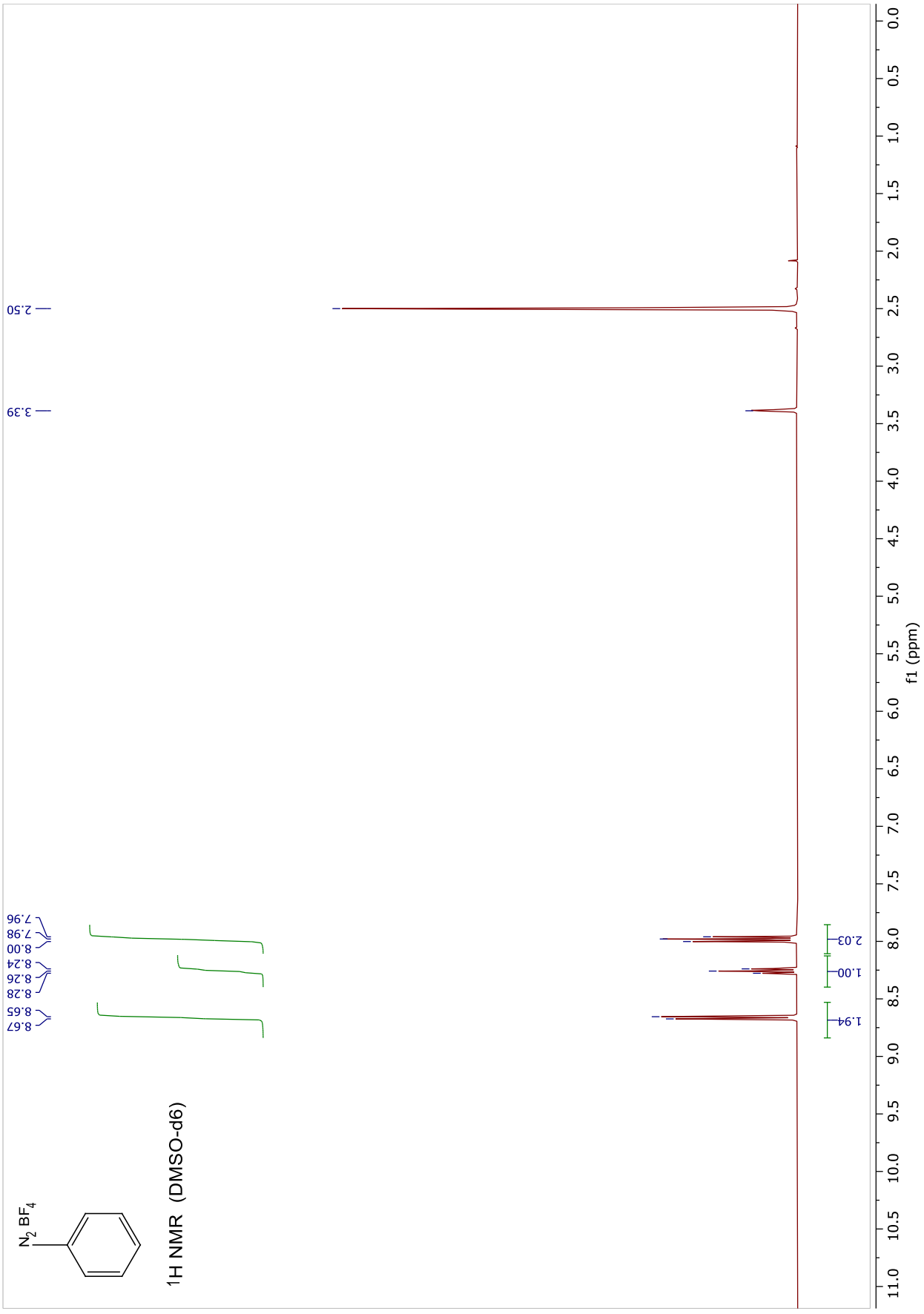
^{1}H NMR (DMSO-d6)
N_2 BF_4
8.67
8.65
8.28
8.26
8.24
8.00
7.98
7.96
2.50
3.39
1.94
1.00
2.03
f1 (ppm)

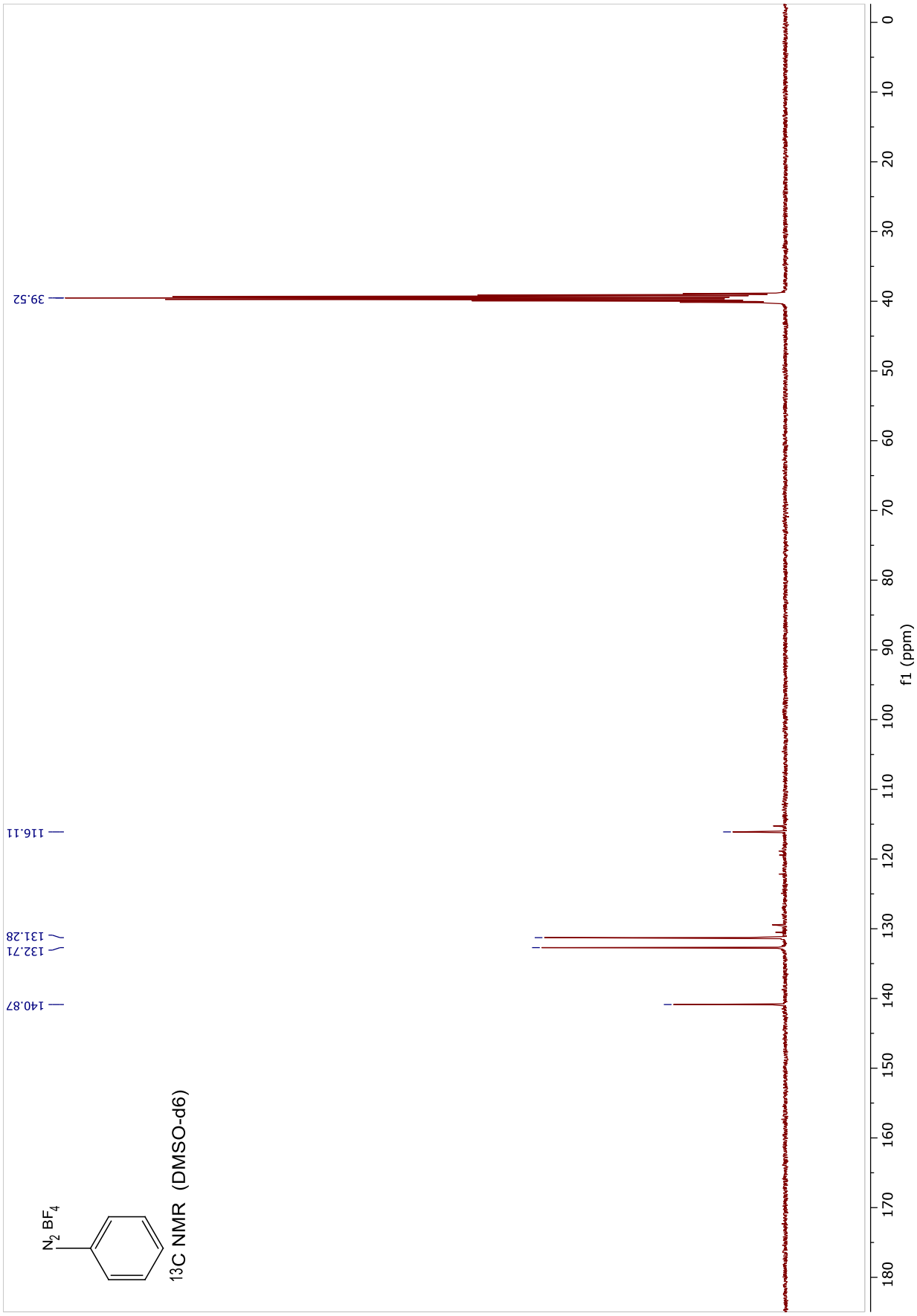
^{13}C NMR (DMSO-d6)
N_2 BF_4
39.52
116.11
131.28
132.71
140.87
f1 (ppm)

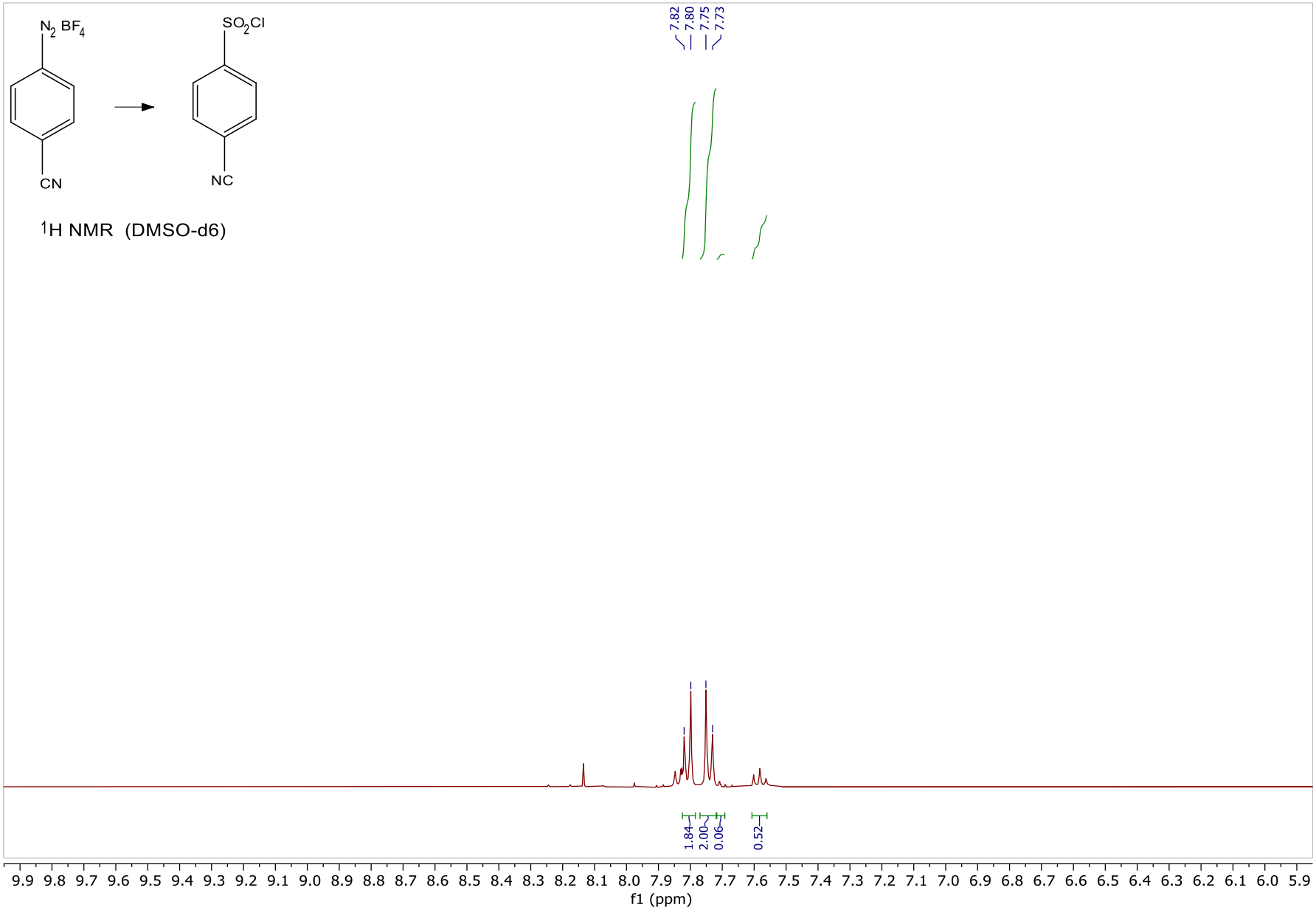
N2 BF4
CN
SO2Cl
NC
1H NMR (DMSO-d6)
7.82
7.80
7.75
7.73
1.84
2.00
0.06
0.52
9.9 9.8 9.7 9.6 9.5 9.4 9.3 9.2 9.1 9.0 8.9 8.8 8.7 8.6 8.5 8.4 8.3 8.2 8.1 8.0 7.9 7.8 7.7 7.6 7.5 7.4 7.3 7.2 7.1 7.0 6.9 6.8 6.7 6.6 6.5 6.4 6.3 6.2 6.1 6.0 5.9
f1 (ppm)

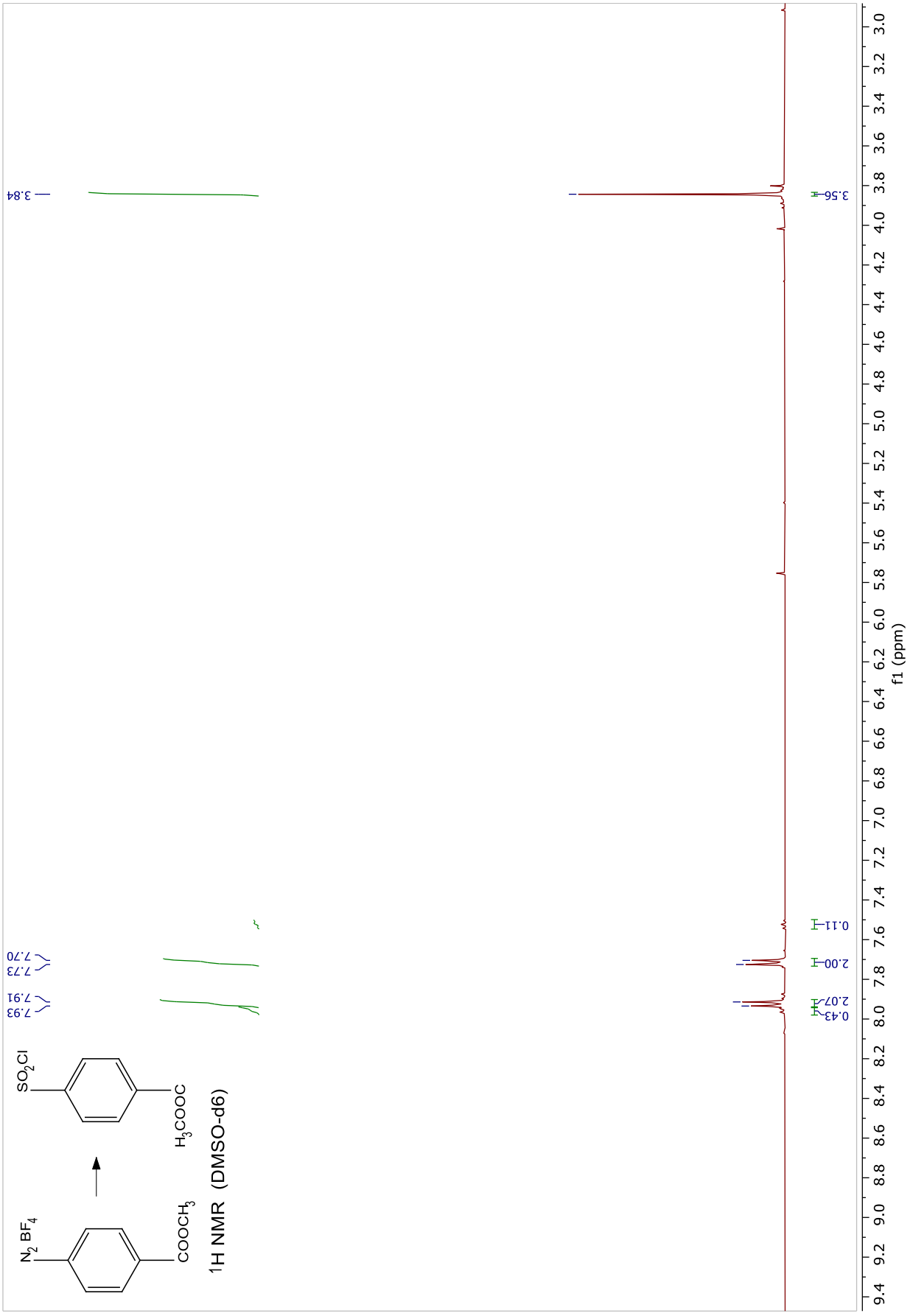
N_2 BF_4
$COOCH_3$
SO_2Cl
H_3COOC
^{1}H NMR (DMSO-d6)
7.93
7.91
7.73
7.70
3.84
3.56
0.11
2.00
2.07
0.43
f1 (ppm)

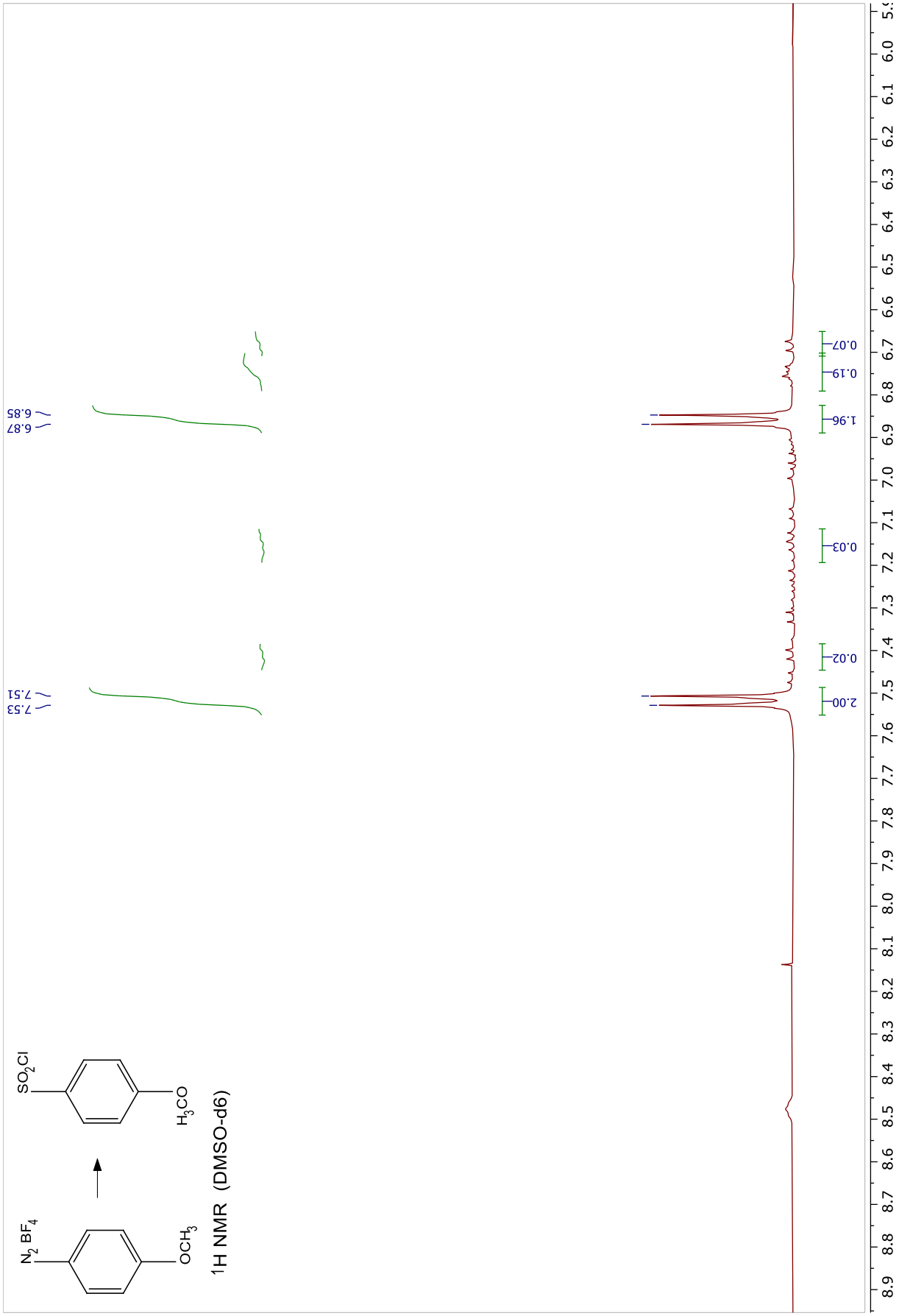
N_2 BF_4
OCH_3
SO_2Cl
H_3CO
^{1}H NMR (DMSO-d6)
7.53
7.51
6.87
6.85
2.00
0.02
0.03
1.96
0.19
0.07
f1 (ppm)

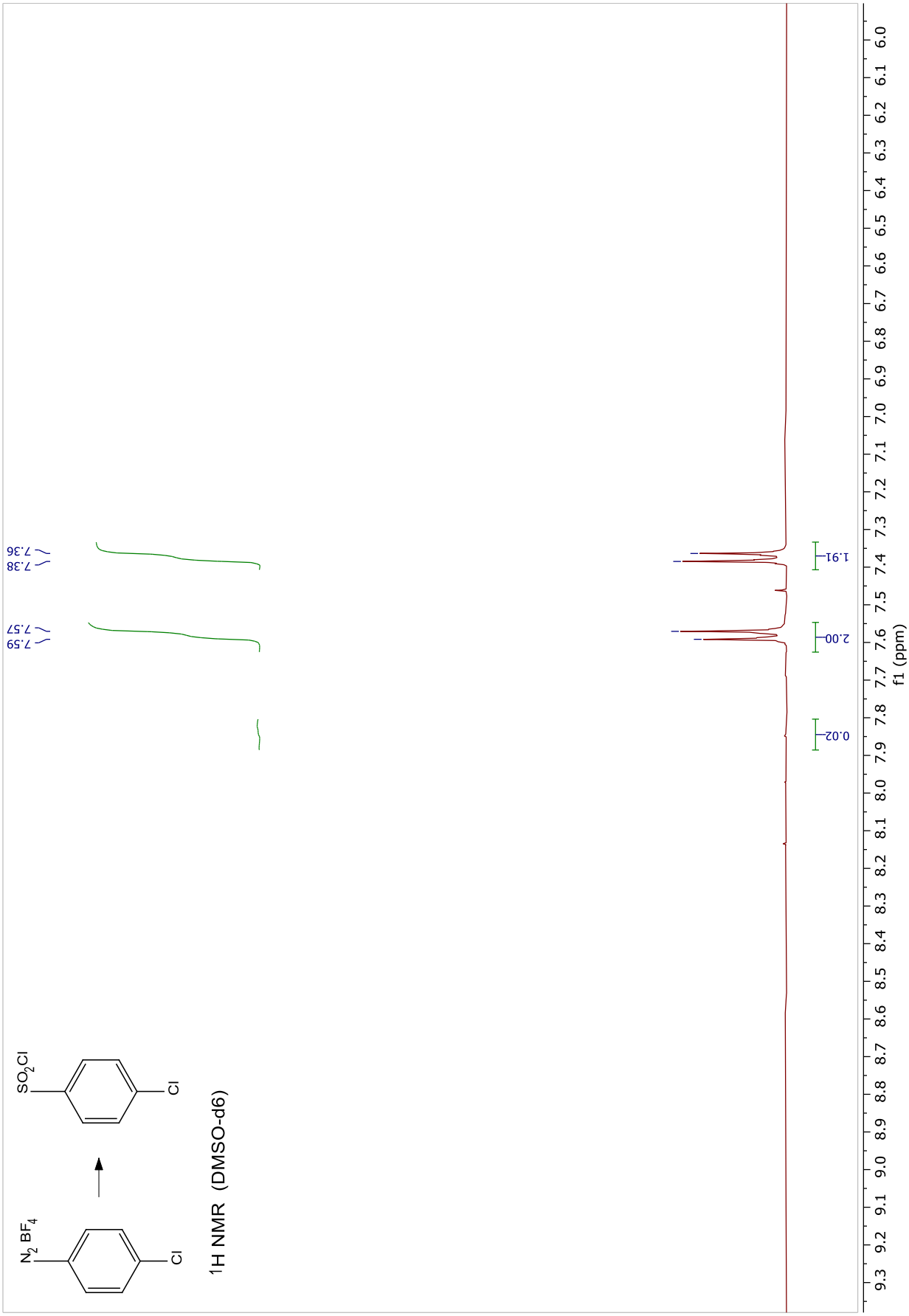
N_2 BF_4
Cl
SO_2Cl
Cl
^{1}H NMR (DMSO-d6)
7.36
7.38
7.57
7.59
1.91
2.00
0.02
f1 (ppm)

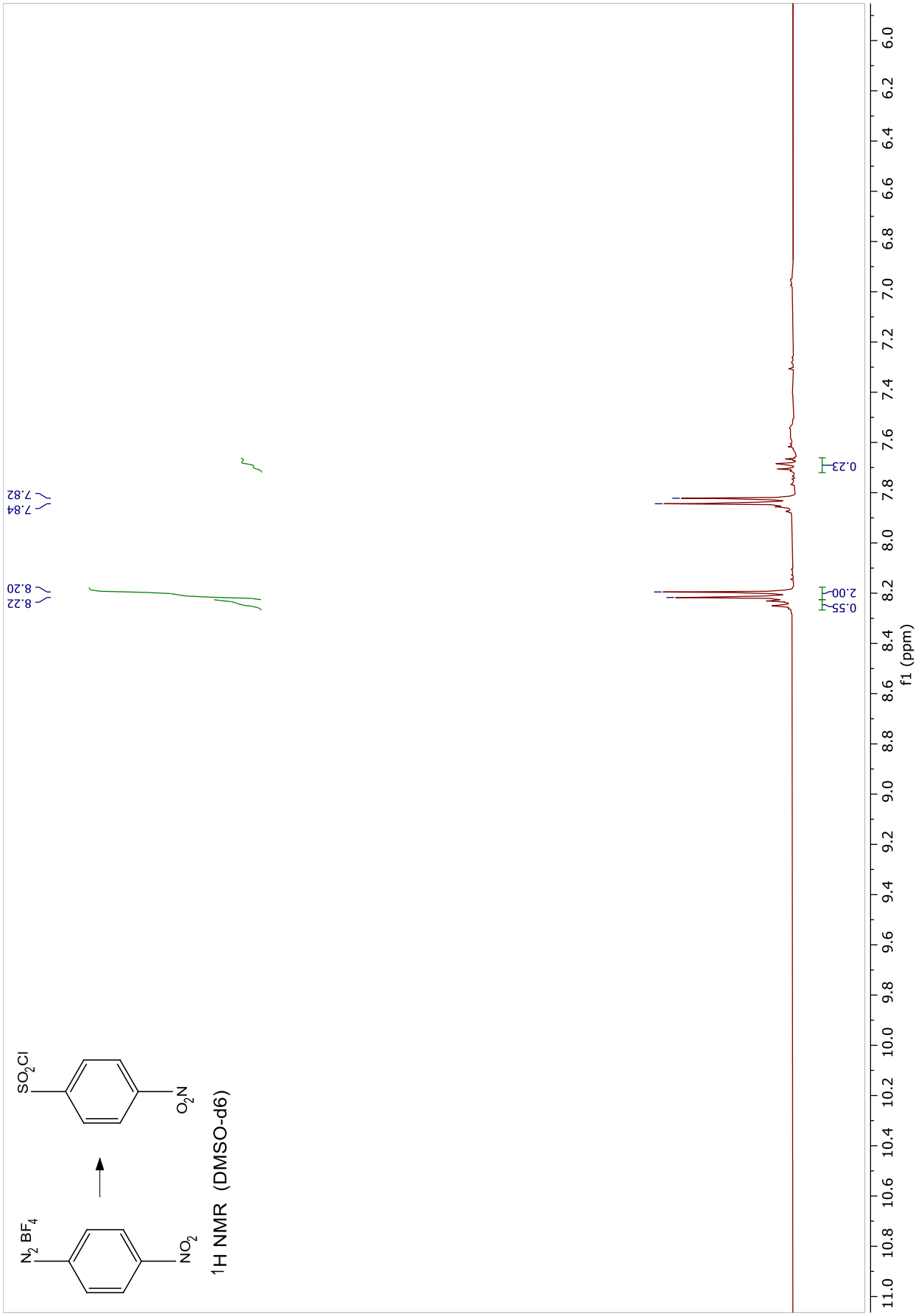
N_2BF_4
NO_2
SO_2Cl
O_2N
^{1}H NMR (DMSO-d6)
8.22
8.20
7.84
7.82
0.23
2.00
0.55
f1 (ppm)

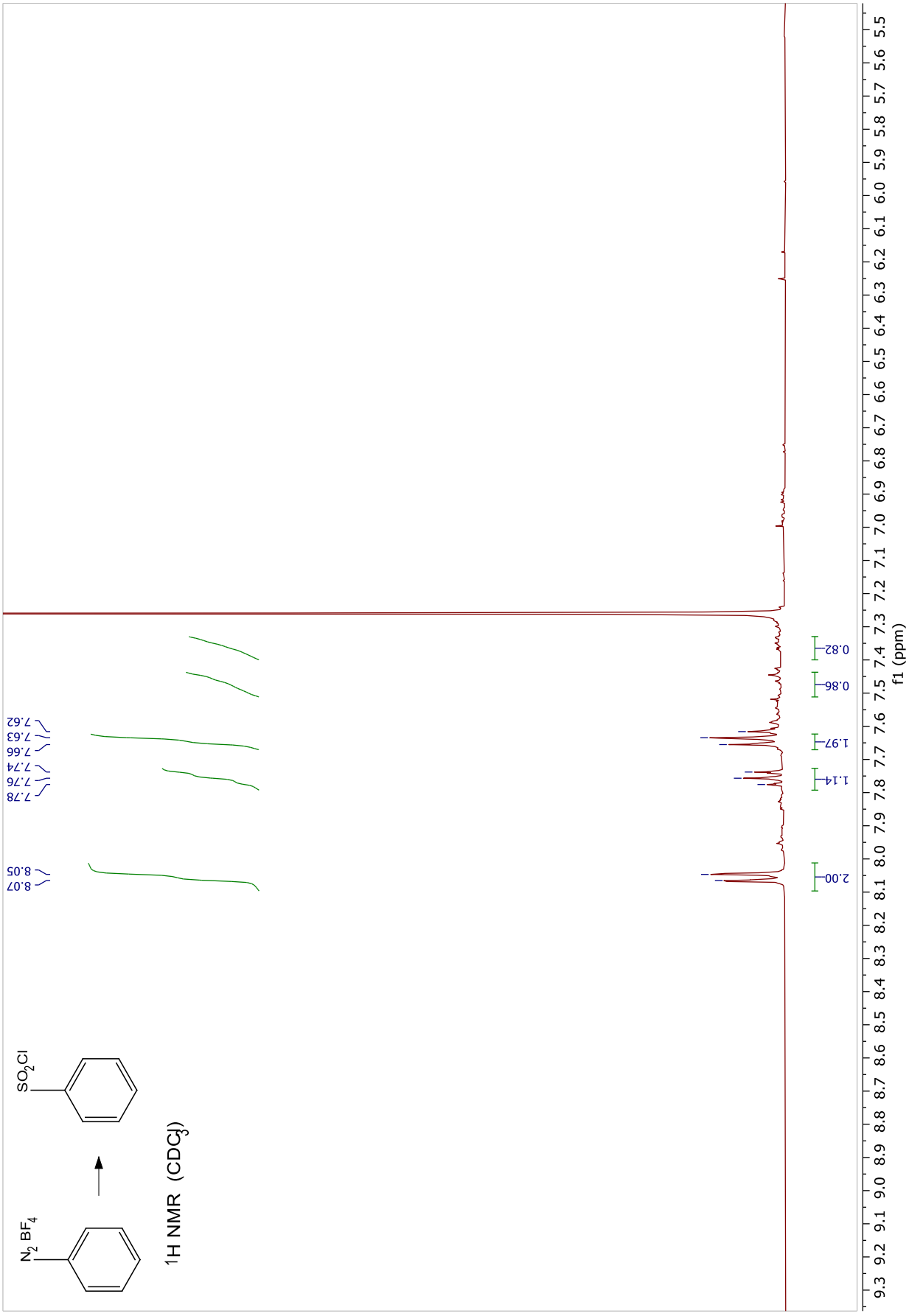
N_2 BF_4
SO_2Cl
^1H NMR (CDCl$_3$)
8.07
8.05
7.78
7.76
7.74
7.66
7.63
7.62
2.00
1.14
1.97
0.86
0.82
f1 (ppm)

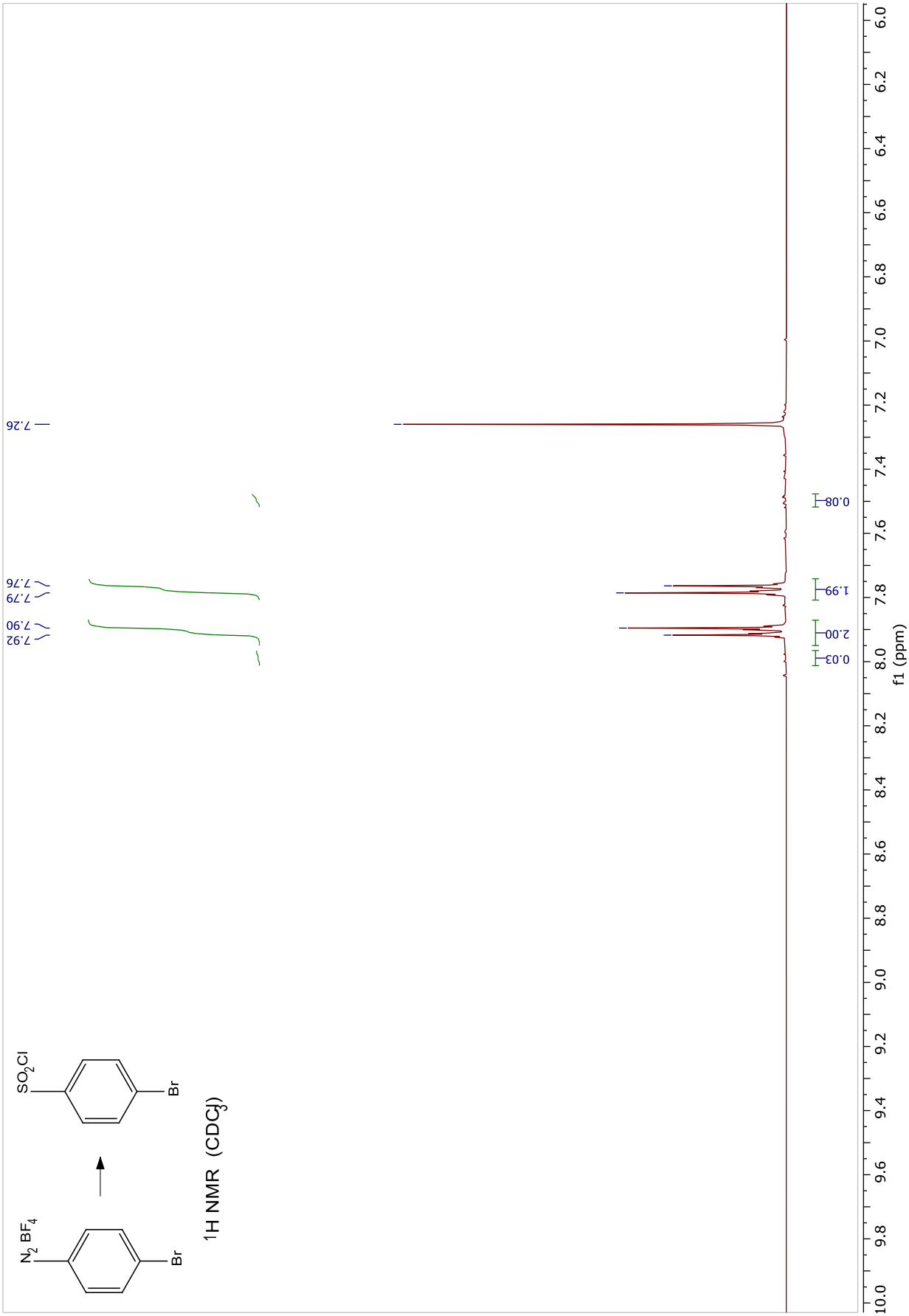
N_2 BF_4
Br
SO_2Cl
Br
^{1}H NMR (CDCl$_3$)
7.26
7.92
7.90
7.79
7.76
0.08
1.99
2.00
0.03
f1 (ppm)

11.11. Publication List

1. Markushyna, Y.; Lamagni, P.; Catalano, J.; Lock, N.; Zhang, G.; Antonietti, M.; Savateev, A.: Advantages in using cheap CO2 to favour photocatalytic oxidation of benzylamines. ACS Catalysis 10, S. 7336 - 7342 (***2020***)

2. Savateev, A.; Tarakina, N.; Strauss, V.; Hussain T.; ten Brummelhuis, K.; Sánchez Vadillo, J.,M.; Markushyna, Y.; Mazzanti S.; Tyutyunnik, A.; Walczak, R.; Oschatz, M.; Guldi, D.; Karton, A.; Antonietti, M.: Potassium Poly(Heptazine Imide) – Transition Metal-free Solid State Triplet Sensitizer in Cascade Energy Transfer and [3+2]-cycloadditions. Angewandte Chemie International Edition 59 (35), S. 15061 - 15068 ***(2020)***

3. Achilleos, D.; Yang, W.; Kasap, H.; Savateev, A.; Markushyna, Y.; Durrant, J.; Reisner, E.: Solar Reforming of Biomass with Homogeneous Carbon Dots. Angewandte Chemie International Edition 59, ***(2020)***

4. Markushyna, Y.; Smith, C. A.; Savateev, A.: Organic photocatalysis: carbon nitride semiconductors versus molecular catalysts. European Journal of Organic Chemistry (10), S. 1294 - 1309 (***2020***)

5. Logvinenko, I. G.; Markushyna, Y.; Kondratov, I. S.; Vashchenko, B. V.; Kliachyna, M.; Tokaryeva, Y.; Pivnytska, V.; Grygorenko, O. O.; Haufe, G.: Synthesis, physico-chemical properties and microsomal stability of compounds bearing aliphatic trifluoromethoxy group. Journal of Fluorine Chemistry 231, 109461 (***2020***)

6. Kurpil, B.; Markushyna, Y.; Savateev, A.: Visible Light Driven Reductive (Cyclo)Dimerization of Chalcones Over Heterogeneous Carbon Nitride Photocatalyst. ACS Catalysis 9, S. 1531 - 1538 (***2019***)

7. Markushyna, Y.; Teutloff, C.; Kurpil, B.; Cruz, D.; Lauermann, I.; Zhao, Y.; Antonietti, M.; Savateev, A.: Halogenation of aromatic hydrocarbons by halide anion oxidation with poly(heptazine imide) photocatalyst. Applied Catalysis B: Environmental 248, S. 211 - 217 (***2019***)

8. Markushyna, Y.; Lamagni, P.; Teutloff, C.; Catalano, J.; Lock, N.; Zhang, G.; Antonietti, M.; Savateev, A.: Green radicals of potassium poly(heptazine imide) by light and benzylamine. Journal of Materials Chemistry A 7 (43), S. 24771 - 24775 (***2019***)

9. Markushyna, Y.; Völkel, A.; Savateev, A.; Antonietti, M.; Filonenko, S.: One-pot photocalalytic reductive formylation of nitroarenes via multielectron transfer by carbon nitride in functional eutectic medium. Journal of Catalysis 380, S. 186 - 194 (***2019***)

10. Markushyna, Y.; Savateev, A.; Strauss, V.; Antonietti, M.: Photocatalysis Inside the Conductive Polymers for Sensing Applications (***in preparation***)

11. Markushyna, Y.; *et al*: Teteramerization of Benzylic Amines to Diazetidines-1,3 Employing Intrinsic Charge Storage Property of Semiconductors Under Visible Light Irradiation (***in preparation***)

12. Markushyna, Y.; et al: Chromoselective Catalytic Synthesis of Sulfonylchlorides and Sulfamides Using Dual Effect of Polyanion and Intrinsic Defects of Potassium Poly(heptazine imide) (***in preparation***)

11.12. Declaration

Die vorliegende Dissertation entstand im Zeitraum zwischen Juli 2018 und Juni 2020 am Max Planck Institut für Kolloid und Grenzflächenforschung unter der Betreuung von Prof. Dr. Dr. h.c. Markus Antonietti.

Hiermit erkläre ich, dass die vorliegende Arbeit selbständig angefertigt wurde und keine anderen als die angegebenen Hilfsmittel und Quellen verwendet wurden.

The present work was carried out and written during the period from July 2018 to June 2020 at the Max Planck Institute of Colloids and Interfaces under supervision of Prof. Dr. Dr. h.c. Markus Antonietti.

I declare that I have written this work on my own using only literature and other aids as described here.

Yevheniia Markushyna,

Potsdam, June 2020

12. References

1. Kannan, N.; Vakeesan, D., Solar energy for future world: - A review. *Renew. Sust. Energ. Rev.* **2016,** *62*, 1092-1105.
2. O'Regan, B.; Grätzel, M., A low-cost, high-efficiency solar cell based on dye-sensitized colloidal TiO2 films. *Nature* **1991,** *353* (6346), 737-740.
3. Yan, C.; Barlow, S.; Wang, Z.; Yan, H.; Jen, A. K. Y.; Marder, S. R.; Zhan, X., Non-fullerene acceptors for organic solar cells. *Nat. Rev. Mater.* **2018,** *3* (3).
4. Hagfeldt, A.; Boschloo, G.; Sun, L.; Kloo, L.; Pettersson, H., Dye-sensitized solar cells. *Chem. Rev.* **2010,** *110* (11), 6595-663.
5. Ahmad, H.; Kamarudin, S. K.; Minggu, L. J.; Kassim, M., Hydrogen from photo-catalytic water splitting process: A review. *Renew. Sust. Energ. Rev.* **2015,** *43*, 599-610.
6. Chen, X.; Shen, S.; Guo, L.; Mao, S. S., Semiconductor-based photocatalytic hydrogen generation. *Chem. Rev.* **2010,** *110* (11), 6503-70.
7. Li, G.; Su, R.; Rao, J.; Wu, J.; Rudolf, P.; Blake, G. R.; de Groot, R. A.; Besenbacher, F.; Palstra, T. T. M., Band gap narrowing of SnS2 superstructures with improved hydrogen production. *J. Mater. Chem. A* **2016,** *4* (1), 209-216.
8. Habisreutinger, S. N.; Schmidt-Mende, L.; Stolarczyk, J. K., Photocatalytic reduction of CO2 on TiO2 and other semiconductors. *Angew. Chem. Int. Ed.* **2013,** *52* (29), 7372-408.
9. Ran, J.; Jaroniec, M.; Qiao, S. Z., Cocatalysts in Semiconductor-based Photocatalytic CO2 Reduction: Achievements, Challenges, and Opportunities. *Adv. Mater.* **2018,** *30* (7).
10. Tu, W.; Zhou, Y.; Zou, Z., Photocatalytic conversion of CO(2) into renewable hydrocarbon fuels: state-of-the-art accomplishment, challenges, and prospects. *Adv. Mater.* **2014,** *26* (27), 4607-26.
11. Bhatkhande, D. S.; Pangarkar, V. G.; Beenackers, A. A. C. M., Photocatalytic degradation for environmental applications - a review. *J. Chem. Technol. Biotechnol.* **2002,** *77* (1), 102-116.
12. Chen, C.; Ma, W.; Zhao, J., Semiconductor-mediated photodegradation of pollutants under visible-light irradiation. *Chem. Soc. Rev.* **2010,** *39* (11), 4206-19.
13. Konstantinou, I. K.; Albanis, T. A., TiO2-assisted photocatalytic degradation of azo dyes in aqueous solution: kinetic and mechanistic investigations. *Appl. Catal. B* **2004,** *49* (1), 1-14.
14. Wang, X.; Sø, L.; Su, R.; Wendt, S.; Hald, P.; Mamakhel, A.; Yang, C.; Huang, Y.; Iversen, B. B.; Besenbacher, F., The influence of crystallite size and crystallinity of anatase nanoparticles on the photo-degradation of phenol. *J. Catal.* **2014,** *310*, 100-108.
15. Bach, T.; Hehn, J. P., Photochemical reactions as key steps in natural product synthesis. *Angew. Chem. Int. Ed.* **2011,** *50* (5), 1000-45.
16. Ciamician, G., The Photochemistry of the Future. *Science* **1912,** *36* (926), 385-94.
17. Albini, A.; Fagnoni, M., 1908: Giacomo Ciamician and the concept of green chemistry. *ChemSusChem* **2008,** *1* (1-2), 63-6.
18. Shaw, M. H.; Twilton, J.; MacMillan, D. W., Photoredox Catalysis in Organic Chemistry. *J. Org. Chem.* **2016,** *81* (16), 6898-926.
19. Wang, X.; Maeda, K.; Thomas, A.; Takanabe, K.; Xin, G.; Carlsson, J. M.; Domen, K.; Antonietti, M., A metal-free polymeric photocatalyst for hydrogen production from water under visible light. *Nat. Mater.* **2009,** *8* (1), 76-80.
20. Savateev, A.; Chen, Z. P.; Dontsova, D., Baking 'crumbly' carbon nitrides with improved photocatalytic properties using ammonium chloride. *RSC Adv.* **2016,** *6* (4), 2910-2913.

21. Zhang, W.; Albero, J.; Xi, L.; Lange, K. M.; Garcia, H.; Wang, X.; Shalom, M., One-Pot Synthesis of Nickel-Modified Carbon Nitride Layers Toward Efficient Photoelectrochemical Cells. *ACS Appl. Mater. Interfaces* **2017,** *9* (38), 32667-32677.
22. Chen, Z.; Mitchell, S.; Vorobyeva, E.; Leary, R. K.; Hauert, R.; Furnival, T.; Ramasse, Q. M.; Thomas, J. M.; Midgley, P. A.; Dontsova, D.; Antonietti, M.; Pogodin, S.; López, N.; Pérez-Ramírez, J., Stabilization of Single Metal Atoms on Graphitic Carbon Nitride. *Adv. Funct. Mater.* **2017,** *27* (8).
23. Li, X.-H.; Baar, M.; Blechert, S.; Antonietti, M., Facilitating room-temperature Suzuki coupling reaction with light: Mott-Schottky photocatalyst for C-C-coupling. *Sci. Rep.* **2013,** *3* (1).
24. Pei, Z.; Zhao, J.; Huang, Y.; Huang, Y.; Zhu, M.; Wang, Z.; Chen, Z.; Zhi, C., Toward enhanced activity of a graphitic carbon nitride-based electrocatalyst in oxygen reduction and hydrogen evolution reactions via atomic sulfur doping. *J. Mater. Chem. A* **2016,** *4* (31), 12205-12211.
25. Savateev, A.; Antonietti, M., Heterogeneous Organocatalysis for Photoredox Chemistry. *ACS Catal.* **2018,** *8* (10), 9790-9808.
26. Larkum, A. W., Limitations and prospects of natural photosynthesis for bioenergy production. *Curr. Opin. Biotechnol.* **2010,** *21* (3), 271-6.
27. Eibner, A., Action of Light on Pigments I. *Chem.-Ztg.* **1911,** *35*, 753-755.
28. Eibner, A., Action of Light on Pigments II. *Chem.-Ztg.* **1911,** *35*, 774-776.
29. Eibner, A., Action of Light on Pigments III. *Chem.-Ztg.* **1911,** *35*, 786-788.
30. Baur, E.; Perret, A., Über die Einwirkung von Licht auf gelöste Silbersalze in Gegenwart von Zinkoxyd. *Helv. Chim. Acta* **1924,** *7* (1), 910-915.
31. Renz, C., Über die Einwirkung von Oxyden auf Silbernitrat und Goldchlorid im Licht. *Helv. Chim. Acta* **1932,** *15* (1), 1077-1084.
32. Fujishima, A.; Zhang, X.; Tryk, D., TiO2 photocatalysis and related surface phenomena. *Surf. Sci. Rep.* **2008,** *63* (12), 515-582.
33. Goodeve, C. F.; Kitchener, J. A., The mechanism of photosensitisation by solids. *Transactions of the Faraday Society* **1938,** *34*.
34. Filimonov, V. N., Photocatalytic oxidation of gaseous isopropanol on ZnO and TiO2. *Dokl. Akad. Nauk SSSR* **1964,** *154:4*, 922–925.
35. Fujishima, A.; Honda, K., Electrochemical photolysis of water at a semiconductor electrode. *Nature* **1972,** *238* (5358), 37-8.
36. Schrauzer, G. N.; Guth, T. D., Photolysis of Water and Photoreduction of Nitrogen on Titanium Dioxide. *J. Am. Chem. Soc.* **2002,** *99* (22), 7189-7193.
37. Inoue, T.; Fujishima, A.; Konishi, S.; Honda, K., Photoelectrocatalytic reduction of carbon dioxide in aqueous suspensions of semiconductor powders. *Nature* **1979,** *277* (5698), 637-638.
38. Wang, Z.; Li, C.; Domen, K., Recent developments in heterogeneous photocatalysts for solar-driven overall water splitting. *Chem. Soc. Rev.* **2019,** *48* (7), 2109-2125.
39. Prier, C. K.; Rankic, D. A.; MacMillan, D. W., Visible light photoredox catalysis with transition metal complexes: applications in organic synthesis. *Chem. Rev.* **2013,** *113* (7), 5322-63.
40. Shaw, M. H.; Twilton, J.; MacMillan, D. W., Photoredox Catalysis in Organic Chemistry. *J. Org. Chem.* **2016,** *81* (16), 6898-926.
41. Lang, X.; Chen, X.; Zhao, J., Heterogeneous visible light photocatalysis for selective organic transformations. *Chem. Soc. Rev.* **2014,** *43* (1), 473-86.
42. Higashimoto, S.; Kitao, N.; Yoshida, N.; Sakura, T.; Azuma, M.; Ohue, H.; Sakata, Y., Selective photocatalytic oxidation of benzyl alcohol and its derivatives into corresponding

aldehydes by molecular oxygen on titanium dioxide under visible light irradiation. *J. Catal.* **2009,** *266* (2), 279-285.
43. Shishido, T.; Miyatake, T.; Teramura, K.; Hitomi, Y.; Yamashita, H.; Tanaka, T., Mechanism of Photooxidation of Alcohol over Nb2O5. *J. Phys. Chem. C* **2009,** *113* (43), 18713-18718.
44. Lang, X.; Ji, H.; Chen, C.; Ma, W.; Zhao, J., Selective formation of imines by aerobic photocatalytic oxidation of amines on TiO2. *Angew. Chem. Int. Ed. Engl.* **2011,** *50* (17), 3934-7.
45. Ohno, T.; Masaki, Y.; Hirayama, S.; Matsumura, M., TiO2-Photocatalyzed Epoxidation of 1-Decene by H2O2 under Visible Light. *J. Catal.* **2001,** *204* (1), 163-168.
46. Parrino, F.; Ramakrishnan, A.; Kisch, H., Semiconductor-photocatalyzed sulfoxidation of alkanes. *Angew. Chem. Int. Ed. Engl.* **2008,** *47* (37), 7107-9.
47. Sarina, S.; Zhu, H.; Zheng, Z.; Bottle, S.; Chang, J.; Ke, X.; Zhao, J.-C.; Huang, Y.; Sutrisno, A.; Willans, M.; Li, G., Driving selective aerobic oxidation of alkyl aromatics by sunlight on alcohol grafted metal hydroxides. *Chem. Sci.* **2012,** *3* (6).
48. Little , L. H.; Kiselev, A. V.; Lygin, V. I., Infrared Spectra of Adsorbed Species. *Academic Press Inc., London, UK* **1966**.
49. Chen, X.; Zhu, H. Y.; Zhao, J. C.; Zheng, Z. F.; Gao, X. P., Visible-light-driven oxidation of organic contaminants in air with gold nanoparticle catalysts on oxide supports. *Angew. Chem. Int. Ed. Engl.* **2008,** *47* (29), 5353-6.
50. Wang, P.; Huang, B.; Qin, X.; Zhang, X.; Dai, Y.; Wei, J.; Whangbo, M. H., Ag@AgCl: a highly efficient and stable photocatalyst active under visible light. *Angew. Chem. Int. Ed. Engl.* **2008,** *47* (41), 7931-3.
51. Ide, Y.; Nakamura, N.; Hattori, H.; Ogino, R.; Ogawa, M.; Sadakane, M.; Sano, T., Sunlight-induced efficient and selective photocatalytic benzene oxidation on TiO2-supported gold nanoparticles under CO2 atmosphere. *Chem. Commun.* **2011,** *47* (41), 11531-3.
52. Irving, H., Historical account of Pharaoh's serpents. *Sci. Prog.* **1935,** *30*, 62-66.
53. Davis, T. L., Pyrotechnic snakes. *J. Chem. Educ.* **1940,** *17* (6).
54. Liebig, J., Uber einige Stickstoff - Verbindungen. *Annalen der Pharmacie* **1834,** *10* (1), 1-47.
55. Liebig, J., Ueber Mellon und Mellonverbindungen. *Liebigs Ann.* **1844,** *50* (3), 337-363.
56. Liebig, J., Ueber die Constitution der Mellonverbindungen. *Liebigs Ann.* **1855,** *95* (3), 257-282.
57. Goettmann, F.; Fischer, A.; Antonietti, M.; Thomas, A., Metal-free catalysis of sustainable Friedel-Crafts reactions: direct activation of benzene by carbon nitrides to avoid the use of metal chlorides and halogenated compounds. *Chem. Commun.* **2006,** (43), 4530-2.
58. Takanabe, K.; Kamata, K.; Wang, X.; Antonietti, M.; Kubota, J.; Domen, K., Photocatalytic hydrogen evolution on dye-sensitized mesoporous carbon nitride photocatalyst with magnesium phthalocyanine. *Phys. Chem. Chem. Phys.* **2010,** *12* (40), 13020-5.
59. Zhang, J.; Zhang, M.; Sun, R. Q.; Wang, X., A facile band alignment of polymeric carbon nitride semiconductors to construct isotype heterojunctions. *Angew. Chem. Int. Ed. Engl.* **2012,** *51* (40), 10145-9.
60. Yan, S. C.; Li, Z. S.; Zou, Z. G., Photodegradation performance of g-C3N4 fabricated by directly heating melamine. *Langmuir* **2009,** *25* (17), 10397-401.
61. Dong, F.; Wu, L.; Sun, Y.; Fu, M.; Wu, Z.; Lee, S. C., Efficient synthesis of polymeric g-C3N4 layered materials as novel efficient visible light driven photocatalysts. *J. Mater. Chem.* **2011,** *21* (39).
62. Zhang, G.; Zhang, J.; Zhang, M.; Wang, X., Polycondensation of thiourea into carbon nitride semiconductors as visible light photocatalysts. *J. Mater. Chem.* **2012,** *22* (16).

63. Sung, C.-M.; Sung, M., Carbon nitride and other speculative superhard materials. *Mater. Chem. Phys.* **1996,** *43* (1), 1-18.
64. Liu, A. Y.; Cohen, M. L., Prediction of new low compressibility solids. *Science* **1989,** *245* (4920), 841-2.
65. Algara-Siller, G.; Severin, N.; Chong, S. Y.; Bjorkman, T.; Palgrave, R. G.; Laybourn, A.; Antonietti, M.; Khimyak, Y. Z.; Krasheninnikov, A. V.; Rabe, J. P.; Kaiser, U.; Cooper, A. I.; Thomas, A.; Bojdys, M. J., Triazine-based graphitic carbon nitride: a two-dimensional semiconductor. *Angew. Chem. Int. Ed. Engl.* **2014,** *53* (29), 7450-5.
66. Kouvetakis, J.; Todd, M.; Wilkens, B.; Bandari, A.; Cave, N., Novel Synthetic Routes to Carbon-Nitrogen Thin Films. *Chem. Mater.* **1994,** *6* (6), 811-814.
67. Thomas, A.; Fischer, A.; Goettmann, F.; Antonietti, M.; Müller, J.-O.; Schlögl, R.; Carlsson, J. M., Graphitic carbon nitride materials: variation of structure and morphology and their use as metal-free catalysts. *J. Mater. Chem.* **2008,** *18* (41).
68. Jurgens, B.; Irran, E.; Senker, J.; Kroll, P.; Muller, H.; Schnick, W., Melem (2,5,8-triamino-tri-s-triazine), an important intermediate during condensation of melamine rings to graphitic carbon nitride: synthesis, structure determination by X-ray powder diffractometry, solid-state NMR, and theoretical studies. *J. Am. Chem. Soc.* **2003,** *125* (34), 10288-300.
69. Lotsch, B. V.; Schnick, W., New light on an old story: formation of melam during thermal condensation of melamine. *Chem. Eur. J.* **2007,** *13* (17), 4956-68.
70. Horvath-Bordon, E.; Riedel, R.; McMillan, P. F.; Kroll, P.; Miehe, G.; van Aken, P. A.; Zerr, A.; Hoppe, P.; Shebanova, O.; McLaren, I.; Lauterbach, S.; Kroke, E.; Boehler, R., High-pressure synthesis of crystalline carbon nitride imide, C2N2(NH). *Angew. Chem. Int. Ed.* **2007,** *46* (9), 1476-80.
71. Zhang, Z.; Leinenweber, K.; Bauer, M.; Garvie, L. A.; McMillan, P. F.; Wolf, G. H., High-pressure bulk synthesis of crystalline C(6)N(9)H(3).HCl: a novel c(3)n(4) graphitic derivative. *J. Am. Chem. Soc.* **2001,** *123* (32), 7788-96.
72. Bojdys, M. J.; Muller, J. O.; Antonietti, M.; Thomas, A., Ionothermal synthesis of crystalline, condensed, graphitic carbon nitride. *Chem. Eur. J.* **2008,** *14* (27), 8177-82.
73. Chong, S. Y.; Jones, J. T. A.; Khimyak, Y. Z.; Cooper, A. I.; Thomas, A.; Antonietti, M.; Bojdys, M. J., Tuning of gallery heights in a crystalline 2D carbon nitride network. *J. Mater. Chem. A* **2013,** *1* (4), 1102-1107.
74. Dontsova, D.; Pronkin, S.; Wehle, M.; Chen, Z.; Fettkenhauer, C.; Clavel, G.; Antonietti, M., Triazoles: A New Class of Precursors for the Synthesis of Negatively Charged Carbon Nitride Derivatives. *Chem. Mater.* **2015,** *27* (15), 5170-5179.
75. Savateev, A.; Pronkin, S.; Epping, J. D.; Willinger, M. G.; Wolff, C.; Neher, D.; Antonietti, M.; Dontsova, D., Potassium Poly(heptazine imides) from Aminotetrazoles: Shifting Band Gaps of Carbon Nitride-like Materials for More Efficient Solar Hydrogen and Oxygen Evolution. *ChemCatChem* **2017,** *9* (1), 167-174.
76. Lau, V. W.; Moudrakovski, I.; Botari, T.; Weinberger, S.; Mesch, M. B.; Duppel, V.; Senker, J.; Blum, V.; Lotsch, B. V., Rational design of carbon nitride photocatalysts by identification of cyanamide defects as catalytically relevant sites. *Nat. Commun.* **2016,** *7*, 12165.
77. Gillan, E. G., Synthesis of Nitrogen-Rich Carbon Nitride Networks from an Energetic Molecular Azide Precursor. *Chem. Mater.* **2000,** *12* (12), 3906-3912.
78. Groenewolt, M.; Antonietti, M., Synthesis of g-C3N4 Nanoparticles in Mesoporous Silica Host Matrices. *Adv. Mater.* **2005,** *17* (14), 1789-1792.
79. Vinu, A.; Ariga, K.; Mori, T.; Nakanishi, T.; Hishita, S.; Golberg, D.; Bando, Y., Preparation and Characterization of Well-Ordered Hexagonal Mesoporous Carbon Nitride. *Adv. Mater.* **2005,** *17* (13), 1648-1652.

80. Goettmann, F.; Fischer, A.; Antonietti, M.; Thomas, A., Chemical synthesis of mesoporous carbon nitrides using hard templates and their use as a metal-free catalyst for Friedel-Crafts reaction of benzene. *Angew. Chem. Int. Ed.* **2006,** *45* (27), 4467-71.
81. Liang, C.; Li, Z.; Dai, S., Mesoporous carbon materials: synthesis and modification. *Angew. Chem. Int. Ed.* **2008,** *47* (20), 3696-717.
82. Antonietti, M., Surfactants for novel templating applications. *Curr. Opin. Colloid Interface Sci.* **2001,** *6* (3), 244-248.
83. Wang, Y.; Wang, X.; Antonietti, M.; Zhang, Y., Facile one-pot synthesis of nanoporous carbon nitride solids by using soft templates. *ChemSusChem* **2010,** *3* (4), 435-9.
84. Wang, Y.; Zhang, J.; Wang, X.; Antonietti, M.; Li, H., Boron- and fluorine-containing mesoporous carbon nitride polymers: metal-free catalysts for cyclohexane oxidation. *Angew. Chem. Int. Ed.* **2010,** *49* (19), 3356-9.
85. Dong, F.; Zhao, Z.; Xiong, T.; Ni, Z.; Zhang, W.; Sun, Y.; Ho, W. K., In situ construction of g-C3N4/g-C3N4 metal-free heterojunction for enhanced visible-light photocatalysis. *ACS Appl. Mater. Interfaces* **2013,** *5* (21), 11392-401.
86. Corkill, J. L.; Cohen, M. L., Calculated quasiparticle band gap of beta -C3N4. *Phys. Rev. B Condens. Matter.* **1993,** *48* (23), 17622-17624.
87. Cao, S.; Low, J.; Yu, J.; Jaroniec, M., Polymeric photocatalysts based on graphitic carbon nitride. *Adv. Mater.* **2015,** *27* (13), 2150-76.
88. Zhang, G.; Li, G.; Heil, T.; Zafeiratos, S.; Lai, F.; Savateev, A.; Antonietti, M.; Wang, X., Tailoring the Grain Boundary Chemistry of Polymeric Carbon Nitride for Enhanced Solar Hydrogen Production and CO2 Reduction. *Angew. Chem. Int. Ed.* **2019,** *58* (11), 3433-3437.
89. Zhang, G.; Lin, L.; Li, G.; Zhang, Y.; Savateev, A.; Zafeiratos, S.; Wang, X.; Antonietti, M., Ionothermal Synthesis of Triazine-Heptazine-Based Copolymers with Apparent Quantum Yields of 60 % at 420 nm for Solar Hydrogen Production from "Sea Water". *Angew. Chem. Int. Ed.* **2018,** *57* (30), 9372-9376.
90. Barrio, J.; Shalom, M., Rational Design of Carbon Nitride Materials by Supramolecular Preorganization of Monomers. *ChemCatChem* **2018,** *10* (24), 5573-5586.
91. Savateev, A.; Pronkin, S.; Epping, J. D.; Willinger, M. G.; Antonietti, M.; Dontsova, D., Synthesis of an electronically modified carbon nitride from a processable semiconductor, 3-amino-1,2,4-triazole oligomer, via a topotactic-like phase transition. *J. Mater. Chem. A* **2017,** *5* (18), 8394-8401.
92. Kurpil, B.; Savateev, A.; Papaefthimiou, V.; Zafeiratos, S.; Heil, T.; Özenler, S.; Dontsova, D.; Antonietti, M., Hexaazatriphenylene doped carbon nitrides—Biomimetic photocatalyst with superior oxidation power. *Appl. Catal. B* **2017,** *217*, 622-628.
93. Barrio, J.; Lin, L.; Amo-Ochoa, P.; Tzadikov, J.; Peng, G.; Sun, J.; Zamora, F.; Wang, X.; Shalom, M., Unprecedented Centimeter-Long Carbon Nitride Needles: Synthesis, Characterization and Applications. *Small* **2018,** *14* (21), e1800633.
94. Wang, B.; Cai, H.; Zhao, D.; Song, M.; Guo, P.; Shen, S.; Li, D.; Yang, S., Enhanced photocatalytic hydrogen evolution by partially replaced corner-site C atom with P in g-C3N4. *Appl. Catal. B* **2019,** *244*, 486-493.
95. Battula, V. R.; Kumar, S.; Chauhan, D. K.; Samanta, S.; Kailasam, K., A true oxygen-linked heptazine based polymer for efficient hydrogen evolution. *Appl. Catal. B* **2019,** *244*, 313-319.
96. Liu, Q.; Shen, J.; Yu, X.; Yang, X.; Liu, W.; Yang, J.; Tang, H.; Xu, H.; Li, H.; Li, Y.; Xu, J., Unveiling the origin of boosted photocatalytic hydrogen evolution in simultaneously (S, P, O)-Codoped and exfoliated ultrathin g-C3N4 nanosheets. *Appl. Catal. B* **2019,** *248*, 84-94.

97. Singh, G.; Ramadass, K.; Lee, J. M.; Ismail, I. S.; Singh, M.; Bansal, V.; Yang, J.-H.; Vinu, A., Convenient design of porous and heteroatom self-doped carbons for CO2 capture. *Microporous and Mesoporous Mater.* **2019,** *287*, 1-8.
98. Ong, W. J.; Tan, L. L.; Ng, Y. H.; Yong, S. T.; Chai, S. P., Graphitic Carbon Nitride (g-C3N4)-Based Photocatalysts for Artificial Photosynthesis and Environmental Remediation: Are We a Step Closer To Achieving Sustainability? *Chem. Rev.* **2016,** *116* (12), 7159-329.
99. Savateev, A.; Kurpil, B.; Mishchenko, A.; Zhang, G.; Antonietti, M., A "waiting" carbon nitride radical anion: a charge storage material and key intermediate in direct C-H thiolation of methylarenes using elemental sulfur as the "S"-source. *Chem. Sci.* **2018,** *9* (14), 3584-3591.
100. Kurpil, B.; Kumru, B.; Heil, T.; Antonietti, M.; Savateev, A., Carbon nitride creates thioamides in high yields by the photocatalytic Kindler reaction. *Green Chem.* **2018,** *20* (4), 838-842.
101. Kurpil, B.; Otte, K.; Mishchenko, A.; Lamagni, P.; Lipiński, W.; Lock, N.; Antonietti, M.; Savateev, A., Carbon nitride photocatalyzes regioselective aminium radical addition to the carbonyl bond and yields N-fused pyrroles. *Nat. Commun.* **2019,** *10* (1), 945.
102. Hari, D. P.; Konig, B., Synthetic applications of eosin Y in photoredox catalysis. *Chem. Commun.* **2014,** *50* (51), 6688-99.
103. Park, J. H.; Ko, K. C.; Kim, E.; Park, N.; Ko, J. H.; Ryu, D. H.; Ahn, T. K.; Lee, J. Y.; Son, S. U., Photocatalysis by phenothiazine dyes: visible-light-driven oxidative coupling of primary amines at ambient temperature. *Org. Lett.* **2012,** *14* (21), 5502-5.
104. Koike, T.; Akita, M., Visible-light radical reaction designed by Ru- and Ir-based photoredox catalysis. *Inorg. Chem. Front.* **2014,** *1* (8), 562-576.
105. Kurpil, B.; Markushyna, Y.; Savateev, A., Visible-Light-Driven Reductive (Cyclo)Dimerization of Chalcones over Heterogeneous Carbon Nitride Photocatalyst. *ACS Catal.* **2019,** *9* (2), 1531-1538.
106. Sobarzo-Sanchez, E.; Soto, P. G.; Valdes Rivera, C.; Sanchez, G.; Hidalgo, M. E., Applied biological and physicochemical activity of isoquinoline alkaloids: oxoisoaporphine and boldine. *Molecules* **2012,** *17* (9), 10958-70.
107. Chrzanowska, M.; Grajewska, A.; Rozwadowska, M. D., Asymmetric Synthesis of Isoquinoline Alkaloids: 2004-2015. *Chem. Rev.* **2016,** *116* (19), 12369-12465.
108. Condie, A. G.; Gonzalez-Gomez, J. C.; Stephenson, C. R., Visible-light photoredox catalysis: aza-Henry reactions via C-H functionalization. *J. Am. Chem. Soc.* **2010,** *132* (5), 1464-5.
109. Hari, D. P.; Konig, B., Eosin Y catalyzed visible light oxidative C-C and C-P bond formation. *Org. Lett.* **2011,** *13* (15), 3852-5.
110. Möhlmann, L.; Baar, M.; Rieß, J.; Antonietti, M.; Wang, X.; Blechert, S., Carbon Nitride-Catalyzed Photoredox C□C Bond Formation with N-Aryltetrahydroisoquinolines. *Adv. Synth. Catal* **2012,** *354* (10), 1909-1913.
111. Rueping, M.; Vila, C.; Koenigs, R. M.; Poscharny, K.; Fabry, D. C., Dual catalysis: combining photoredox and Lewis base catalysis for direct Mannich reactions. *Chem. Commun.* **2011,** *47* (8), 2360-2.
112. Filler, R.; Kobayashi, Y.; Yagupolskii, L. M., Organofluorine Compounds in Medicinal Chemistry and Biomedical Applications. *Elsevier: Amsterdam* **1993**.
113. Nagib, D. A.; MacMillan, D. W., Trifluoromethylation of arenes and heteroarenes by means of photoredox catalysis. *Nature* **2011,** *480* (7376), 224-8.
114. Baar, M.; Blechert, S., Graphitic carbon nitride polymer as a recyclable photoredox catalyst for fluoroalkylation of arenes. *Chem. Eur. J.* **2015,** *21* (2), 526-30.

115. Cai, Y.; Tang, Y.; Fan, L.; Lefebvre, Q.; Hou, H.; Rueping, M., Heterogeneous Visible-Light Photoredox Catalysis with Graphitic Carbon Nitride for α-Aminoalkyl Radical Additions, Allylations, and Heteroarylations. *ACS Catal.* **2018,** *8* (10), 9471-9476.
116. Miyake, Y.; Ashida, Y.; Nakajima, K.; Nishibayashi, Y., Visible-light-mediated addition of α-aminoalkyl radicals generated from α-silylamines to α,β-unsaturated carbonyl compounds. *Chem. Commun.* **2012,** *48* (55).
117. Zhu, S.; Das, A.; Bui, L.; Zhou, H.; Curran, D. P.; Rueping, M., Oxygen Switch in Visible-Light Photoredox Catalysis: Radical Additions and Cyclizations and Unexpected C–C-Bond Cleavage Reactions. *J. Am. Chem. Soc.* **2013,** *135* (5), 1823-1829.
118. Millet, A.; Lefebvre, Q.; Rueping, M., Visible-Light Photoredox-Catalyzed Giese Reaction: Decarboxylative Addition of Amino Acid Derived α-Amino Radicals to Electron-Deficient Olefins. *Chem. Eur. J.* **2016,** *22* (38), 13464-13468.
119. Prier, C. K.; MacMillan, D. W., Amine alpha-heteroarylation via photoredox catalysis: a homolytic aromatic substitution pathway. *Chem. Sci.* **2014,** *5* (11), 4173-4178.
120. Seghers, S.; Protasova, L.; Mullens, S.; Thybaut, J. W.; Stevens, C. V., Improving the efficiency of the Diels–Alder process by using flow chemistry and zeolite catalysis. *Green Chem.* **2017,** *19* (1), 237-248.
121. Lin, S.; Ischay, M. A.; Fry, C. G.; Yoon, T. P., Radical cation Diels-Alder cycloadditions by visible light photocatalysis. *J. Am. Chem. Soc.* **2011,** *133* (48), 19350-3.
122. Zhao, Y.; Antonietti, M., Visible-Light-Irradiated Graphitic Carbon Nitride Photocatalyzed Diels-Alder Reactions with Dioxygen as Sustainable Mediator for Photoinduced Electrons. *Angew. Chem. Int. Ed.* **2017,** *56* (32), 9336-9340.
123. Tucker, J. W.; Nguyen, J. D.; Narayanam, J. M.; Krabbe, S. W.; Stephenson, C. R., Tin-free radical cyclization reactions initiated by visible light photoredox catalysis. *Chem. Commun.* **2010,** *46* (27), 4985-7.
124. Woznica, M.; Chaoui, N.; Taabache, S.; Blechert, S., THF: an efficient electron donor in continuous flow radical cyclization photocatalyzed by graphitic carbon nitride. *Chem. Eur. J.* **2014,** *20* (45), 14624-8.
125. Zhao, G.; Yang, C.; Guo, L.; Sun, H.; Lin, R.; Xia, W., Reactivity insight into reductive coupling and aldol cyclization of chalcones by visible light photocatalysis. *J. Org. Chem.* **2012,** *77* (14), 6302-6.
126. Blum, T. R.; Zhu, Y.; Nordeen, S. A.; Yoon, T. P., Photocatalytic Synthesis of Dihydrobenzofurans by Oxidative [3+2] Cycloaddition of Phenols. *Angew. Chem. Int. Ed.* **2014,** *53* (41), 11056-11059.
127. Song, T.; Zhou, B.; Peng, G.-W.; Zhang, Q.-B.; Wu, L.-Z.; Liu, Q.; Wang, Y., Aerobic Oxidative Coupling of Resveratrol and its Analogues by Visible Light Using Mesoporous Graphitic Carbon Nitride (mpg-C3N4) as a Bioinspired Catalyst. *Chem. Eur. J.* **2014,** *20* (3), 678-682.
128. Murahashi, S.-I., Synthetic Aspects of Metal-Catalyzed Oxidations of Amines and Related Reactions. *Angew. Chem. Int. Ed. Engl.* **1995,** *34* (22), 2443-2465.
129. Patil, R. D.; Adimurthy, S., Catalytic Methods for Imine Synthesis. *Asian J. Org. Chem.* **2013,** *2* (9), 726-744.
130. Nicolaou, K. C.; Mathison, C. J.; Montagnon, T., New reactions of IBX: oxidation of nitrogen- and sulfur-containing substrates to afford useful synthetic intermediates. *Angew. Chem. Int. Ed.* **2003,** *42* (34), 4077-82.
131. Mukaiyama, T.; Kawana, A.; Fukuda, Y.; Matsuo, J.-i., Oxidation of Various Secondary Amines to Imines withN-tert-Butylphenylsulfinimidoyl Chloride. *Chem. Lett.* **2001,** *30* (5), 390-391.

132. Su, F.; Mathew, S. C.; Mohlmann, L.; Antonietti, M.; Wang, X.; Blechert, S., Aerobic oxidative coupling of amines by carbon nitride photocatalysis with visible light. *Angew. Chem. Int. Ed.* **2011,** *50* (3), 657-60.
133. Rueping, M.; Vila, C.; Szadkowska, A.; Koenigs, R. M.; Fronert, J., Photoredox Catalysis as an Efficient Tool for the Aerobic Oxidation of Amines and Alcohols: Bioinspired Demethylations and Condensations. *ACS Catal.* **2012,** *2* (12), 2810-2815.
134. Hagmann, W. K., The many roles for fluorine in medicinal chemistry. *J Med Chem* **2008,** *51* (15), 4359-69.
135. Rueda-Becerril, M.; Mahe, O.; Drouin, M.; Majewski, M. B.; West, J. G.; Wolf, M. O.; Sammis, G. M.; Paquin, J. F., Direct C-F bond formation using photoredox catalysis. *J. Am. Chem. Soc.* **2014,** *136* (6), 2637-41.
136. Movsisyan, M.; Delbeke, E. I. P.; Berton, J. K. E. T.; Battilocchio, C.; Ley, S. V.; Stevens, C. V., Taming hazardous chemistry by continuous flow technology. *Chem. Soc. Rev.* **2016,** *45* (18), 4892-4928.
137. Movsisyan, M.; De Coen, L. M.; Heugebaert, T. S. A.; Verlee, A.; Roman, B. I.; Stevens, C. V., Continuous-Flow Synthesis of Phenothiazine Antipsychotics: A Feasibility Study. *Eur. J. Org. Chem.* **2019,** *2019* (6), 1350-1354.
138. Plutschack, M. B.; Pieber, B.; Gilmore, K.; Seeberger, P. H., The Hitchhiker's Guide to Flow Chemistry. *Chem. Rev.* **2017,** *117* (18), 11796-11893.
139. Pieber, B.; Shalom, M.; Antonietti, M.; Seeberger, P. H.; Gilmore, K., Continuous Heterogeneous Photocatalysis in Serial Micro-Batch Reactors. *Angew. Chem. Int. Ed.* **2018,** *57* (31), 9976-9979.
140. Meyer, A. U.; Jager, S.; Hari, D. P.; Konig, B., Visible Light-Mediated Metal-Free Synthesis of Vinyl Sulfones from Aryl Sulfinates. *Adv. Synth. Catal* **2015,** *357* (9), 2050-2054.
141. Meyer, A. U.; Strakova, K.; Slanina, T.; Konig, B., Eosin Y (EY) Photoredox-Catalyzed Sulfonylation of Alkenes: Scope and Mechanism. *Chem. Eur. J.* **2016,** *22* (25), 8694-9.
142. Meyer, A. U.; Lau, V. W.-h.; König, B.; Lotsch, B. V., Photocatalytic Oxidation of Sulfinates to Vinyl Sulfones with Cyanamide-Functionalised Carbon Nitride. *Eur. J. Org. Chem.* **2017,** *2017* (15), 2179-2185.
143. Li, L.; Cruz, D.; Savateev, A.; Zhang, G.; Antonietti, M.; Zhao, Y., Photocatalytic cyanation of carbon nitride scaffolds: Tuning band structure and enhancing the performance in green light driven C S bond formation. *Appl. Catal. B* **2018,** *229*, 249-253.
144. Fauvarque, J., The Chlorine Industry. *Pure Appl. Chem.* **1996,** *68* (9), 1713-1720.
145. Littke, A. F.; Fu, G. C., Palladium-Catalyzed Coupling Reactions of Aryl Chlorides. *Angew. Chem. Int. Ed.* **2002,** *41* (22), 4176-4211.
146. Gribble, G. W., Natural Organohalogens: A New Frontier for Medicinal Agents? *J. Chem. Educ.* **2004,** *81* (10).
147. Podgorsek, A.; Zupan, M.; Iskra, J., Oxidative halogenation with "green" oxidants: oxygen and hydrogen peroxide. *Angew. Chem. Int. Ed.* **2009,** *48* (45), 8424-50.
148. Hering, T.; Muhldorf, B.; Wolf, R.; Konig, B., Halogenase-Inspired Oxidative Chlorination Using Flavin Photocatalysis. *Angew. Chem. Int. Ed.* **2016,** *55* (17), 5342-5.
149. Zhang, L.; Hu, X., Room temperature C(sp(2))-H oxidative chlorination via photoredox catalysis. *Chem. Sci.* **2017,** *8* (10), 7009-7013.
150. Markushyna, Y.; Teutloff, C.; Kurpil, B.; Cruz, D.; Lauermann, I.; Zhao, Y.; Antonietti, M.; Savateev, A., Halogenation of aromatic hydrocarbons by halide anion oxidation with poly(heptazine imide) photocatalyst. *Appl. Catal. B* **2019,** *248*, 211-217.
151. Ghosh, I.; Khamrai, J.; Savateev, A.; Shlapakov, N.; Antonietti, M.; König, B., Organic semiconductor photocatalyst can bifunctionalize arenes and heteroarenes. *Science* **2019,** *365* (6451), 360-366.

152. Semiconductor Photocatalysis for Organic Synthesis. In *Adv. Photochem.* pp 93-143.
153. Kisch, H., Semiconductor Photocatalysis for Chemoselective Radical Coupling Reactions. *Acc. Chem. Res.* **2017,** *50* (4), 1002-1010.
154. Tasker, S. Z.; Standley, E. A.; Jamison, T. F., Recent advances in homogeneous nickel catalysis. *Nature* **2014,** *509* (7500), 299-309.
155. Rosen, B. M.; Quasdorf, K. W.; Wilson, D. A.; Zhang, N.; Resmerita, A. M.; Garg, N. K.; Percec, V., Nickel-catalyzed cross-couplings involving carbon-oxygen bonds. *Chem. Rev.* **2011,** *111* (3), 1346-416.
156. Twilton, J.; Le, C.; Zhang, P.; Shaw, M. H.; Evans, R. W.; MacMillan, D. W. C., The merger of transition metal and photocatalysis. *Nat. Rev. Chem.* **2017,** *1* (7).
157. Tellis, J. C.; Primer, D. N.; Molander, G. A., Dual catalysis. Single-electron transmetalation in organoboron cross-coupling by photoredox/nickel dual catalysis. *Science* **2014,** *345* (6195), 433-6.
158. Primer, D. N.; Karakaya, I.; Tellis, J. C.; Molander, G. A., Single-electron transmetalation: an enabling technology for secondary alkylboron cross-coupling. *J. Am. Chem. Soc.* **2015,** *137* (6), 2195-8.
159. Karakaya, I.; Primer, D. N.; Molander, G. A., Photoredox Cross-Coupling: Ir/Ni Dual Catalysis for the Synthesis of Benzylic Ethers. *Org. Lett.* **2015,** *17* (13), 3294-7.
160. Caputo, J. A.; Frenette, L. C.; Zhao, N.; Sowers, K. L.; Krauss, T. D.; Weix, D. J., General and Efficient C-C Bond Forming Photoredox Catalysis with Semiconductor Quantum Dots. *J. Am. Chem. Soc.* **2017,** *139* (12), 4250-4253.
161. Liu, Y. Y.; Liang, D.; Lu, L. Q.; Xiao, W. J., Practical heterogeneous photoredox/nickel dual catalysis for C-N and C-O coupling reactions. *Chem. Commun.* **2019,** *55* (33), 4853-4856.
162. Terrett, J. A.; Cuthbertson, J. D.; Shurtleff, V. W.; MacMillan, D. W., Switching on elusive organometallic mechanisms with photoredox catalysis. *Nature* **2015,** *524* (7565), 330-4.
163. Cavedon, C.; Madani, A.; Seeberger, P. H.; Pieber, B., Semiheterogeneous Dual Nickel/Photocatalytic (Thio)etherification Using Carbon Nitrides. *Org. Lett.* **2019,** *21* (13), 5331-5334.
164. Pieber, B.; Malik, J. A.; Cavedon, C.; Gisbertz, S.; Savateev, A.; Cruz, D.; Heil, T.; Zhang, G.; Seeberger, P. H., Semi-heterogeneous Dual Nickel/Photocatalysis using Carbon Nitrides: Esterification of Carboxylic Acids with Aryl Halides. *Angew. Chem. Int. Ed.* **2019,** *58* (28), 9575-9580.
165. Ghosh, I.; Khamrai, J.; Savateev, A.; Shlapakov, N.; Antonietti, M.; Konig, B., Organic semiconductor photocatalyst can bifunctionalize arenes and heteroarenes. *Science* **2019,** *365* (6451), 360-366.
166. Lau, V. W. h.; Klose, D.; Kasap, H.; Podjaski, F.; Pignié, M. C.; Reisner, E.; Jeschke, G.; Lotsch, B. V., Dark Photocatalysis: Storage of Solar Energy in Carbon Nitride for Time-Delayed Hydrogen Generation. *Angew. Chem. Int. Ed.* **2016,** *56* (2), 510-514.
167. Savateev, A.; Kurpil, B.; Mishchenko, A.; Zhang, G.; Antonietti, M., A "waiting" carbon nitride radical anion: a charge storage material and key intermediate in direct C–H thiolation of methylarenes using elemental sulfur as the "S"-source. *Chem. Sci.* **2018,** *9*, 3584-3591
168. Kurpil, B.; Markushyna, Y.; Savateev, A., Visible-Light-Driven Reductive (Cyclo)Dimerization of Chalcones over Heterogeneous Carbon Nitride Photocatalyst. *ACS Catal.* **2019,** *9* (2), 1531-1538.
169. Ou, H.; Tang, C.; Chen, X.; Zhou, M.; Wang, X., Solvated Electrons for Photochemistry Syntheses Using Conjugated Carbon Nitride Polymers. *ACS Catal.* **2019,** *9* (4), 2949-2955.

170. Damavandi, J. A.; Karami, B.; Zolfigol, M. A., Selective Oxidation of N-Alkyl Imines to Oxaziridines using UHP/Maleic Anhydride system. *Synlett* **2002,** *2002* (06), 0933-0934.
171. Wu, G.; Geib, S. J.; Rheingold, A. L.; Heck, R. F., Isoquinolinium salt syntheses from cyclopalladated benzaldimines and alkynes. *J. Org. Chem.* **1988,** *53* (14), 3238-3241.
172. Wang, M.; Li, L.; Lu, J.; Luo, N.; Zhang, X.; Wang, F., Photocatalytic coupling of amines to imidazoles using a Mo–ZnIn2S4 catalyst. *Green Chem.* **2017,** *19* (21), 5172-5177.
173. Annunziata, R.; Benaglia, M.; Cinquini, M.; Cozzi, F.; Raimondi, L., Diastereoselective synthesis of 1,2-diphenyl-1,2-diaminoethanes by Yb(OTf)3 accelerated reductive coupling of imines. *Tetrahedron Lett.* **1998,** *39* (20), 3333-3336.
174. Suh, I.-K.; Ohta, H.; Waseda, Y., High-temperature thermal expansion of six metallic elements measured by dilatation method and X-ray diffraction. *J. Mater. Sci.* **1988,** *23* (2), 757-760.
175. Chen, Z.; Savateev, A.; Pronkin, S.; Papaefthimiou, V.; Wolff, C.; Willinger, M. G.; Willinger, E.; Neher, D.; Antonietti, M.; Dontsova, D., 'The easier the better' preparation of efficient photocatalysts – metastable poly(heptazine imide) salts. *Adv. Mater.* **2017,** *29* (32), 1700555.
176. Burdzhiev, N. T.; Stanoeva, E. R., Reaction between glutaric anhydride and N-benzylidenebenzylamine, and further transformations to new substituted piperidin-2-ones. *Tetrahedron Lett.* **2006,** *62* (35), 8318-8326.
177. Duhamel, L.; Plaquevent, J. C., A method for simple titration of organolithium reagents in ethers or hydrocarbons using metalation of N-benzylidenebenzylamine as colored reaction. *J.Org. Chem.* **1979,** *44* (19), 3404-3405.
178. Raza, F.; Park, J. H.; Lee, H.-R.; Kim, H.-I.; Jeon, S.-J.; Kim, J.-H., Visible-light-driven oxidative coupling reactions of amines by photoactive WS_2 nanosheets. *ACS Catal.* **2016,** *6* (5), 2754-2759.
179. Yang, J.; Mou, C.-Y., Ordered mesoporous Au/TiO_2 nanospheres for solvent-free visible-light-driven plasmonic oxidative coupling reactions of amines. *Appl. Catal. B* **2018,** *231*, 283-291.
180. Kumar, A.; Hamdi, A.; Coffinier, Y.; Addad, A.; Roussel, P.; Boukherroub, R.; Jain, S. L., Visible light assisted oxidative coupling of benzylamines using heterostructured nanocomposite photocatalyst. *J. Photochem. Photobiol. A* **2018,** *356*, 457-463.
181. Furukawa, S.; Ohno, Y.; Shishido, T.; Teramura, K.; Tanaka, T., Selective amine oxidation using Nb_2O_5 photocatalyst and O_2. *ACS Catal.* **2011,** *1* (10), 1150-1153.
182. Liu, H.; Xu, C.; Li, D.; Jiang, H. L., Photocatalytic hydrogen production coupled with selective benzylamine oxidation over MOF composites. *Angew. Chem. Int. Ed.* **2018,** *57* (19), 5379-5383.
183. Riemer, D.; Schilling, W.; Goetz, A.; Zhang, Y.; Gehrke, S.; Tkach, I.; Hollóczki, O.; Das, S., CO_2-catalyzed efficient dehydrogenation of amines with detailed mechanistic and kinetic studies. *ACS Catal.* **2018,** *8* (12), 11679-11687.
184. Thirumoorthi, A.; Elango, K. P., Solvent and substituent effects on the electrochemical oxidation of substituted benzylamines in 2-methylpropan-2-ol/water medium. *Int. J. Chem. Kinet.* **2007,** *39* (7), 371-377.
185. Liu, L.; Zhang, S.; Fu, X.; Yan, C. H., Metal-free aerobic oxidative coupling of amines to imines. *Chem. Commun.* **2011,** *47* (36), 10148-50.
186. Savateev, A.; Antonietti, M., Heterogeneous organocatalysis for photoredox chemistry. *ACS Catal.* **2018,** *8* (10), 9790-9808.
187. Yu, W.; Zhang, D.; Guo, X.; Song, C.; Zhao, Z., Enhanced visible light photocatalytic non-oxygen coupling of amines to imines integrated with hydrogen production over Ni/CdS nanoparticles. *Catal. Sci. Technol.* **2018,** *8* (20), 5148-5154.

188. Savateev, A.; Antonietti, M., Ionic carbon nitrides in solar hydrogen production and organic synthesis: Exciting chemistry and economic advantages. *ChemCatChem* **2019**.
189. Jitaru, M., Electrochemical carbon dioxide reduction - Fundamental and applied topics. *J. Chem. Technol. Metall.* **2007,** *42* (4), 333-344.
190. Ullah, F.; Oprea, A. I.; Kindermann, M. K.; Bajor, G.; Veszprémi, T.; Heinicke, J., Homologues of N-heterocyclic carbenes: Detection and electronic structure of N-bridgehead pyrido[a]-anellated 1,3,2-diazagermol-2-ylidenes. *J. Organomet. Chem.* **2009,** *694* (3), 397-403.
191. Chakraborty, A.; Goswami, K.; Adiyala, A.; Sinha, S., Syntheses of Spiro[cyclopent[3]ene-1,3′-indole]s and Tetrahydrocyclohepta[b]indoles from 2,3-Disubstituted Indoles through Sigmatropic Rearrangement. *Eur. J. Org. Chem.* **2013,** *2013* (31), 7117-7127.
192. Likhosherstov, A. M.; Peresada, V. P.; Vinokurov, V. G.; Skoldinov, A. P., Azacycloalkanes. XXXVII: 3,4-Dihydro-5H-pyrrolo[1,2-a]-diazepine and Its Conversions. *Pharm. Chem. J.* **2005,** *39* (9), 504-507.
193. Hegedus, L. S.; Kramer, A.; Yijun, C., Reactions of chromium carbene complexes with 1-azirines. Synthesis of N-vinylimidates. *Organometallics* **1985,** *4* (10), 1747-1750.
194. Kan, R. O.; Furey, R. L., Photochemical formation of 1,3-diazetidines. *J. Am. Chem. Soc.* **1968,** *90* (6), 1666-1667.
195. Lawrenz, D.; Mohr, S.; Wendländer, B., Formation of 1,3-diazetidines via C–N dimerization of 4-cycloalkylidene-oxazol-5(4H)-ones in the solid state. *Chem. Commun.* **1984,** (13), 863-865.
196. Quast, H.; Eckert, P.; Seiferling, B., Photolyse von 9-Azido-10-methyltriptycen. – Dimerisierung eines extrem gespannten Brückenkopfimins durch verschiedene Cycloadditionen. *Chem. Ber.* **1985,** *118* (9), 3535-3550.
197. Roussilhe, J.; Fargin, E.; Lopez, A.; Despax, B.; Paillous, N., Photochemical behavior of 2-phenylbenzoxazole. Synthesis of 1,3-diazetidine via the intermolecular [2.pi. + 2.pi.] cycloaddition of two carbon-nitrogen double bonds. *J. Org. Chem.* **1983,** *48* (21), 3736-3741.
198. Radziszewski, J. G.; Downing, J. W.; Jawdosiuk, M.; Kovacic, P.; Michl, J., 4-Azahomoadamant-3-ene: spectroscopic characterization and photoresolution of a highly reactive strained bridgehead imine. *J. Am. Chem. Soc.* **1985,** *107* (3), 594-603.
199. Fery-Forgues, S.; Paillous, N., Photodehalogenation and photodimerization of 2-(4-halophenyl)benzoxazoles. Dependence of the mechanism on the nature of the halogen atom. *J. Org. Chem.* **1986,** *51* (5), 672-677.
200. Margaretha, P., Photochemistry of Aliphatic Imines. The Photochemical Behaviour of Fluorinated N-Isopropylidenecyclohexylamines. *Helv. Chim. Acta* **1982,** *65* (1), 290-292.
201. Su, F.; Mathew, S. C.; Möhlmann, L.; Antonietti, M.; Wang, X.; Blechert, S., Aerobic Oxidative Coupling of Amines by Carbon Nitride Photocatalysis with Visible Light. *Angew. Chem. Int. Ed.* **2011,** *50* (3), 657-660.
202. Southwick, P. L.; Sullivan Iii, D. S., Strain-Barrier Stabilized Products from the Fischer Indole Synthesis. Compounds Containing the 4H-Imidazo[1,2-a]pyrrolo[3,4-b]indole and Dipyrrolo [3,4-b:3′,4′-b′][1,3]diazeto[1,2-a:3,4-a′]diindole Ring Systems. *Synthesis* **1986,** *1986* (09), 731-735.
203. Mazzanti, S.; Kurpil, B.; Pieber, B.; Antonietti, M.; Savateev, A., Dichloromethylation of enones by carbon nitride photocatalysis. *Nat. Commun.* **2020,** *11* (1), 1387.
204. Markushyna, Y.; Lamagni, P.; Teutloff, C.; Catalano, J.; Lock, N.; Zhang, G.; Antonietti, M.; Savateev, A., Green radicals of potassium poly(heptazine imide) using light and benzylamine. *J. Mater. Chem. A* **2019,** *7* (43), 24771-24775.

205. Lau, V. W.-h.; Klose, D.; Kasap, H.; Podjaski, F.; Pignié, M.-C.; Reisner, E.; Jeschke, G.; Lotsch, B. V., Dark Photocatalysis: Storage of Solar Energy in Carbon Nitride for Time-Delayed Hydrogen Generation. *Angew. Chem. Int. Ed.* **2017,** *56* (2), 510-514.
206. Yu, L.; Zhang, Q.; Li, S. S.; Huang, J.; Liu, Y. M.; He, H. Y.; Cao, Y., Gold-Catalyzed Reductive Transformation of Nitro Compounds Using Formic Acid: Mild, Efficient, and Versatile. *ChemSusChem* **2015,** *8* (18), 3029-35.
207. Nasir Baig, R. B.; Verma, S.; Nadagouda, M. N.; Varma, R. S., A photoactive bimetallic framework for direct aminoformylation of nitroarenes. *Green Chem.* **2016,** *18* (4), 1019-1022.
208. Tao, L.; Zhang, Q.; Li, S.-S.; Liu, X.; Liu, Y.-M.; Cao, Y., Heterogeneous Gold-Catalyzed Selective Reductive Transformation of Quinolines with Formic Acid. *Adv. Synth. Catal* **2015,** *357* (4), 753-760.
209. Lou, X.-B.; He, L.; Qian, Y.; Liu, Y.-M.; Cao, Y.; Fan, K.-N., Highly Chemo- and Regioselective Transfer Reduction of Aromatic Nitro Compounds using Ammonium Formate Catalyzed by Supported Gold Nanoparticles. *Adv. Synth. Catal* **2011,** *353* (2-3), 281-286.
210. Wang, H.; Jia, J.; Song, P.; Wang, Q.; Li, D.; Min, S.; Qian, C.; Wang, L.; Li, Y. F.; Ma, C.; Wu, T.; Yuan, J.; Antonietti, M.; Ozin, G. A., Efficient Electrocatalytic Reduction of CO2 by Nitrogen-Doped Nanoporous Carbon/Carbon Nanotube Membranes: A Step Towards the Electrochemical CO2 Refinery. *Angew. Chem. Int. Ed. Engl.* **2017,** *56* (27), 7847-7852.
211. Abbott, A. P.; Capper, G.; Gray, S., Design of improved deep eutectic solvents using hole theory. *ChemPhysChem* **2006,** *7* (4), 803-6.
212. Filonenko, S.; Voelkel, A.; Antonietti, M., Valorization of monosaccharides towards fructopyrazines in a new sustainable and efficient eutectic medium. *Green Chem.* **2019,** *21* (19), 5256-5266.
213. Francisco, M.; van den Bruinhorst, A.; Kroon, M. C., Low-transition-temperature mixtures (LTTMs): a new generation of designer solvents. *Angew. Chem. Int. Ed. Engl.* **2013,** *52* (11), 3074-85.
214. Huang, C.; Zhang, W.; Yan, Z.; Gao, J.; Liu, W.; Tong, P.; Zhang, L., Protonated mesoporous graphitic carbon nitride for rapid and highly efficient removal of microcystins. *RSC Adv.* **2015,** *5* (56), 45368-45375.
215. Dong, X.; Wang, Z.; Duan, Y.; Yang, Y., One-pot selective N-formylation of nitroarenes to formamides catalyzed by core-shell structured cobalt nanoparticles. *Chem. Commun.* **2018,** *54* (64), 8913-8916.
216. Kortlever, R.; Balemans, C.; Kwon, Y.; Koper, M. T. M., Electrochemical CO2 reduction to formic acid on a Pd-based formic acid oxidation catalyst. *Catal. Today* **2015,** *244*, 58-62.
217. Podgoršek, A.; Zupan, M.; Iskra, J., Oxidative Halogenation with "Green" Oxidants: Oxygen and Hydrogen Peroxide. *Angew. Chem. Int. Ed.* **2009,** *48* (45), 8424-8450.
218. Moon, G.-h.; Fujitsuka, M.; Kim, S.; Majima, T.; Wang, X.; Choi, W., Eco-Friendly Photochemical Production of H_2O_2 through O_2 Reduction over Carbon Nitride Frameworks Incorporated with Multiple Heteroelements. *ACS Catal.* **2017,** *7*, 2886-2895.
219. Hering, T.; Mühldorf, B.; Wolf, R.; König, B., Halogenase-Inspired Oxidative Chlorination Using Flavin Photocatalysis. *Angew. Chem. Int. Ed.* **2016,** *55* (17), 5342-5345.
220. Savateev, A.; Pronkin, S.; Willinger, M.; Antonietti, M.; Dontsova, D., Towards organic zeolites and inclusion catalysts: heptazine imide salts can exchange metal cations in the solid state. *Chem. - Asian J.* **2017,** *12* (13), 1517-1522.
221. Aldissi, M.; Armes, S. P., X-ray photoelectron spectroscopy study of bulk and colloidal polyaniline. *Macromolecules* **1992,** *25* (11), 2963-2968.
222. Rodríguez, N. A.; Savateev, A.; Grela, M. A.; Dontsova, D., Facile Synthesis of Potassium Poly(heptazine imide) (PHIK)/Ti-Based Metal–Organic Framework (MIL-125-

NH2) Composites for Photocatalytic Applications. *ACS Appl. Mater. Interfaces* **2017,** *9* (27), 22941-22949.
223. Martin, S. T.; Herrmannt, H.; Hoffmann, M. R., Time-resolved Microwave Conductivity. Part 2.-Quantum-sized TiO, and the Effect of Adsorbates and Light Intensity on Charge-carrier Dynamics. *J. Chem. Soc., Faraday Trans.* **1994,** *90* (21), 3323-3330.
224. Zhang, G.; Li, G.; Lan, Z.-a.; Lin, L.; Savateev, A.; Heil, T.; Zafeiratos, S.; Wang, X.; Antonietti, M., Optimizing Optical Absorption, Exciton Dissociation, and Charge Transfer of a Polymeric Carbon Nitride with Ultrahigh Solar Hydrogen Production Activity. *Angew. Chem. Int. Ed.* **2017,** *56* (43), 13445-13449.
225. Bosch, F.; Rosich, L., The contributions of Paul Ehrlich to pharmacology: a tribute on the occasion of the centenary of his Nobel Prize. *Pharmacology* **2008,** *82* (3), 171-9.
226. Scott K.A.; J.T., N., Analysis of US FDA-Approved Drugs Containing Sulfur Atoms. *Jiang X. (eds) Sulfur Chemistry. Topics in Current Chemistry Collections. Springer, Cham* **2019**.
227. Feng, M.; Tang, B.; Liang, S. H.; Jiang, X., Sulfur Containing Scaffolds in Drugs: Synthesis and Application in Medicinal Chemistry. *Curr. Top. Med. Chem.* **2016,** *16* (11), 1200-16.
228. KK, A., Anderson KK. In: Sulfonic Acids and Their Derivatives in Comprehensive Organic Chemistry. Barton DHR, Ollis WD, Jones DN, editors. Vol. 3. Pergamon Press; Oxford: 1979. pp. 331–350.
229. Chaudhary, R.; Natarajan, P., Visible Light Photoredox Activation of Sulfonyl Chlorides: Applications in Organic Synthesis. *ChemistrySelect* **2017,** *2* (22), 6458-6479.
230. Dai, Y.; Li, C.; Shen, Y.; Lim, T.; Xu, J.; Li, Y.; Niemantsverdriet, H.; Besenbacher, F.; Lock, N.; Su, R., Light-tuned selective photosynthesis of azo- and azoxy-aromatics using graphitic C3N4. *Nat. Commun.* **2018,** *9* (1), 60.
231. Martinez-Gualda, A. M.; Cano, R.; Marzo, L.; Perez-Ruiz, R.; Luis-Barrera, J.; Mas-Balleste, R.; Fraile, A.; de la Pena O'Shea, V. A.; Aleman, J., Chromoselective access to Z- or E- allylated amines and heterocycles by a photocatalytic allylation reaction. *Nat. Commun.* **2019,** *10* (1), 2634.
232. Ghosh, I.; Konig, B., Chromoselective Photocatalysis: Controlled Bond Activation through Light-Color Regulation of Redox Potentials. *Angew. Chem. Int. Ed. Engl.* **2016,** *55* (27), 7676-9.
233. Nishiguchi, A.; Maeda, K.; Miki, S., Sulfonyl Chloride Formation from Thiol Derivatives by N-Chlorosuccinimide Mediated Oxidation. *Synthesis* **2006,** *2006* (24), 4131-4134.
234. Choi, J.; Yoon, N. M., A Convenient One-Pot Synthesis of Disulfides from Thioacetates via Nickel Boride Catalyzed Methanolysis and Disproportionation. *Synlett* **1995,** *1995* (10), 1073-1074.
235. Meshram, H. M.; Bandyopadhyay, A.; Reddy, G. S.; Yadav, J. S., Microwave Thermolysis VII: Oxidative Coupling of Thiol Acetates and Esters Using “Clayan” in Dry Media. *Synth. Commun.* **1999,** *29* (15), 2705-2709.
236. Meshram, H. M., An efficient and mild cleavage of thiol acetate with clayfen in the absence of solvent. *Tetrahedron Lett.* **1993,** *34* (15), 2521-2522.
237. Majek, M.; Neumeier, M.; Jacobi von Wangelin, A., Aromatic Chlorosulfonylation by Photoredox Catalysis. *ChemSusChem* **2017,** *10* (1), 151-155.
238. Weidinger, A.; Waiblinger, M.; Pietzak, B.; Murphy, T. A., Atomic nitrogen in C60: N@C60. . *Appl. Phys. A* **1998,** *66*, 287-292.
239. Savateev, A.; Dontsova, D.; Kurpil, B.; Antonietti, M., Highly Crystalline Poly(heptazine imides) by Mechanochemical Synthesis for Photooxidation of Various Organic Substrates Using an Intriguing Electron Acceptor – Elemental Sulfur. *J. Catal.* **2017**.

240. Kurpil, B.; Kumru, B.; Heil, T.; Antonietti, M.; Savateev, A., Carbon Nitride Creates Thioamides in High Yields by Photocatalytic Kindler Reaction. *Green Chem.* **2018,** *20*, 838-842.
241. Savateev, A.; Dontsova, D.; Kurpil, B.; Antonietti, M., Highly Crystalline Poly(heptazine imides) by Mechanochemical Synthesis for Photooxidation of Various Organic Substrates Using an Intriguing Electron Acceptor – Elemental Sulfur. *J. Catal.* **2017,** *350*, 203-211.
242. Schlomberg, H.; Kröger, J.; Savasci, G.; Terban, M. W.; Bette, S.; Moudrakovski, I.; Duppel, V.; Podjaski, F.; Siegel, R.; Senker, J.; Dinnebier, R. E.; Ochsenfeld, C.; Lotsch, B. V., Structural Insights into Poly(Heptazine Imides): A Light-Storing Carbon Nitride Material for Dark Photocatalysis. *Chem. Mater.* **2019,** *31* (18), 7478-7486.
243. Kurpil, B.; Savateev, A.; Papaefthimiou, V.; Zafeiratos, S.; Heil, T.; Özenler, S.; Dontsova, D.; Antonietti, M., Hexaazatriphenylene doped carbon nitrides—Biomimetic photocatalyst with superior oxidation power. *Appl. Catal., B* **2017,** *217*, 622-628.
244. Chen, Z.; Savateev, A.; Pronkin, S.; Papaefthimiou, V.; Wolff, C.; Willinger, M. G.; Willinger, E.; Neher, D.; Antonietti, M.; Dontsova, D., "The Easier the Better" Preparation of Efficient Photocatalysts-Metastable Poly(heptazine imide) Salts. *Adv. Mater.* **2017,** *29* (32).
245. Raza, F.; Park, J. H.; Lee, H.-R.; Kim, H.-I.; Jeon, S.-J.; Kim, J.-H., Visible-Light-Driven Oxidative Coupling Reactions of Amines by Photoactive WS_2 Nanosheets. *ACS Catal.* **2016,** *6*, 2754-2759.
246. He, Z.; Wang, D.; Tang, J.; Song, S.; Chen, J.; Tao, X., A quasi-hexagonal prism-shaped carbon nitride for photoreduction of carbon dioxide under visible light. *Environ. Sci. Pollut. Res.* **2017,** *24* (9), 8219-8229.
247. Fu, J.; Zhu, B.; Jiang, C.; Cheng, B.; You, W.; Yu, J., Hierarchical porous O-doped g-C3N4 with enhanced photocatalytic CO2 reduction activity. *Small* **2017,** *13* (15).
248. Niu, P.; Yang, Y.; Yu, J. C.; Liu, G.; Cheng, H. M., Switching the selectivity of the photoreduction reaction of carbon dioxide by controlling the band structure of a g-C3N4 photocatalyst. *Chem. Commun.* **2014,** *50* (74), 10837-40.
249. Mao, J.; Peng, T.; Zhang, X.; Li, K.; Ye, L.; Zan, L., Effect of graphitic carbon nitride microstructures on the activity and selectivity of photocatalytic CO2 reduction under visible light. *Catal. Sci. Technol.* **2013,** *3* (5).
250. Clarizia, L.; Di Somma, I.; Marotta, R.; Minutolo, P.; Villamaina, R.; Andreozzi, R., Photocatalytic reforming of formic acid for hydrogen production in aqueous solutions containing cupric ions and TiO_2 suspended nanoparticles under UV-simulated solar radiation. *Appl. Catal. A* **2016,** *518*, 181-188.
251. Loges, B.; Boddien, A.; Gärtner, F.; Junge, H.; Beller, M., Catalytic generation of hydrogen from formic acid and its derivatives: Useful hydrogen storage materials. *J. Am. Chem. Soc.* **2010,** *53* (13-14), 902-914.
252. Tsutsumi, K.; Kashimura, N.; Tabata, K., Photo-assisted hydrogen evolution in aqueous solution of formic acid with silicon which is supported with noble metals. *Silicon* **2015,** *7* (1), 43-48.
253. Antao, S. M.; Hassan, I., $BaCO_3$: high-temperature crystal structures and the Pmcn→R3m phase transition at 811°C. *Phys. Chem. Miner.* **2007,** *34* (8), 573-580.
254. Tolbert, T. L.; Houston, B., The Preparation of Aldimines through the Stephen Reaction1. *J. Org. Chem.* **1963,** *28* (3), 695-697.
255. Hari, D. P.; Schroll, P.; Konig, B., Metal-free, visible-light-mediated direct C-H arylation of heteroarenes with aryl diazonium salts. *J. Am. Chem. Soc.* **2012,** *134* (6), 2958-61.
256. Pu, Y.-M.; Christesen, A.; Ku, Y.-Y., A simple and highly effective oxidative chlorination protocol for the preparation of arenesulfonyl chlorides. *Tetrahedron Lett.* **2010,** *51* (2), 418-421.

257. Górski, B.; Basiak, D.; Talko, A.; Basak, T.; Mazurek, T.; Barbasiewicz, M., Olefination with Sulfonyl Halides and Esters: E-Selective Synthesis of Alkenes from Semistabilized Carbanion Precursors. *Eur. J. Org. Chem.* **2018,** *2018* (15), 1774-1784.
258. *CURIS, INC. - WO2009/36016, 2009, A1*.
259. Wang, H. Y.; Pu, X. Q.; Yang, X. J., Rearrangement Reaction Based on the Structure of N-Fluoro- N-alkyl Benzenesulfonamide. *J. Org. Chem.* **2018,** *83* (21), 13103-13110.
260. Bonk, J. D.; Amos, D. T.; Olson, S. J., Convenient One-Pot Synthesis of Sulfonamides from Thiols using Trichloroisocyanuric Acid. *Synth. Commun.* **2007,** *37* (12), 2039-2050.

13. Acknowledgments

I am sincerely grateful to all the people who were supportive throughout my ‘PhD journey’ and without whom it would not have been as pleasant and fruitful as it is.

Firstly, I would like to thank Dr. Aleksandr Savateev for the great supervision and all the support I have got from him. I extremely appreciate the level of freedom in my research and the trust he provided me with. I would also like to acknowledge the quality of scientific discussions we have had. Apart from a very good supervision, thank you Sasha just for being a good person and the warm environment in the group you have organized!

I am thankful to Prof. Markus Antonietti for the opportunity to be a member of MPIKG family and to conduct the research under his supervision. I appreciate the constructive suggestions and ideas I have received in these years. I never cease to be amazed by the level of creativity and intelligence of him.

I would like to acknowledge Prof. Bernd Schmidt for being my second supervisor and providing me the opportunity to teach in the lab course of organic chemistry.

I indeed appreciate being a member of Colloid Chemistry Department, where I not only gained the knowledge needed for my research, but experienced working in an international environment among wonderful researchers of different backgrounds and cultures. I am thankful to each and every MPIKG member! Special thanks to my group members for the help with experiments and fruitful discussions. Many thanks to Stefano, Bogdan, Yajun, Guigang and Katharina!

I am also thankful to my friends for enjoyable company! Thank you Svitlana, Swapnil, Simon and Ivo for the extensive support and wise advises. Thanks to the “table tennis team” for trainings and fun times! Thanks to Hossein, Naresh and Shaowen!

I would also like to thank my close friends in Ukraine, Valik, Sasha, Andrii, and Nazar for the great time spent together, while I was in my home country; many thanks to Valik for the tremendous support and help I have for the last many years. I am also thankful to my previous supervisor at Enamine Ltd for valuable experience and skills. Thank you Vania and we stay in touch!

Finally, I want to thank my family for their invaluable support and love throughout my life. I deeply cherish the moments spent together visiting my parents’ house.